An investigation of the photostabilisation of sunscreen absorbers by plant polyphenols

by

Georges Jasper Mturi

Submitted in fulfilment of the academic
requirements for the degree of
Master of Science in the
School of Chemistry,
University of KwaZulu-Natal,
Durban

July 2005

Hii kazi iwe ukumbusho wa usotaji
wa wazazi wangu kunilea na kunisomesha

ABSTRACT

Commercial sunscreen products are used to protect the skin against harmful ultraviolet (UV) radiation that can induce skin cancer at high dosage. These products contain UV filters that can reflect, scatter or absorb UV light. The chemical UV filters responsible for the absorption of UV radiation can be photochemically modified and as a result reduce the efficacy of the sunscreen formulation. This study focused on the possible use of plant polyphenols as potential stabilisers of photo-unstable sunscreen chemical absorbers.

The photo-instability of some sunscreen absorbers results in radical formation; this prompted the use of the plant, *Sutherlandia microphylla* (Cancer Bush plant), as a potential photostabiliser. The Cancer Bush plant is used by the indigenous people of South Africa to treat AIDS and cancer. The radical scavenging properties of polyphenolic compounds present in the plant are possibly responsible for the plant's anti-tumour and anti-HIV properties. Therefore, these Cancer Bush polyphenols could possibly be used to photostabilise photo-unstable sunscreen absorbers.

Potential polyphenolic photostabilisers from the Cancer Bush plant were extracted by means of various polyphenolic extraction methods. These extracts were analysed by gas chromatography (GC), high-performance liquid chromatography (HPLC), UV spectroscopy and gas chromatography-mass spectrometry (GC-MS). The phenolic content and the antioxidant activity of these extracts were investigated by means of the Folin-Ciocalteu reagent (FCR) and the diphenylpicrylhydrazyl (DPPH) radical assays respectively. Polyphenols were also extracted from various Rooibos teas and compared with those extracted from the Cancer Bush plant. Both the Cancer Bush and various Rooibos tea extracts were found to contain simple phenolics and potential polyphenolic compounds.

The Cancer Bush extracts as well as the Rooibos tea extracts together with the specific polyphenols, epicatechin and rutin, were assessed for their ability to photostabilise sunscreen absorbers. The photostability of the chemical absorbers in the absence and in the presence of the polyphenol extracts was investigated by UV spectroscopy, by monitoring their absorption spectra during irradiation with solar-simulated radiation. These extracts inhibited the photodegradation of the absorber avobenzone. The photostability of avobenzone is solvent-

dependent hence the investigations were carried out in three solvents, namely, cyclohexane, ethyl acetate and dimethylsulfoxide. Additionally, the cause of the instability of avobenzone in these solvents was investigated by means of UV spectroscopy, HPLC and nuclear magnetic resonance spectroscopy. The oxygen dependency of the photo-instability of avobenzone was also determined.

The photo-instability of avobenzone was found to occur as a result of photoisomerisation and/or photodegradation, depending on the solvent. Avobenzone photoisomerised extensively in dimethylsulfoxide and photodegraded appreciably in cyclohexane, whereas both processes occurred to a similar extent in ethyl acetate. Photoisomerisation only occurred in the presence of oxygen whereas photodegradation occurred irrespective of oxygen. The Cancer Bush and various Rooibos tea extracts as well as other polyphenols photostabilised avobenzone in ethyl acetate and dimethylsulfoxide but not in cyclohexane. This photostabilisation effect was potentially due to the radical scavenging ability of polyphenols which prevented the oxygen-dependent photoisomerisation, but not the oxygen independent photodegradation process from occurring.

PREFACE

The experimental work described in this thesis was carried out in the School of Pure and Applied Chemistry, University of KwaZulu-Natal, Durban, from January 2003 to December 2004, under the supervision of Professor B.S. Martincigh.

These studies represent original work by the author and have not otherwise been submitted in any form for any degree or diploma to any tertiary institution. Where use has been made of the work of others it is duly acknowledged in the text.

15ᵗʰ July, 2005

ACKNOWLEDGEMENTS

TABLE OF CONTENTS

CHAPTER 1

INTRODUCTION

The prevalence of skin cancer is relatively high in South Africa as it is in many parts of the world such as Australia, the United States of America (Taylor [1995]) and the Scandinavian countries. The incidence is highest in the fair-skinned population and the principal cause is thought to be long cutaneous exposure to radiation from the sun (Mukhtar and Elmets [1996]). Ultraviolet (UV) radiation constitutes a small band of sunlight that falls on the earth, and it has been implicated to induce skin cancer. Consequently, the incidence of skin cancer is greatest in places where the climate is ideal for people to spend more time outdoors. The use of sunscreens is advocated as a means of protection from the harmful UV light. These products protect the skin because they contain filter compounds that preferentially absorb, reflect or scatter the UV light. However, these sunscreen filters provide protection against UV radiation for a predetermined period of time before they lose their efficacy. It is therefore important to find ways to improve the efficacy of these filters, so as to improve the efficacy of the sunscreen product. In this research, antioxidant polyphenolic substances have been investigated as potential photostabilisers of sunscreen filter compounds. The polyphenols that were specifically investigated were those extracted from the plant, *Sutherlandia microphylla*, commonly known as the Cancer Bush plant, as well as those from various Rooibos teas. They were investigated for their ability to photostabilise photo-unstable filter compounds, and in particular the filter, 4-*tert*-butyl-4'-methoxydibenzoylmethane (avobenzone).

1.1 Photodamage

Solar emission comprises of radiation of various wavelengths, but the shortest wavelengths do not reach the earth's surface since they are absorbed by the oxygen and ozone in the earth's atmosphere. UV radiation forms only 15% of the sun's total radiation that penetrates through the earth's atmosphere (Sayre [1992]). But since UV radiation (see Section 1.1.1) has the shortest wavelength of all the penetrating radiation, it is the most energetic and potentially dangerous to living organisms. The most applicable harm relating to this study is how UV exposure can act as a major inducer of skin cancer in humans (see Section 1.1.2).

1.1.1 UV radiation

UV radiation can be classified into three parts: UVA (320-400 nm), UVB (280-320 nm) and UVC (100-280 nm) radiation. The lowest detectable wavelength of solar radiation at sea level is 290 nm (Martincigh *et al.* [1997]), which implies that only UVA and a portion of UVB radiation enter our atmosphere. Sayre *et al.* [1992] also reported that only 1-2% of the total UV radiation entering our atmosphere is UVB, the rest falls in the UVA range. This amount of UVB radiation is, however, the most affected by depletion of stratospheric ozone.

UVC radiation is the most dangerous of all the UV radiation since it has the highest energy; fortunately, it is absorbed by the ozone layer before it reaches the earth's surface (Martincigh *et al.* [1997]). UVB radiation is mostly absorbed by stratospheric ozone, but the portion that enters the atmosphere, although small, has been implicated to be the most dangerous of all the UV radiation reaching the earth's surface. UVB radiation has been shown to be the major cause of erythema and skin cancer (Martincigh *et al.* [1997]), it has also been implicated as an inhibitor of DNA, RNA and protein synthesis (Woodruff [2001]). On the other hand, low energy UVA radiation, which was once considered harmless, has been implicated in causing wrinkling, photoaging of the skin, erythema (Martincigh *et al.* [1997]) and skin cancer (Setlow *et al.* [1993]).

1.1.2 Skin cancer

Skin cancer is the most widespread type of cancer in many parts of the world. There are three types of skin cancer: squamous cell carcinoma, basal cell carcinoma and malignant melanoma. These cancers differ based on the type of skin cells they originate from within the different layers of the skin.

Only the outer layers of the human skin are affected by UV radiation, namely, the epidermal and dermal layers (see Figure 1.1). The epidermis is the outermost layer which is relatively thin but tough. The epidermis contains three main specialised cells: melanocytes (that produce melanin), Langerhans' cells and keratinocytes (that produce keratin). The epidermis contains a membrane at its base consisting of basal cells that separates it from the dermis, whereas the squamous cells are located more towards the surface of the skin. The outer region of the epidermis is referred to as the stratum corneum; with cells that become increasingly flattened towards the more outer sections of the layer. These cells produce keratin which when in high content causes the cell to die forming the protective stratum corneum layer (Green *et al.*

[1990]). The epidermis also contains the protective melanin substance that gives the skin its colour. The dermis is the thick skin layer beneath the epidermis composed of collagen fibers, elastic tissue as well as reticular fibers (Cancer Research UK [accessed on 28th October 2004]) with specialised structures such as sweat glands, sebaceous glands and hair follicles. UVA radiation is able to penetrate deeper into these two layers than UVB radiation (see Figure 1.2).
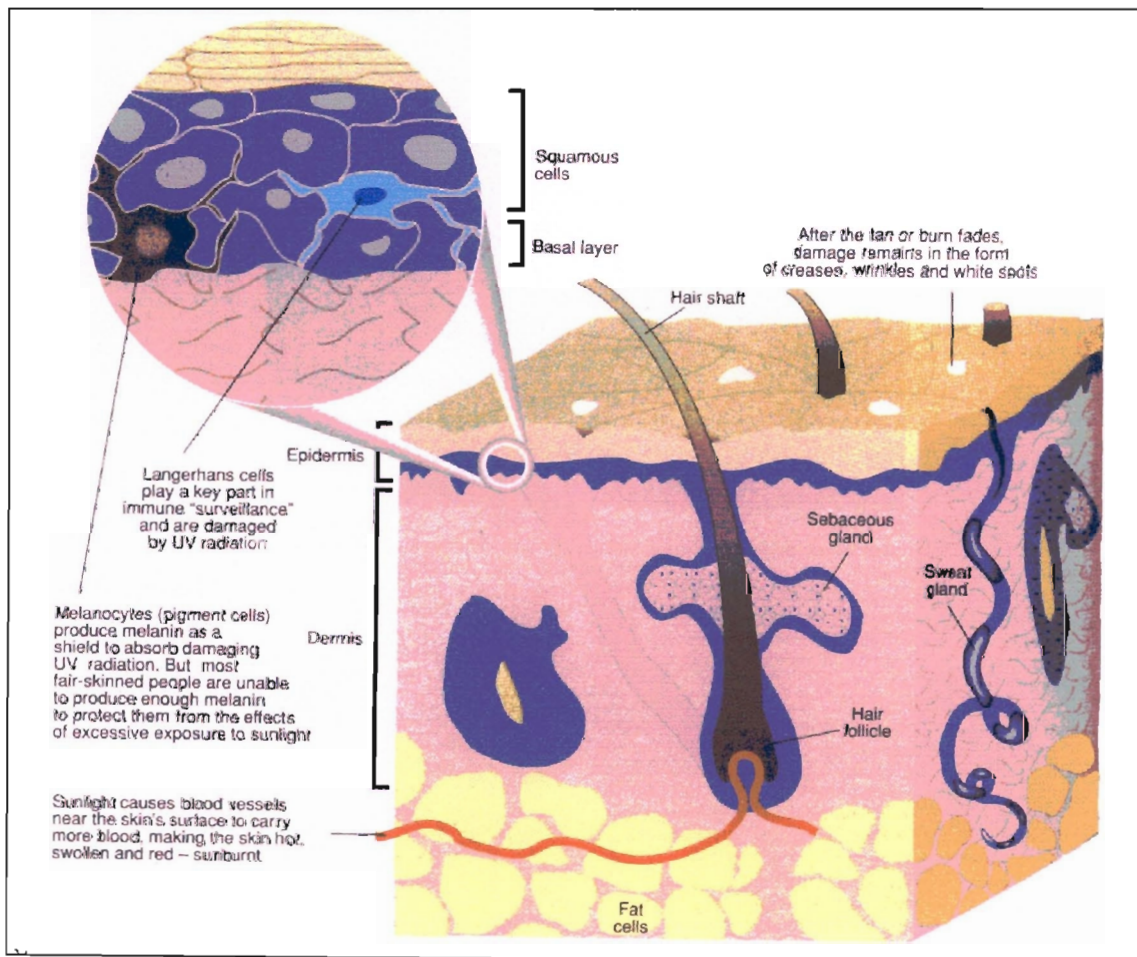
Figure 1.1:   The epidermal and dermal layers of the outer human skin (Concar [1992]).
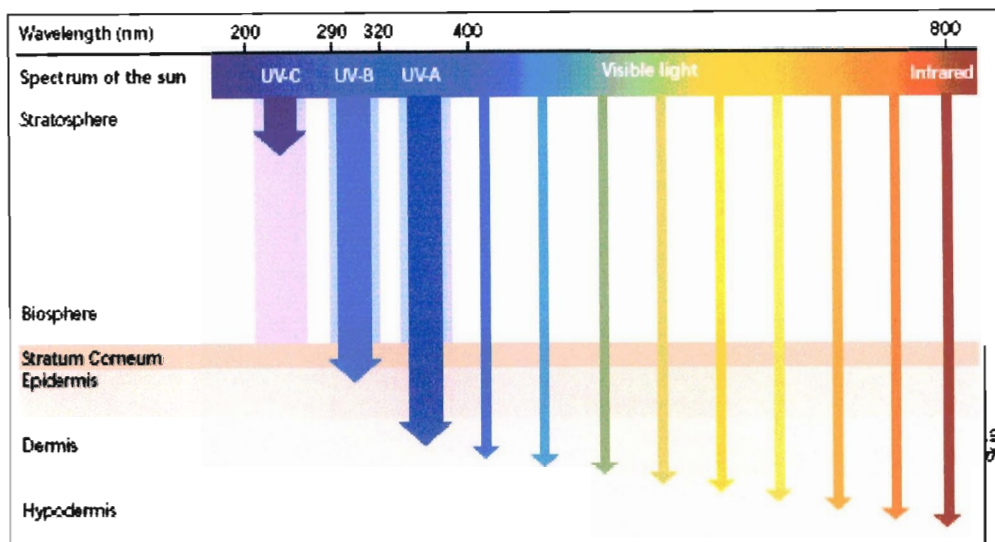
Figure 1.2:   The different levels of penetration of UVA, UVB and UVC through the skin layer (Ciba Specialty Chemicals [accessed on 13th December 2004]).

Carcinoma refers to cancer originating from cells of the tissues lining or covering organs. When skin cancer begins at the basal cells of the epidermis, it is referred to as basal cell carcinoma, whereas that which arises from the squamous cells is called squamous cell carcinoma. On the other hand, malignant melanoma is a skin cancer that develops from melanocytes, it is malignant since it has a tendency to spread to other parts of the body (Sewlall [2003] and CancerNet [accessed on 28th October 2004]). Basal cell carcinoma and squamous cell carcinoma are the most frequently occurring types of skin cancer; they are referred to as non-melanoma skin cancer. In the United Kingdom (UK), 90% of skin cancer cases are non-melanoma skin cancer, with only 10% due to malignant melanoma (Cancer Research UK [accessed on 28th October 2004]). Fortunately, although non-melanoma skin cancers occur abundantly, nearly all diagnoses are cured. On the other hand, in 5 500 malignant melanoma diagnoses in the United Kingdom, about 1 600 die from the skin cancer disease (Cancer Research UK [accessed on 28th October 2004]). Hence, malignant melanoma is the rarest of the skin cancers, but the most dangerous type when not treated early. In South Africa, the risk for a Caucasian male and female to develop malignant melanoma in their lifetime is 2.2% and 1.8%, respectively (Human and Bajic [2002]). Alternatively, there is only a 0.11% and a 0.13% risk of developing melanoma for black males and females, respectively (Human and Bajic [2002]). The rates of non-melanoma skin cancers in Caucasian South Africans varies with age (Human and Bajic [2002]).

UVA as well as UVB radiation have both been implicated in the induction of skin cancer. Animal models have shown UVB radiation, of all the UV radiation entering the earth's

atmosphere, to be the principal cause of skin cancer (Lowe [1990] and de Gruijl and van der Leun [1994]). Setlow *et al.* [1993], on the other hand, observed that the once perceived harmless UVA radiation induced 90-95% malignant melanoma in fish hybrids of the genus, *Xiphophorus*. The occurrence of skin cancer is much more abundant in the fair-skinned population as they have less melanin in their skin. Melanin absorbs UV radiation and in so doing acts as protection against skin cancer. This was observed by Eggset *et al.* [1984] when untanned epidermis showed a several-fold higher UVB light transmission than tanned epidermis.

Skin cancer develops from genetic mutations, which are modifications of the nucleic acids that make up the genes. In humans, the type of nucleic acid present is deoxyribonucleic acid (DNA). DNA is a helical structure containing two adjacent polynucleotide strands anti-parallel to one another, and is present in the nucleus of every body cell (see Figure 1.3). Each nucleotide is made up of a deoxyribose (a five carbon sugar) unit, a phosphate group and a nitrogenous base. The phosphate groups attach the nucleotides together to form a polynucleotide, whereas the nitrogenous bases bind the two adjacent polynucleotides by hydrogen bonding. There are four nitrogenous bases in humans: adenine (A), guanine (G), cytosine (C) and thymine (T). These bases are categorised into two groups; adenine and guanine are purines, whereas cytosine and thymine are pyrimidines. The two DNA polynucleotides are held together by hydrogen bonding between purines and pyrimidines. The purine-pyrimidine base pairs that hydrogen bond with each other are A-T and G-C pairs. There are two hydrogen bonds between the A-T base pairs whereas the G-C base pairs have three (see Figure 1.4).

The DNA base sequence carries the genetic information in the form of genes. This sequence is replicated and passed on to other cells as well as transcribed to ribonucleic acids (RNA) and translated into proteins. It is therefore essential that the correct code is passed on from one stage to another; thereby preventing gene mutations that could be translated to produce mutated proteins that could potentially cause the cell to become cancerous.
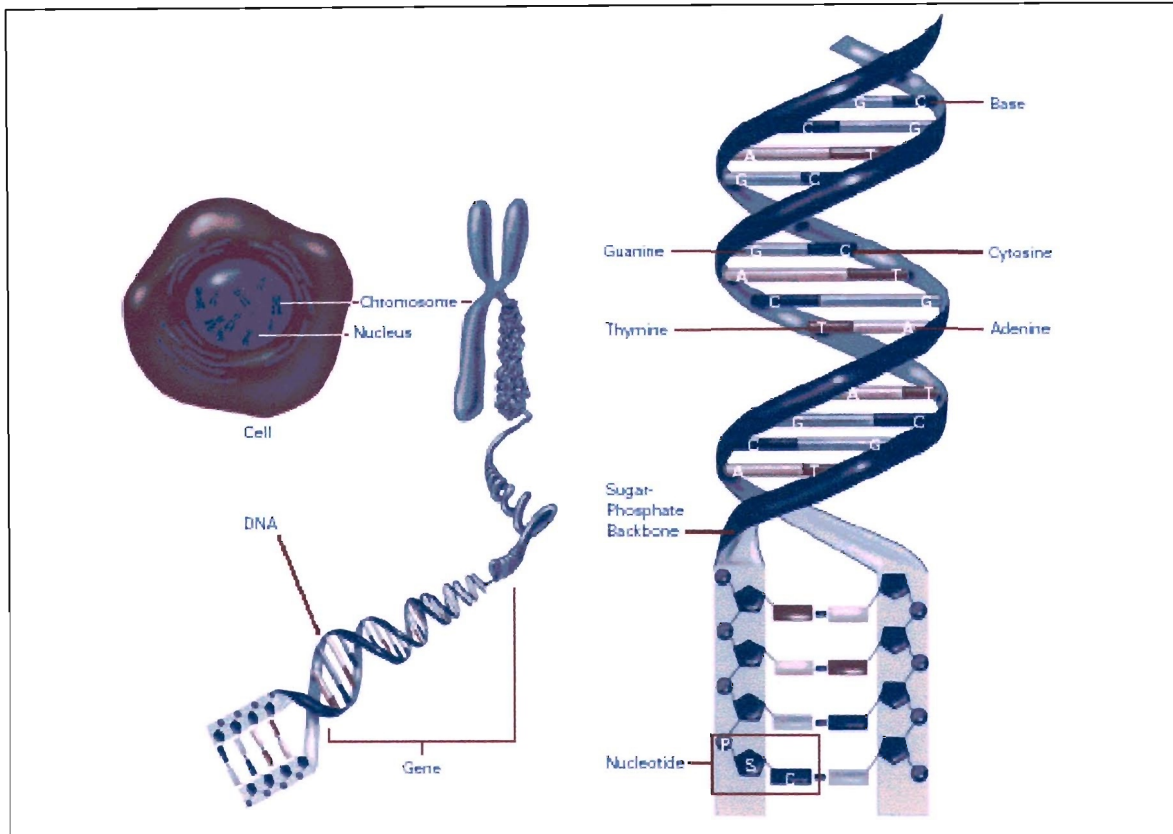
Figure 1.3:   A cell has a nucleus that contains chromosomes with DNA consisting of two nucleotide strands held together by hydrogen bonding (National Institute of Health [accessed on 12th November 2004]).
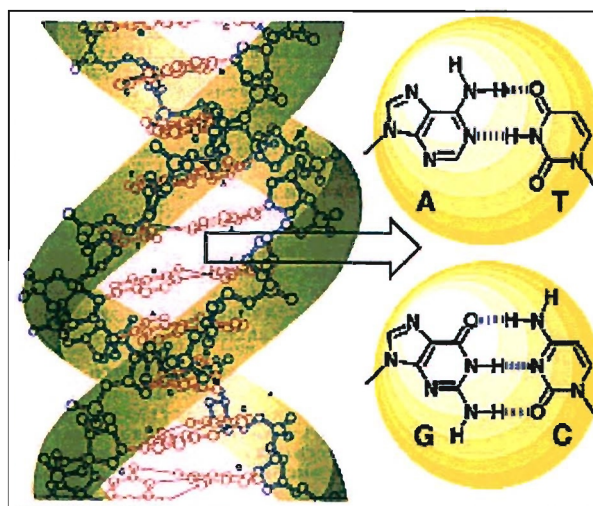
Figure 1.4:   The DNA molecule is composed of two polynucleotides held together by hydrogen bonding between purines and pyrimidines (Toyama Medical and Pharmaceutical University [accessed on 11th November 2004]).

Upon UV exposure, the most likely absorbers in the DNA molecule are the conjugated nitrogenous bases. These bases absorb UV light to form two types of pyrimidine dimers: cyclobutane pyrimidine dimers (see Figure 1.5) and the pyrimidine-(6-4)-pyrimidone photoproduct (see Figure 1.6). Pyrimidine dimerisation occurs when adjacent pyrimidine bases on the same polynucleotide strand of the DNA molecule dimerise by cross-linking to form a cyclobutane ring between them. Thymine photodimerisation has been observed by various researchers (Weinblum and Johns [1966], Lamola A.A. [1969] and Sutherland and Griffin [1984]) and the thymine dimer is the most likely photoproduct to form from pyrimidine dimerisation in the DNA molecule as has been observed experimentally. Other pyrimidine dimers that form subsequent to photo-irradiation are between thymine and cytosine as well as between cytosine and cytosine, with the latter being the most lethal. The pyrimidine-(6-4)-pyrimidone photoproduct forms between adjacent pyrimidine bases when a bond forms between carbon-6 of one base and carbon-4 of another (Taylor [1994]). Although these photoproducts are more mutagenic than the pyrimidine dimers they are formed less frequently by solar radiation (You *et al.* [2001] and Dany *et al.* [2001]).

Potten *et al.* [1993] showed that thymine dimers increased at higher UV dosage in nuclei of human epidermal cells. The formation of any pyrimidine dimers causes uncoiling and bending in the DNA molecule, this effect is both lethal and carcinogenic as it prevents DNA replication. Armstrong and Kricker [2001] reported that pyrimidine dimers occurred at dipyrimidine sites in non-melanoma skin cancers of the human skin; this implicated them as the potential causers of these cancers. De Gruijl *et al.* [2001] reported on how the body contains excision repair enzymes that nick these pyrimidine dimers on each side of the DNA strand (Montelone [accessed on 24th November 2004]). A specialised DNA polymerase enzyme then inserts the appropriate bases using the complementary strand (Montelone [accessed on 24th November 2004]). This repair process is efficient but very slow (Hemminki *et al.* [2002]), so overexposure can easily overburden the skin with this damage and then not all dimers are repaired, which could potentially lead to skin cancer. Some people with the condition called *Xerodema pigmentosa* lack these repair enzymes, and these people are more prone to UV-induced skin cancer.
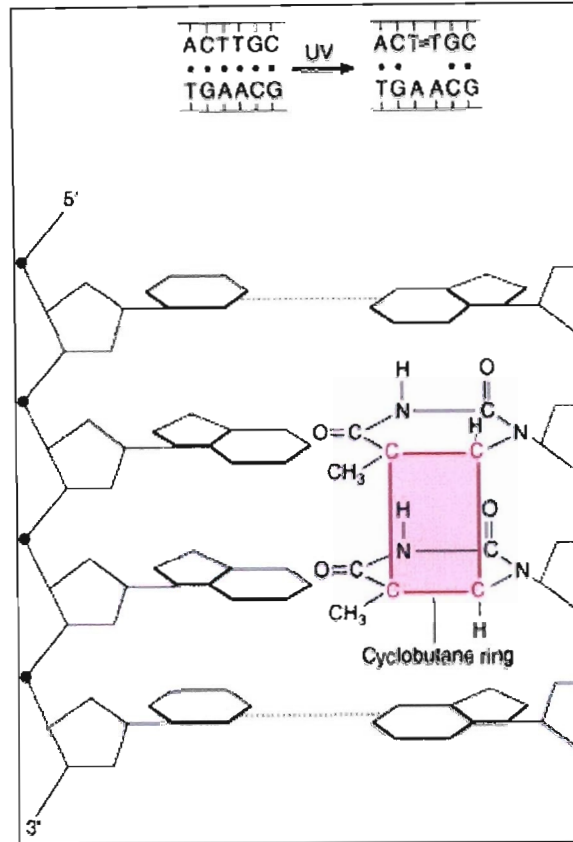
Figure 1.5:   A cyclobutane pyrimidine dimer can form between two adjacent pyrimidine
              bases on the DNA strand when the molecule is exposed to UV radiation
              (Weaver [accessed on 11th November 2004]).
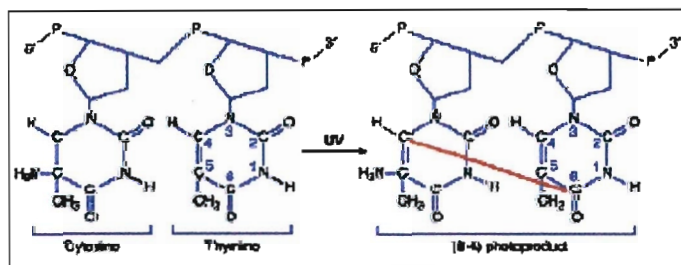
Figure 1.6:   The pyrimidine-(6-4)-pyrimidone adduct can be produced when DNA is
              exposed to UV radiation (Matsumura and Ananthaswamy [accessed on 11th
              November 2004]).

1.2 Photoprotection

Non-Caucasian people have well-pigmented skin which contains a high level of melanin that protects the skin against UV radiation. Caucasians, on the other hand, have relatively less melanin in their skin and they are more prone to the deleterious effects caused by UV radiation. Sunscreens are employed in order to protect the human skin against UV radiation, and this is especially crucial for fair-skinned individuals. In so doing, they minimise the UV radiation that enters the skin that could potentially lead to events, such as described in Section 1.1, that result in the development of skin cancer.

1.2.1 Sunscreens

Sunscreen formulations can take many forms, including oils, gels and aerosols, but the most widespread vehicle used is an emulsion. These emulsions can be in the form of creams or more commonly lotions. These contain emulsifiers, emollients, film formers, stabilisers/protectants, chemical absorbers and physical blockers. Emulsifiers are surface-active agents that promote the formation of sunscreen emulsions; emollients act as the vehicles for introducing the oil-soluble sunscreen absorbers; film formers are materials that are used to form films in sunscreen formulations; stabilisers are materials that preserve and stabilise the emulsions; and chemical absorbers absorb harmful UV radiation whereas physical blockers reflect or scatter the UV light (Klein [1990]).

The UV protection offered by sunscreens is solely dependent upon the action of the physical blockers and chemical absorbers. The former include metal oxides such as titanium dioxide and zinc oxide, which protect throughout the UV region. The latter are normally organic molecules which absorb light of certain wavelengths of UV radiation; consequently, more than one chemical absorber has to be employed in order to achieve protection throughout the UV region. The concentration of physical blockers and chemical absorbers in a sunscreen product has to adhere to international limits for safety reasons. This research focuses specifically on the efficacy of organic chemical absorbers (see Section 1.2.1.1).

The level of protection offered by a sunscreen product is measured in terms of the Sun Protection Factor (SPF). The SPF value is defined as the ratio of the minimal erythemal dose

(MED) of UV radiation in sunscreen-protected skin to that in unprotected skin. The SPF equation is given in Equation 1.1 (Taylor *et al.* [1990]).

$$SPF = \left(\frac{MED \text{ of sunscreen-protected skin}}{MED \text{ of nonprotected skin}} \right)$$
                                                                                                          Equation 1.1

Therefore, a person wearing a sunscreen with an SPF value of 30 will take 30 times longer to redden in the sun compared to unprotected skin.

1.2.1.1 Chemical absorbers

Chemical absorbers are organic molecules that absorb either UVA or UVB light. Organic molecules that absorb UVA radiation are referred to as UVA absorbers; these include benzophenones, anthranilates and dibenzoylmethanes (see Figure 1.7). Those that absorb UVB radiation are called UVB absorbers, and they include the camphor derivatives, salicylates, cinnamates, *para*-aminobenzoic acid and *para*-aminobenzoate derivatives (see Figure 1.7).

Chemical absorbers have conjugated structures with π-electron delocalisation which allow them to absorb photons of UV light. Before absorption, chemical absorbers are in the ground state with paired electrons of opposite spin. Upon absorption of a photon, an electron is promoted from the ground state to an excited state without changing its spin. Organic molecules are normally excited to the first singlet excited state. The electron will return to the ground state by losing this excess energy in various photophysical and photochemical pathways (as seen in Figure 1.8). The electron could relax photophysically by radiative decay, where it emits a photon and fluoresces, or by nonradiative decay, where it emits the energy thermally through a sequence of vibrational relaxation transitions. The excited chemical absorber could also relax to a triplet excited state of lower energy, this process is referred to as intersystem crossing since the electron changes spin. In the excited triplet state, the molecule can return to the ground state as before, through nonradiative decay or radiative decay. The latter process is now referred to as phosphorescence, since it involves emission of a photon when the molecule moves from an excited triplet state to a singlet ground state (Kimbrough [1997]). Ideally, in a sunscreen absorber, the excited state is supposed to lose the energy in the most harmless way possible, mostly via these photophysical processes, then return to its ground state so that it is available for re-absorption of a photon.
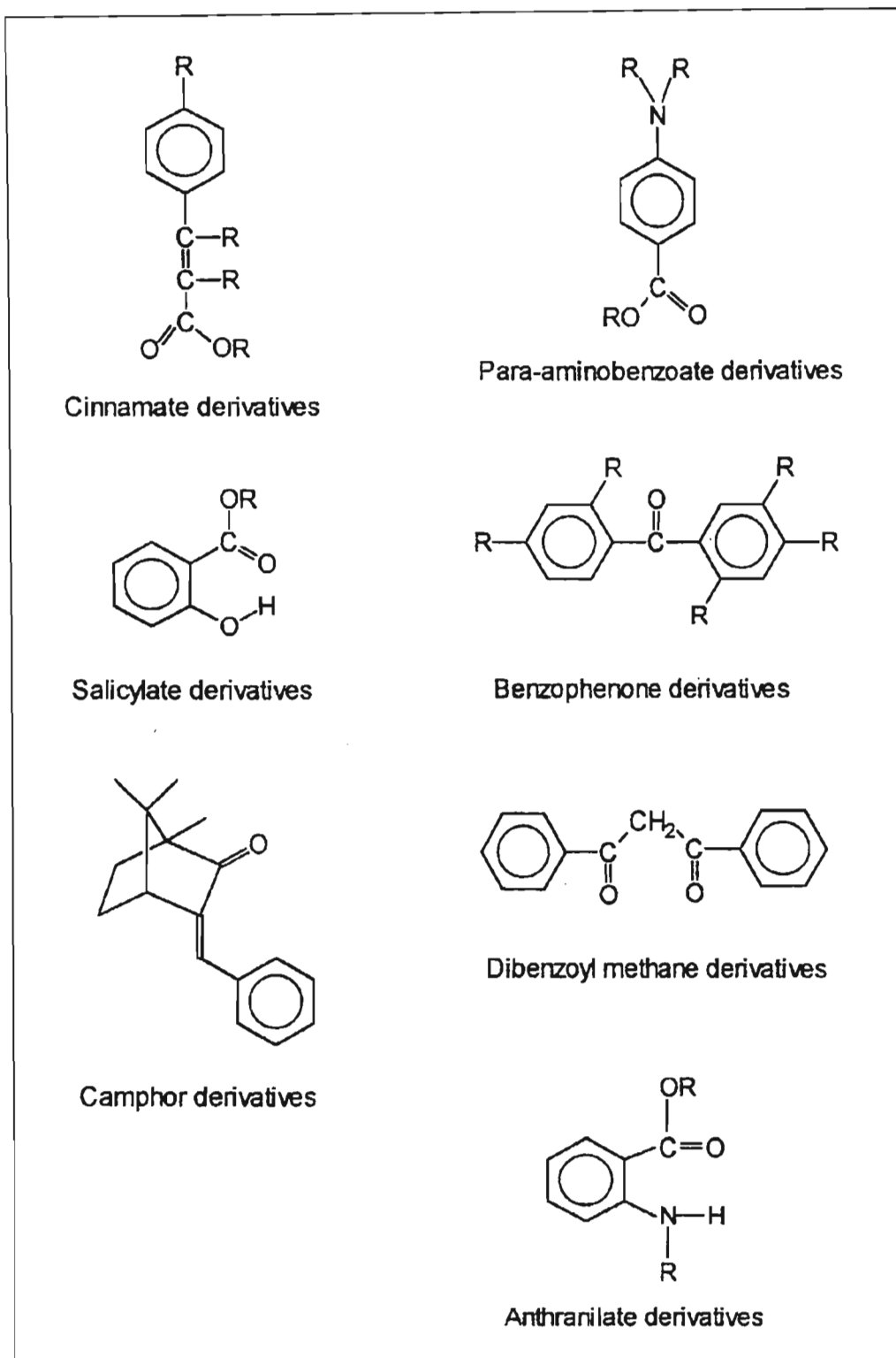
Figure 1 7:   The classes of chemical absorbers used in sunscreen formulations.
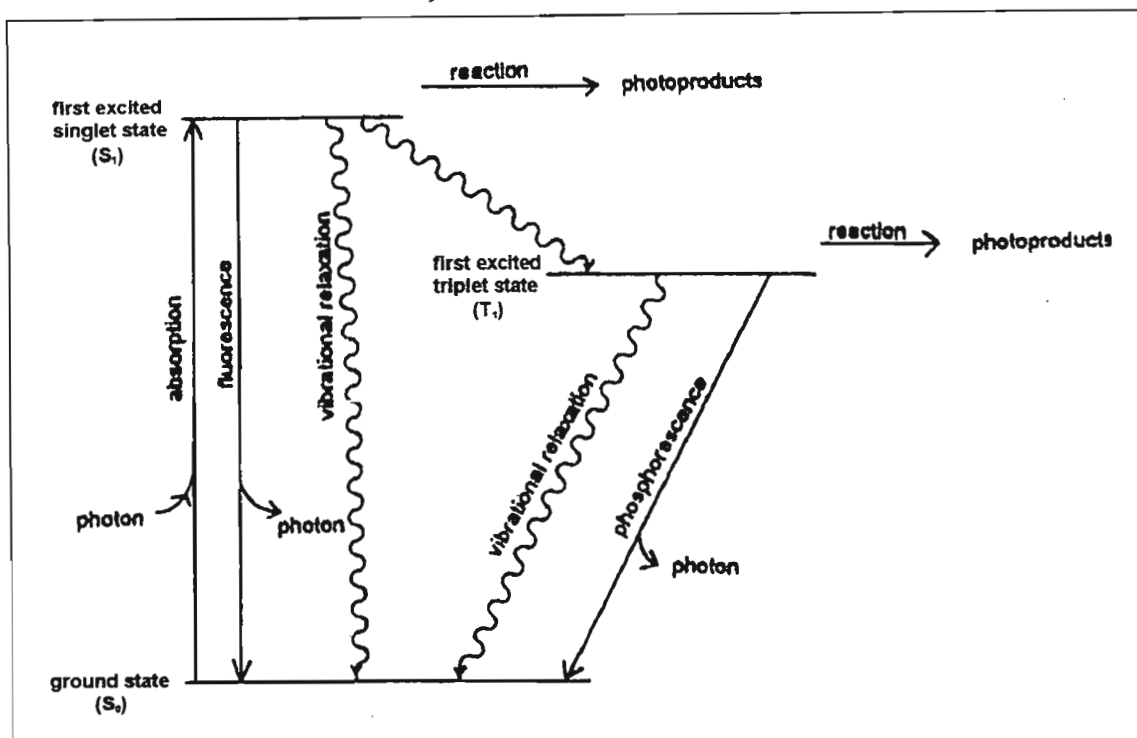
Figure 1.8:   The absorption of UV light by a chemical absorber and the different energy releasing pathways (Kimbrough [1997]).

The singlet and triplet excited states can also relax to the ground state photochemically by interacting with other molecules to form photoproducts or by transfer of energy. The lifetime of the excited triplet state is longer than that of the excited singlet state; therefore it is more likely that the molecule undergoes these photochemical processes from the triplet state. The excited states can lose their excess electronic energy through intramolecular or intermolecular photochemical pathways.

The excited states can be deactivated intramolecularly by fragmenting into low molecular mass compounds, or undergo intramolecular rearrangement of bonds and atomic positions so that other isomers of the absorber are formed. The fragments and isomers produced may not absorb UV radiation with the same capacity or at the same wavelength of absorption as the parent chemical absorber, and hence this would decrease the protective efficacy of the sunscreen.

Intermolecular deactivation of the excited state mainly involves bimolecular reactions. The excited state could react with another molecule (photoreaction), collide with another molecule of the same type (self-quenching) or any other molecule (quenching), or transfer its energy to another molecule as a means of losing its excess energy (photosensitisation). Photochemical pathways are mostly undesirable since they reduce the efficacy of sunscreens. These pathways

could be potentially mutagenic and carcinogenic if they occur within the body, but this would only be possible if these chemical absorbers are able to penetrate human skin. This is more likely when sunscreens are used since the pores of the skin are open during sweating under hot climatic conditions.

Sunscreen absorbers can act as potential photosensitisers of DNA damage. The photo-sensitisation process is illustrated in Equation 1.2.

$$D^*(T_1) + A(S_0) \rightarrow D(S_0) + A^*(T_1) \qquad \text{Equation 1.2}$$
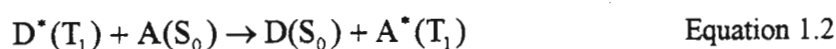
This occurs when a triplet excited state donor molecule $(D^*(T_1))$ relaxes to the ground state $(D(S_0))$ by transferring its energy to a ground state acceptor molecule $(A(S_0))$. The donor molecule, D, in the triplet excited state is known as the photosensitiser and when it relaxes to the ground state, the energy transfer process is referred to as triplet-triplet energy transfer. The acceptor molecule, A, is said to be photosensitised and its triplet state energy must be lower than that of the photosensitiser.

Photosensitisation can act as a harmless deactivation pathway of excited chemical absorbers, but it can also be harmful if it occurs within the nuceus of the cell where the DNA molecule is found, or if the process results in potentially toxic products. Examples of this are the formation of cyclobutane pyrimidine dimers and singlet oxygen respectively. Chemical sunscreen absorbers have been shown to photosensitise the formation of cyclobutane pyrimidine dimers via triplet-triplet energy transfer (Sutherland and Griffin [1984], Aliwell [1991], Bolton [1991] and Bolton et al. [1992]). These dimers are potentially carcinogenic and are the precursors to skin cancer as was discussed in Section 1.1.2. Chemical absorbers in their excited triplet states can also photosensitise the formation of singlet molecular oxygen, $^1O_2$, from triplet ground state oxygen $(^3O_2)$ as shown in Equation 1.3 (Allen et al. [1995, 1996a and 1996b]).

$$D^*(T_1) + {}^3O_2 \rightarrow D(S_0) + {}^1O_2 \qquad \text{Equation 1.3}$$
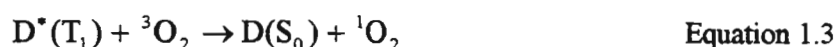
Singlet oxygen is cytotoxic and causes oxidative damage to biological molecules such as lipids, proteins and DNA.

Some chemical absorbers such as *p*-aminobenzoic acid have been shown to lose their efficacy when photo-irradiated (Serpone *et al.* [2002]). These absorbers will consequently decrease the efficacy of the sunscreen formulation, as well as produce compounds which could potentially possess dangerous properties. A number of previous studies have shown that upon irradiation not all sunscreen absorbers are photostable and that this is also exhibited in the finished product (Maier *et al.* [2001]). As the main aim of this investigation was to assess the potential of plant polyphenols to stabilise these photo-unstable absorbers a photostability investigation was conducted. Table 1.1 lists the chemical absorbers tested and indicates those which were found to be photo-unstable. Some background information on the photo-unstable absorbers will now be provided. These are 2-ethylhexyl-*p*-methoxycinnamate (EHMC), menthyl anthranilate, 4-bis(polyethoxy)-*p*-aminobenzoic acid polyethoxyethyl ester (Peg-25 PABA), 3-(4-methylbenzylidene) camphor (MBC), isoamyl *p*-methoxycinnamate (IMC) and 4-*tert*-butyl-4'-methoxydibenzoylmethane (avobenzone).

Table 1.1:   The photostability of chemical absorbers in appropriate solvents when exposed to light of wavelengths greater than 300 nm.

Chemical absorber	Solvent	Photostability
2-ethylhexyl-*p*-methoxycinnamate (EHMC)	Methanol	Photo-unstable
4-bis(polyethoxy)-*p*-aminobenzoic acid polyethoxyethyl ester (Peg-25 PABA)	Millipore water	Photo-unstable
3-(4-methylbenzylidene) camphor (MBC)	Methanol	Photo-unstable
isoamyl *p*-methoxycinnamate (IMC)	Methanol	Photo-unstable
menthyl anthranilate	Methanol	Photo-unstable
octyl dimethyl *p*-aminobenzoic acid	Methanol	Photostable
phenylbenzimidazole sulfonic acid	Millipore water	Photostable
2,4-dihydroxybenzophenone	Methanol	Photostable
2,2',4,4'-tetrahydroxybenzophenone	Methanol	Photostable
2-hydroxy-4-methoxybenzophenone	Methanol	Photostable
2-hydroxy-4-methoxybenzophenone-5-sulfonic acid	Millipore water	Photostable
4-*tert*-butyl-4'-methoxydibenzoylmethane (avobenzone)	Methanol	Photostable
	DMSO, ethyl acetate and cyclohexane	Photo-unstable
2,2'-dihydroxy-4,4'-dimethoxybenzophenone	Methanol	Photostable
2-hydroxy-4-n-octyloxybenzophenone	Methanol	Photostable

Peg-25 PABA

This is one of the esters of *p*-aminobenzoic acid (PABA) which has been used as a UVB absorber in sunscreens to replace PABA. PABA was once widely used as a chemical absorber in sunscreens before it was shown to photofragment (Shaw *et al.* [1992]) as well as act as a triplet sensitizer capable of forming singlet oxygen (Allen *et al.* [1996a and 1996b]). Sutherland [1982] further showed that PABA was able to penetrate mammalian cells and photosensitise thymine to form thymine dimers. Aliwell [1991] also showed that thymine dimers were produced from the photosensitisation of thymine in solutions of the free base, nucleotides and plasmid DNA (Aliwell *et al.* [1993a and 1993b]). However, the major reason for the absorber's non-usage nowadays is due to its side-effects, since it acts as an irritant and also causes allergic reactions. Consequently PABA was replaced as an active ingredient in sunscreens by its esters. The esters of PABA include octyl dimethyl PABA (Padimate-O) and Peg-25 PABA (see Figure 1.9). Padimate-O has also been shown to photodegrade (Roscher *et al.* [1994]), and act as a mutagen by damaging DNA directly when irradiated (Knowland *et al.* [1993]). However, Padimate-O was found to be relatively more photostable than aqueous solutions of Peg-25 PABA (Vanquerp *et al.* [1999]). Couteau *et al.* [2001] showed that Peg-25 PABA penetrates through the skin when dissolved in an aqueous solution as well as when in an oil-in-water emulsion, since only 20% of the absorber remained in the stratum corneum of human volunteers seven hours after application. Therefore, if Peg-25 PABA has the potential to react with DNA either directly or indirectly it will be able to cause damage when used as a sunscreen ingredient. The photostability of aqueous solutions of Peg-25 PABA were investigated in this research.
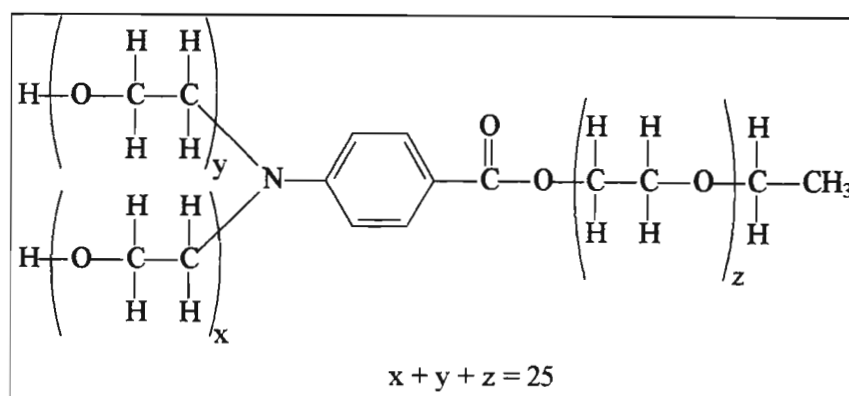

Figure 1.9:   The chemical structure of Peg-25 PABA.

MBC

The chemical absorber, MBC, is used in sunscreen formulations as a UVB absorber. Benzylidene camphor derivatives, in general, have been shown to be stable to photodegradation

(Beck *et al.* [1985]). But Beck *et al.* [1981 and 1985] have reported the photoisomerising capability of these derivatives. Deflandre and Lang [1988a] showed that this photoisomerisation occurs minimally and rapidly reaches a photostable equilibrium, and that irreversible photodegradation was insignificant especially for MBC. Deflandre and Lang [1988b] further showed that the photoisomerisation and photodegradation of benzylidene camphor derivatives were neither oxygen nor concentration dependent. They also reported that the photoisomerisation was solvent dependent in some instances whereas the photodegradation was minimally affected. Vanquerp *et al.* [1999] reported that a 10% decrease in the initial concentration of MBC, upon photo-irradiation, occurred at a faster rate than five other chemical absorbers that included Padimate-O and Peg-25 PABA. Tarras-Wahlberg *et al.* [1999] showed how MBC in a thin film of an appropriate emulsion underwent an initial loss in absorbance due to *cis-trans* photoisomerisation (see Figure 1.10), prior to reaching a photostationary state. In this research, this photoisomerisation of MBC was investigated by UV spectroscopy.
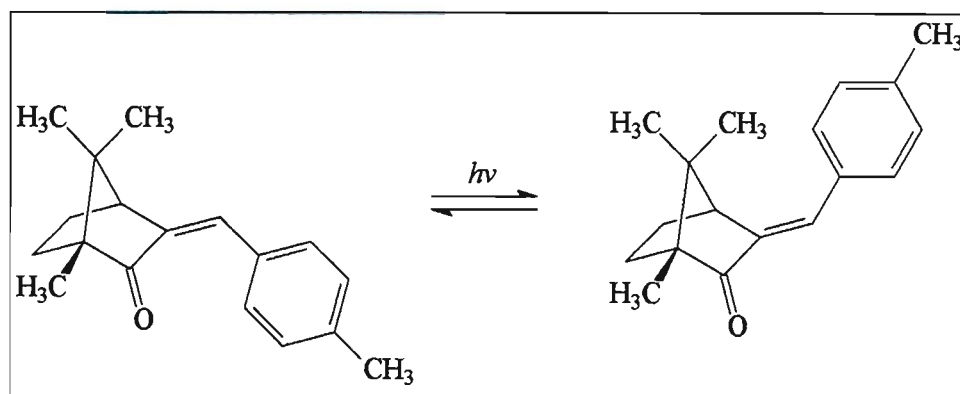
Figure 1.10:   MBC undergoes *cis-trans* photoisomerisation when exposed to UV light (Tarras-Wahlberg *et al.* [1999]).

Cinnamates

IMC and EHMC are UVB absorbers that fall in the cinnamate group of sunscreen absorbers. Cinnamates exist in two forms as *cis-* and *trans*-isomers. In sunscreen formulations they occur as the *trans*-isomer, but when photo-irradiated they photoisomerise to the *cis*-isomer, a less efficient UVB absorber (see Figure 1.11). EHMC is the most commonly used chemical absorber in sunscreen products. When *trans*-EHMC is photo-irradiated it has been shown to undergo photoisomerisation (Broadbent [1994], Kowlaser [1998], Ingouville [1995] and Tarras-Wahlberg *et al.* [1999]) as well as photo-induced self-dimerisation (see Figure 1.12) by means of a [2+2] cycloaddition reaction (Broadbent *et al.* [1996]). Both processes reduce the UV absorption ability of EHMC. EHMC has also been reported to produce singlet oxygen (Allen *et*

al. [1996a]) and to form a photo-adduct with DNA bases (Kowlaser [1998]), thereby making it a potential mutagen and carcinogen if it enters the human body. Bonin *et al.* [1982] substantiated EHMC's mutagenicity in the Ames *Salmonella typhimurium* test and Butt and Christensen [2000] further showed the absorber to be toxic when in mouse cells, whether photo-irradiated or not. But Ingouville [1995] reported that when a similar concentration of the absorber was used as found in most sunscreen products, namely a 5% EHMC solution, the photostationary equilibrium lies towards the *trans*-isomer. This implies that formulations containing EHMC only minimally reduce their efficacy in the UVB region.
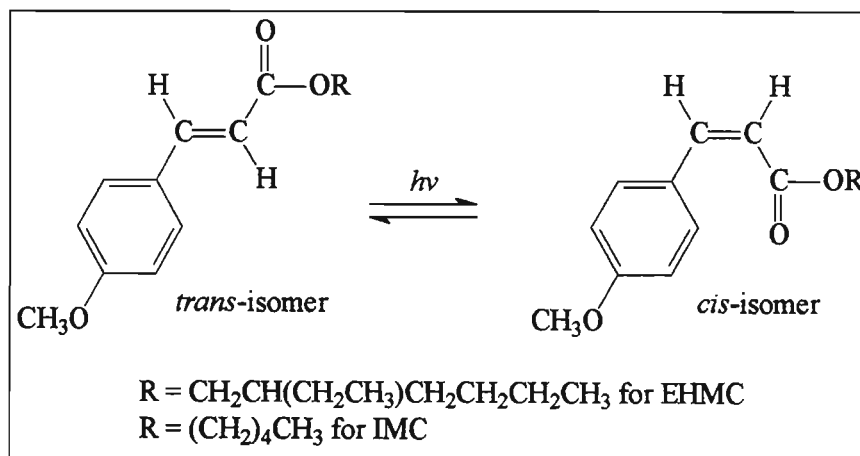

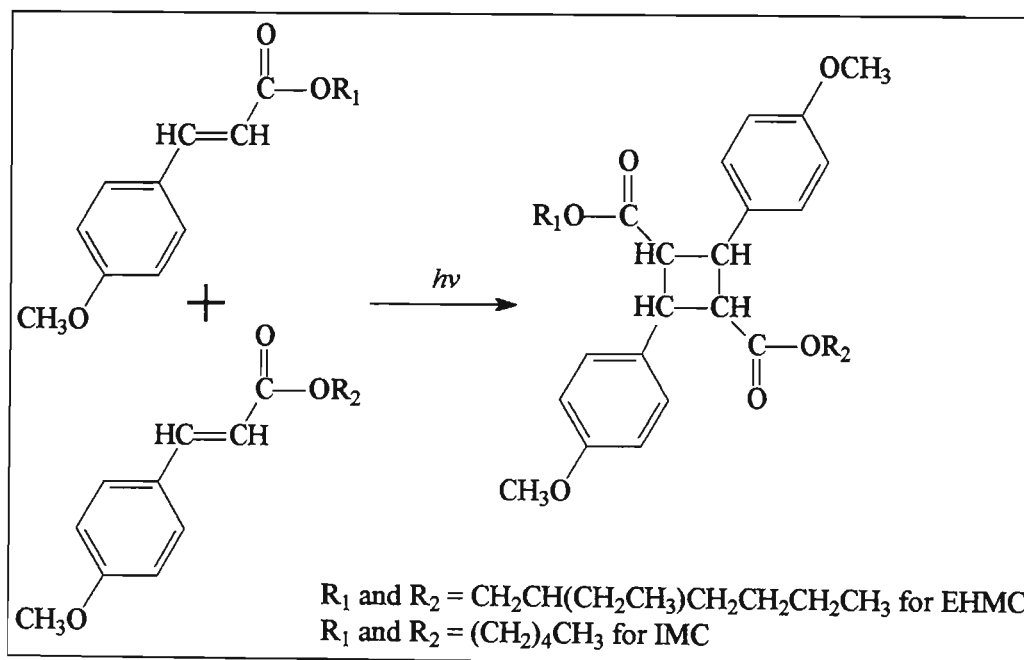Figure 1.11: Cinnamates undergo a *cis-trans* photoisomerisation when exposed to UV light.

Figure 1.12: Cinnamates undergo self-dimerisation when exposed to UV light.

In this research, the photostability of EHMC and IMC was investigated by UV spectroscopy since they are potentially photo-unstable as a result of photoisomerisation and photodimerisation. These photostability investigations were conducted in methanol since Panday [2002] had successfully shown the photo-instability of EHMC in methanol.

Avobenzone

Avobenzone is part of the dibenzoylmethane group of sunscreens. It is the most popular UVA absorber with a wavelength of maximum absorption (λ_{max}) ranging from 350 nm to 365 nm depending on the solvent used. Avobenzone exists in two tautomeric forms, the enol-tautomer (or enol form) and the keto-tautomer (or keto form). The keto form occurs only in one geometric form whereas the enol form has been postulated to occur in many geometric configurations (Dubois et al. [1998], Cantrell and McGarvey [2001] and Andrae et al. [1997]). The enol form is unsymmetrical hence it has two obvious isomeric forms, namely, two cis-enols as reported by Dubois et al. [1998], enol form A and enol form B as shown in Figure 1.13. Cantrell and McGarvey [2001] and Andrae et al. [1997] proposed that transient enol forms were also possible isomers of the enol form of avobenzone. These transient species were either produced as a result of rotation about a single bond (between carbon 8 and 9 in enol form A or 7 and 8 in enol form B of Figure 1.13) or isomerisation at the double bond of the enol form (between carbon 7 and 8 in enol form A or 8 and 9 in enol form B of Figure 1.13) as displayed in Figure 1.14 (Cantrell and McGarvey [2001]).

In a sunscreen formulation, avobenzone exists in the enol form which absorbs in the UVA wavelength range. Andrae et al. [1995] showed by high-performance liquid chromatography (HPLC) analysis that avobenzone exists to a large extent as the enol form in acetonitrile (λ_{max} = 355 nm), although the keto form (λ_{max} = 270 nm) was also present but to a very small extent. Tarras-Wahlberg et al. [1999] showed how the UVA absorption efficiency of avobenzone is reduced upon irradiation. Andrae et al. [1997] further showed by absorption spectroscopy that a loss in absorption of the enol form in acetonitrile (λ_{max} = 350 nm) is replaced by an increase in absorption at 260 nm attributed to the keto form. This was substantiated by Dubois et al. [1998] who showed this photoisomerisation of avobenzone in dilute acetonitrile solutions by ^{1}H and ^{13}C nuclear magnetic resonance (NMR) spectroscopy.
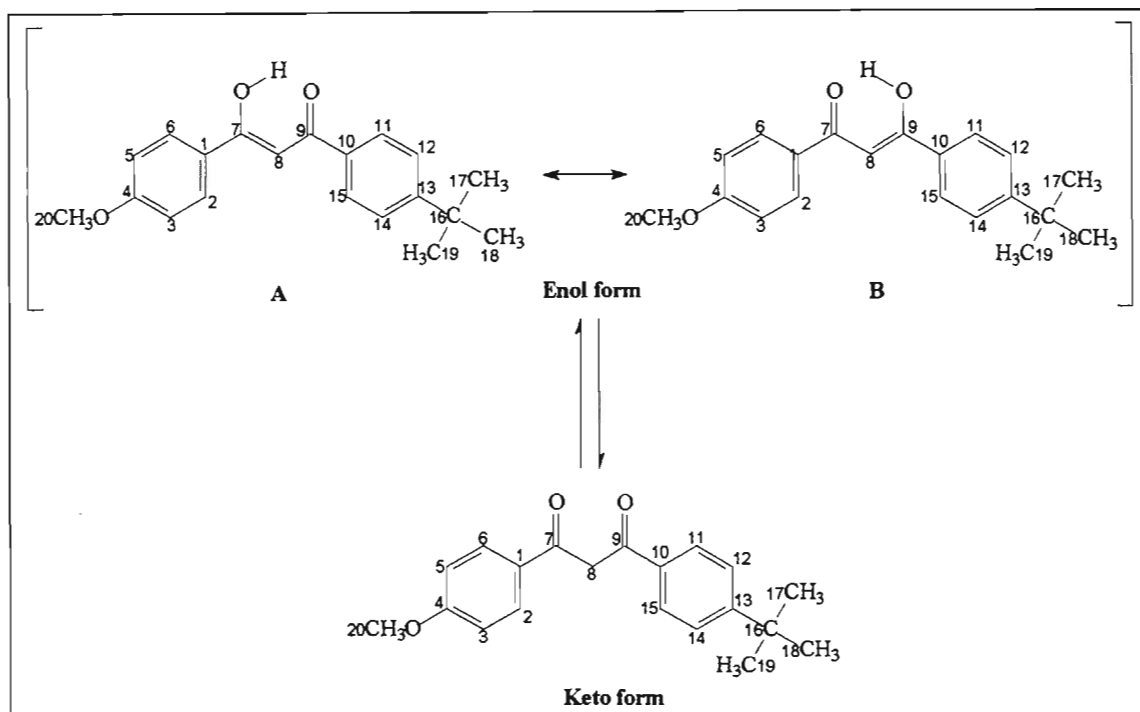
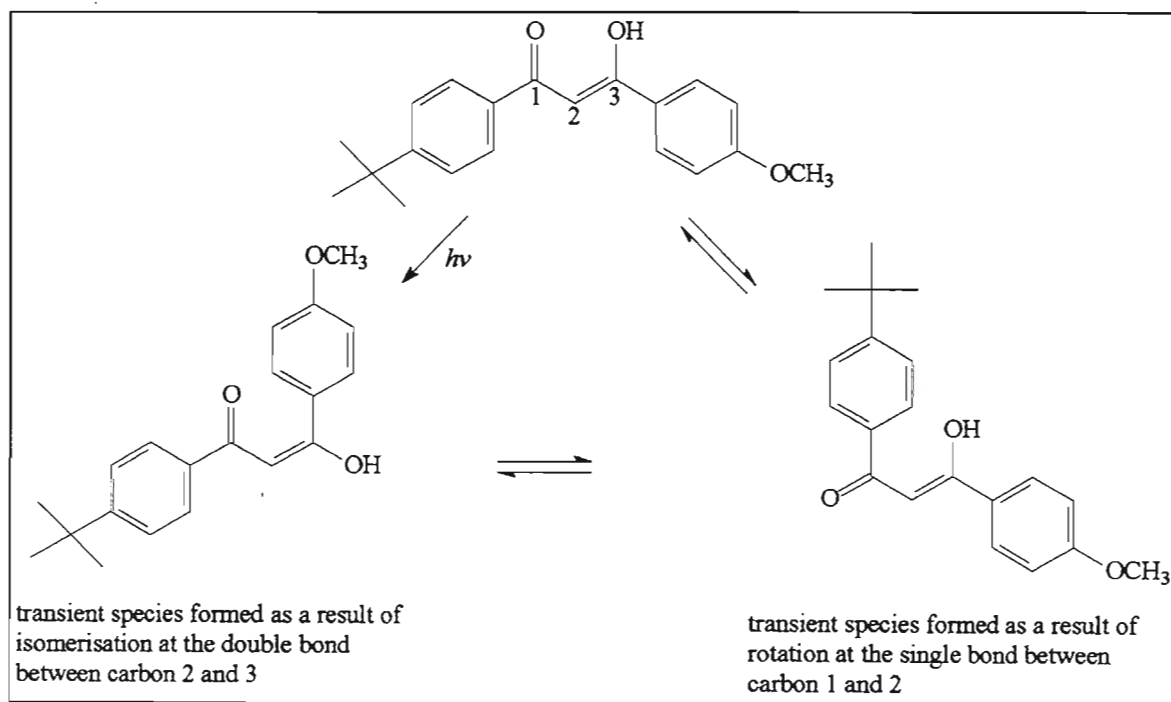Figure 1.13:   The keto-enol tautomerism of avobenzone.

Figure 1.14:   The proposed equilibrium between the enol form of avobenzone and its transient forms (Cantrell and McGarvey [2001]).

Andrae *et al.* [1997] showed that laser excitation at 355 nm of avobenzone produced a species that absorbed maximally at 300 nm and hence could not be the keto form. This species is short-lived with a solvent-dependent lifetime; it was proposed to be either one of the transient enol isomers. Andrae *et al.* [1997] also reported that a high concentration of avobenzone reduced UVA- and UVB-induced deaths of human lympoid cells by over 30%. These cells were not protected from UVA radiation at low concentrations of the absorber, whereas there was an increase in UVB protection. This supports the evidence for the presence of the transient enol form in solutions that absorb at 300 nm. Cantrell and McGarvey [2001] proposed that the transient enol species is formed as a result of isomerisation about the double bond, since the transient enol species formed through rotation can easily revert back to the enol form through rapid rotation about a single bond. They also proposed that the two transient species are in equilibrium with each other, and the one formed by rotation is in equilibrium with the enol form; they defended this proposal by temperature dependence studies (see Figure 1.14).

Roscher *et al.* [1994] reported that when avobenzone is irradiated for 100 hours in cyclohexane several photoproducts are formed. Schwack and Rudolph [1995] further showed that avobenzone photodegrades when irradiated with a solar simulator in non-polar solvents (cyclohexane and isooctane), but appeared photostable in polar media (methanol and isopropanol). They investigated the photoproducts by high-performance liquid chromatography (HPLC) and gas chromatography-mass spectrometry (GC-MS) techniques. They deduced that the photoproducts were formed likely from α-cleavage of the photo-excited keto form of avobenzone as they all stem from either a benzoyl or a phenacyl radical. Cantrell and McGarvey [2001] laser excited avobenzone at 266 nm and observed the formation of the triplet state of the keto form. This is why triplet state quenchers, such as 3-(4-methybenzylidene) camphor were able to photostabilise avobenzone (Chatelain and Gabard [2001]).

Damiani *et al.* [1999] reported that avobenzone, when illuminated *in vitro*, caused DNA strand breaks as a result of the formation of carbon-centered radicals, which most likely are benzoyl and phenacyl radicals as proposed by Schwack and Rudolph [1995]. Indolinonic nitroxide radicals were able to trap these radicals and hence reduce DNA damage. These nitroxide radicals were also able to prevent the oxidative modification of the bovine serum albumin protein by avobenzone when illuminated (Damiani *et al.* [2000]). The photodegradation of avobenzone resulted in the absorber only displaying some degree of inhibition to UVA-induced lipid peroxidation (Damiani *et al.* [2002]), and complete failure to stop UVA-induced cytotoxic effects in keratinocytes, such as apoptosis (Armeni *et al.* [2004]).

Deflandre and Lang [1988a] showed that avobenzone in an emulsion had a 36% irreversible loss in absorption at 355 nm for a one hour exposure to wavelengths greater than 290 nm. This loss was less than for 4-isopropyldibenzoylmethane, but it was greater than that of all the benzylidene camphor derivatives, the rest of the dibenzoylmethane derivatives and other sunscreen agents such as EHMC. On the other hand, Vanquerp *et al.* [1999] reported that avobenzone in ethanol took the second longest time to decrease to 10% its initial concentration upon photo-irradiation, after 3-(4-methybenzylidene) camphor, Peg-25 PABA and octyl dimethyl PABA but before benzophenone-3 (2-hydroxy-4-methoxybenzophenone). This confirms the photostability of avobenzone in polar solvents as reported by Schwack and Rudolph [1995].

Sayre and Dowdy [1999] found that upon UVA exposure not only did avobenzone in sunscreen products photodegrade but that UVB absorbers, such as EHMC, also photodegraded when in the presence of avobenzone. This was supported by Panday [2002] who showed that avobenzone photosensitises the photoisomerisation of *trans*-EHMC. Chatelain and Gabard [2001] were able to photostabilise these avobenzone-EHMC combinations by the addition of bis-ethylhexyloxyphenol methoxyphenyl triazine (Tinosorb S).

The efficacy of chemical absorbers can be solvent dependent (Shaath [1990]) as observed with avobenzone that shows different photochemical behaviour in different solvents. Avobenzone has been reported to photodegrade in non-polar solvents such as mineral oil (Agrapidis-Paloympis *et al.* [1987]) and cyclohexane (Panday [2002]), but has shown very good stability in polar solvents such as methanol (Panday [2002]). The wavelength of maximum absorption of avobenzone undergoes a red or bathochromic shift in moving from non-polar to polar solvents (Shaath [1990] and Agrapidis-Paloympis *et al.* [1987]) which is characteristic of less polar chemical absorbers (Agrapidis-Paloympis *et al.* [1987]). This shift in λ_{max} of the absorber is insufficient to reduce its SPF as a UVA absorber in any solvent.

The photostability of avobenzone was investigated in various solvents in this research, including dimethyl sulfoxide (DMSO), ethyl acetate, cyclohexane and methanol, since its photochemical behaviour is solvent dependent (Shaath [1990], Agrapidis-Paloympis *et al.* [1987] and Panday [2002]).

1.3 Photostabilisation

The photostabilisation of chemical absorbers is crucial for improving the efficacy of sunscreen formulations. In an attempt to improve the photostability of chemical absorbers various methods have been used. One such method has been to synthesise new chemical absorbers based on the presently available absorbers. For instance, esters of PABA were synthesised in order to replace PABA and Mexoryl® SX (terephthalylidene dicamphor sulfonic acid), a UVA absorber which is structurally based on the benzylidene camphor absorbers (Cantrell et al. [1999]) was synthesised as a new UVA absorber because of the problems associated with avobenzone. Another method has been to add other substances, including other absorbers, to solutions of photo-unstable chemical absorbers in an attempt to photostabilise them. For example, avobenzone has been photostabilised by the addition of methylbenzylidene camphor, diethylhexyl 2,6-naphthalate (Bonda and Steinberg [2000]), or alternatively Tinosorb S (Chatelain and Gabard [2001]) (see Section 1.2.1.1). A third method has been to encapsulate photo-unstable absorbers, for example, in the cavity of cyclodextrins (Simeoni et al. [2004]).

An ideal photostabiliser is one which not only photostabilises photo-unstable absorbers but also acts as a photoprotector itself. Consequently, other chemical absorbers as well as antioxidants have been considered as potential photostabilisers. Antioxidants are more favoured in skin care products since they also offer other benefits. They have been shown to act as stabilisers/protectants of sunscreen formulations in the form of emulsions (Klein [1990]) and, unlike chemical absorbers, they can offer complete spectral protection throughout the UV region (Pinnell [2003]).

1.3.1 Antioxidants as photoprotectors

Antioxidants are found in humans as well as in plants. The human body naturally uses antioxidants such as vitamin C and E that photoprotect us daily. Topical application of vitamin C (L-ascorbic acid) has been reported to offer photoprotection upon UV irradiation of porcine skin, and similarly vitamin E (humans use mainly its α-tocopherol molecular form) provides the same kind of photoprotection for various animal skins ([Pinnell [2003]). In combination, they have been shown to prevent erythema and the formation of thymine dimers in UV-exposed porcine skin ([Pinnell [2003]). Plants also utilise antioxidants for their photoprotection and

these include vitamin C, vitamin E and polyphenols. There are various classes of polyphenols including phenolic acids, flavonoids ([Pinnell [2003]) and polymeric polyphenols.

1.3.1.1 Polyphenols

Polyphenols are substances with phenolic rings that act as pigments and sunscreens in plants. There are many types of polyphenolics, including flavanoids, gallic acid and its esters, as well as derivatives of hydroxycinnamic acids. Flavanoids consist of proanthocyanidins and flavonoids, and they display a common structure as shown in Figure 1.15.
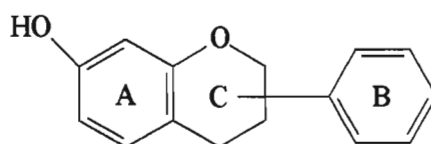

Figure 1.15:   The tricyclic $C_6.C_3.C_6$ flavanoid skeleton showing rings A, B and C.

Catechins (such as catechins and epicatechins) and gallocatechins which are catechins with a galloyl group (such as gallocatechins, epigallocatechins and epigallocatechin gallates), are also important polyphenolic compounds. They are found in large amounts in green tea and their polymers are known as procyanidins (catechin polymers) and prodelphinidins (gallocatechin polymers) and they fall within the group called proanthocyanidins. This group has the basic flavan-3-ol structure (see Figure 1.16A).

Flavonoids are polyphenolic substances that naturally exist as glycosides (with a sugar), and they are based on a flavone ring. When the sugar is removed through hydrolysis of the glycoside for instance, aglycones such as quercetin, myricetin and kaempferol are formed (see Figure 1.16B).

The esters, glycosides and amides of hydroxycinnamic acids have a $C_3.C_6$ system and they include ferulic and caffeic acids (see Figure 1.16C). Gallic acid (see Figure 1.16D) and its esters, such as gallic esters of the catechins, are also considered as polyphenolics.

R = R' = H; catechin or epicatechin
R = OH, R' = H; gallocatechin or epigallocatechin
R = H, R' = galloyl group; epicatechin gallate
R = OH, R' = galloyl group; epigallocatechin gallate

galloyl group

(A)

R = R' = H; kaempferol
R = OH, R' = H; quercetin
R = R' = OH; myricetin

(B)

R' = R = H; p-coumaric acids
R' = OH, R = H; caffeic acids
R' = OCH₃, R = H; ferulic acid
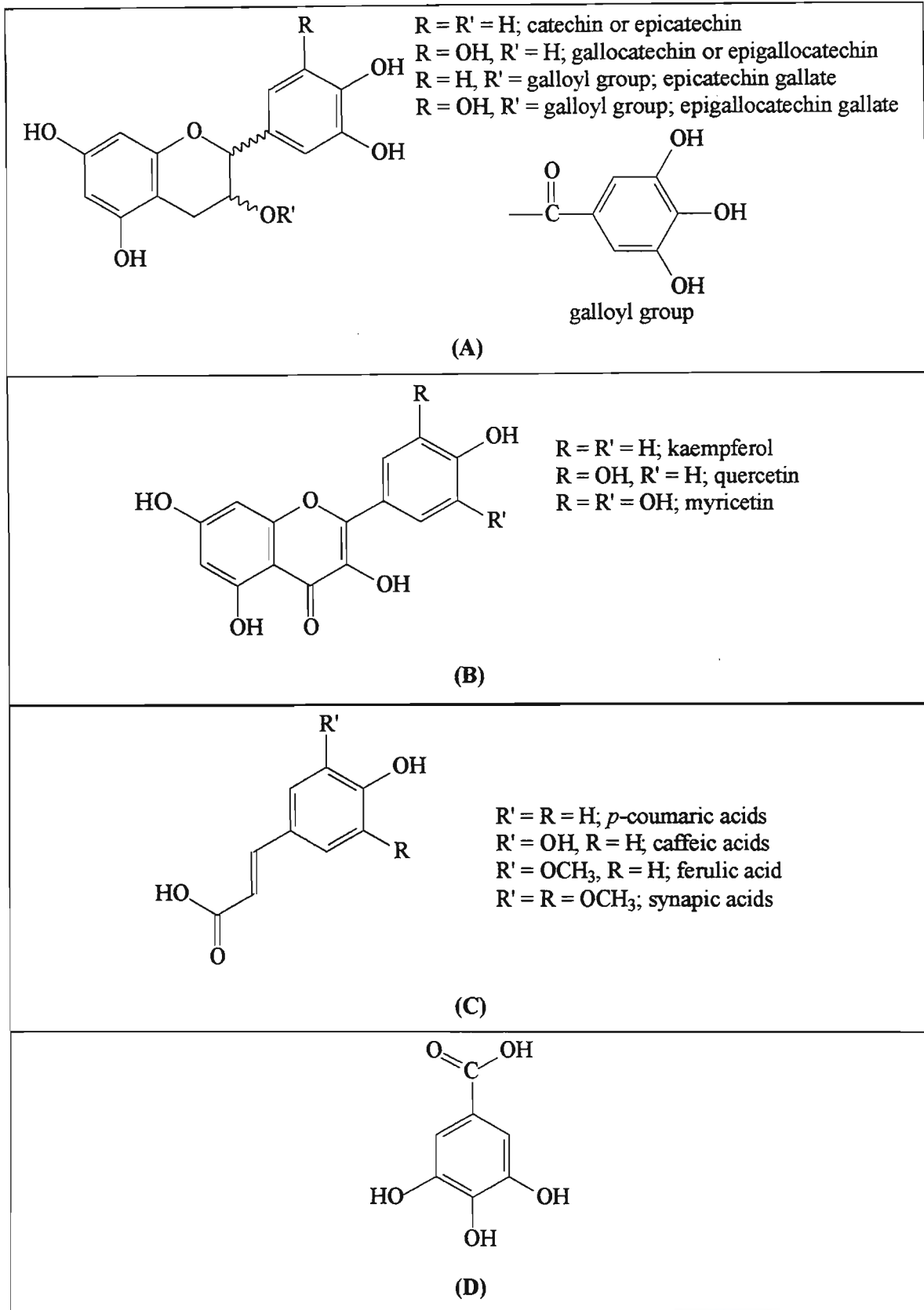R' = R = OCH₃; synapic acids

(C)

(D)

Figure 1.16: The flavan-3-ol skeleton of proanthocyanidins (A), the flavone skeleton of flavonoids (B), the skeleton of hydroxycinnamic acid derivatives (C) and gallic acid (D).

1.3.1.2 Polyphenolic photoprotection

Polyphenolic compounds are major constituents of teas, wines, seaweeds and various other plants. They have been shown to generally possess photoprotective properties, and those properties have been widely investigated for tea polyphenols. Tea polyphenolics vary with the type of tea at hand; green tea (*Camellia sinensis*) contains predominantly catechin monomers, black tea (*Camellia sinensis*) has largely polyphenolic polymers ([Pinnell [2003]) whereas Rooibos tea (*Aspalathus linearis*) contains phenolic acids and flavonoids (Erickson [2003]).

Polyphenolics present in *Camellia sinensis* tea have been shown to prevent skin cancer in animal models as well as decrease erythematic levels in UV-exposed human skin ([Pinnell [2003]). Picard [1996] showed specifically that green tea polyphenols were able to prevent skin cancer throughout its multistage processes in mouse skin models. Katiyar *et al.* [2001] reported that these green tea polyphenols were not only able to inhibit the formation of cyclobutane pyrimidine dimers, but were also able to prevent the penetration of UV rays when applied topically. Green tea polyphenols have also been shown to prevent inflammation and immunosuppression in the skin of C3H/HeN mice in a dose-dependent way (Katiyar *et al.* [1995]). When taken orally they have also afforded great protection against UVB-induced inflammatory responses in SKH-1 hairless mice (Agarwal *et al.* [1993]). Green tea contains the polyphenolic compound, epigallocatechin gallate (EGCG), which has been shown to inhibit erythema in UVB-exposed human skin when topically applied (Katiyar *et al.* [1999]). EGCG has also been shown to reduce UVB induced non-malignant and malignant tumours per SKH-1 hairless mouse by 55% and 66%, respectively (Lu *et al.* [2002]). Alternatively, Zhao *et al.* [1999] showed that a standardised black tea extract was able to inhibit erythema and edema in SKH-1 mice, as well as decrease erythema in humans, when exposed to UVB radiation. Svobodová *et al.* [2003] went on to show how the phenolic acids, caffeic and ferulic acid, were able to inhibit erythema in UV-exposed human skin.

Flavonoids have been shown to potentially offer photoprotection. Ryan *et al.* [2002] have shown how, in the leaves of the plant *Petunia*, UVB radiation stimulated an increase in the amounts of flavonoids present. It specifically increased dihydroxylated flavonoids as opposed to their complementary mono-hydroxylated flavonoids. The cytochrome P_{450} enzyme, flavonoid 3'hydroxylase, converts mono-hydroxylated flavonoids to their dihydroxylated counterparts. In the absence of this enzyme, kaempferol glycosides (monohydroxylated) predominated in *Petunia* leaves and these plants grew at a slower rate when exposed to UVB radiation. In the presence of the enzyme, quercetin glycosides (*ortho*-dihydroxylated) were

abundant and these plants grew at a much faster rate when UVB-exposed. It seems that the presence of quercetin glycosides offered better photoprotection than kaempferol glycosides in the plant. These *ortho*-dihydroxylated flavonoids have been shown to be better antioxidants than the mono-hydroxylated flavonoids (Ryan *et al.* [2002]).

Aquino *et al.* [2002] also verified the photoprotective properties of flavonoids based on the activities of a flavonol-rich extract. Aquino *et al.* [2002] showed how an ethanolic extract from the leaves of the plant *Culcitium reflexum* H.B.K. showed strong antioxidant activity in various antioxidant tests. This extract was also found to prevent erythema on human skin when exposed to UVB radiation. The extract was found to contain flavonols such as rutin, quercetin and others, which were thought to be the major contributors of the plant's radical scavenging properties.

1.3.2 Antioxidants as radical scavengers

Radical scavenging antioxidants are capable of potentially photostabilising chemical absorbers such as avobenzone which lose some of their UV absorption efficiency through radical production. Vitamin C is known to scavenge free radicals whereas vitamin E can inhibit lipid peroxidation as well as quench singlet oxygen (Pinnell [2003]). Tea (*Camellia sinensis*) polyphenols have been reported to quench singlet oxygen and various radicals such as superoxide and hydroxyl radicals (Pinnell [2003]).

Rooibos tea contains polyphenolics that contribute to its antioxidant activity. Rooibos tea phenolic acids, such as ferulic and syringic acid, and flavonoids, such as quercetin and luteolin, are all potent antioxidants. This antioxidant activity has been shown by Joubert *et al.* [2004] when Rooibos tea quenched diphenylpicrylhydrazyl (DPPH) and superoxide anion radicals. Marnewick *et al.* [2000] showed that the aqueous extracts of fermented and unfermented Rooibos tea and honeybush tea exhibit antimutagenic properties against metabolically activated mutagens. However, they were less effective in preventing the mutagenic effect of mutagens that acted directly without activation. Marnewick *et al.* [2004] took processed and unprocessed Rooibos, honeybush, black and green teas and fed them to male Fischer rats for 10 weeks. The anti-mutagenic activities of these teas were determined by means of the *Salmonella* mutagenicity assay. These teas possessed anti-mutagenic properties in some tests but some teas enhanced mutagenicity in others. The results varied from one tea to another perhaps as a result of different polyphenolic compositions.

Polyphenols have been shown not only to possess antioxidant activities but prooxidant properties as well. Azam *et al.* [2004] showed how the catechins, epicatechin and EGCG, were able to reduce copper to produce hydroxyl radicals which are dangerous to DNA. They were also able to form superoxide anions as well as cleave DNA oxidatively. Polymerisation of these catechins was thought to occur when oxidised by copper, and in their oxidised form they showed an even higher prooxidant activity. In general, EGCG was a better prooxidant than epicatechin. This prooxidant activity has also to be considered when using antioxidants as photostabilisers, as they may portray a potentially harmful effect.

1.3.2.1 The Cancer Bush plant

The plant, *Sutherlandia frutescens* subspecies *microphylla*, is common to the southern African region where it is referred to as the Cancer Bush plant. It is used by the indigenous people medicinally as an anti-cancer and an immune booster for HIV-infected individuals. It is thought that the radical scavenging properties of polyphenols could be responsible for the plant's anti-tumour promoting activity. This plant was investigated in this research as these polyphenols could act as potential photostabilisers of photo-unstable chemical absorbers.

Fernandes *et al.* [2004] obtained a hot water extract from the Cancer Bush plant and showed that the extract could inhibit the chemiluminescence of oxygen species produced from the stimulation of neutrophils and cell free systems. The implication was that this hot water extract showed potential antioxidant activity. The activity was most likely the result of the presence of phenolic compounds, and they specifically referred to tannins and flavonoids. The Medical Research Council of South Africa (Seier *et al.* [April 2002]) reported that the consumption of *Sutherlandia* leaf powder displayed no toxicity at concentrations of up to 81 mg per kg body mass of vervet monkeys (*Chlorocebus aethiops*). This lack of toxicity implies that the plant can potentially be used medicinally.

Since flavonoids were thought to be some of the most probable polyphenolics present in the Cancer Bush leaves (Fernandes *et al.* [2004]), Rooibos tea which is a known flavonoid-rich source was also investigated in order to compare the photostabilisation activity as well as its polyphenolic composition. The various Rooibos teas investigated included: plain Rooibos tea, Rooibos with honeybush tea and Rooibos with honeybush and black tea, so as to offer diverse polyphenolic substances which in turn could affect the tea's photostabilisation potential.

1.4   Outline of this study

The purpose of this study was to investigate whether plant polyphenol extracts could act as photostabilisers of photo-unstable chemical absorbers. Potential polyphenolics were extracted from the Cancer Bush leaves by means of various extraction methods. The different extracts were characterised by UV spectroscopy and HPLC analysis, and suitable extracts were chosen for further analysis accordingly. The extract considered to contain the greatest concentration of polyphenolics was further characterised by gas chromatography (GC) and gas chromatography-mass spectrometry (GC-MS). The best extraction method was then used to extract polyphenols from the various Rooibos teas, in order to compare them with those from the Cancer Bush leaves.

The photostability of a number of chemical absorbers (listed in Table 1.1) was investigated in appropriate solvents. Attempts were then made to photostabilise those absorbers that degraded by the addition of an appropriate Cancer Bush extract. These photostability studies were monitored by UV absorption spectroscopy.

Since the polyphenolic extracts exhibited the greatest photostabilising effect with avobenzone, this chemical absorber was investigated in detail. As previously mentioned, see Section 1.2.1.1, the photochemical behaviour of avobenzone is solvent dependent. The photostability of this absorber was therefore investigated in DMSO, ethyl acetate, cyclohexane and methanol. Various techniques, including UV spectroscopy, HPLC, GC-MS and nuclear magnetic resonance (NMR) spectroscopy, were employed in order to determine the mechanism that gives rise to the photo-instability in most of these solvents. Consequently, the mechanism that led to the photostabilisation of avobenzone in certain solvents by appropriate Cancer Bush extracts was deduced. The photostabilisation effect was in turn compared with that observed with known polyphenols, which included the various Rooibos tea extracts and the specific polyphenols, epicatechin and rutin.

In order to further comprehend the photo-instability mechanism observed with avobenzone and to explain the results of the photostabilisation research, various experiments were conducted. The effect that the presence and the absence of oxygen has towards the photo-instability of avobenzone was investigated by UV spectroscopy in the various solvents. The phenolics present in the photostabilising Cancer Bush extract were quantified by using a Folin-Ciocalteu

reagent. The presence of antioxidants in the Cancer Bush extract was verified by reacting the extract with a stable free radical, DPPH, and monitoring the amount scavenged. These results were used to determine a possible mechanism that could explain the photostabilisation results observed.

The details of the experiments performed are given in Chapter 2 and the results are presented and discussed in Chapter 3.

CHAPTER 2

EXPERIMENTAL

This chapter describes the materials, equipment and methods used to investigate the photostability of sunscreen chemical absorbers with polyphenols.

2.1 Materials and equipment

The materials and equipment used in this study are listed in Appendix A.

2.2 Cancer Bush extraction methods and properties

The Cancer Bush plant (see Figure 2.1) was used as a potential source of polyphenols for photostabilising the chemical absorbers. Like other plants, the Cancer Bush plant consists of chemical substances that aid in its growth, metabolism, structure and mechanism of survival. In photostabilising chemical absorbers, only the antioxidant polyphenolic chemical substances of the plant are essential. In order to work with the Cancer Bush polyphenols solely, an experimental procedure was developed for their isolation and extraction. There is little research done on this plant therefore extractions were either adapted or adopted from similar procedures conducted mainly on tea leaves. The appropriate extraction method was subsequently used to extract polyphenols from various Rooibos teas, namely: plain Rooibos tea, Rooibos-honeybush tea, Rooibos-black tea (Rooibos with honeybush and black tea). Subsequently the Cancer Bush and Rooibos tea extracts were compared for their polyphenolic composition and photostabilising effect.

The Cancer Bush plant was considered a likely source of antioxidant polyphenols because of its use for the treatment of Cancer and AIDS by the indigenous people of southern Africa. In order to verify the presence of antioxidant polyphenolics in the extracts, an experiment measuring the antioxidant activity was conducted in which the extracts were reacted with a stable free radical, diphenylpicrylhydrazyl (DPPH). This assay is described in Section 2.2.5.1. Since most plants

contain polyphenols, a phenol quantitation experiment was also performed in order to assign the type of antioxidants present in the sample (see Section 2.2.5.2). Four extraction methods were attempted and these are described in Sections 2.2.1 to 2.2.4.

Figure 2.1:   The Cancer Bush plant growing naturally in the wild (Finebush [2003]).

2.2.1 Methanol-water extraction

This extraction method was adopted from that used by Zuo *et al*. [2002] in preparing extracts of tea samples. The aqueous methanol solvents used for the solvent extraction of the Cancer Bush leaves were prepared using water purified through a Millipore Milli-Q[50] ultra pure water apparatus, that will be referred to as Millipore water. Ground Cancer Bush leaves (1.9 – 3.8 g) were extracted three times by shaking, using an orbital shaker, with 20 ml portions of 80:20 (v/v) methanol:Millipore water for 3 hours each, then two times with 20 ml of 80:20 (v/v) methanol:Millipore water also containing 0.15% HCl for 3 more hours each. The extracts were combined, filtered through cotton wool and a 0.45 μm Durapore membrane filter. The filtered extract (50 μl) was diluted to 1 ml with Millipore water, then re-filtered through a 0.45 μm Millex syringe filter, and 10 μl of this solution was injected into the HPLC for analysis (see Section 3.1.1.3). The UV absorption spectrum of 1 ml of the filtered extract diluted to 25 ml with Millipore water was also obtained on a Perkin Elmer Lambda 35 UV/Visible (UV/VIS) spectrophotometer.

2.2.2 Boiling water extraction

Liang *et al.* [1990] used a boiling distilled water extraction method to determine the composition of green teas. In this research, a similar method was adapted where boiling Millipore water (40 ml) was added to about 5 g of extractable material and left stirring overnight. The mixture was then filtered under suction through Whatman filter paper. In the case of the Cancer Bush extract, 0.2 ml of this filtered extract in Millipore water was diluted to 25 ml by an appropriate solvent (including Millipore water, methanol and DMSO) for UV absorption spectroscopy investigations. A portion of the filtrate was re-filtered through a 0.45 μm Millex filter and a 10 μl aliquot of this re-filtered solution was injected into the HPLC directly for analysis. The efficiency of this method was investigated by attempting to extract caffeine from JOKO tea before attempting to extract polyphenols from both ground Cancer Bush leaves as well as non-ground leaves.

2.2.3 High temperature extraction

This extraction procedure was adapted from that of Mukhtar *et al.* [1992] and Lin *et al.* [1996] who isolated polyphenolic catechins from green tea leaves. The adapted method involved immersing 5 g of Cancer Bush leaves in 40 ml Millipore water at 65 – 75 °C for 30 minutes. The mixture was filtered under suction through Whatman filter paper and the extraction was repeated two more times on the same sample. The filtrates were combined and filtered through a 0.45 μm Millex filter before a 10 μl aliquot was injected into the HPLC for analysis. The UV absorption spectrum of a 70 μl portion of the filtrate diluted to 25 ml with Millipore water was also obtained.

2.2.4 Ethanol-water extraction

This method was adapted from the method used to extract polyphenols from tea leaves and tea flowers by Lin *et al.* [2003a and 2003b]. About 5 g of extractable material were ground using a pestle and mortar, then immersed in 40 ml 75:25 (v/v) ethanol:Millipore water solution. The mixture was placed in an oil bath at 65 °C with stirring for 30 minutes. The mixture was then filtered through Whatman filter paper and the filtrate evaporated under reduced pressure by means of a rotavapor. The crude extract was re-dissolved in 25 ml Millipore water (Miketova *et al.* [1998]). The aqueous solution was extracted three times with an equal volume of ethyl acetate (Mukhtar *et al.* [1992], Lin *et al.* [1996] and Miketova *et al.* [1998]) to extract the polyphenols. The ethyl acetate extracts were combined and filtered through Whatman filter

paper. The ethyl acetate was evaporated under reduced pressure in a rotavapor. A few drops of dichloromethane were added to ensure complete removal of water (Soleas et al. [1997 and 1999]) leaving a solid extract. This method was tested for its ability to extract gallic acid from a gallic acid-containing Rooibos-black tea (Miller [1996]). When this method was used to extract potential polyphenols from Cancer Bush leaves, a dark green solid (0.3308 g) was extracted.

A portion of the Cancer Bush solid extract was re-dissolved in methanol and a 10 µl aliquot of the solution injected into the HPLC for analysis. A further 32 mg portion of the extract was dissolved in 25 ml methanol and analysed by the Perkin Elmer Lambda 35 UV/VIS spectrophotometer in order to obtain a UV absorption spectrum of the extract. The same quantity of extract sample used for UV absorption spectroscopy was subsequently irradiated in various solvents of interest with wavelengths greater than 300 nm (see Sections 2.3 and 2.4). UV spectra of the irradiated extract solutions were recorded at set time intervals, in order to assess the photostability of the extract in the spectral region of interest.

The extraction methods were assessed based on the ability of the resulting extracts to absorb in the UV region of interest and the diversity of compounds extracted. The UV spectra and HPLC chromatograms of all the extracts are compared in Section 3.1.1. The boiling water and the ethanol-water extracts were chosen for subsequent photostability investigations, but the ethanol-water extracts also offered various other advantages. Therefore, the ethanol-water extraction method was used to extract antioxidant polyphenols from the various Roooibos teas including: Rooibos-honeybush tea, Rooibos-black tea and plain Rooibos tea (see discussion in Section 3.1.1.3).

2.2.5 Properties of the Cancer Bush extract

In order to understand the mechanism by which the ethanol-water Cancer Bush extract could photostabilise chemical absorbers, it was important to investigate some properties of this extract. The two parameters investigated were the antioxidant activity and the polyphenol content.

The antioxidant activity offers a relative measure of the ethanol-water Cancer Bush extract's ability to scavenge radicals. The result obtained provides insight into the mechanistic pathway involved by which the extract is able to photostabilise chemical absorbers. In this work the

ethanol-water Cancer Bush extract was tested for its ability to scavenge the stable free radical, diphenylpicrylhydrazyl (DPPH).

It was necessary to determine the phenolic content of the ethanol-water Cancer Bush extract in order to establish whether phenols were the potential photostabilisers in the extract. These phenols were quantified by the Folin-Ciocalteu reagent (FCR) method. This method measures the phenolic content based on the reduction of a phosphomolybdic-tungstic mixed acid chromagen to the reduced form that absorbs maximally around 750 nm (Peterson [1983]). The absorbance produced by a certain amount of the extract was compared with those obtained from a calibrated standard and the results are reported in equivalent amounts of that standard.

2.2.5.1 Antioxidant activity

The method employed for determining the antioxidant activity of the extract was based on the recommendations made by Molyneux [2004]. A 4.1 mg sample of DPPH was measured, then dissolved and the solution was diluted to the mark in a 100 ml volumetric flask with 80% aqueous ethanol solution (Guan and Whiteman [accessed on 1st March 2005]). Ethanol could be used as the solvent because it does not interfere with the radical scavenging reaction (Molyneux [2004]). Ethanol is miscible with ethyl acetate which enabled it to dissolve the ethyl acetate extracted ethanol-water Cancer Bush extract. Aqueous ethanol was required for complete dissolution of the extract. An initial DPPH solution with a concentration of 52 µM was prepared by diluting 2 ml of the 41 mg l^{-1} solution with 2 ml of 80% aqueous ethanol. This concentration gave an absorbance reading less than 1. The UV absorption spectrum of this purple solution of DPPH was recorded and it showed a maximum absorbance at 522 nm (shown in Figure 2.2).

A mass of 45.3 mg of the ethanol-water Cancer Bush extract was measured into a 25 ml volumetric flask and diluted to the mark with 80% aqueous ethanol solution. A 1 ml aliquot of this solution was added into a plastic vial by means of a 1000 µl micropipette and diluted to 2 ml with 80% aqueous ethanol solution. A 2 ml aliquot of the 41 mg l^{-1} DPPH solution was added to the diluted extract sample, and the whole solution turned purple (colour of DPPH). An equal volume of the 41 mg l^{-1} DPPH solution and the ethanol-water Cancer Bush extract was always used, since different volume ratios compromise the accuracy of the relative volumes (Molyneux [2004]). The absorbance at 522 nm was measured 15 seconds from mixing the extract with DPPH. Absorbance readings at this wavelength were followed for four hours at

23 °C, until equilibrium was reached and the sample displayed an insignificant change in absorbance. Since the ethanol-water extract also absorbed at 522 nm, blank samples of the extract without DPPH were prepared (see Table 2.1) separately from the extract samples with DPPH (Table 2.2). The absorbances at 522 nm were recorded after 4 hours for each set of samples. Tables 2.1 and 2.2 show how the total volume in the vials was always kept constant, as well as how radical scavenging results in loss of the purple DPPH colour (Molyneux [2004] and Lu *et al.* [2003]) at the end of the 4 hours. The results of the ethanol-water Cancer Bush extract's ability to scavenge the DPPH radical are discussed in Section 3.1.3.2.
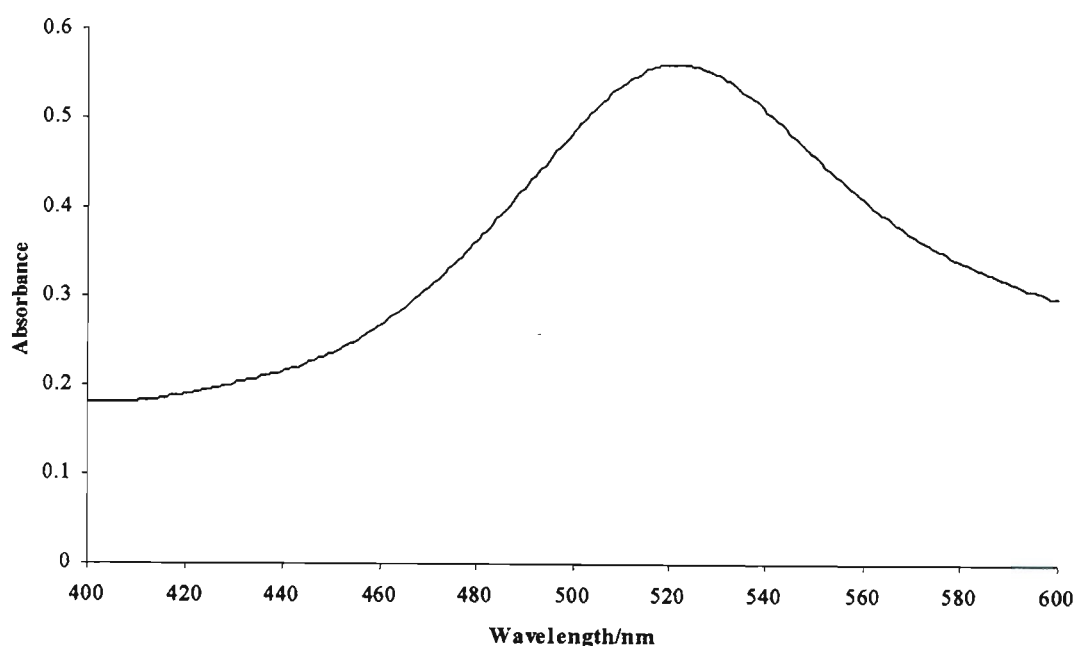
Figure 2.2:   UV absorption spectrum of 52 μM DPPH in 80% aqueous ethanol.

Table 2.1:   The volumes of the ethanol-water Cancer Bush extract that were made up to a constant volume of 4 ml with 80% aqueous ethanol in a glass vial in order to prepare the sample blanks for the measurement of antioxidant activity. The solutions were incubated at 23 °C for 4 hours and their colour noted.

Sample Number	Volume of extract diluted to 4 ml with 80% aqueous ethanol/μl	Colour generated after 4 hours at 23 °C
0	0	Green
1	100	Green
2	200	Green
3	300	Green
4	400	Green
5	500	Green
6	600	Green
7	700	Green
8	800	Green
9	900	Green
10	1000	Green

Table 2.2:   The volumes of the ethanol-water Cancer Bush extract that were made up to 2
               ml with 80% aqueous ethanol and added to 2 ml of 41 mg l^{-1} DPPH to maintain
               a constant volume of 4 ml in a glass vial for the measurement of antioxidant
               activity. The solutions were incubated at 23 °C for 4 hours and their colour
               noted.

Sample Number	Volume of extract diluted to 2 ml with 80% aqueous ethanol then to 4 ml with DPPH solution/µl	Colour observed after 4 hours at 23 °C
0	0	Purple
1	100	Purple
2	200	Purple
3	300	Light purple
4	400	Light green
5	500	Green
6	600	Green
7	700	Green
8	800	Green
9	900	Green
10	1000	Green/yellow

2.2.5.2 Phenol Quantitation

The method used to quantify the phenolic content of the ethanol-water extract was adapted from
that of Singleton *et al.* [1999]. Gallic acid was employed as the standard as was done by Reddy
et al. [2000], Nigdikar *et al.* [1998], and Morais *et al.* [1999]. Singleton *et al.* [1999] reported
that linear calibration curves for gallic acid are only obtained between concentrations ranging
from 300 mg l^{-1} to 3 mg l^{-1}. Hence, a 507 mg l^{-1} stock solution of gallic acid was prepared by
dissolving 50.7 mg gallic acid in 80% aqueous methanol in a 100 ml volumetric flask, and
diluting to the mark. Different concentrations of gallic acid were prepared from this stock
solution, ranging from 5 mg l^{-1} to 50 mg l^{-1} (in steps of 5 mg l^{-1}).

A mass of 17.5 mg of the dry, green ethanol-water extract was dissolved in 80% aqueous
methanol and diluted to the mark in a 25 ml volumetric flask. A 100 µl aliquot of the extract

solution as well as each standard solution was measured by means of a 100 μl micropipette into about 7 ml Millipore water in a 10 ml volumetric flask. A 500 μl volume of the Folin-Ciocalteu reagent (FCR) was added to the diluted extract and each of the standard solutions, and the mixtures were mixed thoroughly. All the solutions exhibited the green/yellow colour of the FCR. Between 1 and 8 minutes, a 1500 μl volume of the 20% sodium carbonate solution (20.04 g sodium carbonate dissolved and made up to 100 ml in a volumetric flask with Millipore water) was added to each sample solution. The volumetric flasks were then made up to volume with Millipore water, shaken and left at 23 °C (room temperature) for 2 hours. Once shaken, the green/yellow colour disappeared leaving a colourless solution. After 2 hours, a blue colour developed in all the samples (except the blank) increasing in intensity with the highly concentrated gallic acid standards. The wavelength of maximum absorbance of the solution having the most concentrated gallic acid standard, namely 50 mg l^{-1}, was used as the wavelength of detection due to the reduced impact of absorbing interferences. This wavelength was found to be 765 nm as shown in Figure 2.3. The absorbances of the sample solution and all the gallic acid standard solutions containing the FCR were recorded at 765 nm. The gallic acid standard solutions gave a calibration curve of absorbance at 765 nm against the volume of the gallic acid stock solution initially measured into the 10 ml volumetric flask (see Table 2.3 and Figure 2.4). The equivalent gallic acid amount that gave the same absorbance as the ethanol-water Cancer Bush extract amount was obtained from the gallic acid calibration curve. The results of the phenol quantitation of the ethanol-water Cancer Bush extract by the FCR method are reported and discussed in Section 3.1.3.1.
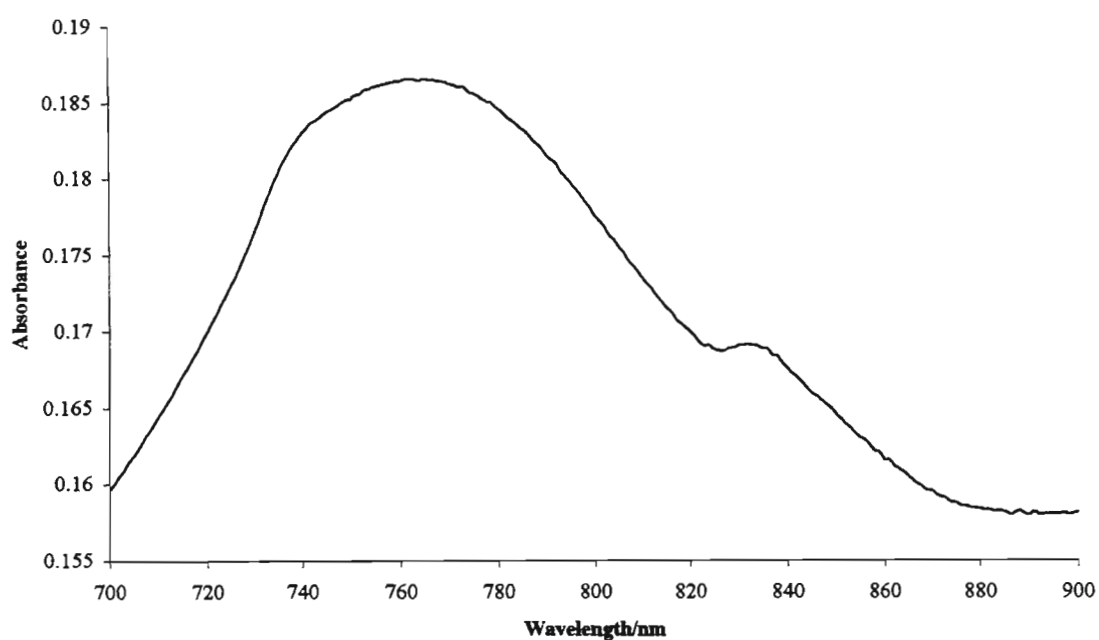
Figure 2.3: The visible absorption spectrum of the total phenol content of a 50 mg l^{-1} gallic acid standard solution after two hours at 23 °C.

Table 2.3: Absorbances at 765 nm of the Folin-Ciocalteu reagent with different volumes of a 507 mg l^{-1} stock solution of gallic acid.

Volume of a 507 mg l^{-1} gallic acid stock solution/μl	Gallic acid Absorbance			Standard deviation
	Trial 1	Trial 2	Average	
100	0.0889	0.0937	0.0913	0.0034
200	0.0967	0.102	0.0994	0.0037
300	0.110	0.113	0.112	0.002
500	0.118	0.132	0.125	0.010
600	0.136	0.142	0.139	0.004
700	0.147	0.150	0.149	0.002
800	0.165	0.172	0.169	0.005
1000	0.183	0.187	0.185	0.003

The graph shows:
y = 0.0106x + 0.078
R² = 0.9869

(y-axis: Absorbance at 765 nm, values from 0 to 0.2)
(x-axis: Volume of a 507 mg per liter gallic acid stock solution/100 µl, values from 0 to 10)
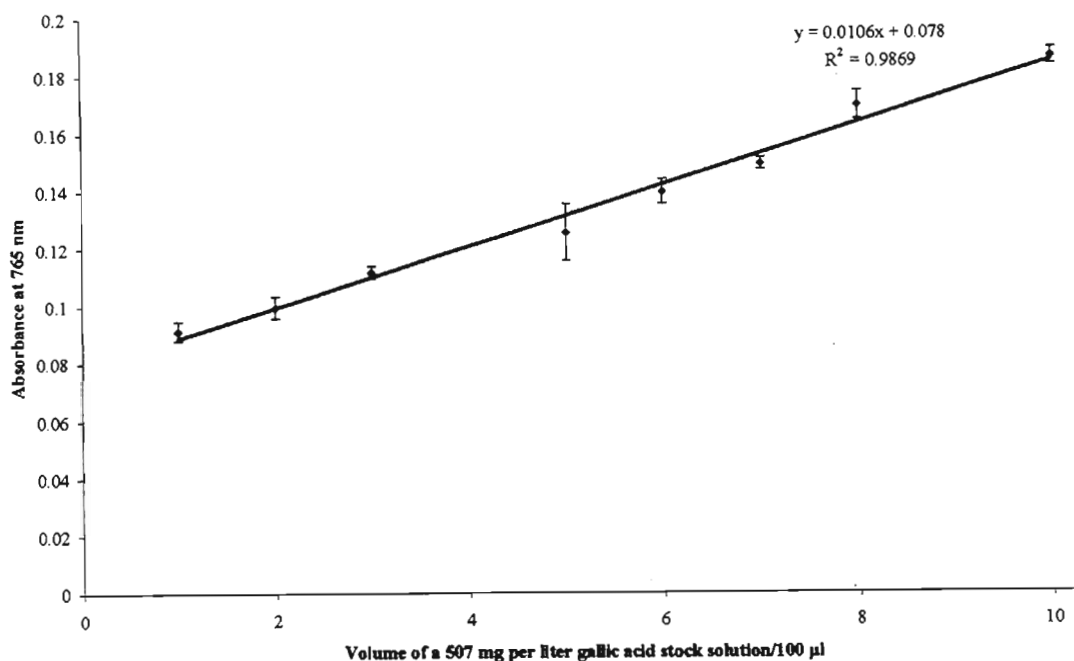
Figure 2.4:   Calibration curve for the Folin-Ciocalteu reagent method of phenolic quantitation in gallic acid solutions.

2.3 UV irradiation

Chemical absorbers are incorporated in sunscreen preparations in order to absorb solar UV radiation. A UV radiation source is therefore required for determining the protective efficacy of chemical absorbers.

An Osram HBO 500 W/2 high pressure mercury lamp was used as a source of UV radiation. This lamp was suitable for irradiations because it provided high radiant light in the UV region. The lamp is described in Section 2.3.1 and the sample holders are described in Section 2.3.2.

2.3.1 UV light source and filter

The Osram HBO 500 W/2 high pressure mercury lamp (shown in Figure 2.5) is part of a group of mercury short arc lamps, whereby the discharge arc burns in an atmosphere of mercury vapour at high pressure (Osram [accessed on 23rd August 2004a]). The lamp emits radiation in the form of a multi-line spectrum of wavelengths ranging from 260 nm to 610 nm (Figure 2.6). In order to mimic solar UV radiation falling on the earth, a 10 mm thick Pyrex filter was placed

between the lamp and sample to be irradiated. The filter allowed only wavelengths greater than 300 nm to pass through (Figure 2.7).

The Osram lamp functions optimally within set time limits; it requires at least a 15 minute warm-up time and has a 400 hour lifetime. The lamp maintains a significantly consistent intensity range, which was monitored with a Black-Ray J-221 Longwave UV intensity meter, throughout the 400 hours. Once the lamp had been used for over 400 hours it was replaced.

The Osram light source is housed in an insulated steel box (Figure 2.8). The radiation emitted by the lamp passes through an opening on one end of the steel box to the Pyrex filter to reach the sample to be irradiated contained in a cuvette. This only occurs when the shutter gate is open to let the light through. The shutter gate, filter holder and cuvette holder are part of an external bracket (Figure 2.9) attached in front of the steel box opening. The steel box is connected to an extractor. The equipment also consists of a fan, a Schreiber power supply and an igniter.

The insulated steel box, the fan and the extractor insure safety in the operation of the equipment. The steel box prevents potentially harmful UV radiation from being scattered in the room. The fan cools the equipment from the heat produced by the radiation. The extractor removes potentially harmful gases produced (e.g. ozone).
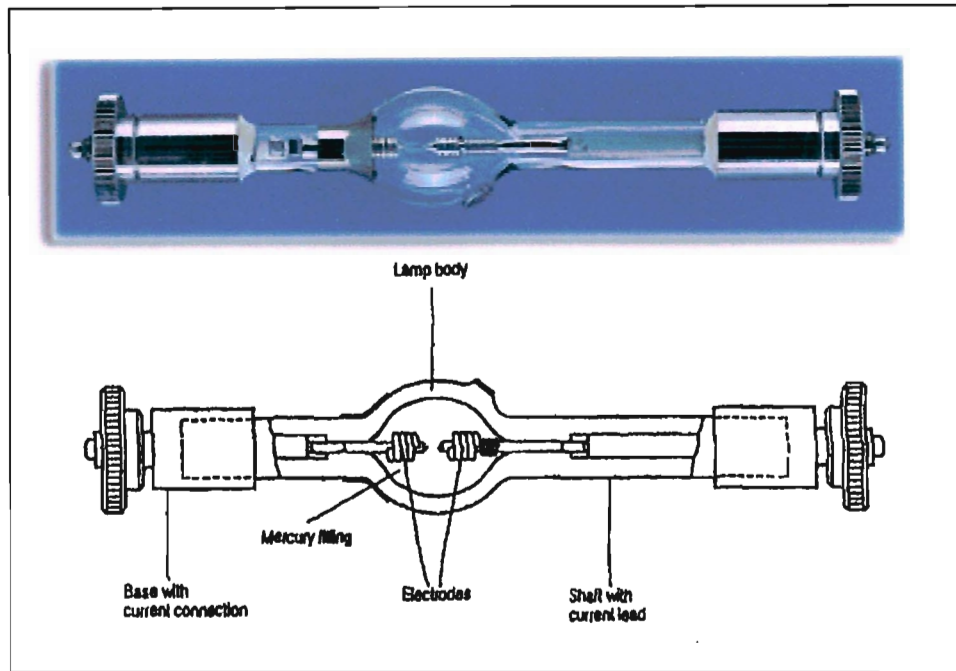
Figure 2.5:   A diagram of the Osram 500 W/2 high pressure mercury lamp (Osram [accessed on 23rd August 2004b]) and schematic drawing (Aliwell [1991]).
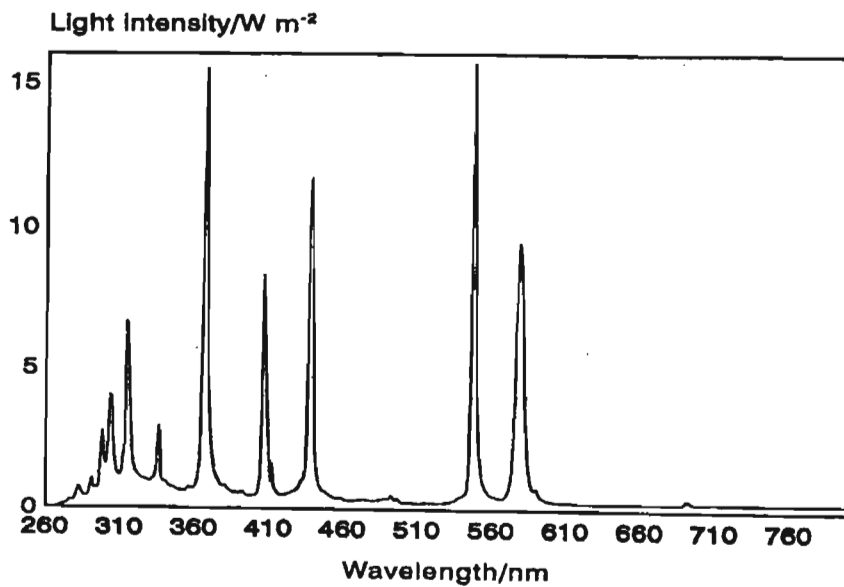
Figure 2.6:   Output of the Osram HBO 500 W/2 high pressure mercury lamp (Broadbent [1994]).
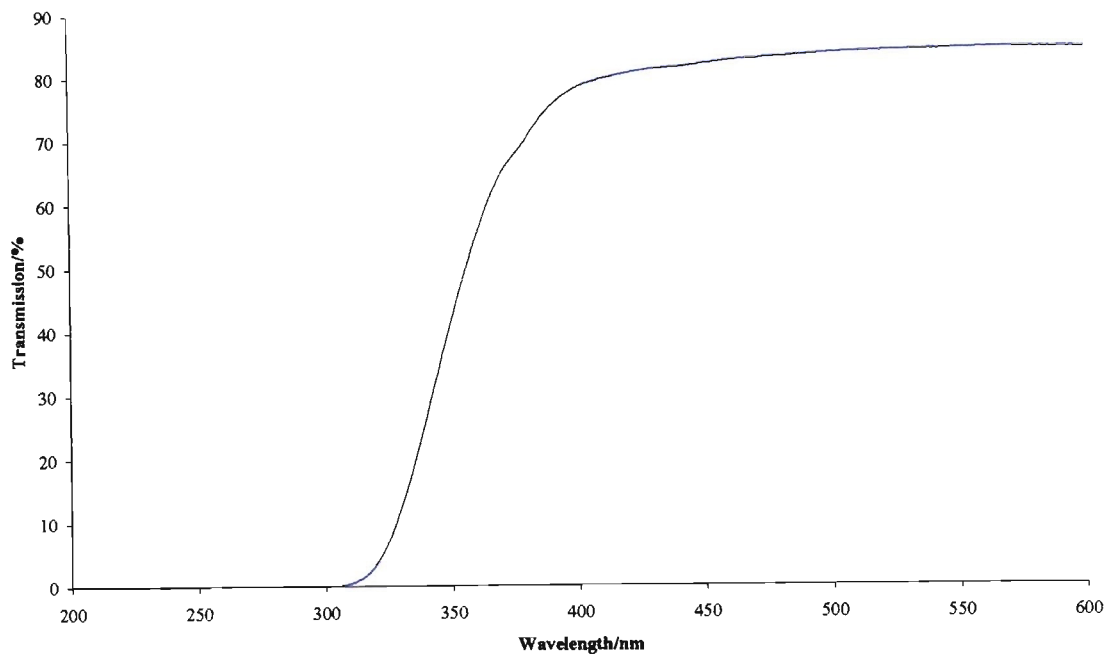
Figure 2.7:   Transmission spectrum of the 10 mm thick Pyrex filter.
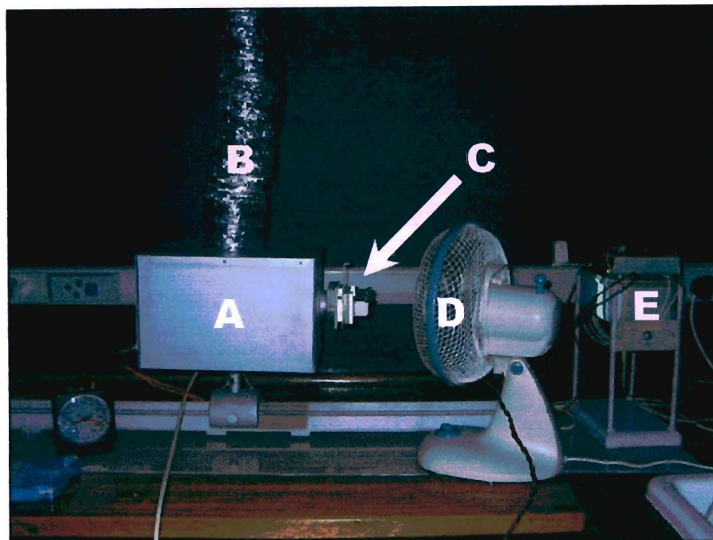
Figure 2.8:   A photograph of the irradiation equipment showing the insulated steel box (A), containing the lamp, connected to an extractor (B) and the external bracket (C) which holds the filter, shutter and sample cuvette. The photograph also shows the fan (D) and the igniter (E).
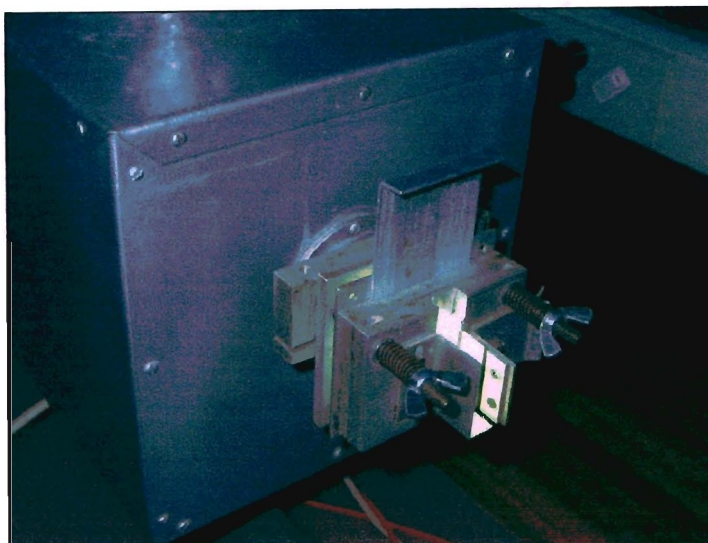
Figure 2.9:   Close-up of the external bracket holding the shutter gate, filter and cuvette.

2.3.2 Sample holders

The suitability of a cuvette depends upon the wavelength range of the radiation it allows to pass through. Quartz cuvettes are appropriate for usage in the ultraviolet region (Skoog *et al.* [2004a]). A 1 mm pathlength quartz cuvette was used for small as well as concentrated samples, whilst 10 mm pathlength quartz cuvettes were used for dilute and abundant samples. Because of the hygroscopic nature of NMR solvents, NMR tubes were used as irradiation sample holders when irradiated samples were to be analysed by NMR spectroscopy. This allowed direct transfer to the NMR instrument following irradiation. Use was made of a glass cuvette for the photostability investigations performed at the maximum absorption wavelength of the UVA absorber avobenzone, which ranged from 350 nm to 365 nm, where the cuvette does not absorb. The UV absorption spectra of the 1 mm and the 10 mm pathlength quartz cuvettes, the 10 mm pathlength glass cuvette and the NMR tube are shown in Figures 2.10, 2.11, 2.12 and 2.13 respectively. These spectra were acquired with a Perkin Elmer Lambda 35 UV/VIS spectrophotometer. All these sample holders absorb below 300 nm hence allowing radiation in the appropriate spectral region to pass through the sample.

Samples were irradiated at suitable time intervals for adequate degradation in different solvents, and then examined by UV absorption spectroscopy (see Section 2.4).
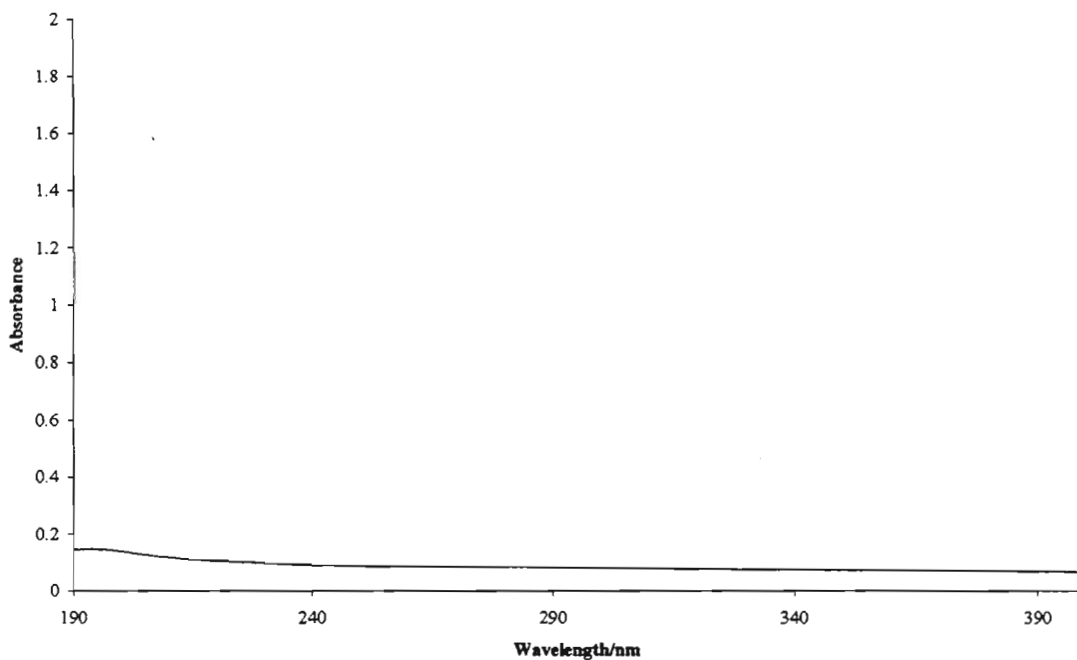
Figure 2.10: The UV absorption spectrum of a 1 mm pathlength quartz cuvette used in irradiation experiments with chemical absorbers absorbing between wavelengths of 190 nm and 400 nm.
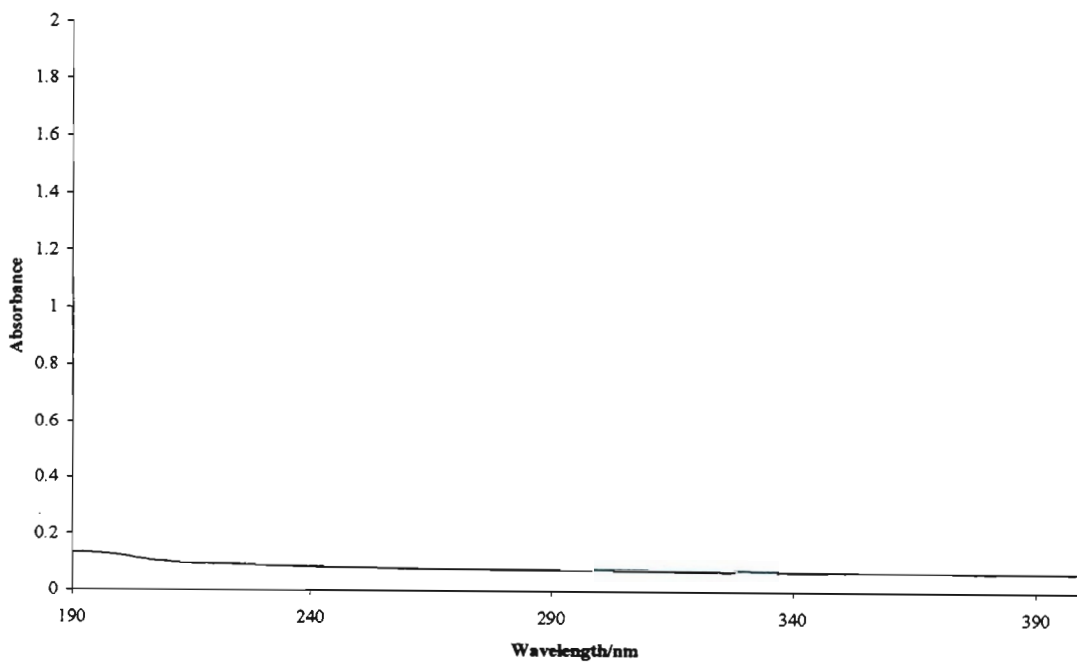
Figure 2.11: The absorption spectrum of a 10 mm pathlength quartz cuvette used for irradiation experiments with chemical absorbers absorbing in the range between 190 to 400 nm.
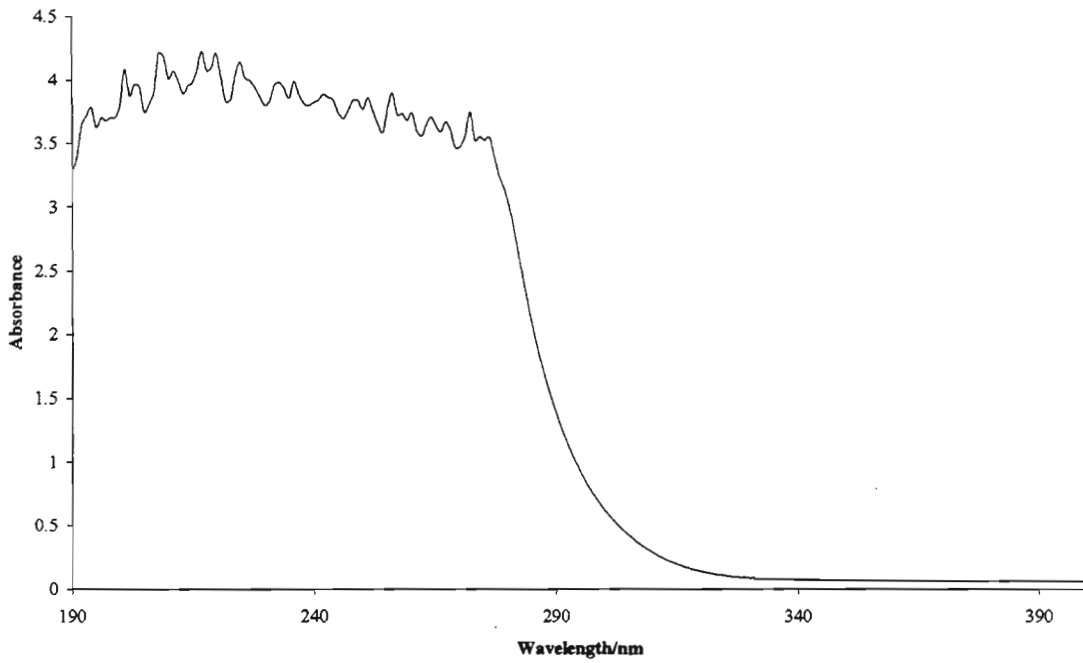
Figure 2.12:   The absorption spectrum of a 10 mm pathlength glass cuvette used for irradiation analyses with avobenzone only.
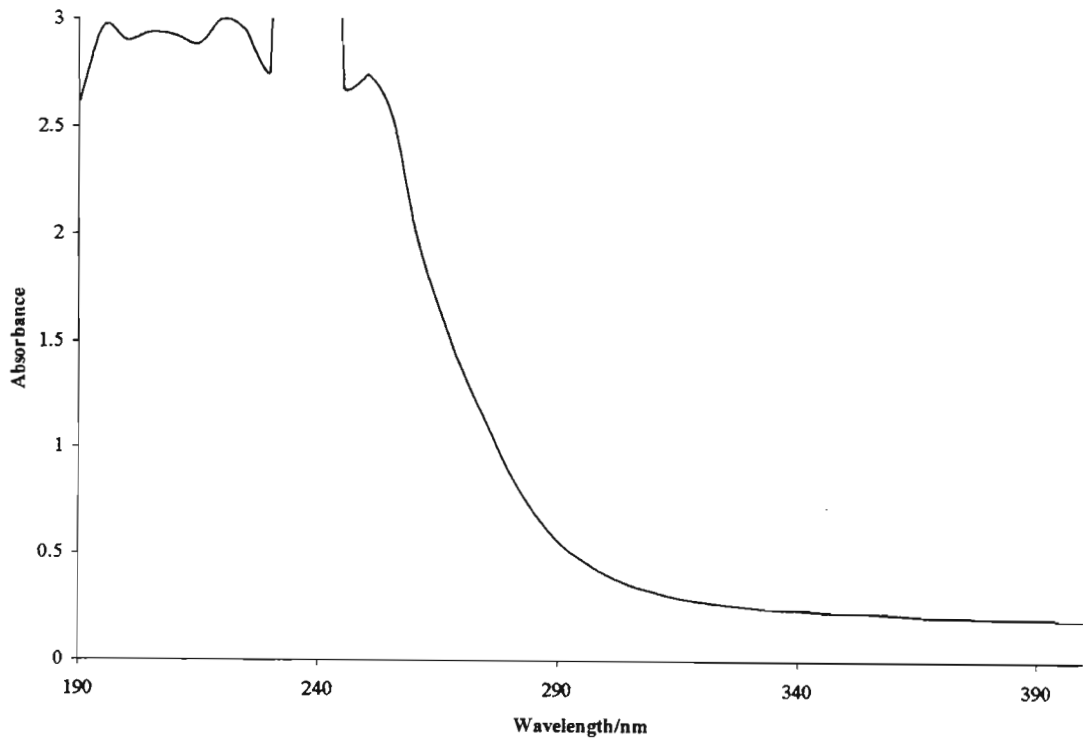
Figure 2.13:   The absorption spectrum of a typical NMR tube used for the UV irradiation of solutions of avobenzone that were analysed by NMR spectroscopy.

2.4 UV absorption spectroscopy

Chemical absorbers protect one's skin through the absorption of UV radiation. The UV absorption of a compound is measured by means of UV absorption spectrophotometers, and the data is recorded in the form of a UV spectrum. UV spectra are essential not only in characterising UV absorbers but also in determining the efficacy of these absorbers when exposed to UV radiation. This section is divided into three parts that introduce UV absorption spectroscopy (Section 2.4.1), show the UV spectra of solvents used in this research (Section 2.4.2) and describe how samples were prepared for UV experiments (Section 2.4.3).

2.4.1 An introduction to the theory and instrumentation of UV absorption spectroscopy

Electromagnetic radiation refers to discrete particles of energy, called photons, transmitted through space. This energy is transmitted in waves and can therefore be characterised by its wavelength or frequency (Fessenden and Fessenden [1998]), as expressed by Equation 2.1.

$$E = h\nu = h\frac{c}{\lambda} \quad \text{since } \nu = \frac{c}{\lambda} \qquad \text{Equation 2.1}$$

where E is energy in J, ν is frequency in s^{-1}, h is a constant known as Planck's constant, c is the speed of light in m s^{-1} and λ is the wavelength in m.

Absorption can be looked at as the removal of specific frequencies of electromagnetic radiation by chemical substances (Skoog and West [1982]). UV absorption is hence the removal of radiation frequencies from the UV portion of the electromagnetic radiation by chemical species appropriately termed as UV absorbers.

Chemical species, such as atoms, ions or molecules, possess electronic energy levels. These chemical species will absorb a photon of light with energy equivalent to the energy gap between their lowest (ground) and one of their higher (excited) electronic energy levels. The absorption of a photon of light of energy, *h*ν, will convert the species from its ground state (M) to an excited state (M*) as shown in Equation 2.2:

$$M \; + \; h\nu \; \rightarrow \; M^{\bullet} \qquad\qquad \text{Equation 2.2}$$

When the radiation absorbed falls within the wavelength range of UV light; the chemical species is a UV absorber and the absorption spectrum produced is a UV absorption spectrum.

The excited species loses its excitation energy very fast (10^{-6} to 10^{-9} s) mostly as undetectable heat (Skoog and West [1982]) as it returns to its ground state depicted by Equation 2.3. It could also photochemically decompose to form new species.

$$M^{\bullet} \; \rightarrow \; M \; + \; heat \qquad\qquad \text{Equation 2.3}$$

Ultraviolet absorption bands are broad since chemical species can undergo an electronic transition from a number of ground state sub-levels (vibrational and rotational states), to a number of sub-levels of a higher electronic state (Morrison and Boyd [1983]).

The UV absorption bands of chemical absorbers were measured by means of a double-beam Perkin Elmer Lambda 35 UV/VIS spectrophotometer and a Cary 1E UV/VIS spectrophotometer. The components of a double beam spectrophotometer are illustrated in Figure 2.14.
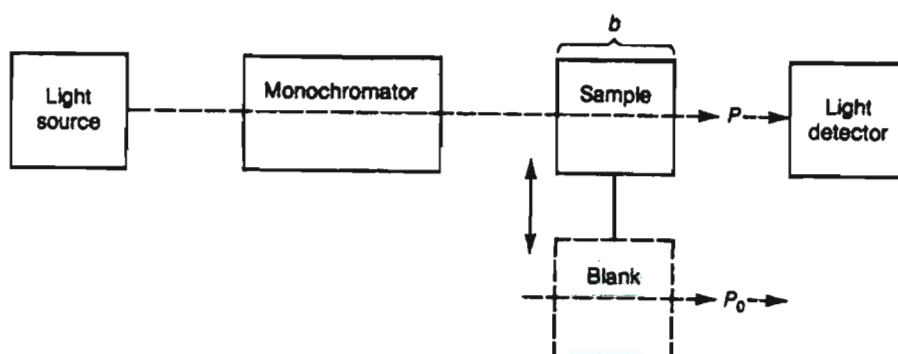
Figure 2.14:   A block diagram of the different components of a double-beam spectrophotometer (Manahan [1986]).

In a double-beam spectrophotometer, light from a light source passes through a monochromator which filters the light leaving a narrow wavelength range. This filtered radiation is split into

two light beams, one goes through the sample and the other through the blank or reference (normally the solvent). The final absorbance obtained from the detector is the beam transmitted through the sample having compensated for the beam transmitted through the blank. This can be expressed through Equation 2.4.

$$A = \log \frac{P_\circ}{P} = \log \frac{P_{Solvent}}{P_{Sample}}$$ Equation 2.4

Absorbance (A) is hence related to the ratio between the radiant power of the light beam that passes through the sample (P) to that through the solvent ($P_\circ$).

Absorbance (A) is also directly proportional to the concentration (c) of the absorbing sample and the optical pathlength (b) through which the sample absorbs the light; this is referred to as Beer's law (Equation 2.5). When the concentration is in moles per litre and the pathlength is in centimetres, the proportionality constant is referred to as the absorptivity (ε) in $l\ cm^{-1}\ mol^{-1}$.

$$A = \varepsilon b c$$ Equation 2.5

According to Beer's law, the total absorbance at a specified wavelength is the sum of the absorbances of all absorbing species at that wavelength (Equation 2.6).

$$A^\lambda = \varepsilon_1^\lambda b c_1 + \varepsilon_2^\lambda b c_2$$ Equation 2.6

where the subscripts refer to substances 1 and 2, respectively, whose absorbances add up to the overall absorbance at a particular wavelength.

All absorbance readings of samples and sample mixtures were kept below the value of 2, to limit deviations of Beer's law observed at high concentrations (Skoog *et al.* [2004b]).

2.4.2 UV spectra of solvents used for absorption spectroscopy

In this work two factors needed to be considered in the choice of solvent, apart from its ability to dissolve the chemical absorber and antioxidant extract, namely its spectral region of

absorption and its photostability. The solvent should be transparent over the wavelength range in which the chemical absorber absorbs, as well as being relatively photostable so as not to mask the photostability of the absorber. The absorption spectra of the solvents were obtained in a 1 mm pathlength quartz cuvette against air as a reference by using the Perkin Elmer Lambda 35 UV/VIS spectrophotometer. All spectra were obtained over the wavelength range of 190 nm to 400 nm at a scan rate of 240 nm min^{-1}. The solvents used in this research and the figures showing their absorption spectra are as follows: cyclohexane (Figure 2.15), ethyl acetate (Figure 2.16), DMSO (Figure 2.17) methanol (Figure 2.18) and Millipore water (Figure 2.19). All the solvents were transparent over both the UVB and UVA region where chemical absorbers absorb. The photostability of these solvents is discussed in Section 2.4.2.1.
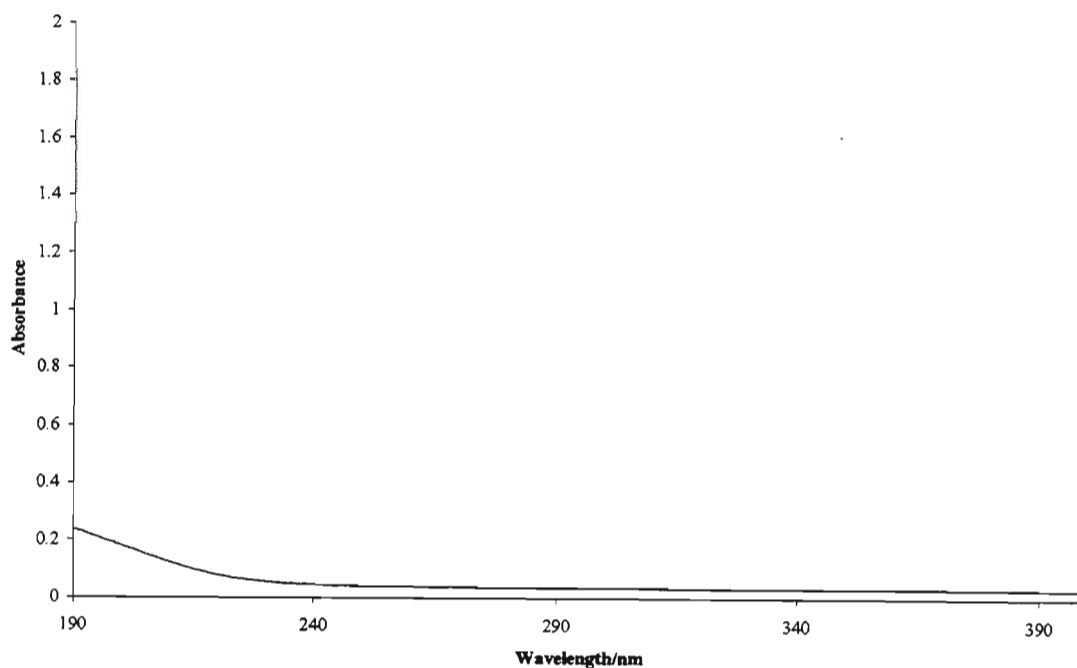
Figure 2.15:   The UV absorption spectrum of cyclohexane measured in a 1 mm pathlength quartz cuvette.
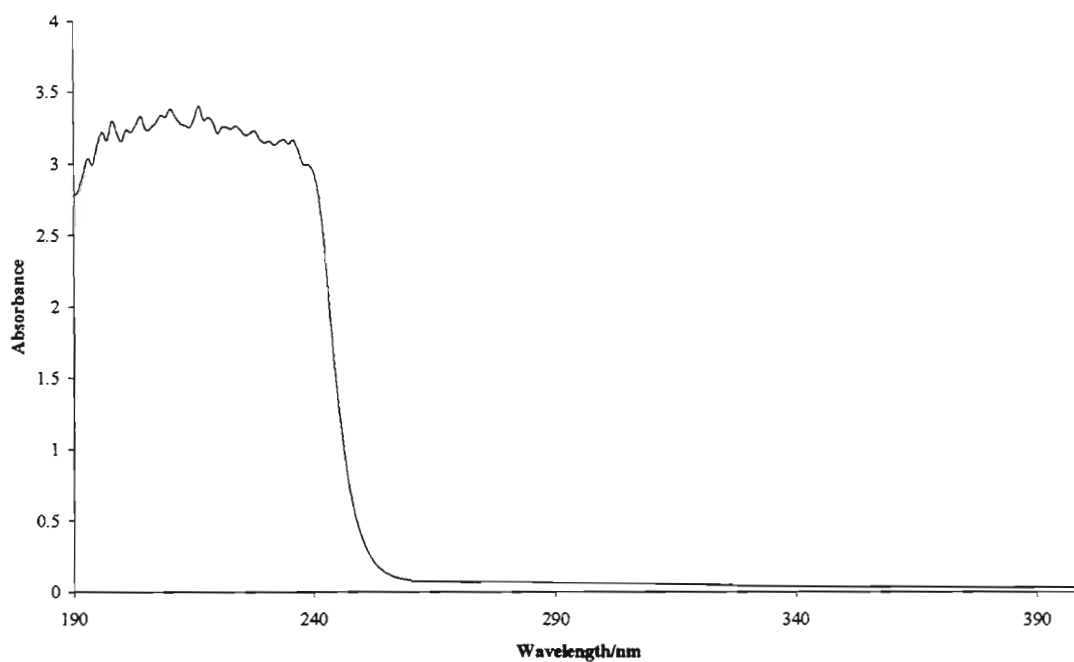
Figure 2.16:   The UV absorption spectrum of ethyl acetate measured in a 1 mm pathlength quartz cuvette.
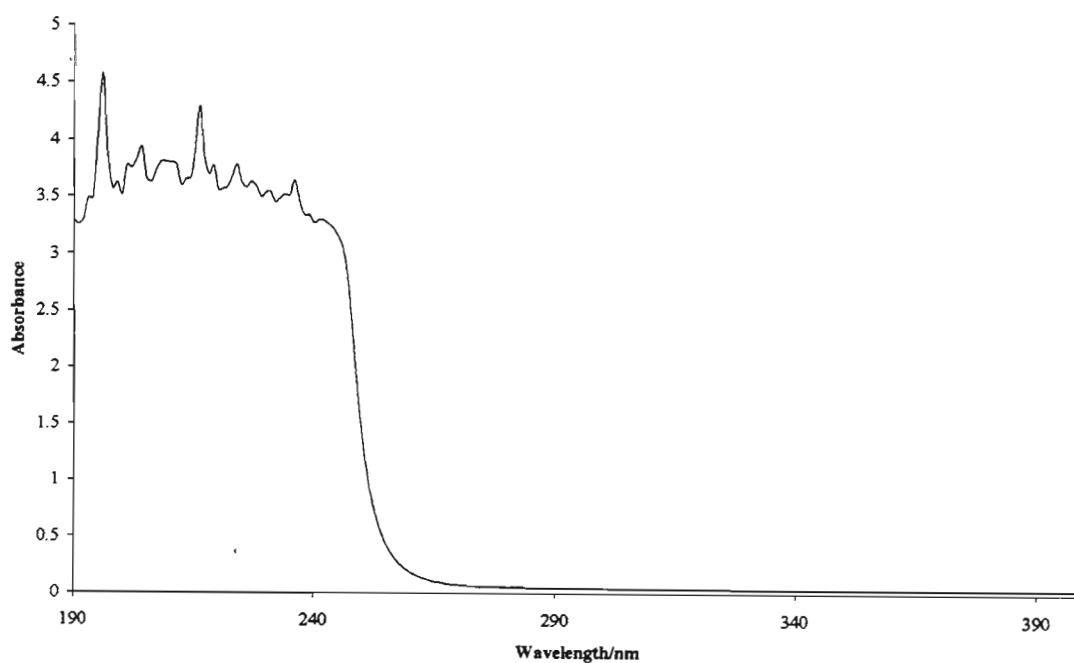
Figure 2.17:   The UV absorption spectrum of DMSO measured in a 1 mm pathlength quartz cuvette.
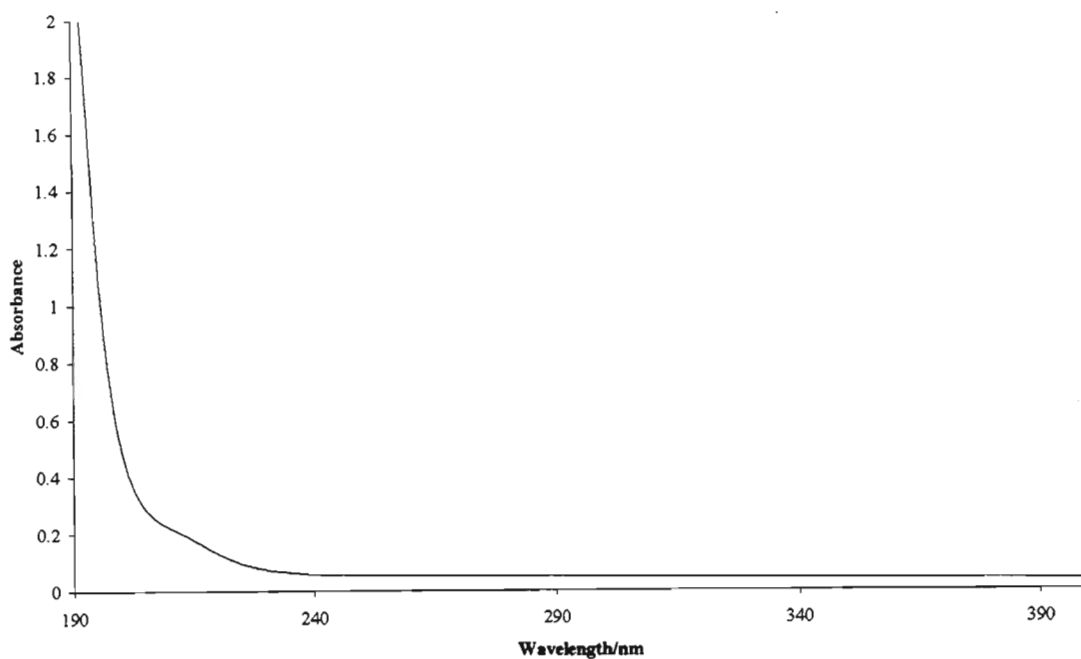
Figure 2.18:   The UV absorption spectrum of methanol measured in a 1 mm pathlength quartz cuvette.
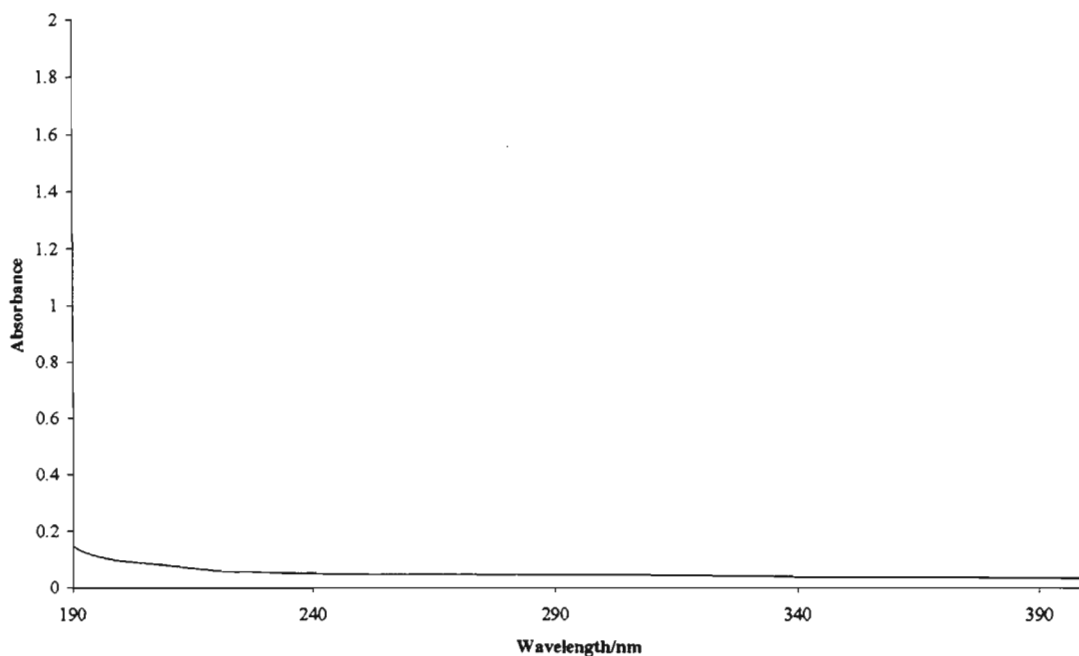
Figure 2.19:   The UV absorption spectrum of Millipore water measured in a 1 mm pathlength quartz cuvette.

2.4.2.1 Solvent photostability

It is crucial to investigate the photostability of the solvent so as to determine whether the solvent masks or influences the photostability of a chemical absorber. Photo-unstable solvents can photodegrade to produce reactive chemical species that can react with the absorber. Consequently, the absorber is observed as being photo-unstable whereas the photo-instability is that of the solvent. The photostability of the following solvents: cyclohexane, ethyl acetate and DMSO, was investigated by irradiating them with light of wavelengths greater than 300 nm in a 1 mm pathlength quartz cuvette. All UV spectra were obtained with the Perkin Elmer Lambda 35 UV/VIS spectrophotometer. The UV spectra of these irradiated solvents are displayed in Figures 2.20, 2.21, 2.22, 2.23 and 2.24 for cyclohexane, ethyl acetate, DMSO, methanol and Millipore water respectively. All solvents in this work can be regarded as photostable for a total irradiation period of 5 hours.
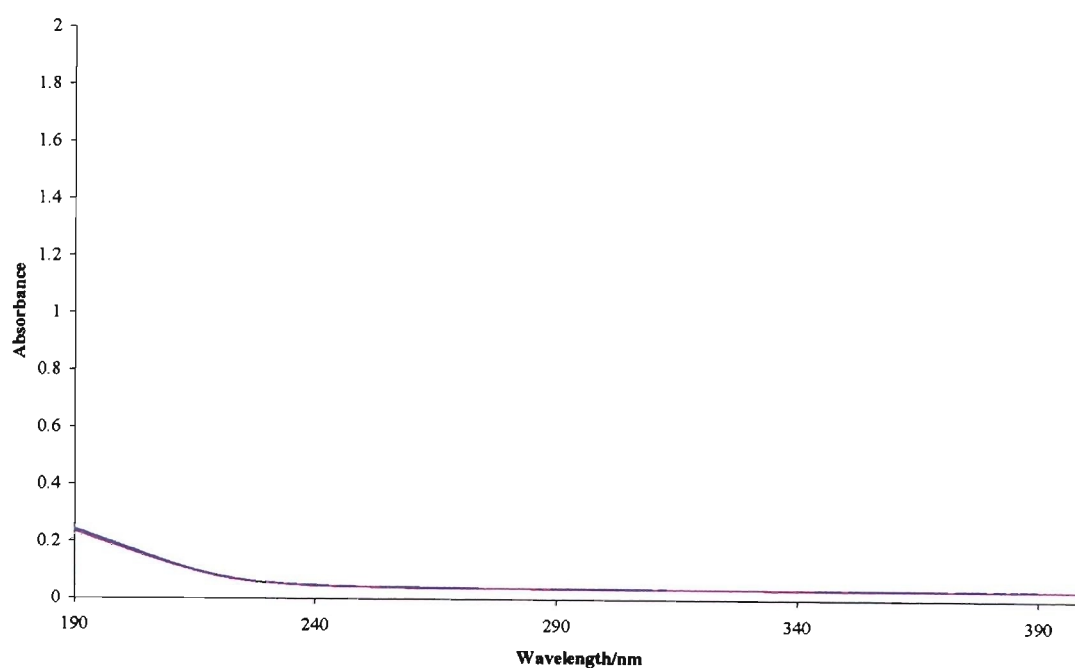
Figure 2.20:   The UV spectra of cyclohexane obtained at one hour irradiation intervals for a total irradiation period of 5 hours. The spectra were acquired in a 1 mm pathlength quartz cuvette against air in the reference beam.
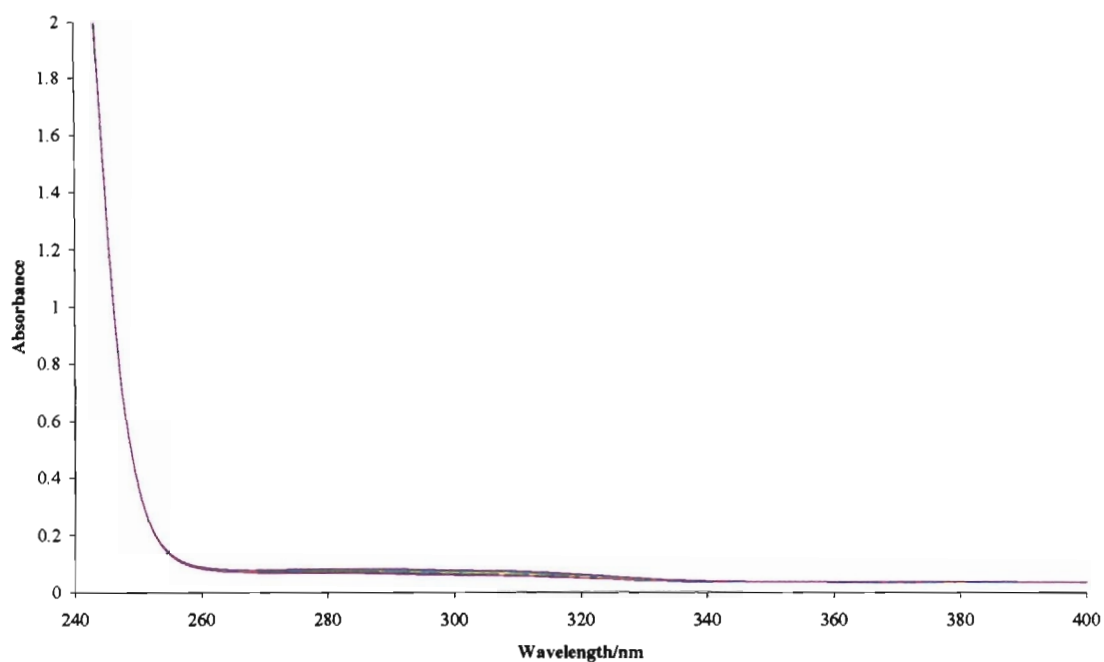
Figure 2.21:   The UV spectra of ethyl acetate obtained at one hour irradiation intervals for a total irradiation period of 5 hours.   The spectra were acquired in a 1 mm pathlength quartz cuvette against air in the reference beam.
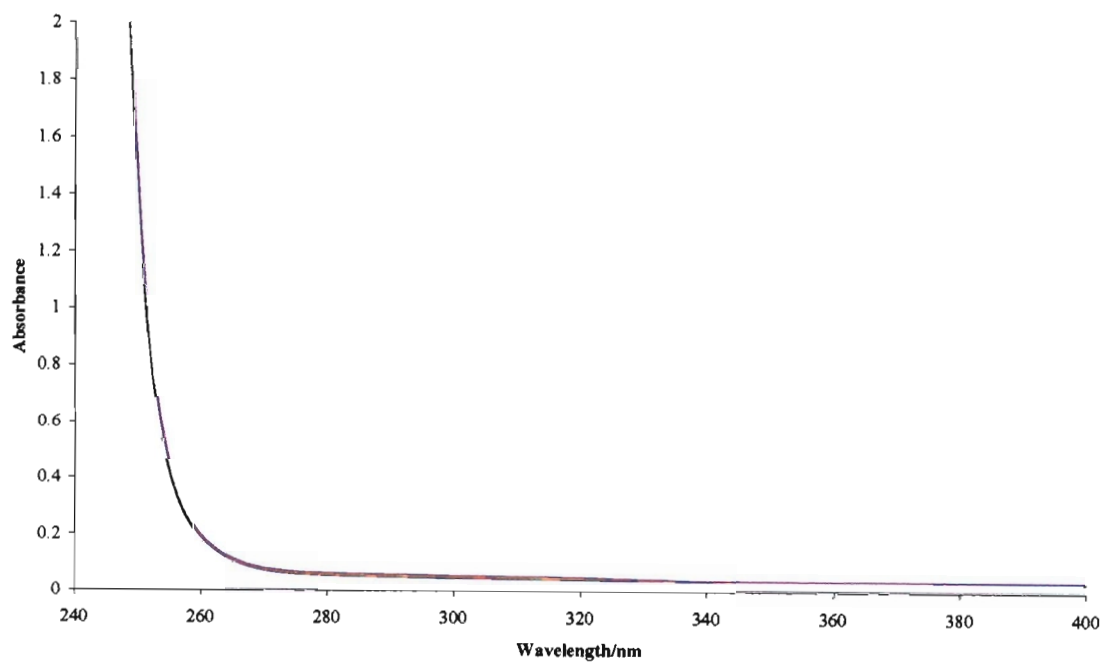
Figure 2.22:   The UV spectra of DMSO obtained at one hour irradiation intervals for a total irradiation period of 5 hours. The spectra were acquired in a 1 mm pathlength quartz cuvette against air in the reference beam.
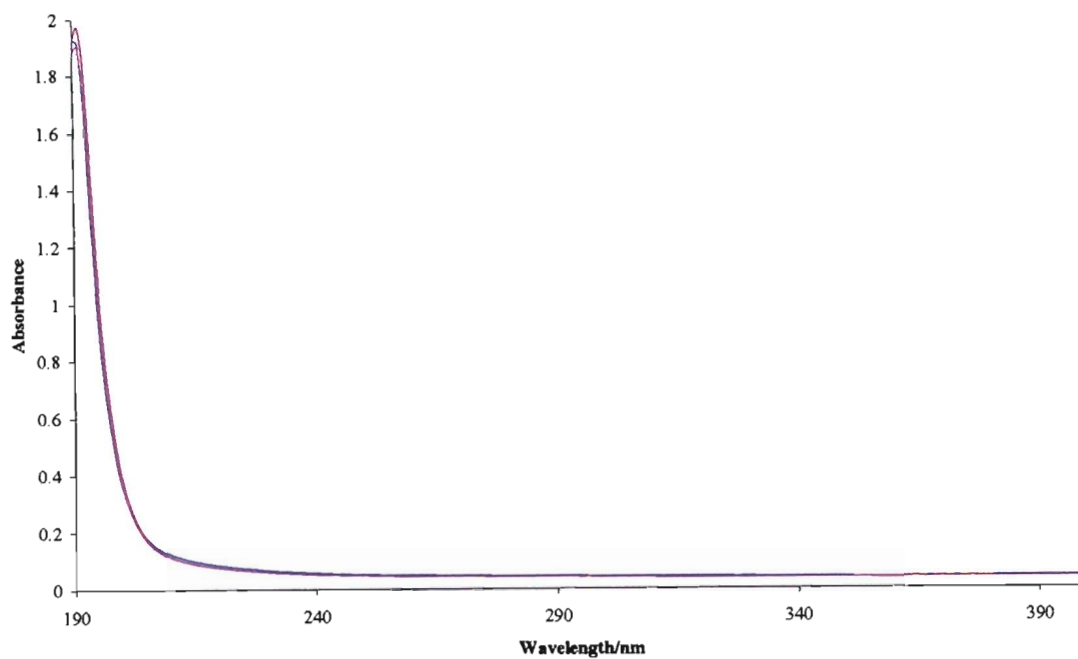
Figure 2.23: The UV spectra of methanol obtained at one hour irradiation intervals for a total irradiation period of 5 hours. The spectra were acquired in a 1 mm pathlength quartz cuvette against air in the reference beam.
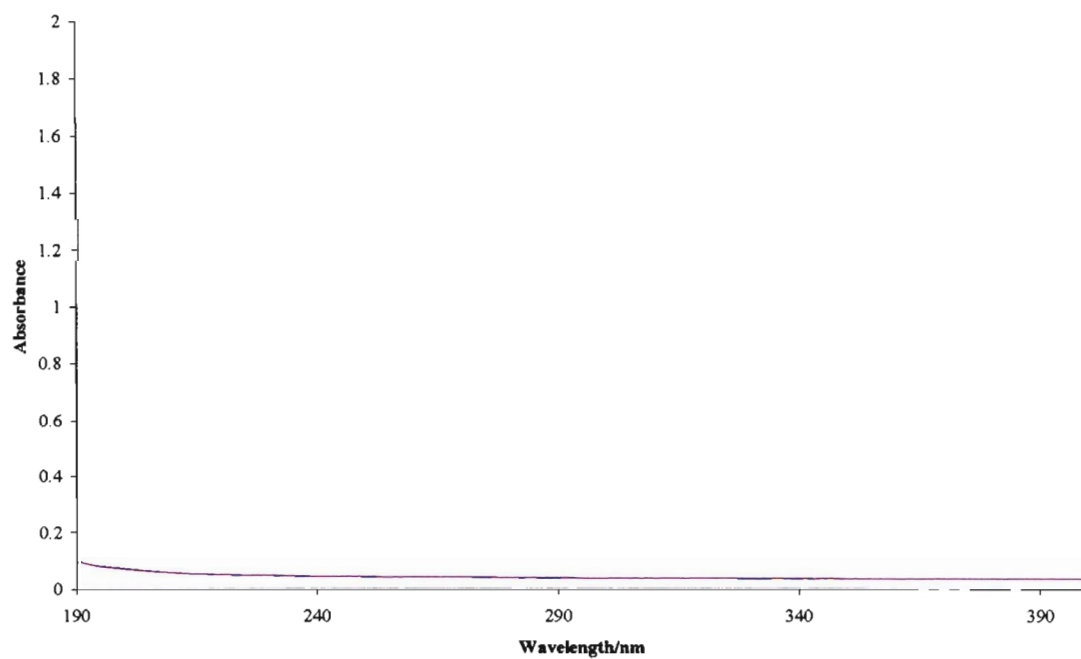
Figure 2.24: The UV spectra of Millipore water obtained at one hour irradiation intervals for a total irradiation period of 5 hours. The spectra were acquired in a 1 mm pathlength quartz cuvette against air in the reference beam.

2.4.3 Sample preparation for UV absorption spectroscopy

Solutions of the chemical absorbers were prepared from 1×10^{-3} M stock solutions made up by mass in the different solvents. The stock solutions were serially diluted to make solutions of appropriate concentrations, such that their absorbance readings at maximum wavelength fell below 2. These solutions were irradiated for set time intervals and their UV spectra obtained after each irradiation period. Those chemical absorbers that photodegraded were further investigated with the antioxidant polyphenolic extracts of Cancer Bush leaves as well as the extracts of various Rooibos teas. Mixtures of each photodegrading chemical absorber with the appropriate extract were prepared and irradiated. The absorbance of the mixture at the wavelength of maximum absorption of the chemical absorber was kept below 2. The results of the photostability analyses by UV absorption spectroscopy of various chemical absorbers with and without appropriate Cancer Bush extracts are reported and discussed in Section 3.2 and 3.3.2.1.

For the chemical absorber avobenzone absorption measurements of oxygenated and deoxygenated samples were performed in order to investigate the mechanisms of photodegradation and photostabilisation. Samples were deoxygenated by flushing with nitrogen gas, which had previously passed through a Dreschel bottle (Figure 2.25) containing only the solvent. This ensured that the nitrogen was pre-saturated with the solvent and therefore did not evaporate the solution.
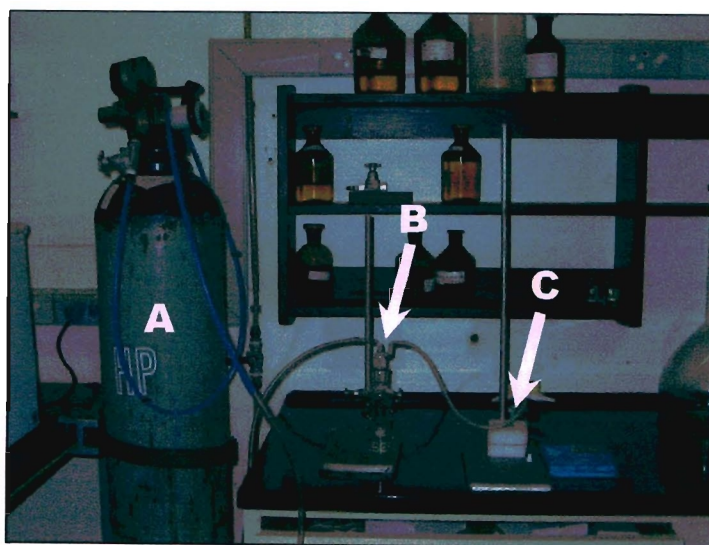
Figure 2.25:   Set-up for deoxygenating samples with nitrogen gas. The nitrogen gas (A) was presaturated by passing it through a Dreschel bottle (B) containing only solvent and then flushed through the sample (C).

The cuvette containing the sample to be deoxygenated was stoppered with a silicone rubber septum which had a syringe inlet to introduce the nitrogen gas and a very small outlet to prevent pressure building up in the cuvette.

The photostability investigations of avobenzone in ethyl acetate and DMSO were conducted in a 1 cm pathlength glass cuvette. The UV absorbance of avobenzone in ethyl acetate was measured at 356 nm before irradiation, and after 1, 2, 4, 8, 16 and 32 minutes of irradiation. The UV absorbance of avobenzone in DMSO was measured at 363 nm before irradiation, then subsequently after each 10-minute irradiation interval for a total duration of 40 minutes. The avobenzone solution in cyclohexane was irradiated in a 1 mm pathlength quartz cuvette. The UV absorbance of avobenzone in cyclohexane was recorded at 351 nm before irradiation, and after 10, 20, 30 and 60 minutes of irradiation. The absorbance measurements for the photostability of the absorber in the various solvents were conducted both in the presence and in the absence of oxygen. The photostability of the avobenzone solutions in the absence of oxygen were then compared at an irradiation time where an adequate loss in absorption of these solutions was observed in the presence of oxygen. All absorbance reading readings were obtained with the Perkin Elmer Lambda 35 UV/VIS spectrophotometer. The results of the photostability analyses for these deoxygenated solutions of avobenzone in the various solvents are reported and discussed in Section 3.3.1.2.

2.5 High-performance liquid chromatography

The photostability of the chemical absorber, avobenzone, and the efficiency of the various methods utilised to extract antioxidant polyphenols from the Cancer Bush plant had to be analysed appropriately. Both the Cancer Bush extracts and avobenzone photoproducts contain a mixture of materials; hence they required a chromatographic method of separation. High-performance liquid chromatography (HPLC) was considered as the appropriate technique for separating and identifying the different substances in these mixtures.

2.5.1 An introduction to the theory and instrumentation of HPLC

Liquid chromatography involves separating a mixture by using two phases. The two phases are referred to as the mobile phase (since it moves) and the stationary phase (since it is motionless). The mobile phase and the stationary phase differ in polarity. In normal operation, the mobile

phase moves through the stationary phase carrying with it the liquid sample. The solutes in the sample vary in polarity and, as the mobile phase passes, they are retained differently by the stationary phase. Subsequently, the solutes are detected separately depending on the time it took for them to reach the detector. The weakly retained solutes reach the detector faster than the strongly retained solutes.

The particle size of the stationary phase has been extremely reduced in order to increase the efficiency of chromatographic columns. This decrease in particle size has led to instruments needing much higher pumping pressures in order to obtain adequate flow rates. These instruments requiring higher pressures are referred to as high-performance liquid chromatographs.

A typical HPLC instrument has the following components: a mobile phase reservoir, an injector, a guard column, a column, a detector and a data system.

The mobile phase is normally in a glass bottle where it is sparged (degassed by an inert gas) to remove dissolved gases. Dissolved gases lead to bubbles in the column which result in band broadening. These gases can also affect the normal functioning of the detector (Skoog *et al.* [2004c]). The mobile phase is pumped to the injector where it carries the sample through the guard column. The guard column removes dust and other contaminants from the mobile phase, making the column last longer. The mobile phase then passes through the column and detector into a waste bottle reservoir. The HPLC instrument used in this research is illustrated in Figure 2.26.

The HPLC instrument used for this research consisted of a Perkin Elmer series 200 autosampler, a Waters 600 multisolvent delivery system, a Waters 996 photodiode array detector (PDA) linked to a De'Mark Pentium II computer where the results were analysed by the Waters Millennium Version 4.00 software.

Figure 2.26:   The high-performance liquid chromatograph (HPLC) used in this research.

All samples were filtered through 0.45 μm Millex syringe filters and solvents were filtered through 0.45 μm Durapore membrane filters before being used in the HPLC. Helium gas was used to sparge the mobile phase prior to use. The solvent flow rate was increased gradually to 1 ml min^{-1} before injection. The HPLC instrument was then primed (removing some of the solvent in the system) to remove dissolved gases in the solvent so as to keep the pressure in the system constant. Once the pressure reading was more or less constant, a 10 μl aliquot of the sample was injected by means of the autosampler into the HPLC. The sample was carried through the HPLC by the mobile phase, passing through a Waters Guard-Pak μ-Bondapak C18 column before entering the analytical column.

The samples to be analysed by HPLC were largely non-polar, hence a reverse phase separation method was employed with a non-polar stationary phase and a polar mobile phase. The analytical column used was a non-polar Nucleosil 100 C18 (18-carbon alkyl group attached to the surfaces of silica particles) column of 250 mm length, 4.6 mm internal diameter and 5 μm particle size. This column had previously been used successfully by Panday [2002] for the analysis of avobenzone.

The analytical column was cleaned and conditioned prior to use by running the following gradient through it at 1 ml min^{-1}: Millipore water for 30 minutes, Millipore water to methanol changed linearly over 5 minutes, methanol for 30 minutes, methanol to acetonitrile changed linearly over 5 minutes, acetonitrile for 30 minutes, acetonitrile to tetrahydrofuran changed linearly over 5 minutes and tetrahydrofuran for 30 minutes. The whole gradient was then

repeated in reverse order. The column was then equilibrated by passing five times the column volume of the eluent to be used before analysing the samples.

The Waters 600 multisolvent delivery system was programmed to control the sparging of solvents in the different solvent bottles, and the composition and flow rate of the mobile phase to be used in different runs through the HPLC.

The photodiode array detector detected the components of the sample coming out of the column. The detector required a 1 hour warm-up period for the lamp to function optimally, and the components of the sample were detected based on their absorption abilities at a particular wavelength. This meant the larger the absorptivity of a solute, the larger its peak area in the chromatogram. Peak areas were determined by integrating the area covered by the peak using the Waters Millennium Version 4.00 software. The wavelength of detection was changed based on the material being eluted. The extracts of the Cancer Bush leaves and Rooibos teas were analysed at 272 nm whereas avobenzone was sometimes detected at 350 nm close to its wavelength of maximum absorption.

2.5.2 HPLC elution methods and techniques

When the solvent composition remains the same throughout a run in the HPLC, this is referred to as isocratic elution. A solvent composition of 85:15% (v/v) methanol:Millipore water was used for the isocratic analysis of avobenzone photoproducts obtained after irradiation in different solvents (see Section 3.3.1.4). Panday [2002] successfully used the same isocratic elution for monitoring avobenzone and 2-ethylhexyl-p-methoxycinnamate (EHMC).

In order to quantify the amount of avobenzone that had photodegraded (see Section 3.3.1.4), a calibration curve of avobenzone concentration against peak area was developed. A stock solution of 1×10^{-2} M avobenzone was prepared by mass in a 25 ml volumetric flask and this was serially diluted by the autosampler to various concentrations in HPLC vials. Each of these solutions of different concentration was injected into the HPLC. Table 2.4 lists the avobenzone concentrations used and the corresponding peak area values obtained, and Figure 2.27 shows the corresponding calibration curve.

Table 2.4:   Peak areas of 10 μl aliquots of different concentrations of avobenzone injected into a C18 Nucleosil 100 column with an isocratic mobile phase of 85:15% (v/v) methanol:Millipore water at a flow rate of 1 ml min^{-1}, and detected at a wavelength of 350 nm.

Concentration/ 10^{-4}M	Peak Area/10^5 μV s			Standard deviation
	Trial 1	Trial 2	Average	
101	1797	1810	1804	9.20
50.5	974.9	985.0	980.0	7.14
25.3	466.3	480.0	473.2	9.69
12.6	219.2	210.0	214.6	6.51
6.31	97.89	102.8	98.85	3.47
3.16	53.66	50.01	51.84	2.58
1.58	23.01	24.61	23.81	1.13
0.789	11.85	12.19	12.02	0.24
0.395	4.919	5.132	5.026	0.15

$y = 18.168x + 0.1106$
$R^2 = 0.9982$
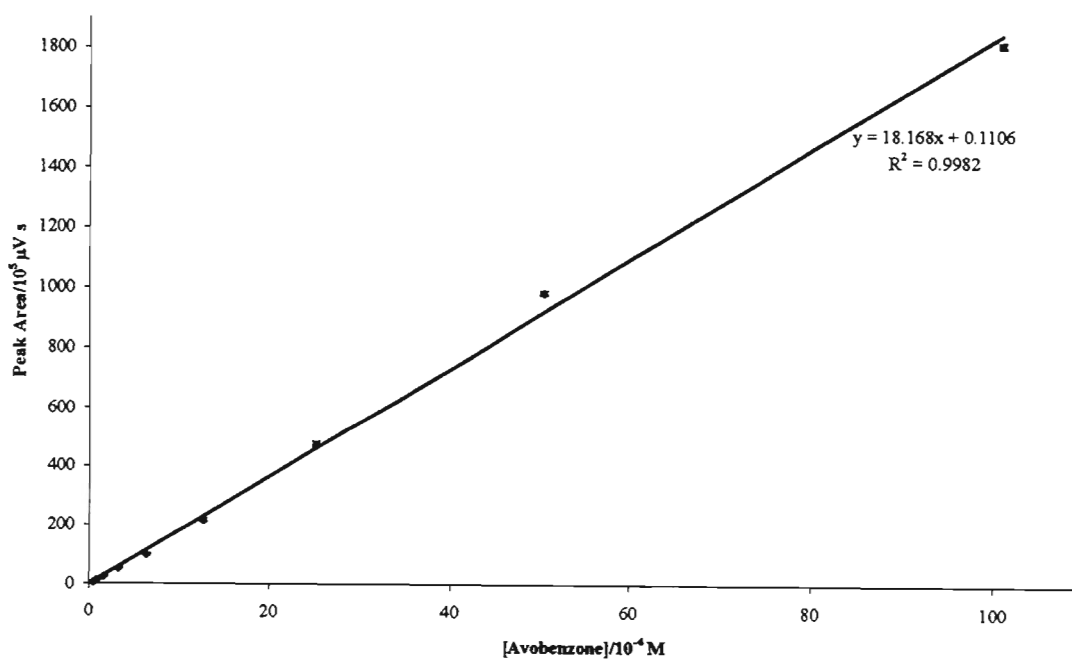
Figure 2.27:   Calibration curve of avobenzone obtained on the Nucleosil 100 C18 column using an isocratic mobile phase of 85:15% (v/v) methanol:Millipore water at a flow rate of 1 ml min^{-1}, and a detection wavelength of 350 nm.

When one solvent does not satisfactorily elute all the solutes to reach the detector in reasonable time, other solvents are employed to carry the solutes so they come out much earlier. When the composition of the mobile phase changes continuously, or in a stepwise manner between different solvents, during an HPLC run, the technique is referred to as gradient elution.

The separation of the Cancer Bush polyphenols required gradient elution. The gradient elution program employed was adopted from Zuo *et al.* [2002] in the analyses of green, Oolong, black and pu-erh teas. The mobile phase was set at a flow rate of 1 ml min^{-1} with 100% solvent A (97:3% (v/v) Millipore water:acetic acid) for 1 minute. The solvent composition was changed linearly to 33:67% (v/v) solvent A:solvent B (methanol) in 27 minutes then back to 100% solvent A in 2 minutes. The gradient elution program was modified depending on the resolution of peaks in the final chromatogram. The adapted gradient started with 100% solvent A for 1 minute then linearly changed to 37:63% (v/v) solvent A:solvent B in 56 minutes and reverted back to 100% solvent A for up to 70 minutes to make sure all compounds eluted. Both the adapted and adopted gradient elution programs were used to obtain HPLC chromatograms displayed and discussed in Sections 3.1.1.2 and 3.1.1.3.

In order to quantify the amount of the polyphenol rutin possibly present in the ethanol-water Cancer Bush extract (see Section 3.1.2.1), a calibration curve of rutin concentration against peak area was acquired. A mass of 0.0154 g of rutin was dissolved in methanol and made up to 25 ml in a volumetric flask to make a 1.01×10^{-3} M stock solution. This stock solution was serially diluted using the HPLC autosampler to prepare various concentrations of rutin as shown in Table 2.5. A 10 µl aliquot of each concentration was eluted through the Nucleosil 100 C18 column using the adopted gradient method from Zuo *et al.* [2002] to elute the extracts. A rutin calibration curve of peak area against rutin molarity was plotted for detection wavelengths of both 272 nm and 350 nm (as shown in Figures 2.28 and 2.29). These detection wavelengths were chosen since the Cancer Bush and Rooibos tea extracts were monitored at 272 nm whereas rutin absorbs maximally at around 350 nm.

Table 2.5:   Peak areas of the different concentrations of rutin injected onto a Nucleosil 100 C18 column and eluted with a gradient mobile phase adopted from Zuo *et al.* [2002]. Detection was monitored at both 272 nm and 350 nm.

Rutin concentration /10^{-5} M	Peak Area at 350 nm/10^4 µV s			Peak Area at 272 nm/10^4 µV s			Standard deviation	
	Trials		Average	Trials		Average	350 nm	272 nm
	1	2		1	2			
50.5	557.0	569.6	563.3	475.6	488.4	482.0	8.9	9.0
25.3	267.5	280.7	274.1	231.0	241.6	236.3	9.3	7.5
12.6	120.6	123.0	121.8	103.1	103.8	103.45	1.7	0.49
6.31	54.95	52.10	53.53	47.43	45.47	46.45	2.02	1.39
3.16	29.30	26.24	27.77	24.18	21.67	22.93	2.16	1.77
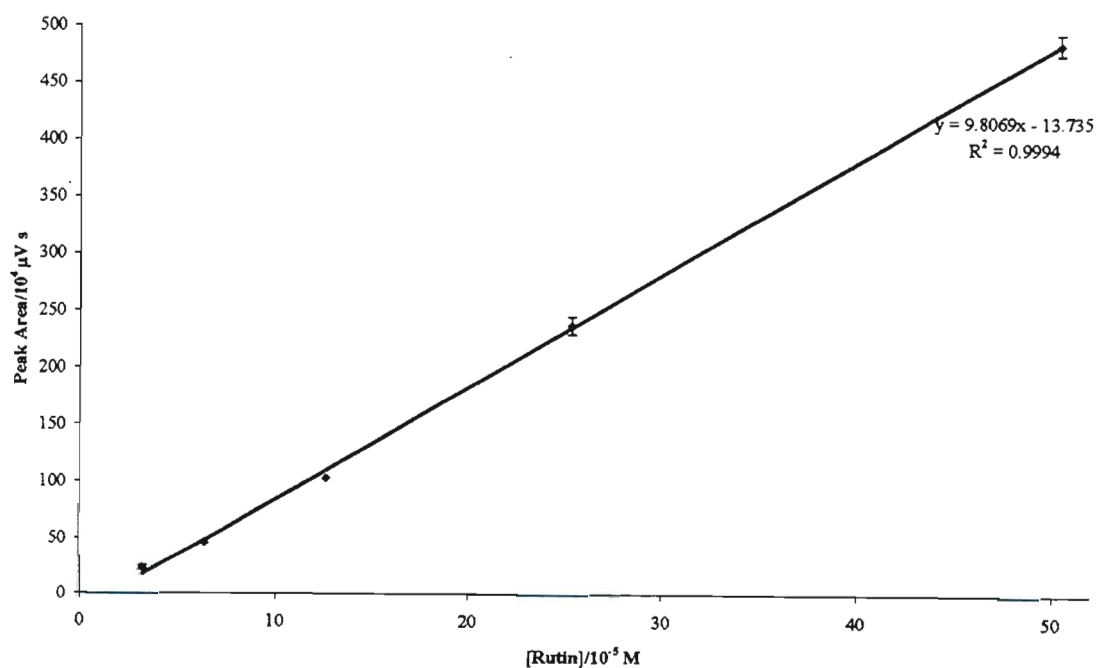
Figure 2.28:   Calibration curve of rutin obtained when different concentrations of rutin were eluted through a Nucleosil 100 C18 column using an adopted gradient method from Zuo *et al.* [2002]. The wavelength of detection was 272 nm.
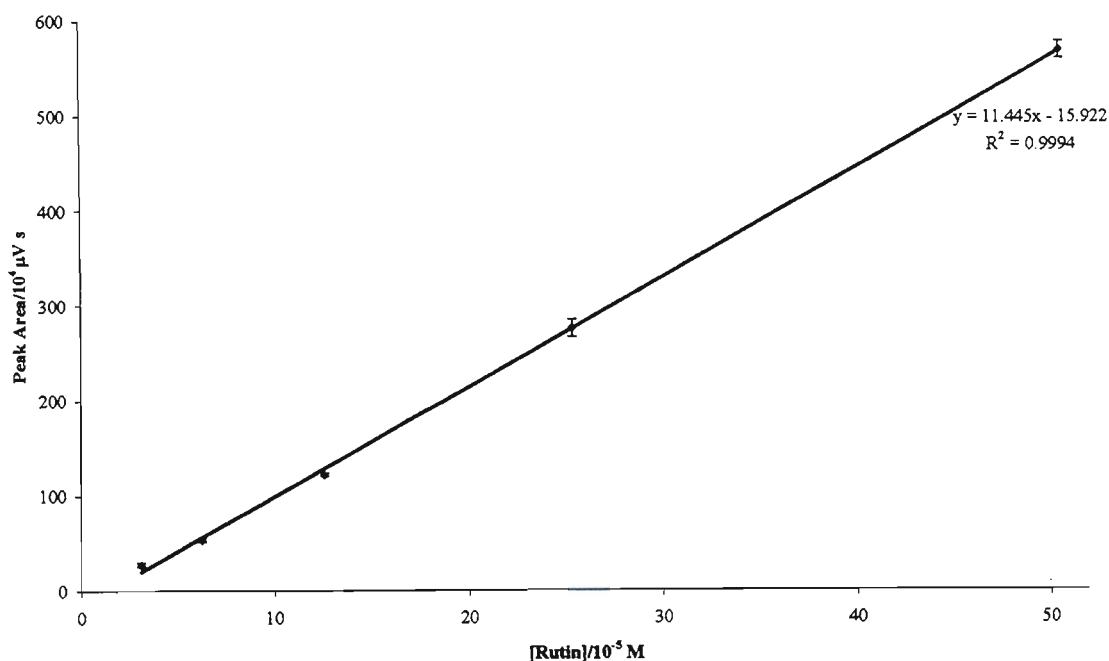
Figure 2.29:   Calibration curve of rutin obtained when different concentrations of rutin were eluted through a Nucleosil 100 C18 column using an adopted gradient method from Zuo *et al.* [2002]. The wavelength of detection was 350 nm.

2.6   Gas chromatography

HPLC investigations were inadequate for characterising the components of the Cancer Bush extracts due to the lack of standards for each substance present in the mixtures. The components of the ethanol-water Cancer Bush extract were therefore analysed by GC-MS since this method does not require standards as it is based on the fragmentation patterns of each constituent. Before GC-MS analysis was performed, the extracts were analysed by more accessible GC instruments in order to insure appropriate derivatisation techniques and temperature programs.

2.6.1   An introduction to the theory and instrumentation of GC

In gas chromatography, the mobile phase is a gas and the stationary phase can either be a liquid or a solid. When the stationary phase is a liquid, the GC method is referred to as gas-liquid chromatography and when it is a solid it is called gas-solid chromatography.

In gas-liquid chromatography, the liquid stationary phase is adsorbed or chemically bonded to the surface of the column inner wall, or to the surface of any other type of packing used. When the sample is vaporized, it is carried by an inert gas (mobile phase) through a liquid stationary phase, where the solutes are separated, then detected by an appropriate detector. All GC instruments used in this research employed a gas-liquid chromatographic method of separation, which is commonly referred to as gas chromatography.

A gas chromatograph (Figure 2.30) consists of a carrier gas (mobile phase) supply, a flow regulator, a sample injector, an injection chamber, an appropriate column, an oven, a detector and a data processor.

The carrier gas is the gaseous mobile phase that carries the sample without interaction in the GC. The carrier gas has to be an inert gas so as to prevent modifying the sample. The most common gases used in GC instruments are helium, argon, nitrogen and hydrogen gas (Skoog *et al.* [2004d]). In this study, nitrogen was always used as the carrier gas. The carrier gas is released from a tank and passes through a flow-controlling pressure regulator which sets the flow rate before it enters the instrument.
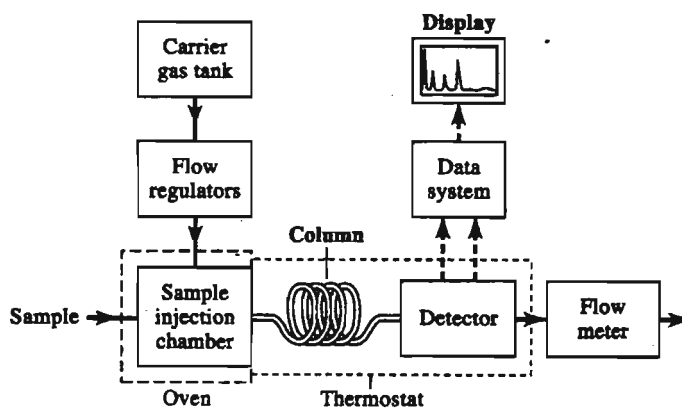
Figure 2.30:   A diagram of the different components of a gas chromatograph (Skoog *et al.* [2004d]).

A sample of suitable size and discrete amount is injected and evaporated in the sample injection chamber and is carried by the carrier gas into the column. Capillary columns require low carrier gas flow rates hence minimal injection volumes are used to prevent column overload. Split injection can be employed to split the sample volume so only a certain amount reaches the

column. Splitless injection (without splitting the sample) was the only method employed during injection in the GC instruments used in this work.

Capillary columns are open tubular columns with a liquid stationary phase of high boiling point coated on the inner walls of the tube. In comparison to packed columns, open tubular columns increase the gas-liquid surface area, increasing adsorption and column efficiency (Perry [1981]). Column efficiency is greatly determined though by the amount injected and the method of injecting the sample. In the column, the sample solutes are separated by partition (between the mobile phase and the stationary phase) or adsorption chromatography into the stationary phase (Schwedt [1997]). This distribution is temperature dependent implying there is a correlation between the vapour pressures of the solutes in the sample and their retention times in the GC (Schwedt [1997]). Therefore, sample separation depends upon the stationary phase and the temperature(s) employed during separation.

There are different types of detectors that can be used in gas chromatography. These include: flame ionization detectors (FID), thermal conductivity detectors (TCD) and mass spectrometry detectors. The most important features of a detector are sensitivity and reproducibility.

A flame ionisation detector (Figure 2.31) is best suited for the detection of hydrocarbons. The carrier gas transporting the sample emerges from the column and is mixed with hydrogen, then directed to an air-hydrogen flame. Organic compounds produce ionic species when burned in an air-hydrogen flame, which conduct electricity and their current can be detected and measured. These ions are produced between two electrodes, an anode (the burner) and a cathode above the flame, and at a particular voltage they move towards their respective electrodes creating a measurable current. This current is monitored throughout the set run time and it is given out in the form of a chromatogram.

The two GC instruments employed in this research were the Perkin Elmer Autosystem XL (Figure 2.32) and the Fisons GC 8000 Series gas chromatography instrument (Figure 2.33). These instruments will be referred to as the PE Autosystem GC and the Fisons GC instrument, respectively. Both these instruments employed flame ionisation detectors.
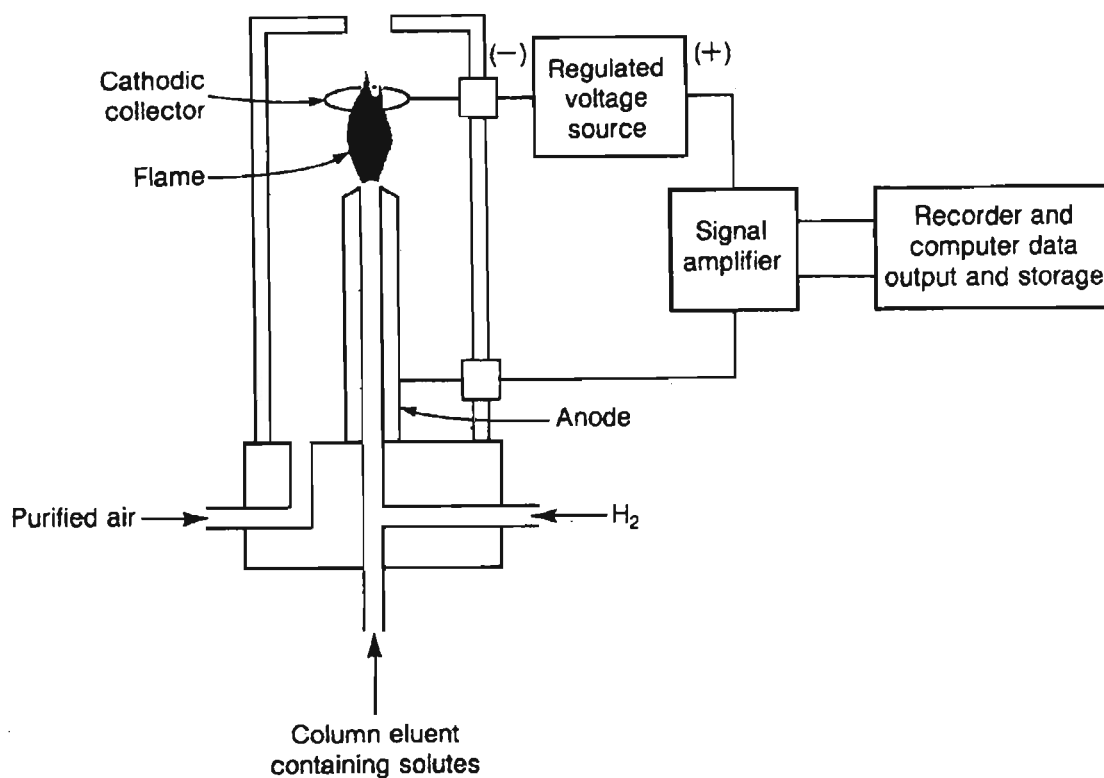
Figure 2.31:   A diagram of the flame ionisation detector showing how the sample ends up between the two electrodes (Manahan [1986]).

Figure 2.32:   The Perkin Elmer Autosystem XL gas chromatograph.

Figure 2.33:   The Fisons GC 8000 Series chromatograph.

2.6.2 Sample preparation and GC operation

The analyte has to be appropriately prepared before being injected through the GC column for GC analysis. Suitable sample preparation depends on the type of compounds being analysed (see Section 2.6.2.1) and the subsequent GC analysis requires proper operation of the GC instrument (see Section 2.6.2.2).

2.6.2.1 Sample preparation

Analytes are derivatised prior to GC injection in order to improve their volatility or develop their chromatographic features by reducing their polarity and/or increasing detector sensitivity towards them (Wells [1999]).

GC analysis with non-polar columns was employed to characterise the constituents of the ethanol-water Cancer Bush extract. The extract was expected to be rich in polyphenolic substances, which meant a derivatising procedure was required in order to reduce their polarity and increase their volatility. The first derivatising procedure employed was from Pierce *et al.* [1969]. In this procedure, the volume of solvent and silylating agent was too high for detection

of the extract constituents by GC, and the reaction temperature too low for effective derivatisation. An effective derivatising method was adapted from the GC-derivatising procedures of Regis Technologies (Regis Technologies [accessed on 15th October 2003]). The extract was kept in the dark prior to derivatisation to avoid polymerisation of some phenolics when exposed to light. The extract was further dried by means of a rotavapor to completely remove all moisture - potential competition of water with polyphenolic hydroxyl groups during derivatisation reduces the efficiency of the process. A 10-50 mg sample of the ethanol-water Cancer Bush extract was then weighed and placed in a relatively small vessel together with 100 μl each of pyridine (solvent) and silylating reagent. The vessel was closed and heated to 65 – 70 °C in an oil bath for 25 minutes. A portion of the derivatised sample was injected into the GC. The silylating agents used were bis(trimethylsilyl)acetamide, BSA (Pierce *et al.* [1969] and Klebe *et al.* [1966]) and bis(trimethylsilyl)trifluoroacetamide, BSTFA (Stremple [1996], Donovan *et al.* [1999] and Helaleh *et al.* [2001]).

2.6.2.2 GC techniques and operation

The FID flame has to be switched on both GC instruments prior to injection. In the Fisons GC instrument, this was done by pressing the ignition button on the instrument, after the hydrogen and air supply had been turned on for a few minutes, until a 'pop' sound was heard. With the PE Autosystem GC instrument, prior to ignition the air valve is turned off and the hydrogen left open. The air is slowly turned on until two 'pop' sounds are heard, then the air valve is quickly twisted to fully open the air supply.

A 1 μl sample volume was injected manually each time, by using a 1 μl syringe through a silicone rubber septum. This process had to be fast and consistent in order to minimise errors in reproducing chromatograms. The sample enters the injection chamber where it is vaporized and carried by the carrier gas into the column. Both GC instruments used nitrogen as the gaseous mobile phase with a flow rate of 2 ml min^{-1}.

The column in the Fisons GC was a DB-5 capillary column with 30 m length, 0.25 mm diameter and a 0.25 μm thick film of stationary phase. This column was relatively non-polar comprising of bonded and cross-linked (5%-phenyl)-methylsiloxane stationary phase. The column used in the PE Autosystem GC was the Elite 5 capillary column with a length of 30 m, a diameter of 0.53 mm and a film thickness of 1.5 μm. This column was also relatively non-polar with crossbound 5% diphenyl-95% dimethyl polysiloxane.

Both GC instruments used Turbochrom Workstation Version 6.1 software to analyse samples and, in the case of the PE Autosystem GC instrument, this software was also used to set-up the chromatographic conditions.

2.6.3 Temperature programs for GC

Separation of analytes depends not only on the stationary phase but also on the temperature employed during a sample run in the GC. Solutes of different polarity have different retention times when an isothermal temperature procedure is used during separation. Since the derivatised Cancer Bush extract was expected to contain various polyphenolic substances of diverse polarity, temperature programming was essential for the complete elution of all the material. Temperature programming is the constant or stepwise changing of column temperature during a GC run.

The ethanol-water Cancer Bush extract derivatised by the Pierce *et al.* [1969] method was eluted through the DB-5 capillary column by a temperature program adapted from Luthria *et al.* [1997]. This involved the following temperature program: 100 °C held for 3 minutes, followed by an increase at 30 °C/minute to 260 °C, and maintaining 260 °C for 17 minutes.

The total run time was set at 30 minutes to insure complete elution of all components. The injector and detector zone were maintained at a temperature of 250 °C. The temperature program is illustrated in Figure 2.34.

This program proved to be unsuccessful in separating the derivatised phenolics present in the extract. A second derivatising technique (Regis Technologies [2000]) and temperature program from Soleas *et al.* [1997 and 1999] was adapted to accommodate the column's maximum temperature of 300 °C. The detector zone temperature was set at 295 °C to avoid condensation and the injector zone temperature was set at 280 °C to insure complete vaporization. The temperature program used was as follows: 60 °C held for 1 minute, an increase of 20 °C/minute to 280 °C, 280 °C held for 2 minutes, an increase of 6 °C/minute to 295 °C and a temperature of 295 °C maintained for 4 minutes.

The total run time was also set at 30 minutes for the run to finish way after the temperature program had ceased. The temperature program is depicted in Figure 2.35. This temperature program was used to obtain the gas chromatograms displayed and discussed in Section 3.1.2.2.

The gas chromatograms of pyridine alone and with BSA obtained with the Fisons GC, by using the adapted temperature programs from Soleas *et al.* [1997 and 1999] and Luthria *et al.* [1997], are displayed in Figures 2.36 and 2.37, respectively.
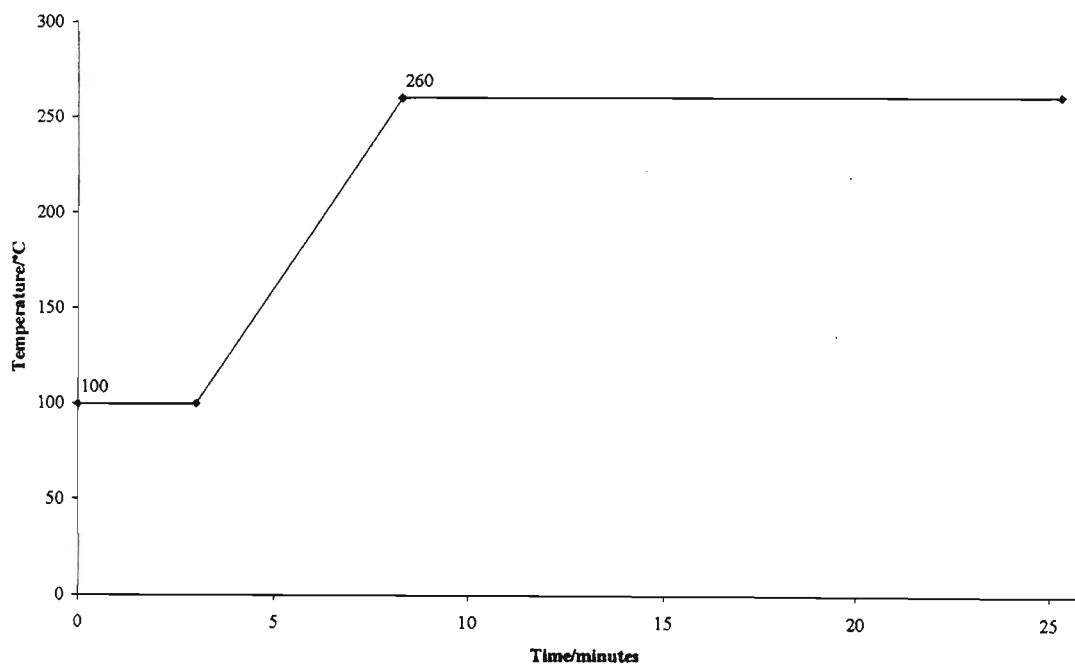
Figure 2.34: Temperature program adapted from Luthria *et al.* [1997] for separating the Cancer Bush extract with the Fisons GC instrument.
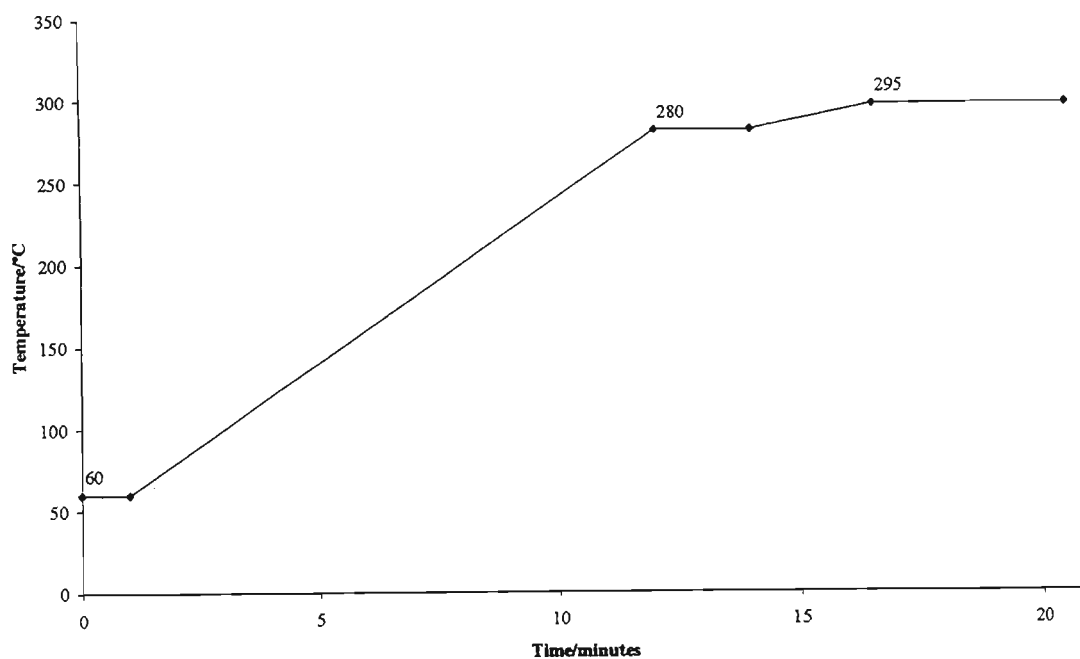
Figure 2.35: Temperature program modified from that of Soleas *et al.* [1997 and 1999] employed for separating the Cancer Bush extract with the Fisons gas chromatograph.
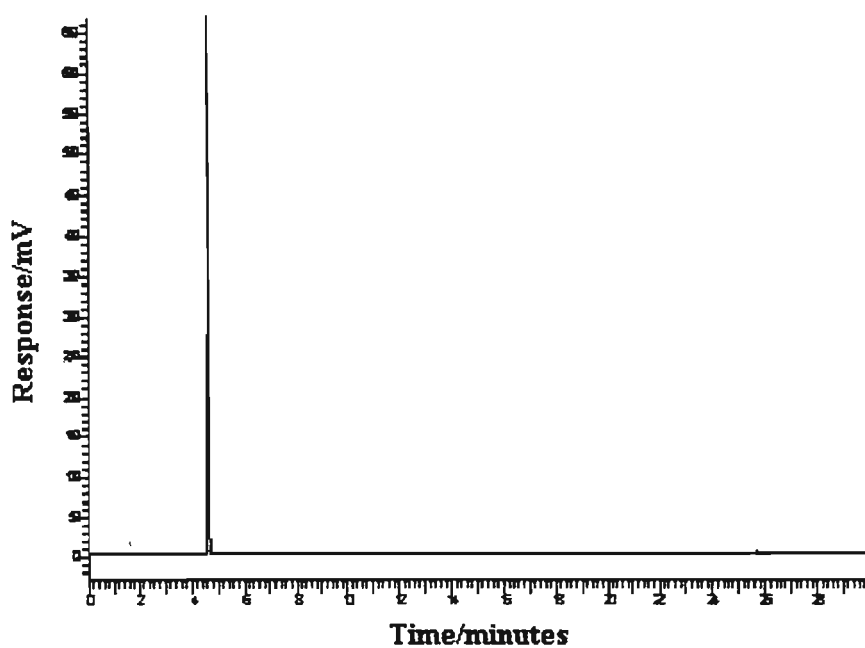
Figure 2.36: The gas chromatogram of pyridine alone obtained by the adapted temperature program of Soleas *et al.* [1997 and 1999] with the Fisons GC instrument. Pyridine elutes at about 4.6 minutes.

Time/minutes
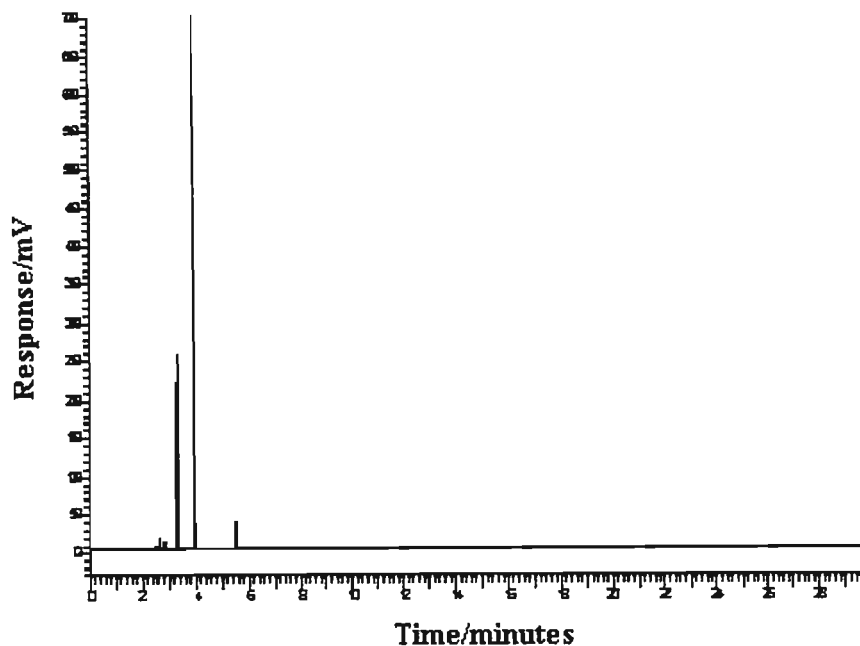
Figure 2.37: The gas chromatogram of BSA and pyridine obtained by the temperature program adapted from Luthria *et al.* [1997] with the Fisons GC instrument. BSA peaks occur at about 2.5 (2.5) minutes, 3.5 (3.8) minutes and 5.5 (6.4) minutes and pyridine elutes at about 4.0 (4.6) minutes with the values in brackets representing the retention times of the respective peaks with the modified temperature program of Soleas *et al.* [1997 and 1999].

The temperature program adapted from Soleas *et al.* [1997 and 1999] was also employed and modified for the Cancer Bush samples derivatised with BSA and BSTFA and analysed with the Perkin Elmer GC. The GC column used with this instrument has a maximum temperature of 330 °C and hence could not achieve the high temperature used by Soleas *et al.* [1997 and 1999]. The injector and detector temperatures were set at high temperatures to achieve complete vaporization and prevent condensation, respectively. The injector chamber temperature was set at 280 °C whereas the detector was set at 310 °C and the temperature program employed is illustrated in Figure 2.38 and was: 80 °C held for 1 minute, an increase of 20 °C/minute to 250 °C, 250 °C held for 1 minute, an increase of 6 °C/minute to 300 °C, 300 °C held for 2 minutes, an increase of 20 °C/minute to 310 °C and a final temperature of 310 °C held for 4 minutes. The total run time was 25.33 minutes.

The chromatograms of pyridine, BSA with pyridine and BSTFA alone obtained with the PE Autosystem GC instrument by using the adapted Soleas *et al.* [1997 and 1999] temperature program are shown in the Figures 2.39, 2.40 and 2.41, respectively. This temperature program was used to obtain the gas chromatograms displayed and discussed in Section 3.1.2.2.
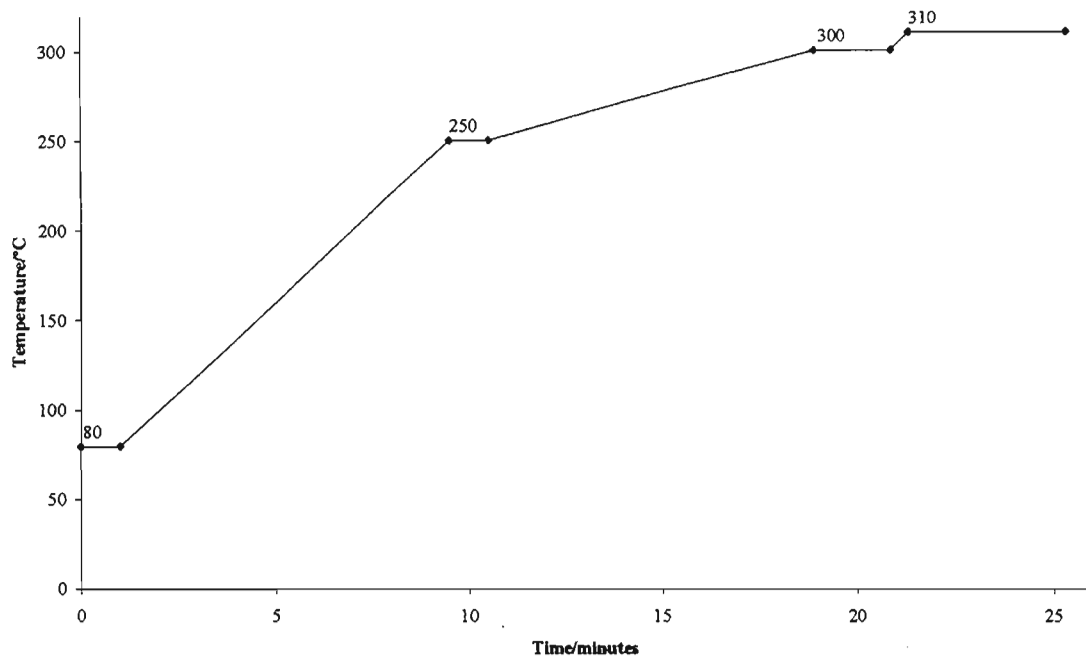
Figure 2.38:   Temperature program employed for separating the Cancer Bush extract in the PE Autosystem gas chromatograph.
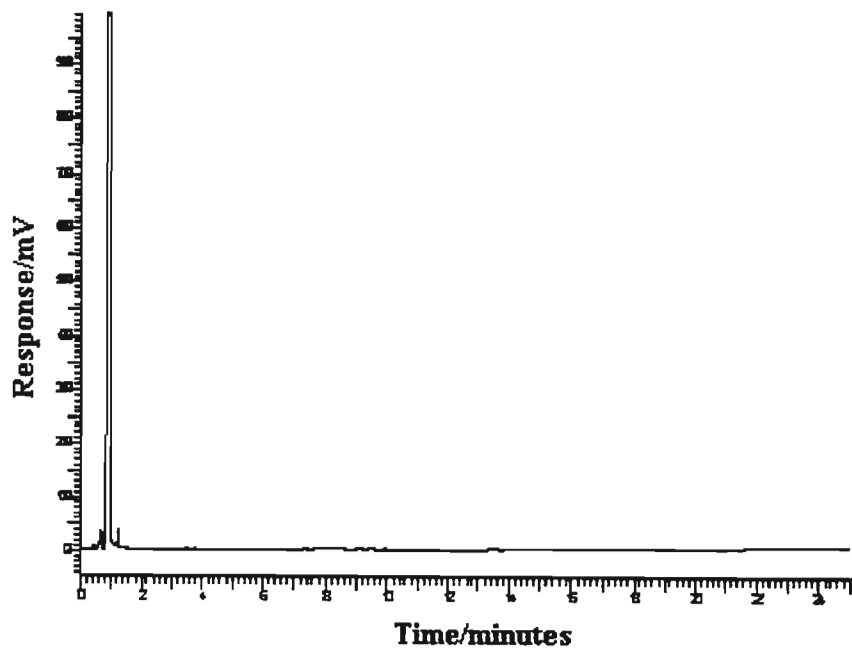
Figure 2.39:   Gas chromatogram of pyridine injected in the PE Autosystem GC instrument and separated by the adapted temperature program of Soleas *et al.* [1997 and 1999]. Pyridine eluted at about 0.4 minutes.
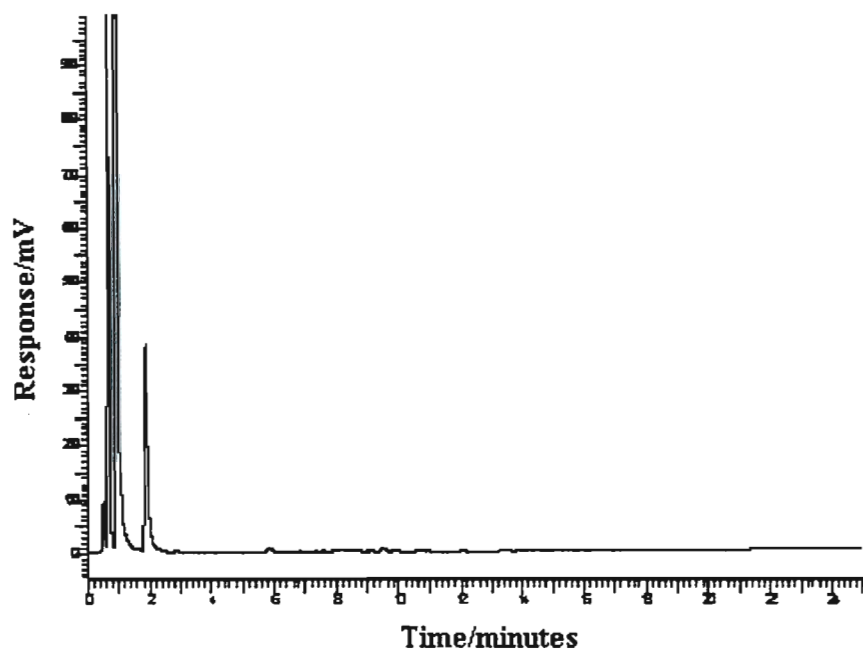
Figure 2.40: The gas chromatogram of BSA together with pyridine obtained with the PE Autosystem GC using the adapted temperature program of Soleas *et al.* [1997 and 1999]. Pyridine eluted at about 0.4 minutes and the rest of the peaks at 0.3 minutes and 2 minutes are due to the BSA agent.
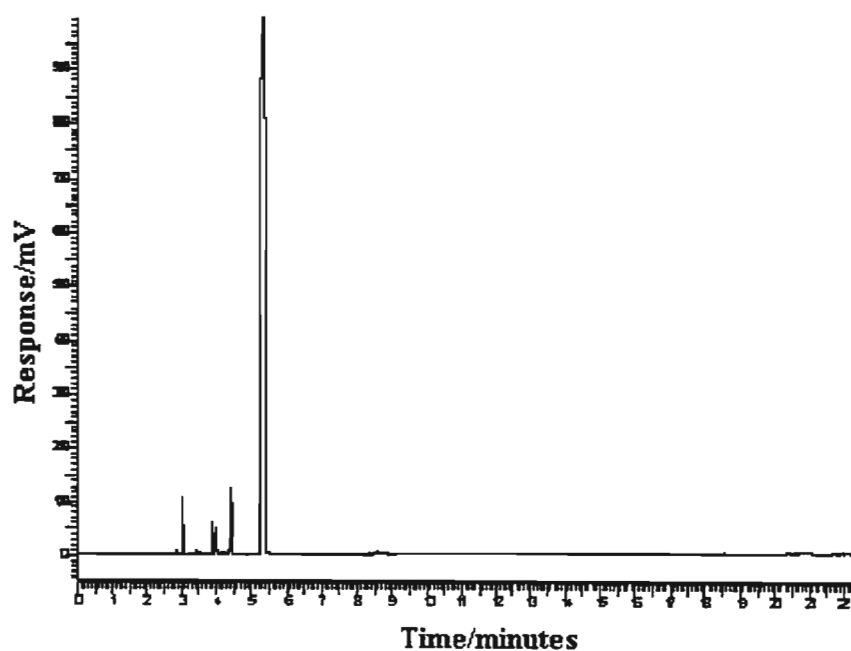
Figure 2.41: The gas chromatogram of BSTFA alone injected in the PE Autosystem GC and separated by the adapted temperature program from Soleas *et al.* [1997 and 1999]. All the peaks (at 3.0, 3.5, 4.0, 4.4 and 5.4 minutes) are due to BSTFA.

2.7 Gas chromatography-mass spectrometry

A gas chromatograph-mass spectrometry instrument combines a gas chromatographic method of separation (Section 2.6) and a mass spectrometric method of detection. This type of detection is based on the fact that each compound has a unique fragmentation pattern, and hence can be characterised. A mass spectrum illustrates the fragmentation of a compound as discussed in Section 2.7.1, and the temperature programs and GC-MS functioning are discussed in Section 2.7.2.

2.7.1 An introduction to the theory and operation of MS detectors

In mass spectrometry, compounds are ionized to molecular ions which are broken-up to produce fragment ions. The mass-to-charge ratios (m/z) of these ions along with their relative intensities are measured and the resulting fragmentation pattern is used to characterise the compound in the sample. Each ion has a m/z value that gives a single line signal whose intensity is proportional to the abundance of the ion. The ion with a m/z value equal to the molecular mass of the compound being investigated is called the molecular ion. The m/z signal of highest intensity is referred to as the base peak and designated 100% abundance. All other signals have abundances relative to that of the base peak. The final mass spectrum gives a plot of abundance against m/z ratio characteristic of the compound.

In a GC-MS, vaporized samples are introduced into the MS after having been separated in the GC. The sample entering the MS is ionized by an ionisation source, separated by an analyzer, based on the mass-to-charge ratios of the fragments, and detected by an ion detector.

2.7.2 GC-MS instruments, operation and temperature programs

Two GC-MS instruments were employed in this work for different analyses. The first GC-MS instrument consisted of an Agilent 6890 gas chromatograph coupled to an Agilent 5973 mass selective detector (see Figure 2.42). The GC-MS operation and data analysis were carried out by using the Agilent Enhanced ChemStation software (Version C.00.00) coupled with the National Institute of Standards and Technology MS library known as NIST98. This GC-MS instrument was used to analyse the ethanol-water Cancer Bush and plain Rooibos tea extracts as discussed in Section 2.7.2.1.

The second GC-MS (see Figure 2.43) contained a Hewlett Packard 6890 series GC system, an injector (with a 10 µl syringe) and a mass selective detector. The computer system used for analysing and producing mass spectral data contained the Standard Hewlett Packard ChemStation software (Version B.01.00) coupled with a Wiley library known as Wiley275. This GC-MS was used to investigate the photo-instability of avobenzone in various solvents and the method of analysis is discussed in Section 2.7.2.2.
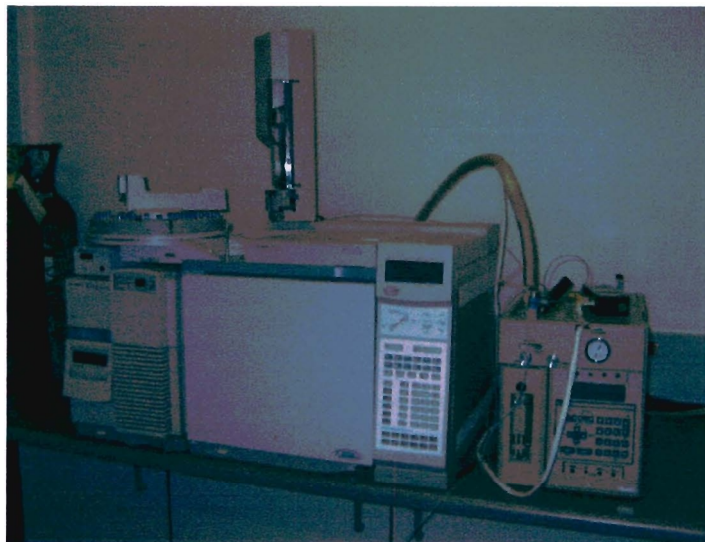
Figure 2.42:   The Agilent 6890 gas chromatography instrument coupled to an Agilent 5973 mass-selective detector.

Figure 2.43:   The Hewlett Packard 6890 gas chromatography instrument coupled to a Hewlett Packard 6890 mass-selective detector.

2.7.2.1 GC-MS analysis of the ethanol-water Cancer Bush and Rooibos tea extracts

The Agilent 6890 GC-MS instrument was used to characterise the derivatised polyphenols in the ethanol-water Cancer Bush and plain Rooibos tea extracts. A 1 μl aliquot of the sample was injected into the Agilent 6890 GC set at a 1:50 split mode ratio. The helium mobile phase carried the sample from the injector (at 250 °C) into a non-polar HP-5MS capillary column. The column consists of (5%-phenyl)-methylpolysiloxane stationary phase in a capillary of 30 metres in length, 250 μm diameter and 0.25 μm stationary phase film thickness. The HP-5MS column was chosen because its phase was similar to those of the two columns (DB-5 and PE-5 capillary columns) that were used to establish the GC separation method. The temperature program (see Figure 2.44) employed was: 50 °C held for 2 minutes, an increase of 20 °C/minute to 300 °C and 300 °C held for 10 minutes. This temperature program was used to obtain the GC-MS spectra displayed in Appendix C and discussed in Section 3.1.2.3.
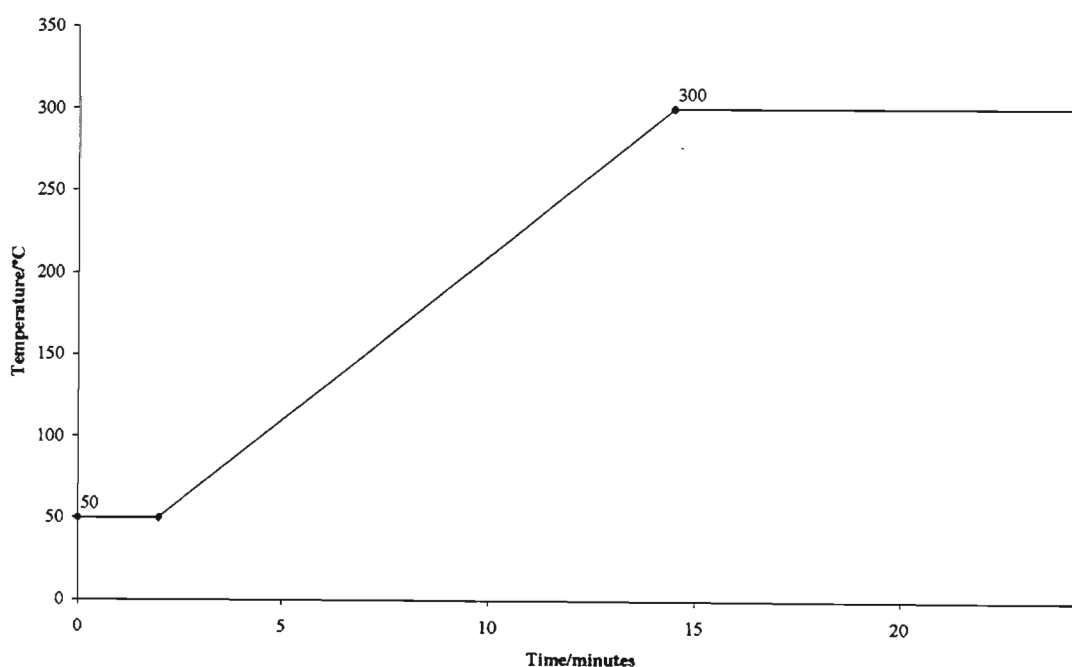
Figure 2.44:   Temperature program employed for separating the Cancer Bush extract in the Agilent 6890 gas chromatograph coupled to an Agilent 5973 mass-selective detector.

The separated vaporized sample reached an Agilent 5973 MS where an electron impact source (at 230 °C) ionized the sample. A quadrupole mass filter at 150 °C separated the ions produced based on their mass-to-charge ratios. Detection followed by an ion detector and the data was given out as a mass spectrum of the sample. The MS was only able to scan compounds within

35 to 500 u. The total ion chromatogram of BSTFA and the corresponding mass spectra are shown in Figures 2.45 and 2.46 respectively.
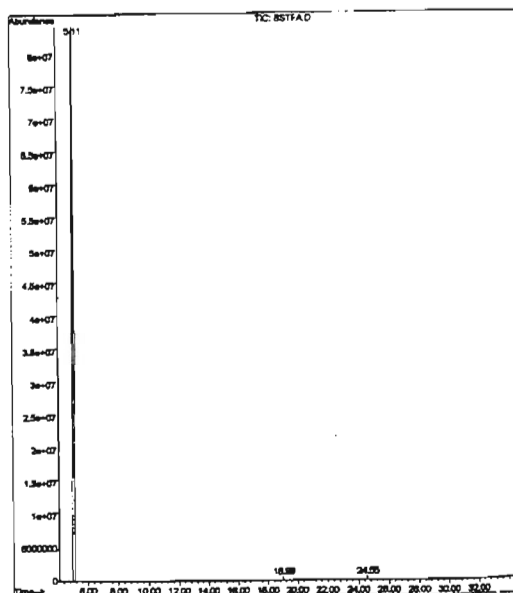
Figure 2.45:   Total ion chromatogram of BSFTA (at 5.11 minutes) eluted through the HP-5MS column of the Agilent 6890 gas chromatograph according to the conditions described in Section 2.7.2.1.
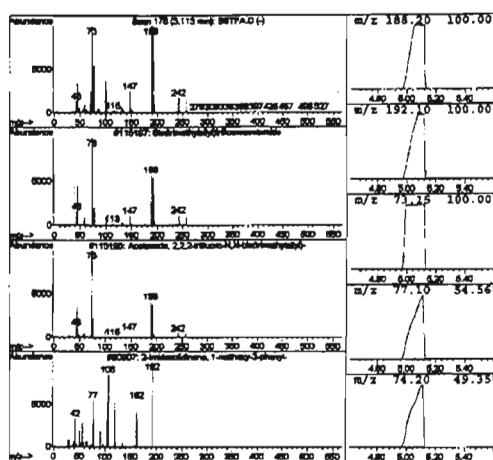
Figure 2.46:   The mass spectrum of BSTFA which eluted at 5.11 minutes in the total ion chromatogram is displayed in the top-left window. The library mass spectral matches are displayed in the windows below it on the left-hand side; they are arranged in descending order starting with the best match at the top. The windows on the right-hand side are the fragment peaks of BSTFA; they are arranged in descending order of abundance starting with the most abundant fragment at the top.

2.7.2.2 GC-MS analysis of the photodegradation of avobenzone

The photostability of avobenzone in various solvents was investigated by means of the Hewlett Packard 6890 GC-MS instrument. The GC also used an HP-5MS column with a similar MS detection procedure as the Agilent 6890 GC-MS instrument, scanning compounds of mass range 50 to 550 amu. Only splitless injection was employed in this GC-MS since avobenzone concentrations were of the order of 10^{-2} M, which were sufficiently low to avoid column overloading. The total ion chromatogram and MS spectra were gathered 3 minutes from sample injection in order to allow the solvent to elute. All solvents used had boiling points below 200 °C (as shown in Table 2.6) and hence eluted within 3 minutes of the run. This meant a 3 minute solvent delay prior to data gathering was adequate to avoid solvent peaks.

Table 2.6:   Solvents used for avobenzone photostability investigations by GC-MS analysis and their respective boiling points.

Solvent	Boiling point (Lide [1992-1993]) /°C
Cyclohexane	80.8
Ethyl acetate	77.2
DMSO	189

A modified temperature program from that of Soleas *et al.* [1999] was found to be adequate for eluting all the photoproducts that resulted from the photodegradation of avobenzone. The injector was set at 280 °C in order to evaporate the injected sample and the detector was kept at 310 °C to maintain the sample in vaporized form. The temperature program is illustrated in Figure 2.47 and was: 80 °C held for 1 minute, an increase of 20 °C/minute to 250 °C, 250 °C held for 1 minute, an increase of 6 °C/minute to 280 °C, 280 °C held for 2 minutes, an increase of 10 °C/minute to 290 °C, and 290 °C maintained for 4 minutes. This temperature program was used to obtain the GC-MS spectra shown in Appendix B and discussed in Section 3.3.1.3.
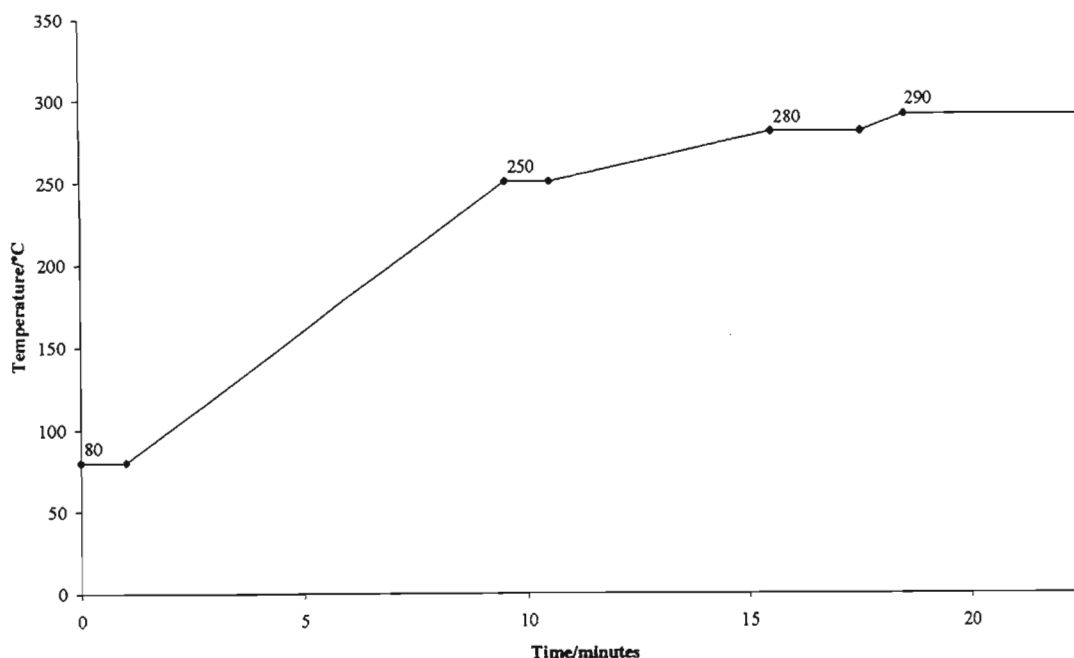
Figure 2.47:   Temperature program used for separating avobenzone and its photoproducts in the Hewlett Packard 6890 gas chromatograph coupled to a Hewlett Packard 6890 mass-selective detector.

2.8 Nuclear Magnetic Resonance Spectroscopy

Nuclear magnetic resonance (NMR) spectroscopy was employed in order to characterise the avobenzone structure before and after irradiation. The theory concerning NMR is outlined in Section 2.8.1 and the instruments, method and solvents used are discussed in Section 2.8.2.

2.8.1 An introduction to the theory of NMR spectroscopy

An atom can be used for NMR spectroscopy if it has a nuclear spin that creates a magnetic field along its spin axis, referred to as a nuclear magnetic moment. The existence of the nuclear magnetic moment depends on the nucleus of the atom possessing an odd number of either protons or neutrons. The most important of these nuclei are the isotopes of hydrogen, ^{1}H, and carbon, ^{13}C. NMR spectroscopy based on ^{1}H is known as proton nuclear magnetic resonance (^{1}H NMR) and that of ^{13}C is referred to as carbon nuclear magnetic resonance (^{13}C NMR).

When an external magnetic field is applied to protons in a sample, half the protons nuclear magnetic moments will align in the same direction with the field and half in the opposite direction. Aligning with the field is a more stable position of less energy; hence more energy is required to flip these nuclear magnetic moments to align opposing the external field. This energy can be provided in the form of radiofrequency waves and the amount depends upon the strength of the external magnetic field. The greater the external magnetic field, the more energy is required to flip the nuclear magnetic moments of the protons to oppose the field. A proton is said to be in resonance when it is flipped to oppose the external magnetic field.

The magnetic field of a proton in a compound is the combination of the external and the environmental magnetic field (known as the induced molecular magnetic field) felt by the proton. Protons in a sample are exposed to the same external field but they are not necessarily in the same environmental magnetic field. The latter depends on the electron density around the proton.

An NMR spectrum is obtained at set radiofrequency energy whilst varying the external magnetic field. Protons in different environments will resonate at different strengths of the external field and will appear at different positions in the NMR spectrum. A proton engulfed in a high electron density environment is said to be shielded and will require a larger external field to bring it into resonance. A shielded proton gives a peak upfield, towards the right hand side, of an NMR spectrum and the opposite applies to a deshielded proton (its peak appears downfield).

In an NMR spectrum, the position of tetramethylsilane (TMS) is the set point of reference, and all protons appear relative to this peak in what is referred to as their chemical shift. In modern NMR instruments, NMR solvents of known chemical shifts are used as reference points. The chemical shift of a proton is given in δ values, with units in parts per million, ppm, of the external field (Fessenden and Fessenden [1998]).

^{1}H NMR shows all the protons in chemically different environments, all the integrals of proton signals give the number of protons at the same environment and all the splitting of signals (occurs between adjacent protons) chemically explain the proton environment.

In ^{13}C NMR spectroscopy, the fundamental difference from ^{1}H NMR is the ^{13}C isotope of carbon exists only as 1.1% of naturally occurring carbon, compared to a 99.985% abundance of

the hydrogen isotope, ^{1}H. ^{13}C NMR therefore requires very sensitive instruments and long periods of time for generating spectra. As a result of this abundance, ^{13}C NMR spectra do not show ^{13}C - ^{13}C splitting, nor the number of carbons in a chemically identical environment that generate a single peak in the spectrum.

In ^{13}C NMR, proton decoupled spectra show only the ^{13}C peaks in different environments in the compound, whereas the off-resonance decoupled spectra show splitting of ^{13}C signals by ^{1}H atoms. Additionally, carbon based distortionless enhancement by polarisation transfer (DEPT) NMR, and attached proton test (APT) NMR can be done with modern instruments. Modern NMR methods give more information on the carbon-hydrogen groups in a sample.

2.8.2 NMR instruments, solvents and techniques used

The NMR instruments used during this research were a 300 MHz Varian Gemini NMR and a 400 MHz Varian Unity Inova NMR instrument (see Figures 2.48 and 2.49, respectively).
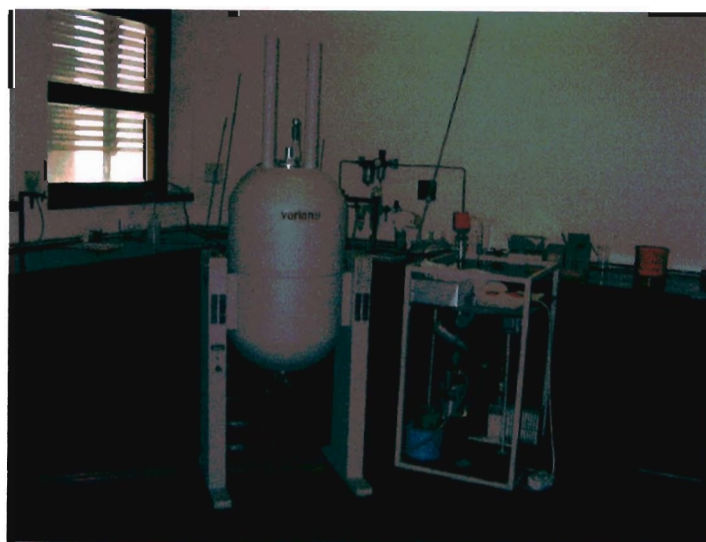
Figure 2.48:   The 300 MHz Varian Gemini NMR.
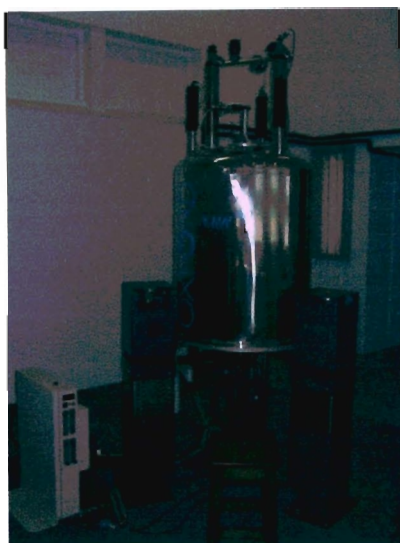
Figure 2.49:   The 400 MHz Varian Unity Inova NMR.

Only deuterated solvents were used for NMR analysis to avoid solvent protons appearing with the sample protons in the NMR spectra. These deuterated solvents are very hygroscopic, consequently they were kept in a desiccator. This minimised water contamination which results in large broadened peaks in the NMR spectra. The solvents used were deuterated DMSO and cyclohexane since avobenzone photodegrades in these two solvents.

A sample for NMR analysis was prepared by weighing about 20 mg of avobenzone, and dissolving it in an NMR solvent inside a fume hood to minimise water contamination. The NMR tube was flushed with nitrogen to remove any possible water contamination before introducing the sample. The avobenzone solution was placed in the NMR tube by means of a Pasteur pipette, and an NMR spectrum of the sample in the tube was recorded. The sample was then irradiated in the NMR tube and an NMR spectrum was re-obtained.

In order to illustrate avobenzone degradation, the NMR peaks were set at the same vertical and integral scale (width and height, respectively) before and after irradiation. The NMR spectra were obtained by locking the radiofrequency signal which depends on the solvent used, and setting a homogenous magnetic field around the sample before data acquisition. The ^{1}H NMR spectra were obtained at 300 MHz and 400 MHz for the 300 MHz Varian Gemini and 400 MHz Varian Unity Inova NMR instruments, respectively. The ^{13}C NMR spectra were, on the other hand, obtained at the following radiofrequencies: 75 MHz (for the 300 MHz Varian Gemini NMR) and 100 MHz (for the 400 MHz Varian Unity Inova NMR). The NMR spectra obtained

for avobenzone in DMSO and cyclohexane, before and after irradiation, included ^{1}H NMR and DEPT spectra. The NMR spectra are displayed and discussed in Section 3.3.1.5.

Avobenzone keto-enol tautomerism can easily be followed by ^{1}H NMR, but can also be shown through ^{13}C NMR if the extent of isomerisation is great. The APT and DEPT are specialised ^{13}C NMR that show the presence of CH_3, CH_2 and CH groups in a compound, and in the case of the APT, also saturated carbon peaks (Figure 2.50).
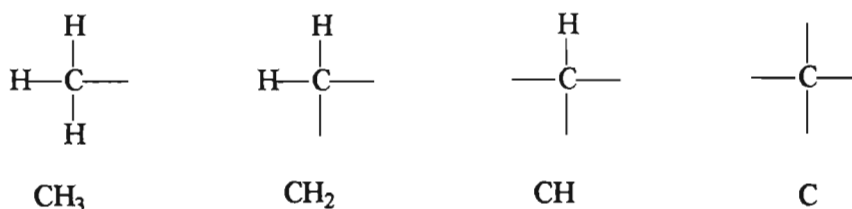
Figure 2.50:   APT and DEPT spectra can distinguish between a CH_3, CH_2, CH and a C, a carbon not bonded to any hydrogen, in a compound.

When avobenzone isomerises, a CH interchanges with a CH_2 group, and if this occurs to a significant extent then the APT and DEPT spectra can show this phenomenon.

CHAPTER 3

RESULTS AND DISCUSSION

Sunscreens are a necessity since they offer protection against some of the adverse effects of UV radiation. As they are used by a large proportion of the population worldwide, it is imperative that they act as indicated and do not photodegrade on use. Photo-unstable chemical absorbers (Serpone et al. [2002] and Maier et al. [2001]) reduce the efficacy of the sunscreen product they are contained in by decreasing its protective ability. In keeping with the increasing usage of plant antioxidants in skin care products the possibility of photostabilising photo-unstable sunscreen absorbers with plant polyphenols was investigated in this work. The photo-unstable chemical absorbers: 2-ethylhexyl-*p*-methoxycinnamate (EHMC), 4-bis(polyethoxy)-*p*-aminobenzoic acid polyethoxyethyl ester (Peg-25 PABA), 3-(4-methylbenzylidene) camphor (MBC), isoamyl *p*-methoxycinnamate (IMC) and avobenzone, were investigated in this respect. The polyphenolic extracts were derived from the Cancer Bush plant. In addition, various Rooibos teas including: Rooibos-black tea, Rooibos-honeybush tea and plain Rooibos tea as well as the specific polyphenols, epicatechin and rutin, were investigated as potential photostabilisers of the absorber avobenzone. These Rooibos tea extracts were used since they are known sources of polyphenols (Erickson [2003]) and were used to compare the polyphenolic extraction efficiency as well as the photostabilising potential of the Cancer Bush extracts.

This chapter examines the results of the experimental work described in Chapter 2. The chapter is divided into four sections. The first examines the content and photostability of various Cancer Bush and Rooibos tea extracts. The second investigates the ability of the Cancer Bush extracts to photostabilise various photo-unstable chemical absorbers. The third section deals specifically with the chemical absorber, avobenzone, and the photostabilising effect observed with the Cancer Bush and Rooibos tea extracts, as well as the polyphenols, rutin and epicatechin. The fourth section concludes with a discussion of a possible mechanism for the photostabilising effect of the Cancer Bush extracts.

3.1 Analysis of the Cancer Bush leaves

The Cancer Bush plant is thought to be a potential source of polyphenolic antioxidants. The leaves of this plant were extracted via several methods (as described in Section 2.2) in an attempt to isolate these possible polyphenolics. The various extracts acquired, henceforth referred to as polyphenolic extracts, were analysed by UV spectroscopy and HPLC (Section 3.1.1). The ethanol-water extract was further compared with similarly extracted polyphenols from various Rooibos teas, and then characterised by GC-FID and GC-MS analysis (Section 3.1.2). The phenolic content and the radical scavenging ability of the ethanol-water Cancer Bush extract were measured (Section 3.1.3). The photostability of the ethanol-water extract and the boiling water extract of ground Cancer Bush leaves were subsequently investigated by UV spectroscopy (Section 3.1.4). The results of these analyses will be discussed in this section.

3.1.1 Polyphenolic extracts from the Cancer Bush leaves

UV spectroscopy and high-performance liquid chromatography were the techniques employed to characterise the Cancer Bush polyphenolic extracts and to assess their photostabilising potential. Polyphenols that absorb at similar wavelengths as photo-unstable chemical absorbers could act as potential photostabilisers by shielding the absorbers and scavenging any free radicals formed. HPLC analysis was important for characterising the type of compounds isolated, based on their retention times together with their corresponding UV spectra. This data could then be used to choose the appropriate method of extracting diverse polyphenolic substances.

3.1.1.1 UV analysis of the Cancer Bush extracts

The UV spectra of the various Cancer Bush extracts were obtained by diluting portions of these extracts in their respective solvents, so as to obtain absorbances within the boundaries of Beer's law. All extracts were diluted with Millipore water except for the solid obtained from the ethanol-water extraction which was dissolved in methanol prior to UV analysis. Figure 3.1 compares the UV spectra of the methanol-water extract, the boiling water extract of non-ground and that of ground Cancer Bush leaves, the high temperature extract and the ethanol-water extract of Cancer Bush leaves. These UV spectra show that all the extracts absorb strongly in the UVB as well as most of the UVA region. The ethanol-water extract consistently showed strong absorption up to 400 nm where the other extracts failed to absorb strongly. These

extracts can therefore compete against UVA as well as UVB absorbers for absorption of radiation at these wavelengths as a means of photostabilising them.
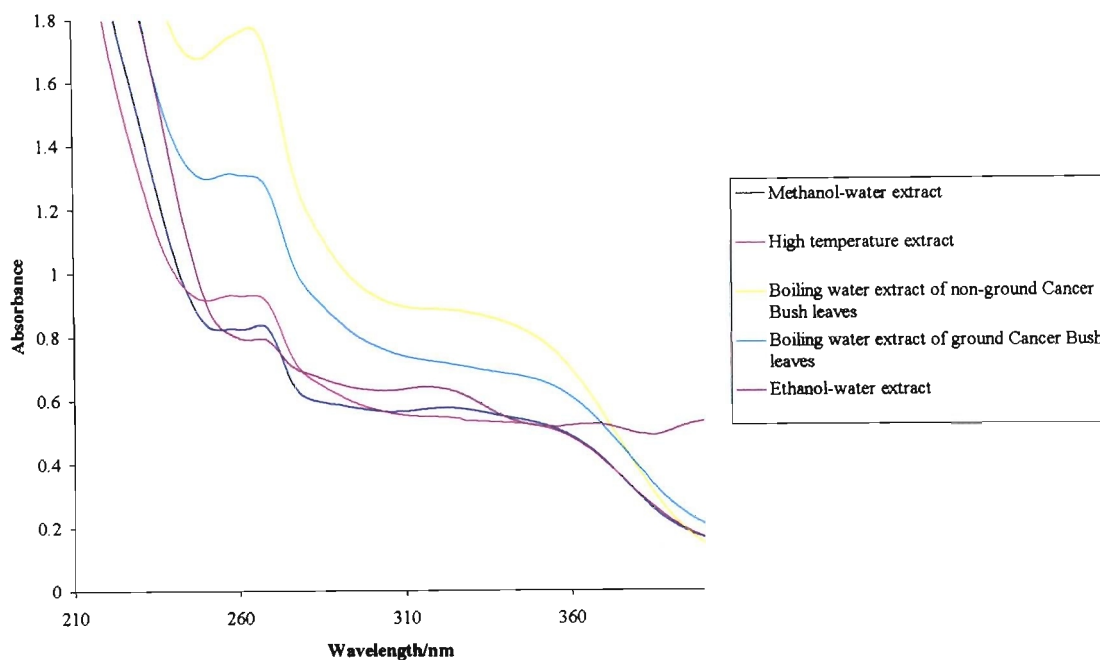
Figure 3.1:   UV spectra of the Cancer Bush extracts: the methanol-water extract (in Millipore water), the high temperature extract (in Millipore water), the boiling water extract of non-ground and ground Cancer Bush leaves (in Millipore water) and the ethanol-water extract (in methanol). The spectra were acquired in a 1 cm pathlength quartz cuvette against air as the reference.

3.1.1.2 Suitability of extraction methods as determined by HPLC

Before extracting the polyphenols from the Cancer Bush leaves it was necessary to assess whether the envisaged extraction methods were indeed suitable for this purpose. Two of the envisaged extraction methods were assessed by means of HPLC. The boiling water extraction method was investigated for its ability to extract caffeine from a caffeine-containing JOKO tea. On the other hand, the ethanol-water extraction method was investigated for its ability to extract gallic acid from a gallic acid-containing Rooibos-black tea (Miller [1996]). The two methods were both successful in extracting each respective compound. Caffeine eluted at 25 minutes in both the standard sample (see Figure 3.2) and the boiling water extract of JOKO tea (see Figure 3.3). The HPLC gradient used for the elution was that of Zuo et al. [2002]. Gallic acid eluted at about 10 minutes for both the standard sample (Figure 3.4) and the ethanol-water Rooibos-

black tea extract (Figure 3.5) using an adapted gradient from Zuo *et al.* [2002] (see Section 2.5.2).
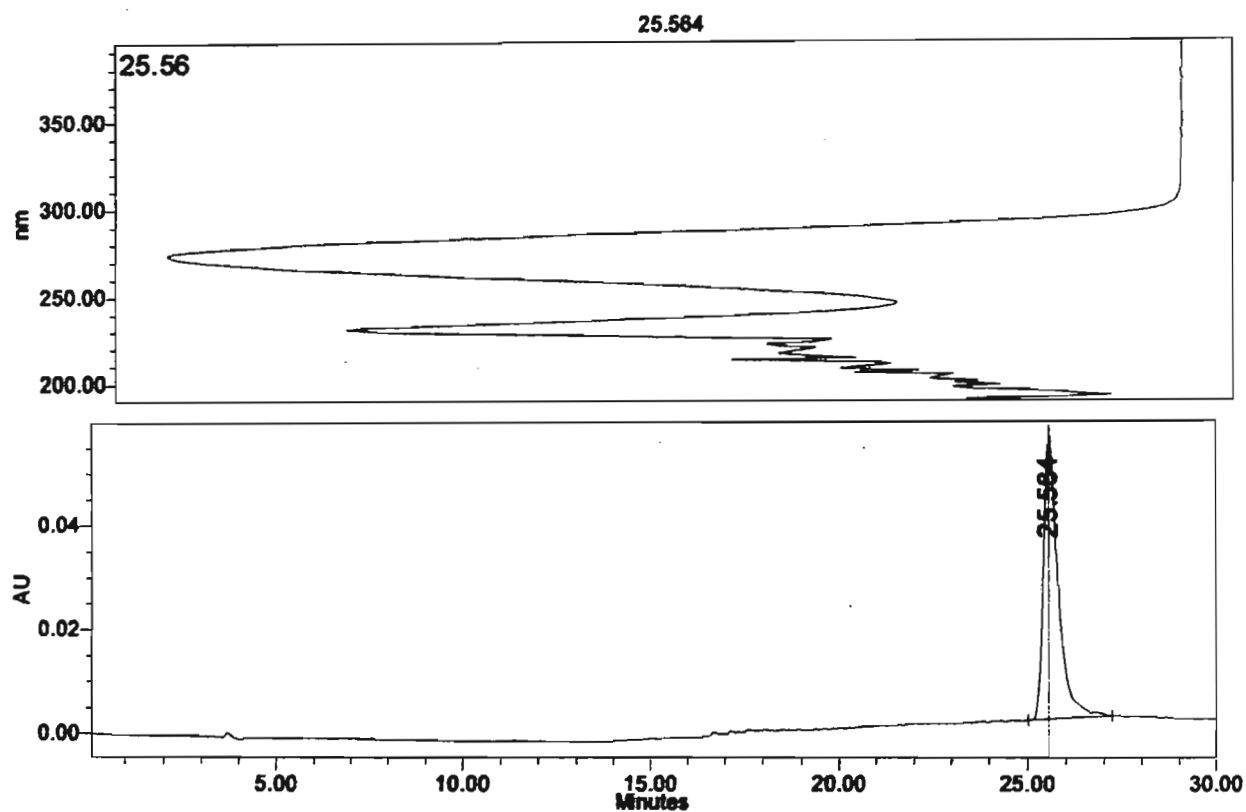
Figure 3.2:   HPLC chromatogram of the elution of caffeine through a Nucleosil 100 C18 column by a gradient mobile phase adopted from Zuo *et al.* [2002]. The chromatogram was monitored at a detection wavelength of 272 nm. The bottom window shows caffeine eluting at around 25 minutes and the top window has its corresponding UV spectrum with the wavelength of maximum absorption at 273.8 nm.
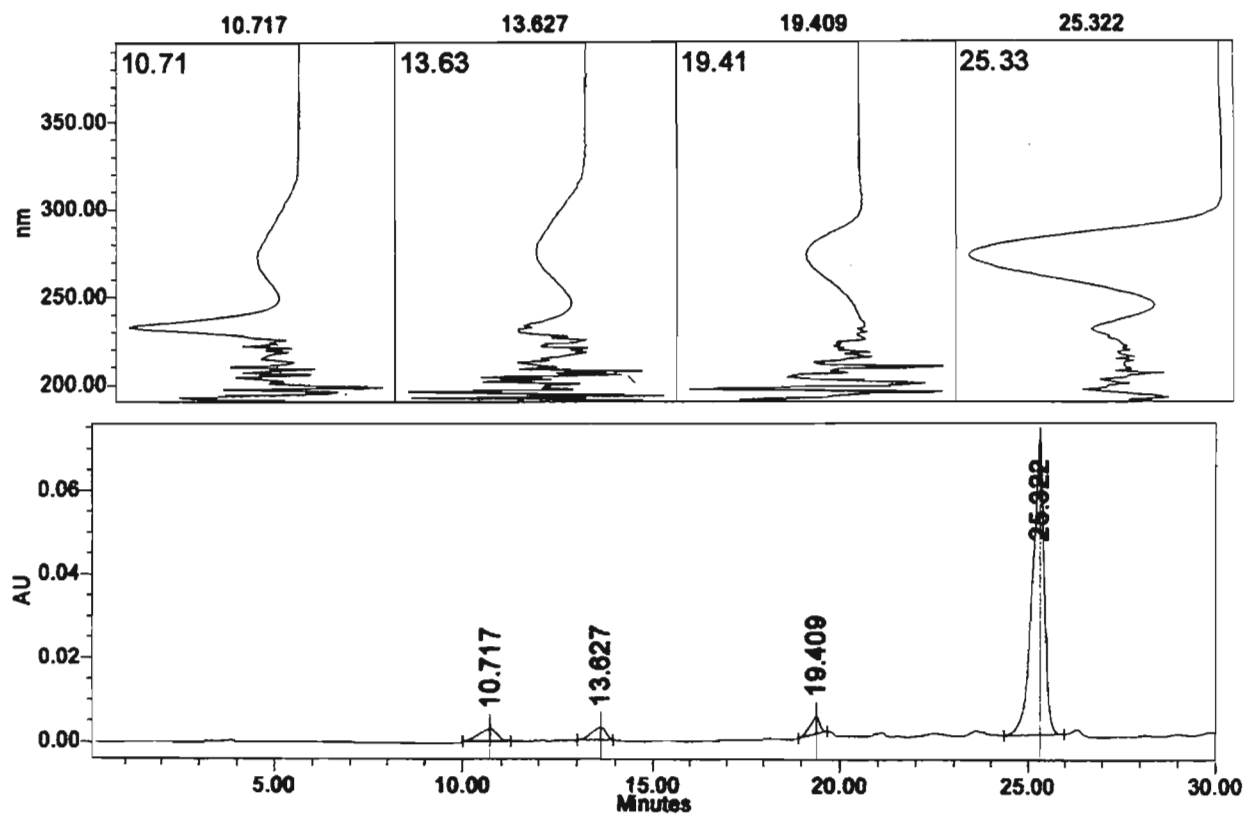
Figure 3.3:   HPLC chromatogram of the elution of the boiling water JOKO tea extract
through a Nucleosil 100 C18 column by a gradient mobile phase adopted from
Zuo *et al.* [2002]. The chromatogram was monitored at a detection wavelength
of 272 nm and shows caffeine eluting at 25 minutes.
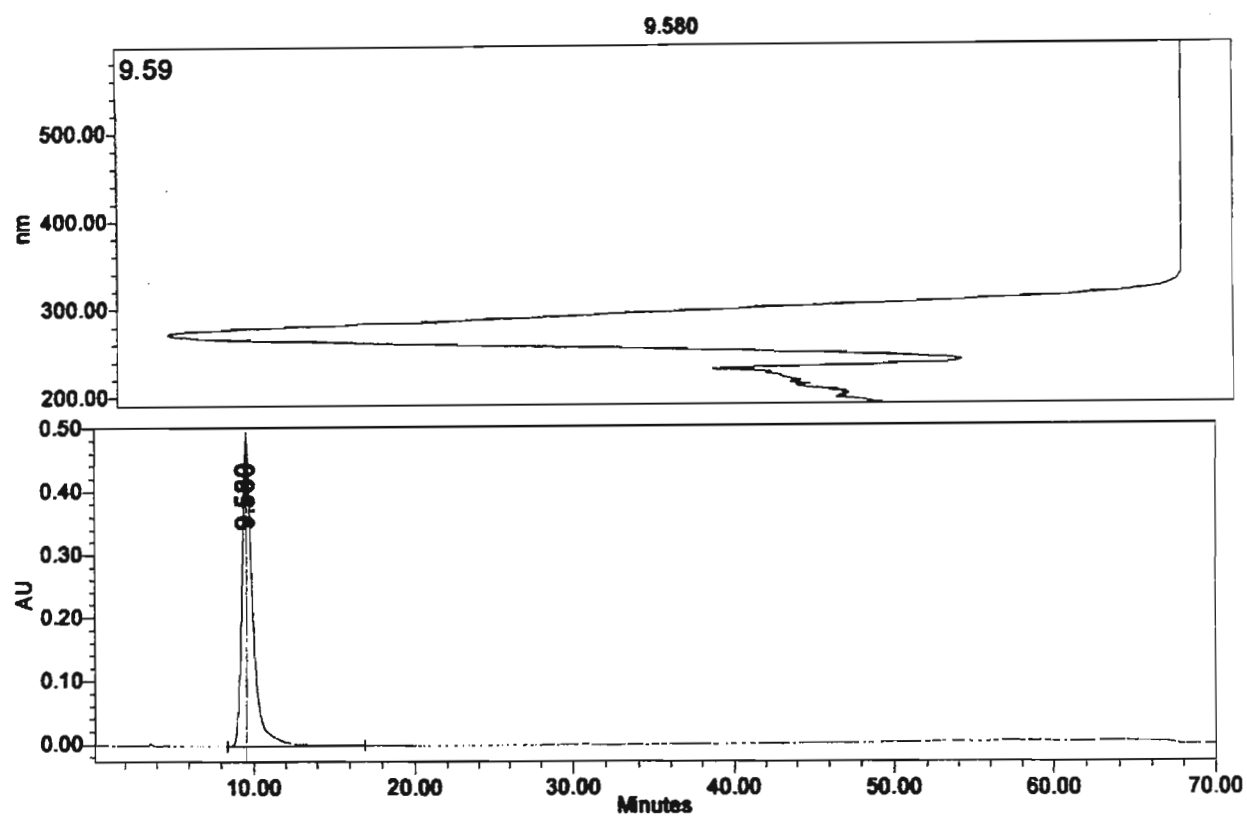
Figure 3.4: HPLC chromatogram of the elution of gallic acid through a Nucleosil 100 C18 column by a gradient mobile phase adapted from that used by Zuo *et al*. [2002]. The chromatogram was monitored at a detection wavelength of 272 nm. Gallic acid elutes at 9.6 minutes and the top window shows its UV spectrum.
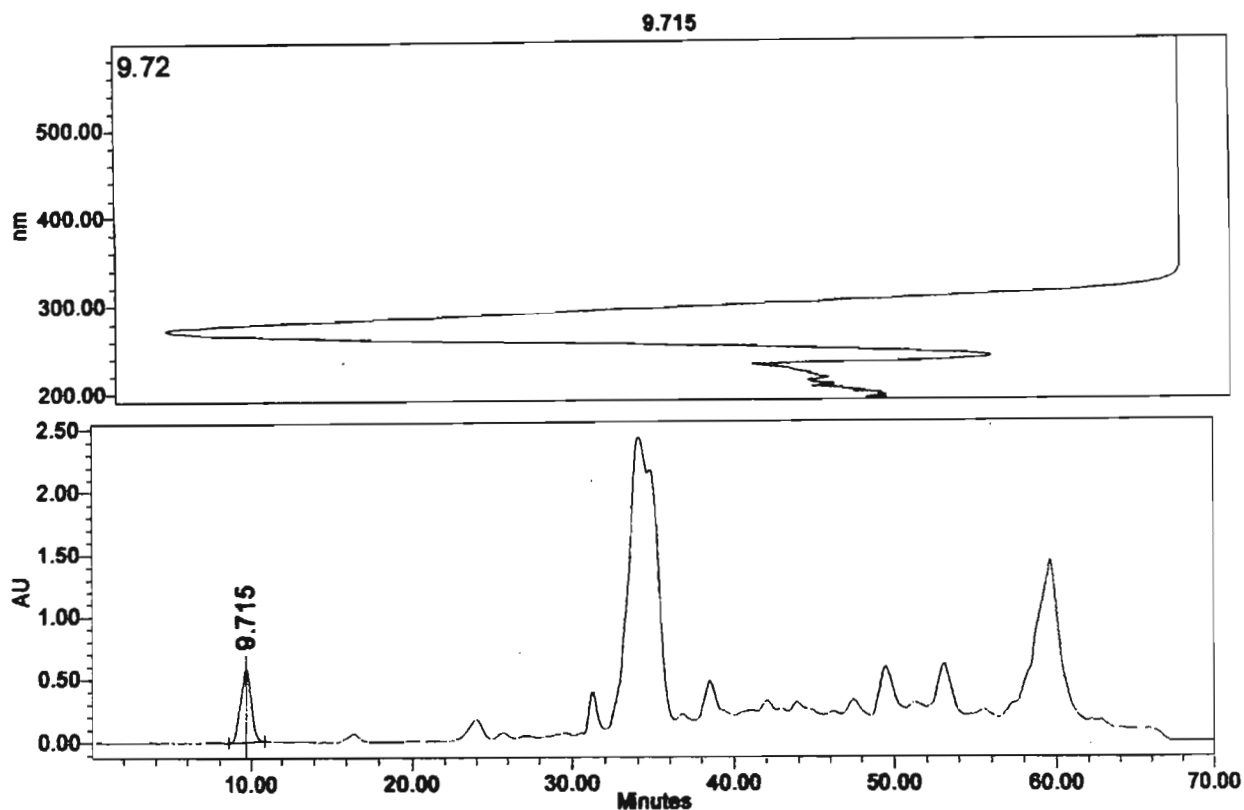
Figure 3.5: HPLC chromatogram of the ethanol-water Rooibos-black tea extract eluted through a Nucleosil 100 C18 column by a gradient mobile phase adapted from that used by Zuo *et al.* [2002]. The chromatogram was monitored at a detection wavelength of 272 nm and shows gallic acid eluting at 9.7 minutes.

3.1.1.3 HPLC analysis of the Cancer Bush extracts

The methanol-water extract, the high temperature extract and the boiling water extract of both ground and non-ground Cancer Bush leaves, were all eluted through a Nucleosil 100 C18 column by the gradient program adopted from Zuo *et al.* [2002]. These extracts were injected into the HPLC instrument as described in Sections 2.2 and 2.5, and their HPLC chromatograms are displayed in Figures 3.6-3.9.

Potential polyphenolic substances extracted from the Cancer Bush leaves by means of the various extraction methods were categorised according to their UV spectra. Each UV spectrum was compared with standard UV spectra of known polyphenols (Ryan and Robards [1998], Mozetič and Trebše [2004] and Macheix *et al.* [1990]) and allocated a potential class to which it could belong. Those peaks with UV spectra not easily categorised were left unassigned to lessen speculation. The compounds isolated in each extract were compared and grouped based on their UV spectra and retention times. Since the methanol-water extract, high temperature

extract, boiling water extract of ground and non-ground leaves, were all separated by the same gradient method in the HPLC, they were compared together. The results of this comparison are listed in Table 3.1. From Table 3.1 and the associated chromatograms it is evident that the boiling water extracts of the Cancer Bush leaves contained the largest diversity of substances isolated, and in particular that of the ground Cancer Bush leaves. The methanol-water extraction method isolated the lowest number of compounds followed by the high temperature extraction method.

The compounds eluting between 4.5 – 5.0 minutes and between 30 – 33 minutes were consistently present in all the extracts. A comparison of the UV spectra of these compounds with those of known polyphenols indicated the possible presence of flavan-3-ols, benzoic acids, hydroxycinnamic acids, isoflavones, flavonols as well as chalcones.
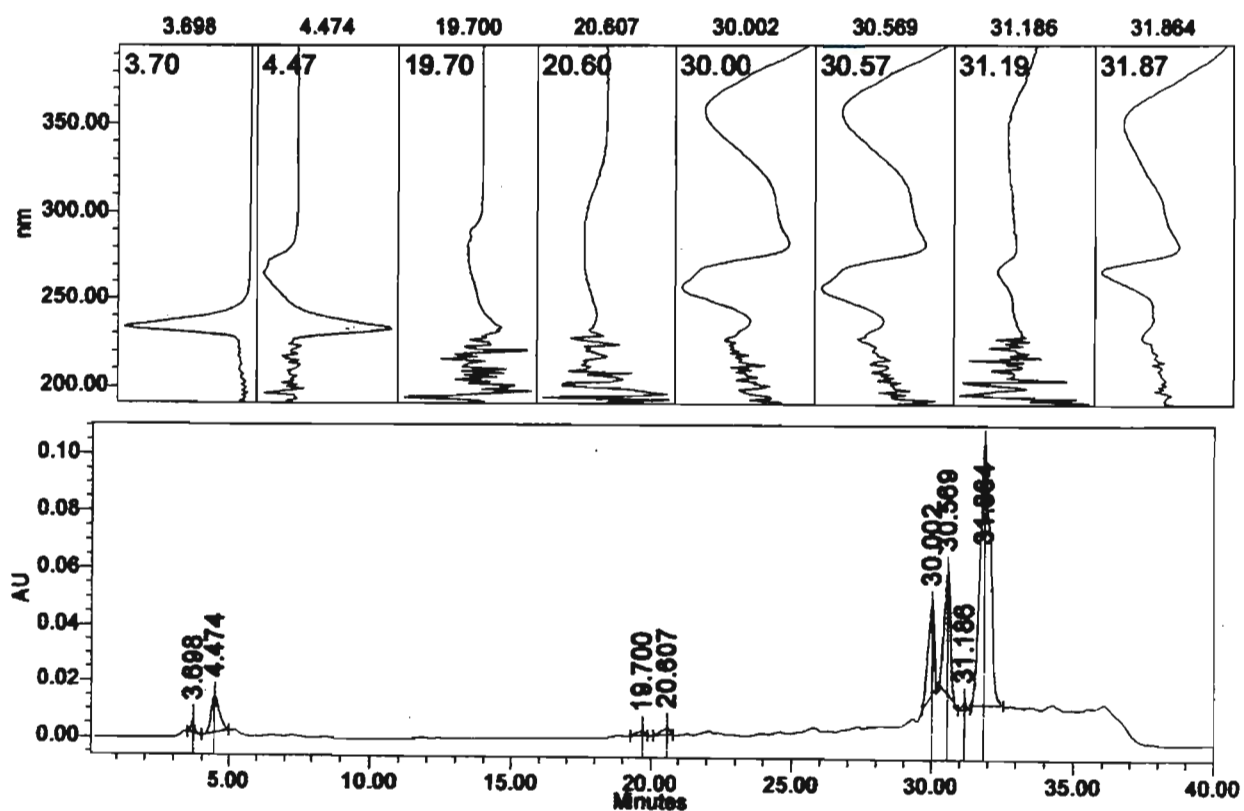
Figure 3.6:   HPLC chromatogram of the methanol-water Cancer Bush extract eluted through a Nucleosil 100 C18 column by a gradient method adopted from Zuo *et al.* [2002]. The wavelength of detection was 272 nm.
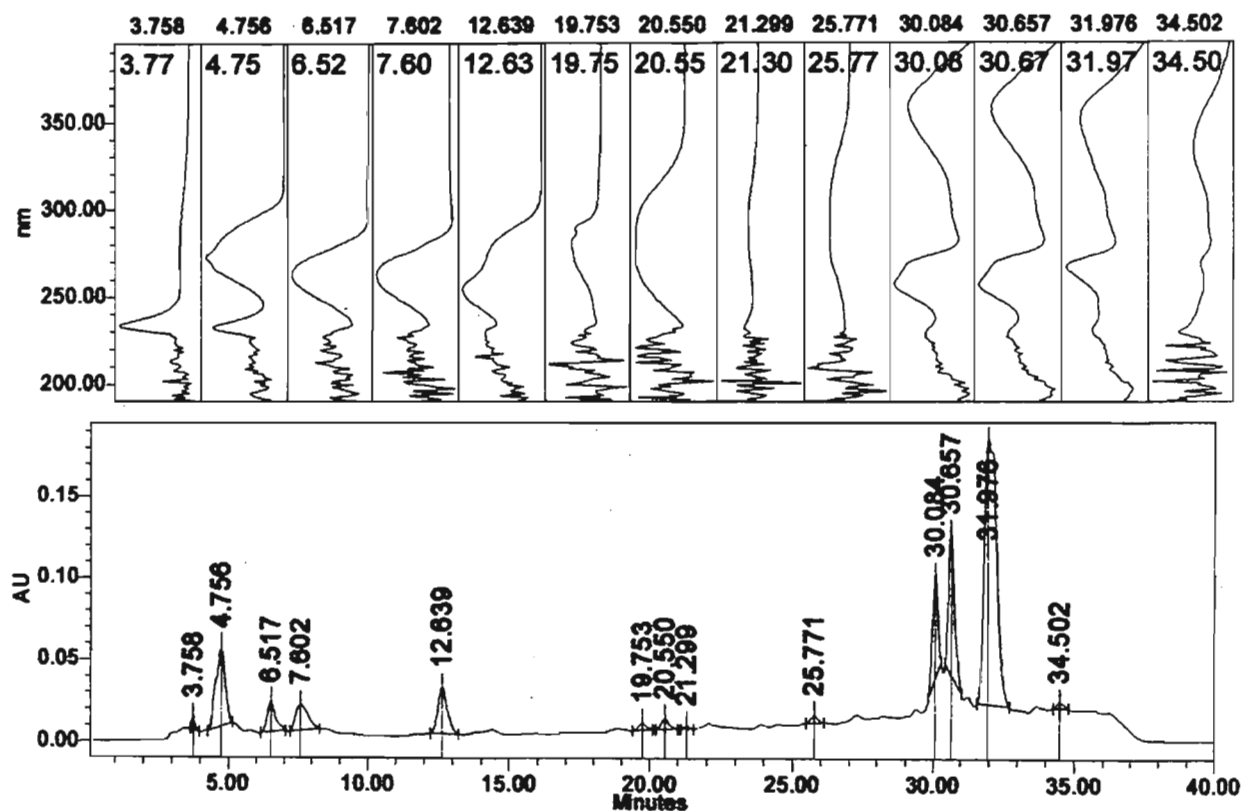
Figure 3.7:   HPLC chromatogram of the high temperature Cancer Bush extract eluted
through a Nucleosil 100 C18 column by a gradient method adopted from Zuo *et
al.* [2002]. The wavelength of detection was 272 nm.
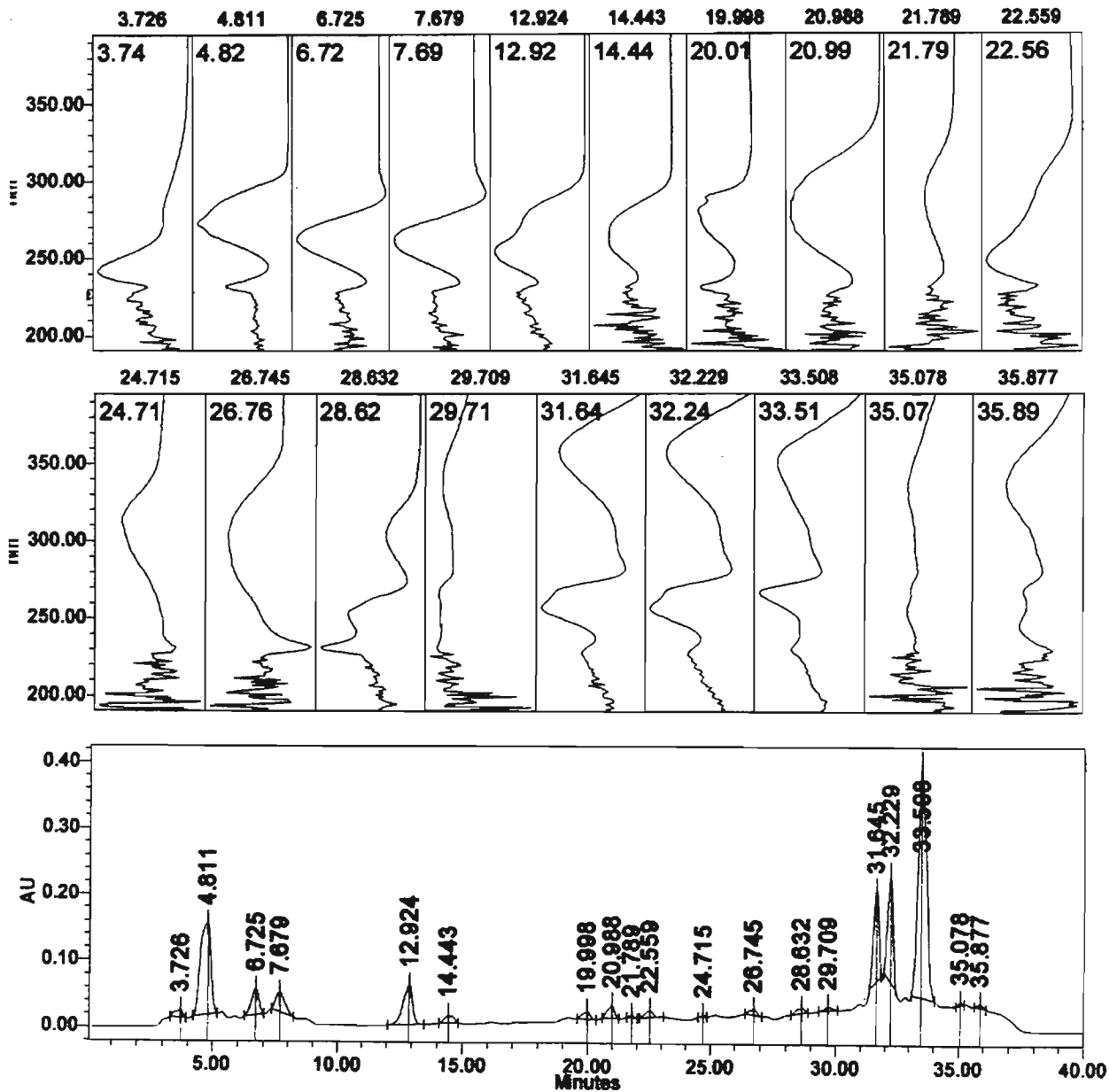
Figure 3.8:   HPLC chromatogram of the boiling water extract of non-ground Cancer Bush leaves eluted through a Nucleosil 100 C18 column by a gradient method adopted from Zuo *et al.* [2002]. The wavelength of detection was 272 nm.
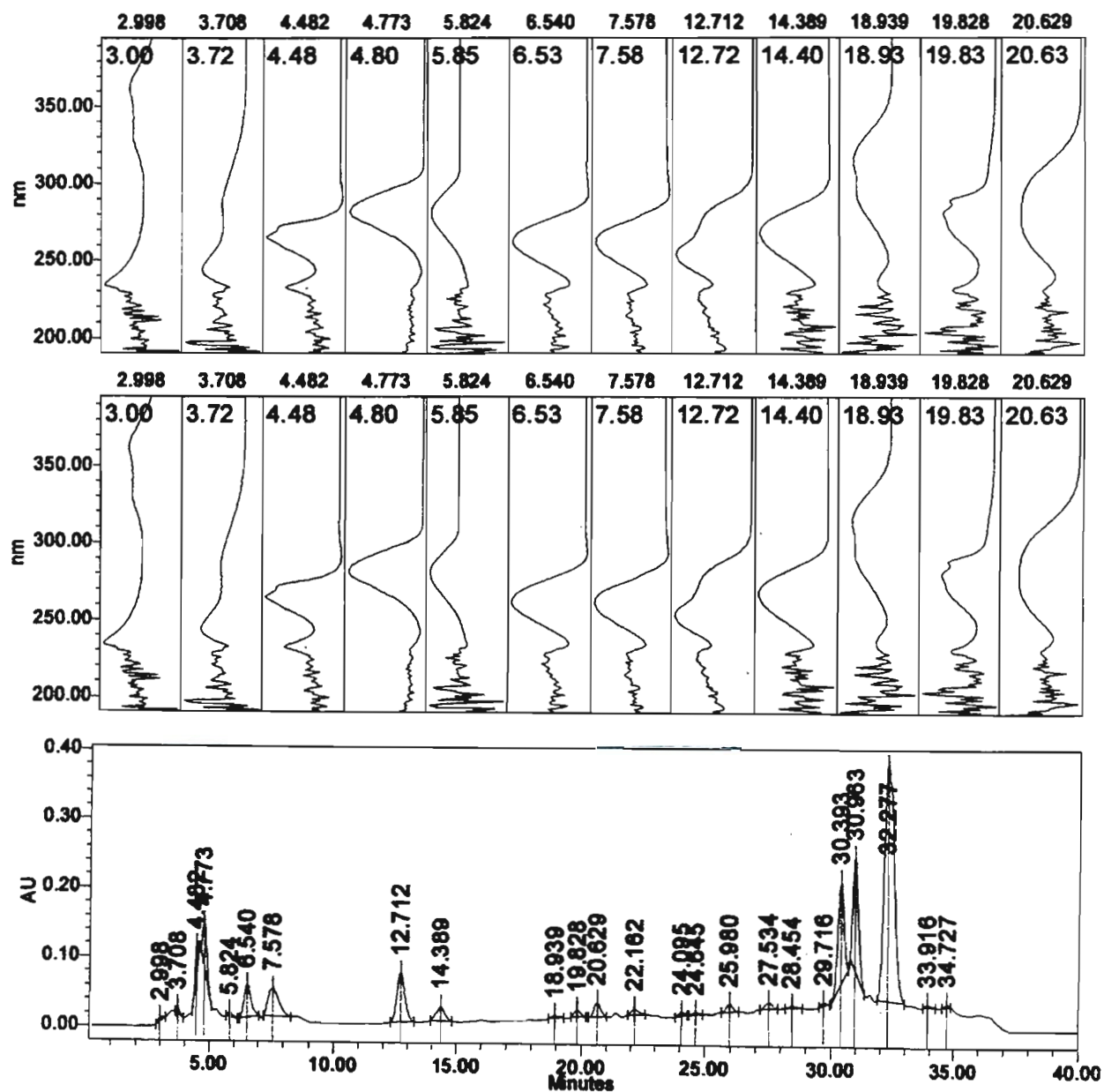
Figure 3.9: HPLC chromatogram of the boiling water extract of ground Cancer Bush leaves eluted through a Nucleosil 100 C18 column by a gradient method adopted from Zuo *et al.* [2002]. The wavelength of detection was 272 nm.

Table 3.1: Matched HPLC retention times based on the UV spectra of compounds extracted from the Cancer Bush leaves by the methanol-water, high temperature and boiling water (for ground and non-ground leaves) extraction methods and their assigned class of polyphenols.

Polyphenolic group	Retention times of compounds extracted from the Cancer Bush leaves/minutes			
	Methanol-water extract	High temperature extract	Boiling water extract (non-ground leaves)	Boiling water extract (ground leaves)
1	-	-	-	2.998
2	-	-	3.726	-
3	3.698	3.758	-	-
4	-	-	-	3.708
5	4.474	4.756	4.811	4.482
6	4.474	4.756	4.811	4.773
7	-	-	-	5.824
8	-	6.517	6.725	6.54
9	-	7.602	7.679	7.578
10	-	12.639	12.924	12.712
11	-	-	14.443	14.389
12	-	-	-	18.939
13	-	19.753	19.998	19.828
Flavan-3-ol/Benzoic acid (Ryan and Robards [1998] and Macheix et al. [1990])	20.607	20.550	20.988	20.629
15	-	21.299	21.789	-
16	-	-	22.559	22.162
Hydroxycinnamic acid (Ryan and Robards [1998], Mozetič and Trebše [2004] and Macheix et al. [1990])	-	-	24.715	24.095
18	-	-	-	24.645
19	-	25.771	-	25.980
20	-	-	26.745	-

Isoflavone (Ryan and Robards [1998] and Macheix et al. [1990])	-	-	28.632	27.534
22	-	-	-	28.454
Isoflavone (Ryan and Robards [1998] and Macheix et al. [1990])	-	-	29.709	-
Flavonol (Ryan and Robards [1998] and Macheix et al. [1990])	-	-	-	29.716
Flavonol (Ryan and Robards [1998] and Macheix et al. [1990])	30.002	30.084	31.645	30.393
Rutin[a]	30.569	30.657	32.229	30.963
Flavonol/Chalcone (Ryan and Robards [1998] and Macheix et al. [1990])	31.864	31.976	33.508	32.277
28	-	-	35.078	33.916
29	-	34.502	35.877	34.727

[a] See Section 3.1.2.1

The ethanol-water Cancer Bush extract

The ethanol-water Cancer Bush extract showed better resolution of peaks when eluted using the adapted gradient from Zuo et al. [2002].

In order to set a comparison point, the boiling water extract was injected into the HPLC and eluted with the adapted gradient program used to elute the ethanol-water extract. The resulting HPLC chromatogram was compared with that obtained for the ethanol-water extract under the same conditions. The HPLC chromatograms are displayed in Figures 3.10 and 3.11. Table 3.2 shows the various compounds isolated by these two extraction methods, and the compounds have been matched and categorised into different groups of polyphenols based on their UV spectra and retention times.
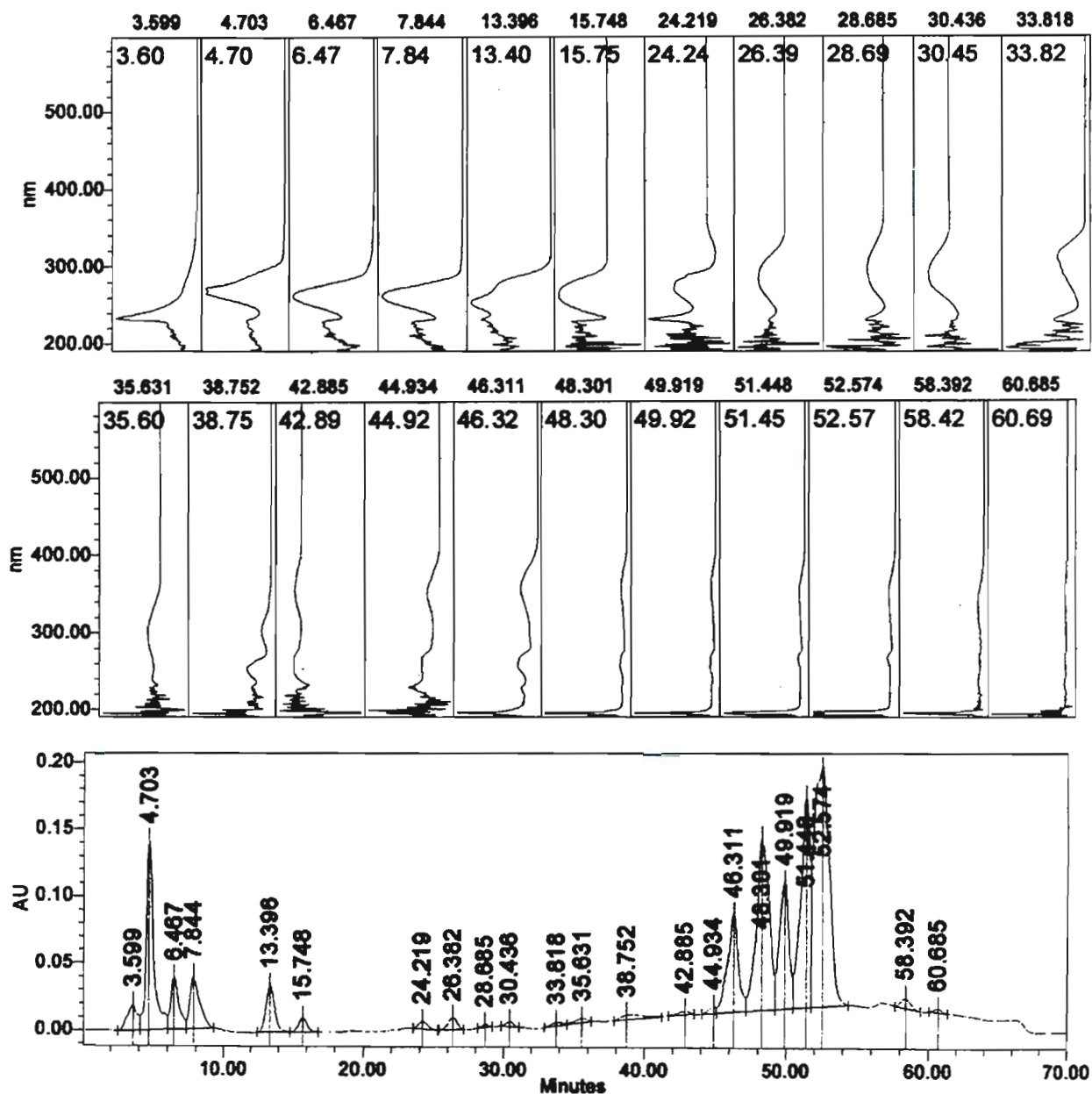
Figure 3.10:   HPLC chromatogram of the boiling water extract of ground Cancer Bush leaves
eluted through a Nucleosil 100 C18 column by a gradient mobile phase adapted
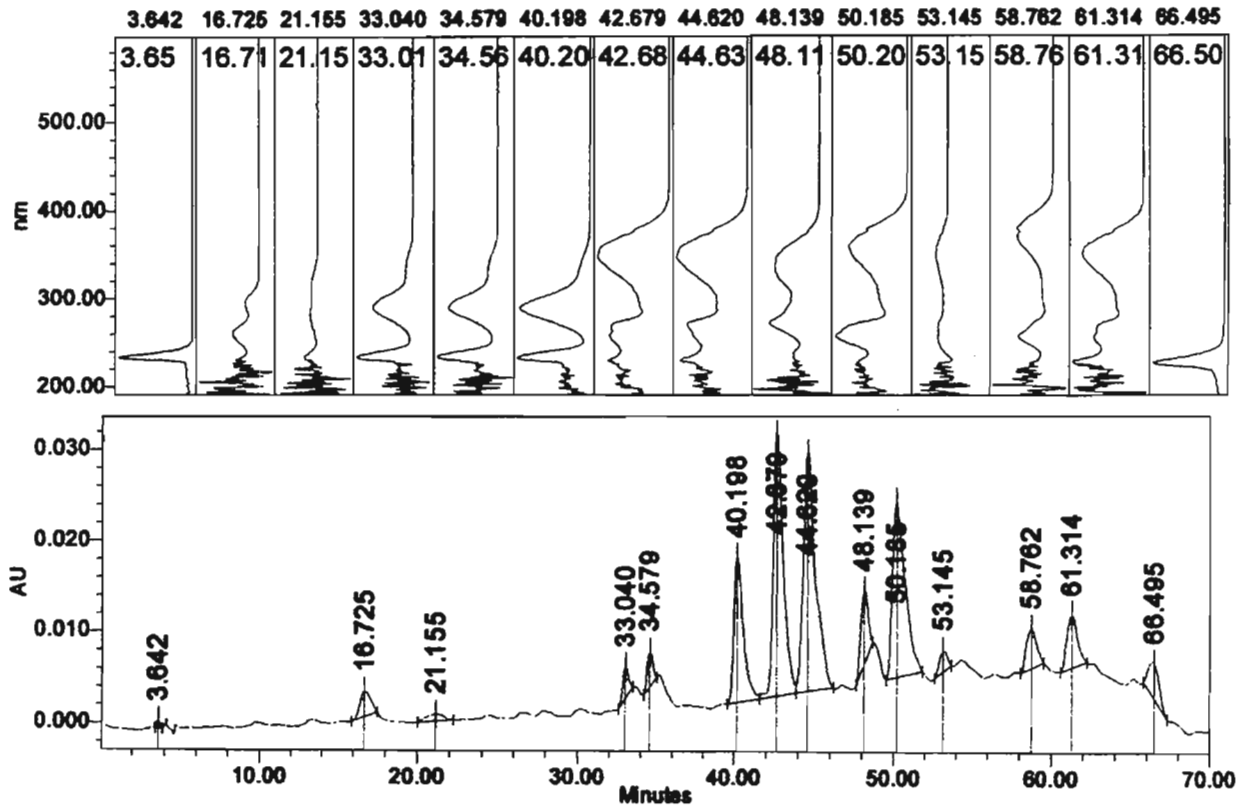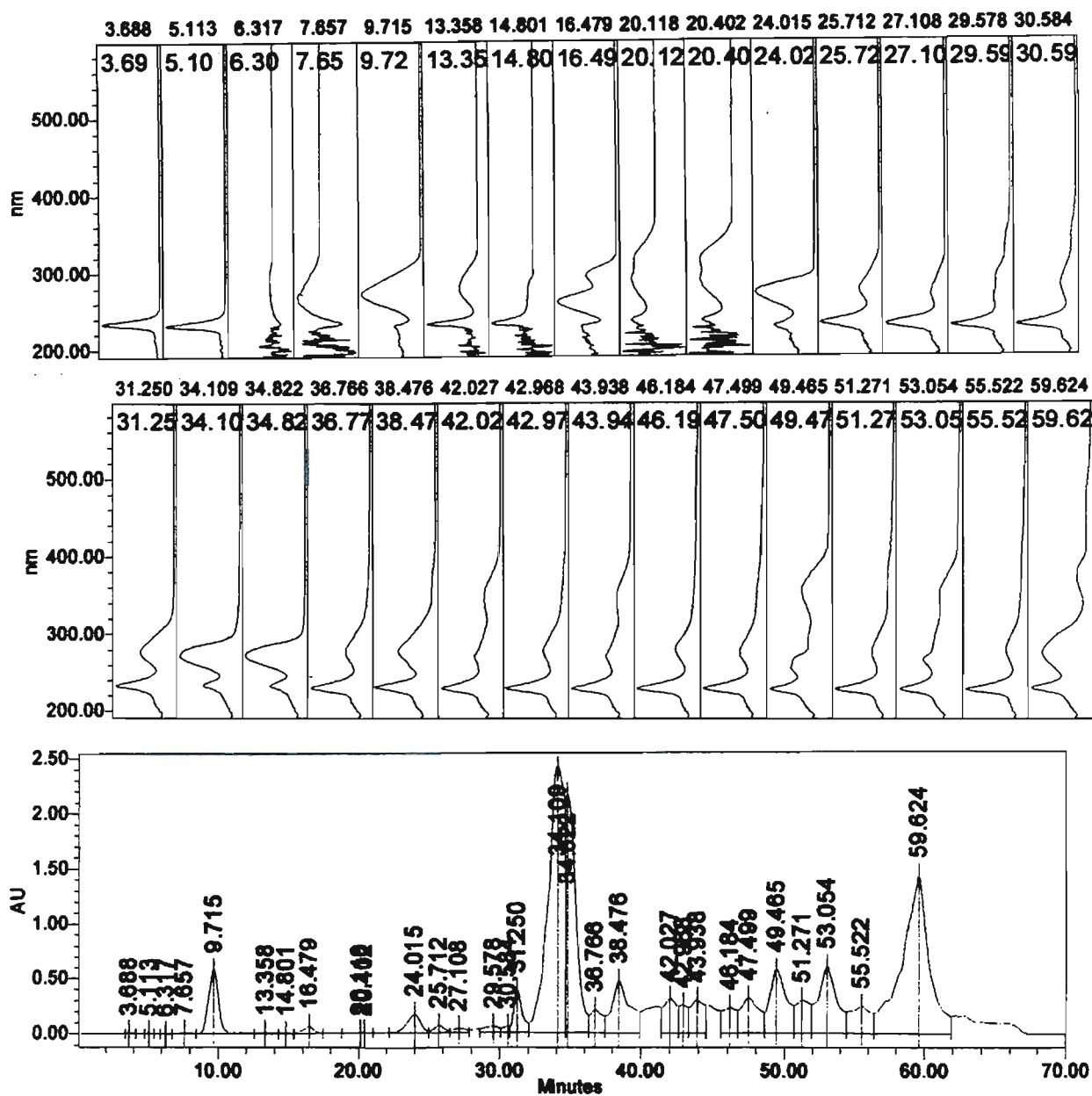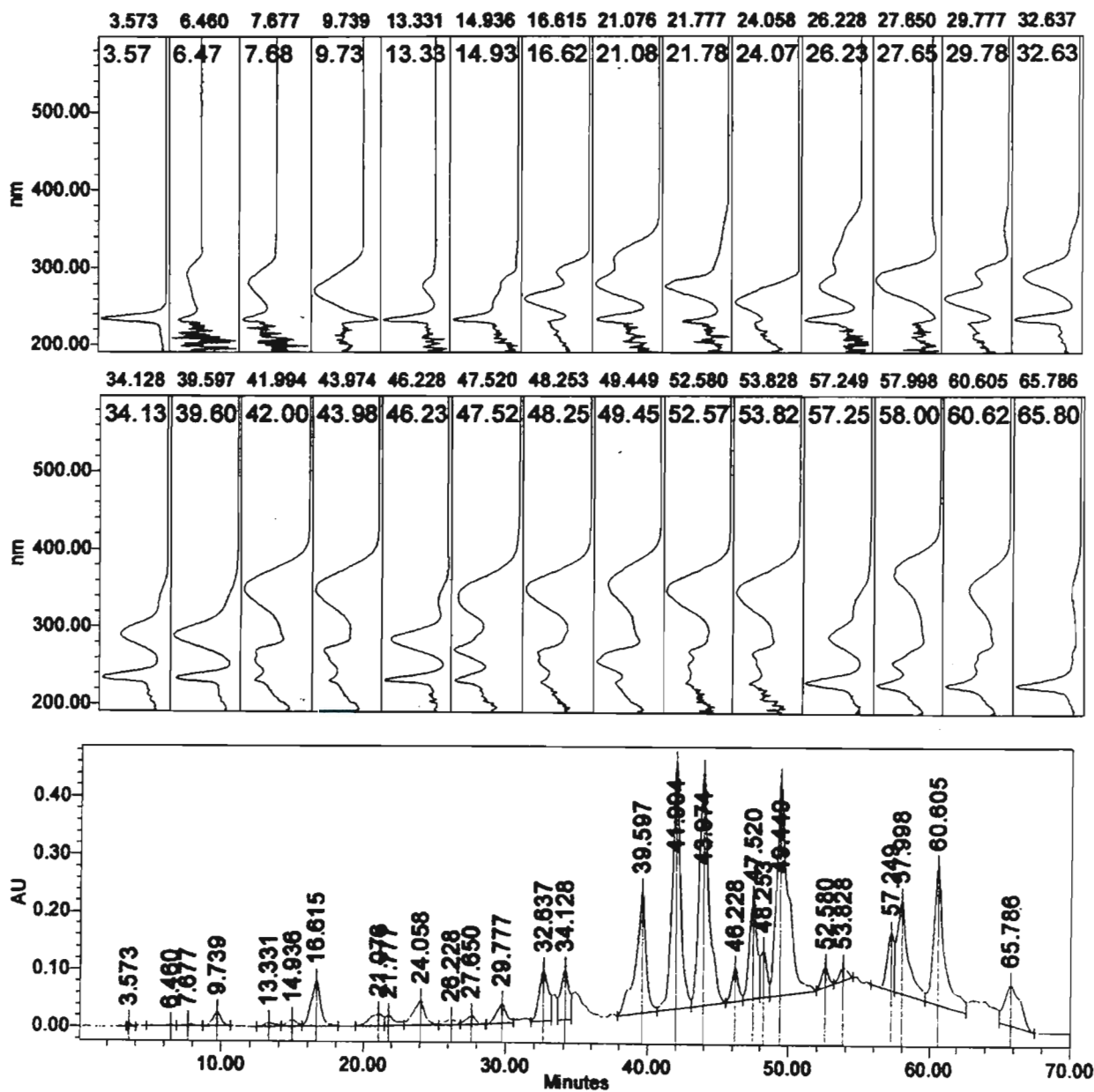from Zuo *et al.* [2002]. The wavelength of detection was 272 nm.
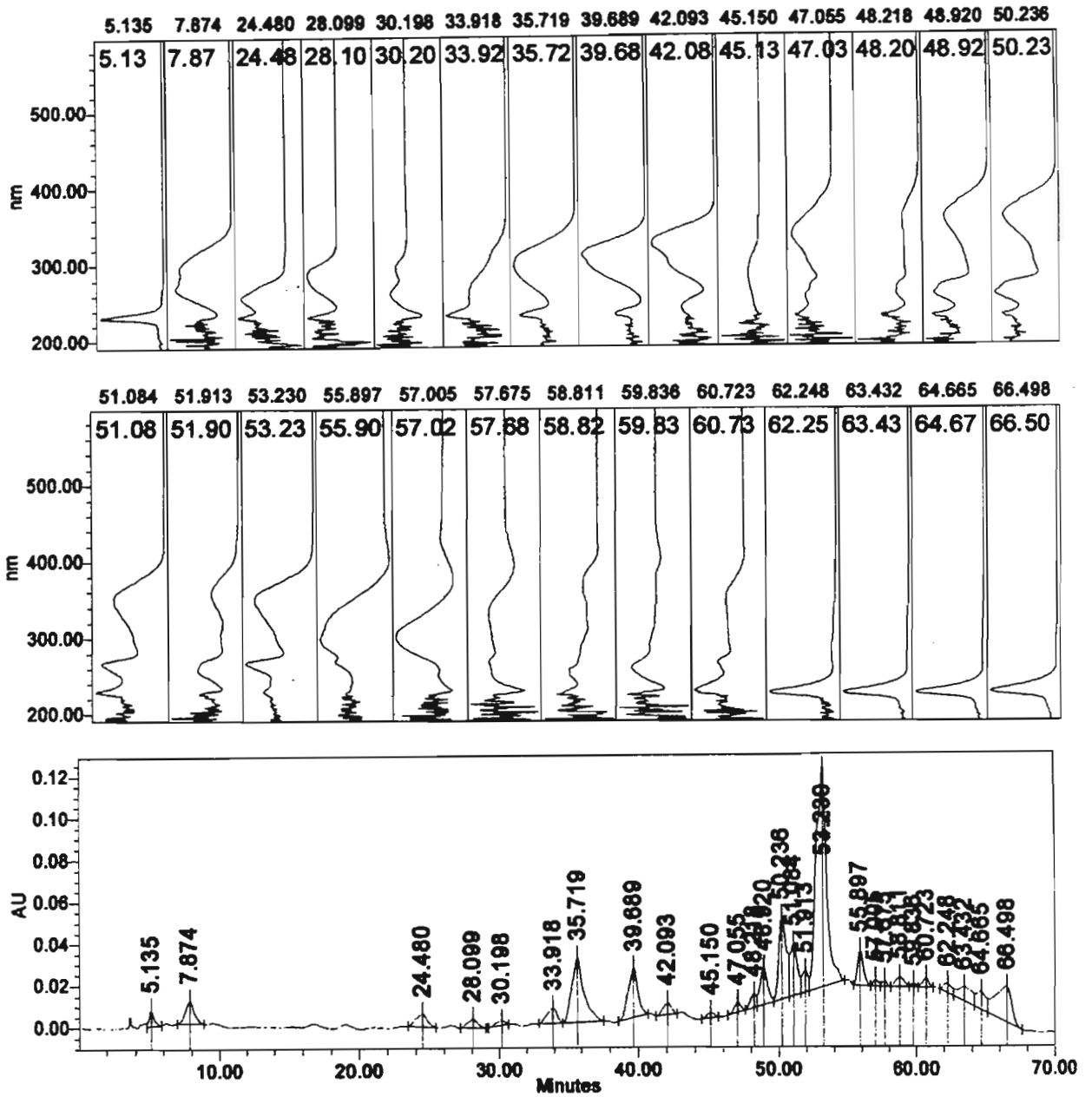
Figure 3.11:   HPLC chromatogram of the ethanol-water Cancer Bush extract eluted through a
                Nucleosil 100 C18 column by a gradient mobile phase adapted from Zuo et al.
                [2002]. The wavelength of detection was 272 nm.

The boiling water extract eluted compounds within 0 – 8 minutes and between 45 – 54 minutes
in very high amounts. The ethanol-water extract also contained the compounds that eluted
between 45 – 54 minutes, based on their retention times and UV spectra, but in much smaller
quantities. The extract, however, did not contain any of the compounds that eluted between 0 –
8 minutes in the boiling water extract but it did contain compounds that consistently eluted
throughout the 70 minutes of the HPLC run.

The compounds that eluted within 30 minutes of the elution run of the boiling water extract were not easily categorised into any of the polyphenolic groups based on their UV spectra. In general, the polyphenolic compounds isolated by the two methods were potential hydroxycinnamic acids, isoflavones, flavonols, chalcones, flavan-3-ols, benzoic acids and flavanones and flavanonols.

Table 3.2   Matched HPLC retention times based on the UV spectra of compounds extracted from the Cancer Bush leaves by the boiling water (ground leaves) and ethanol-water extraction methods and their assigned polyphenolic groups.

Polyphenolic group	Retention times of compounds extracted from Cancer Bush leaves/minutes	
	Boiling water extract (ground leaves)	Ethanol-water extract
1	3.599	-
2	4.703	-
3	-	5.135
4	6.467	-
5	7.844	-
6	-	7.874
7	13.396	-
8	15.748	-
9	24.219	-
10	-	24.480
11	26.382	28.099
12	28.685	-
13	30.445	-
14	-	30.198
Hydroxycinnamic acid (Ryan and Robards [1998], Mozetič and Trebše [2004] and Macheix et al. [1990])	33.752	-
16	-	33.918
17	35.626	35.719

Isoflavones (Ryan and Robards [1998] and Macheix et al. [1990])	38.752	-
Hydroxycinnamic acid (Ryan and Robards [1998] and Macheix et al. [1990])	-	39.689
Hydroxycinnamic acid (Ryan and Robards [1998] and Macheix et al. [1990])	-	42.093
Flavonol/Chalcone (Ryan and Robards [1998] and Macheix et al. [1990])	42.885	-
23	44.934	-
Flavanones/Flavanonols (Ryan and Robards [1998] and Macheix et al. [1990])	-	45.150
24	46.311	-
25	-	47.055
Flavonol (Ryan and Robards [1998] and Macheix et al. [1990])	-	48.218
Flavonol (Ryan and Robards [1998] and Macheix et al. [1990])	48.301	48.920
Rutin[a]	49.919	50.236
Chalcone (Ryan and Robards [1998] and Macheix et al. [1990])	-	51.084
Flavonol/Chalcone (Ryan and Robards [1998] and Macheix et al. [1990])	51.448	51.913
Flavonol/Chalcone (Ryan and Robards [1998] and Macheix et al. [1990])	52.574	53.230

Flavanones/Flavanonols (Ryan and Robards [1998] and Macheix *et al.* [1990])	-	55.897
33	-	57.005
Chalcone/Flavone (Ryan and Robards [1998] and Macheix *et al.* [1990])	-	57.675
35	58.392	-
Flavonol/Chalcone (Ryan and Robards [1998] and Macheix *et al.* [1990])	-	58.811
37	-	59.836
Flavonol/Chalcone (Ryan and Robards [1998] and Macheix *et al.* [1990])	60.685	60.723
39	-	62.248
Flavan-3-ol/Benzoic acid (Ryan and Robards [1998] and Macheix *et al.* [1990])	-	63.432
41	-	64.665
42	-	66.498

[a] See Section 3.1.2.1

Table 3.2 shows that the ethanol-water and the boiling water extraction methods of ground Cancer Bush leaves extracted more compounds than any of the other extraction methods attempted. The UV spectra in Figure 3.1 further show that both these extracts absorbed in both the UVB and UVA regions. In the ethanol-water extraction method, an additional extraction step with ethyl acetate was performed. Consequently, any polyphenolics present in the aqueous extract of the Cancer Bush leaves were extracted into ethyl acetate which was easily evaporated to leave a solid extract (see Section 2.2.4). The ethanol-water solid extract was easily stored and having been extracted into ethyl acetate meant it was soluble in non-polar solvents as well as most polar solvents such as methanol. This was important for investigating the photostability of chemical absorbers soluble in either polar and/or non-polar solvents.

From the above arguments it can be concluded that both the ethanol-water and the boiling water extraction methods (of ground Cancer Bush leaves) were the ideal methods of extracting potential polyphenolics from the Cancer Bush leaves. It was therefore decided to investigate these extracts further for their possible use as photostabilisers for both UVA as well as UVB chemical absorbers.

In order to determine whether any photostabilising effect observed was due to the presence of polyphenols it was also necessary to extract a substance known to be rich in polyphenols.

The ethanol-water Rooibos tea extracts

The ethanol-water extraction method was used to extract polyphenols from a known polyphenolic source, namely Rooibos tea (Erickson [2003]). Polyphenols were extracted from different Rooibos tea combinations: Rooibos tea alone, Rooibos-black tea and Rooibos-Honeybush tea. These Rooibos tea extracts were compared with the Cancer Bush extract for their photostabilising effects. This would verify that the photostabilisation effect arises as a result of the presence of polyphenols.

The HPLC chromatograms of the various Rooibos tea extracts are displayed in Figures 3.12 (for Rooibos tea), 3.13 (for Rooibos-black tea) and 3.14 (for Rooibos-honeybush tea). Table 3.3 summarises the chromatograms by listing and categorising all the compounds present in the various extracts and compares them with those obtained from the ethanol-water extract of the Cancer Bush leaves. The table shows that the extracts from Rooibos tea and Rooibos-honeybush tea contain similar compounds unlike that of Rooibos-black tea. However, the Rooibos-black tea extract contains the most compounds compared to the other two.

Some compounds present in the ethanol-water Cancer Bush extract had matching retention times and UV spectra to those in the Rooibos tea extracts (see Table 3.3). Rooibos tea is a rich source of flavonoids (Erickson [2003]), and honeybush tea is also known to contain various polyphenols (Ferreira *et al.* [1998] and Kamara *et al.* [1998]) such as hydroxycinnamic acids, isoflavones, flavanones, flavones, coumestans and xanthones. The polyphenolic substances in black tea are different from those in Rooibos and honeybush tea - they tend to be rich in dimeric flavonols and polymeric polyphenols (Zhao *et al.* [1999]). This is the reason that the Rooibos-black tea chromatogram showed a greater variation of compounds than those of the other Rooibos teas.

Figure 3.12:   HPLC chromatogram of the ethanol-water Rooibos tea extract eluted through a
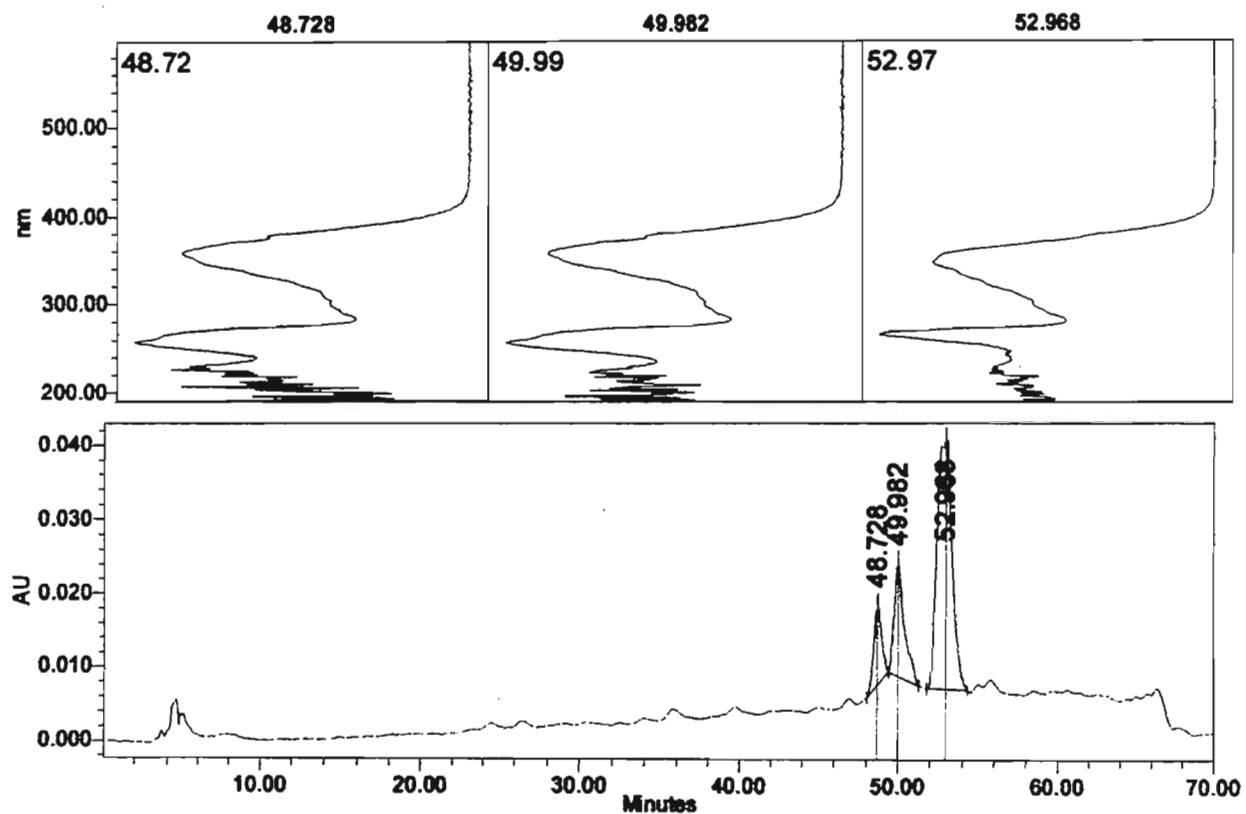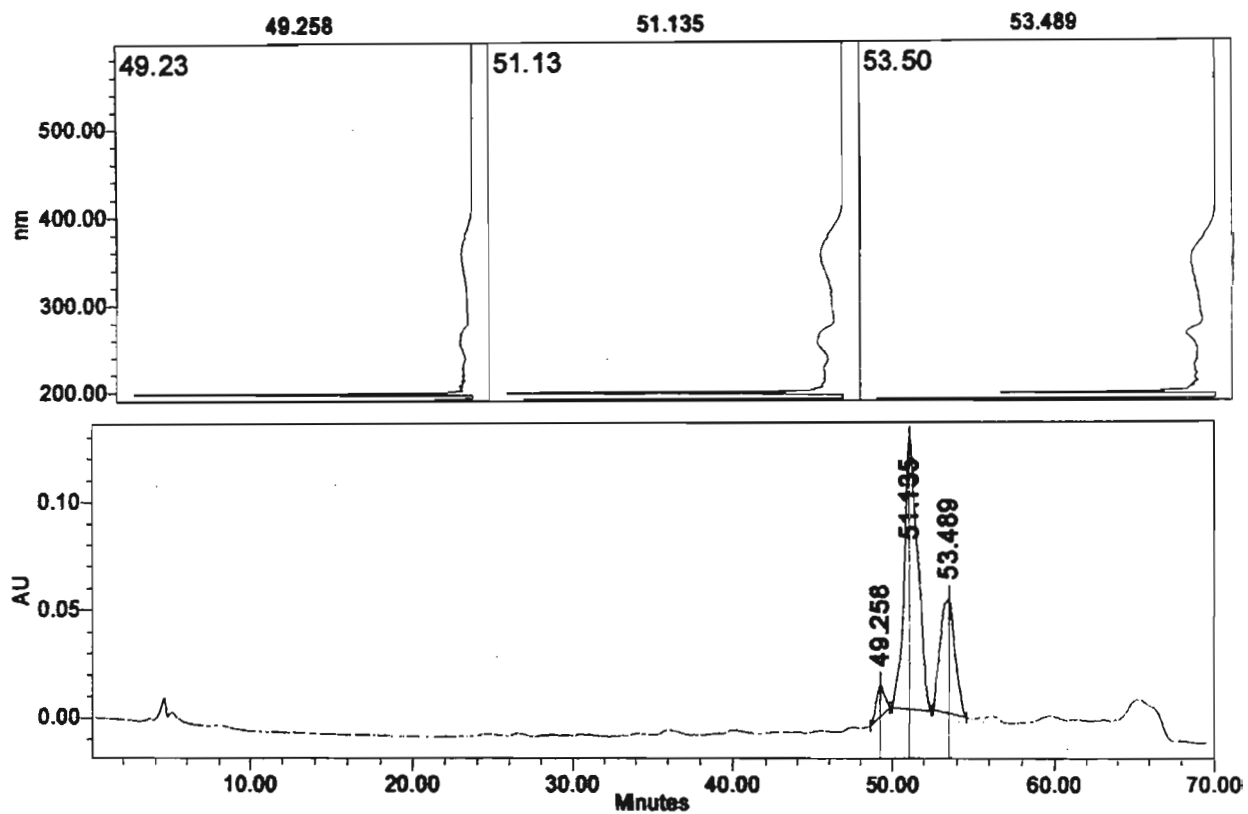Nucleosil 100 C18 column by a gradient method adapted from Zuo *et al.*
[2002]. The wavelength of detection was 272 nm.

Figure 3.13: HPLC chromatogram of the ethanol-water Rooibos-black tea extract eluted through a Nucleosil 100 C18 column by a gradient method adapted from Zuo *et al.* [2002]. The wavelength of detection was 272 nm.

Figure 3.14: HPLC chromatogram of the ethanol-water Rooibos-honeybush tea extract eluted through a Nucleosil 100 C18 column by a gradient method adapted from Zuo *et al.* [2002]. The wavelength of detection was 272 nm.

Table 3.3: Matched HPLC peaks, based on their retention times and UV spectra, from extracts of various Rooibos teas and the ethanol-water extract of ground Cancer Bush leaves. These compounds are grouped into known polyphenolic groups based on their UV spectra.

Polyphenolic group	Retention times of compounds extracted by the ethanol-water extraction method/minutes			
	Rooibos tea	Rooibos-black tea	Rooibos-honeybush tea	Cancer Bush leaves
1	3.642	3.688	3.573	3.645
2	-	5.113	-	5.135
3	-	6.317	6.460	6.184
4	-	7.657	-	-
5	-	-	7.677	-
Gallic acid[a]	-	9.715	9.739	-
7	-	13.358	13.331	-
8	-	14.801	14.936	-
9	16.725	16.479	16.615	16.789
10	-	20.118	-	-
11	-	20.402	-	-
Flavan-3-ol/Benzoic acid (Ryan and Robards [1998] and Macheix et al. [1990])	21.155	-	21.076	-
Flavan-3-ol/Benzoic acid (Ryan and Robards [1998] and Macheix et al. [1990])	-	-	21.777	-
14	-	-	24.058	24.48
Flavan-3-ol/Benzoic acid (Ryan and Robards [1998] and Macheix et al. [1990])	-	24.015	-	-
Flavan-3-ol/Benzoic acid (Ryan and Robards [1998] and Macheix et al. [1990])	-	25.712	-	-
17	-	27.108	-	-
Flavan-3-ol/Benzoic acid	-	-	26.228	-

(Ryan and Robards [1998] and Macheix *et al.* [1990])				
19	-	-	27.650	28.099
20	-	29.578	29.777	30.198
Flavan-3-ol/Benzoic acid (Ryan and Robards [1998] and Macheix *et al.* [1990])	-	30.584	-	-
Flavan-3-ol/Benzoic acid (Ryan and Robards [1998] and Macheix *et al.* [1990])	-	31.250	-	-
23	33.040	-	32.637	-
Flavan-3-ol/Benzoic acid (Ryan and Robards [1998] and Macheix *et al.* [1990])	-	34.109	-	-
25	34.579	-	34.128	-
Flavan-3-ol/Benzoic acid (Ryan and Robards [1998] and Macheix *et al.* [1990])	-	34.822	-	-
Flavan-3-ol/Benzoic acid (Ryan and Robards [1998] and Macheix *et al.* [1990])	-	36.766	-	-
Flavan-3-ol/Benzoic acid (Ryan and Robards [1998] and Macheix *et al.* [1990])	-	38.476	-	-
29	40.198	-	39.597	-
Flavone/Flavonol/Chalcone (Ryan and Robards [1998] and Macheix *et al.* [1990])	42.679	42.027	41.994	-
Flavan-3-ol/Benzoic acid (Ryan and Robards [1998] and Macheix *et al.* [1990])	-	42.968	-	-
Flavone/Flavonol/Chalcone (Ryan and Robards [1998] and Macheix *et al.* [1990])	44.620	43.938	43.974	-

33	-	46.184	46.228	-
34	-	47.499	-	-
Flavone/Isoflavone (Ryan and Robards [1998] and Macheix et al. [1990])	48.139	-	47.520	-
Flavone/Flavonol/Chalcone (Ryan and Robards [1998] and Macheix et al. [1990])	-	-	48.253	-
Rutin[b]	50.185	49.465	49.449	50.236
Flavonol/Chalcone (Ryan and Robards [1998] and Macheix et al. [1990])	-	51.271	-	-
Flavone/Flavonol/Chalcone (Ryan and Robards [1998] and Macheix et al. [1990])	-	-	52.580	-
Flavone/Flavonol/Chalcone (Ryan and Robards [1998] and Macheix et al. [1990])	53.145	53.054	53.828	53.23
41	-	55.522	-	-
42	-	-	57.249	-
Flavonol/Chalcone (Ryan and Robards [1998] and Macheix et al. [1990])	58.762	-	57.998	58.811
44	-	59.624	-	-
Flavonol/Chalcone (Ryan and Robards [1998] and Macheix et al. [1990])	61.314	-	60.605	-
46	66.495	-	65.786	66.498

[a] see section 3.1.1.2

[b] see section 3.1.2.1

3.1.2 Characterising the Cancer Bush extracts

The characterisation of compounds in the ethanol-water Cancer Bush extract was conducted by UV, HPLC, GC and GC-MS analysis. UV analysis of the extract has been discussed in Section 3.1.1. The retention times of the various compounds separated by HPLC are tabulated in Tables 3.2 and 3.3.

3.1.2.1 HPLC analysis of the ethanol-water extract

The Cancer Bush plant has not been well characterised; meaning its constituents have to be confirmed and verified. A proper way to characterise the ethanol-water Cancer Bush extract was to spike the extract with known standards. Of the standards available, rutin was the only standard possibly present in the ethanol-water extract; this was verified through spiking experiments. A mass of about 30 mg of the ethanol-water Cancer Bush extract was dissolved in 2 ml methanol. A 1 µl portion of this liquid extract was eluted through the HPLC instrument with the adapted gradient from Zuo *et al.* [2002]. A small amount of solid rutin was added to 1 ml of the ethanol-water extract dissolved in methanol, the mixture was sonicated for complete dissolution and injected into the HPLC instrument using the same gradient.

The rutin standard was found to elute at 50 minutes (see Figure 3.15) when eluted through the Nucleosil 100 C18 column. Figures 3.16* and 3.17 show the HPLC chromatograms of the ethanol-water Cancer Bush extract before and after the addition of rutin. The addition of rutin resulted in the increase of the flavonol peak (Ryan and Robards [1998]) at about 51 minutes (50 minutes before addition). But the peak may not have been rutin since the retention time of the flavonol peak changed slightly in the spiked sample. The UV spectrum of the peak eluting at 50 minutes, which is characteristic of flavonol compounds (Ryan and Robards [1998], Macheix *et al.* [1990] and Paganga and Rice-Evans [1997]) (family of rutin), also matches that of the flavonol, rutin (Figure 3.18). Therefore this peak could be rutin or a rutin-like compound. The retention times of the peak due to rutin or a rutin-like compound (in the case of Cancer Bush leaves) in the chromatograms of the various Cancer Bush and Rooibos tea extracts have been summarised in Table 3.4.

---

* This chromatogram although the same as that in Figure 3.11 is for a much more dilute sample and hence does not show all the peaks seen there.
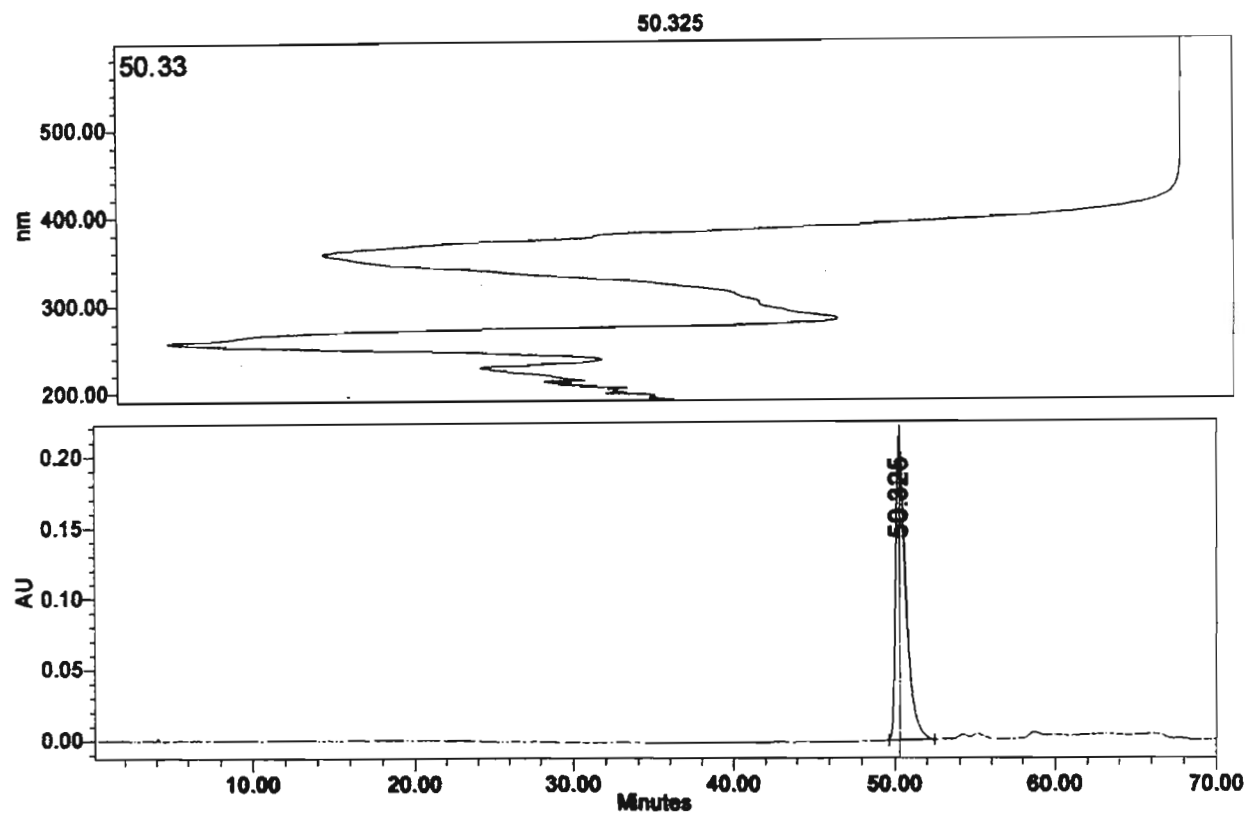
Figure 3.15: HPLC chromatogram of rutin eluted through a Nucleosil 100 C18 column with the adapted gradient method from Zuo *et al.* [2002]. The wavelength of detection was 272 nm.

Figure 3.16:   HPLC chromatogram of the ethanol-water Cancer Bush extract eluted through a Nucleosil 100 C18 column by a gradient mobile phase adapted from Zuo *et al.* [2002]. The wavelength of detection was 272 nm and the chromatogram was obtained before the addition of rutin.

Figure 3.17:   HPLC chromatogram of the ethanol-water Cancer Bush extract eluted through a
                Nucleosil 100 C18 column by a gradient mobile phase adapted from Zuo *et al.*
                [2002]. The wavelength of detection was 272 nm and the chromatogram was
                obtained after the addition of rutin.
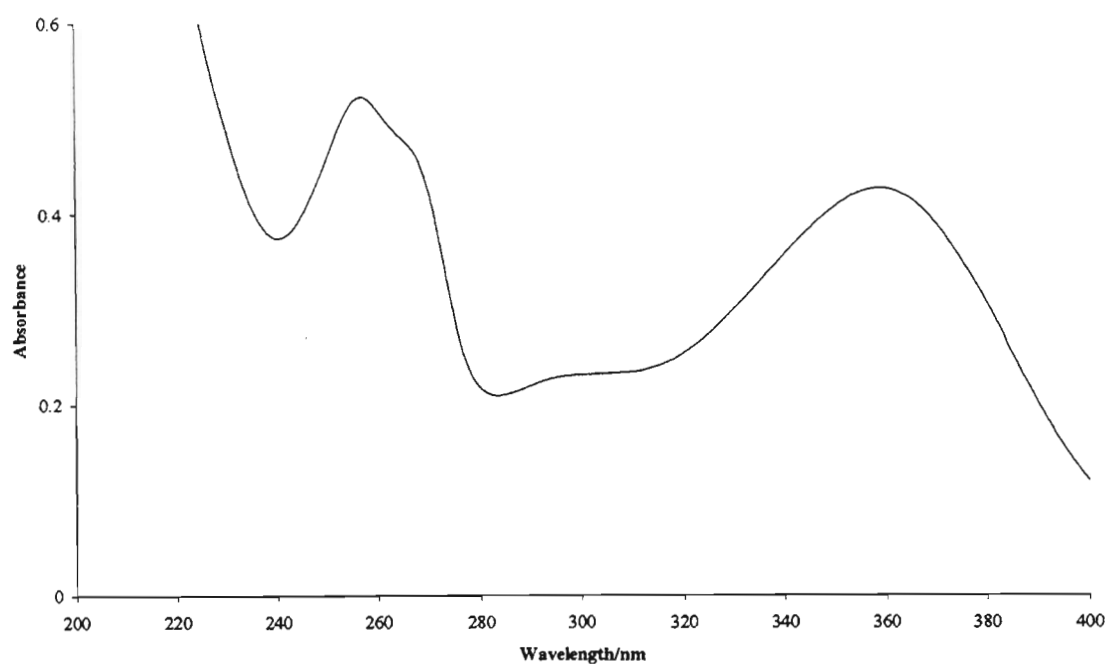
Figure 3.18:   UV spectrum of rutin dissolved in methanol obtained with the Perkin Elmer
                Lambda 35 UV/VIS spectrophotometer in a 1 cm pathlength quartz cuvette with
                air as the reference.

Table 3.4:   The retention times for rutin or a rutin-like compound in the various
                chromatograms of Cancer Bush and Rooibos tea extracts analysed by HPLC.

Extract	Retention time of rutin or a rutin-like compound/minutes	
	Gradient of Zuo *et al.* [2002]	Adapted gradient from Zuo *et al.* [2002]
Methanol-water Cancer Bush extract	30.569	-
High temperature Cancer Bush extract	30.657	-
Boiling water extract of non-ground Cancer Bush leaves	32.229	-
Boiling water extract of ground Cancer Bush leaves	30.963	-
Ethanol-water Cancer Bush extract	-	50.236
Ethanol-water Rooibos tea extract	-	50.185
Ethanol-water Rooibos-black extract	-	49.462
Ethanol-water Rooibos-honeybush extract	-	49.449

Based on the assumption that the flavonol peak eluting at about 50 minutes in the ethanol-water Cancer Bush extract (see Figure 3.16) was rutin, quantification was carried out by means of a calibration curve (see Figures 2.28 and 2.29 in Section 2.5.2).

The peak area of rutin if present in a 0.3308 g ethanol-water Cancer Bush extract dissolved in 2 ml methanol (see Figure 3.16) was 60.7×10^4 µV s. This peak area corresponds to $7.59 \pm 0.10 \times 10^{-5}$ M or $9.27 \pm 0.12 \times 10^{-5}$ g of rutin. Therefore if rutin is present in the ethanol-water Cancer Bush extract, it occurs in 0.0280% (by mass) of the extract corresponding to 0.280 mg rutin per gram of extract. This rutin concentration is much less than that found in an aqueous extract of fermented Rooibos tea (Erickson [2003]).

3.1.2.2 GC-FID analysis of the ethanol-water extract

Natural polyphenols have high molecular masses and are non-volatile and very polar. They contain a large number of hydroxyl groups in their structure that need to be derivatised to form the more volatile silyl derivatives for GC analysis.

The ethanol-water Cancer Bush extract was derivatised with both bis(trimethylsilyl)acetamide (BSA) and bis(trimethylsilyl)trifluoroacetamide (BSTFA) as explained in Section 2.6. A small amount of the ethanol-water extract was weighed (between 10-50 mg) and derivatised by each silylating agent. A 1 µl portion of the derivatised extract was injected into both the Fisons and the PE Autosystem GC instruments, and eluted by a temperature program adapted from Soleas *et al.* [1997 and 1999]. The gas chromatograms in Figures 3.19-3.22 show how both BSA and BSTFA were able to derivatise the extract as well as confirm the presence of polyphenols in the extract.

The gas chromatograms obtained with BSA and BSTFA derivatised extracts using the PE Autosystem GC instrument showed remarkable resemblance, as did those obtained using the Fisons GC instrument. This could be the result of similarly derivatised compounds since both methods involved the formation of trimethyl silyl derivatives.

This GC-FID analysis showed that it was possible to successfully derivatise the ethanol-water Cancer Bush extract and separate the components. However, without a wide range of standard polyphenols that could be used to authenticate the components it was impossible to identify

them. Hence GC-MS analysis was performed as it would indicate the fragmentation pattern of the various components which would aid in identifying them.
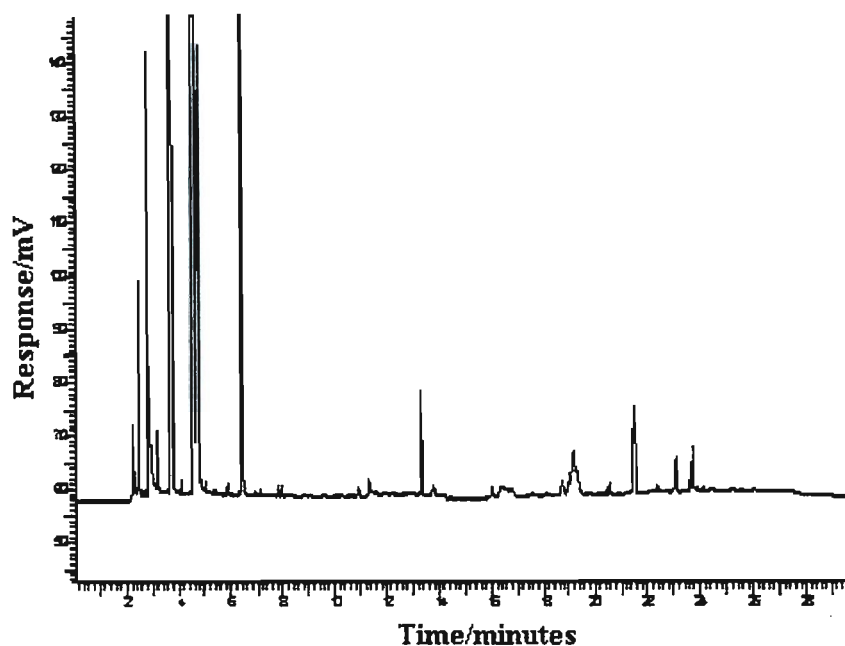
Figure 3.19: The gas chromatogram of the ethanol-water Cancer Bush extract derivatised by BSA/pyridine obtained by the temperature program adapted from Soleas *et al.* [1997 and 1999] with the Fisons GC instrument. The peak eluting at 4.4 minutes is due to pyridine and the rest of the peaks before 6.5 minutes are due to BSA.
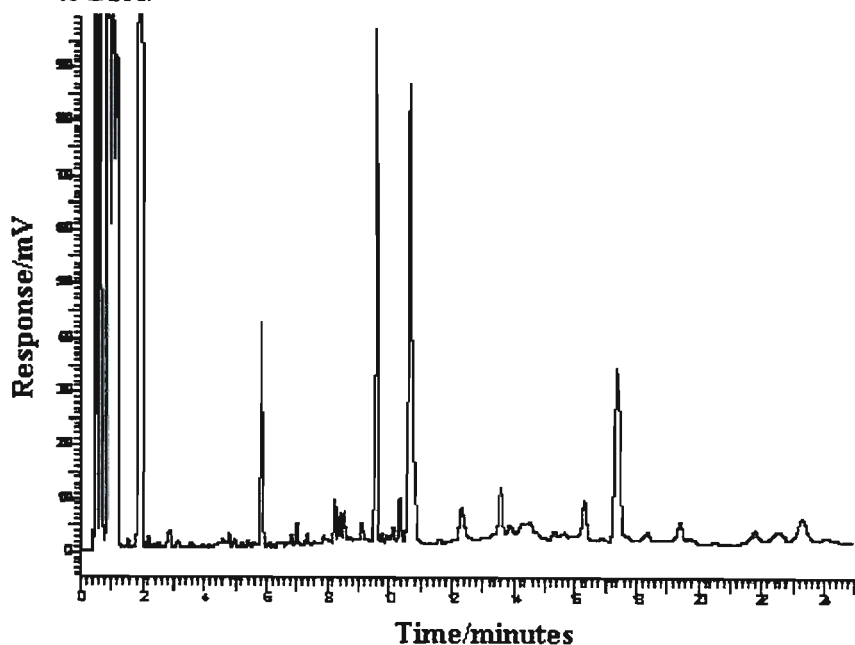
Figure 3.20: The gas chromatogram of the ethanol-water Cancer Bush extract derivatised by BSA/pyridine obtained by the temperature program adapted from Soleas *et al.* [1997 and 1999] with the PE Autosystem GC instrument. The peak eluting at 0.5 minutes and those below 2 minutes are due to pyridine and BSA respectively.
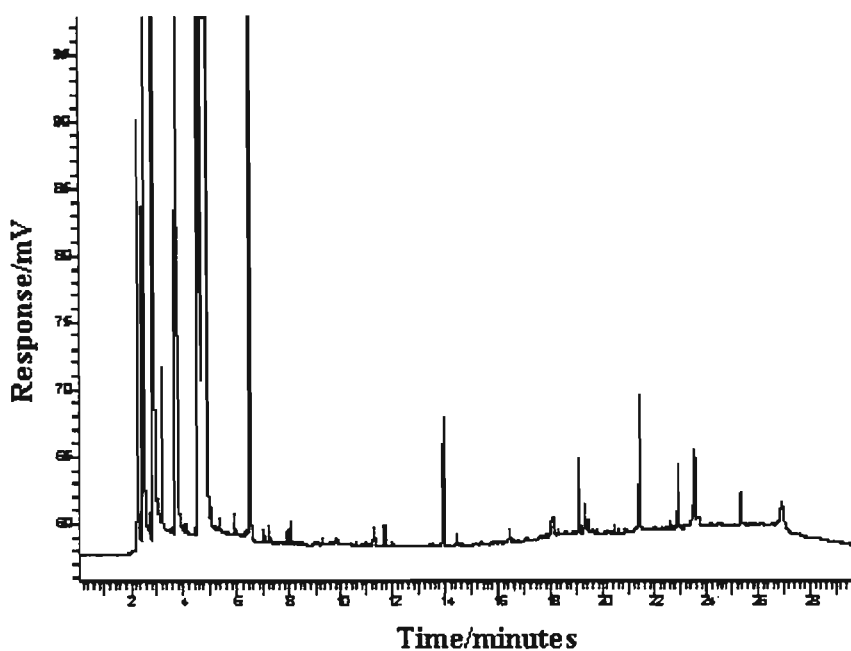
Figure 3.21:   The gas chromatogram of the ethanol-water Cancer Bush extract derivatised by BSTFA/pyridine obtained by the temperature program adapted from Soleas *et al.* [1997 and 1999] with the Fisons GC instrument. The peak eluting at 4.4 minutes is due to pyridine and the rest of the peaks before 6.5 minutes are due to BSA.
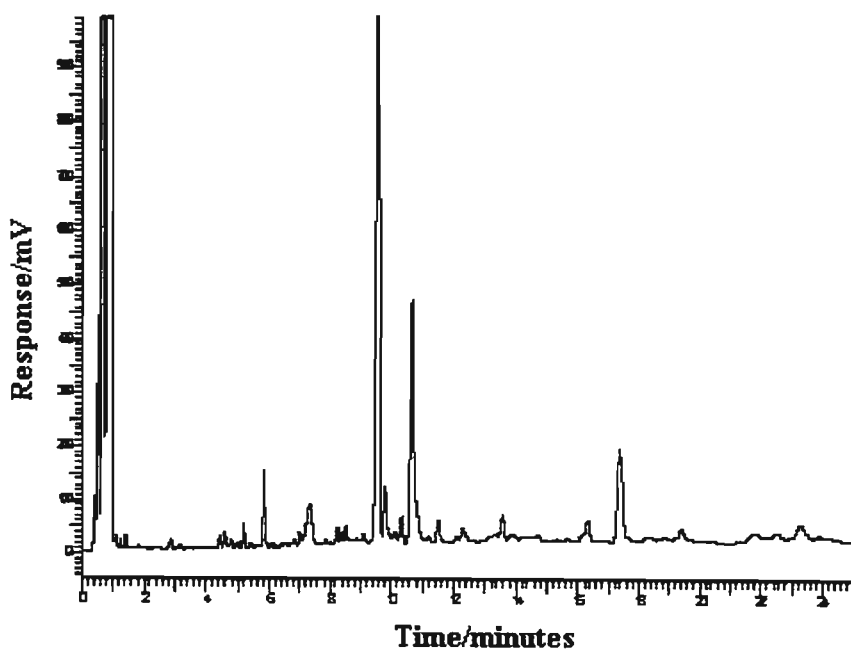
Figure 3.22:   The gas chromatogram of the ethanol-water Cancer Bush extract derivatised by BSTFA/pyridine obtained by the temperature program adapted from Soleas *et al.* [1997 and 1999] with the PE Autosystem GC instrument. The peak eluting at 0.4 minutes and those below 6 minutes are due to pyridine and BSTFA respectively.

3.1.2.3 GC-MS analysis of the ethanol-water extract

The ethanol-water Cancer Bush extract was re-derivatised for GC-MS analysis. The general mechanism of silylation by BSA and BSTFA is illustrated in Figure 3.23.

$$
\begin{array}{l}
\overset{\text{O—TMS}}{\underset{|}{}} \\
X_3C-C{=}N-TMS \;+\; H-O-R \\
m/z\ 204\ (BSA) \\
m/z\ 257\ (BSTFA)
\end{array}
$$

$$
\begin{array}{l}
\overset{\text{O—TMS}}{\underset{|}{}} \\
X_3C-C{=}N-H \quad + \quad TMS-O-R \xrightarrow{\;+\;H-O-R\;}
\end{array}
\quad
\begin{array}{l}
\overset{\text{O—H}}{\underset{|}{}} \\
X_3C-C{=}N-H \quad + \quad TMS-O-R
\end{array}
$$

m/z 132 (BSA) m/z 59 (BSA)
m/z 185 (BSTFA) m/z 113 (BSTFA)

R = Alkyl or Aromatic
X = H (BSA) or F (BSTFA)
TMS = Si(CH$_3$)$_3$, m/z 73
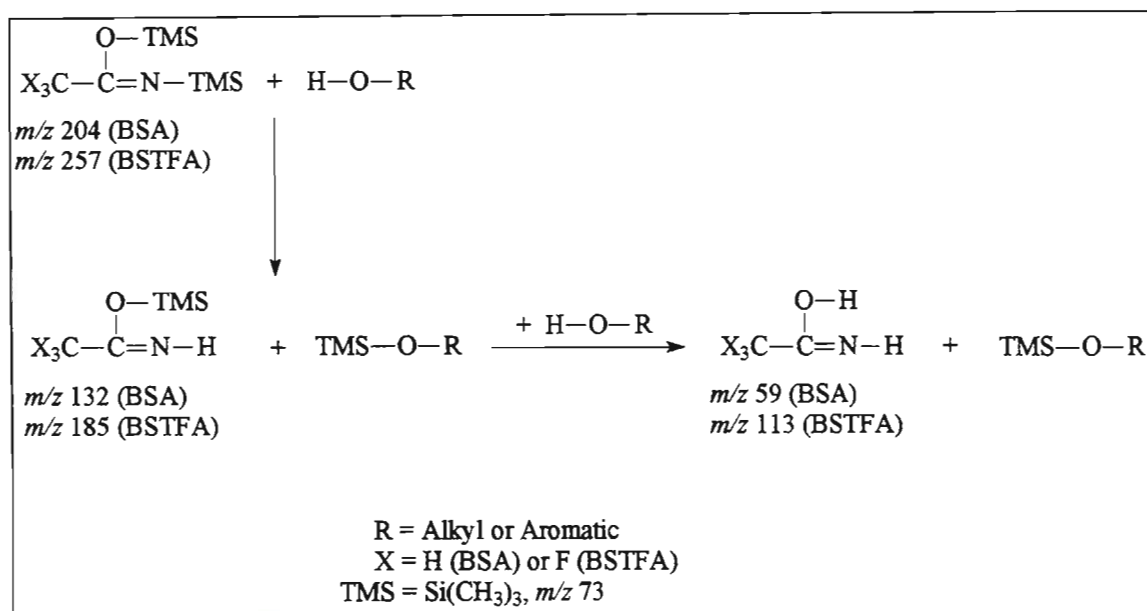
Figure 3.23:   Silylation mechanism of phenolics by BSA and BSTFA.

Derivatised polyphenols are of even higher molecular mass than the corresponding free polyphenols, such that their molecular ions are beyond the maximum detectable mass of 550 amu of the Agilent GC-MS used to analyse them. Therefore, the presence of high molecular mass polyphenolic compounds in the ethanol-water extract had to be assigned based on their fragmentation patterns. All fragmentations were compared with those available in the NIST98 library available on the Agilent GC-MS instrument. HPLC and UV spectroscopy analysis (see Section 3.1.1) provided an indication of the polyphenols that could be present in the ethanol-water Cancer Bush extract. Common polyphenols in plants include flavonoids such as catechins, flavonols and flavones.

The pyridine solvent used during the derivatisation procedures eluted quickly through the GC columns investigated in Section 3.1.2.2. Consequently, a three-minute solvent delay was adequate for eluting the solvent before GC-MS analysis of the samples.

Before the GC-MS analysis of the ethanol-water Cancer Bush extract, Rooibos tea was analysed since a lot is known about its polyphenolic composition (Erickson [2003]).

MS fragmentation of Rooibos tea

Rooibos tea is a known source of polyphenolic substances. Gallic acid was shown, in Section 3.1.1.2, to be present in the ethanol-water extract of Rooibos tea. Hence, the suitability of the derivatisation technique employed was assessed based on the derivatisation of gallic acid in the ethanol-water Rooibos tea extract.

The total ion chromatogram of the BSTFA/pyridine derivatised ethanol-water Rooibos tea extract, together with the mass spectra of each compound in the extract are displayed in Appendix C in Figures C1.1 and C1.2-C1.69 respectively. Gallic acid was successfully derivatised (to the structure shown in Figure 3.24) and eluted at 13.750 minutes. Figure C1.39 shows its MS fragmentation pattern which matches that of a trimethyl silylated gallic acid standard present in the NIST98 library as well as that obtained by Owen *et al.* [2003].
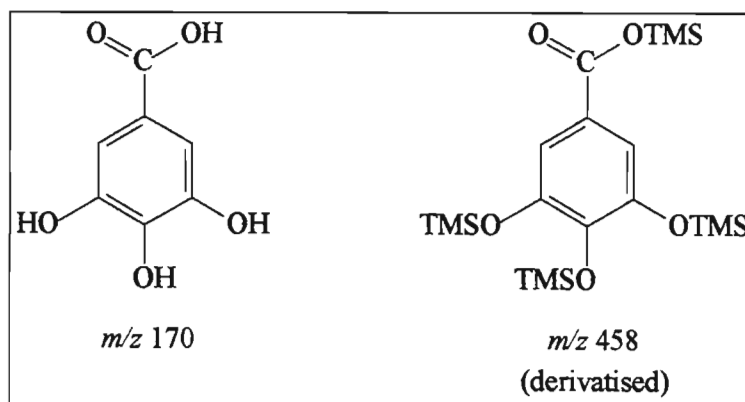
Figure 3.24: The chemical structure and molecular mass of gallic acid before and after silylation.

Other compounds that were successfully derivatised include various benzoic acids (Figures C1.10, C1.15, C1.20 and C1.26), 4-hydroxyphenyl ethanol (Figure C1.18), benzenepropanoic acid (Figures C1.19 and C1.36), benzeneacetic acid (Figure C1.21), *p*-coumaric acid (Figure C1.28), tetradecanoic acid (Figure C1.32), syringic acid (Owen *et al.* [2003]) (Figure C1.35), cinnamic acid (Figure C1.37), hexadecanoic acid (Figure C1.41), ferulic acid (Owen *et al.* [2003]) (Figure C1.44), octadecanoic acid (Figure C1.52), cholesta-3,5-diene (Figure C1.53) and 4-hydroxy-3-methoxyphenethylene glycol (Figure C1.61). These compounds identified were simple phenolics and fatty acids with *m/z* values of their molecular ions within the detectable limit of the Agilent GC-MS. The phenolic acids: syringic acid, ferulic acid and p-coumaric acid, are known to exist in Rooibos tea (Erickson [2003]).

A possible catechin or epicatechin fragmentation pattern was seen with the compound shown in Figure C1.69, as was observed by Donovan *et al.* [1999] and Luthria *et al.* [1997]. Catechins undergo a retro-Diels-Alder (RDA) fragmentation to form two principal fragments (Miketova *et al.* [1998]): an A-ring ion and a B-ring ion (see Figure 3.25), as illustrated by the mechanism from Zeeb *et al.* [2000]. When these catechins are derivatised prior to fragmentation, the *m/z* values of the RDA fragments appear as displayed in Table 3.5.

Donovan *et al.* [1999] and Luthria *et al.* [1997] derivatised catechin and epicatechin with a similar method as was used in this work with BSTFA/pyridine. They obtained similar fragmentation patterns; the *m/z* values of these fragments with their respective abundances are displayed in Table 3.6. These fragmentation patterns were found to be similar to that of the compound in Figure C1.69.
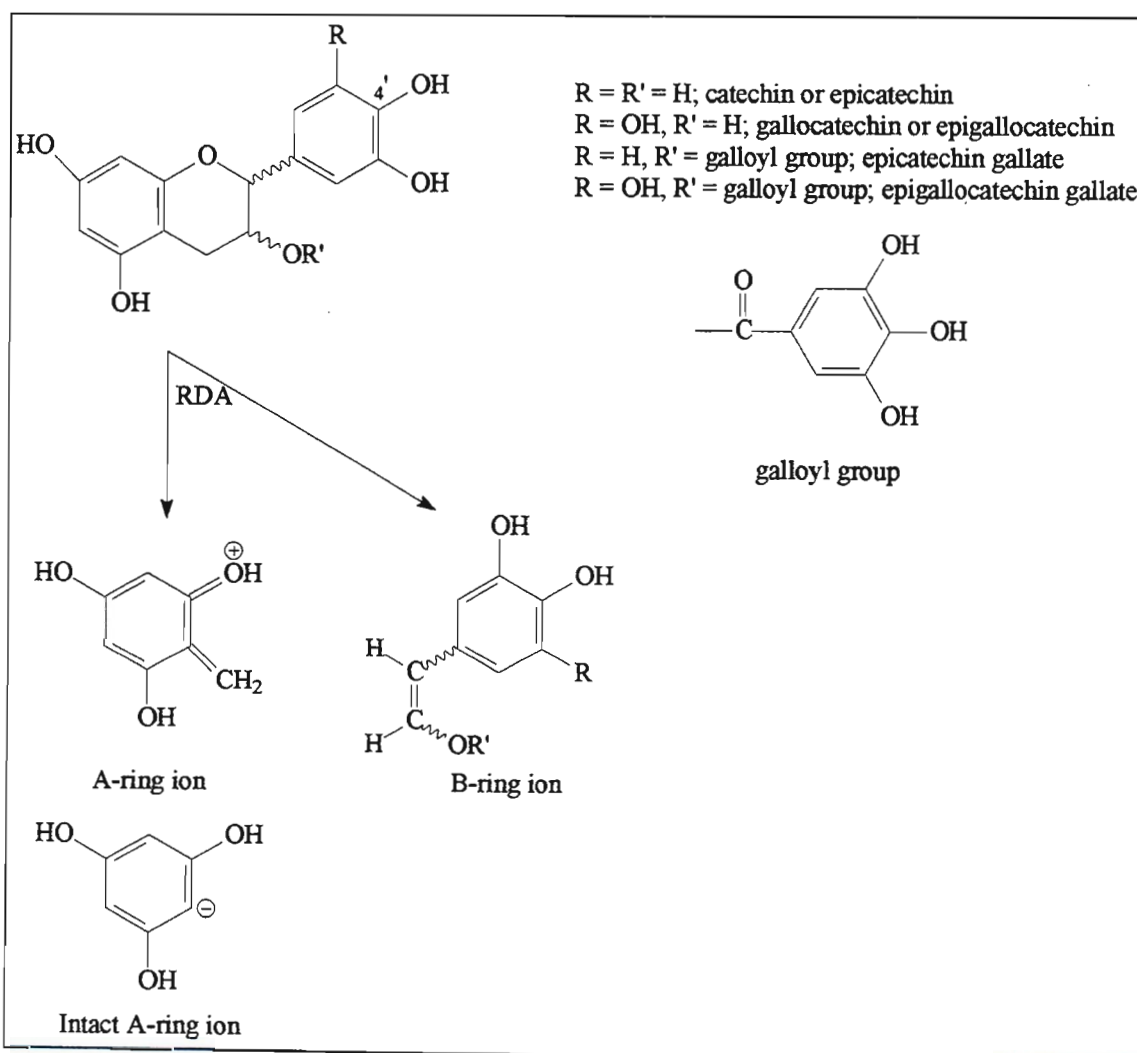
Figure 3.25: Retro-Diels-Alder fragmentation of typical catechin compounds showing their respective mass spectral fragments (Miketova *et al.* [1998]).

Table 3.5:   The *m/z* values of derivatised and non-derivatised fragments from the retro-
              Diels-Alder fragmentation of catechins.

m/z values				Catechin
A-ring ion		B-ring ion		
Non-derivatised	Derivatised	Non-derivatised	Derivatised	
139	283	152	368	Catechin, epicatechin
139	283	168	456	Gallocatechin, epigallocatechin
139	283	304	664	Epicatechin gallate
139	283	320	752	Epigallocatechin gallate

Table 3.6:   The *m/z* values of catechin and epicatechin fragments with their respective
              abundances when derivatised by BSTFA/pyridine by Donovan *et al.* [1999] and
              Luthria *et al.* [1997].

m/z values	Abundances/%	
	Donovan *et al.* [1999]	Luthria *et al.* [1997]
650 (Molecular ion)	5-6	2-4 (catechin) 2-9 (epicatechin)
368 (B-ring ion)	100	100 (Catechin) 100 (epicatechin)
355	30-37	31 (catechin) 37 (epicatechin)
283 (A-ring ion)	1-3	0.9 (catechin) 1.5 (epicatechin)

MS fragmentation of BSA- and BSTFA-derivatised Cancer Bush extract

The total ion chromatogram obtained when the ethanol-water Cancer Bush extract was derivatised by BSTFA and with the mass spectra of all compounds present in the extract are displayed in Appendix C, Figures C2.1 and C2.2-C2.28 respectively. The total ion chromatogram of the BSA-derivatised ethanol-water Cancer Bush extract with mass spectra of

all compounds in the extract are displayed in Appendix C, Figures C3.1 and C3.2-C3.50 respectively.

BSTFA successfully derivatised alpha-linolenic acid in the ethanol-water Cancer Bush extract (Figure C2.24). A possible quercetin fragmentation pattern was also observed for the compound in Figure C2.5, as was observed by Tokuşoğlu et al. [2003] (as shown in Table 3.7). This compound could be rutin or a rutin-like compound which was shown to be present by HPLC in the ethanol-water Cancer Bush extract in Section 3.1.2.1. The flavonol O-glycosides such as rutin, possibly present in both the ethanol-water Cancer Bush and Rooibos tea extracts, fragment (Sánchez-Rabaneda et al. [2003]) into the deprotonated glycoside and aglycoside. The rutin aglycone is quercetin, hence rutin would fragment as quercetin thereafter.

Owen et al. [2003] and Tokuşoğlu et al. [2003] showed fragments of BSTFA/pyridine derivatised flavonoids. The m/z values and the abundances for each of the fragments are given in Table 3.7. Tokuşoğlu et al. [2003] identified the presence of quercetin, myricetin and kaempferol in tomato pastes and other tomato-based products from fragments of low m/z values only, as in this research. The fragmentation of these flavonoids are very different from those of non-derivatised flavonoids, whose principal structures were formed from a retro-Diels-Alder fragmentation (Fabre and Rustan [2001]). Hence fragmentation patterns of the compounds in the derivatised extracts in this work were only compared with those of derivatised flavonoids in the literature.

Table 3.7:   The m/z values of the fragmentation of gallic acid, quercetin, myricetin and kaempferol derivatised by BSTFA/pyridine.

Polyphenol	m/z values (Abundance in percent, %)	
	Owen et al. [2003]	Tokuşoğlu et al. [2003]
Quercetin	662(0.96), 661(1.2), 647(100), 559(12)	281(100), 273, 207, 95, 81
Myricetin	750(1), 749(1.2), 745(100), 647(18)	279(100), 167, 149, 71, 40
Kaempferol	574(0.90), 573(1.4), 559(100), 487(6), 272(6)	281, 207(100), 200, 73, 55

BSA successfully derivatised benzoic acid (Figure C3.5), benzofuranone (Figure C3.8), dodecanoic acid (Figure C3.9), hexadecanoic acid (Figure C3.24), octadecatrienoic acid (Figure C3.26), octadecanoic acid (Figures C3.27 and C3.31), alpha-linolenic acid (Figure C3.30), squalene (Figure C3.39) and cyclotetracosane (Figure C3.40).

Alpha-Linolenic acid is an essential fatty acid that was present in both the BSA- and BSTFA-derivatised ethanol-water Cancer Bush extracts. This compound did not elute at the same retention time when the two derivatised extracts were eluted by the same temperature program, meaning they were either not the same compound or they may have been derivatised differently. Most of the compounds identified in the derivatised Cancer Bush extracts were simple phenolics and fatty acids, as was observed with the derivatised Rooibos tea extract. These compounds have molecular ions with m/z values in the detectable range of the Agilent GC-MS, hence their whole fragmentation patterns were reported.

3.1.3 Antioxidant properties of the Cancer Bush extracts

The presence of potential polyphenols in the Cancer Bush extracts has been shown by UV and HPLC analyses, whereas GC-MS investigations showed the presence of simple phenols in the ethanol-water Cancer Bush extract. These phenolics are antioxidants (Erickson [2003]) hence they could act as potential photostabilisers of photo-unstable chemical absorbers. In this section, the results of the phenol quantitation (see Section 3.1.3.1) and the antioxidant activity analyses (see Section 3.1.3.2) of the ethanol-water Cancer Bush extract are discussed. The phenolics present in the extract were quantified by the Folin-Ciocalteu reagent (FCR) as described in Section 2.2.5.2. The antioxidant activity of the extract was measured by its ability to scavenge a stable free radical as described in Section 2.2.5.1.

3.1.3.1 Phenol Quantitation

The Folin-Ciocalteu reagent (FCR) method is a simple, yet accurate, method for quantitating phenols in a sample. This method, however, lacks specificity in the type of phenolics it quantitates (Peterson [1983]). Therefore it will not discriminate between the presence of polyphenols or just simple phenols present in the ethanol-water Cancer Bush extract.

The procedure for quantitating phenols in the ethanol-water Cancer Bush extract by the FCR method was outlined in Section 2.2.5.2. In this method, gallic acid was used as the standard for

obtaining a calibration curve (see Table 2.3 and Figure 2.4 in Chapter 2), and the phenolic quantity in the extract is reported in milligram gallic acid equivalents per liter (mg GAE/liter).

The ethanol-water Cancer Bush extract had an average absorbance of 0.107 at 765 nm when determined by the FCR method. This corresponds to a volume of 274 ± 39 μl of the 507 mg l^{-1} gallic acid solution from the calibration curve displayed in Figure 2.4. Equation 3.1 shows how the concentration of gallic acid in μg/ml corresponding to this volume of gallic acid is obtained when account is taken of the dilution factors (see Section 2.2.5.2) involved in this experiment.

$$\text{Concentration GAE} = \left(\frac{50700\,\mu g}{100\,\text{ml}}\right)\left(\frac{274 \times 10^{-3}\,\text{ml}}{10\,\text{ml}}\right) = 13.9 \pm 2\,\mu g\,\text{GAE/ml}$$

<div align="right">Equation 3.1</div>

Hence, a mass of 0.0175 g of the total extracted 0.3308 g ethanol-water Cancer Bush extract (see Section 2.2.4) had a phenolic content that corresponded to 13.9 ± 2 μg GAE/ml. This would mean that a 0.3308 g extract of 5 g Cancer Bush leaves would contain 262 ± 38 μg GAE/ml. If it is assumed that all polyphenolics were extracted into the ethanol-water Cancer Bush extract, then the initial 5 g of the Cancer Bush leaves that were extracted (see Section 2.2.4) will contain 262 ± 38 μg GAE/ml. But the ethanol-water Cancer Bush extract was dissolved in 25 ml aqueous ethanol, then a 100 μl aliquot of this solution was further diluted in 10 ml during the phenol quantitation experiment (see Section 2.2.5.2). Therefore the phenolic content, 262 ± 38 μg GAE/ml, would correspond to the concentration of the Cancer Bush extract calculated in Equation 3.2 and the phenolic content can be expressed as in Equation 3.3.

$$\text{Concentration Cancer Bush} = \left(\frac{5\,g}{25\,\text{ml}}\right)\left(\frac{100 \times 10^{-3}\,\text{ml}}{10\,\text{ml}}\right) = 0.002\,\text{g/ml} = 2000\,\mu g/\text{ml}$$

<div align="right">Equation 3.2</div>

$$\text{Concentration GAE} = \left(\frac{262 \ \mu g \ \text{GAE/ml}}{2000 \ \mu g/\text{ml}} \right) = 0.131 \pm 0.019 \ \mu g \ \text{GAE per gram Cancer Bush leaves}$$

$$= 131 \ \text{mg GAE per gram Cancer Bush leaves}$$

<div align="right">Equation 3.3</div>

Hence, the Cancer Bush leaves will contain a phenolic concentration equivalent to 131 ± 19 mg GAE per gram of Cancer Bush leaves. This phenolic content exceeds those reported for caneberries which ranged between 30.94 – 57.65 mg GAE per gram of dry matter (Wada and Ou [2002]) and date fruits which ranged from 2.49 to 8.36 mg GAE per 100 g fresh fruit (Mansouri et al. [2005]). But the phenolic content was much less than the total polyphenol content of ethyl acetate extracts of fermented and unfermented rooibos tea which were reported to be 558.2 and 483.0 mg GAE per gram soluble solids (Joubert et al. [2004]).

3.1.3.2 Radical scavenging property

The Cancer Bush extract was investigated for its radical scavenging ability by reacting it with a stable free radical, namely diphenylpicrylhydrazyl radical (DPPH). The progress of the reaction can be monitored by measuring the loss of DPPH absorption at its wavelength of maximum absorption (λ_{max}) at 522 nm. When the radical was reacted with the Cancer Bush extract, a loss in absorbance at its λ_{max} was observed with time. Figure 3.26 shows how the DPPH radical contained in a 52 μM aqueous ethanol solution was scavenged by a 453 μg/ml ethanol-water Cancer Bush extract. After four hours the Cancer Bush extract had scavenged all the DPPH radicals. This implies that the Cancer Bush extract (CB) acted as a hydrogen donor towards the DPPH radical, $D^{\bullet}$ (see Equation 3.4). The stoichiometry of the reaction depends on the number of sites for hydrogen abstraction on the donor compound. Polyphenols would therefore act as ideal donors since they contain conjugated phenyl rings, hydroxyl groups and carbonyl groups that are able to delocalise the radical electron left on the compound (Valcic et al. [1999]).

$$D^{\bullet} + CB - H \rightarrow D - H + CB^{\bullet}$$

<div align="right">Equation 3.4</div>
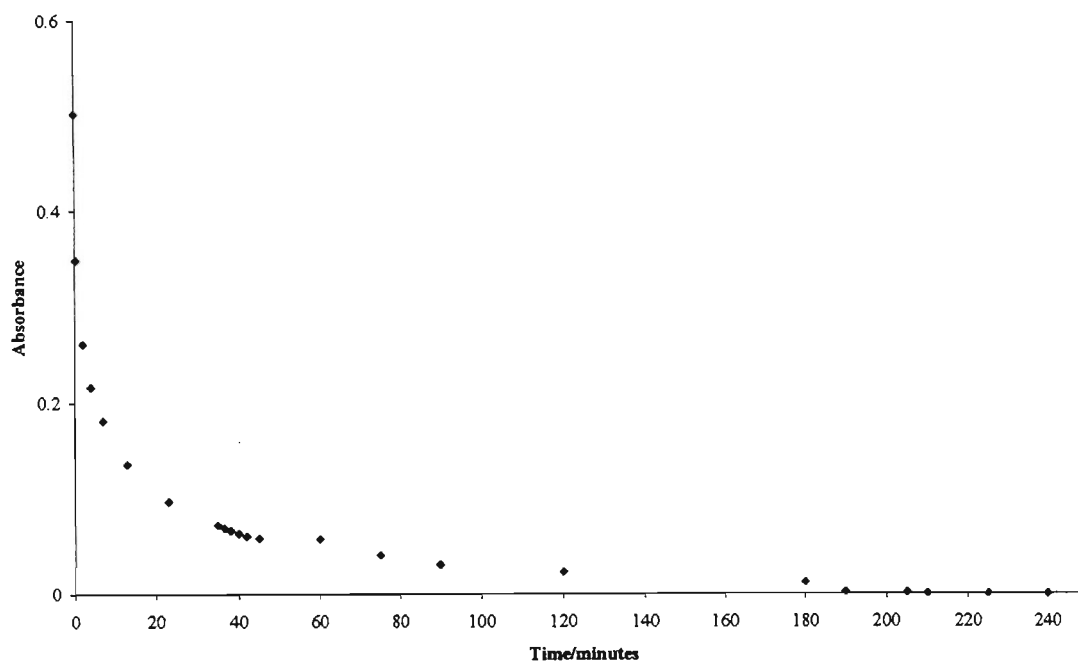
Figure 3.26:   Loss in absorbance of the DPPH radical at 522 nm in the presence of the ethanol-water Cancer Bush extract with time.

The reaction with the DPPH radical was investigated with differing amounts of the ethanol-water Cancer Bush extract in order to determine the amount of extract required to cause the complete loss of the radical absorption at 522 nm. Table 3.8 shows the resulting UV absorbances for solutions containing the DPPH radical and different amounts of the ethanol-water Cancer Bush extract. Each mixture was allowed to stand for 4 hours after being mixed to allow the reaction to reach completion. In order to calculate the concentration of extract required to decrease the initial DPPH absorption at 522 nm by 50%, IC_{50}, Equation 3.5 was employed.

$$\text{DPPH scavenged} / \% = 100\left[1 - \left(\frac{A_{522}\ \text{control} - A_{522}\ \text{sample}}{A_{522}\ \text{control}}\right)\right]\qquad \text{Equation 3.5}$$

Table 3.9 shows the amount of DPPH scavenged, in percentage, by different amounts of the extract, and the results of both Tables 3.8 and 3.9 have been plotted together in Figure 3.27. The volume of the ethanol-water Cancer Bush extract required for 50% scavenging of the DPPH radical was determined to be 260 ± 21 µl. This was done by interpolating the points on the graph of absorbance/percentage DPPH scavenged against volume of extract shown in Figure

3.27, and reading off the volume of extract at the point of intersection of the two curves. A 260 µl aliquot of the 0.0453 g ethanol-water Cancer Bush extract in 25 ml aqueous ethanol was diluted to 1 ml, and was further diluted to a total volume of 4 ml for the DPPH reaction. Equation 3.6 shows how the IC_{50} value of the ethanol-water Cancer Bush extract was calculated, keeping in mind all the dilution factors involved.

$$IC_{50}\,(\mu g/ml) = \left(\frac{45300\ \mu g}{25\ ml}\right)\left(\frac{260\ \mu l}{1\ ml}\right)\left(\frac{1\ ml}{4\ ml}\right)\left(\frac{1\ ml}{1000\ \mu l}\right) = 118 \pm 9\ \mu g/ml$$

Equation 3.6

Therefore, 118 ± 9 µg/ml of the ethanol-water Cancer Bush extract was required to scavenge the DPPH radical by 50% in a 52 µM aqueous ethanol solution. Lu *et al.* [2003] reported that the IC_{50} values for ethanolic extracts of propolis (a substance utilised by bees for safeguarding their hives (Chang *et al.* [2002])) ranged between 17.90 and 108.05 µg/ml with a 300 µM DPPH methanol solution. By comparison, the Cancer Bush extract showed a much lower scavenging ability.

Table 3.8:   DPPH absorbance values at 522 nm of 52 µM DPPH solutions prepared with different volumes of the ethanol-water Cancer Bush extract. The absorbance readings were recorded four hours after mixing the reagents.

Volume of Extract/100 µl	DPPH absorbance			Standard deviation
	Trial 1	Trial 2	Average	
0	0.4979	0.4769	0.4874	0.0148
1	0.3921	0.3941	0.3931	0.0014
2	0.3040	0.3170	0.3105	0.0092
3	0.2032	0.2332	0.2182	0.0212
4	0.1090	0.1540	0.1315	0.0318
5	0.1150	0.1140	0.1145	0.0007
6	0.0740	0.0800	0.0770	0.0042
7	0.0460	0.0570	0.0515	0.0078
8	0.0300	0.0390	0.0345	0.0064
9	0.0250	0.0310	0.0280	0.0042
10	0.0260	0.0310	0.0285	0.0035

Table 3.9:   Percentage DPPH scavenged by 52 μM DPPH solutions prepared with different volumes of the ethanol-water Cancer Bush extract.

Volume of Extract/100 μl	DPPH scavenged/%			Standard deviation
	Trial 1	Trial 2	Average	
0	0.00	0.00	0.00	0.00
1	21.25	17.36	19.31	2.75
2	38.94	33.53	36.24	3.82
3	59.19	51.10	55.15	5.72
4	78.11	67.71	72.91	7.35
5	76.90	76.10	76.50	0.57
6	85.14	83.22	84.18	1.36
7	90.76	88.05	89.41	1.92
8	93.97	91.82	92.90	1.52
9	94.98	93.5	94.24	1.05
10	94.78	93.5	94.14	0.91
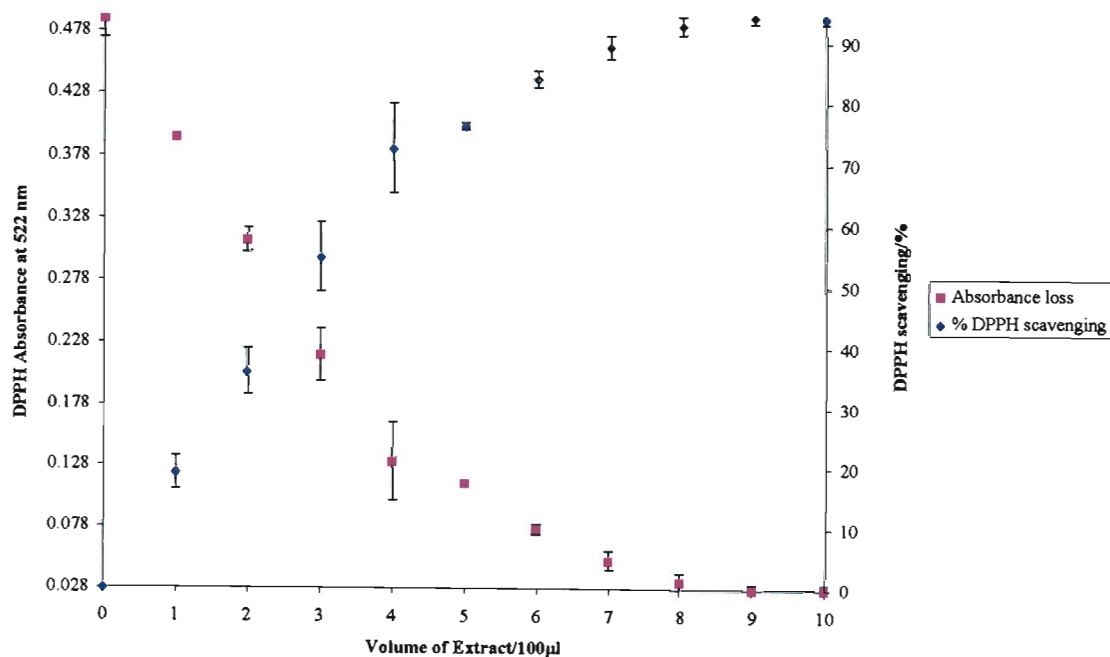
Figure 3.27:   Loss in absorbance and percent DPPH radical scavenged after 4 hours equilibration of solutions containing different volumes of the ethanol-water Cancer Bush extract to make up a 52 μM DPPH solution each time.

3.1.4 Photostability of the Cancer Bush extracts

The ethanol-water extract and the boiling water extract of ground Cancer Bush leaves were found to give the most diverse yields of potential polyphenolic substances. The photostability of these extracts was determined in order to understand the mechanism involved and to be able to distinguish the photo-instability due to the chemical absorbers in mixtures with the extracts. The photostability of the extracts was investigated by UV spectroscopy and high-performance liquid chromatography.

3.1.4.1 Photostability of the Cancer Bush extract investigated by UV spectroscopy

UV spectroscopy requires samples of relatively low concentration. The ethanol-water extract and the boiling water extract of ground Cancer Bush leaves were therefore adequately diluted so that their UV absorptions conformed to Beer's law as described in Section 2.2. The photostability of each extract was investigated when irradiated by the Osram HBO 500 W/2 high pressure mercury lamp, with light of wavelengths greater than 300 nm in a 1 cm pathlength quartz cuvette. Each extract was irradiated in every solvent where it would be used to photostabilise photo-unstable chemical absorbers. The boiling water extract of ground Cancer Bush leaves was irradiated in methanol (see Figure 3.28), DMSO (see Figure 3.29) and Millipore water (see Figure 3.30). On the other hand, the ethanol-water Cancer Bush extract was irradiated in ethyl acetate (see Figure 3.31) and cyclohexane (see Figure 3.32).

Figures 3.28-3.30 show that the boiling water extract of ground Cancer Bush leaves is more photostable in Millipore water than in methanol or DMSO. After the total one and a half hours of irradiation, the extract in methanol showed its greatest absorbance loss of about 0.13 at around 353 nm, whereas in DMSO a loss of 0.16 was observed at around 281 nm. The extract dissolved in Millipore water was relatively photostable throughout the one and a half hours of irradiation, showing not more than a loss of 0.05. The boiling water extract of ground Cancer Bush leaves was relatively photostable in all solvents investigated compared with the ethanol-water Cancer Bush extract.

The ethanol-water Cancer Bush extract was photo-unstable in both ethyl acetate and cyclohexane. In both solvents, the photo-instability of the extract increased towards 400 nm. In cyclohexane, an absorbance loss of 0.45 was observed at 400 nm at the end of the one and a half hour irradiation period. In ethyl acetate, the loss was of an even higher magnitude of 0.85 at the same wavelength after the total one and a half hours of irradiation. In both solvents though, the

extract appeared photostable towards shorter wavelengths. In cyclohexane, isosbestic points were observed at shorter wavelengths, indicating the possible formation of photoproducts in this solvent.
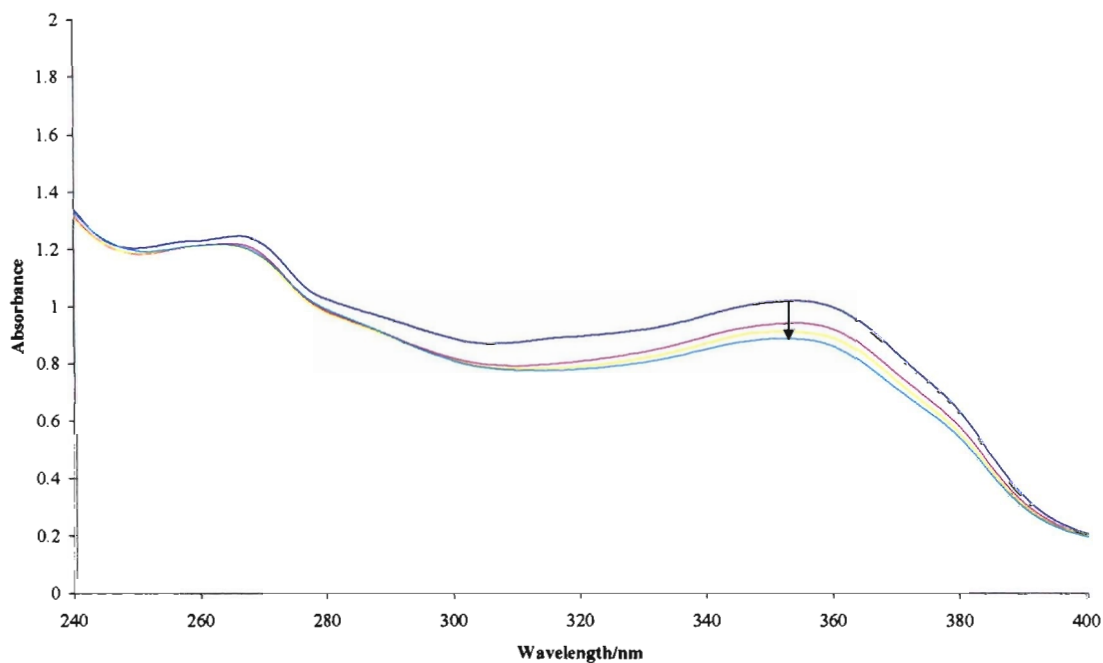
Figure 3.28:   The UV spectra of the boiling water Cancer Bush extract dissolved in methanol obtained after each 30 minute irradiation interval for a total period of one and a half hours. The spectra were recorded in a 1 cm pathlength quartz cuvette against air as the reference.
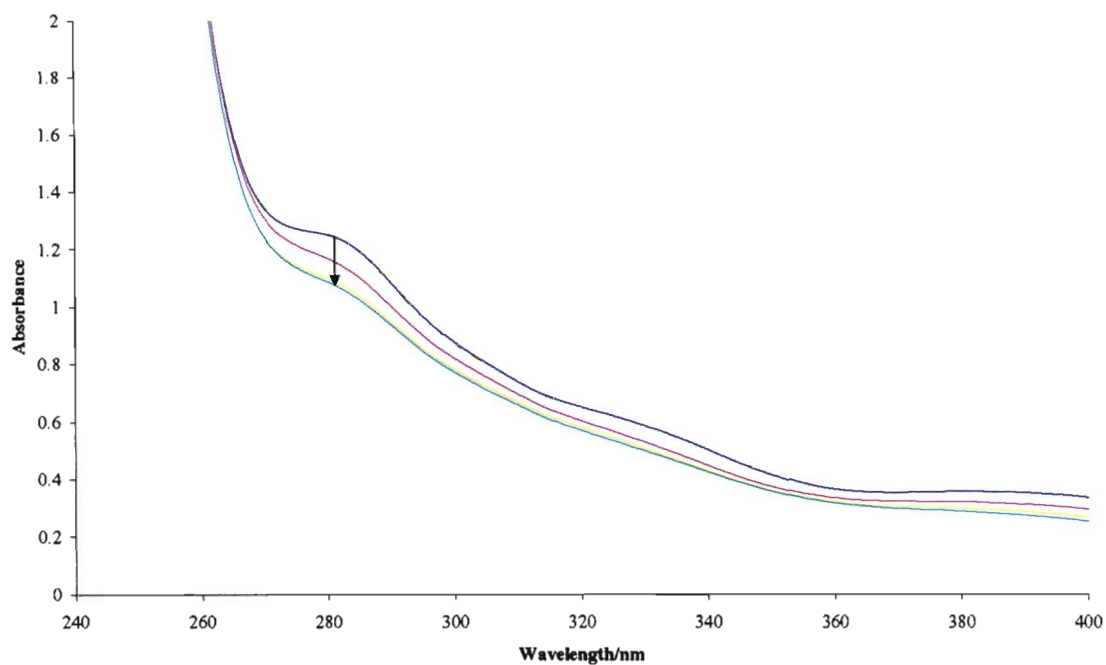
Figure 3.29:   The UV spectra of the boiling water Cancer Bush extract dissolved in DMSO obtained after each 30 minute irradiation interval for a total period of one and a half hours. The spectra were recorded in a 1 cm pathlength quartz cuvette against air as the reference.
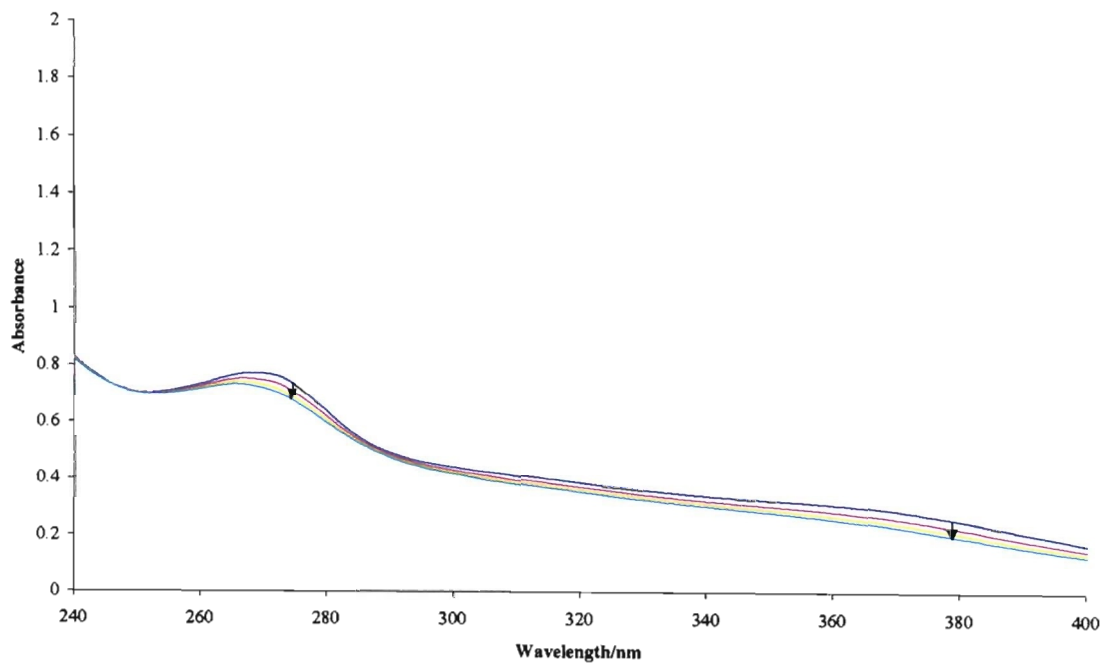
Figure 3.30:   The UV spectra of the boiling water Cancer Bush extract dissolved in Millipore water obtained after each 30 minute irradiation interval for a total period of one and a half hours. The spectra were recorded in a 1 cm pathlength quartz cuvette against air as the reference.
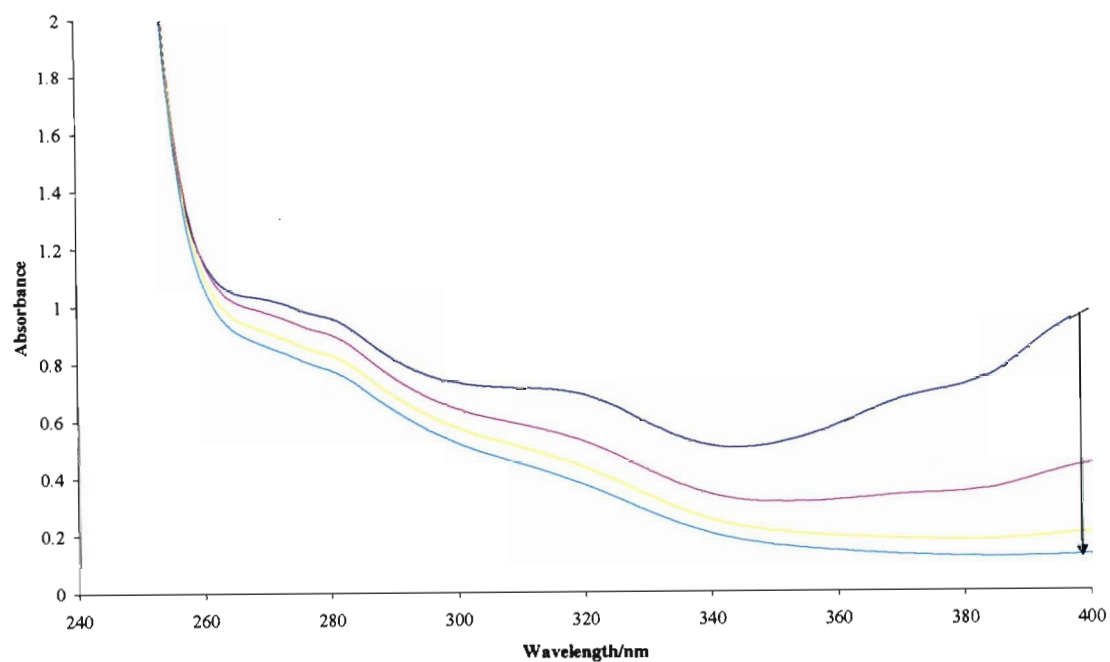
Figure 3.31:   The UV spectra of the ethanol-water Cancer Bush extract dissolved in ethyl
                acetate obtained after each 30 minute irradiation interval for a total period of
                one and a half hours. The spectra were recorded in a 1 cm pathlength quartz
                cuvette against air as the reference.
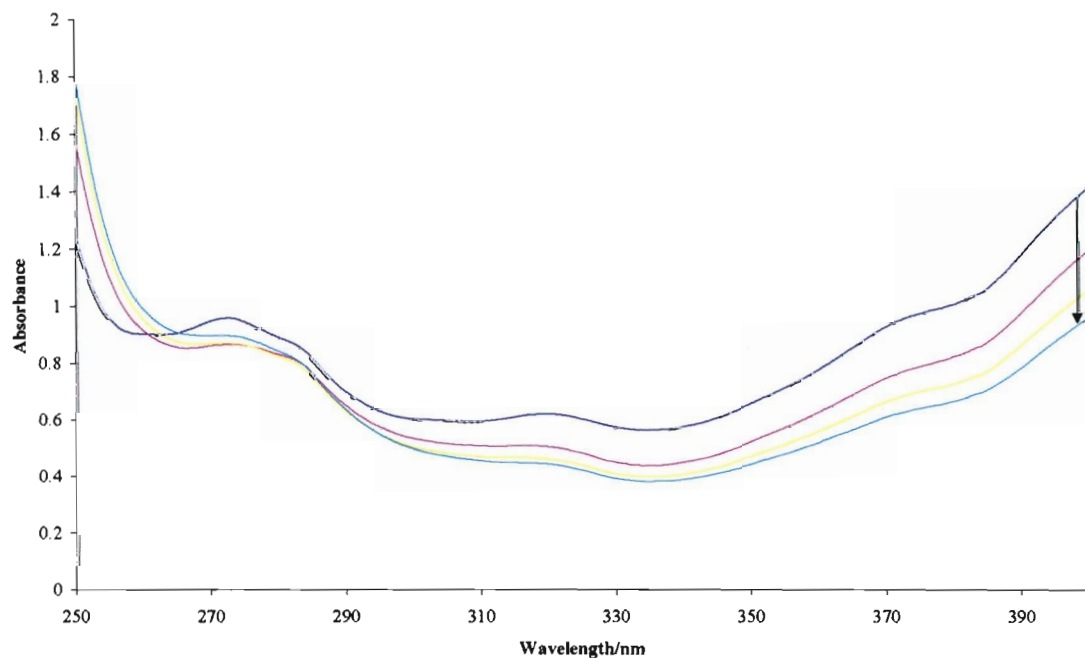
Figure 3.32:   The UV spectra of the ethanol-water Cancer Bush extract dissolved in
                cyclohexane after each 30 minute irradiation interval for a total period of one
                and a half hours. The spectra were recorded in a 1 cm pathlength quartz cuvette
                against air as the reference.

3.1.4.2 Photostability of the Cancer Bush extract investigated by HPLC

The photostability of the ethanol-water Cancer Bush extract was investigated further by HPLC. In order to do this a much more concentrated sample than was used in the UV spectroscopic analysis was required so as to obtain chromatograms with reasonable peaks. These HPLC investigations were only conducted in ethyl acetate since it was the only solvent that could be injected directly without exhaustive sample preparation, which could have compromised the accuracy of these results. Samples in cyclohexane required complete evaporation of the solvent and re-dissolution of the solid sample in another solvent that could be injected into the HPLC. On the other hand, DMSO solutions had to be diluted by another solvent, such as methanol, prior to injection into the HPLC.

The extract in ethyl acetate was concentrated by evaporating off the solvent with the rotavapor to an extract amount equivalent to 60 mg in 2 ml. A 10 µl portion of the solution was injected and eluted through the Nucleosil 100 C18 column by an isocratic mobile phase of 85:15% (v/v) methanol:Millipore water. All the extract components eluted together without separation at about 3 minutes as shown in Figure 3.33. Since this mobile phase can satisfactorily elute the sunscreen absorber avobenzone, it was necessary to determine the photostability of the extract when eluted by this mobile phase prior to conducting the photostabilising experiments of this absorber with the extract. After a one hour irradiation period of the extract in a 1 mm pathlength quartz cuvette, the extract peak height and area were reduced by 22% (see Figure 3.34) and 26%, respectively.

In order to analyse the photostability of each specific substance in the extract, a more concentrated extract sample was prepared in ethyl acetate. About 300 mg of the ethanol-water Cancer Bush extract was dissolved in 2 ml ethyl acetate, then a 10 µl aliquot was injected into the HPLC. The extract sample was eluted through the Nucleosil 100 C18 column by the method adapted from Zuo *et al.* [2002] at a detection wavelength of 272 nm (see Figure 3.35). After a one hour irradiation period of the extract in a 1 mm pathlength quartz cuvette, there was no obvious loss in peak height and area for any of the extracted compounds (see Figure 3.36), and no apparent formation of any new peaks. Hence, photostability was observed with concentrated extract samples in ethyl acetate whereas the dilute extract sample used for UV analysis (see Figure 3.31 in Section 3.1.4.1) and HPLC analysis above (see Figure 3.34) was largely photo-unstable. However, the period of irradiation of the concentrated samples may have been insufficient to observe photodegradation.
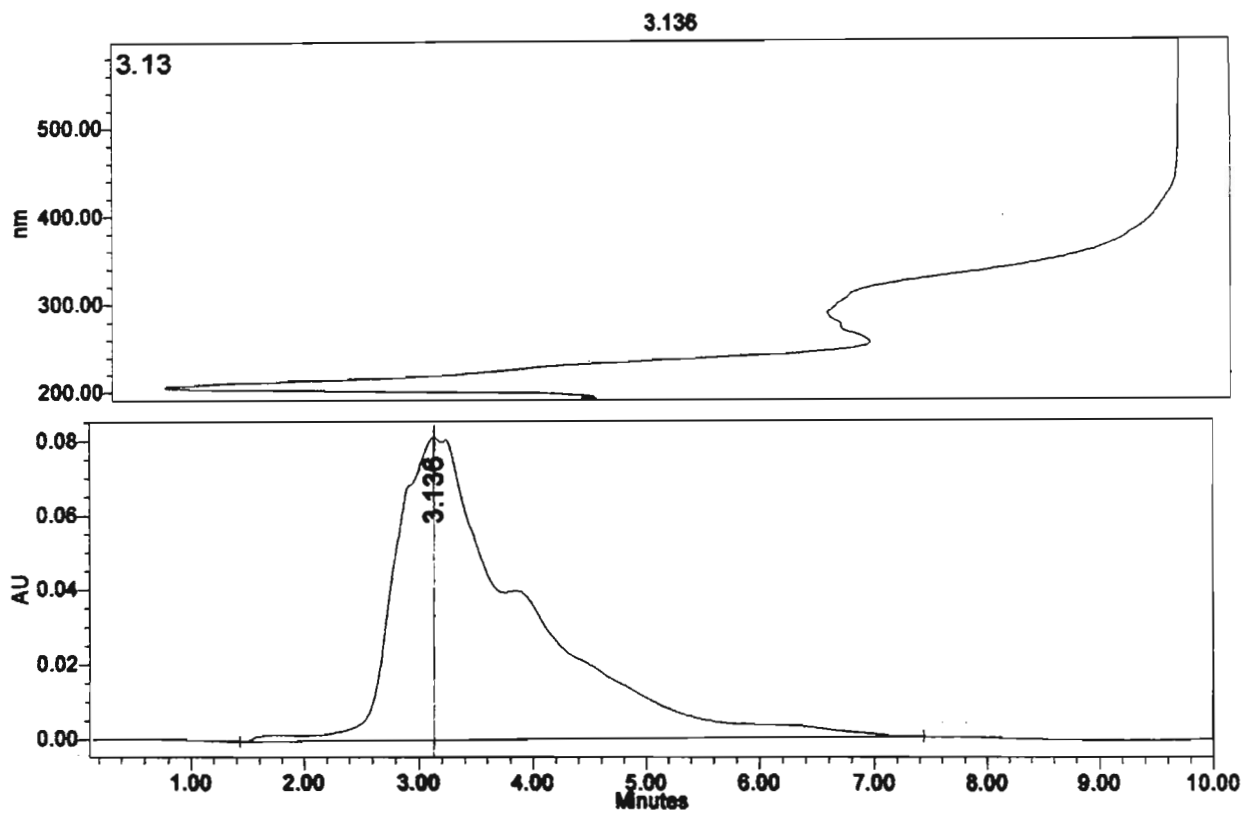
Figure 3.33:   HPLC chromatogram of the ethanol-water Cancer Bush extract eluted through a Nucleosil 100 C18 column by an isocratic mobile phase of 85:15% (v/v) methanol:Millipore water. The wavelength of detection was 272 nm and the chromatogram was obtained before irradiation of the sample.
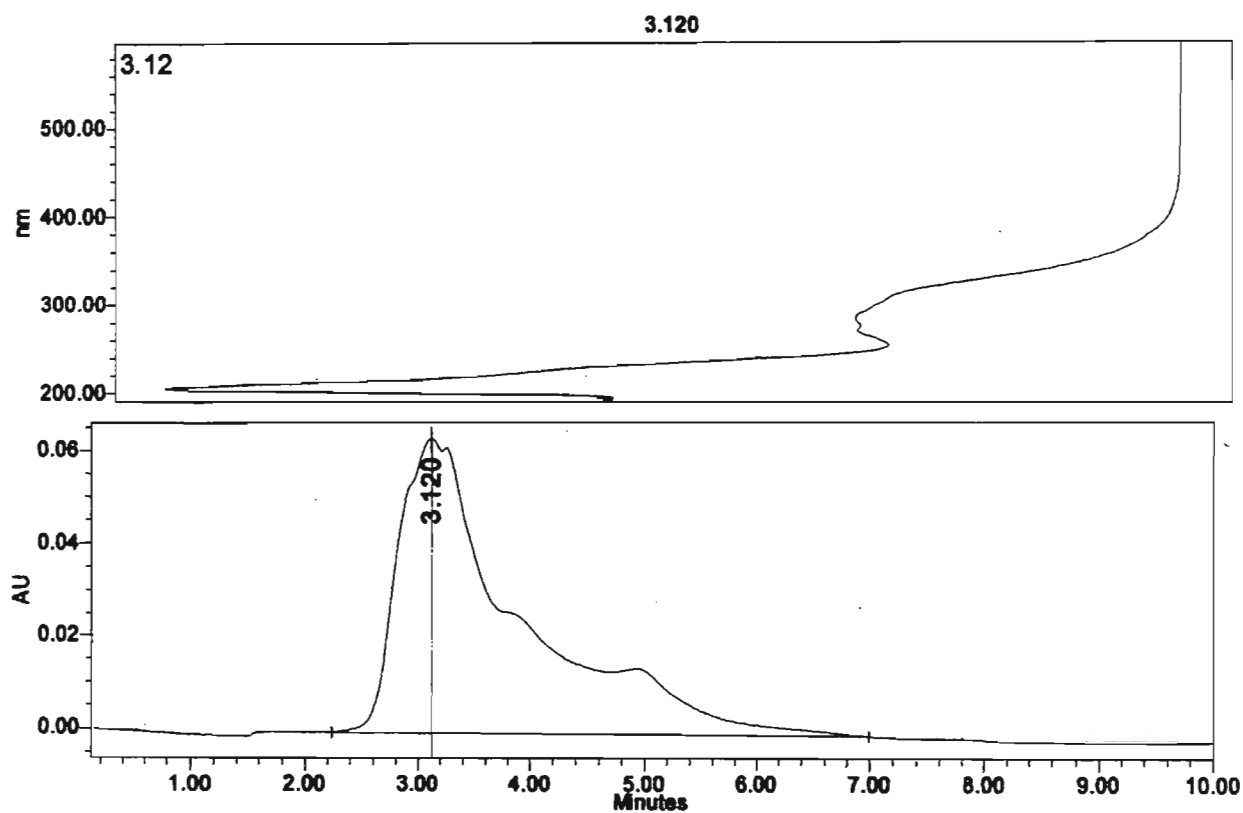
Figure 3.34:   HPLC chromatogram of the ethanol-water Cancer Bush extract eluted through a Nucleosil 100 C18 column with an isocratic mobile phase of 85:15% (v/v) methanol:Millipore water. The wavelength of detection was 272 nm and the chromatogram was obtained after a one hour irradiation period of the sample.
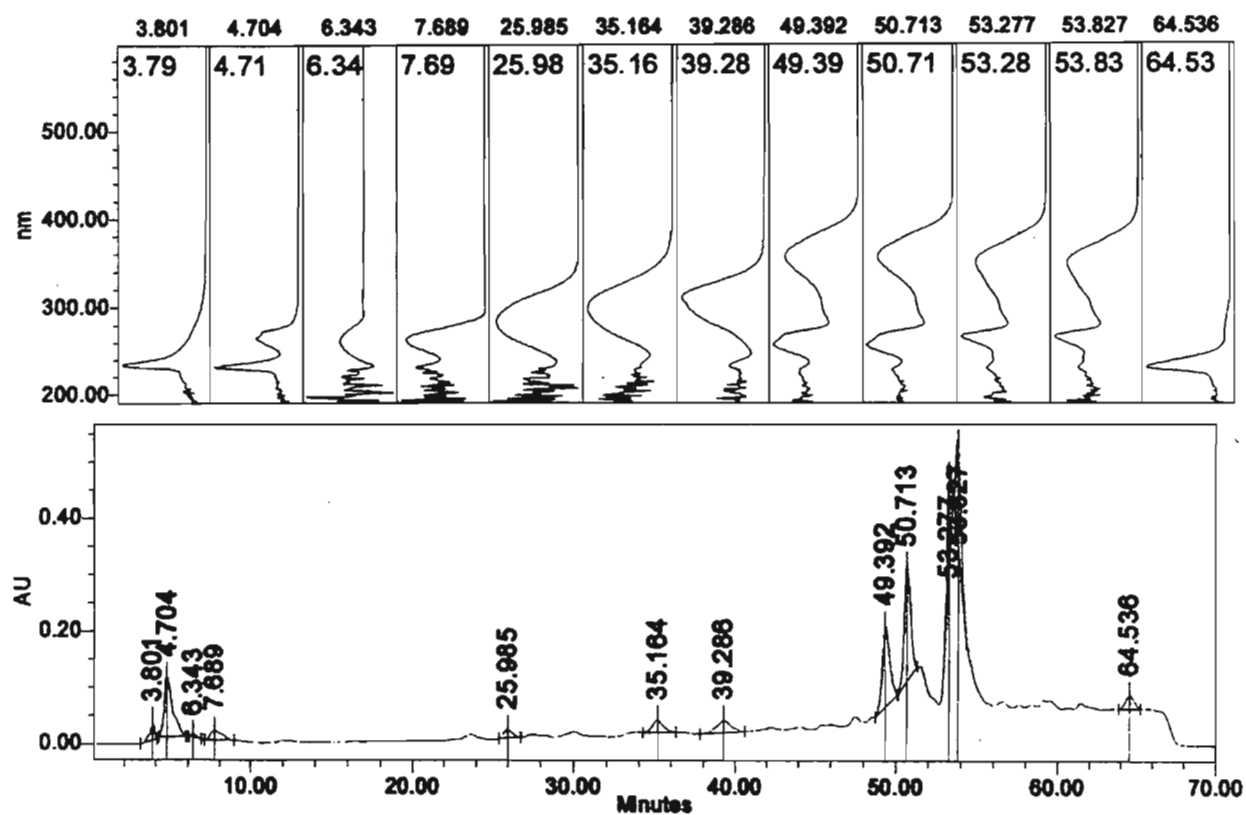
Figure 3.35: HPLC chromatogram of the ethanol-water Cancer Bush extract eluted through a Nucleosil 100 C18 column with a gradient method adapted from Zuo *et al.* [2002]. The wavelength of detection was 272 nm and the chromatogram was obtained before irradiation of the sample.
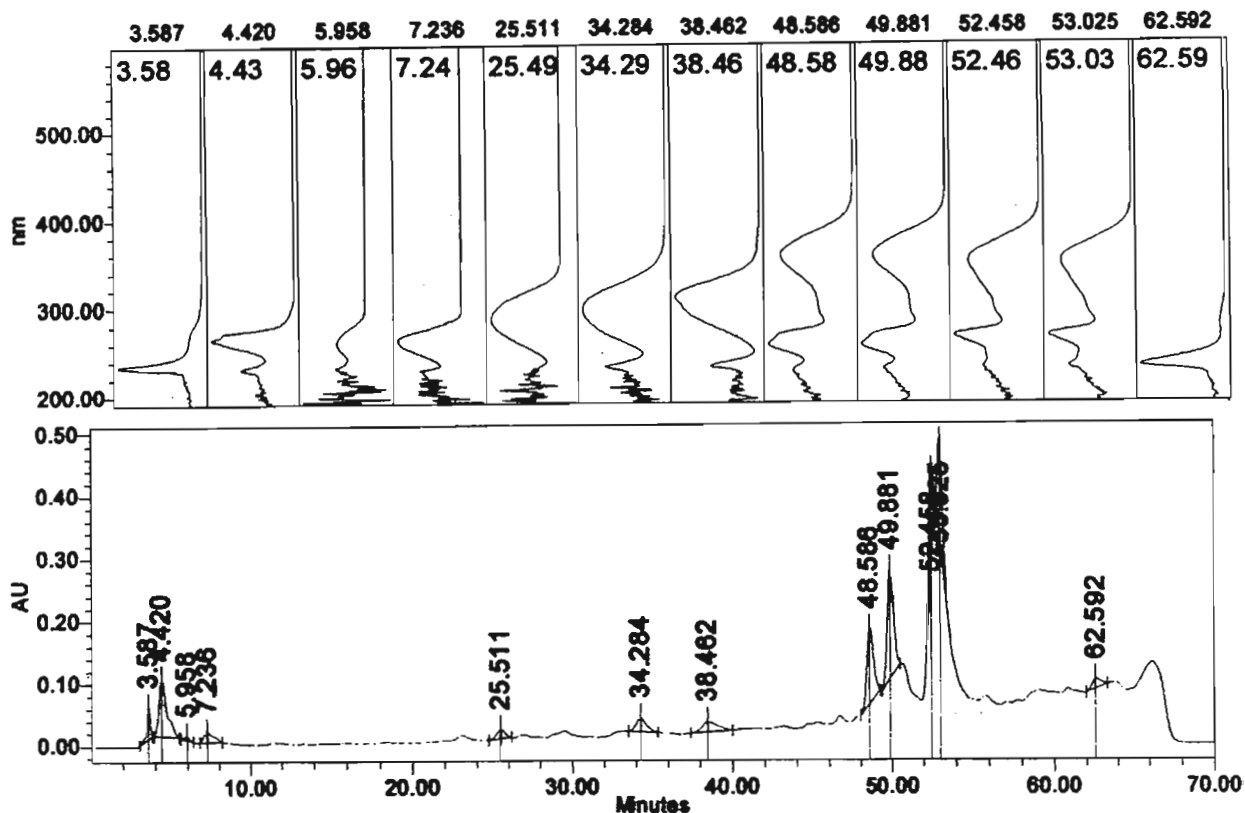
Figure 3.36:   HPLC chromatogram of the ethanol-water Cancer Bush extract eluted through a
               Nucleosil 100 C18 column with a gradient method adapted from Zuo *et al.*
               [2002]. The wavelength of detection was 272 nm and the chromatogram was
               obtained after a one hour irradiation period of the sample.

3.1.5 Summary of Section 3.1

HPLC and UV analysis suggested that potential polyphenolic compounds, such as flavonoids,
were present in the Cancer Bush leaves. The flavonoid rutin or a rutin-like compound was
shown to be present in the ethanol-water Cancer Bush extract. GC-MS studies additionally
showed the presence of simple phenolics as well as tentatively verifing the presence of a rutin-
like compound in the ethanol-water Cancer Bush extract. It is important to note that simple
phenolics such as benzoic acids also portray antioxidant activity (Erickson [2003]). The
phenolics present in the ethanol-water Cancer Bush extract were quantified by the Folin-
Ciocalteu reagent, and the extract was also shown to scavenge the diphenylpicrylhydrazyl
radical.

The boiling water extract of ground Cancer Bush leaves as well as the ethanol-water Cancer
Bush extract were deemed suitable for use in photostabilising photo-unstable chemical
absorbers. The boiling water extract of ground Cancer Bush leaves was more photostable in

various solvents compared with the ethanol-water Cancer Bush extract. The ethanol-water Cancer Bush extract was photo-unstable in cyclohexane and even more so in ethyl acetate, but the extract appeared photostable at high concentrations in ethyl acetate when investigated by HPLC analysis.

3.2 Photostability of chemical absorbers with and without the Cancer Bush extract

Photo-unstable chemical absorbers reduce the efficacy of sunscreen products. The procedures involved in obtaining the approved use of new absorbers are long and tedious. It is therefore much easier to photostabilise already approved absorbers. Photostabilising these absorbers not only increases the efficacy of the products but also decreases the potential adverse effects derived from the photoproducts formed. In this section the results of experiments performed to assess the photostabilising effect of the boiling water extract from ground Cancer Bush leaves on some photo-unstable absorbers will be discussed. The plant extracts have been shown to contain polyphenols (see Section 3.1) which could act as potent antioxidants capable of scavenging various radicals. Depending on the pathway of photoproduct formation for these photo-unstable absorbers, polyphenols could be potential photostabilisers. The photostability of various sunscreen absorbers were investigated by UV spectroscopy. Table 3.10 shows a summary of the results.

The photostabilisation of the following photo-unstable chemical absorbers was investigated in this work: 2-ethylhexyl-*p*-methoxycinnamate (EHMC), 4-bis(polyethoxy)-*p*-aminobenzoic acid polyethoxyethyl ester (Peg-25 PABA), 3-(4-methylbenzylidene) camphor (MBC) and isoamyl *p*-methoxycinnamate (IMC). The boiling water extract of ground Cancer Bush leaves was used to photostabilise these absorbers. UV absorption spectroscopy was used to monitor the photostabilisation experiments. The extract was prepared for these UV absorption spectroscopy investigations as described in Section 2.2.

Table 3.10:   The photostability of chemical absorbers in appropriate solvents when exposed
                to light of wavelengths greater than 300 nm.

Chemical absorber	Solvent	Photostability
2-ethylhexyl-*p*-methoxycinnamate (EHMC)	Methanol	Photo-unstable
4-bis(polyethoxy)-*p*-aminobenzoic acid polyethoxyethyl ester (Peg-25 PABA)	Millipore water	Photo-unstable
3-(4-methylbenzylidene) camphor (MBC)	Methanol	Photo-unstable
isoamyl *p*-methoxycinnamate (IMC)	Methanol	Photo-unstable
menthyl anthranilate	Methanol	Photo-unstable
octyl dimethyl *p*-aminobenzoic acid	Methanol	Photostable
phenylbenzimidazole sulfonic acid	Millipore water	Photostable
2,4-dihydroxybenzophenone	Methanol	Photostable
2,2',4,4'-tetrahydroxybenzophenone	Methanol	Photostable
2-hydroxy-4-methoxybenzophenone	Methanol	Photostable
2-hydroxy-4-methoxybenzophenone-5-sulfonic acid	Millipore water	Photostable
4-*tert*-butyl-4'-methoxydibenzoylmethane (avobenzone)	Methanol	Photostable
	DMSO, ethyl acetate and cyclohexane	Photo-unstable
2,2'-dihydroxy-4,4'-dimethoxybenzophenone	Methanol	Photostable
2-hydroxy-4-n-octyloxybenzophenone	Methanol	Photostable

3.2.1 Photostability of EHMC

2-Ethylhexyl-*p*-methoxycinnamate is the most commonly used UVB absorber since it absorbs maximally in the UVB region of the electromagnetic spectrum.

Upon irradiation, EHMC loses its absorbing ability through *trans-cis* photoisomerisation (Tarras-Wahlberg *et al.* [1999], Kowlaser [1998], Ingouville [1995] and Broadbent [1994]) (see Figure 1.11), and self-dimerisation (Broadbent *et al.* [1996] and Ingouville [1995]) (see Figure 1.12). Panday [2002] showed EHMC to be photo-unstable in methanol, hence attempts to photostabilise this absorber with the boiling water Cancer Bush extract were conducted in methanol. A 2×10^{-5} M methanolic solution of EHMC was irradiated with and without the boiling water extract of ground Cancer Bush leaves at one minute irradiation intervals for a total period of four minutes. The resulting UV spectra given in Figure 3.37 show the photostability

of the boiling water extract of ground Cancer Bush leaves alone, EHMC alone, and the two together.

The UV spectrum of EHMC shows maximum absorption at 310 nm due to the *trans*-isomer, with a shoulder peak at 300 nm due to the *cis*-isomer. After the first minute of irradiation, there was a rapid loss of absorbance at 310 nm of about 0.15, attributed to photoisomerisation. This loss was accompanied by an absorbance increase at 250 nm creating isosbestic points (points of intersection) at 220 nm and 240 nm. This increase in absorbance could be due to self-dimerisation since the compound would lose conjugation and absorb at a much lower wavelength. EHMC remained photostable during subsequent irradiations indicating that a photostationary state had been reached for this photoisomerisation.

The boiling water Cancer Bush extract was thoroughly mixed with EHMC by manual shaking. Photostabilisation of EHMC in the mixture was not observed when irradiated for the same time intervals as was EHMC alone. The same photodegradation pattern for the peak at 310 nm was observed - it decreased in absorbance rapidly from 0.97 to 0.81 in the first minute of irradiation and then remained photostable afterwards. Hence, EHMC must have photoisomerised in the mixture in the same way, to reach a photostationary state between the isomers that prevented further loss in absorbance.

3.2.2 Photostability of MBC

The chemical absorber, 3-(4-methylbenzylidene) camphor (MBC), absorbs maximally at 300 nm hence it is a UVB absorber.

A 2×10^{-5} M solution of MBC was prepared in methanol and irradiated with and without the Cancer Bush extract for 30 minute intervals for a total period of one and a half hours. The resulting UV spectra showing the photostability of the boiling water extract of ground Cancer Bush leaves alone, MBC alone, and the two combined, are shown in Figure 3.38. Figure 3.38B shows the loss in absorbance of MBC as a result of UV irradiation with wavelengths greater than 300 nm. This loss in absorbance is significant in the first 30 minutes, reducing the absorbance from 0.69 to 0.59 at 300 nm, and then stabilises thereafter which is characteristic of photoisomerising absorbers. The photo-instability of MBC is due to photoisomerisation (Deflandre and Lang [1988a]) (see Figure 1.10) which occurs until a photostationary state is

reached. A small increase in absorption at 230 nm was also observed creating isosbestic points at 222 nm and 237 nm. This can be attributed to the formation of another product.
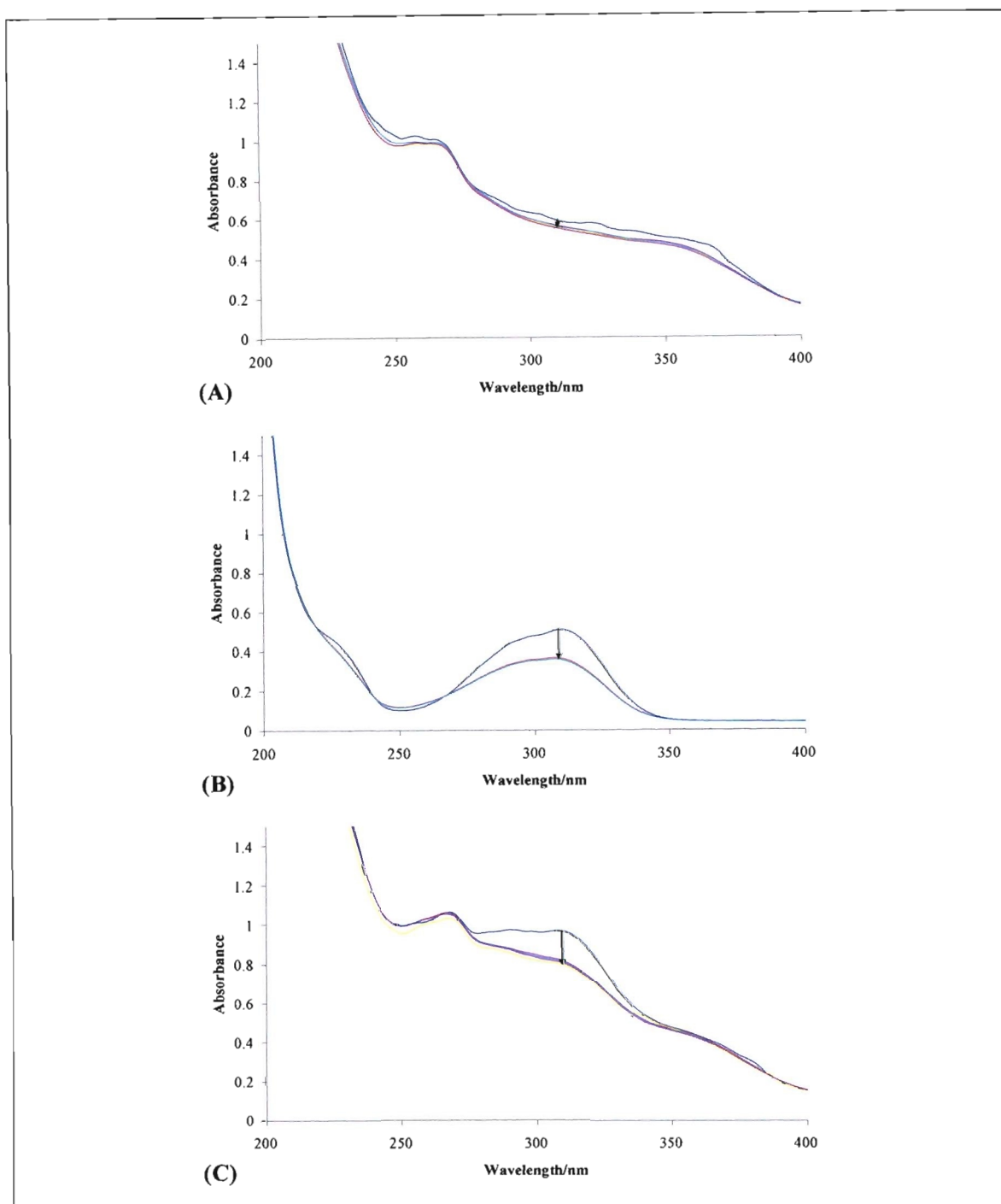
Figure 3.37:   The boiling water extract of ground Cancer Bush leaves (A), 2×10^{-5} M EHMC (B) and 2×10^{-5} M EHMC with the extract (C). Each sample was irradiated at one minute irradiation intervals in methanol in a 1 cm pathlength quartz cuvette. All UV spectra were obtained with the Perkin Elmer Lambda 35 UV/VIS spectrophotometer.
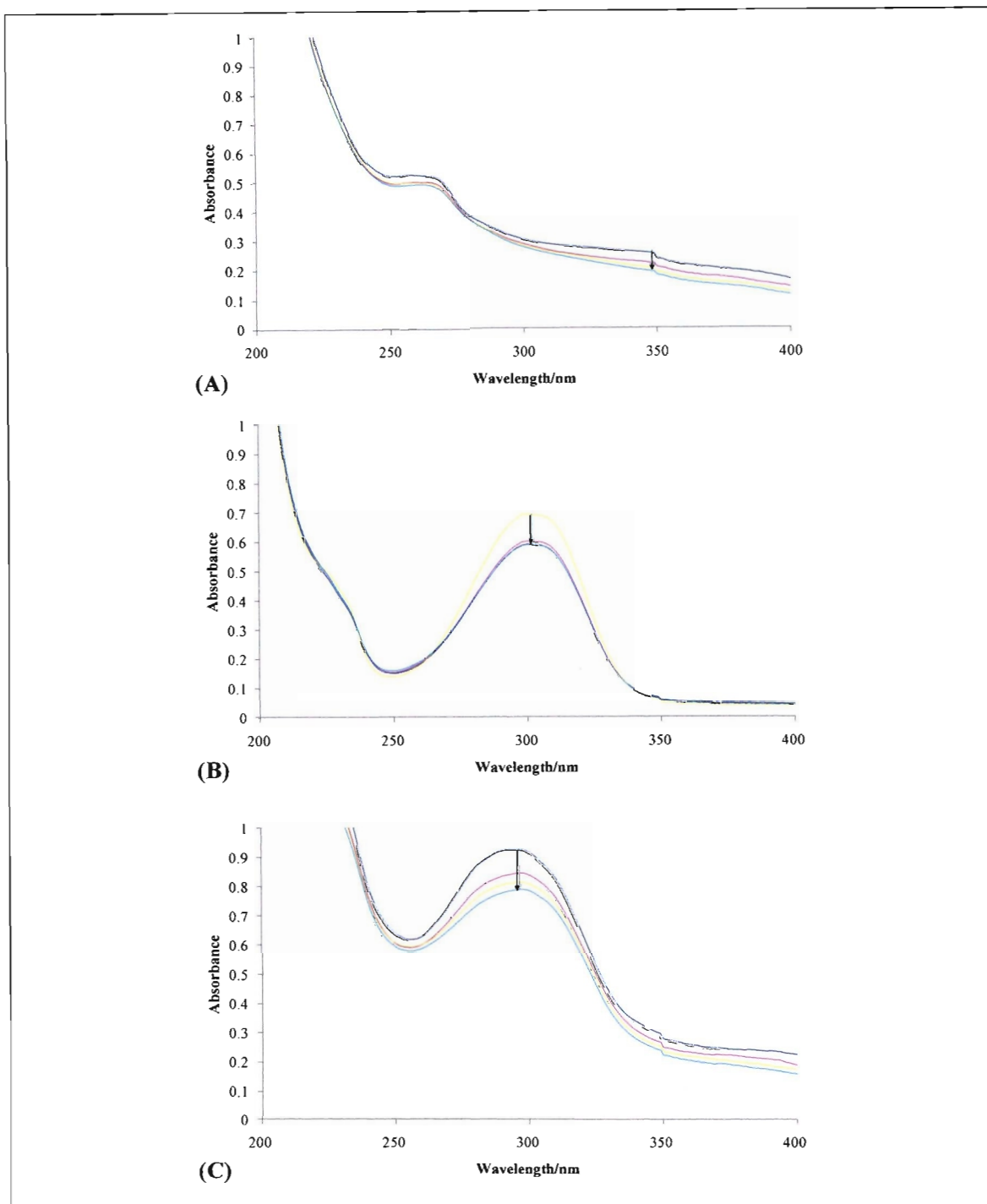
Figure 3.38:   The boiling water extract of ground Cancer Bush leaves (A), 2×10^{-5} M MBC (B) and 2×10^{-5} M MBC with the extract (C). Each sample was irradiated at 30 minutes irradiation intervals in methanol in a 1 cm pathlength quartz cuvette. All UV spectra were obtained with the Cary 1E UV/VIS spectrophotometer.

The boiling water Cancer Bush extract did not photostabilise MBC. The irradiated mixture showed a large decrease in absorbance after the first 30 minutes of irradiation, similar to that of the absorber alone, i.e. from 0.92 to 0.84 at 300 nm. Subsequent irradiations showed relatively minor instabilities at 300 nm which could be attributed to the photodegradation of the boiling water Cancer Bush extract.

3.2.3 Photostability of IMC

The chemical absorber, isoamyl p-methoxycinnamate (IMC), has a wavelength of maximum absorption at 309 nm making it an efficient UVB absorber.

A 2×10^{-5} M solution of IMC in methanol was irradiated with and without the Cancer Bush extract at 30 minutes intervals for a total period of one hour. The UV spectra showing the photostability of the boiling water extract of ground Cancer Bush leaves alone, IMC alone, and the two combined, are displayed in Figure 3.39. The UV spectrum of IMC shown in Figure 3.39B is typical of cinnamates such as EHMC. There is an absorption maximum at 309 nm with a shoulder peak at 300 nm. Upon irradiation, there was loss in absorbance at 309 nm accompanied by a minor increase at 226 nm. This initial absorbance loss of 0.12 was rapid, subsequently reaching a photostationary state. This photo-instability pattern is characteristic of photoisomerisation (Deflandre and Lang [1988a]) (see Figure 1.11). Photodimerisation (see Figure 1.12) can also occur in isoamyl p-methoxycinnamate as it is common with cinnamic acid derivatives upon irradiation (Cohen *et al.* [1964]), possibly resulting in the absorbance increase observed at 226 nm. In cinnamates and benzylidene camphor derivatives, a photostationary state is reached shortly after exposure to UV radiation, potentially due to photoisomerisation (Tarras-Wahlberg *et al.* [1999]).

When IMC was analysed in the presence of the boiling water Cancer Bush extract, photoisomerisation still occurred. There was a loss in absorbance of the mixture at 309 nm from 0.86 to 0.66 during the first 30 minutes of irradiation. The mixture remained photochemically stable afterwards as was the case when IMC was irradiated alone.

3.2.4 Photostability of Peg-25 PABA

The absorber, 4-bis(polyethoxy)-p-aminobenzoic acid polyethoxyethyl ester (Peg-25 PABA), is used as a water-soluble UVB absorber in various skin-care products.
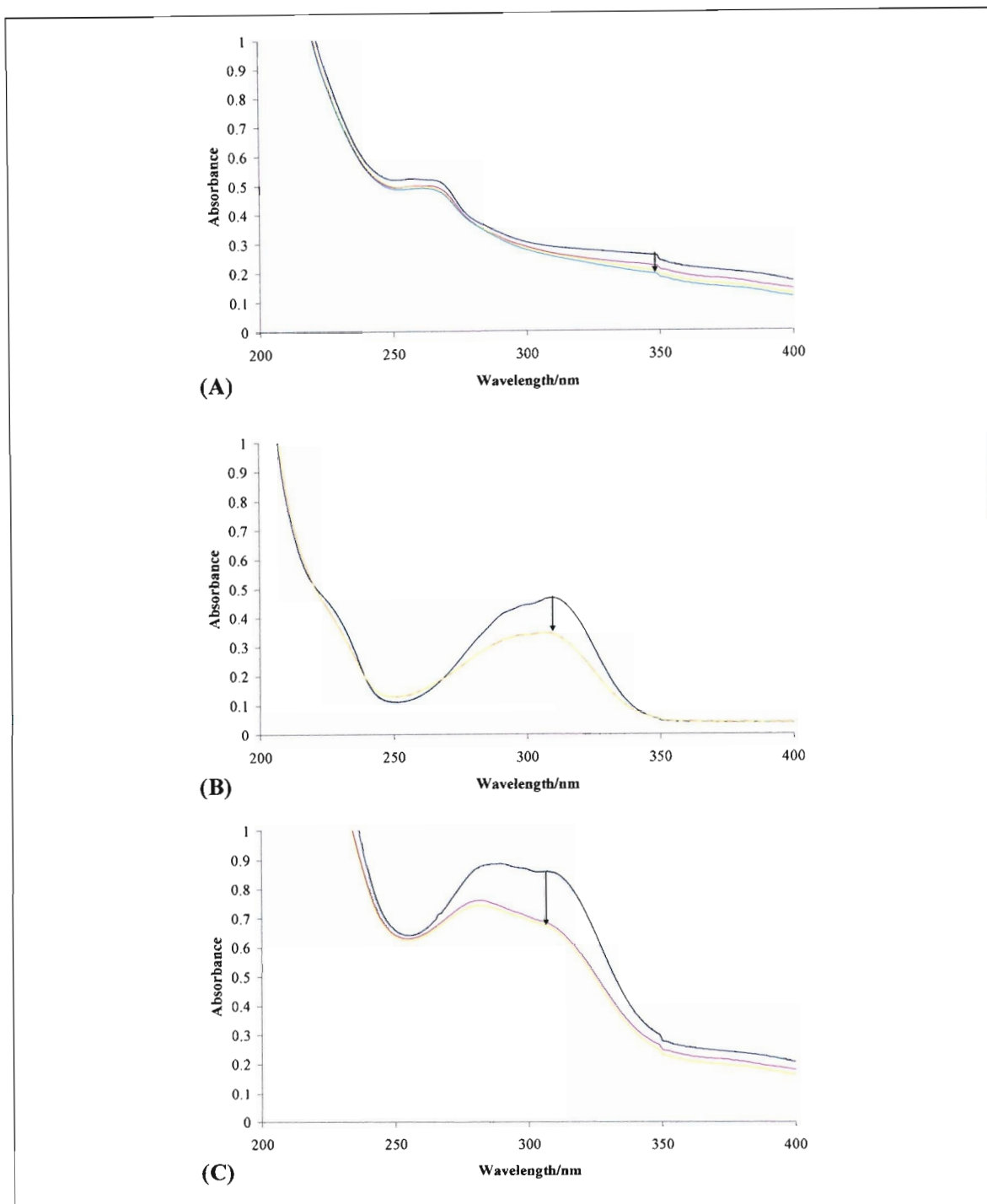
Figure 3.39:   The boiling water extract of ground Cancer Bush leaves (A), 2×10^{-5} M IMC (B) and 2×10^{-5} M IMC with the extract (C). Each sample was irradiated at 30 minute irradiation intervals in methanol in a 1 cm pathlength quartz cuvette. All UV spectra were obtained with the Cary 1E UV/VIS spectrophotometer.

A 3.6 × 10^{-5} M solution of the absorber was prepared in Millipore water and irradiated with and without the Cancer Bush extract at 30 minute intervals for a total period of two hours. The UV spectra showing the photostability of the boiling water extract of ground Cancer Bush leaves alone, Peg-25 PABA alone, and the two combined, are displayed in Figure 3.40. There are few reports about this absorber but photo-instability of the parent structure, *p*-aminobenzoic acid, is well known (Shaw *et al.* [1992]). The UV spectrum of Peg-25 PABA shows two UV absorption peaks at 308 nm and at 225 nm. Upon irradiation, a small loss in absorption was observed at 308 nm and an even smaller loss occurred at 225 nm. Three isosbestic points occur at 215 nm, 248 nm and 283 nm in the combined spectra of irradiated Peg-25 PABA. A minor increase in absorbance was observed at 267 nm. The decrease in absorbance at 308 nm is due to the loss of Peg-25 PABA to form a photoproduct(s) that absorbs at 267 nm.

The boiling water Cancer Bush extract was added to Peg-25 PABA in Millipore water. The mixture was irradiated for the same irradiation intervals as for Peg-25 PABA alone. UV spectra of the irradiated mixture showed photo-instability at 308 nm of the same magnitude as the combined instability of Peg-25 PABA and the extract at this wavelength. Loss in absorption of the mixture was observed between 240 nm and 400 nm similar to the photodegradation undergone by the extract alone. The extract therefore did not photostabilise Peg-25 PABA in Millipore water.

3.2.5 Summary of Section 3.2

The results in this section show that the boiling water extract of ground Cancer Bush leaves failed to photostabilise the photo-unstable absorbers EHMC, MBC, IMC and Peg-25 PABA.

3.3 Photostabilising avobenzone

The UVA chemical absorber, avobenzone, has been reported to be photo-unstable in acetonitrile (Andrae *et al.* [1995 and 1997] and Dubois *et al.* [2002]) and cyclohexane (Panday [2002]). This section deals with the photostability of avobenzone in DMSO, ethyl acetate, methanol and cyclohexane (discussed in Section 3.3.1). In those solvents where photo-instability was observed, avobenzone was investigated in the presence and absence of extracts from the Cancer Bush leaves and Rooibos tea, as well as specific polyphenols, namely epicatechin and rutin (see Section 3.3.2 and 3.3.3).
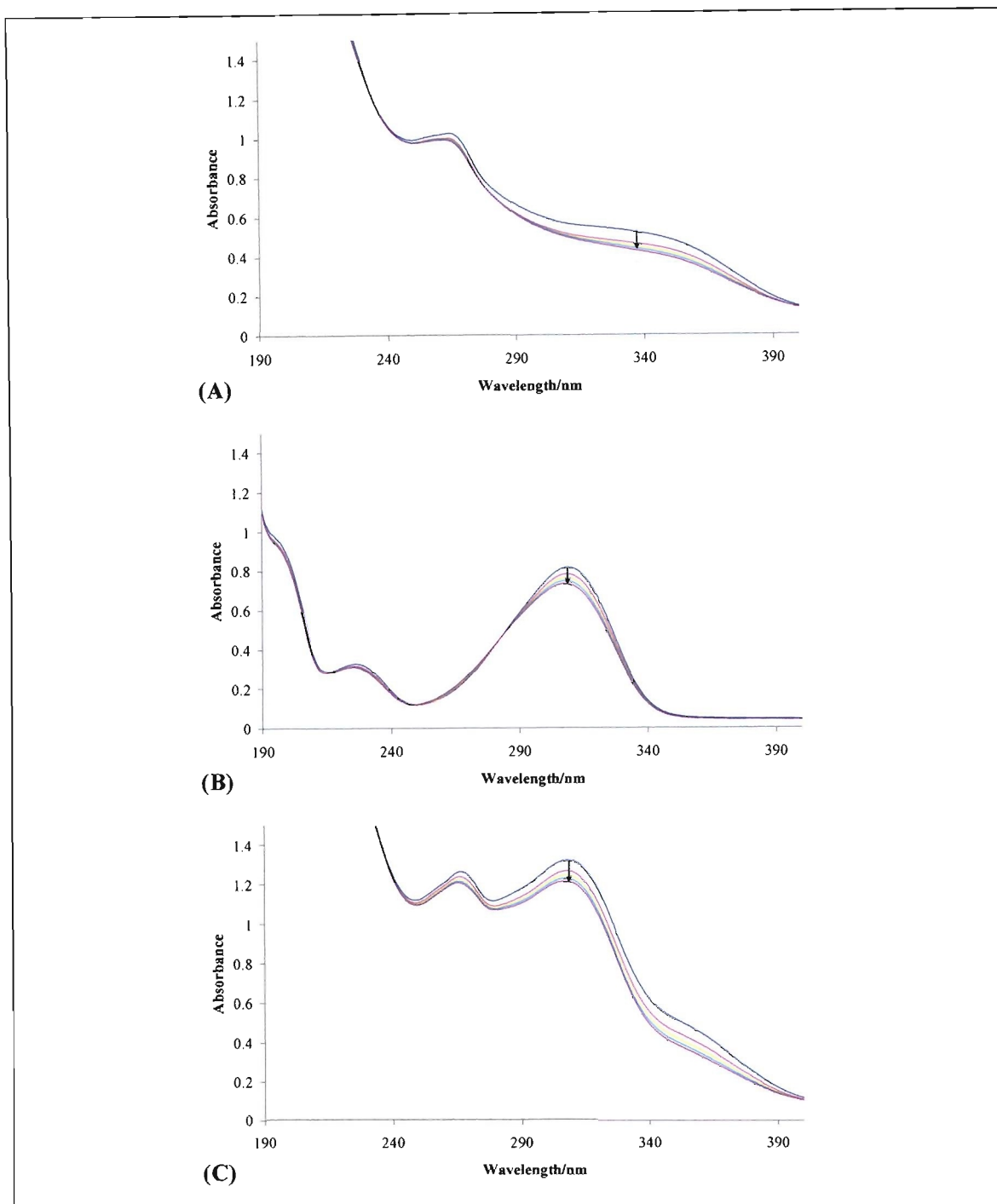
Figure 3.40:   The boiling water extract of ground Cancer Bush leaves (A), 2 × 10⁻⁵ M Peg-25 PABA (B) and 2 × 10⁻⁵ M Peg-25 PABA with the extract (C). Each sample was irradiated at 30 minute irradiation intervals in Millipore water in a 1 cm pathlength quartz cuvette. All UV spectra were obtained with the Perkin Elmer Lambda 35 UV/VIS spectrophotometer.

3.3.1 Photostability of avobenzone in different solvents

The photostability of avobenzone in DMSO, ethyl acetate and cyclohexane was investigated by various techniques, namely UV spectroscopy for oxygen independent analyses (discussed in Section 3.3.1.1) and for oxygen-dependent investigations (discussed in Section 3.3.1.2), GC-MS (discussed in Section 3.3.1.3), HPLC (discussed in Section 3.3.1.4) and NMR spectroscopy (discussed in Section 3.3.1.5).

3.3.1.1 Photostability shown by UV spectroscopy

UV spectra can be used to assign substances as UVA or UVB absorbers depending on their wavelengths of maximum absorption. The efficacy of a substance used as a chemical absorber can be determined by assessing how well it retains its absorption capacity, upon irradiation of the absorber with wavelengths such as those that fall on the earth's surface.

The UV absorbance spectrum of avobenzone in different solvents was measured with the Perkin Elmer Lambda 35 UV/VIS spectrophotometer. The wavelengths of maximum absorption (λ_{max}) of avobenzone in cyclohexane, ethyl acetate, methanol and DMSO are listed in Table 3.11. These results show that the λ_{max} of avobenzone in ethyl acetate, methanol and DMSO show a bathochromic shift relative to that in cyclohexane, which increases with increasing polarity of the solvent. This feature is in accordance with most sunscreens (Agrapidis-Paloympis *et al.* [1987]).

The λ_{max} of avobenzone in the various solvents shown in Table 3.11 substantiates that it is a UVA absorber, that is, it absorbs UV radiation between 320 – 400 nm. The efficacy of avobenzone as a sunscreen absorber was investigated in different solvents by irradiating with wavelengths greater than 300 nm and monitoring the resulting absorption spectrum.

Table 3.11: The wavelengths of maximum absorption of avobenzone in different solvents.

Solvent	Wavelength of maximum absorption of avobenzone, λ_{max}/nm
Cyclohexane	351
Ethyl acetate	356
Methanol	358
DMSO	363

Photo-instability of avobenzone in ethyl acetate

A solution of 1.8×10^{-5} M avobenzone was prepared in ethyl acetate and irradiated with UV radiation of wavelengths greater than 300 nm. The UV absorption spectra of the avobenzone solution after every 1 minute irradiation interval were obtained, and the combined spectra are displayed in Figure 3.41. These spectra show an isosbestic point at 295 nm separating a decrease in absorbance at 356 nm, accompanied by an increase in absorbance at around 269 nm with increasing irradiation time. The absorbance values at the two wavelengths of 356 nm and 269 nm have been plotted against irradiation time in Figure 3.42. The wavelength of 269 nm was chosen arbitrarily (and is not a wavelength of maximum absorbance) to show the change in absorbance observed around these wavelengths with increasing irradiation time. A possible correlation exists between the decreasing absorbance values at 356 nm with the increasing absorbance values at 269 nm observed with increasing irradiation time.
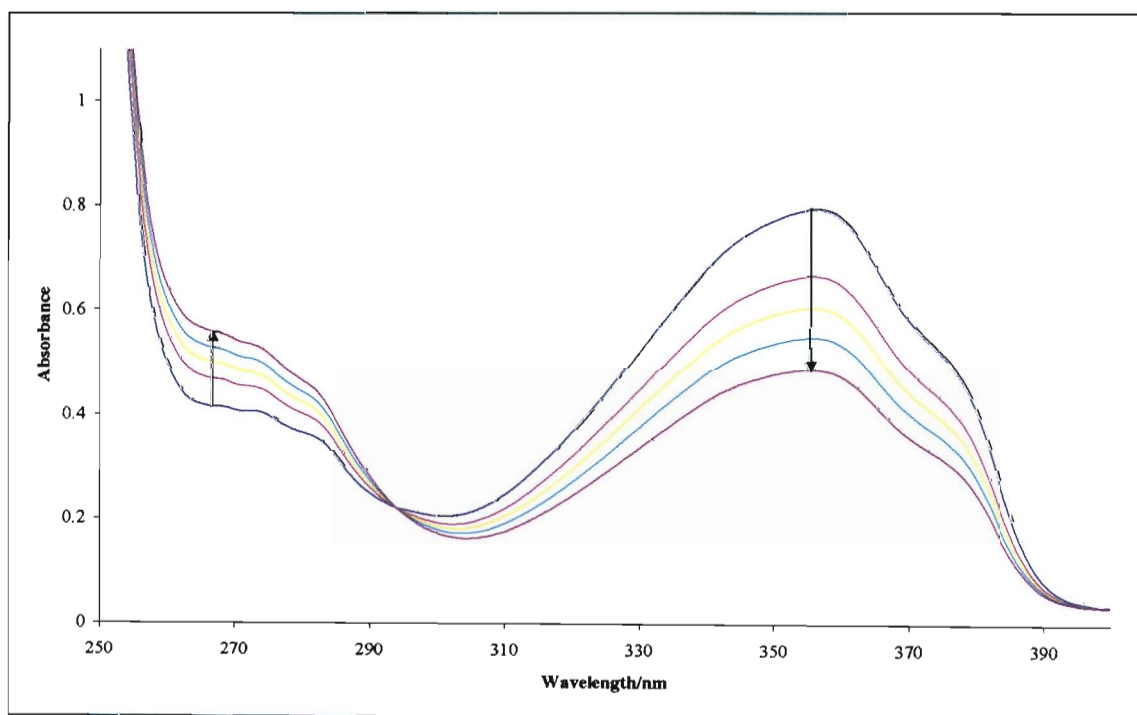
Figure 3.41:   UV absorption spectra of 1.8×10^{-5} M avobenzone dissolved in ethyl acetate obtained after one minute irradiation intervals. Irradiation was with UV light of wavelengths greater than 300 nm. The spectra were recorded in a 1 cm pathlength quartz cuvette against air as the reference.
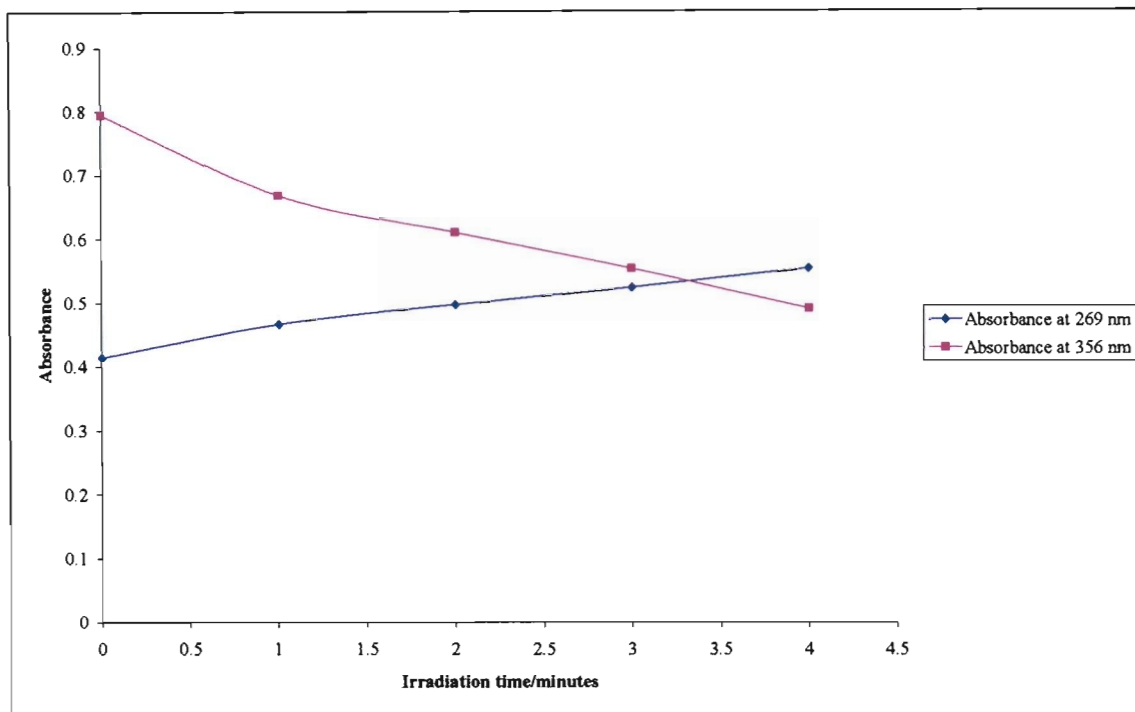
Figure 3.42: Absorbance of a 1.8×10^{-5} M solution of avobenzone dissolved in ethyl acetate monitored at 356 nm and at 269 nm after each one minute irradiation interval with wavelengths of light greater than 300 nm.

Photo-instability of avobenzone in DMSO

A 1.5×10^{-5} M solution of avobenzone dissolved in DMSO was prepared. This solution was irradiated with light of wavelengths greater than 300 nm at 5 minute intervals. UV spectra were obtained after each irradiation interval. The combined spectra (see Figure 3.43) show a decline in the absorbance at 363 nm accompanied by an increase in absorbance at 280 nm with increasing irradiation time as shown in Figure 3.44.
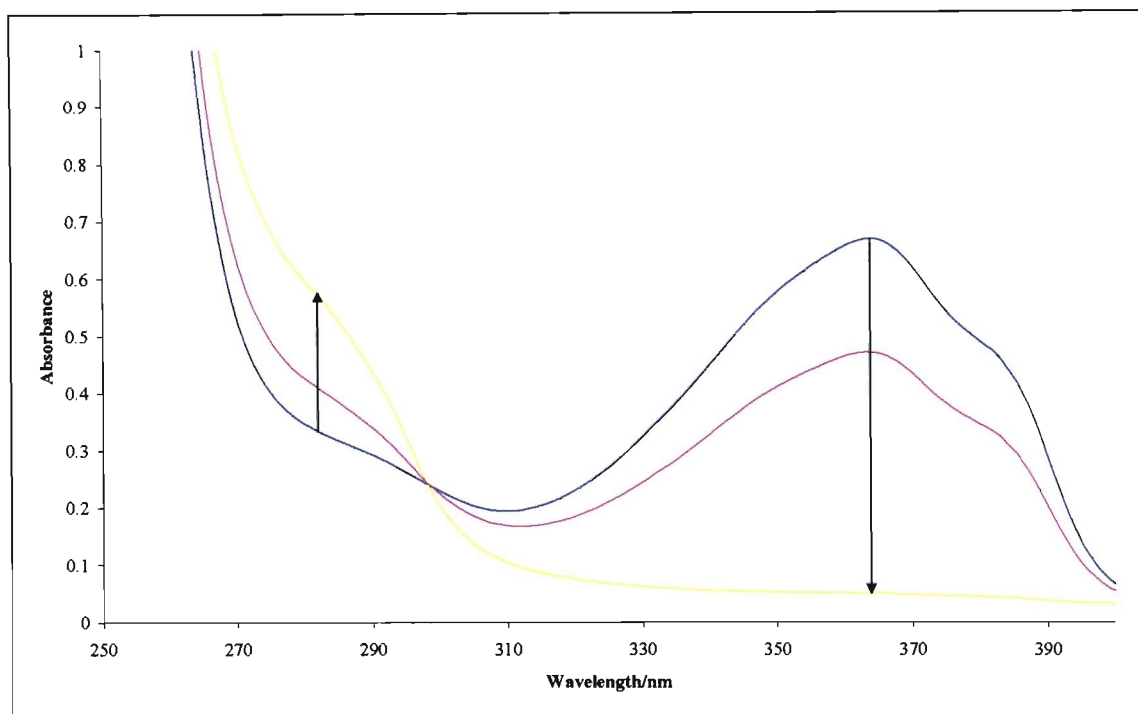
Figure 3.43:   UV absorption spectra of 1.5×10^{-5} M avobenzone dissolved in DMSO obtained after five minute irradiation intervals. Irradiation was with UV light of wavelengths greater than 300 nm. The spectra were recorded in a 1 cm pathlength quartz cuvette against air as the reference.
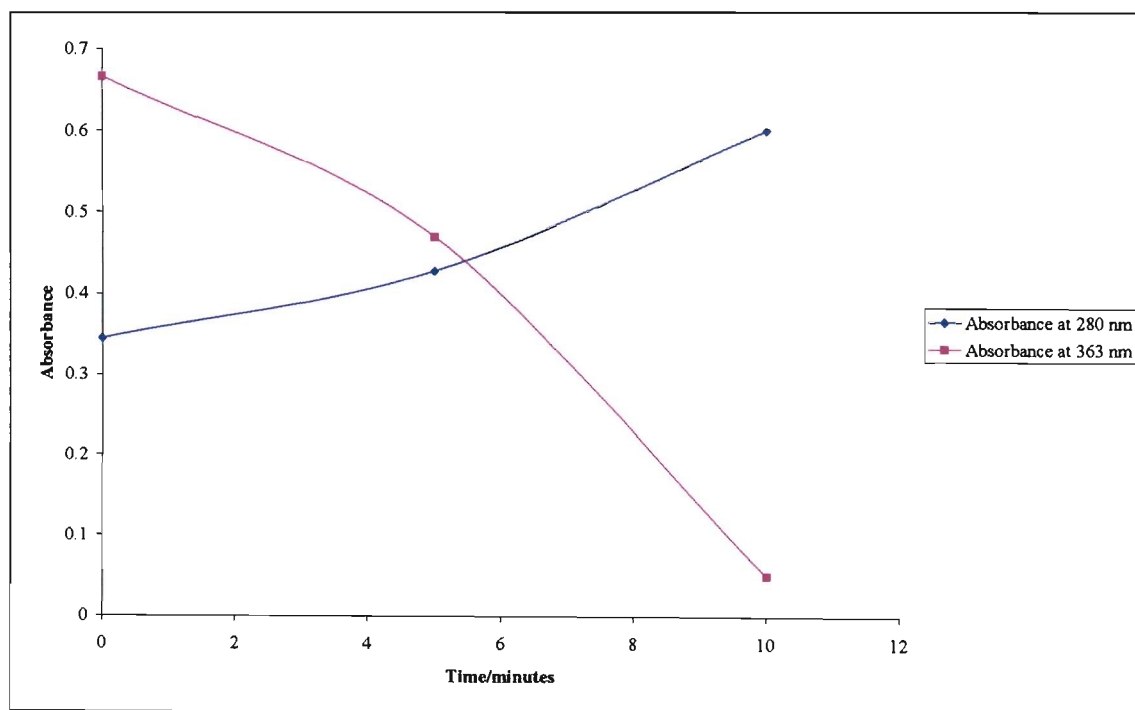
Figure 3.44:   Absorbance of a 1.5×10^{-5} M solution of avobenzone dissolved in DMSO monitored at 363 nm and at 280 nm after each five minute irradiation interval with wavelengths of light greater than 300 nm.

Photo-instability of avobenzone in cyclohexane

A 2.0×10^{-5} M solution of avobenzone dissolved in cyclohexane was irradiated for 30 minute intervals with UV light of wavelengths greater than 300 nm. Figure 3.45 shows the UV spectrum of avobenzone obtained after each irradiation interval. A decline in absorbance at 351 nm was accompanied by an increase in absorbance at 263 nm with irradiation time, and this correlation is shown in Figure 3.46. Upon the last thirty minutes of irradiation, there were losses in absorbance at 351 nm and at 263 nm. The loss in absorption at 263 nm may have been due to the formation of intermediate photoproducts which also absorbed above 300 nm. Consequently, these photoproducts further photodegraded upon subsequent irradiation with light of wavelengths greater than 300 nm.
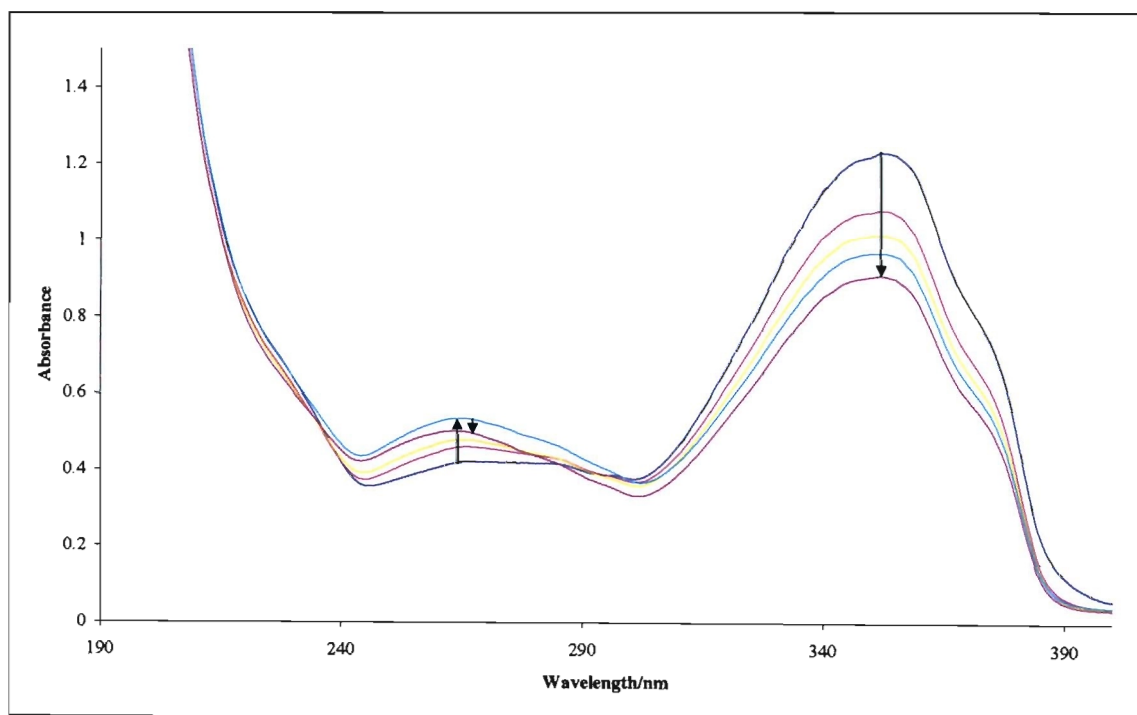
Figure 3.45:   UV absorption spectra of 2.0×10^{-5} M avobenzone dissolved in cyclohexane obtained after thirty minute irradiation intervals. Irradiation was with UV light of wavelengths greater than 300 nm. The spectra were recorded in a 1 cm pathlength quartz cuvette against air as the reference.
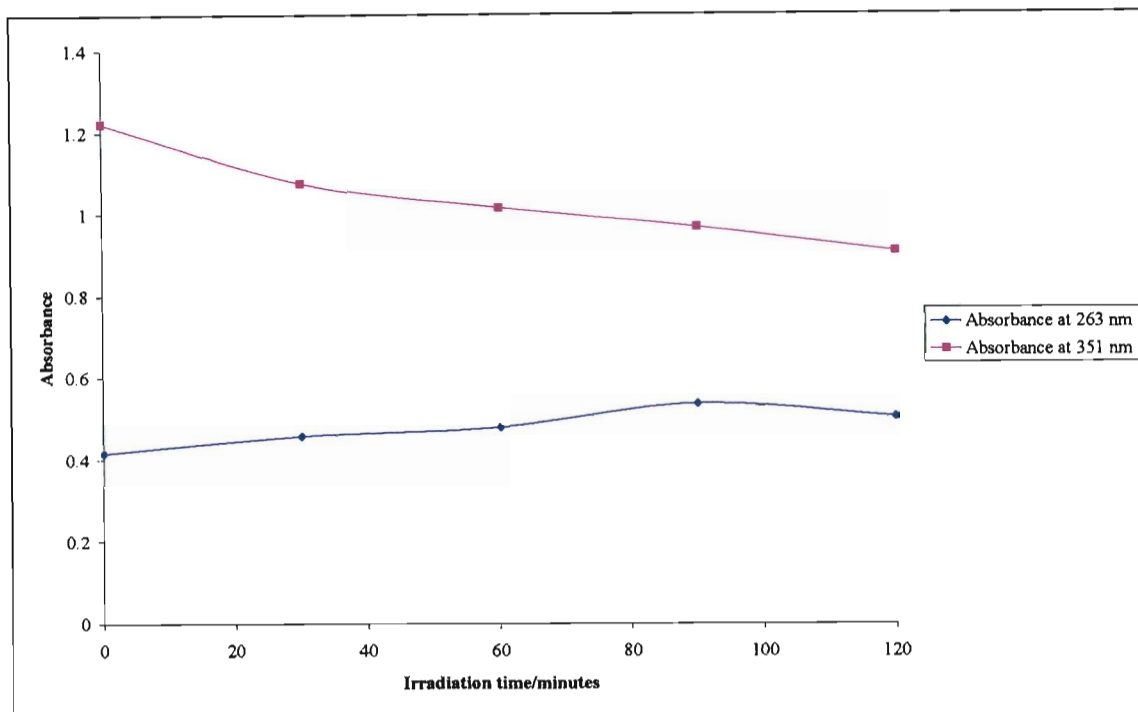
Figure 3.46:   Absorbance of a 2.0×10^{-5} M solution of avobenzone dissolved in cyclohexane monitored at 351 nm and at 263 nm after each 30 minute irradiation interval with wavelengths of light greater than 300 nm.

Photo-instability of avobenzone in methanol

A 2.6×10^{-5} M solution of avobenzone dissolved in methanol was prepared and irradiated at 30 minute intervals with UV radiation of wavelengths greater than 300 nm. The UV spectra (see Figure 3.47) of this solution acquired after each irradiation interval show a much smaller loss in absorption at the wavelength of maximum absorption than for the other solvents investigated. The loss in absorption at the λ_{max} of avobenzone in methanol, 358 nm, is accompanied by an increase in absorbance at 259 nm, and this correlation is shown in Figure 3.48. Apart from the initial loss in absorbance at the λ_{max} of avobenzone, the absorber appears relatively photostable thereafter.

Avobenzone was observed to be photo-unstable in ethyl acetate, DMSO and cyclohexane but relatively photostable in methanol. Therefore, further investigations regarding the absorber were conducted in only those solvents where photo-instability was observed.
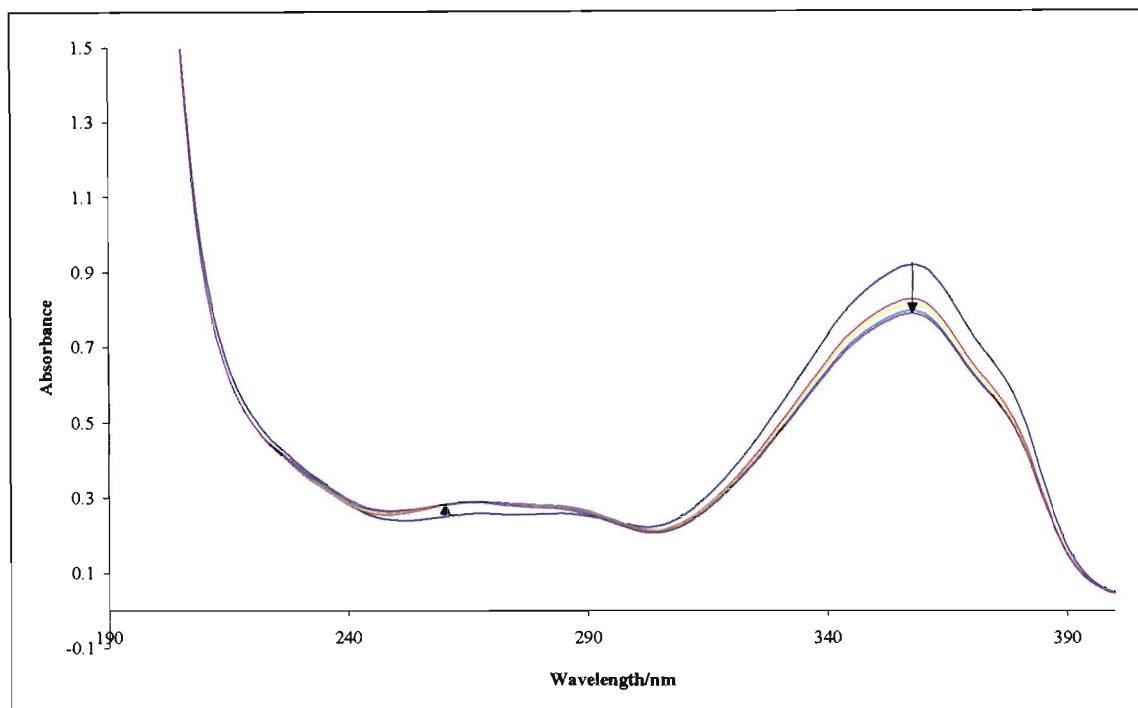
Figure 3.47:   UV absorption spectra of 2.6 × 10^{-5} M avobenzone dissolved in methanol measured after each thirty minute irradiation interval. Irradiation was with UV light of wavelengths greater than 300 nm. The spectra were recorded in a 1 cm pathlength quartz cuvette against air as the reference.
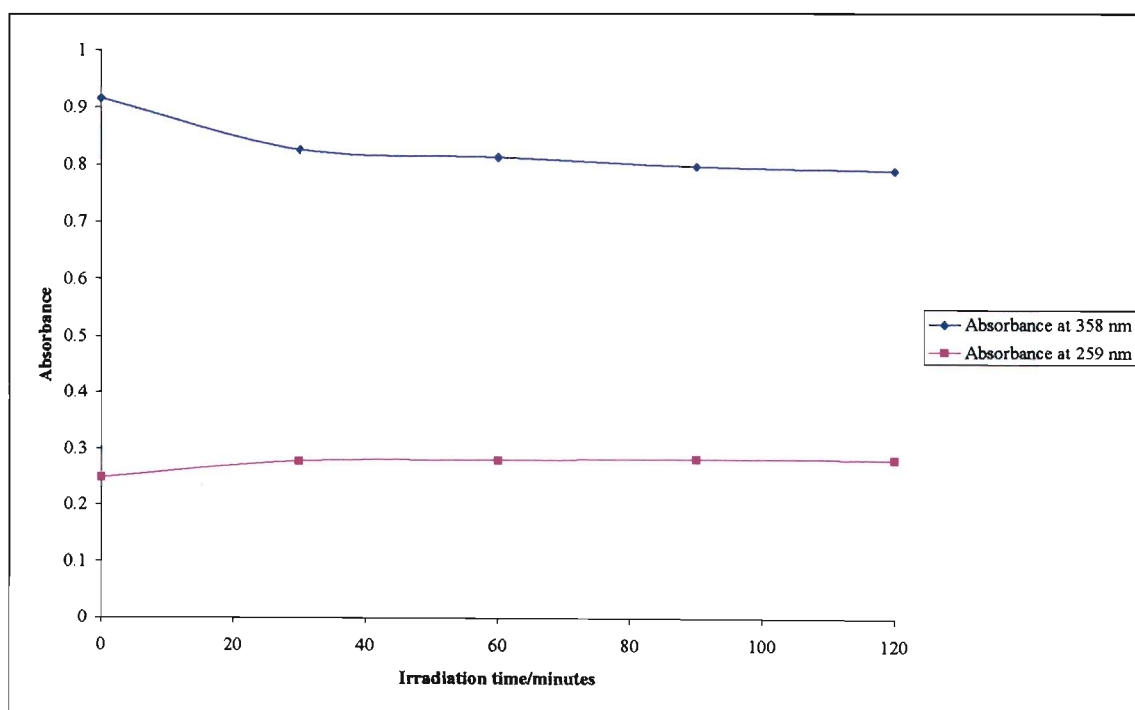
Figure 3.48:   Absorbances of a 2.6 × 10^{-5} M avobenzone solution in methanol monitored at 358 nm and at 259 nm during thirty minute irradiation intervals with wavelengths of light greater than 300 nm.

3.3.1.2 Oxygen dependence of photo-instability shown by UV spectroscopy

Singlet oxygen ($^1O_2$) is a higher energy excited state of molecular ground-state oxygen ($^3O_2$), and can be generated photochemically to further degrade avobenzone (Puccetti and Chaudhuri [2004]). This section discusses whether the absence of oxygen has an effect on the loss in absorbance at the λ_{max} of irradiated solutions of avobenzone dissolved in DMSO, ethyl acetate and cyclohexane.

Avobenzone solutions of concentrations: 2.4×10^{-5} M in ethyl acetate, 5.0×10^{-5} M in DMSO and 1.0×10^{-4} M in cyclohexane, were prepared and irradiated in the presence and in the absence of oxygen. Solutions were deoxygenated by bubbling nitrogen through them for three-minutes. The absorbance of each solution was measured at the λ_{max} value before and after each irradiation interval.

The results of these deoxygenation experiments are tabulated in Tables 3.12 (ethyl acetate), 3.13 (DMSO) and 3.14 (cyclohexane). The results in Table 3.12 have been plotted in Figures 3.49 and 3.50, those in Table 3.13 have been plotted in Figures 3.51 and 3.52, and those in Table 3.14 have been plotted in Figures 3.53 and 3.54.

The photostability of avobenzone increased by 6%, 43% and 10% in ethyl acetate (see Figure 3.50), DMSO (see Figure 3.52) and cyclohexane (see Figure 3.54) respectively in the absence of oxygen at the irradiation time where a 45% loss in absorbance was observed in the presence of oxygen. These results indicate that avobenzone is more photostable in all solvents in the absence of oxygen but, this photostabilisation is only significant in DMSO. In the absence of oxygen the loss in absorbance of avobenzone was decreased by 90% in DMSO for an irradiation period of 40 minutes.

Table 3.12:   Variation in the absorbance readings at 356 nm with irradiation time for a 2.4 × 10^{-5} M solution of avobenzone in ethyl acetate contained in a 1 cm pathlength glass cuvette.

Irradiation time/ minutes	In the absence of oxygen		In the presence of oxygen	
	Absorbance, A	% photodegradation $100[1 - (A/0.95390)]$	Absorbance, A	% photodegradation $100[1 - (A/0.98826)]$
0	0.95390	0	0.98826	0
1	0.92657	2.87	0.96139	2.72
2	0.89977	5.94	0.92500	6.40
4	-	-	0.87009	12.0
8	0.79557	16.6	0.79047	20.0
16	0.68991	27.7	0.66448	32.8
32	0.52193	45.3	0.47502	51.9
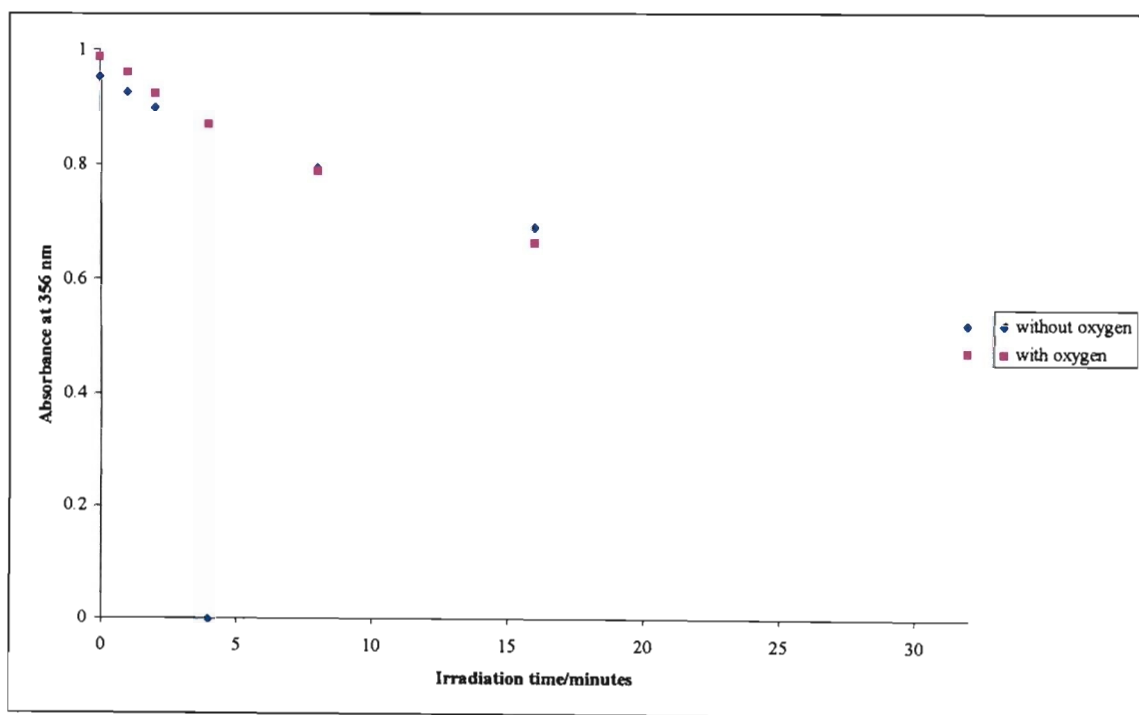
Figure 3.49:   Change in absorbance at 356 nm with irradiation time for a 2.4 × 10^{-5} M avobenzone solution in ethyl acetate in the presence and absence of oxygen.
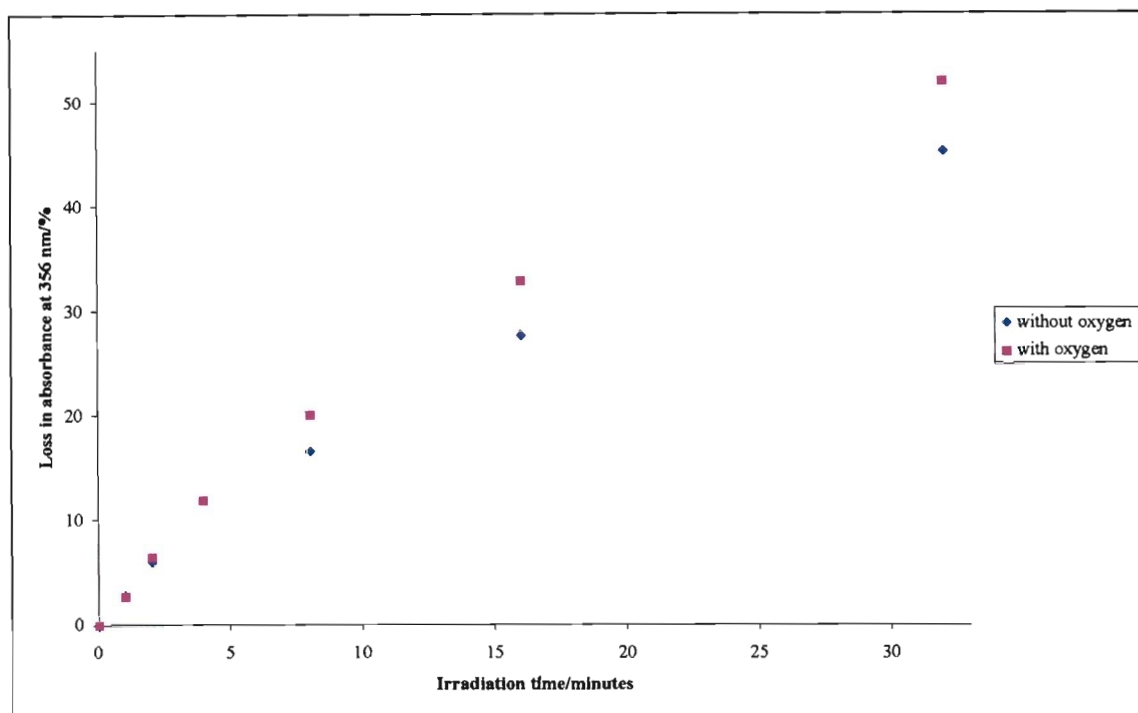
Figure 3.50:   Percentage loss in absorbance of a 2.4 × 10⁻⁵ M solution of avobenzone in ethyl acetate with increasing irradiation time in the presence and absence of oxygen.

Table 3.13:   Variation in the absorbance readings at 363 nm with irradiation time for a 5.0×10^{-5} M solution of avobenzone in DMSO contained in a 1 cm pathlength glass cuvette.

Irradiation time/ minutes	In the absence of oxygen		In the presence of oxygen	
	Absorbance, A	% photodegradation $100[1 - (A/1.64763)]$	Absorbance, A	% photodegradation $100[1 - (A/1.66720)]$
0	1.64763	0	1.66720	0
10	1.61476	1.99	1.19472	28.3
20	1.58014	4.10	0.15958	90.4
30	1.55773	5.46	0.06501	96.1
40	1.52961	7.16	0.06874	95.9
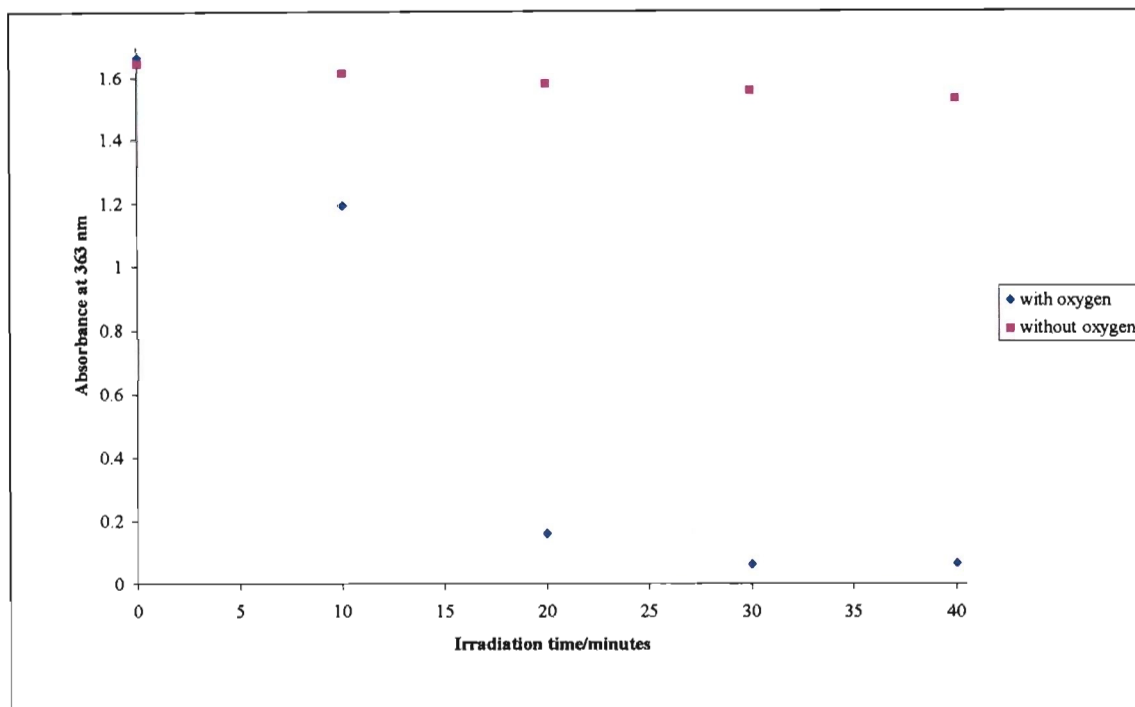
Figure 3 51:   Change in absorbance at 363 nm with irradiation time for a 5.0×10^{-5} M solution of avobenzone in DMSO in the presence and absence of oxygen.
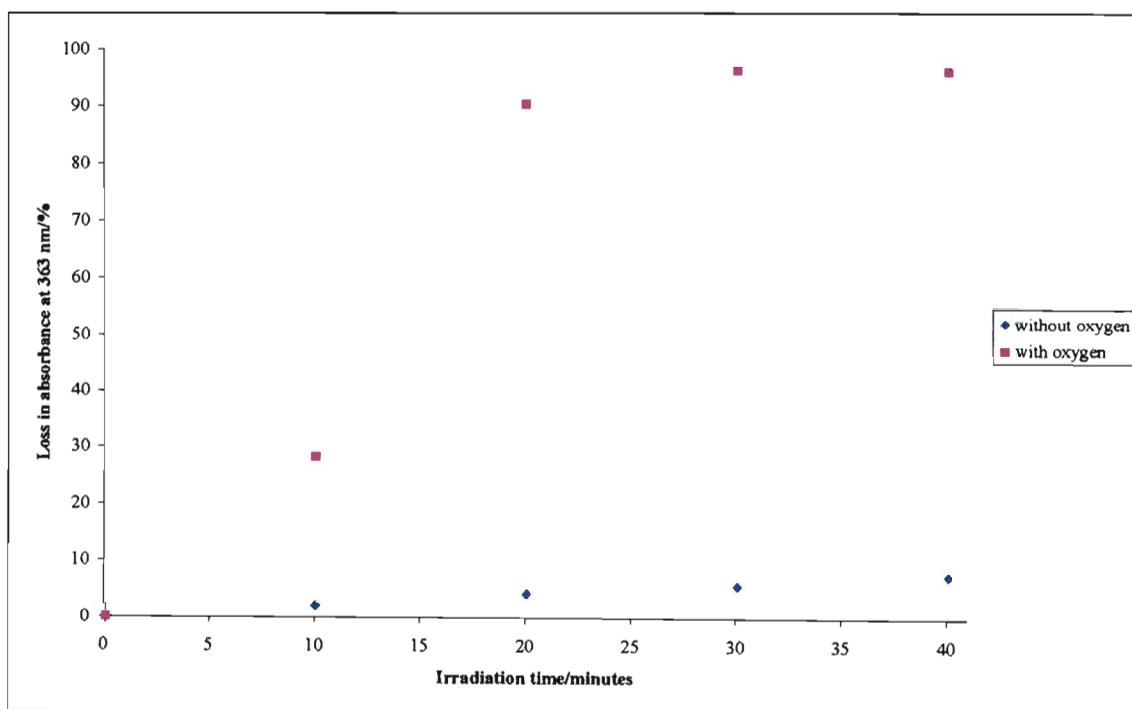
Figure 3.52:   Percentage loss in absorbance of a 5.0×10^{-5} M solution of avobenzone in DMSO with increasing irradiation time in the presence and absence of oxygen.

Table 3.14:   Variation in the absorbance readings at 351 nm with irradiation time for a 1.0 × 10^{-4} M solution of avobenzone in cyclohexane contained in a 1 mm quartz cuvette.

Irradiation time/ minutes	In the absence of oxygen		In the presence of oxygen	
	Absorbance, A	% photodegradation 100[1 − (A/1.57208]	Absorbance, A	% photodegradation 100[1 − (A/1.55030)]
0	1.57208	0	1.55030	0
10	1.51912	3.37	1.46412	5.56
20	1.41081	10.3	1.34362	13.3
30	1.25381	20.2	1.10409	28.8
60	0.93273	40.7	0.79241	48.9
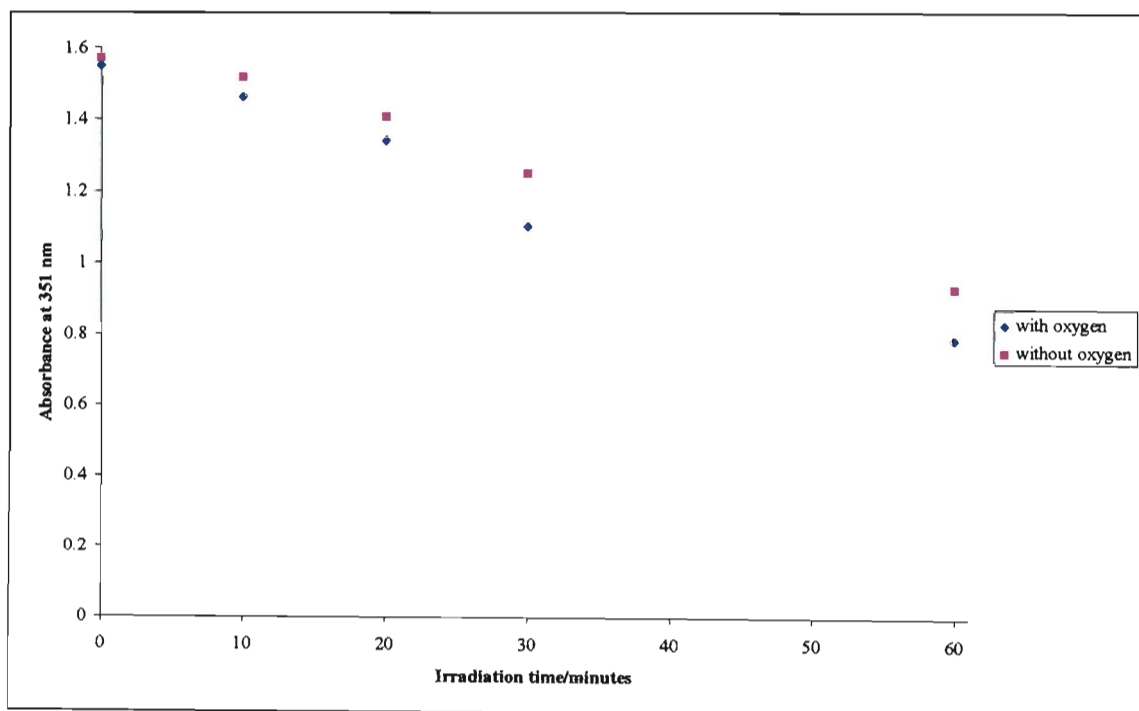
Figure 3.53:   Change in absorbance at 351 nm with irradiation time for a 1.0 × 10^{-4} M avobenzone solution in cyclohexane in the presence and absence of oxygen.
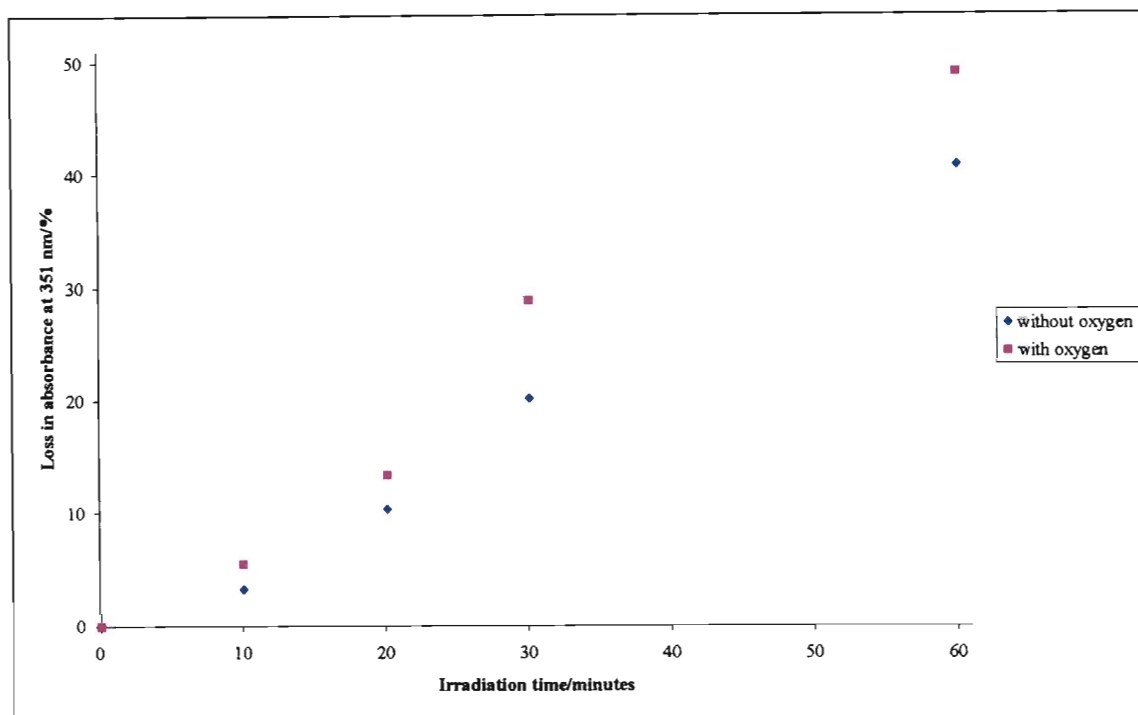
Figure 3.54:   Percentage loss in absorbance of a 1.0×10^{-4} M avobenzone solution in cyclohexane with increasing irradiation time in the presence and absence of oxygen.

3.3.1.3 Photo-instability shown by GC-MS

UV analyses have shown that avobenzone loses its UVA absorbance capacity significantly in DMSO, ethyl acetate and cyclohexane and to a smaller extent in methanol. In order to photostabilise avobenzone, it is important to understand the pathway followed that results in this loss in absorbance. The UV spectra in Section 3.3.1.1 show a decrease in absorbance of avobenzone at around 350 nm accompanied by an increase in absorbance at much lower wavelengths, in the UVB range. The loss in absorption could be due to the loss of one substance and the formation of another or other ones. GC-MS analyses became essential for characterising the photoproduct(s) which in turn helped to elucidate their path of formation. These analyses were performed for avobenzone in each solvent where photo-instability was observed, in order to determine the nature of the photoproducts formed. This section will therefore discuss the GC-MS analyses of irradiated avobenzone in ethyl acetate, DMSO and cyclohexane.

The column and temperature program employed for the GC-MS analyses of avobenzone photoproducts have been discussed in Section 2.7.

A 1×10^{-2} M avobenzone solution in each of DMSO, ethyl acetate and cyclohexane was prepared and injected into the Hewlett Packard GC-MS prior to irradiation. The GC-MS results are displayed in Appendix B. The total ion chromatograms of avobenzone in cyclohexane, ethyl acetate and DMSO are displayed in Figures B1.1, B3.1 and B5.1, respectively, and their corresponding MS spectra are shown in Figures B1.2, B3.2 and B5.2 respectively. Avobenzone was found to elute at 15 minutes with the temperature program employed.

Avobenzone was irradiated for 18 hours in each of cyclohexane, ethyl acetate and DMSO. The total ion chromatograms of irradiated avobenzone in cyclohexane, ethyl acetate and DMSO are displayed in Figures B2.1, B4.1 and B6.1 respectively. The MS fragmentation patterns of each peak in the total ion chromatogram in Figure B2.1 are displayed in Figures B2.2 to B2.12; and those in Figure B4.1 are displayed in Figures B4.2 to B4.6. The MS fragmentation of the peak in Figure B6.1 is displayed in Figure B6.2. The fragmentation of each photoproduct was compared with the electron impact fragmentations in the Wiley275 library of the Hewlett Packard GC-MS instrument, as well as other literature (Schwack and Rudolph [1995]), and are summarised in Table 3.15.

Schwack and Rudolph [1995] have also investigated the photostability of avobenzone in cyclohexane. They identified the major photoproducts to be various forms of benzaldehydes, benzoic acids, phenylglyoxals, acetophenones, benzils, a dibenzoyl methane and a dibenzoyl ethane. These photoproducts were formed as a result of α-cleavage of the keto form of avobenzone followed by either recombination or oxidation. In this study the photoproducts formed in cyclohexane were also mainly the result of α-cleavage of the keto form of avobenzone (as shown in Figure 3.55) to form benzils, a phenylglyoxal and a benzaldehyde. These radicals may have recombined to form the compounds, dibenzoyl ethane and 1,4-bis(4-methoxyphenyl)butane-1,4-dione. The ester at 9.1 minutes was the combined product from the photoproducts of avobenzone and cyclohexane. Dicyclohexyl ether was also formed and it was attributed to be the product of the solvent, cyclohexane. It is unclear how anthracene and phenanthrene were formed, but since avobenzone was the only phenyl containing substance it can be assumed that these compounds were formed from avobenzone. The compound eluting at 9.5 minutes could not be categorised by either the Wiley275 library or the MS fragmentation reported by Schwack and Rudolph [1995].

Table 3.15: Retention times of chemical substances present in irradiated solutions of avobenzone (for 18 hours) dissolved in cyclohexane, ethyl acetate and DMSO and their identities as determined from the fragmentation patterns reported in the literature (Schwack and Rudolph [1995]) and the Wiley275 library.

Retention times of substances in irradiated avobenzone solutions/minutes			Matched fragmentation pattern*	Compound characterisation
Cyclohexane	Ethyl acetate	DMSO		
5.5	-	-	162 (M^+, 12), 147 (100), 119 (45), 103 (10), 91 (94), 77 (17), 65 (11), 57 (7)	4-t-butyl benzaldehyde
5.7	-	-	Wiley275 library	dicyclohexyl ether
	8.3	-	Wiley275 library	anthracene
8.5	8.5	-	Wiley275 library	phenanthrene
9.1	-	-	Wiley275 library	4-methoxy benzoic acid, cyclohexyl ester
9.5	-	-	unknown	unknown
12.8	12.8	-	296 (M^+, 2), 161 (26), 146 (6), 135 (100), 118 (9), 107 (6), 92 (13), 91 (6), 77 (16)	4-t-butyl-4'-methoxy benzil
13.1	13.1	-	161 (M^+, 100), 146 (29), 133 (3), 131 (6), 118 (32), 105 (17), 91 (33), 76 (8), 57 (15)	4-t-butyl phenylglyoxal
15.1	15.1	15.1	310 (M^+)	avobenzone
15.4	-	-	Wiley275 library	1,4-bis(4-methoxyphenyl)butane-1,4-dione
15.9	-	-	324 (M^+, 6), 161 (32), 146 (5), 135 (100), 118 (7), 92 (11), 77 (17)	4-t-butyl-4'-methoxydibenzoyl ethane
16.6	-	-	161 (M^+, 100), 146 (8), 118 (17), 105 (6), 91 (11), 77 (4)	4,4'-di-t-butyl benzil**

* Matched fragmentation pattern from either literature (Schwack and Rudolph [1995]), given as *m/z* value with its percentage abundance in brackets, or the Wiley275 library.

** tentative assignment
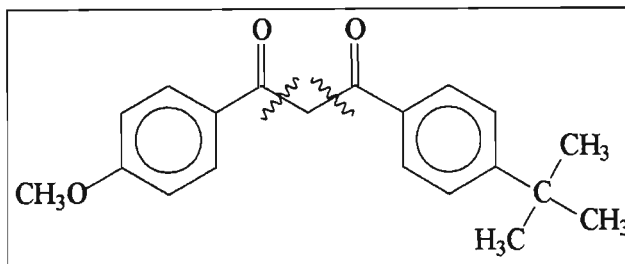
Figure 3.55:   Schematic diagram showing α-cleavage of avobenzone when irradiated with UV light of wavelengths greater than 300 nm.

Avobenzone photoproducts were formed in large quantity and diversity in cyclohexane but they were greatly reduced in ethyl acetate. In DMSO, avobenzone photoproducts were not detected even after 18 hours of irradiation. The avobenzone peak heights in the mass spectra were greatly reduced after irradiation in ethyl acetate and cyclohexane but not in DMSO. The most likely explanation is that avobenzone photoisomerises to the keto form which would therefore elute together with the enol form through the HP-5MS column. Therefore, photoisomerisation possibly occurs solely in DMSO which is why the avobenzone peak does not reduce after irradiation and there were no photoproducts detected. In Section 3.3.1.1, avobenzone was shown to lose a significant amount of its UVA absorption capacity after only one minute of irradiation in ethyl acetate, whereas in cyclohexane the photo-instability was only observed following a thirty minute irradiation interval. However, the number of photoproducts identified by GC-MS following the same irradiation interval is smaller in ethyl acetate than in cyclohexane. This could mean that either avobenzone is photostable at high concentrations in ethyl acetate or that it photodegrades and also photoisomerises in this solvent.

3.3.1.4 Photo-instability shown by HPLC/PDA

Avobenzone photoproducts formed during the irradiation of avobenzone in cyclohexane and ethyl acetate were identified from their mass spectra. However, none were identified in DMSO to account for the loss in absorbance of avobenzone with irradiation. The mass spectra were also not able to show where these photoproducts absorbed maximally.

In UV analysis, avobenzone was shown to lose absorbance at its wavelength of maximum absorption, λ_{max}, upon irradiation in ethyl acetate, DMSO and cyclohexane. This loss in absorbance was accompanied by an increase in absorbance at around 270 nm. These changes in

absorbance could be as a result of the decrease in concentration of one compound associated with the formation of a different compound(s). Compounds of varied polarity can be separated by an HPLC column and the corresponding UV spectra obtained as the compounds pass through the photodiode array (PDA) detector. HPLC/PDA analysis was therefore vital in determining the nature of the loss in absorbance shown by avobenzone upon irradiation.

The GC-MS results show that avobenzone could photodegrade or possibly photoisomerise upon irradiation depending on the solvent. The isomers of avobenzone vary in polarity, hence the equilibrium between these isomers would shift depending on the polarity of the solvent. Subsequently, these isomers would be resolved to different extents by different mobile phases. HPLC analysis was therefore the ideal method to analyse these isomers. Andrae et al. [1995 and 1997] reported different λ_{max} for the enol and keto isomers of avobenzone in acetonitrile. A PDA detector was hence appropriately employed in order to obtain the ultraviolet spectra of the different isomers eluted through the HPLC. In DMSO, the loss in absorbance of avobenzone at its wavelength of maximum absorption could be due to photoisomerisation based on the GC-MS results.

As seen in the previous section (see Section 3.3.1.3), avobenzone photodegrades in cyclohexane (as reported by Schwack and Rudolph [1995] and Roscher et al. [1994]) and ethyl acetate and gives rise to a number of photoproducts. This photodegradation would reduce the efficacy of avobenzone if it forms photoproducts that do not absorb in the UVA region. HPLC analysis is therefore also important for these two solvents in order to determine the ultraviolet spectra of photoproducts formed after irradiation.

HPLC analysis of avobenzone in cyclohexane, DMSO and ethyl acetate before irradiation
The avobenzone solutions in ethyl acetate were injected directly through the Nucleosil 100 C18 column of the HPLC instrument for these photostability investigations. On the other hand, solutions of avobenzone in cyclohexane and DMSO required sample preparation before HPLC analysis. These solutions failed to produce clear chromatograms and they were either diluted or re-dissolved in methanol prior to HPLC studies. The cyclohexane solutions required solvent evaporation and re-dissolution of the left-over solid extract in the same volume of methanol prior to HPLC analysis. Avobenzone solutions in DMSO were diluted in methanol, since the two solvents are miscible, before being injected into the HPLC instrument.

The high-performance liquid chromatogram of avobenzone before irradiation in all three solvents displayed two peaks. These peaks were identified as the enol form and the keto form of avobenzone based on their UV spectra and the HPLC studies of the absorber done by Andrae *et al.* [1995]. The enol form of avobenzone eluted at about 21, 16, and 24 minutes in ethyl acetate (Figure 3.56), DMSO (Figure 3.57) and cyclohexane (Figure 3.58) respectively, with a λ_{max} of 360 nm. On the other hand, the keto form eluted much earlier between 5 and 7 minutes with a λ_{max} of 269 nm. The two isomers of avobenzone occurred in all three solvents before irradiation. The retention time for the enol form of avobenzone increased moving from polar to non-polar solvents since a polar mobile phase was used. The concentration of avobenzone before and after irradiation in each respective solvent was determined from the calibration curve (Figure 2.27) given in Section 2.5.2.
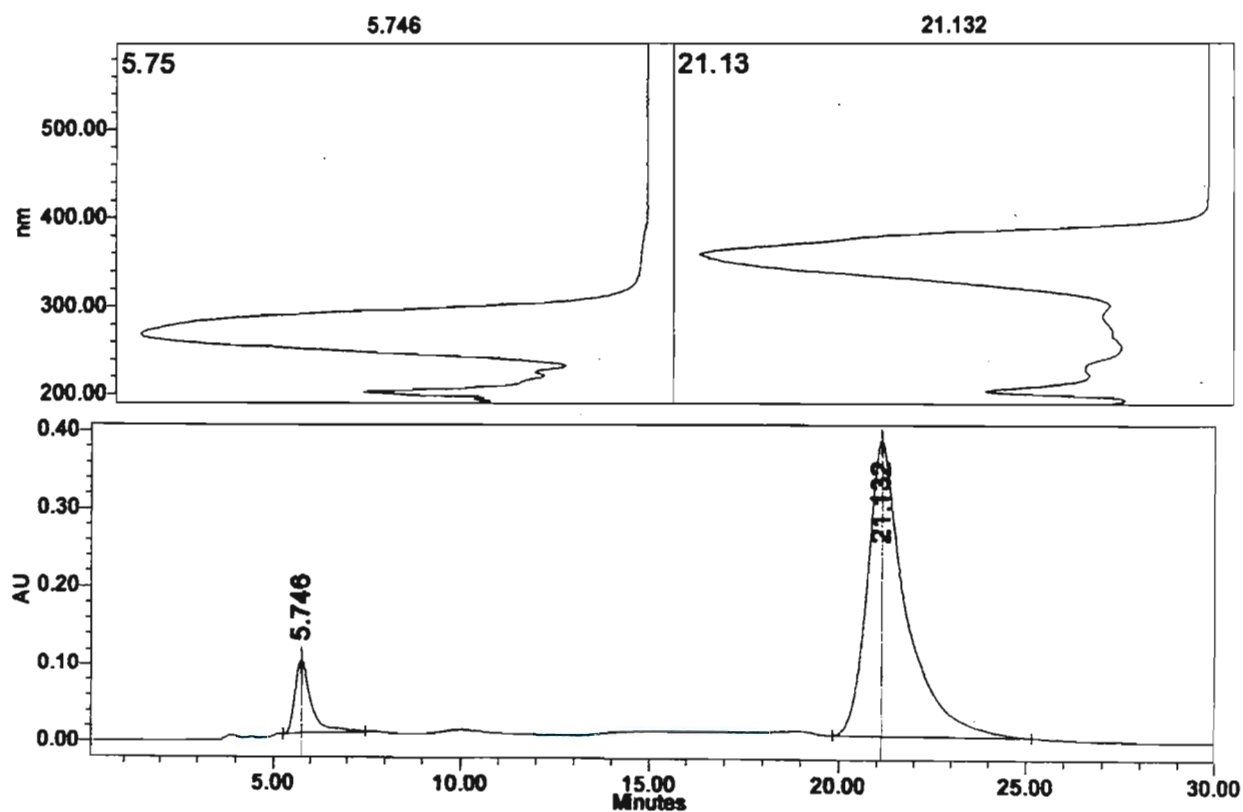
Figure 3.56:   High-performance liquid chromatogram of 0.785×10^{-2} M avobenzone dissolved in ethyl acetate before irradiation (detected at 272 nm) eluted by a mobile phase of 85:15% (v/v) methanol:Millipore water. The keto form elutes at 5.7 minutes and the enol form at 21 minutes.
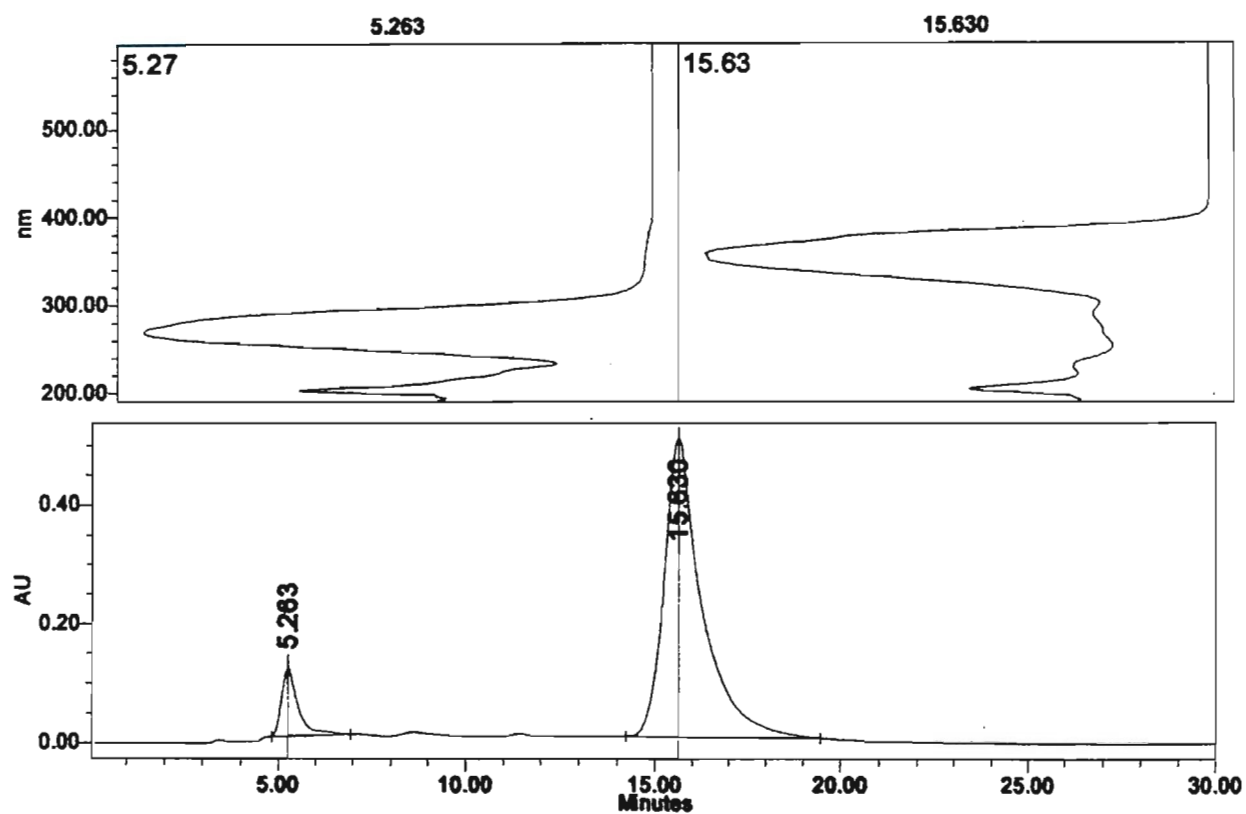
Figure 3.57: High-performance liquid chromatogram of 1.02×10^{-2} M avobenzone dissolved in DMSO before irradiation (detected at 272 nm) eluted by a mobile phase of 85:15% (v/v) methanol:Millipore water. The keto form elutes at 5.3 minutes and the enol form at 16 minutes.
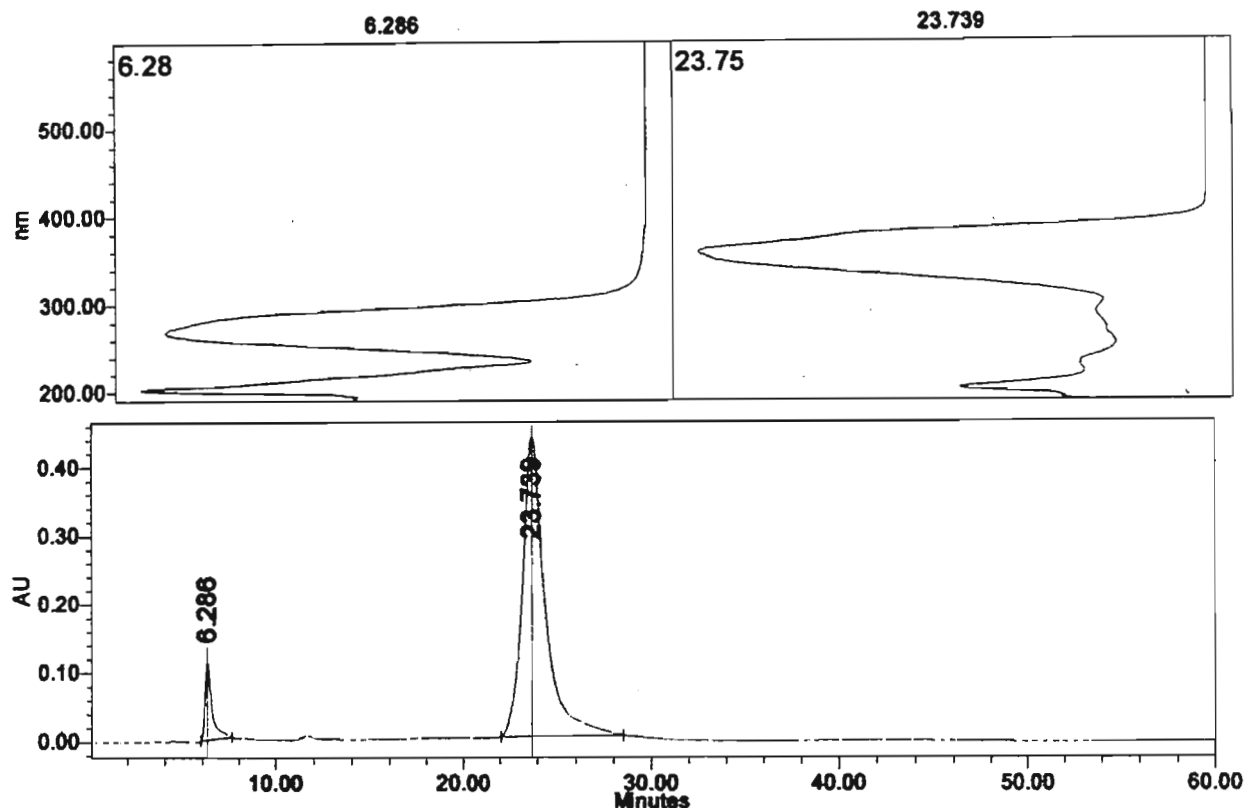
Figure 3.58   High-performance liquid chromatogram of 1.15×10^{-2} M avobenzone dissolved in cyclohexane before irradiation (detected at 272 nm) eluted by a mobile phase of 85:15% (v/v) methanol:Millipore water. The keto form elutes at 6.3 minutes and the enol form at 24 minutes.

Avobenzone in ethyl acetate after irradiation

The high-performance liquid chromatogram of avobenzone dissolved in ethyl acetate after 15 hours of irradiation is shown in Figure 3.59. After irradiation, the peak due to the enol form of avobenzone which elutes at 21 minutes had decreased by 33% and the peak at approximately 5.7 minutes with a λ_{max} of 269 nm had increased. However, a number of new peaks also appeared. Since the peak at 5.7 minutes represents the keto form of avobenzone, photoisomerisation must have occurred. The other peaks seen in the chromatogram are potential photoproducts resulting from the photodegradation of avobenzone. The photoproducts detected eluted at 2.5 minutes (λ_{max} of 285 nm), 2.8 minutes (λ_{max} of 259 nm), 3.6 minutes (λ_{max} of 250 nm), 4.9 minutes (λ_{max} of 240 nm), 7.9 minutes (λ_{max} of 280 nm), 9.2 minutes (λ_{max} of 263 nm), 10 minutes (λ_{max} of 270 nm) and 14 minutes (λ_{max} of 273 nm).
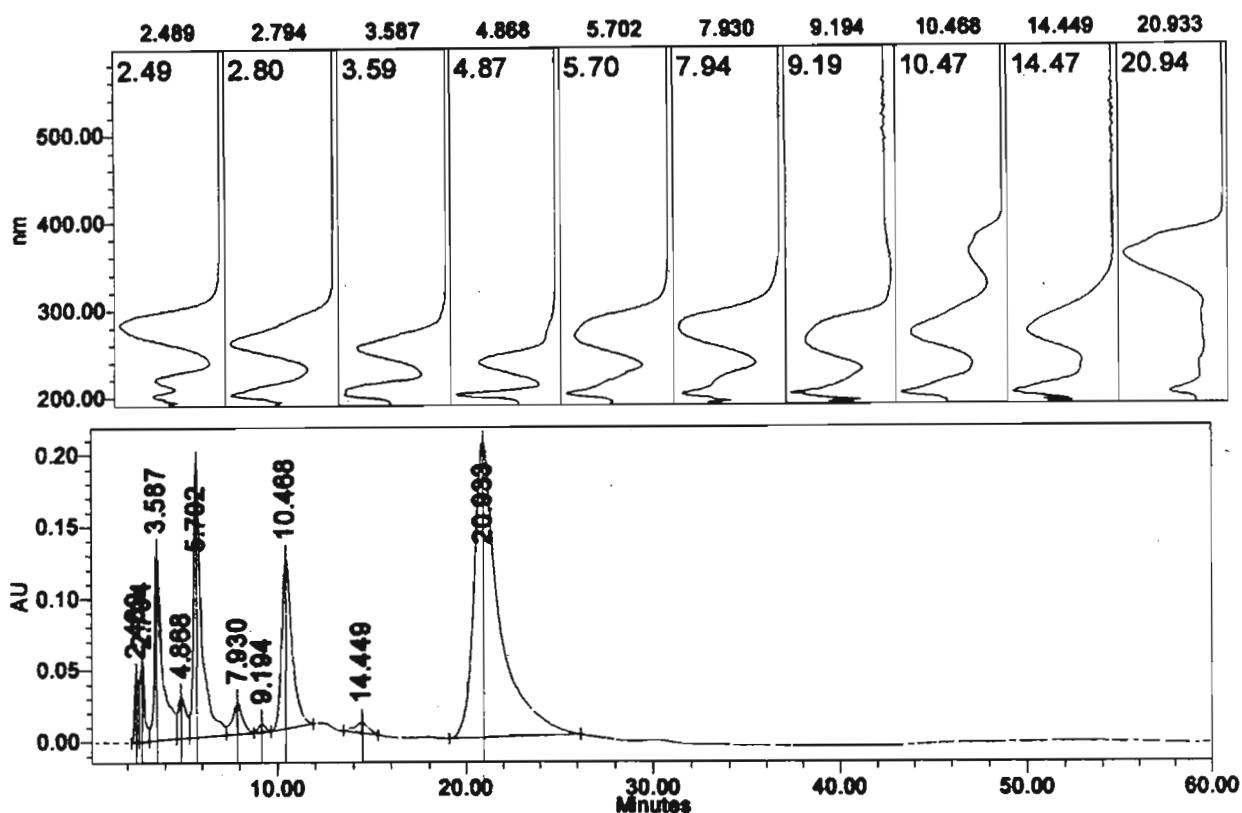
Figure 3.59:   High-performance liquid chromatogram of 0.531×10^{-2} M avobenzone irradiated for 15 hours in ethyl acetate, eluted with a mobile phase composition of 85:15% (v/v) methanol:Millipore water and detected at 272 nm. The keto form elutes at 5.7 minutes and the enol form at 21 minutes; the rest of the peaks are photoproducts.

The photoisomerisation of a 1×10^{-3} M avobenzone solution in ethyl acetate was further investigated by HPLC analysis, following irradiations of 5, 20 and 60 minute intervals with wavelengths of light greater than 300 nm. The peak area for the enol form of avobenzone was determined from the peak eluting at 20 minutes through the Nucleosil 100 C18 column at a detection wavelength of 350 nm. The peak area for the keto form was measured from the peak eluting at 6 minutes at a detection wavelength of 270 nm. Table 3.16 shows the peak areas for the keto and enol form with irradiation time and the corresponding concentrations of the enol form, determined from the avobenzone calibration curve (Figure 2.27) in Section 2.5.2. Table 3.16 and Figure 3.60 show a decrease in the enol form accompanied by an increase in the keto form of avobenzone with irradiation time, indicating that photoisomerisation of the absorber is taking place.

Table 3.16:   Variation in the HPLC peak areas with irradiation time for the enol and keto forms of avobenzone, detected at 350 nm and 272 nm respectively. The concentrations of the enol form in ethyl acetate were determined from Figure 2.27 in Section 2.5.2.

| Irradiation time/minutes | Peak Area/10^5 µV s | | Concentration of the enol form/10^{-4} M |
	Enol form detected at a wavelength of 350 nm	Keto form detected at a wavelength of 270 nm	
0	209.0	3.646	11.50
5	191.3	4.410	10.52
20	163.3	26.55	8.982
60	138.6	37.07	7.623
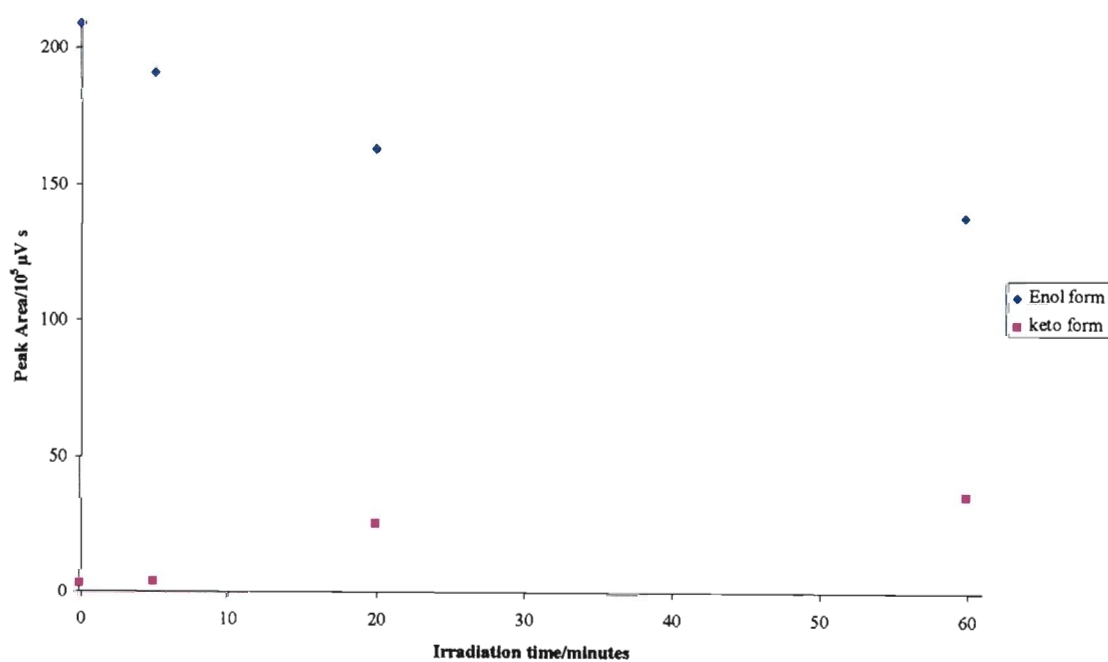
Figure 3.60:   Peak areas of the isomeric forms of avobenzone recorded after 5, 20 and 60 minute irradiation periods. The enol form of avobenzone was detected at 350 nm and the keto form at 270 nm. They were eluted through a Nucleosil 100 C18 column by an isocratic mobile phase of 85:15% (v/v) methanol:Millipore water with a flow rate of 1 ml min^{-1}.

Avobenzone in DMSO after irradiation

The high-performance liquid chromatogram of avobenzone after irradiation for 15 hours in DMSO is displayed in Figure 3.61. The peak area due to the enol form of avobenzone appears to have decreased by 75% after irradiation. The major peak is of the keto form of avobenzone which elutes at 5.4 minutes (λ_{max} = 269 nm), and other photoproducts appear at 2.5 minutes (267 nm), 3.8 minutes (231 nm), 4.5 minutes (267 nm) and 9.1 minutes (363 nm) in the chromatogram of the irradiated sample. The number of photoproducts formed here is smaller than in ethyl acetate in keeping with the GC-MS results.

Avobenzone and its photoproducts were eluted much earlier in DMSO than in ethyl acetate, since it is a more polar solvent and would elute polar compounds at an earlier time.
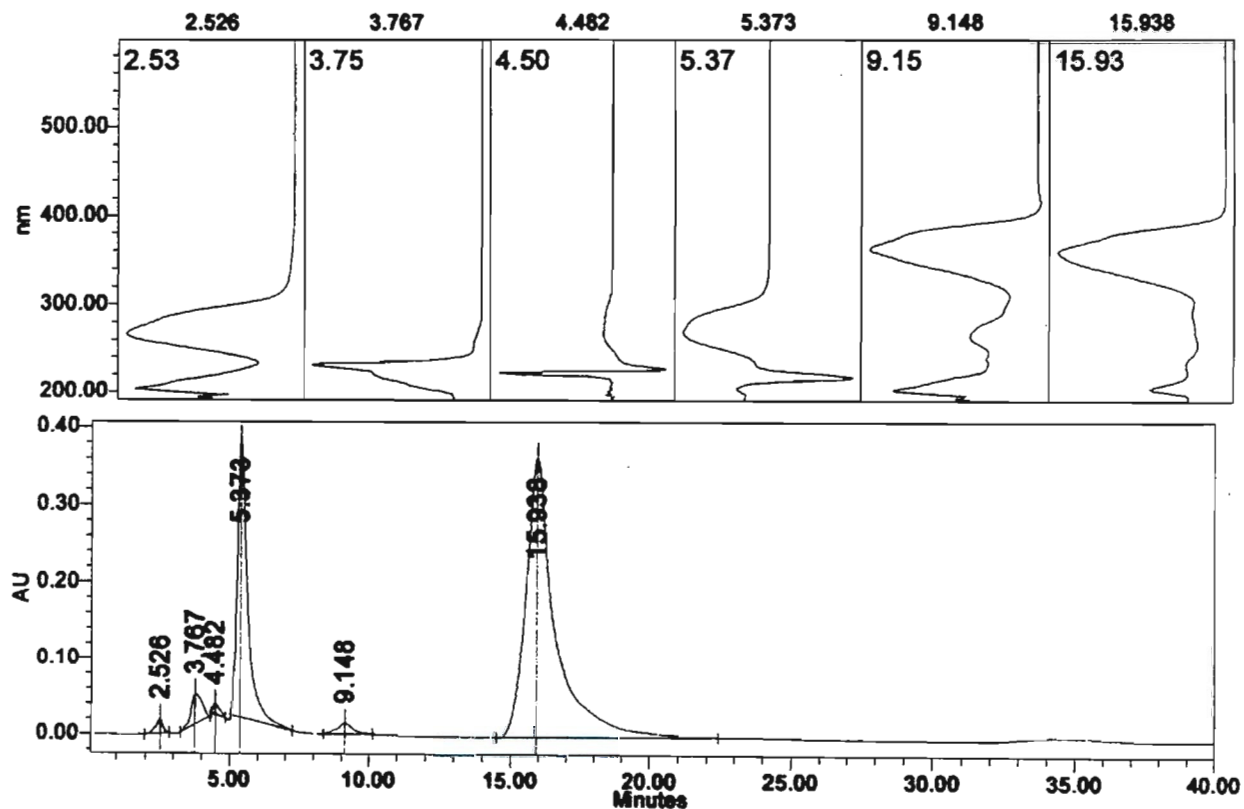
Figure 3.61: High-performance liquid chromatogram of 0.761 × 10^{-2} M avobenzone irradiated for 15 hours in DMSO, eluted with a mobile phase composition of 85:15 (v/v) methanol:Millipore water and detected at 272 nm. The keto form elutes at 5.4 minutes and the enol form at 15.9 minutes.

Avobenzone in cyclohexane after irradiation

Figure 3.62 shows the HPLC chromatogram of avobenzone after 18 hours of irradiation in cyclohexane. The peak due to the enol form of avobenzone is reduced by 56% following irradiation. Avobenzone has disintegrated into various photoproducts of much lower λ_{max} than that of the enol form of avobenzone (λ_{max} = 360 nm) responsible for absorbing UVA radiation.

The avobenzone isomers elute at 23.8 minutes (enol form) and at 6.3 minutes (keto form). Irradiation of avobenzone in cyclohexane also causes photoisomerisation since the peak area at 6.3 minutes has increased. Most photoproducts formed after irradiation absorbed maximally at low wavelengths, mostly in the UVC range. These photoproducts eluted at 3.9 minutes (256 nm), 5.2 minutes (239 nm), 5.7 minutes (241 nm), 9.0 minutes (276 nm), 10.4 minutes (268 nm), 11.9 minutes (363 nm), 14.6 minutes (287 nm), 16.7 minutes (269 nm), 28.8 minutes (360 nm) and 36.4 minutes (273 nm). The number of photoproducts formed here is more than in ethyl acetate in keeping with the GC-MS results.
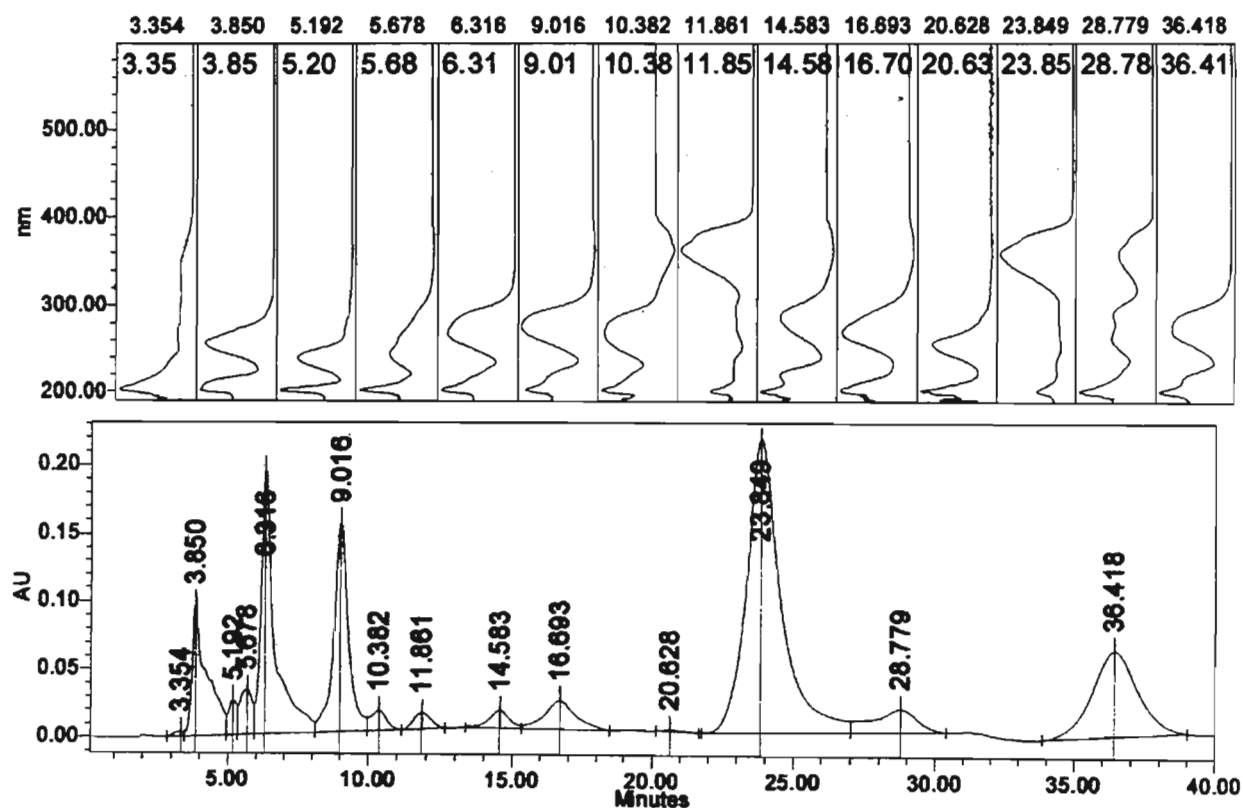
Figure 3.62: High-performance liquid chromatogram of 0.570 × 10^{-2} M avobenzone dissolved in cyclohexane after 18 hours of irradiation, eluted with a mobile phase composition of 85:15% (v/v) methanol:Millipore water and detected at 272 nm. The keto form elutes at 6.3 minutes and the enol form at 24 minutes.

HPLC analysis of avobenzone in DMSO, ethyl acetate and cyclohexane verified the photo-instability observed for this absorber by UV spectroscopy analysis in Section 3.3.1.1. The HPLC results also showed that the number of avobenzone photoproducts formed in the different solvents is in agreement with the GC-MS results in Section 3.3.1.3. Avobenzone was found to primarily photoisomerise in DMSO and to mainly photodegrade in cyclohexane, but in ethyl acetate it equally photoisomerised and photodegraded in significant amounts. Additionally, this HPLC investigation showed that when avobenzone photoisomerises or photodegrades, it loses efficacy as a UVA absorber. The absorber loses efficacy by forming photoproducts with λ_{max} largely below 290 nm.

3.3.1.5 Photo-instability shown by NMR

The position of the equilibrium between the isomers of avobenzone (see Figure 3.63) depends on the solvent avobenzone is dissolved in. Solutions of 1×10^{-2} M avobenzone in deuterated cyclohexane and in deuterated DMSO were prepared in NMR tubes and investigated by means of NMR spectroscopy. The photostability of avobenzone during irradiation with wavelengths of light greater than 300 nm was investigated by means of the 300 MHz Varian Gemini NMR and the 400 MHz Varian Unity Inova NMR instruments. Samples were irradiated in the NMR tubes with the Osram HBO 500 W/2 high pressure mercury lamp in combination with a 10 mm thick Pyrex filter.
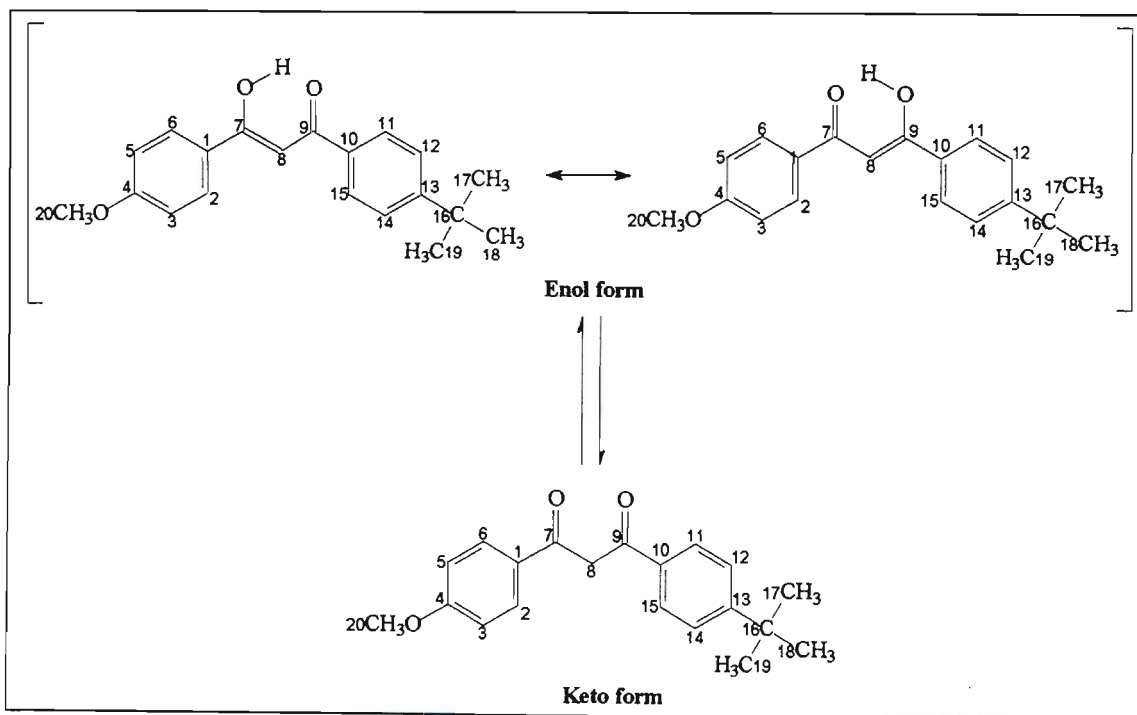
Figure 3.63:   The equilibrium between the keto and enol forms of avobenzone.

¹H NMR spectrum of avobenzone in deuterated cyclohexane

The proton NMR spectrum in Figure 3.64 shows seven sets of avobenzone peaks in deuterated cyclohexane. All peaks are referenced to the solvent peak appearing at 1.39 ppm. The nine methyl protons (attached to C-17, C-18 and C-19) resonate as a singlet farthest upfield at 1.33 ppm. The circulating σ-bond electrons in the *tert*-butyl group create a strong electron density around the hydrogens, acting as a molecular magnetic field opposing the external field. In turn, a stronger external magnetic field is required to bring the protons into resonance; and they appear farther upfield. The nine methyl protons exist in a magnetically equivalent environment and so they resonate at the same chemical shift, appearing as a singlet with integration equivalent to nine protons. The three methoxy protons (attached to C-20) appear relatively downfield at 3.72 ppm due to the electron withdrawing oxygen atom that inductively reduces the electron density around the protons. The integral trace of the singlet resonating at 6.65 ppm is due to a single proton. This peak is due to the proton attached to carbon-8 (C-8) confirming avobenzone occurs as the enol form in deuterated cyclohexane. The peak appears downfield due to the electron withdrawing carbonyl groups as well as the anisotropic effect as a result of the π-electrons. The π-electrons are delocalized (circulate) around the double bond, moving the electron density away from the proton (attached to C-8) hence deshielding it. The doublets at 6.8 ppm, 7.4 ppm, 7.8 ppm and 7.9 ppm are due to the aromatic protons attached to C-11, C-12, C-14, C-15, C-2, C-3, C-5 and C-6. These protons appear as doublets since they are split by adjacent nonequivalent protons. Protons attached to C-12 and C-14 are magnetically equivalent hence resonate together and are each split into a doublet by the equivalent protons at C-11 and C-15. The protons at C-11 and C-15 are in turn split into a doublet by those at C-12 and C-14. The protons at C-3 and C-5 are equivalent and are split into a doublet by those at C-2 and C-6, and those at C-2 and C-6 in turn are split by protons at C-3 and C-5. The aromatic protons appear much more downfield due to the anisotropic effect as a result of the π-electrons. The aromatic electrons delocalize above and below the ring leaving the protons protruding out naked from the plane of the ring. There is a small peak at 5.10 ppm that could possibly represent the two protons attached to the carbon at C-8 of the keto form of avobenzone, based on the results obtained by Andrae *et al.* [1995 and 1997] and Dubois *et al.* [1998]. The small peak at around 4.3 ppm is an unknown and could possibly be an impurity. Hence the ¹H NMR potentially shows the keto form of avobenzone in minute amounts in solution. This keto form was easily seen from HPLC analyses when the chromatograms were monitored at around wavelengths (i.e. 272 nm) where it absorbs maximally.
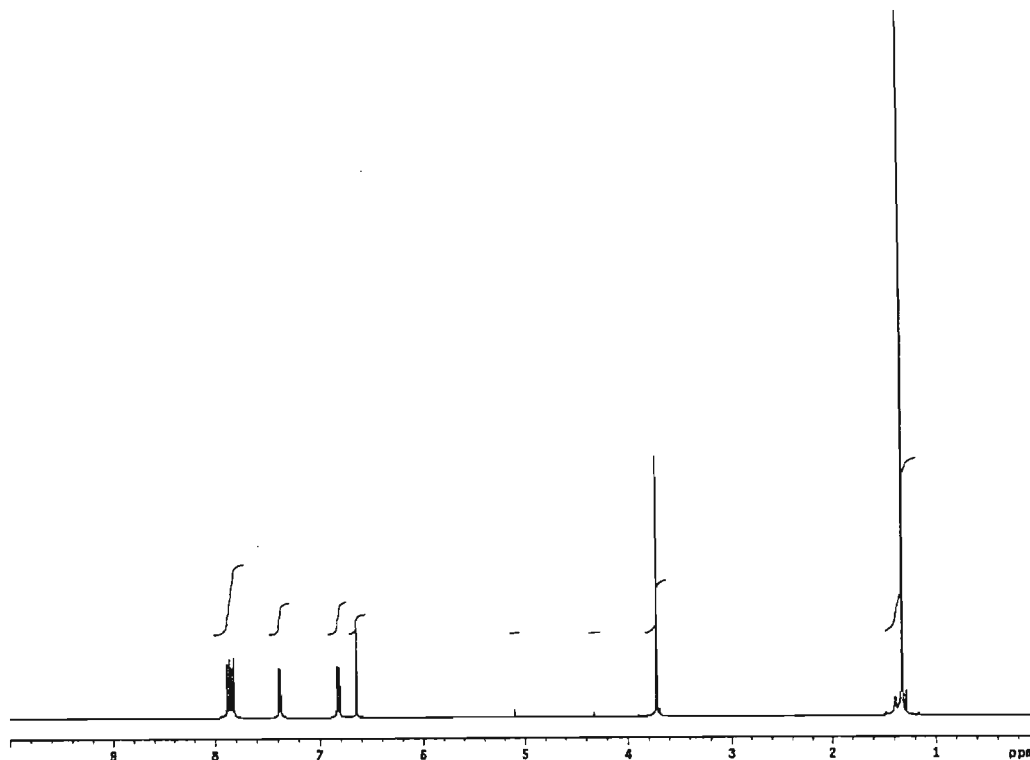
Figure 3.64:   ¹H NMR spectrum of 1 × 10⁻² M avobenzone in deuterated cyclohexane obtained with the 400 MHz Varian Unity Inova NMR spectrometer.

DEPT NMR spectrum of avobenzone in deuterated cyclohexane

The DEPT NMR spectrum of avobenzone (shown in Figure 3.65) in deuterated cyclohexane conforms to the proton NMR sepctrum. The DEPT NMR spectrum shows only the protonated carbons in a compound. The first row only displays the CH_3 carbon groups, the next row shows the CH_2 groups, then the CH groups and the last row shows all protonated carbons in the compound. Only two CH_3 groups appear in the first row of Figure 3.65, the peak resonating upfield (at 32 ppm) with respect to the other is due to the carbons of the three methyl groups at C-17, C-18 and C-19. These carbons are magnetically equivalent hence appear as a singlet, they are also much more shielded by the electron density of the C-H σ-bond hence appear upfield. The other CH_3 group is from the methoxy group, which appears downfield (at 55 ppm) due to the presence of an electron withdrawing oxygen. The DEPT NMR spectrum did not display any CH_2 carbons but showed the CH carbon (at C-8) of the enol form of avobenzone at 92 ppm. This confirms the enol form of avobenzone predominates in cyclohexane. The spectrum also shows four CH carbons due to the aromatic carbon groups at 114 ppm, 126 ppm, 128 ppm and 130 ppm. C-12 and C-14 occur in an equivalent magnetic environment hence resonate to give a single peak. The same applies to C-11 and C-15, C-6 and C-2, and C-5 and C-3; as a result only four aromatic proton peaks occur in the DEPT NMR spectrum.
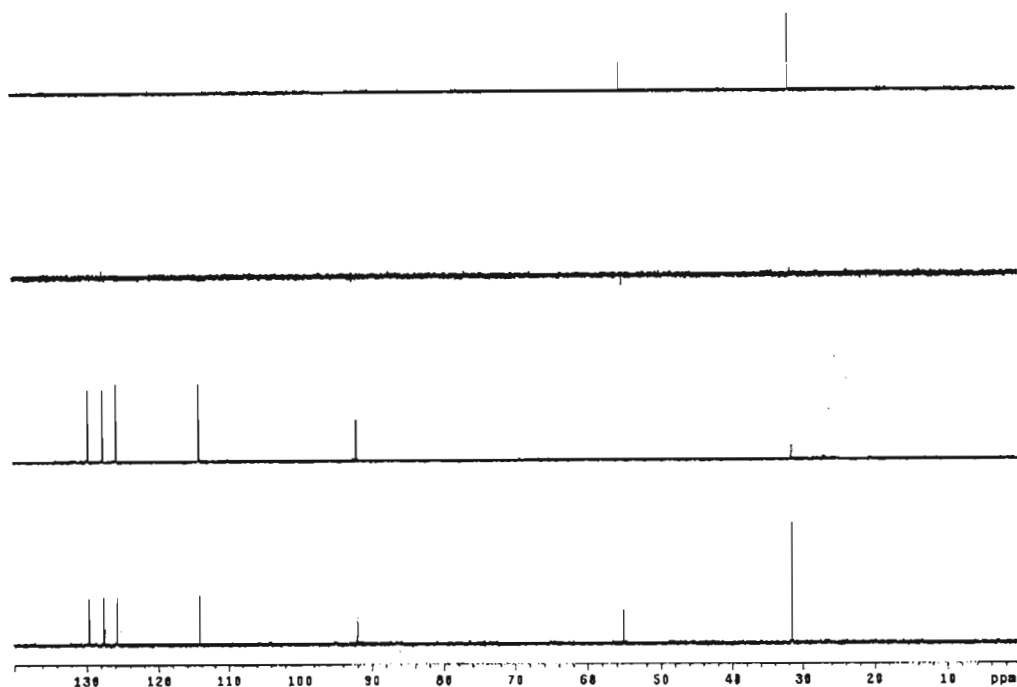
Figure 3.65:   DEPT NMR spectrum of 1×10^{-2} M avobenzone in deuterated cyclohexane obtained with the 400 MHz Varian Unity Inova NMR spectrometer.

^{1}H NMR spectrum of avobenzone in deuterated DMSO

The ^{1}H NMR spectrum of avobenzone dissolved in deuterated DMSO is shown in Figure 3.66. All peaks in Figure 3.66 were referenced to the DMSO peak at 2.5 ppm. The nine methyl protons (attached to C-17, C-18 and C-19) resonate at 1.31 ppm. There is a water peak at 3.36 ppm as a result of water having been absorbed into the sample from moisture in the air due to the hygroscopic nature of the solvent. The methoxy peak (attached to C-20) appears as singlet at 3.86 ppm and the two protons at C-8 of the keto form of avobenzone resonate as a singlet at 4.75 ppm (Andrae *et al.* [1995 and 1997] and Dubois *et al.* [1998]). The aromatic protons resonate as doublets at 7.10 ppm, 7.54 ppm, 8.06 ppm and 8.14 ppm. The single proton peak at C-8 due to the enol form of avobenzone appears as a singlet at 7.23 ppm. This confirms the predominance of the enol form of avobenzone in DMSO as opposed to the keto form. Andrae *et al.* [1995 and 1997] and Dubois *et al.* [1998] showed by ^{1}H NMR that avobenzone also exists in the enol form in acetonitrile.
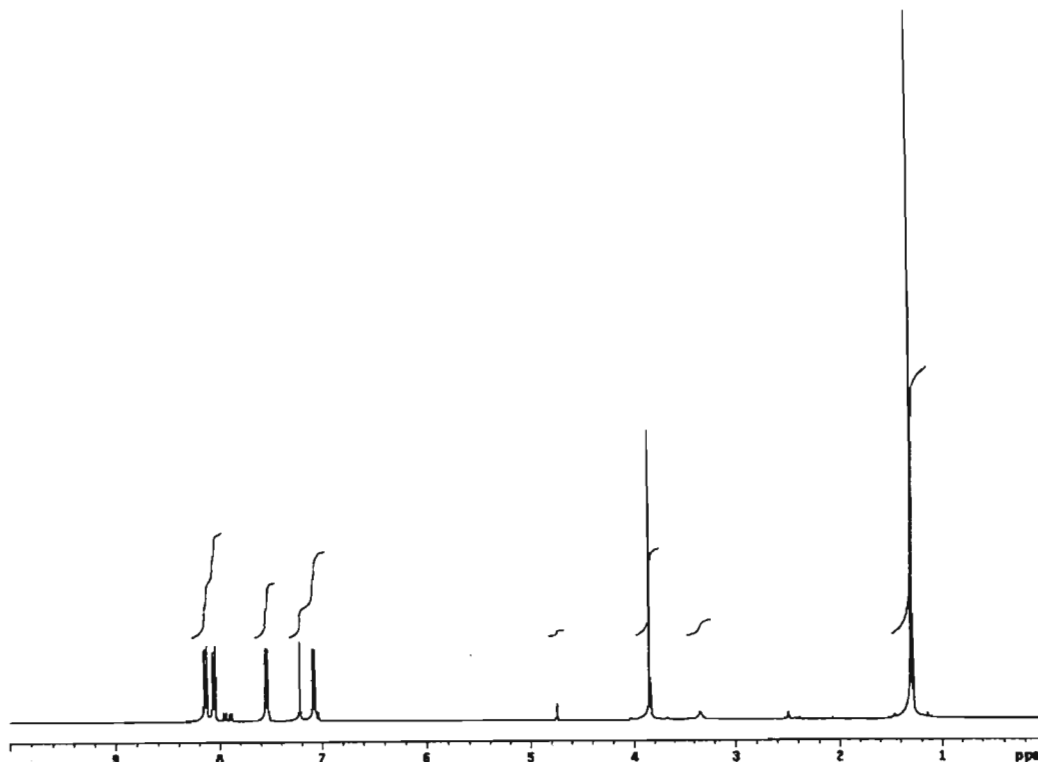
Figure 3.66: ^{1}H NMR spectrum of 1×10^{-2} M avobenzone in deuterated DMSO obtained with the 400 MHz Varian Unity Inova NMR spectrometer.

DEPT NMR spectrum of avobenzone in deuterated DMSO

The DEPT NMR spectrum of avobenzone in deuterated DMSO is shown in Figure 3.67. The single peak of a CH_3 group resonating upfield at 31 ppm in the first row of the DEPT NMR spectrum is due to the three methyl carbons (C-17, C-18 and C-19). The three methyl carbons are in a magnetically equivalent environment and so resonate into a singlet. The second CH_3 group relatively downfield at 56 ppm is the carbon of the methoxy group that is deshielded due to the electron withdrawing oxygen group. The DEPT NMR spectrum shows a carbon peak at around 92 ppm as a result of the resonating carbon at the C-8 position in the enol form of avobenzone. The eight aromatic CH carbons fall in four magnetically equivalent groups and as a result appear only as four peaks at 114 ppm, 126 ppm, 127 ppm and 130 ppm in the DEPT NMR spectrum. The four aromatic equivalent groups are C-12 and C-14, C-11 and C-15, C-6 and C-2 and C-5 and C-3. The DEPT NMR spectrum verifies that avobenzone exists in the enol form in DMSO due to the peak at 92 ppm and the absence of any CH_2 peak.
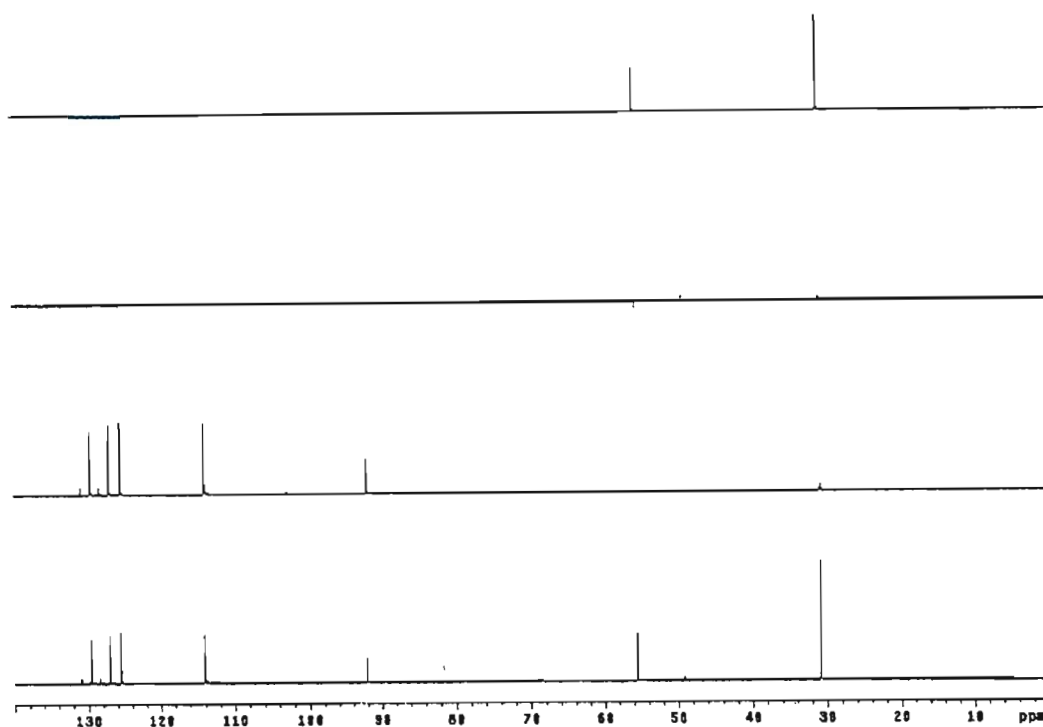
Figure 3.67:   DEPT NMR spectrum of 1×10^{-2} M avobenzone in deuterated DMSO obtained with the 400 MHz Varian Unity Inova NMR spectrometer.

Determination of the equilibrium constant for the tautomerism of avobenzone before irradiation

Since avobenzone exhibits keto-enol tautomerism, the relative amounts of the isomers were quantified in solution. ^{1}H NMR spectra of avobenzone solutions in deuterated DMSO and cyclohexane were obtained as described in Section 2.8.2. The relative amounts of the vinylic and methylene protons were obtained from the integrated areas of the respective peaks in the proton NMR spectrum. The relative abundances of the two isomers in each solvent were determined by calculating the equilibrium constant (K_e) through Equation 3.7 (Grushow [2002]).

$$K_e = \frac{\% \text{ enol - form}}{\% \text{ keto - form}}$$

(Equation 3.7)

Since the ratio of the methylene protons to the vinylic proton is 2:1, the integrated area for the keto form was divided by two as it is due to two protons. The ^{1}H NMR spectra were obtained with the 400 MHz NMR instrument (see Section 2.8).

Table 3.17 shows a decrease in equilibrium constant with an increase in permittivity of the solvent, indicating that the relatively polar keto form is stabilized by the relatively polar deuterated DMSO solvent. On the other hand, the relatively non-polar enol form was stabilized by the non-polar deuterated cyclohexane solvent.

Table 3.17: Integrated areas of methylene and vinylic protons of avobenzone keto and enol form in deuterated cyclohexane and deuterated DMSO together with the calculated values of the equilibrium constant between the tautomers and the permittivity (Grushow [2002]) of the solvents.

Solvent	Relative Integrated Area		K_e	Permittivity
	Methylene proton	Vinyl proton		
C_6D_6	0.22	5.1	46	2.28
DMSO-d_6	0.89	4.7	10	47.24

^{1}H NMR spectrum and DEPT NMR spectrum of irradiated avobenzone in deuterated cyclohexane

Avobenzone was irradiated in deuterated cyclohexane for 25 hours as described in Section 2.8.2. The proton NMR spectrum obtained after irradiation is displayed in Figure 3.68. The proton NMR spectrum shows more peaks than the equivalent spectrum for unirradiated avobenzone. This indicates that avobenzone has been modified during irradiation from the predominantly enol form characterized from Figure 3.64. The single peak due to the nine methyl protons has divided to form three singlet peaks all between 1.0 ppm and 1.4 ppm. The methoxy peak has also broken up to form three major singlet peaks and the same applies to the doublets due to the aromatic protons. This suggests the existence of three major photoproducts of avobenzone potentially arising from photodegradation as was observed with GC-MS and HPLC investigations (see Sections 3.3.1.3 and 3.3.1.4 respectively). The methylene proton peak intensity due to the keto form of avobenzone showed a slight increase. The vinylic proton peak was engulfed by other peaks making it impossible to relate the two forms of avobenzone.
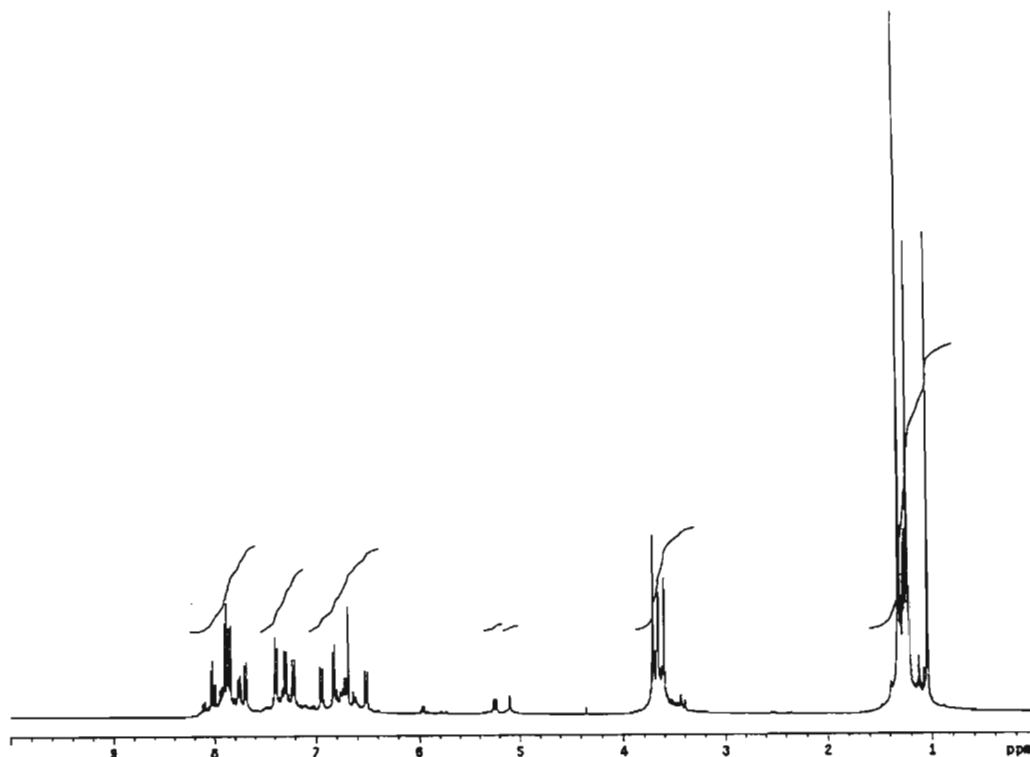
Figure 3.68: ^{1}H NMR spectrum of a UV-irradiated solution of 1×10^{-2} M avobenzone in deuterated cyclohexane obtained with the 400 MHz Varian Unity Inova NMR spectrometer. The avobenzone solution was irradiated for 25 hours as described in Section 2.3.1.

The solution of 1×10^{-2} M avobenzone in deuterated cyclohexane was continuously monitored during irradiation with the 300 MHz Varian NMR spectrometer, so as to compare the methylene proton peak with that of the vinylic proton peak. The decrease or increase of these peaks upon irradiation would directly correspond to the photostability of their respective isomers. The change with irradiation of these peaks was determined by manually measuring their integrated areas. The integrated area for each peak was measured at a constant vertical and integral scale so that they could be compared. The integrated areas were measured twice, as shown in Table 3.18. These integrated areas of the methylene protons and vinylic proton peak were plotted against irradiation time in Figure 3.69. After the first 3 hours of irradiation, the integrated areas for both peaks were halved, suggesting that both isomers were consumed during irradiation. Subsequent irradiations decreased the integrated area of the vinylic proton peak whereas that of the methylene protons remained constant. The vinylic proton peak was reduced from an integrated area of 7.0 to 3.1 after 12 hours of irradiation. After 25 hours of irradiation multiple peaks were observed in the NMR spectrum, masking the vinylic proton peak and as a result its integrated area could not be determined. However, after irradiation for 25 hours, the methylene

proton peak increased in integrated area by about eight times that observed at 12 hours irradiation. Therefore photoisomerisation of the enol form produces the keto form which possibly gets consumed through photodegradation, hence why an increase in the keto form was only observed after it accumulated from long hours of continuous irradiation.

Table 3.18:   Variation with increasing UV-irradiation time of the integrated areas monitored for the methylene and vinylic proton peaks by means of the 300 MHz Varian Gemini NMR spectrometer.

Irradiation time/hours	Integrated Area							
	CH peak				CH_2 peak			
	Trial 1	Trial 2	Average	STD*	Trial 1	Trial 2	Average	STD*
0	6.9	7.1	7.0	0.1	0.2	0.2	0.2	0
3	3.6	3.8	3.7	0.1	0.1	0.1	0.1	0
6	4.4	-	4.4	-	0.1	-	0.1	-
9	3.9	3.7	3.8	0.1	0.1	0.1	0.1	0
12	3.1	-	3.1	-	0.1	-	0.1	-
25	-	-	-	-	0.8	0.8	0.8	0

*   Standard deviation
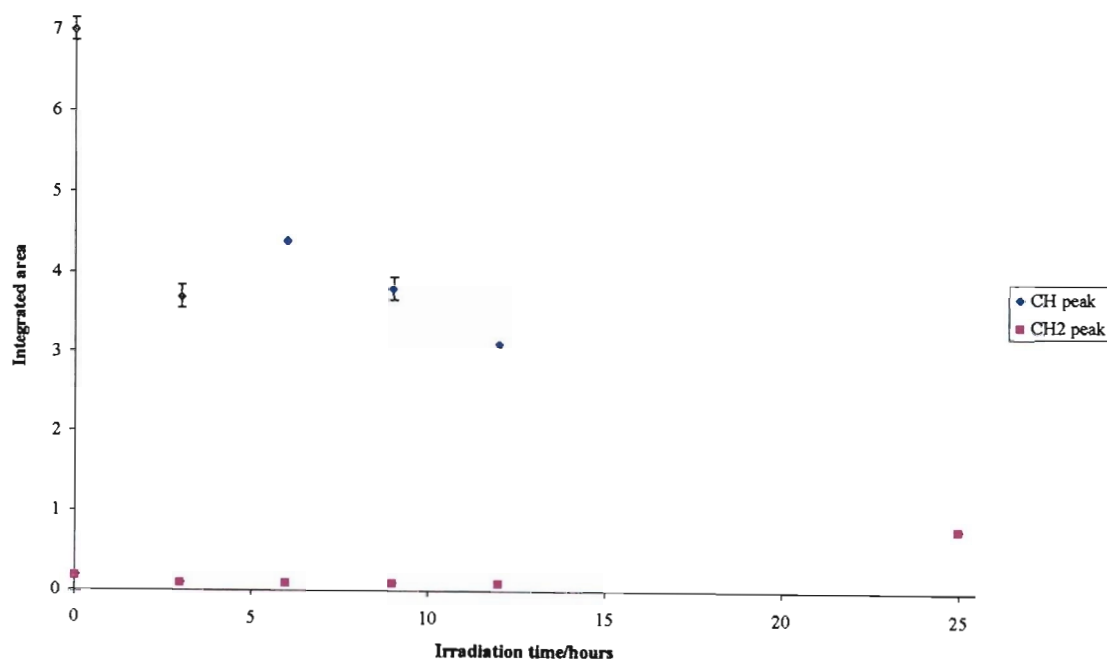
Figure 3 69:   The integrated areas of the methylene and vinylic proton peaks of a 1×10^{-2} M avobenzone solution in deuterated cyclohexane recorded by the 300 MHz Varian Gemini NMR spectrometer for increasing periods of UV-irradiation.

The DEPT NMR spectrum of irradiated avobenzone in deuterated cyclohexane (see Figure 3.70) shows five methyl peaks; three due to the nine methyl protons from the *tert*-butyl group and two from the methoxy methyl group. The spectrum shows seventeen CH groups inclusive of the vinylic proton of the enol form of avobenzone. Only the vinylic proton peak remained intact in the irradiated DEPT spectrum, all the other aromatic CH protons have been split up to almost triple the number they were initially. The ^{1}H NMR and the DEPT spectra show a possible break at the C-8 carbon of avobenzone, hence the reason there is lack of multiple carbon-8 peaks whereas the other peaks re-occur. There must be two major photoproducts in solution that have arisen through a break at the C-8 position, making three major compounds in solution (including avobenzone). The presence of three compounds justifies the existence of three sets of each peak.
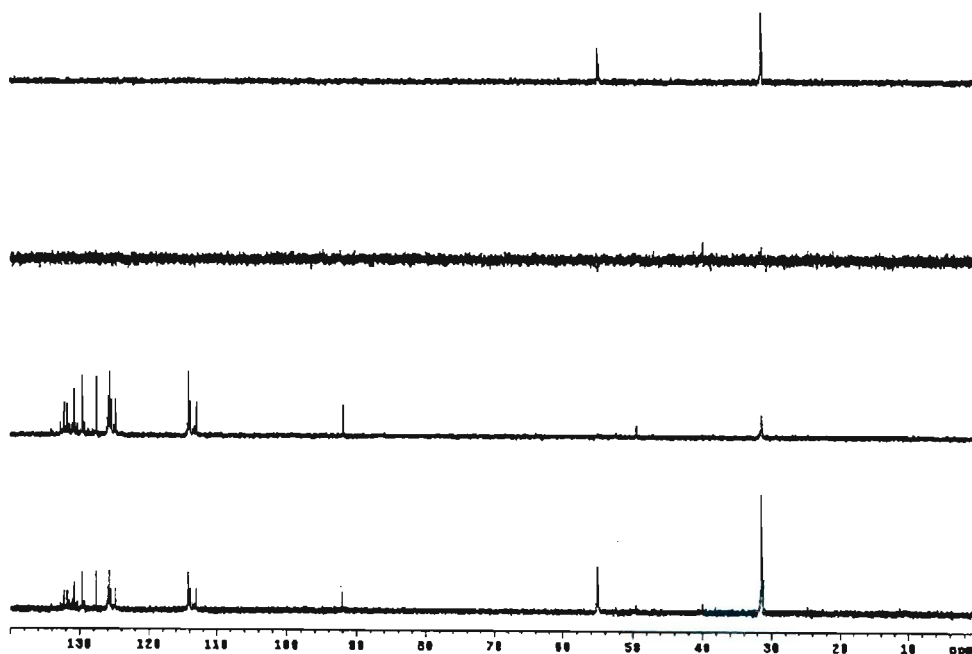
Figure 3.70:   DEPT NMR spectrum of UV-irradiated 1×10^{-2} M avobenzone in deuterated cyclohexane obtained with the 400 MHz Varian Unity Inova NMR spectrometer. The avobenzone solution was irradiated for 25 hours as described in Section 2.3.1.

¹H NMR spectrum and DEPT NMR spectrum of irradiated avobenzone in deuterated DMSO

The proton NMR spectrum (shown in Figure 3.71) of avobenzone dissolved in DMSO after 21 hours of irradiation shows only one major difference from that of unirradiated avobenzone and that is the increase in the methylene proton peak at 4.75 ppm. This suggests irradiation solely results in photoisomerisation of the enol form to the keto form. Since it was not possible to determine whether after 21 hours, there was equilibrium between the two forms, the constant calculated from the integrated areas of the methylene and vinylic peaks will be arbitrarily named as K_{21}. K_{21} was calculated in the same way as K_e given by Equation 3.7, and it has the value of 4.1. If this value is compared to the value of 10 obtained before irradiation, one observes that the constant has decreased by more than half thereby indicating a significant amount of keto form is created upon irradiation. The DEPT NMR spectrum (Figure 3.72) does not show any detectable difference in the avobenzone structure.
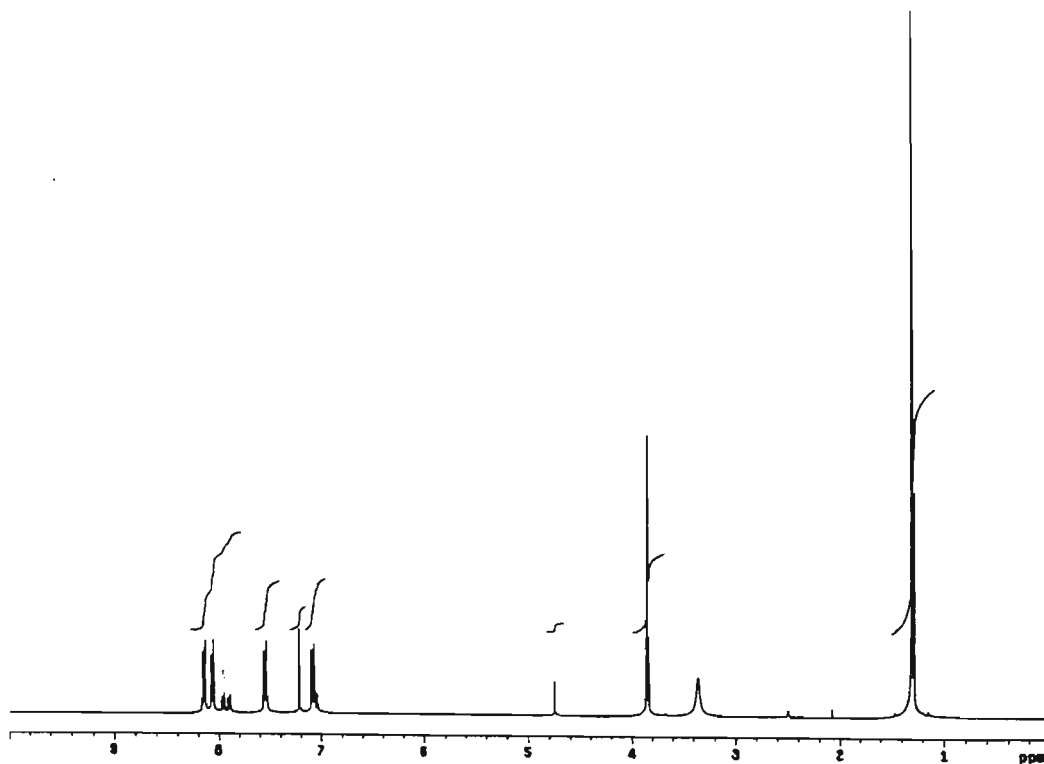
Figure 3.71:   ¹H NMR spectrum of UV-irradiated 1×10^{-2} M avobenzone in deuterated DMSO obtained with the 400 MHz Varian Unity Inova NMR spectrometer. The avobenzone solution was irradiated for 21 hours as described in Section 2.3.1.
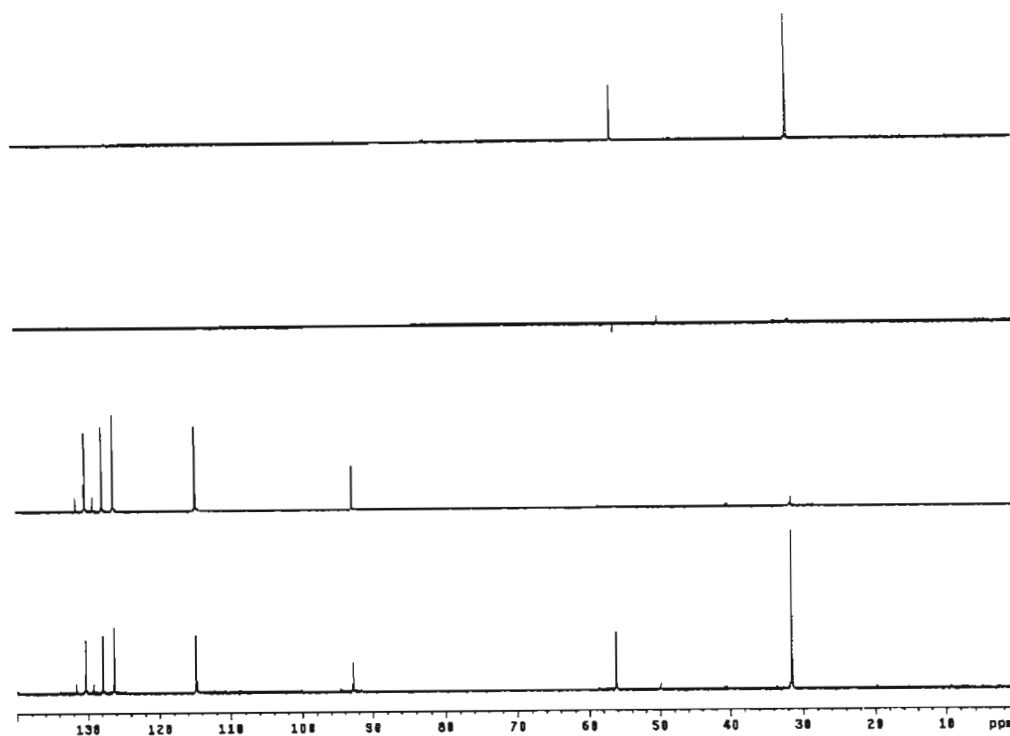
Figure 3.72:   DEPT NMR spectrum of UV-irradiated 1×10^{-2} M avobenzone in deuterated DMSO obtained with the 400 MHz Varian Unity Inova NMR spectrometer. The avobenzone solution was irradiated for 21 hours as described in Section 2.3.1.

3.3.2 Photostablising avobenzone with the Cancer Bush extract

Photostabilisation experiments were conducted by preparing appropriate concentrations of avobenzone in those solvents where instability was observed. In these solvents, avobenzone was irradiated in the presence and in the absence of a suitable Cancer Bush extract, and its photostability at the wavelength of maximum absorption compared. The boiling water and ethanol-water Cancer Bush extracts were used for these analyses. Avobenzone concentrations were prepared of the order of 10^{-5} M and the Cancer Bush extract was made up so as to achieve absorbances within a measurable range on the UV/VIS spectrophotometer. These experiments were investigated with the Perkin Elmer Lambda 35 UV/VIS spectrophotometer, and avobenzone solutions in ethyl acetate were further investigated by HPLC/PDA.

3.3.2.1 Photostabilisation shown by UV spectroscopy

The following avobenzone solutions were prepared: 1.5×10^{-5} M in DMSO, 1.8×10^{-5} M in ethyl acetate and 2.0×10^{-5} M in cyclohexane, through serial dilution from stock solutions of the order of 10^{-3} M. The photostability of avobenzone in these solvents was investigated by irradiating the solutions at appropriate irradiation intervals (see Section 3.3.1.1). The extract was then diluted to absorb in a similar absorbance range as avobenzone, and the photostability of the extract was investigated at the same irradiation intervals as for avobenzone (Section 3.1.4.1 discusses the photostability of the Cancer Bush extracts). The same concentrations of avobenzone and the extract were re-prepared in each solvent together, and the resulting mixtures re-irradiated at the same irradiation intervals.

From Figures 3.73, 3.74 and 3.75, one observes that avobenzone was photostabilised by the boiling water Cancer Bush extract in DMSO, and by the ethanol-water Cancer Bush extract in ethyl acetate but not in cyclohexane.

DMSO

Figure 3.73B shows the change in the UV spectrum arising as a result of irradiating avobenzone in DMSO. What can be observed is that avobenzone loses absorbance at 363 nm and gains it at 280 nm upon irradiation. The photostability of the extract with avobenzone in DMSO was also investigated, and the UV spectra recorded after each 10-minute irradiation interval are displayed in Figure 3.73C. The loss in absorbance at 363 nm of the mixture occurs to a lesser extent than the sum of the extract (see Figure 3.73A) and avobenzone separately. The loss in absorbance at 363 nm was from 0.46 to 0.10 after 10 minutes of irradiation when avobenzone was in solution alone. When avobenzone was mixed with the extract, the absorbance loss observed was only from 0.74 to 0.66 after 10 minutes of irradiation. The loss in absorbance of the mixture throughout the UV spectrum was similar to that of the extract alone. The increase in absorbance at 280 nm as well as the isosbestic point at 295 nm observed in the avobenzone spectra, were absent in the spectra of the mixture. This appears to indicate that the extract prevents the photoisomerisation of avobenzone and that any loss in absorbance is predominantly due to degradation of the Cancer Bush extract.
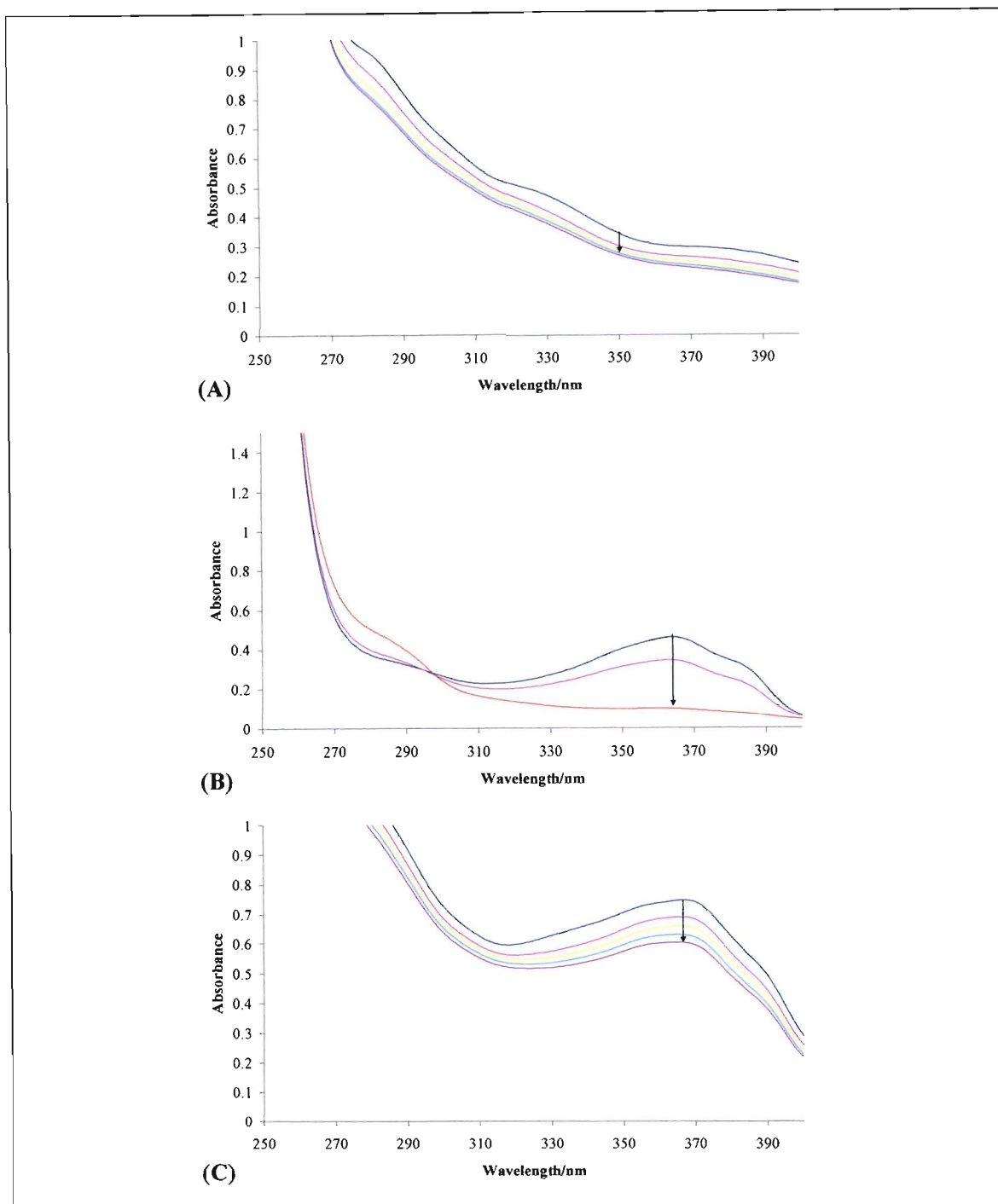
Figure 3.73: UV spectra of the boiling water Cancer Bush extract (A), 1.5×10^{-5} M avobenzone (B) and a mixture of the two (C) in DMSO. Each solution was irradiated at 10 minute intervals in a 1 cm pathlength quartz cuvette and all spectra were obtained with the Perkin Elmer Lambda 35 UV/VIS spectrophotometer.

Ethyl acetate

In ethyl acetate, the extract was found to be photostable at short wavelengths up to 290 nm and photo-unstable thereafter at longer wavelengths (see Figure 3.74A). On the other hand, avobenzone lost absorbance at 356 nm and gained it at 269 nm during irradiations (see Figure 3.74B) largely due to photoisomerisation, but some photodegradation also occurred. When the extract was mixed with avobenzone, the irradiated mixture showed a smaller loss in absorption at 356 nm (see Figure 3.74C). This loss was more than that observed for the extract alone, but much less than that of avobenzone alone. This signified that avobenzone did lose absorbance at 356 nm, but was photostabilised to some extent by the extract. The loss in absorbance of the mixture at 400 nm was most likely due to the photo-instability of the extract in this region, since avobenzone is relatively photostable at these wavelengths and absorbs minimally. The isosbestic point at 292 nm accompanied by an increase in absorption at 269 nm is due to avobenzone solely, since the extract is stable in this region. This again indicates that at least two compounds are present in equilibrium.

Cyclohexane

The photo-instability of avobenzone in cyclohexane was seen by the loss in absorbance at 351 nm accompanied by a slight increase in absorbance at 263 nm (see Figure 3.75B). Similarly, the ethanol-water Cancer Bush extract showed great photo-instability in cyclohexane (see Figure 3.75A). The loss in absorbance of the extract was about 0.4 at 400 nm after one and a half hours of irradiation, whereas there appears to be an increase in absorption below 270 nm. The loss in absorbance of the extract was also significant in the mixture with avobenzone (see Figure 3.75C). The loss in absorbance of the mixture at 351 nm was from 1.75 to 1.25, more than the 0.2 loss observed with the extract alone. This suggested that avobenzone was also significantly losing absorbance here. The 0.3 loss in absorbance at 351 nm of avobenzone and the extract separately were approximately equal to the loss in absorbance of the mixture observed at 351 nm. The UV spectra of the irradiated mixture also showed a large increase in absorbance below 270 nm, since both avobenzone and the extract showed an increase at these wavelengths. An isosbestic point occurred at 285 nm for all the UV spectra excluding the one obtained before irradiation of the mixture in cyclohexane. Avobenzone was therefore not photostabilised by the ethanol-water Cancer Bush extract in cyclohexane.
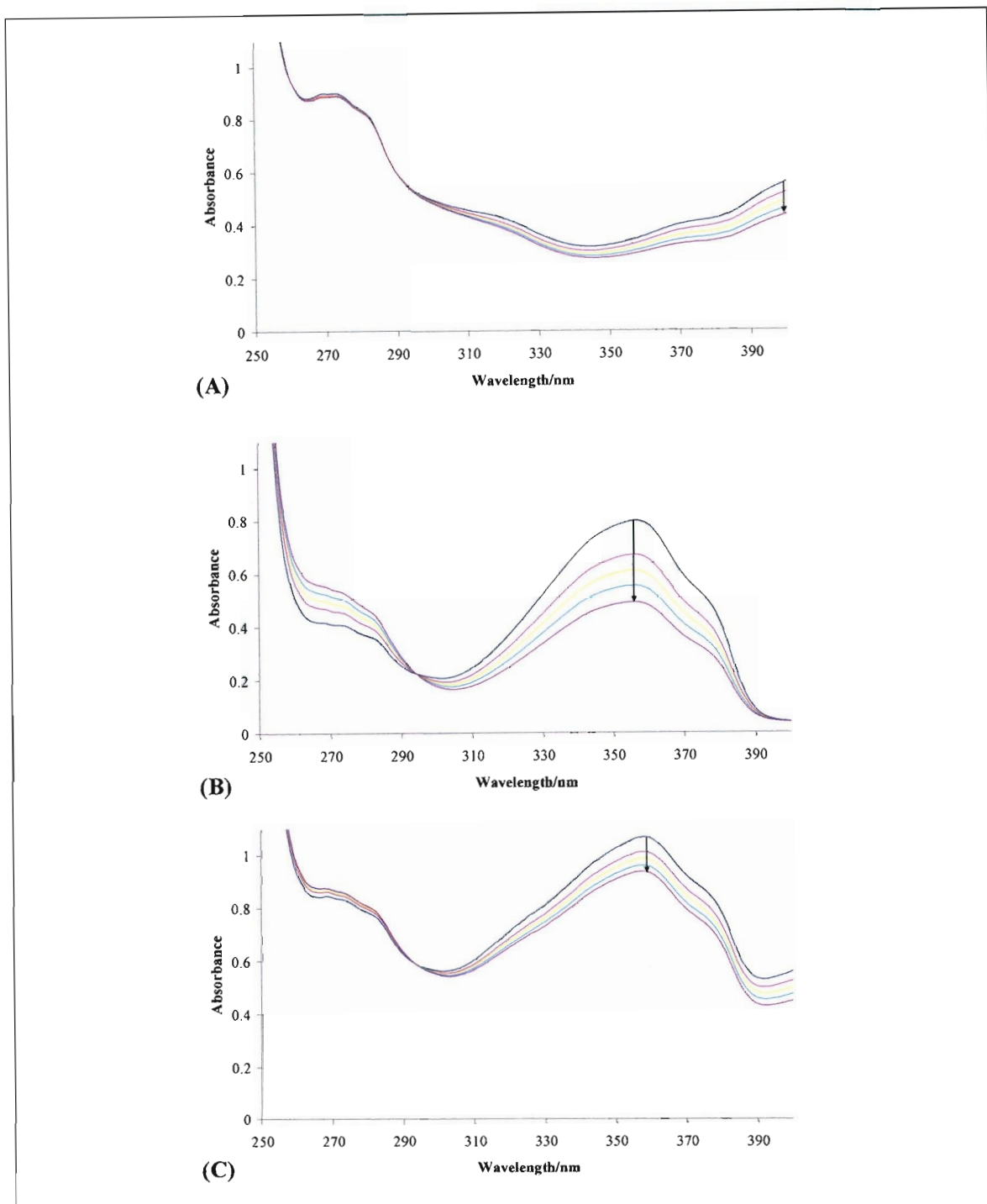
Figure 3.74: UV spectra of the ethanol-water Cancer Bush extract (A), 1.8×10^{-5} M avobenzone (B) and a mixture of the two (C) in ethyl acetate. Each solution was irradiated at one minute intervals in a 1 cm pathlength quartz cuvette and all spectra were obtained with the Perkin Elmer Lambda 35 UV/VIS spectrophotometer.
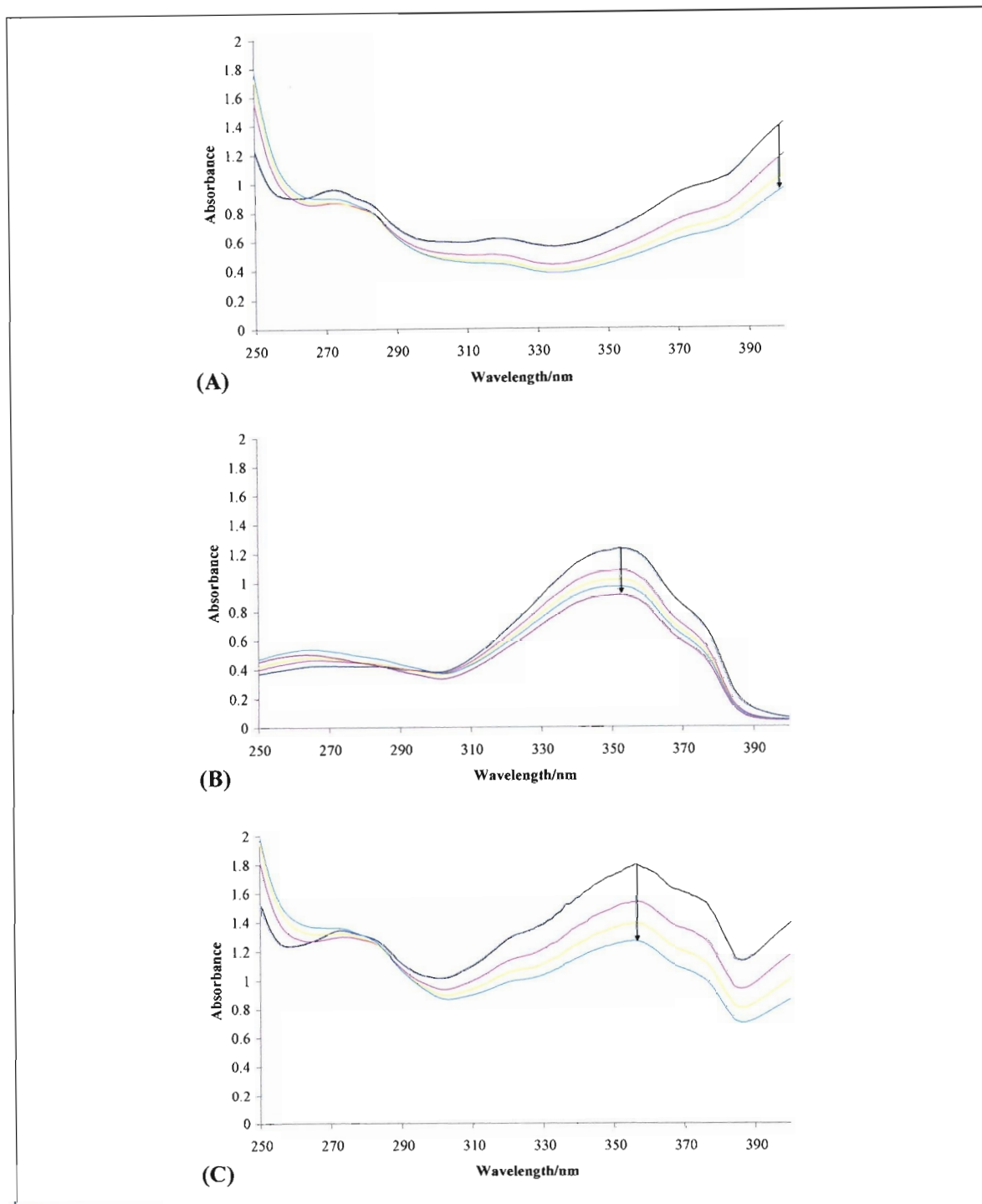
Figure 3.75:   UV spectra of the ethanol-water Cancer Bush extract (A), 2.0×10^{-5} M
                avobenzone (B) and a mixture of the two (C) in cyclohexane. Each solution
                was irradiated at 30 minute intervals in a 1 cm pathlength quartz cuvette and all
                spectra were obtained with the Perkin Elmer Lambda 35 UV/VIS
                spectrophotometer.

3.3.2.2 Photostabilisation shown by HPLC/PDA

The photostabilisation of avobenzone in ethyl acetate was further investigated by HPLC/PDA. Blank runs of ethyl acetate produced clear chromatograms through the Nucleosil 100 C18 column when eluted with a mobile phase composition of 85:15% (v/v) methanol:Millipore water, hence this allowed the photostability of avobenzone in ethyl acetate to be investigated. Low concentrations of the extract and avobenzone were used during these photostabilisation investigations, since these required only short irradiation times for the photostabilisation effect to be observed. Short irradiation times were used to prevent the complete photodegradation of the extract yet allow sufficient photodegradation of avobenzone for analysis with the extract.

These photostabilisation experiments were only conducted in ethyl acetate since the other solvents compromised the accuracy of the results (see Section 3.1.4.2) due to the sample preparation procedures required (see Section 3.3.1.4). These errors would have been greatly enhanced with the small avobenzone concentration, extract amount and irradiation times.

Avobenzone of a concentration of 1×10^{-3} M in ethyl acetate solution before irradiation (see Figure 3.76) elutes at 19 minutes, and has a peak height of 0.15 units. This avobenzone solution was then irradiated in a 1 mm pathlength quartz cuvette with light of wavelengths greater than 300 nm. After a 1 hour irradiation period, the peak height had reduced by 34% to 0.10 units (Figure 3.77). Figures 3.78 and 3.79 show avobenzone mixed with the ethanol-water Cancer Bush extract (about 100 mg in 2 ml ethyl acetate) before and after a 1 hour irradiation period, respectively. Under the elution conditions used the extract did not separate into its components. Avobenzone was photostabilised by the extract since its peak height remained at 0.15/0.16 units before and after irradiation. The extract was also relatively photostable since its peak height remained at about 0.15 units and the peak area reduced by only 8% after irradiation.
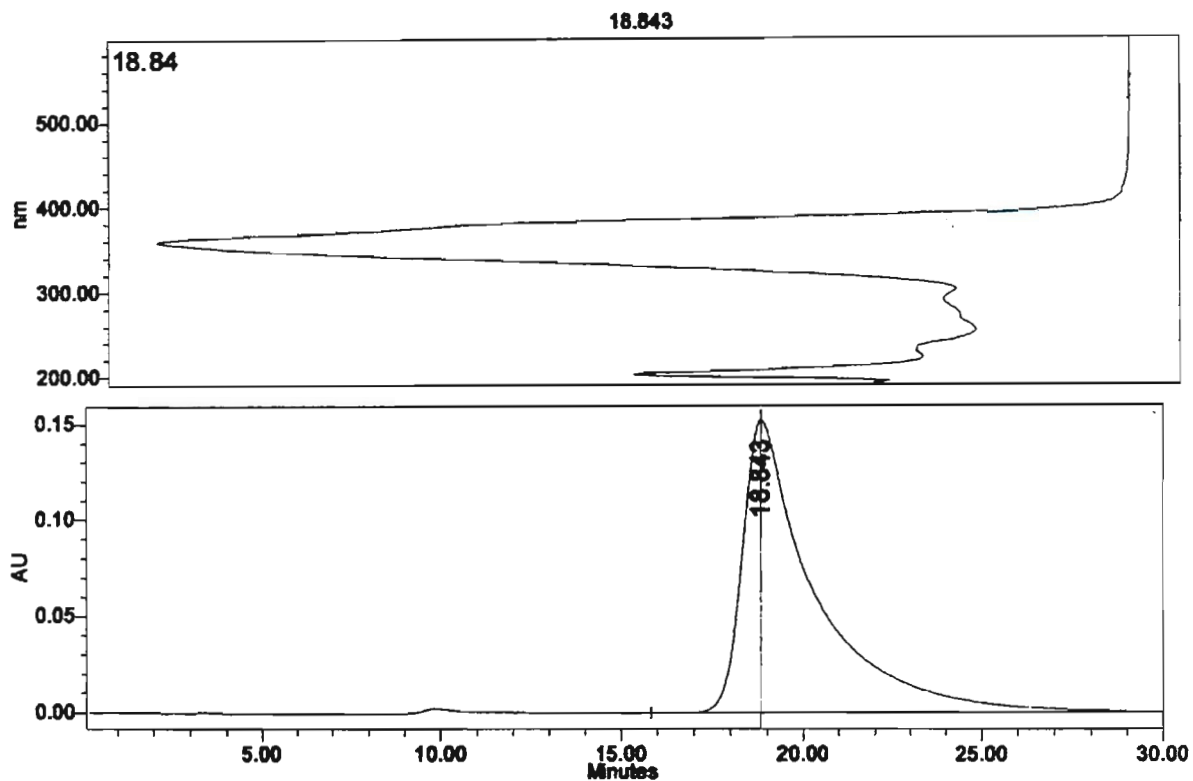
Figure 3.76:   HPLC chromatogram of a 1×10^{-3} M avobenzone solution in ethyl acetate injected through the Nucleosil 100 C18 column with a mobile phase composition of 85:15% (v/v) methanol:Millipore water. Avobenzone eluted at 19 minutes with a peak height of 0.15 units (before irradiation) at a flow rate of 1 ml min^{-1} with a detection wavelength of 350 nm.
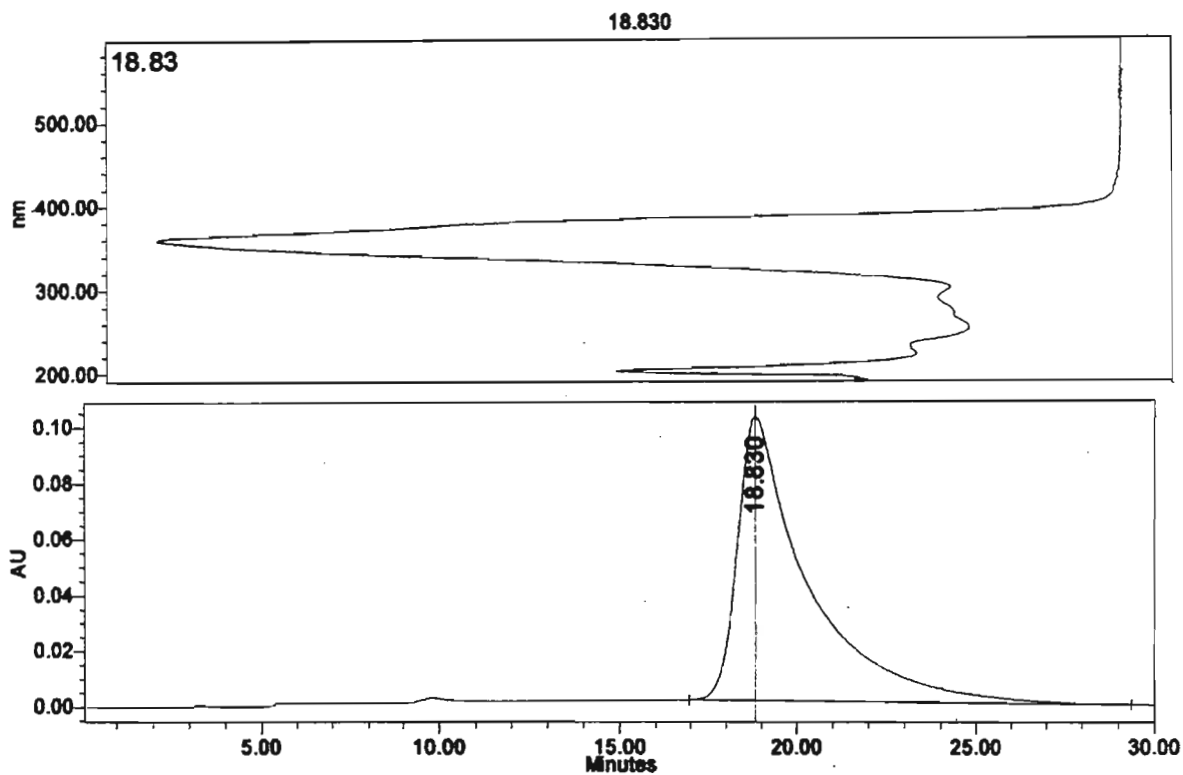
Figure 3.77: HPLC chromatogram of a 1×10^{-3} M avobenzone solution in ethyl acetate injected through the Nucleosil 100 C18 column with a mobile phase composition of 85:15% (v/v) methanol:Millipore water. Avobenzone eluted at 19 minutes with a peak height of 0.10 units, after a 1 hour irradiation interval, at a flow rate of 1 ml min^{-1} and a detection wavelength of 350 nm.
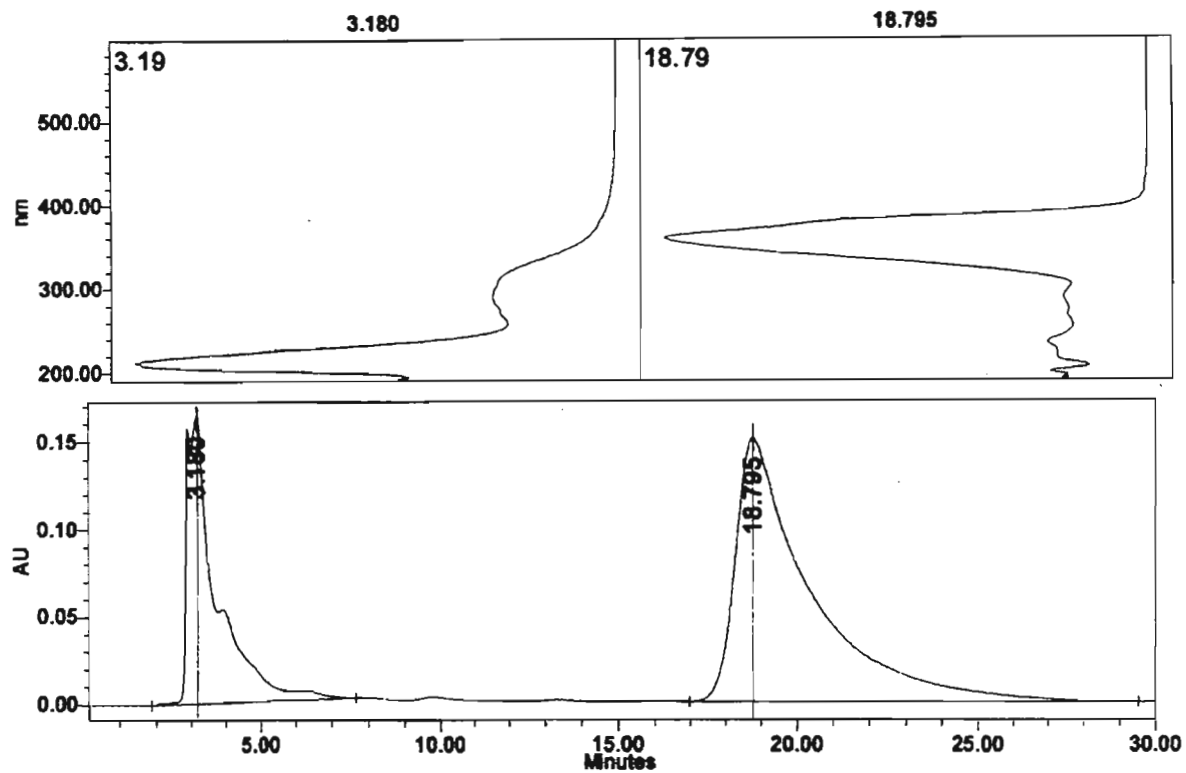
Figure 3.78: HPLC chromatogram of 1×10^{-3} M avobenzone with the ethanol-water Cancer Bush extract injected through the Nucleosil 100 C18 column with a mobile phase composition of 85:15% (v/v) methanol:Millipore water. Avobenzone eluted at 19 minutes with a peak height of 0.15 units and the ethanol-water Cancer Bush extract eluted at 3 minutes with a peak height of 0.16 units (before irradiation) at a flow rate of 1 ml min^{-1} and a detection wavelength of 350 nm.
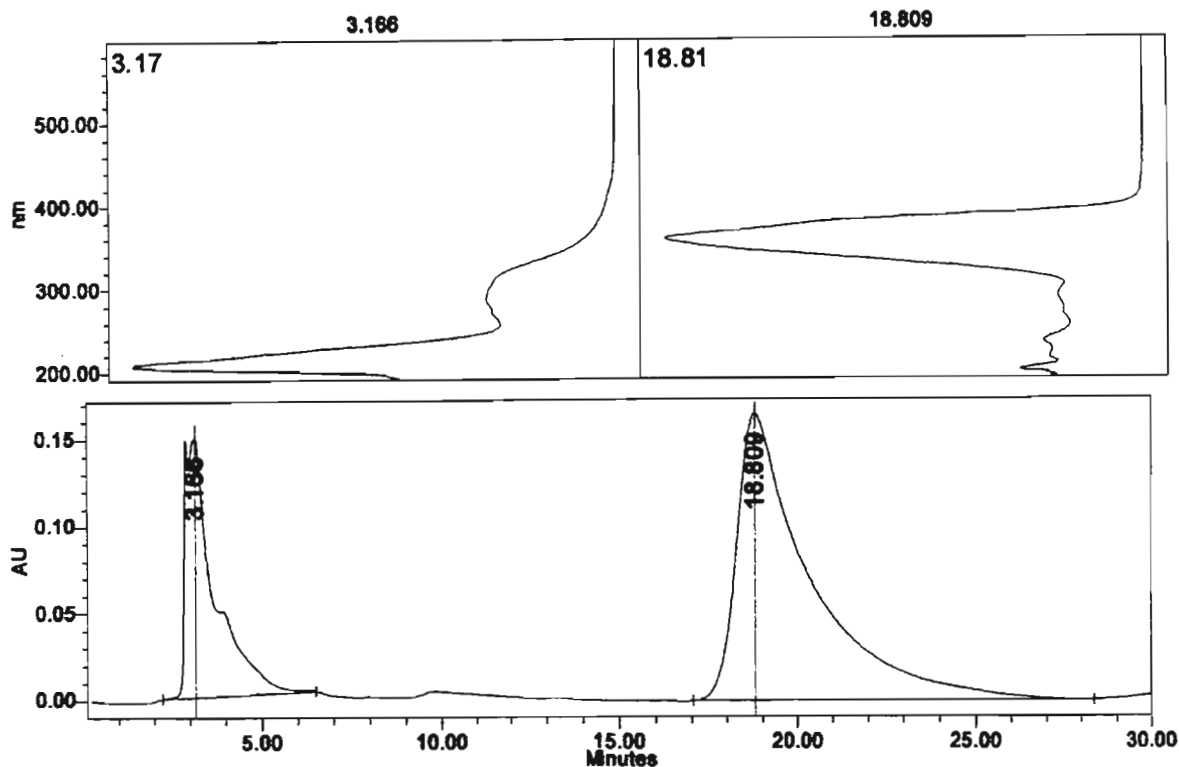
Figure 3.79:   HPLC chromatogram of 1×10^{-3} M avobenzone with the ethanol-water Cancer
                Bush extract injected through the Nucleosil 100 C18 column with a mobile
                phase composition of 85:15% (v/v) methanol:Millipore water.   Avobenzone
                eluted at 19 minutes with a peak height of 0.16 units and the extract eluted at 3
                minutes with a peak height of 0.15 units, after a 1 hour irradiation interval, at a
                flow rate of 1 ml min^{-1} and a detection wavelength of 350 nm.

3.3.3 Photostabilising avobenzone with known polyphenols

Since it was shown that avobenzone could be photostabilised by the boiling water and ethanol-
water Cancer Bush extracts, it was necessary to investigate the photostabilisation with known
polyphenolic compounds in order to ascertain whether the polyphenols are the candidates that
exert the photostabilising effect of the Cancer Bush extract.   Hence, a known polyphenolic
source namely: various types of Rooibos tea (Rooibos-honeybush, Rooibos-black and plain
Rooibos tea), as well as the specific polyphenols, rutin and epicatechin, were investigated with
avobenzone.

Rooibos tea

Rooibos tea is known to contain polyphenolic substances (Erickson [2003]) which could act as
potential photostabilisers. Various Rooibos teas were extracted and the extracts combined with

avobenzone in order to compare their photostabilising abilities. Polyphenols were extracted from the various Rooibos teas by the ethanol-water extraction method, and the extracts were investigated with avobenzone dissolved in ethyl acetate.

The solid extracts extracted from the various Rooibos teas were dissolved in ethyl acetate, and diluted appropriately for UV spectroscopy analysis. Figures 3.80A and 3.81A display the UV spectra of plain Rooibos-tea and Rooibos-honeybush tea when irradiated at one minute intervals in ethyl acetate. These tea extracts have similar UV absorption spectra; there are three main absorption bands at 273 nm, 280 nm and at 320 nm (Rooibos-honeybush tea) or 328 nm (Rooibos-tea). The Rooibos-black tea extract on the other hand has a single absorption peak at 273 nm (see Figure 3.82A) without any major absorption bands at longer wavelengths. All the tea extracts were relatively photostable when irradiated with UV light of wavelengths greater than 300 nm at 1 minute irradiation intervals, and showed a loss in absorption of less than 0.1 throughout the UV spectrum.

Figures 3.80B, 3.81B and 3.82B show the photo-instability of avobenzone in ethyl acetate as discussed in Section 3.3.1.1. Figures 3.80C, 3.81C and 3.82C show the photostabilisation of avobenzone by plain Rooibos tea, Rooibos-honeybush tea and Rooibos-black tea, respectively. Photostabilisation was evident since the loss in absorption at the λ_{max} of avobenzone (356 nm) in the mixture was of a smaller magnitude than that observed for avobenzone alone. Plain Rooibos tea, as well as Rooibos-honeybush tea, showed a significant photostabilisation effect at 356 nm relative to the very minimal effect observed with Rooibos-black tea. The gain in absorbance at 269 nm observed in the UV spectra of irradiated avobenzone solutions was greatly minimised in all these avobenzone-extract mixtures, including Rooibos-black tea. But all the teas did manage to photostabilise avobenzone.

Rutin

The flavonoid, rutin, was possibly present in the ethanol-water Cancer Bush extract and is known to be present in Rooibos tea (Erickson [2003]). An investigation of the photostability of avobenzone in the presence of rutin was imperative in order to understand how avobenzone was photostabilised by the extracts.
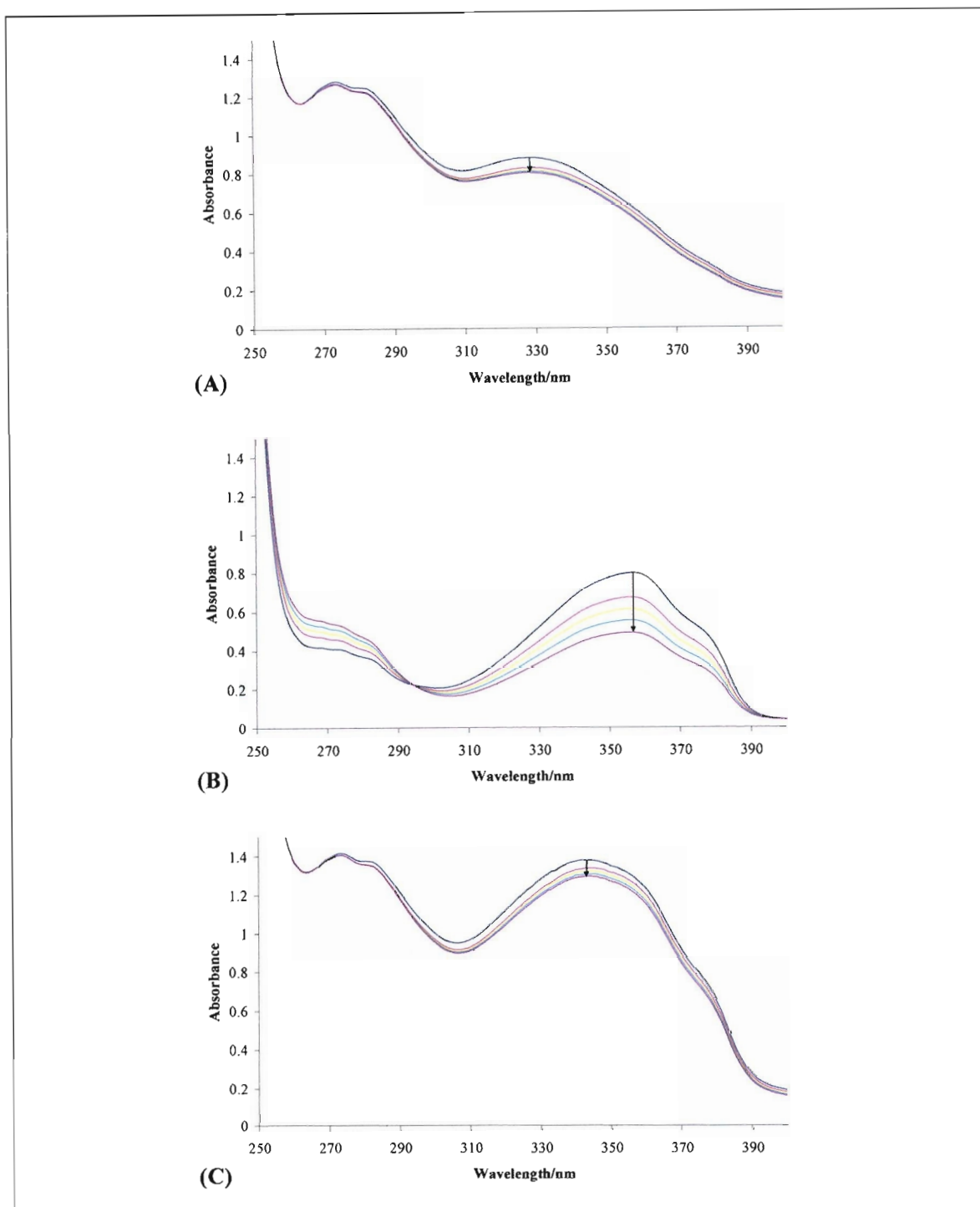
Figure 3.80:   UV spectra of the ethanol-water Rooibos tea extract (A), 1.8×10^{-5} M
                avobenzone (B) and a mixture of the two (C) in ethyl acetate. Each solution
                was irradiated at one minute intervals in a 1 cm pathlength quartz cuvette and
                all spectra were obtained with the Perkin Elmer Lambda 35 UV/VIS
                spectrophotometer.
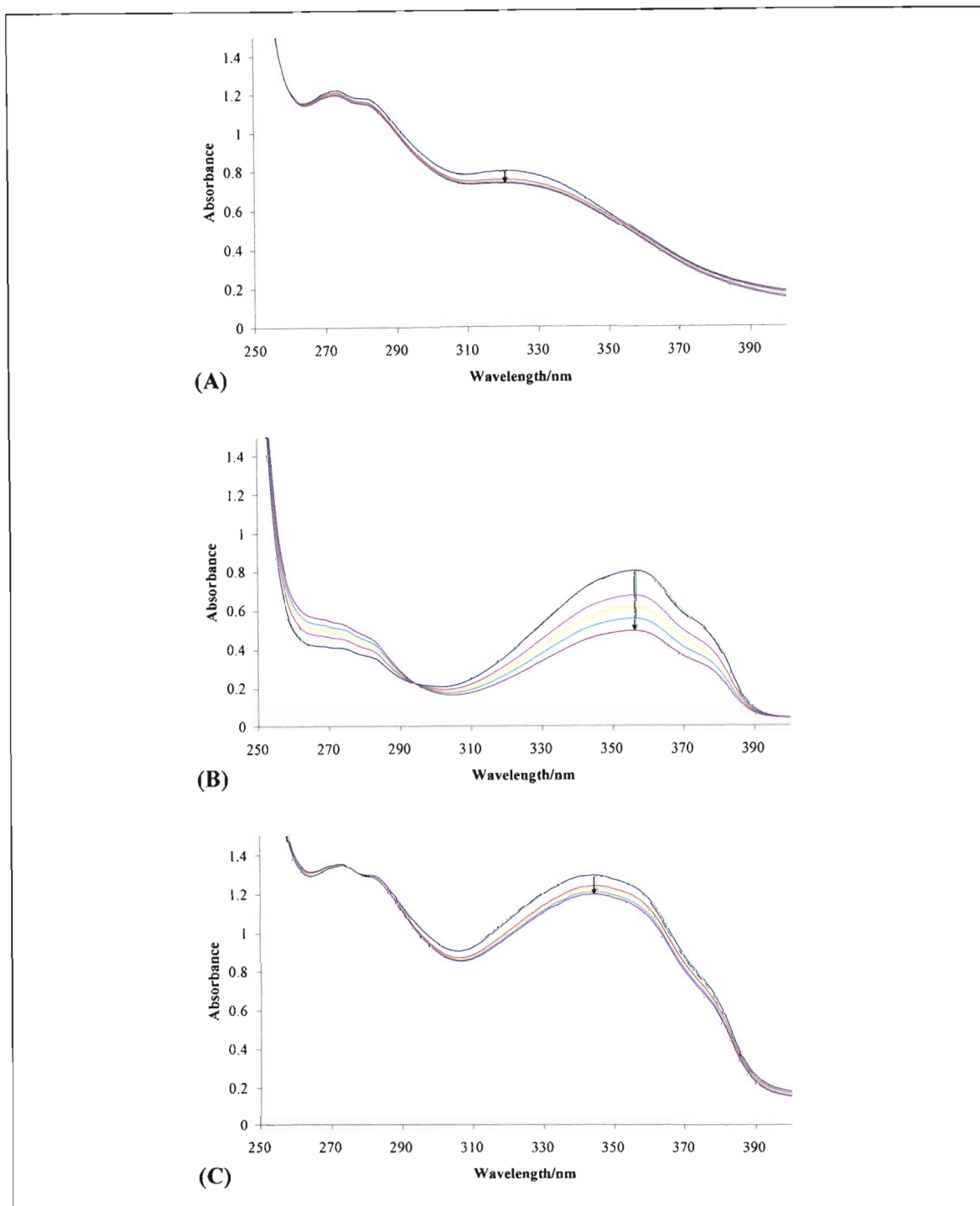
Figure 3.81:   UV spectra of the ethanol-water Rooibos-honeybush tea extract (A), 1.8×10^{-5} M avobenzone (B) and a mixture of the two (C) in ethyl acetate. Each solution was irradiated at one minute intervals in a 1 cm pathlength quartz cuvette and all spectra were obtained with the Perkin Elmer Lambda 35 UV/VIS spectrophotometer.

(A)

(B)

(C)
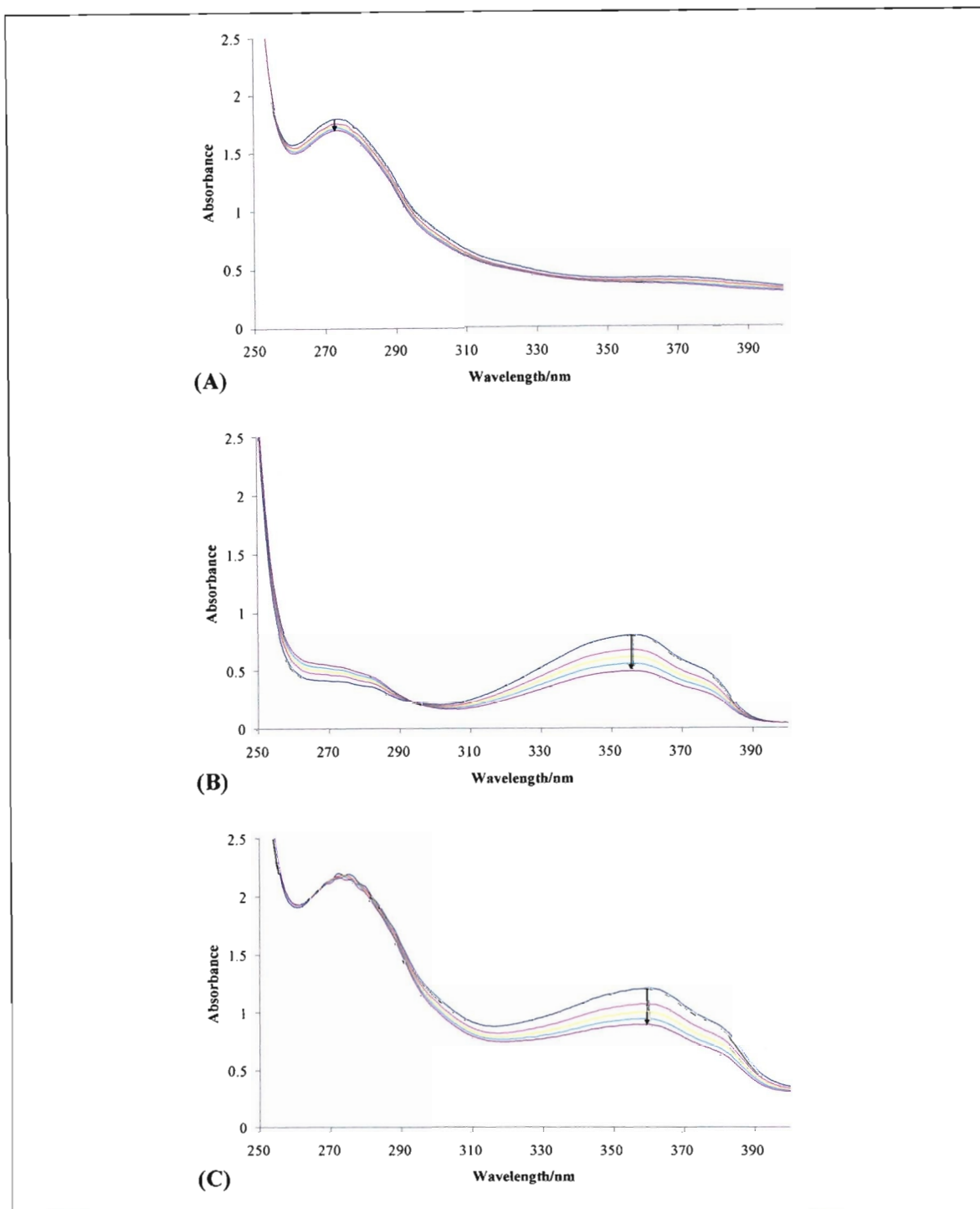
Figure 3.82:   UV spectra of the ethanol-water Rooibos-black tea extract (A), 1.8×10^{-5} M avobenzone (B) and a mixture of the two (C) in ethyl acetate. Each solution was irradiated at one minute intervals in a 1 cm pathlength quartz cuvette and all spectra were obtained with the Perkin Elmer Lambda 35 UV/VIS spectrophotometer.

Rutin was photostable when irradiated with UV light of wavelengths greater than 300 nm in DMSO (as shown in Figure 3.83A). When rutin was mixed with avobenzone, photostabilisation of avobenzone was observed at 363 nm (λ_{max} of avobenzone in DMSO). The loss in absorbance of avobenzone at 363 nm in the mixture with rutin was 0.2 (see Figure 3.83C), compared with an absorbance loss of 0.6 when avobenzone was irradiated alone in DMSO (see Figure 3.83B).

Epicatechin

Rutin could arguably photostabilise avobenzone through competitive absorption of photons at wavelengths greater than 300 nm. In order to verify whether this was the mechanism of avobenzone photostabilisation by the Cancer Bush extracts, a polyphenolic compound, epicatechin, with a λ_{max} of 281 nm, was used to photostabilise avobenzone.

Epicatechin was stable when irradiated in DMSO as shown in Figure 3.84A. The UV spectra of the irradiated mixture of avobenzone with epicatechin showed only a 0.1 loss in absorbance at 365 nm after 10 minutes of irradiation (see Figure 3.84C). On the other hand, solutions of avobenzone alone showed an absorbance loss of 0.6 after the same irradiation time (see Figure 3.84B). As epicatechin does not absorb in the same wavelength region as avobenzone in DMSO (i.e. it does not absorb at wavelengths greater than 320 nm), its ability to photostabilise avobenzone means that the photostabilisation mechanism is not through competitive absorption of photons.

3.3.4 Summary of Section 3.3

In this section, the photo-instability of avobenzone was investigated by UV spectroscopy, GC-MS, HPLC and NMR analysis. Avobenzone was found to photoisomerise in ethyl acetate as well as DMSO, whereas it photodegraded in cyclohexane and to a smaller extent in ethyl acetate. Avobenzone was found to be more photostable in all these solvents in the absence of oxygen, but photostabilised significantly only in DMSO. This indicates photoisomerisation could be oxygen-dependent whereas photodegradation is less dependent on the presence of oxygen. Avobenzone was photostabilised by the Cancer Bush extracts in DMSO and ethyl acetate, but not in cyclohexane. Avobenzone was also photostabilised by various Rooibos tea extracts as well as the polyphenols, rutin and epicatechin.
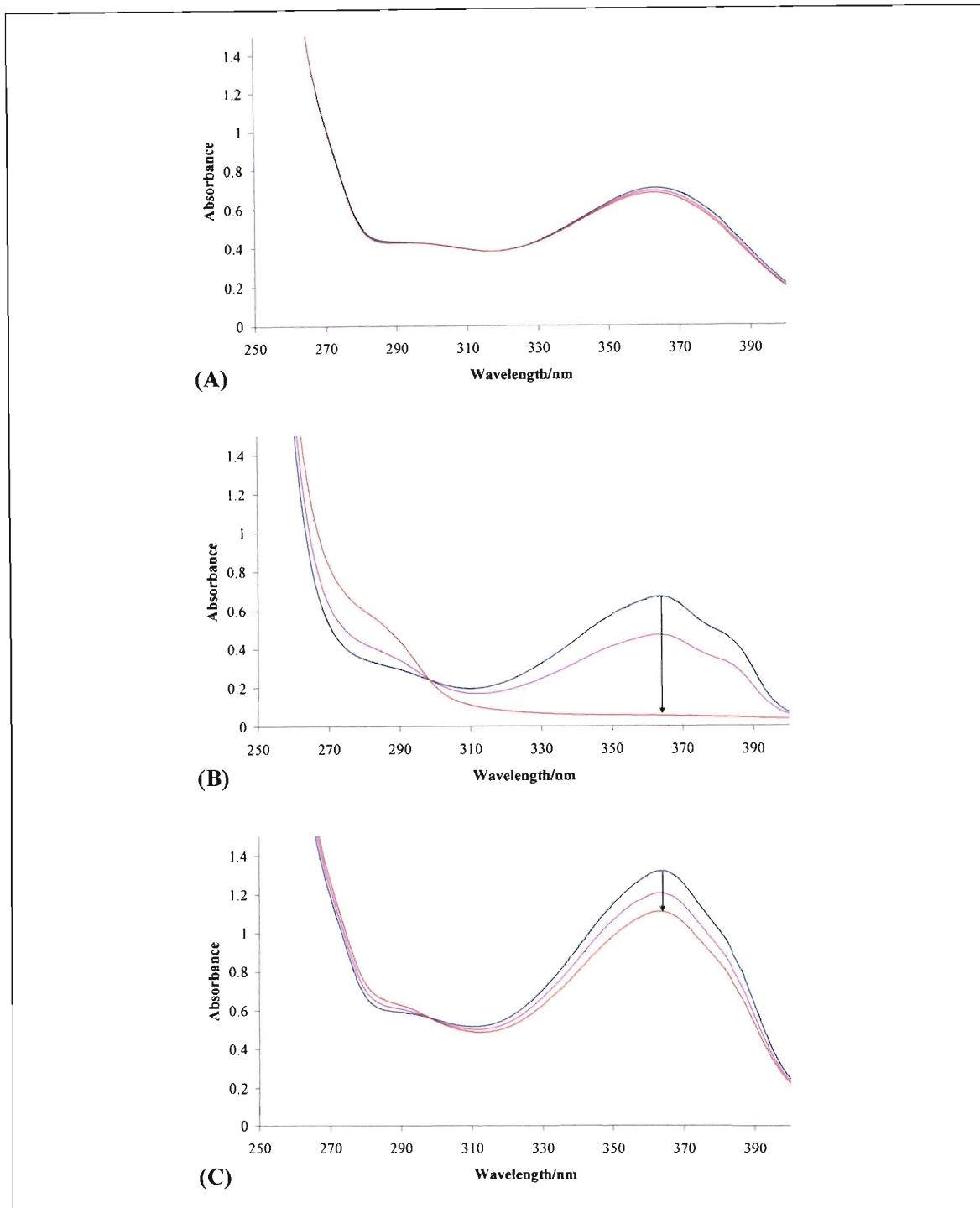
Figure 3.83:   UV spectra of 3.7 × 10^{-5} M rutin (A), 1.6 × 10^{-5} M avobenzone (B) and a mixture of the two (C) in DMSO. Each solution was irradiated at five minute intervals in a 1 cm pathlength quartz cuvette and all spectra were obtained with the Perkin Elmer Lambda 35 UV/VIS spectrophotometer.
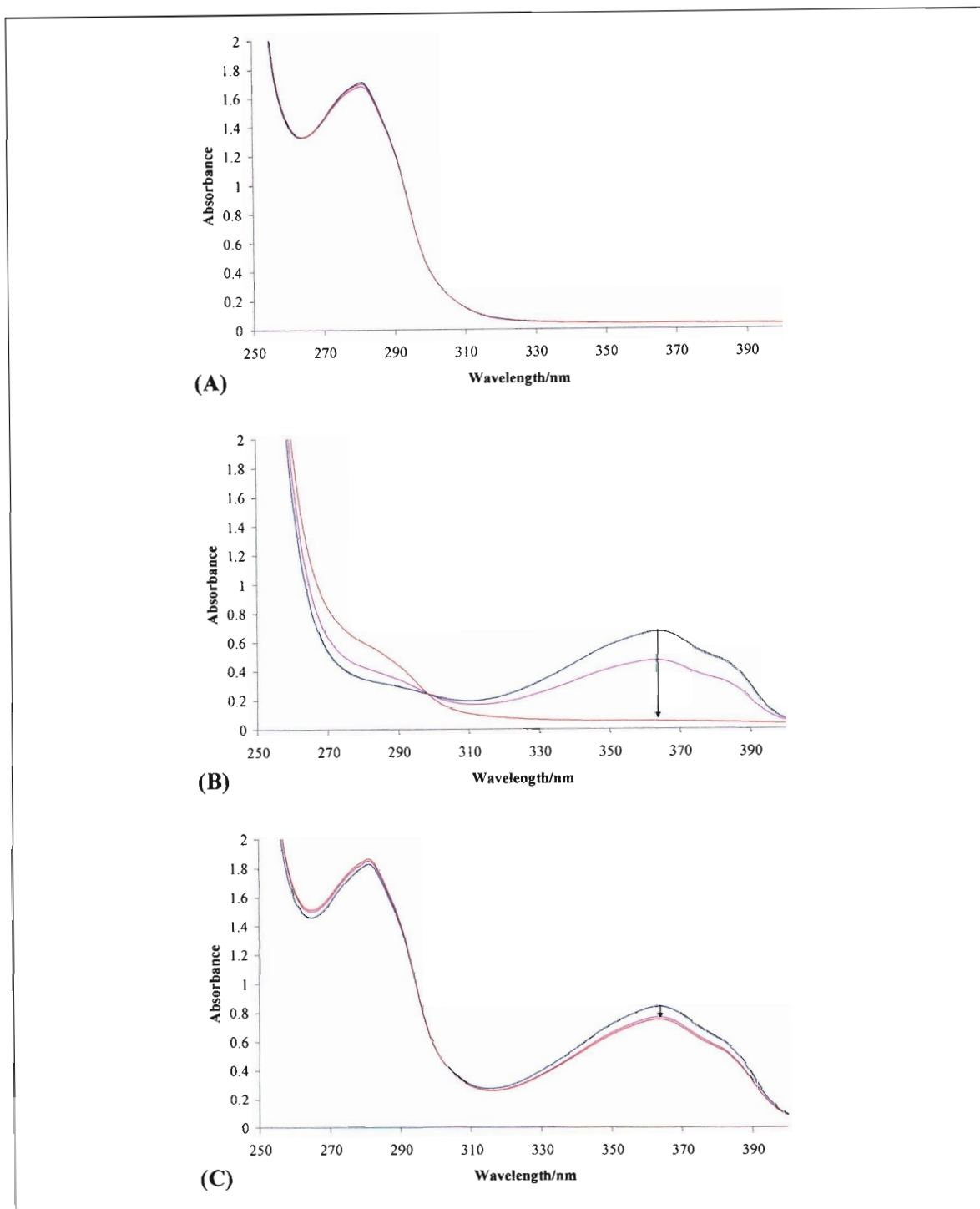
Figure 3.84:   UV spectra of 1.8×10^{-5} M epicatechin (A), 1.7×10^{-5} M avobenzone (B) and a mixture of the two (C) in DMSO. Each solution was irradiated at five minute intervals in a 1 cm pathlength quartz cuvette and all spectra were obtained with the Perkin Elmer Lambda 35 UV/VIS spectrophotometer.

3.4 Proposed mechanism for the photochemistry observed with avobenzone

The Cancer Bush plant, Rooibos tea, Rooibos-honeybush tea and Rooibos-black tea as well as the specific polyphenols, rutin and epicatechin, photostabilised avobenzone. This photostabilising property could be due to the fact that polyphenolics are potent antioxidants.

Avobenzone photostabilisation by epicatechin (see Section 3.3.3) dismisses the argument that photostabilisation occurs when another compound absorbs in competition with avobenzone. The deoxygenation experiments described in Section 3.3.1.2 show that avobenzone photoisomerisation occurs only in the presence of oxygen. This indicates that photoisomerisation possibly occurs through a triplet excited state. This is in agreement with research performed by Chatelain and Gabard [2001]. Cantrell and McGarvey [2001] also reported a triplet state prior to photodegradation of avobenzone, since it was quenched by oxygen to produce singlet oxygen, $^1O_2$. However, Pucetti and Chaudhuri [2004] have reported that $^1O_2$ causes degradation of avobenzone, yet found that $^1O_2$ was not generated by avobenzone in aqueous ethanol. But, it was unclear how the irradiation technique was performed hence difficult to conclude whether avobenzone degraded due to $^1O_2$ or UVA light.

A possible photoisomerisation mechanism is suggested in Figure 3.85. The enol form of avobenzone, A (enol), is excited to its first excited singlet state by UV radiation of wavelengths greater than 300 nm to form ^1A (enol)*. In the excited state, avobenzone undergoes intramolecular proton transfer, followed by intersystem crossing to the triplet state of the keto form, ^3A (keto)*. The triplet state of the keto form of avobenzone can be quenched by ground-state oxygen (through triplet-triplet energy transfer) to form the ground-state keto form, A (keto), and singlet oxygen, $^1O_2$. Therefore, in the absence of oxygen, photoisomerisation of avobenzone will not take place, as was observed in DMSO solvent (see Section 3.3.1.2).

$$A \text{ (enol)} + h\nu \rightarrow {}^1A \text{ (enol)}^*$$

$$^1A \text{ (enol)}^* \rightarrow {}^3A(\text{keto})^* \text{ (photoisomerisation)}$$

$$^3A(\text{keto})^* + {}^3O_2 \rightarrow A \text{ (keto)} + {}^1O_2 \quad \text{(energy transfer)}$$
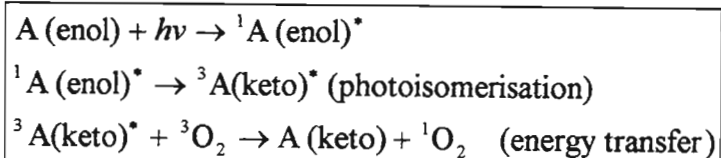
Figure 3.85:   Suggested mechanism for the photoisomerisation of avobenzone.

In DMSO, only photoisomerisation was observed, which could be due to the solvent effect. The photostabilisation of avobenzone in DMSO and ethyl acetate by polyphenolics was therefore the prevention of photoisomerisation.

McGarry *et al.* [1997] reported that DMSO has a strong hydrogen bonding accepting affinity. The photoisomerisation mechanism in DMSO has been displayed in Figure 3.86, based on a similar mechanism reported by McGarry *et al.* [1997]. The enol form is intermolecularly hydrogen bonded to DMSO in solution prior to irradiation. The enol-DMSO complex splits when irradiated, to form the enol anion and a protonated DMSO molecule. The enol anion is then oxidised by singlet oxygen to form the keto form. Singlet oxygen is produced through triplet-triplet energy transfer of ground state oxygen, $^3O_2$, with the triplet state of the keto form (see Figure 3.85). The relatively polar keto form is subsequently stabilised in the relatively polar DMSO solvent. In the absence of oxygen, the enol anion re-captures the proton from the protonated DMSO molecule and reverts back to the enol form. Therefore polyphenolics could act as proton donors for the enol anion (see Section 3.1.3.2), or quenchers of singlet oxygen; reverting the enol anion back to the enol form. Consequently, the absence of oxygen or the presence of polyphenolics prevents photoisomerisation.
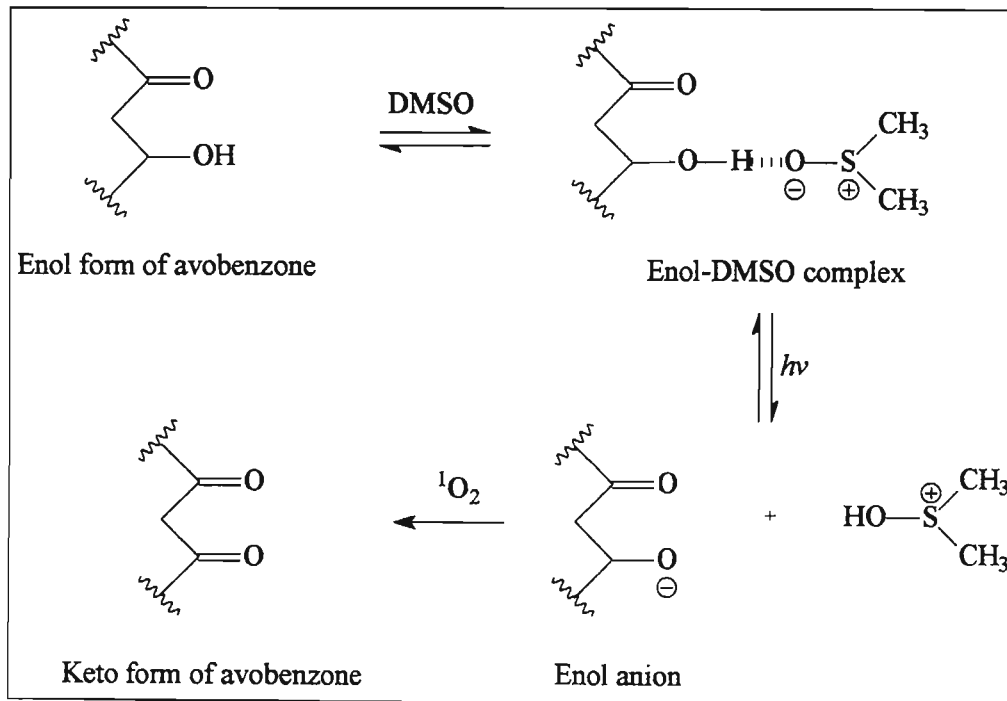
Figure 3.86:   Possible mechanism for the formation of the keto isomer in DMSO when the enol isomer is irradiated in the presence of oxygen.

Photoisomerisation of avobenzone also occurs in ethyl acetate. This could be the result of ethyl acetate hydrogen bonding with the enol form of avobenzone to form a complex, although it is a relatively non-polar solvent. Upon irradiation, the complex splits to form the enol anion and a protonated ethyl acetate molecule. The enol anion can then be oxidised by singlet oxygen to produce the polar keto form (see Figure 3.87). In cyclohexane, the solvent can not hydrogen bond with the enol form and as a result photoisomerisation can not occur through this pathway. The keto form would be relatively more photostable in DMSO than in ethyl acetate and more photostable in ethyl acetate compared to the less polar cyclohexane solvent. Ethyl acetate also possesses proton donating properties (Amyes and Richard [1996]), as shown in Figure 3.88, which could reconvert the enol anion back to the enol form in the absence of oxygen.
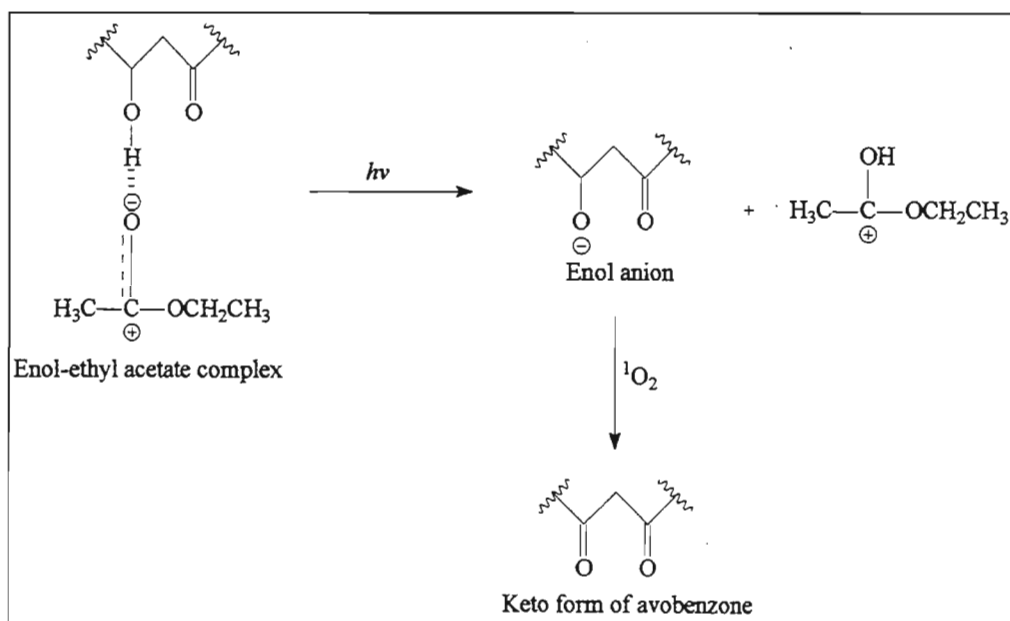
Figure 3.87:   Possible mechanism for the formation of the keto isomer in ethyl acetate when the enol isomer is irradiated in the presence of oxygen.
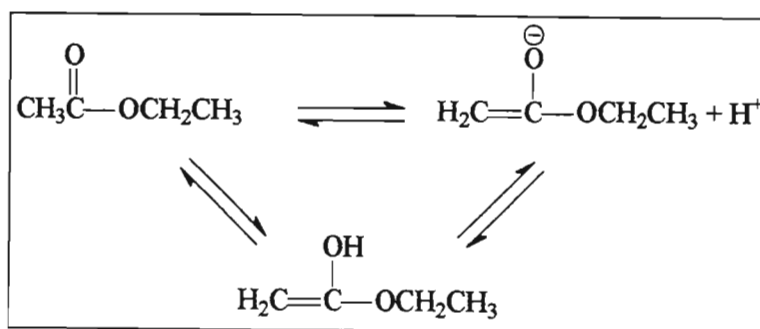
Figure 3.88:   The equilibrium between three different forms of ethyl acetate.

The mechanisms in Figures 3.86 and 3.87 suggest that avobenzone is expected to photoisomerise in non-hydrogen bonding aprotic solvents but should be photostable in polar protic solvents. In these polar protic solvents the enol form is involved in hydrogen exchange through intermolecular hydrogen bonding with the solvent and as a result does not photoisomerise to the keto form. This possibly explains the comparatively higher photostability of avobenzone in methanol (see Section 3.3.1.1).

Photodegradation of avobenzone occurred through α-cleavage (see Section 3.3.1.3) when solutions of the absorber were irradiated in cyclohexane and in ethyl acetate. The structures of the photoproducts suggest that they either originated from a benzoyl radical or a phenacyl radical (Schwack and Rudolph [1995]). Therefore, the photoproducts identified (see Section 3.3.1.3) were characteristic of photodegradation occurring from the keto state (the keto form or the triplet state of the keto form), as has been observed when avobenzone is irradiated in cyclohexane (Schwack and Rudolph [1995], Roscher *et al.* [1994] and Panday [2002]). Since the keto form does not get excited upon irradiation (absorbs below 300 nm), photodegradation possibly occurs from the triplet state of the keto form which is generated from photoisomerisation (see Figure 3.85). Cantrell and McGarvey [2001] reported a triplet state of the keto form which absorbed broadly from 300 to 500 nm. Therefore the triplet state of the keto form could be excited during irradiation by UV light of wavelengths greater than 300 nm. The triplet excited state of the keto form can therefore photodegrade to various photoproducts via two routes; when irradiated or when it collides with singlet oxygen (see Figure 3.89). Hence, in the absence of oxygen, one route is stopped but photodegradation of avobenzone still occurs through the irradiation route, as was seen in cyclohexane and ethyl acetate in Section 3.3.1.2. Consequently, even when antioxidant polyphenols scavenge singlet oxygen photodegradation upon irradiation still occurs. This is why polyphenols failed to photostabilise avobenzone in cylohexane.

$$^3A\,(keto)^* + hv \rightarrow Photodegradation$$
$$^3A\,(keto)^* + {}^1O_2 \rightarrow Photodegradation$$
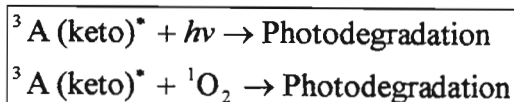
Figure 3.89:   Suggested pathways for photodegradation of avobenzone.

CHAPTER 4

CONCLUSION

This research investigated the potential of polyphenolic extracts derived from Cancer Bush plant to photostabilise the photo-unstable chemical absorbers EHMC, IMC, MBC, Peg-25 PABA and avobenzone.

Appropriate Cancer Bush extracts for photostability analyses were obtained by the boiling water and the ethanol-water extraction methods. These extracts were considered suitable from their UV absorption spectra, HPLC chromatograms and that the extraction methods were able to extract known compounds present in certain substances.

The Folin-Ciocalteu reagent showed the presence of phenolics in the ethanol-water Cancer Bush extract. However, only simple phenolics, such as fatty acids and a phenolic acid, were identified by GC-MS analyses. The presence of rutin or a rutin-like molecule in the Cancer Bush extract was verified by spiking with an authentic sample and from mass spectral analysis which showed the fragmentation of a quercetin (rutin aglycone)-like molecule.

UV spectral analyses showed that EHMC, IMC, MBC and Peg-25 PABA are photo-unstable when dissolved in methanol and Peg-25 PABA when dissolved in water. This photo-instability was not stopped by the addition of polyphenolic extracts from the Cancer Bush plant. On the other hand, avobenzone was found to be photostable in methanol but not in DMSO, ethyl acetate or cyclohexane. The photo-instability of avobenzone was minimised by the addition of Cancer Bush extracts in DMSO and ethyl acetate but not in cyclohexane.

Photostabilisation was only observed in some solvents because of the differing mechanisms of photo-instability of avobenzone in different solvents. HPLC, UV, NMR and GC-MS studies have shown that avobenzone predominantly photoisomerises in DMSO and ethyl acetate but principally photodegrades in cyclohexane. The photoisomerisation of avobenzone in DMSO was found to depend on the presence of oxygen. This suggests that photoisomerisation occurs via a triplet state precursor. In the presence of the ethanol-water Cancer Bush extract, avobenzone was photostabilised in ethyl acetate, and the boiling water Cancer Bush extract photostabilised it in DMSO. The Cancer Bush extracts acted as photostabilisers of avobenzone

by either proton donation or quenching of singlet oxygen (see Section 3.4). Other polyphenolic-rich sources, namely various Rooibos tea extracts, as well as the specific polyphenols, epicatechin and rutin, were also able to photostabilise avobenzone possibly by a similar mechanism. The photostabilisation of avobenzone by epicatechin occurred even though the two compounds do not absorb maximally at the same wavelength, implying an indirect mechanism, in effect supporting the proposed suggestions.

Avobenzone is one of the few approved UVA absorbers; consequently it is used in most sunscreen formulations. Avobenzone's photo-instability in various solvents has been well documented (Schwack and Rudolph [1995], Roscher et al. [1994] and Deflandre and Lang [1988a]) but since there are few UVA absorbers in the market, it is a much easier process to photostabilise this absorber than getting a new one approved. In this study, it has been shown that antioxidant polyphenols could act as potential photostabilisers of avobenzone but more in depth research with sunscreen formulations is required.

Avobenzone is photostable in polar protic solvents (Panday [2002] and Schwack and Rudolph [1995]), but polar sunscreen vehicles could mix with bodily fluids and penetrate into the skin, hence non-polar vehicles are preferable in sunscreen formulations. Unfortunately, avobenzone loses absorbance in non-polar and aprotic solvents by photodegradation and photoisomerisation, either simultaneously or separately. This work has shown that polyphenolic antioxidants can prevent the loss in absorbance arising from the photoisomerisation of avobenzone but not that arising from photodegradation. Alternatively, Damiani et al. [2000] reduced the harmful effects on bovine serum albumin protein and DNA from radicals produced from the photodegradation of avobenzone, by use of antioxidant nitroxide radicals. Therefore avobenzone can be photostabilised when photoisomerising and its harmful effects decreased when photodegrading, by use of appropriate photostabilisers depending on the absorber's behaviour in that non-polar sunscreen vehicle.

The incorporation of antioxidant polyphenolic substances in sunscreen formulations could be a means of offering enhanced photoprotection. However, this should only be done after thorough in vivo experiments have been carried out to determine the safety of polyphenols. The need for caution is apparent because antioxidants are unstable compounds (Pinnell [2003]) and they are also potential prooxidants (Azam et al. [2004]), hence care must be taken in formulation if they are to be used in topical skin applications. It should also be taken into consideration that not all antioxidants are potential photoprotectors, some like simple phenols mainly absorb maximally

in the UVC region (Robards and Antolovich [1997]). Additionally it should be noted that not all antioxidants can enhance photoprotection of the absorber at the particular UV region where it absorbs. The polyphenolic compound epicatechin can photostabilise avobenzone but cannot offer enhanced UVA photoprotection since it absorbs maximally at around 280 nm. Therefore, if antioxidants are to be used as photostabilisers of avobenzone and also provide enhanced UVA photoprotection, then only those that absorb in the appropriate UV region should be used, for instance polyphenols such as rutin.

REFERENCES

Agarwal R., Katiyar S.K., Khan S.G. and Mukhtar H., 1993, Protection against ultraviolet B radiation-induced effects in the skin of SKH-1 hairless mice by a polyphenolic fraction isolated from green tea, *Photochemistry and Photobiology*, **58** (5), 695-700.

Agrapidis-Paloympis L.E, Nash R.A. and Shaath N.A, 1987, The effect of solvents on the ultraviolet absorbance of sunscreens, *Journal of the Society of Cosmetic Chemists*, **38**, 209-221.

Aliwell S.R., 1991, Para-aminobenzoic acid photosensitised dimerization of thymine, *M.Sc. Thesis*, University of Natal, Durban, South Africa.

Aliwell S.R., Martincigh B.S. and Salter L.F., 1993a, Para-aminobenzoic acid-photosensitised dimerization of thymine I. In DNA-related model systems, *Journal of Photochemistry and Photobiology A: Chemistry*, **71**, 137-146.

Aliwell S.R., Martincigh B.S. and Salter L.F., 1993b, Para-aminobenzoic acid-photosensitised dimerization of thymine II. In pUC19 plasmid DNA, *Journal of Photochemistry and Photobiology A: Chemistry*, **71**, 147-153.

Allen J.M., Engenolf S. and Allen S.K., 1995, Rapid reaction of singlet molecular oxygen ($^1O_2$) with p-aminobenzoic acid (PABA) in aqueous solution, *Biochemical and Biophysical Research Communications*, **212** (3), 1145-1151.

Allen J.M., Gossett C.J. and Allen S.K., 1996a, Photochemical formation of singlet molecular oxygen in illuminated aqueous solutions of several commercially available sunscreen active ingredients, *Chemical Research in Toxicology*, **9** (3), 605-609.

Allen J.M., Gossett C.J. and Allen S.K., 1996b, Photochemical formation of singlet molecular oxygen ($^1O_2$) in illuminated aqueous solutions of p-aminobenzoic acid (PABA), *Journal of Photochemistry and Photobiology B: Biology*, **32**, 33-37.

Amyes T.L. and Richard J.P., 1996, Determination of the pK_a of ethyl acetate: Brønsted correlation for deprotonation of a simple oxygen ester in aqueous solution, *Journal of the American Chemical Society*, **118**, 3129-3141.

Andrae I., Böhn F., Brighen A.O., Gonzenbach H., Hill T., Mulroy L. and Truscott T.G., 1995, V-1p/20 Poster, *6th Congress of the European Society for Photobiology*, Churchill College, University of Cambridge, UK.

Andrae I., Brighen A., Böhm F., Gonzenbach H., Hill T., Mulroy L. and Truscott T.G., 1997, A UVA filter (4-tert-butyl-4'-methoxydibenzoylmethane: photoprotection reflects photophysical properties, *Journal of Photochemistry and Photobiology B: Biology*, **37**, 147-150.

Aquino R., Morelli S., Tomaino A., Pellegrino M., Saija A., Grumetto L., Puglia C., Ventura D. and Bonina F., 2002, Antioxidant and photoprotective activity of a crude extract of Culcitium reflexum H.B.K. leaves and their major flavonoids, *Journal of Ethnopharmacology*, **79**, 183-191.

Armeni T., Damiani E., Battino M., Greci L. and Principato G., 2004, Lack of *in vitro* protection by a common sunscreen ingredient on UVA-induced cytotoxicity in keratinocytes, *Toxicology*, **203**, 165-178.

Armstrong B.K. and Kricker A., 2001, The epidemiology of UV induced skin cancer, *Journal of Photochemistry and Photobiology B: Biology*, **63**, 8-18.

Azam S., Hadi N., Khan N.U. and Hadi S.M., 2004, Prooxidant property of green tea polyphenols epicatechin and epigallocatechin-3-gallate: implications for anticancer properties, *Toxicology in Vitro*, **18**, 555-561.

Beck I., Deflandre A., Lang G., Arnaud R. and Lemaire J., 1981, Study of the photochemical behaviour of sunscreens. Benzylidene camphor and derivatives, *International Journal of Cosmetic Science*, **3**, 139-152.

Beck I., Deflandre A., Lang G., Arnaud R. and Lemaire J., 1985, Study of the photochemical behaviour of sunscreens benzylidene camphor and derivatives II: photosensitised isomerisation by aromatic ketones and deactivation of the 8-methoxy psoralin triplet state, *Journal of Photochemistry*, **30**, 215-227.

Bolton K., 1991, Studies of the photochemical reactions of thymine with selected sensitisers, *M.Sc. Thesis*, University of Natal, Durban.

Bolton K., Martincigh B.S. and Salter L.F., 1992, The potential carcinogenic effect of Uvinul DS49–a common UV absorber used in cosmetics, *Journal of Photochemistry and Photobiology A: Chemistry*, **63** (2), 241-248.

Bonda C. and Steinberg D.C., 2000, A new photostabilizer for full spectrum sunscreens, *Cosmetics and Toiletries*, **115**, 37-45.

Bonin A.M., Arlauskas A.P., Angus D.S., Baker R.S.U., Gallagher C.H., Greenoak G., Brown M.M.L., Meher-Homji K.M. and Reeve V., 1982, UV-absorbing and other sun-protecting substances: genotoxicity of 2 ethylhexyl-*p*-methoxycinnamate. *Mutation Research*, **105** (5), 303-308.

Broadbent J.K., 1994, Photochemical studies of sunscreen constituents, *M.Sc. Thesis*, University of Natal, Durban, South Africa.

Broadbent J.K., Martincigh B.S., Raynor M.W., Salter L.F., Moulder R., Sjöberg P. and Markides K.E., 1996, Capillary supercritical fluid chromatography combined with atmospheric pressure chemical ionisation mass spectrometry for tne investigation of photoproduct formation in the sunscreen absorber 2-ethylhexyl-*p*-methoxycinnamate, *Journal of Chromatography A*, **732**, 101-110.

Butt S.T. and Christensen T., 2000, Toxicity and phototoxicity of chemical sun filters, *Radiation Protection Dosimetry*, **91**(1-3), 283-286.

Cantrell A. and McGarvey D.J., 2001, Photochemical studies of 4-*tert*-butyl-4'-methoxydibenzoylmethane (BM-DBM), *Journal of Photochemistry and Photobiology B: Biology*, **64**, 117-122.

Cantrell A., McGarvey D.J., Mulroy L. and Truscott T.G., 1999, Laser flash photolysis studies of the UVA sunscreen mexoryl® SX, *Photochemistry and Photobiology*, **70** (3), 292-297.

Chang C., Yang M., Wen H. and Chern J., 2002, Estimation of total flavonoid content in propolis by two complementary colorimetric methods, *Journal of Food and Drug Analysis*, **10** (3), 178-182.

Chatelain E. and Gabard B., 2001, Photostabilisation of butyl methoxydibenzoylmethane (avobenzone) by bis-ethylhexyloxyphenol methoxyphenyl triazine (tinosorb S), a new UV broadband filter, *Photochemistry and Photobiology*, **74** (3), 401-406.

Cohen M.D., Schmidt G.M.J. and Sonntag F.I., 1964, Topochemistry. Part II. The photochemistry of *trans*-cinnamic acids, *Journal of the Chemical Society*, 2000-2013.

Concar D., 16th May 1992, The resistible rise of skin cancer, *New Scientist*, 23-28.

Couteau C., Cullel N.P., Connan A.E. and Coiffard L.J.M., 2001, Stripping method to quantify absorption of two sunscreens in human, *International Journal of Pharmaceutics*, **222**, 153-157.

Damiani E., Greci L., Parsons R. and Knowland J., 1999, Nitroxide radicals protect DNA from damage when illuminated *in vitro* in the presence of dibenzoylmethane and a common sunscreen ingredient, *Free Radical Biology and Medicine*, **26** (7-8), 809-816.

Damiani E., Carloni P., Biondi C. and Greci L., 2000, Increased oxidative modification of albumin when illuminated in vitro in the presence of a common sunscreen ingredient: protection by nitroxide radicals, *Free Radical Biology and Medicine*, **28** (2), 193-201.

Damiani E., Castagna R. and Greci L., 2002, The effects of derivatives of the nitroxide tempol on UVA-mediated *in vitro* lipid and protein oxidation, *Free Radical Biology and Medicine*, **33** (1), 128-136.

Dany A., Douki T., Triantaphylides C. and Cadet J., 2001, Repair of the main UV-induced thymine dimeric lesions within *Arabidopsis thaliana* DNA: evidence for the major involvement of photoreactivation pathways, *Journal of Photochemistry and Photobiology B: Biology*, **65**, 127-135.

Deflandre A. and Lang G., 1988a, Photostability assessment of sunscreens. Benzylidene camphor and dibenzoylmethane derivatives, *International Journal of Cosmetic Science*, **10**, 53-62.

Deflandre A. and Lang G., 1988b, Photoisomerization of benzylidene camphor and derivatives, *Cosmetics and Toiletries*, **103**, 69-75.

De Gruijl F.R. and Van der Leun J.C., 1994, Estimate of the wavelength dependency of ultraviolet carcinogenesis in humans and its relevance to the risk assessment of a stratospheric ozone depletion, *Health Physics*, **67**, 319-325.

De Gruijl F.R., van Kranen H.J. and Mullenders L.H.F., 2001, UV-induced DNA damage, repair, mutations and oncogenic pathways in skin cancer, *Journal of Photochemistry and Photobiology B: Biology*, **63**, 19-27.

Donovan J.L., Luthria D.L., Sremple P. and Waterhouse A.L., 1999, Analysis of (+)-catechin, (-)-epicatechin and their 3'- and 4'-O-methylated analogs: A comparison of sensitive methods, *Journal of Chromatography B*, **726**, 277-283.

Dubois M., Gilard P., Tiercet P., Deflandre A. and Lefebvre M.A., 1998, Photoisomerisation of the sunscreen filter PARSOL® 1789, *Journal de Chimie Physique et de Physico-Chimie Biologique*, **95**, 388-394.

Eggset G., Kavli G., Krokan H. and Volden G., 1984, Ultraviolet and visible light penetration of epidermis, *Photobiochemistry and Photobiophysics*, **8**, 163-167.

Erickson L., 2003, Rooibos tea: research into antioxidant and antimutagenic properties, *HerbalGram*, **59**, 34-45.

Fabre N. and Rustan I., 2001, Determination of flavone, flavonol, and flavanone aglycones by negative ion liquid chromatography electrospray ion trap mass spectrometry, *Journal of the American Society for Mass Spectrometry*, **12**, 707-715.

Fernandes A.C., Cromarty A.D., Albrecht C. and van Rensburg C.E.J., 2004, The antioxidant potential of Sutherlandia frutescens, *Journal of Ethnopharmacology*, **95**, 1-5.

Ferreira D., Kamara B.I., Brandt E.V. and Joubert E., 1998, Phenolic compounds from *Cyclopia intermedia* (honeybush tea), *Journal of Agricultural and Food Chemistry*, **46** (9), 3406-3410.

Fessenden R.J., and Fessenden J.S., 1998, *Organic Chemistry*, Dodson K. (editor), 6th edition, Brooks/Cole Publishing Company, Pacific Grove, United States of America, pp. 337-412.

Green N.P.O., Stout G.W. and Taylor D.J., 1990, *Biological Science: Systems, Maintenance and Change*, Soper R. (editor), 2nd edition, Volume 2, Cambridge University Press, Cambridge, New York, Port Chester, Melbourne, Sydney, pp. 667-695.

Grushow A., 2002, Hydrogen bonding using NMR: a new look at the 2,4-pentanedione keto-enol tautomer experiment, *Journal of Chemical Education*, **79** (6), 707-714.

Helaleh M.I.H., Tanaka K., Fujii S. and Korenaga T., 2001, GC-MS determination of phenolic compounds in soil samples using soxhlet extraction and derivatisation techniques, *Analytical Sciences*, **17**, 1225-1227.

Hemminki K., Xu G., Kause L., Koulu L.M., Zhao C. and Jansen C.T., 2002, Demonstration of UV-dimers in human skin DNA in situ 3 weeks after exposure, *Carcinogenesis*, **23** (4), 605-609.

Human S. and Bajic V.B., 2002, Contribution to skin cancer prevention in South Africa: modelling the UV index utilizing imprecise data, *Austrian Journal of Statistics*, **31** (2 and 3), 169-175.

Ingouville N.A., 1995, The photochemical behaviour of the sunscreen absorber 2-ethylhexyl-*p*-methoxycinnamate, *M.Sc. Thesis*, University of Natal, Durban, South Africa.

Joubert E., Winterton P, Britz T.J. and Ferreira D., 2004, Superoxide anion and α,α-diphenyl-β-picrylhydrazyl radical scavenging capacity of rooibos (*Aspalathus linearis*) aqueous extracts, crude phenolic fractions, tannin and flavonoids, *Food Research International*, **37**, 133-138.

Kamara B.I., Brandt E.V., Ferreira D. and Joubert E., 1998, Polyphenols from honeybush tea (*Cyclopia intermedia*), *Journal of Agricultural and Food Chemistry*, **51** (13), 3874-3879.

Katiyar S.K., Elmets C.A., Agarwal R. and Mukhtar H., 1995, Protection against ultraviolet-B radiation-induced local and systemic suppression of contact hypersensitivity and edema responses in C3H/HeN mice by green tea polyphenols, *Photochemistry and Photobiology*, **62** (5), 855-861.

Katiyar S.K., Matsui M.S., Elmets C.A. and Mukhtar H., 1999, Polyphenolic antioxidant (-)-epigallocatechin-3-gallate from green tea reduces UVB-induced inflammatory responses and infiltration of leukocytes in human skin, *Photochemistry and Photobiology*, **69** (2), 148-153.

Katiyar S.K., Bergamo B.M., Vyalil P.K. and Elmets C.A., 2001, Green tea polyphenols: DNA photodamage and photoimmunology, *Journal of Photochemistry and Photobiology B: Biology*, **65**, 109-114.

Kimbrough D.R., 1997, The photochemistry of sunscreens, *Journal of Chemical Education*, **74** (1), 51-53.

Klebe J.F., Finkbeiner H. and White D.M., 1966, Silylations with bis(trimethylsilyl)acetamide – a highly reactive silyl donor, *Journal of the American Chemical Society*, **88** (14), 3390-3395.

Klein K., 1990, Formulating sunscreen products in: *Sunscreens: Development, Evaluation and Regulatory Aspects*, Lowe N.J. and Shaath N.A. (editors), Volume 10, Marcel Dekker, New York, United States of America, pp. 235-266.

Knowland J., McKenzie E.A., McHugh P.J. and Cridland N.A, 1993, Sunlight-induced mutagenicity of a common sunscreen ingredient, *Federation of European Biochemical Societies Letters*, **324** (3), 309-313.

Kowlaser K., 1998, Photoproduct formation in the irradiated sunscreen absorber 2-ethylhexyl-*p*-methoxycinnamate, *M.Sc. Thesis*, University of Natal, Durban, South Africa.

Lamola A.A., 1969, Specific formation of thymine dimers in DNA, *Photochemistry and Photobiology*, **9**, 291-294.

Liang Y.R., Liu Z.S., Xu Y.R. and Hu Y.L., 1990, A study on chemical composition of two special green teas (*Camellia sinensis*), *Journal of Science and Food Agriculture*, **53**, 541-548.

Lide D.R. (editor), 1992-1993, CRC Handbook of Chemistry and Physics, 73rd Edition, CRC Press Inc., Boca Raton, Florida, pp. 3-12 to 3-523.

Lin Y., Juan I., Chen Y., Liang Y. and Lin J., 1996, Composition of Polyphenols in Fresh Tea Leaves and Associations of Their Oxygen-Radical-Absorbing Capacity with Antiproliferative Actions in Fibroblast Cells, *Journal of Agricultural and Food Chemistry*, **44**, 1387-1394.

Lin Y., Tsai Y., Tsay J. and Lin J., 2003a, Factors Affecting the Levels of Tea Polyphenols and Caffeine in Tea Leaves, *Journal of Agricultural and Food Chemistry*, **51**, 1864-187.

Lin Y., Wu S. and Lin J., 2003b, Determination of Tea Flowers (Camellia sinensis) and Their Hydroxyl Radical Scavenging and Nitric Oxide Suppressing Effects, *Journal of Agricultural and Food Chemistry*, **51**, 975-980.

Lowe N.J., 1990, The need for photoprotection, in: *Sunscreens: Development, Evaluation and Regulatory Aspects*, Lowe N.J. and Shaath N.A. (editors), Volume 10, Marcel Dekker, New York, United States of America, pp. 37-39.

Lu Y., Lou Y., Xie J., Peng Q., Liao J., Yang C.S., Huang M and Conney A.H., 2002, Topical applications of caffeine or (-)-epigallocatechin gallate (EGCG) inhibit carcinogenesis and selectivity increase apoptosis in UVB-induced skin tumors in mice, *Proceedings of the National Academy of Sciences*, **99** (19), 12455-12460.

Lu L., Chen Y. and Chou C., 2003, Antibacterial and DPPH free radical-scavenging activities of the ethanol extract of propolis collected in Taiwan, *Journal of Food and Drug Analysis*, **11** (4), 277-282.

Luthria D.L., Jones A.D., Donovan J.L. and Waterhouse A.L., 1997, GC-MS determination of catechin and epicatechin levels in human plasma, *Journal of High Resolution Chromatography*, **20**, 621-623.

Macheix J.J., Fleuriet A. and Billot J., 1990, *Fruit Phenolics*, CRC Press, Boca Raton, Florida.

Maier H., Schauberger G., Brunnhofer K. and Hönigsmann H., 2001, Change of ultraviolet absorbance of sunscreens by exposure to solar-simulated radiation, *The Journal of Investigative Dermatology*, **117** (2), 256-262.

Manahan S.E., 1986, *Quantitative Chemical Analysis*, Ewing S., Sky P. and Hancharick M.K. (editors), Brooks/Cole Publishing Company, Monterey, California, United States of America, pp. 545-566.

Mansouri A., Embarek G., Kokkalou E. and Kefalas P., 2005, Phenolic profile and antioxidant activity of the Algerian ripe date palm fruit (*Phoenix dactylifera*), *Food Chemistry*, **89**, 411-420.

Marnewick J.L., Gelderblom W.C.A. and Joubert E., 2000, An investigation on the antimutagenic properties of South African herbal teas, *Mutation Research*, **471**, 157-166.

Marnewick J.L., Batenburg W., Swart P., Joubert E., Swanevelder S. and Gelderblom W.C.A., 2004, *Ex vivo* modulation of chemical-induced mutagenesis by subcellular liver fractions of rats treated with rooibos (*Aspalathus linearis*) tea, honeybush (*Cyclopia intermedia*) tea, as well as green and black (*Camellia sinensis*) teas, *Mutation Research*, **558**, 145-154.

Martincigh B.S., Allen J.M. and Allen S.K., 1997, Sunscreens: the molecules and their photochemistry, in: *Sunscreen photobiology: molecular, cellular and physiological aspects*, Gasparro F.P. (editor), Springer-Verlag and Landes Bioscience, Berlin, pp. 11-45.

McGarry P.F., Jockusch S., Fujiwara Y., Kaprinidis N.A. and Turro N.J., 1997, DMSO solvent induced photochemistry in highly photostable compounds. The role of intermolecular hydrogen bonding, *Journal of Physical Chemistry A*, **101**, 764-767.

Miller A.L., 1996, Antioxidant flavonoids: structure, function and clinical usage, *Alternative Medicine Review*, **1** (2), 103-111.

Miketova P., Schram K.H., Whitney J.L., Kerns E.H., Valcic S., Timmermann B.N. and Volk K.J., 1998, Mass Spectrometry of Selected Components of Biological Interest in Green Tea Extracts, *Journal of Natural Products*, **61**, 461-467.

Molyneux P., 2004, The use of the stable free radical diphenylpicrylhydrazyl (DPPH) for estimating antioxidant activity, *Journal of Science and Technology*, **26** (2), 211-219.

Morais S.A.L., Nascimento E.A., Queiroz C.R.A.A., Piló-Veloso D. and Drumond M.G., 1999, Studies on polyphenols and lignin of *Astronium urundeuva* wood, *Journal of the Brazilian Chemical Society*, **10** (6), 447-452.

Morrison R.T., Boyd R.N., 1983, *Organic Chemistry*, Hill M. (editor), 4th edition, Allyn and Bacon, Inc., Singapore, pp. 675-732.

Mozetič B. and Trebše P., 2004, Identification of sweet cherry anthocyanins and hydroxycinnamic acids using HPLC coupled with DAD and MS detector, *Acta Chimica Slovenica*, **51**, 151-158.

Mukhtar H.M., Wang Z.-Y., Katiyar S.K. and Agarwal R., 1992, Tea Components: Antimutagenic and Anticarcinogenic Effects, *Preventive Medicine*, **21**, 351-360.

Mukhtar H. and Elmets C.A., 1996, Photocarcinogenesis: mechanisms, models and human health implications, *Photochemistry and Photobiology*, **63** (4), 356-357.

Nigdikar S.V., Williams N.R., Griffin B.A. and Howard A.N., 1998, Consumption of red wine polyphenols reduces the susceptibility of low-density lipoproteins to oxidation *in vivo*, *American Journal of Clinical Nutrition*, **68**, 258-265.

Owen R.W., Haubner R., Hull W.E., Erben G., Spiegelhalder B., Bartsch H. and Haber B., 2003, Isolation and structure elucidation of the major individual polyphenols in carob fibre, *Food and Chemical Toxicology*, **41**, 1727-1738.

Paganga G. and Rice-Evans C.A., 1997, The identification of flavonoids as glycosides in human plasma, *Federation of European Biochemical Societies Letters*, **401**, 78-82.

Panday R., 2002, A photochemical investigation of two sunscreen absorbers in a polar and a non-polar medium, *M.Sc. Thesis*, University of Natal, Durban, South Africa.

Perry J.A., 1981, *Introduction to Analytical Gas Chromatography*, Cazes J. (editor), Volume 14, Marcel Dekker, Inc., New York, United States of America, pp. 55-76.

Peterson G.L., 1983, Determination of total protein, *Methods in Enzymology*, **91**, 95-119.

Picard D., 1996, The biochemistry of green tea polyphenols and their potential application in human skin cancer, *Alternative Medicine Review*, **1** (1), 31-42.

Pierce A.R., Graham H.N., Glassner S., Madlin H. and Gonzalez J.G., 1969, Analysis of tea flavonols by gas chromatography of their trimethylsilyl derivatives, *Analytical Chemistry*, **41** (2), 298-302.

Pinnell S.R., 2003, Cutaneous photodamage, oxidative stress, and topical antioxidant protection, *Journal of the American Academy of Dermatology*, **48** (1), 1-22.

Potten C.S., Chadwick C.A., Cohen A.J., Nikaido O., Matsunaga T., Schipper N.W., and Yound A.R., 1993, DNA damage in UV-irradiated human skin in vivo: automated direct measurement by image analysis (thymine dimers) compared with indirect measurement (unscheduled DNA synthesis) and protection by 5-methoxypsoralen, *International Journal of Radiation Biology*, **63** (3), 313-324.

Puccetti G. and Chaudhuri R.K., 2004, Singlet oxygen and singlet oxygen quenchers, *International Federation of Societies of Cosmetic Chemists*, EMD Chemicals, Florida, United States of America.

Reddy M.B., Hurrell R.F. and Cook J.D., 2000, Estimation of nonheme-iron bioavailability from meal composition, *American Journal of Clinical Nutrition*, **71**, 937-943.

Robards K. and Antolovich M., 1997, Critical review: Analytical chemistry of fruit bioflavonoids, *Analyst*, **122**, 11R-34R.

Roscher N.M., Lindemann M.K.O., Kong S.B., Cho C.G. and Jiang P., 1994, Photodecomposition of several compounds commonly used as sunscreen agents, *Journal of Photochemistry and Photobiology A: Chemistry*, **80**, 417-421.

Ryan D. and Robards K., 1998, Critical review: phenolic compounds in olives, *Analyst*, **123**, 31R-44R.

Ryan K.G., Swinny E.E., Markham K.R. and Winefield C., 2002, Flavonoid gene expression and UV photoprotection in transgenic and mutant *Petunia* leaves, *Phytochemistry*, **59**, 23-32.

Sánchez-Rabaneda F., Jáuregui O., Casals I., Andrés-Lacueva C., Izquierdo-Pulido M. and Lamuela-Raventós R.M., 2003, Liquid chromatographic/electrospray ionization tandem mass spectrometric study of the phenolic composition of cocoa (*Theobroma cacao*), *Journal of Mass Spectrometry*, **38**, 35-42.

Sayre R.M., 1992, Sunlight risk and how sunscreens work, *Cosmetics and Toiletries*, **107**, 105-109.

Sayre R.M. and Dowdy J.C., 1999, Photostability testing of avobenzone, *Cosmetics and Toiletries*, **114** (5), 85-91.

Schwack W. and Rudolph T., 1995, Photochemistry of dibenzoyl methane UVA filters. Part 1, *Journal of Photochemistry and Photobiology B: Biology*, **28**, 229-234.

Schwedt G., 1997, *The Essential Guide to Analytical Chemistry*, John Wiley and Sons, Chichester, England, pp. 140-183.

Serpone N., Salinaro A., Emeline A.V., Horikoshi S., Hidaka H. and Zhao J., 2002, An *in vitro* systematic spectroscopic examination of the photostabilities of a random set of commercial sunscreen lotions and their chemical UVB/UVA active agents, *Photochemical and Photobiological Sciences*, **1**, 970-981.

Setlow R.B., Grist E., Thompson K. and Woodhead A.D., 1993, Wavelengths effective in induction of malignant melanoma, *Proceedings of the National Academy of Sciences*, **90**, 6666-6670.

Sewlall A., 2003, DNA cleavage photoinduced by benzophenone based sunscreens, *M.Sc. Thesis*, University of Natal, Durban, South Africa.

Shaath N.A., 1990, The chemistry of sunscreens, in: *Sunscreens: Development, Evaluation and Regulatory Aspects*, Lowe N.J. and Shaath N.A. (editors), Volume 10, Marcel Dekker, New York, United States of America, pp. 211-233.

Shaw A., Wainschel L.A. and Shetlar M.D., 1992, The photochemistry of *p*-aminobenzoic acid, *Photochemistry and Photobiology*, **55** (5), 647-656.

Simeoni S., Scalia S. and Benson H.A.E., 2004, Influence of cyclodextrins on in vitro human skin absorption of the sunscreen, butyl-methoxydibenzoylmethane, *International Journal of Pharmaceutics*, **280**, 163-171.

Singleton V.L., Orthofer R. and Lamuela-Raventós R.M., 1999, Analysis of total phenols and other oxidation substrates and antioxidants by means of Folin-Ciocalteu reagent, *Methods in Enzymology*, **299**, 152-178.

Skoog D.A. and West D.M., 1982, Optical spectroscopic instruments, *Fundamentals of Analytical Chemistry*, Vondeling J., Smith P.L. and Kesselring L. (editors), 4th edition, Saunders College Publishing, Tokyo, pp. 504-524.

Skoog D.A, West D.M., Holler F.J. and Crouch S.R., 2004a, *Fundamentals of Analytical Chemistry*, Kiselica S. and White A. (editors), 8th edition, Brooks/Cole Publishing, Belmont, California, United States of America, pp. 744-783.

Skoog D.A, West D.M., Holler F.J. and Crouch S.R., 2004b, *Fundamentals of Analytical Chemistry*, Kiselica S. and White A. (editors), 8th edition, Brooks/Cole Publishing, Belmont, California, United States of America, pp. 710-743.

Skoog D.A, West D.M., Holler F.J. and Crouch S.R., 2004c, *Fundamentals of Analytical Chemistry*, Kiselica S. and White A. (editors), 8th edition, Brooks/Cole Publishing, Belmont, California, United States of America, pp. 973-995.

Skoog D.A, West D.M., Holler F.J. and Crouch S.R., 2004d, *Fundamentals of Analytical Chemistry*, Kiselica S. and White A. (editors), 8th edition, Brooks/Cole Publishing, Belmont, California, United States of America, pp. 947-972.

Soleas G.J., Diamandis E.P., Karumanchiri A. and Goldberg D.M., 1997, A Multiresidue Derivatization Gas Chromatographic Assay for Fifteen Phenolic Constituents with Mass Selective Detection, *Analytical Sciences*, **69**, 4405-4409.

Soleas G.J., and Goldberg D.M., 1999, Analysis of Antioxidant Wine Polyphenols by Gas Chromatography-Mass Spectrometry, *Methods of Enzymology*, **299**, 137-151.

Stremple P., 1996, Improved separation and identification of aglycon flavonoids by gas chromatography on phenylmethylsilicone copolymers, *Journal of High Resolution Chromatography*, **19**, 581-584.

Sutherland B.M., 1982, *p*-Aminobenzoic acid-sunlamp sensitization of pyrimidine dimmer formation and transformation in human cells, *Photochemistry and Photobiology*, **36**, 95-97.

Sutherland J.C., and Griffin K.P., 1984, *p*-Aminobenzoic acid can sensitise the formation of pyrimidine dimers in DNA: direct chemical evidence, *Photochemistry and Photobiology*, **40**, 391-394.

Svobodová A., Psotová J. and Walterová D., 2003, Natural phenolics in the prevention of UV-induced skin damage - a review, *Biomedical Papers*, **147** (2), 137-145.

Tarras-Wahlberg N., Stenhagen G., Larkö O., Rosén A., Wennberg A. and Wennerström O., 1999, Changes in ultraviolet absorption of sunscreens after ultraviolet irradiation, *The Journal of Investigative Dermatology*, **113** (4), 547-553.

Taylor C.R., Stern R.S., Leyden J.J. and Gilchrest B.A., 1990, Photoaging/photodamage and photoprotection, *Journal of the American Academy of Dermatology*, **22** (1), 1-15.

Taylor J., 1994, Unraveling the molecular pathway from sunlight to skin cancer, *Accounts of Chemical Research*, **27**, 76-82.

Taylor J.S., 1995, DNA, sunlight and skin cancer, *Pure and Applied Chemistry*, **67** (1), 183-190.

Tokuşoğlu Ö., Ünal M.K. and Yıldırım Z., 2003, HPLC-UV and GC-MS characterization of the flavonol aglycons quercetin, kaempferol, and myricetin in tomato pastes and other tomato-based products, *Acta Chromatographica*, **13**, 196-207.

Valcic S., Muders A., Jacobsen N.E., Liebler D.C. and Timmermann B.N., 1999, Antioxidant chemistry of green tea catechins – Identification of products of the reaction of (-)-epigallocatechin gallate with peroxyl radicals, *Chemical Research in Toxicology*, **12**, 382 – 386.

Vanquerp V., Rodriguez C., Coiffard C., Coiffard L.J.M. and de Roeck-Holtzhauer Y., 1999, Technical note: high performance liquid chromatographic method for the comparison of the photostability of five sunscreen agents, *Journal of Chromatography A*, **832**, 273-277.

Wada L. and Ou B., 2002, Antioxidant activity and phenolic content of Oregon caneberries, *Journal of Agricultural and Food Chemistry*, **50**, 3495-3500.

Weinblum D. and Johns H.E., 1966, Isolation and properties of isomeric thymine dimers, *Biochimica et Biophysica Acta*, **114**, 450-459.

Wells R.J., 1999, Review: recent advances in non-silylation derivatisation techniques for gas chromatography, *Journal of Chromatography A*, **843** (1-2), 1-18.

Woodruff J., 2001, Creative developments (cosmetics) limited, *Sun Products: Chemistry in Britain 2002*, **37** (7), 58-61. (Also accessed at: http://www.creative-developments.co.uk/papers/RSC%20Sun%20Products.htm on the 16th September, 2003)

You Y., Lee D., Yoon J., Nakajima S., Yasui A. and Pfeifer G.P., 2001, Cyclobutane pyrimidine dimers are responsible for the vast majority of mutations induced by UVB irradiation in mammalian cells, *The Journal of Biological Chemistry*, **276** (48), 44688-44694.

Zeeb D.J., Nelson B.C., Albert K. and Dalluge J.J., 2000, Separation and identification of twelve catechins in tea using liquid chromatography/atmospheric pressure chemical ionization-mass spectrometry, *Analytical Chemistry*, **72** (20), 5020-5026.

Zhao J., Jin X., E Y., Zheng Z.S., Zhang Y.J., Athar M., DeLeo V.A., Mukhtar H., Bickers D.R. and Wang Z.Y., 1999, Photoprotective effect of black tea extracts against UVB-induced phototoxicity in skin, *Photochemistry and Photobiology*, **70** (4), 637-644.

Zuo Y., Chen H., and Deng Y., 2002, Simultaneous determination of catechins, caffeine and gallic acids in green, Oolong, black and pu-erh teas using HPLC with a photodiode array detector, *Talanta*, **57**, 307-316.

Web-sites

CancerNet (accessed on 28th October 2004), Skin Cancer, web-site:

http://www.pueblo.gsa.gov/cic_text/health/skin-cancer/skin.htm

Cancer Research UK (accessed on 28th October 2004), web-site:

http://www.cancerresearchuk.org/aboutcancer/speci.../melanoma_skincance

Ciba Specialty Chemicals (accessed on 13th December 2004), web-site:

http://www.cibasc.com/pf/pf_docMDMS.asp?itemnumber=6942254&docnumber=80&app_id=
ACROBAT&targetlibrary=CHBS_HP_MADS&dt=BR&ind=23

Finebush (accessed on 28th October 2004), web-site:

www.finebush.com/Sutherlandia.htm

Guan T.T. and Whiteman M., (accessed on 1st March 2005), Antioxidant activities of some tropical fruits, web-site:

http://staff.science.nus.edu.sg/~scilooe/srp2002/sci_paper/Biochem/research_paper/Tan%20Tze
%20Guan1.pdf

Matsumura Y. and Ananthaswamy H.N. (accessed on 11th November 2004), Structure of the major UV-induced photoproducts in DNA, web-site:

http://www-ermm.cbcu.cam.ac.uk/0200533lh.htm

Montelone (accessed on 24th November 2004), Mutation, Mutagens and DNA repair, copyright 1998 by Montelone B.A., Kansas University, web-site:

http://www-personal.ksu.edu/~bethmont/mutdes.html

National Institute of Health (accessed on 12th November 2004), Genetics basics: a science called genetics, web-site:

http://www.nigms.nih.gov/news/science_ed/genetics/science.html

Osram (accessed on 23rd August 2004a), Osram Mercury Short Arc Lamps: HBO® 500 W/2, web-site:

http://www.osram.com.tw/pdf/service_corner/technicalinfo/500W2e.pdf

Osram (accessed on 23rd August 2004b) Mercury lamps / HBO mercury short-arc lamps from Osram, web-site:

http://www.msscientific.de/mercurylamps.htm

Regis Technologies (accessed on 15th October 2003), web-site:
http://www.registech.com/gc/

Seier J.V., Mdhluli M., Dhansay M.A., Loza J. and Laubscher R., April 2002, Final Report: a toxicity study of *Sutherlandia* leaf powder (*Sutherlandia microphylla*) consumption, Medical Research Council of South Africa, web-site:
http://www.sahealthinfo.org/traditionalmeds/firststudy.htm

Toyama Medical and Pharmaceutical University (accessed on 11th November 2004), web-site:
http://www.toyama-mpu.ac.jp/ph/yakka/research/dna.jpg

Weaver R.F. (accessed on 11th November 2004), Molecular Biology, web-site:
http://www.mhhe.com/biosci/cellmicro/weavermolbio/fig3.mhtml

APPENDIX A

A.1: Chemicals used for spectroscopic analysis

Chemical	Information
Methanol	HPLC grade, BDH, 99.8%
Ethyl acetate	GC grade, Riedel-de Haën, 99.5%
Ethyl acetate	H.W.O. Kleber chemicals
Cyclohexane	HPLC grade, Aldrich
Dichloromethane	HPLC grade, Lab-scan, Analytical sciences
Acetone	UnivAR, Saarchem, 99.5%
Ethanol	AnalaR, BDH, 99.7-100%
Ethanol	Spectro grade, Janssen Chimica, 90%
DMSO	GC grade, Merck, 99.8%
DMSO	GC grade, Riedel-de Haën, 99.7%
DMSO	HPLC grade, Sigma-Aldrich
Nitrogen	Afrox
Millipore water	Water purified by the Milli-Q^{50} ultra pure water apparatus
EHMC	BASF
Peg-25 PABA	BASF
MBC	Merck
IMC	Haarmann & Reimer
Menthyl anthranilate	Haarmann & Reimer
Octyl dimethyl *p*-aminobenzoic acid	Edenchem
Phenylbenzimidazole sulfonic acid	Haarmann & Reimer
2,4-dihydroxybenzophenone	BASF
2,2',4,4'-tetrahydroxybenzophenone	BASF
2-hydroxy-4-methoxybenzophenone	BASF
2-hydroxy-4-methoxybenzophenone-5-sulfonic acid	BASF

Chemical	Information
2,2'-dihydroxy-4,4'-dimethoxybenzophenone	Lancaster, 98%
2-hydroxy-4-n-octyloxybenzophenone	Lancaster, 98%
Avobenzone	BASF

A.2: Chemicals used for gas chromatographic analysis

Chemical	Information
Avobenzone	BASF
BSA	Sigma, GC grade, minimum 90%
BSTFA	Aldrich, 99+%
Pyridine	BDH, AnalaR, 99.5%
Ethyl acetate	GC grade
Cyclohexane	HPLC grade, Aldrich
DMSO	GC grade, Merck, 99.8%
Air	Fedgas
Hydrogen	Fedgas
Nitrogen	Fedgas

A.3: Chemicals used for HPLC analysis

Chemical	Information
Avobenzone	BASF
Methanol	HPLC grade, BDH, 99.8%
Millipore water	Water purified by the Milli-Q^{50} ultra pure water apparatus
Acetic acid glacial	BDH, 99.7%
Acetonitrile	HPLC grade, BDH, 99.9%
Tetrahydrofuran	HPLC grade, Riedel-de Haën, 99.9%
Caffeine	Lancaster, 99+%
Hydrochloric acid	BDH, 33%
Helium	High purity, Instrument grade, Afrox, 99.999%

A.4: Chemicals used for NMR analysis

Chemical	Information
Methyl sulfoxide-d_6	Acros, 99.9 atom %
Cyclohexane-d_{12}	Aldrich, 99.6 atom %

A.5: Other products, chemicals and reagents

Chemical	Information
Folin-Ciocalteu reagent	Merck
Rooibos tea	Tea4kids, Phendula tea (for kids)
Rooibos-honeybush tea	Tea4kids, Phendula tea (for kids)
Rooibos-black tea	Tea4kids, Phendula tea (for kids)
Rutin	Donated by Doctor Carl Albrecht
Epicatechin	Donated by Doctor Carl Albrecht
Gallic acid	Donated by Doctor Carl Albrecht
Cancer Bush leaves	Donated by Doctor Carl Albrecht
JOKO tea	JOKO top quality tea bags
Sodium carbonate	UniLAB, 99%
DPPH	Aldrich, 95%

A.6: Equipment

Osram HBO 500 W/2 high pressure mercury lamp

Perkin Elmer Lambda 35 UV/VIS spectrophotometer

Cary 1E UV/VIS spectrophotometer

HPLC instrument: a Perkin Elmer series 200 autosampler, a Waters 600 multisolvent delivery system, a Waters 996 photodiode array detector (PDA)

Perkin Elmer Autosystem XL gas chromatograph

Fisons GC 8000 Series gas chromatograph

Agilent 6890 gas chromatograph coupled to an Agilent 5973 mass selective detector

Hewlett Packard 6890 series GC system coupled to a Hewlett Packard 6890 mass selective detector

300 MHz Varian Gemini NMR

400 MHz Varian Unity Inova NMR Instrument

Milli-Q^{50} ultra pure water apparatus

Mettler orbital shaker apparatus

APPENDIX B

B.1: GC-MS results for the photostability of avobenzone in different solvents
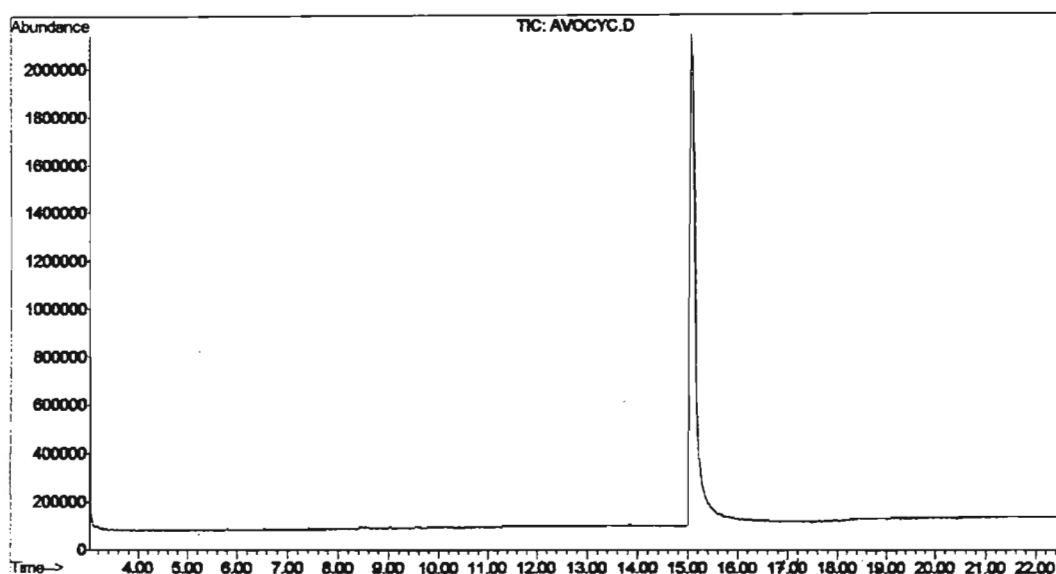
Figure B1.1: Total ion chromatogram of a 1×10^{-2} M avobenzone solution in cyclohexane before irradiation, eluted through an HP-5MS column according to the conditions described in Section 2.7.
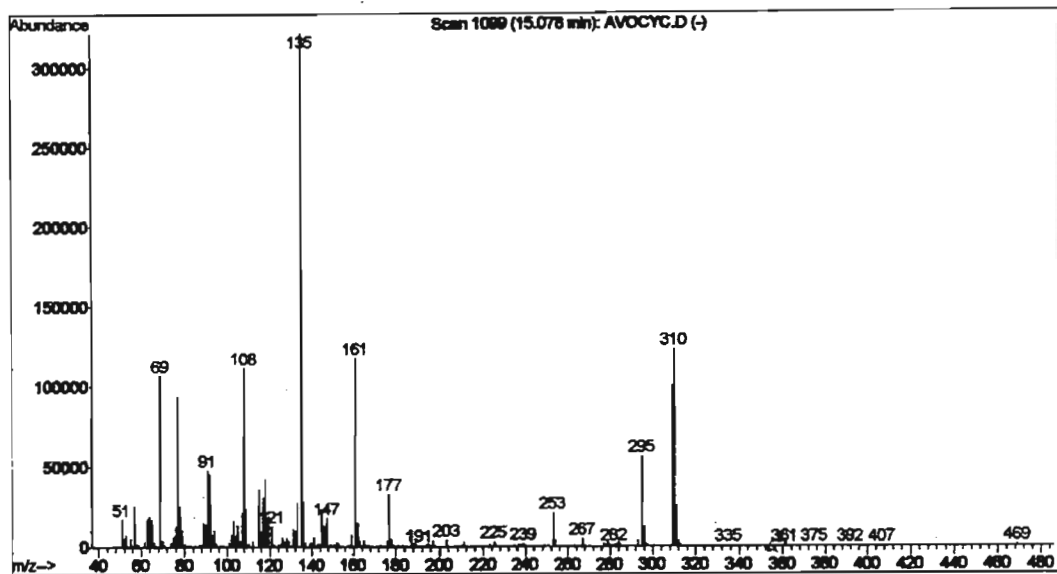
Figure B1.2:   Mass spectrum of avobenzone that eluted at 15.078 minutes in the chromatogram in Figure B1.1.
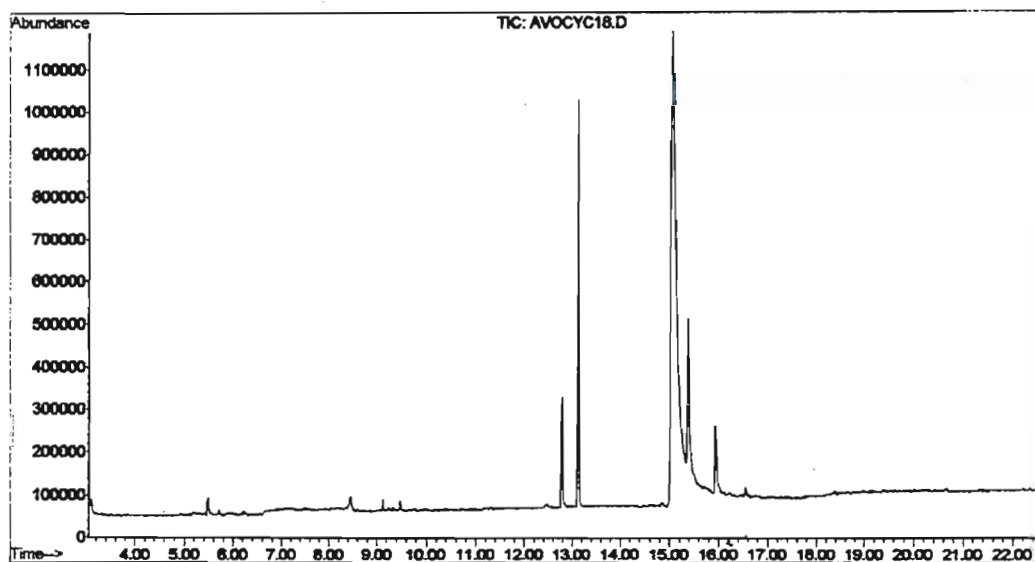
Figure B2.1:   Total ion chromatogram of a 1×10^{-2} M avobenzone solution in cyclohexane after 18 hours of irradiation, eluted through the HP-5MS column according to the conditions described in Section 2.7.
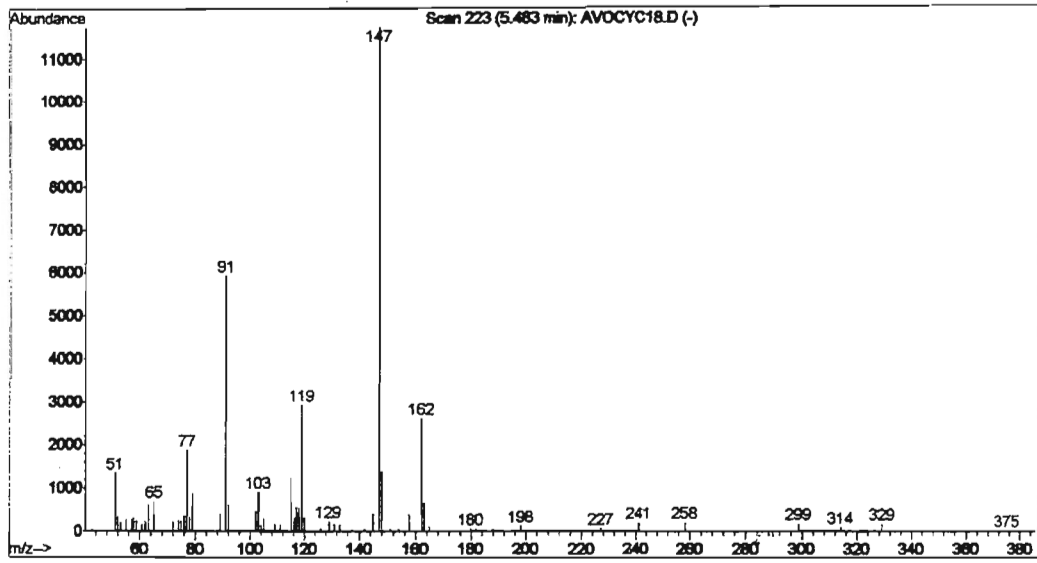
Figure B2.2:   Mass spectrum of 4-*t*-butyl benzaldehyde (Schwack and Rudolph [1995]) that eluted at 5.483 minutes in the chromatogram in Figure B2.1.
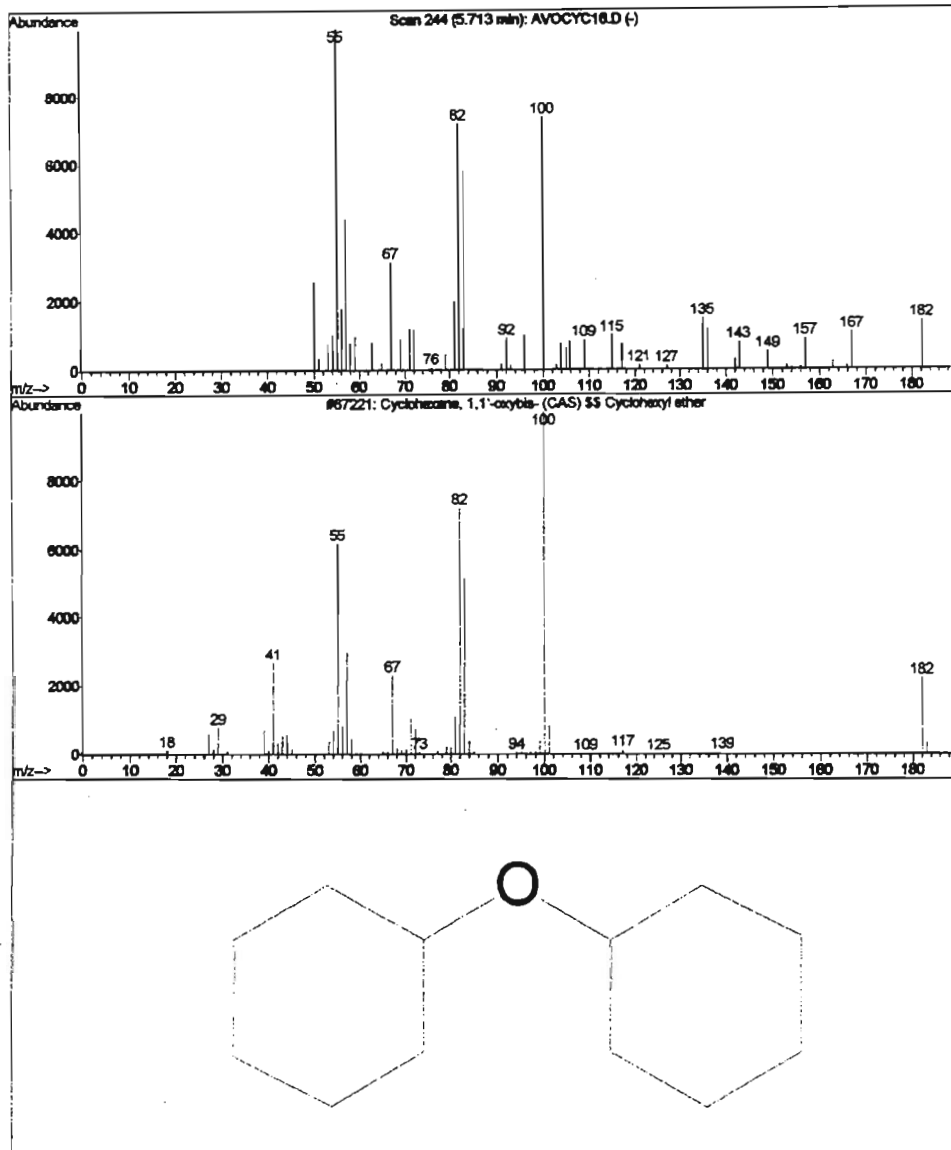
Figure B2.3:   Mass spectrum of dicyclohexyl ether, as matched by the Wiley275 library, which eluted at 5.713 minutes in the chromatogram in Figure B2.1.
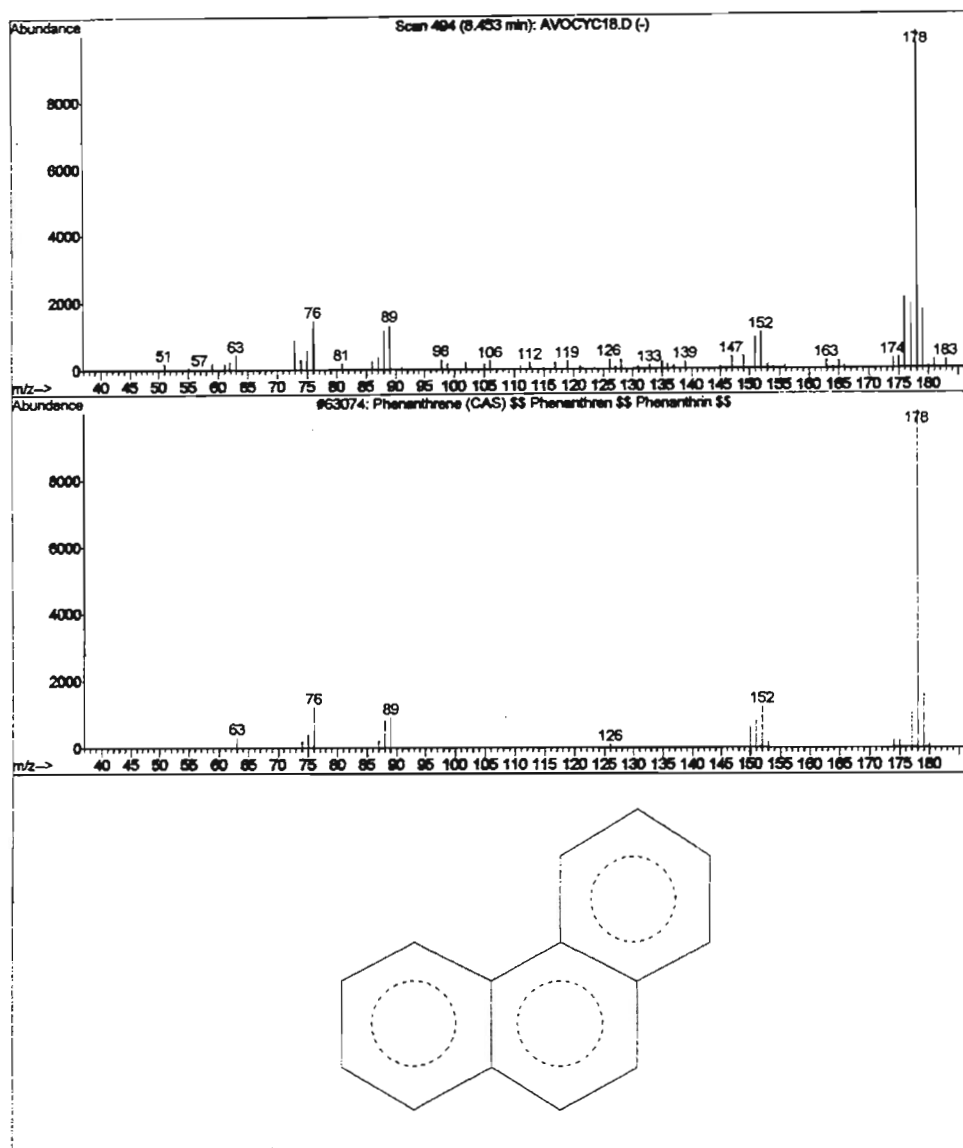
Figure B2.4:   Mass spectrum of phenanthrene, as matched by the Wiley275 library, which eluted at 8.453 minutes in the chromatogram in Figure B2.1.
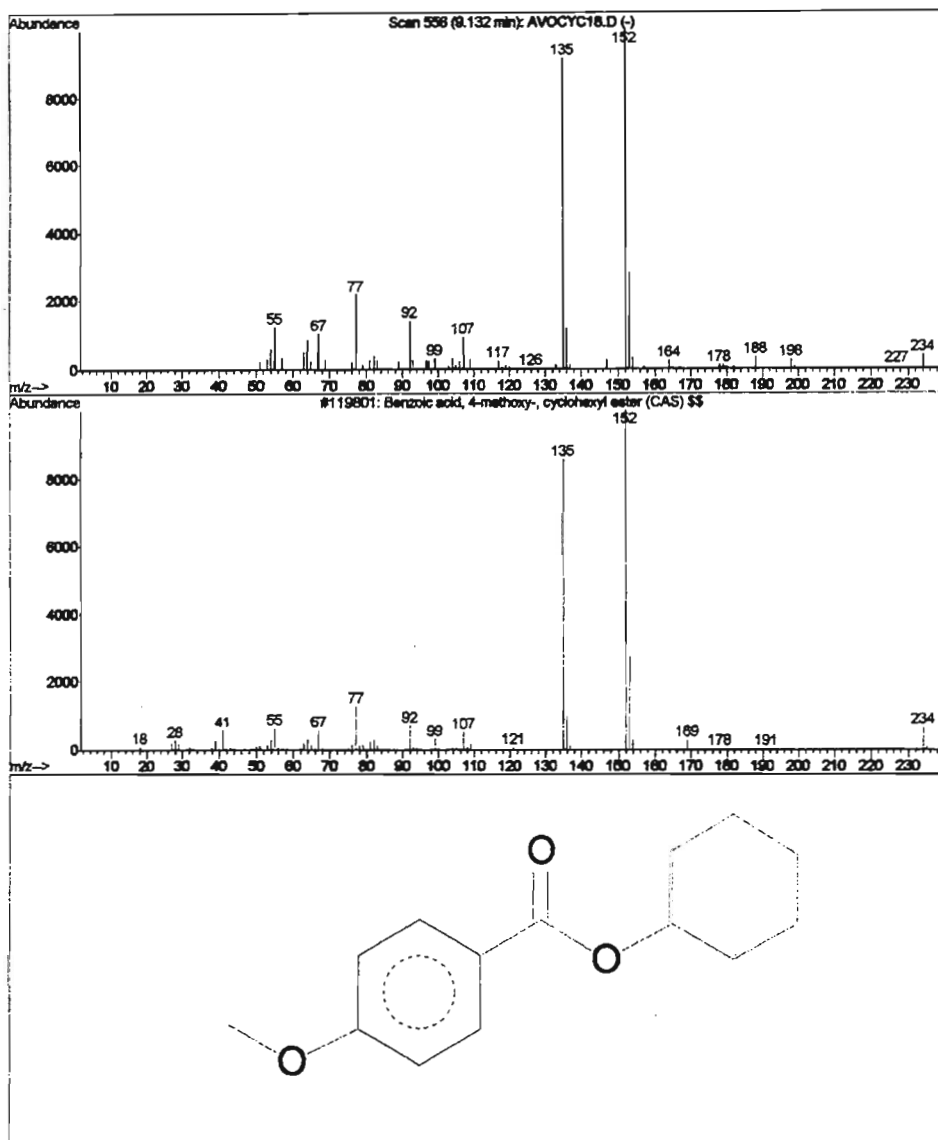
Figure B2.5:   Mass spectrum of 4-methoxy benzoic acid (Schwack and Rudolph [1995]), as matched by the Wiley275 library, which eluted at 9.132 minutes in the chromatogram in Figure B2.1.
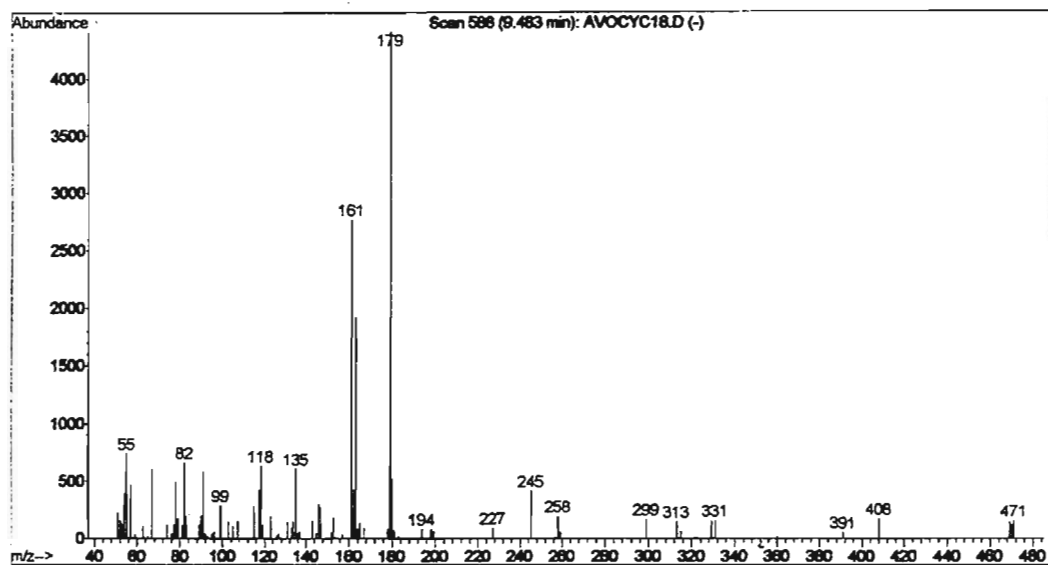
Figure B2.6: Mass spectrum of an unknown compound that eluted at 9.483 minutes in the chromatogram in Figure B2.1.
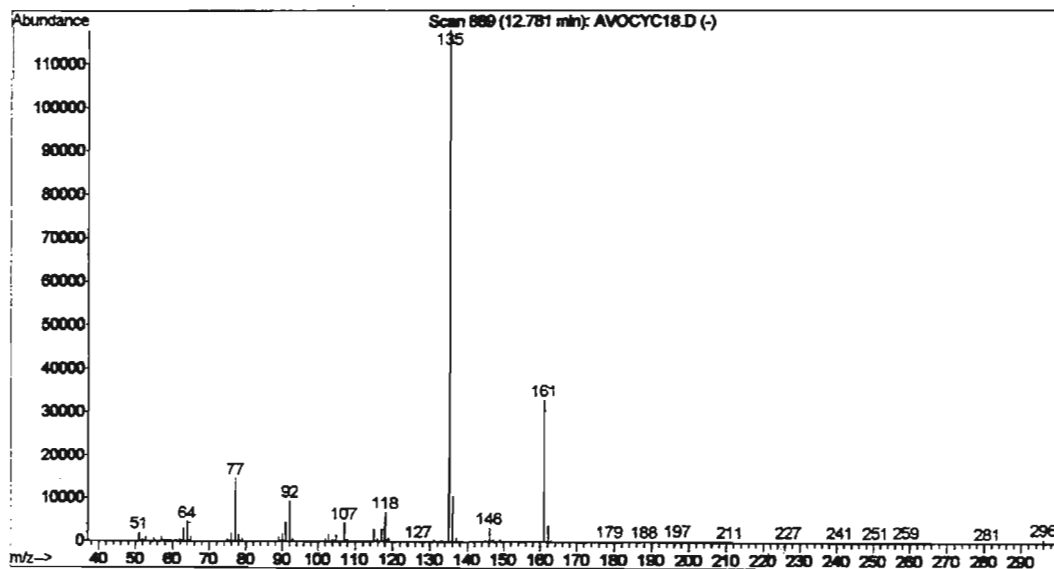
Figure B2.7: Mass spectrum of 4-*t*-butyl-4'-methoxy benzil (Schwack and Rudolph [1995]) that eluted at 12.781 minutes in the chromatogram in Figure B2.1.
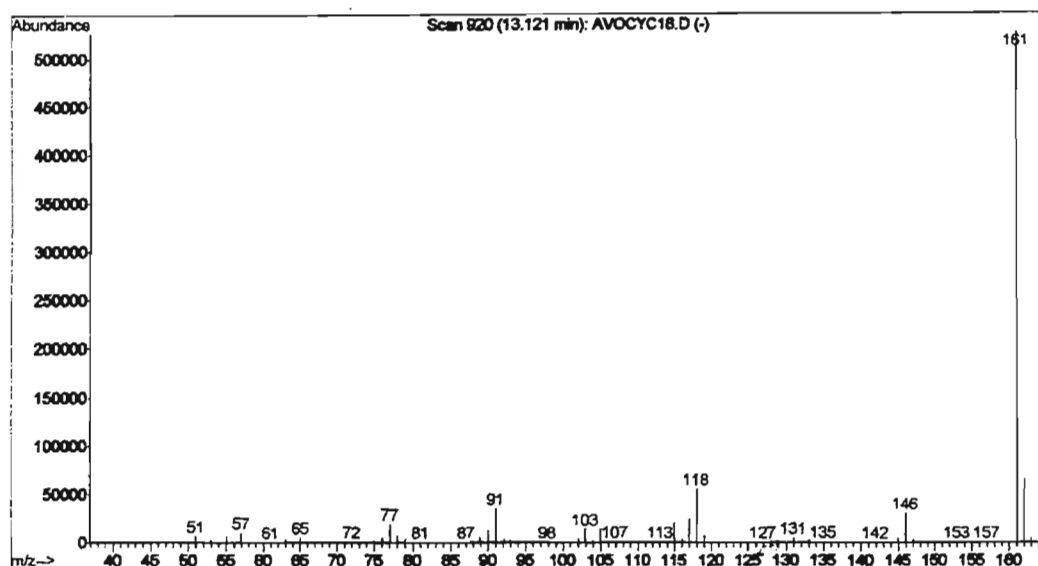
Figure B2.8:   Mass spectrum of 4-*t*-butyl phenyglyoxal (Schwack and Rudolph [1995]) that eluted at 13.121 minutes in the chromatogram in Figure B2.1.
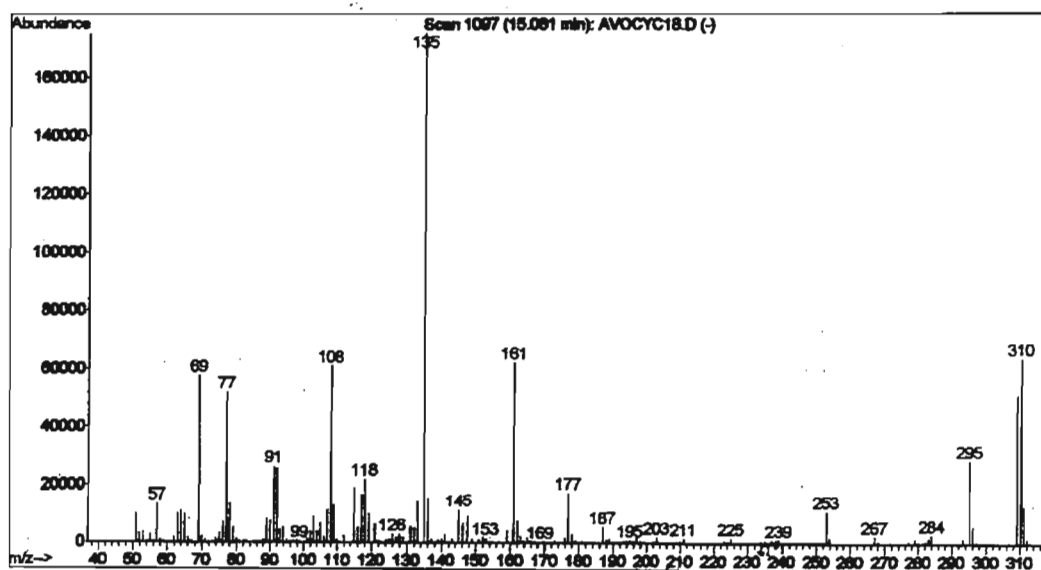
Figure B2.9:   Mass spectrum of avobenzone that eluted at 15.081 minutes in the chromatogram in Figure B2.1.
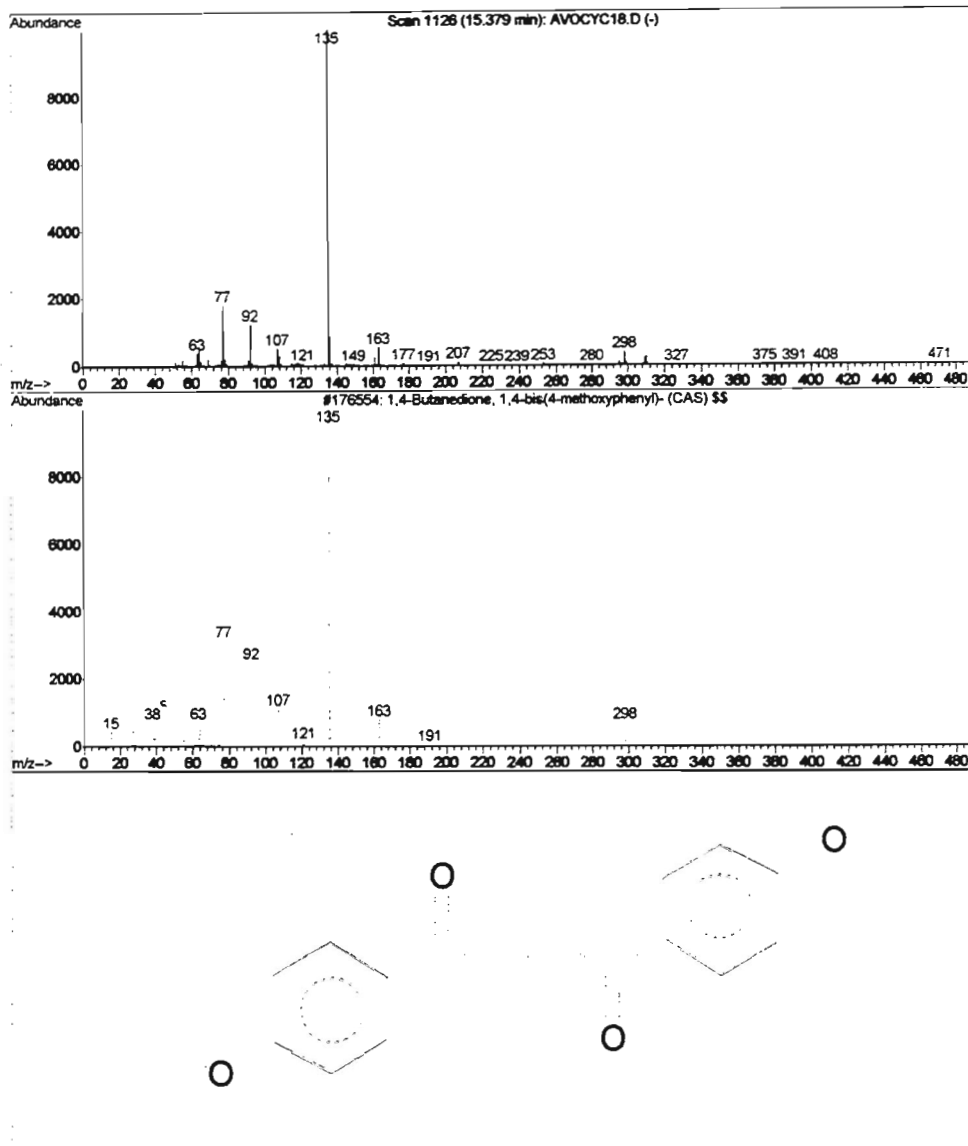
Figure B2.10:   Mass spectrum of 4-methoxy benzyl compound that eluted at 15.379 minutes in the chromatogram in Figure B2.1, as matched from the Wiley275 library.
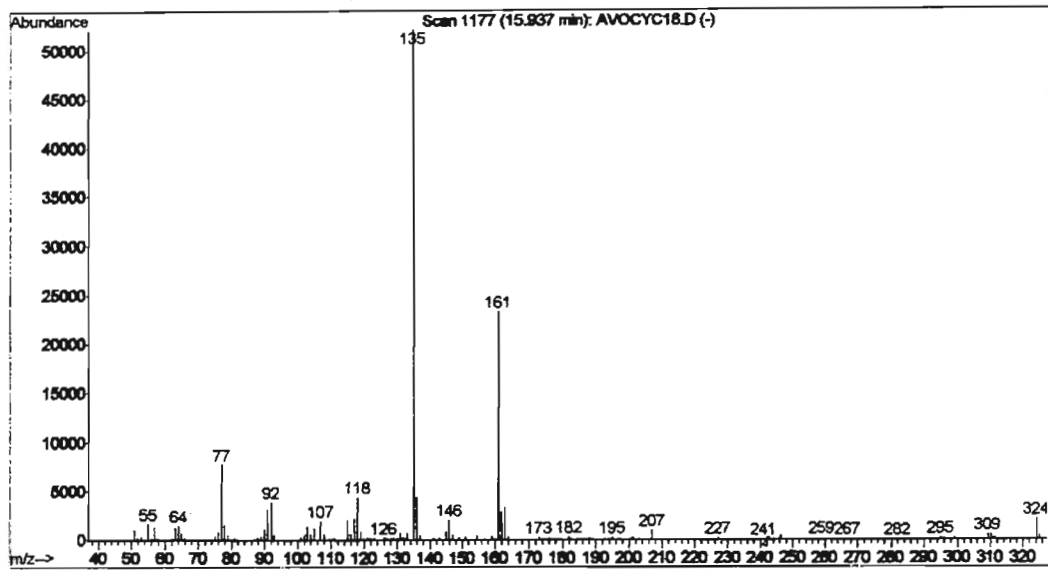
Figure B2.11:   Mass spectrum of 4-*t*-butyl-4'-methoxydibenzoyl ethane (Schwack and Rudolph [1995]) that eluted at 15.937 minutes in the chromatogram in Figure B2.1.
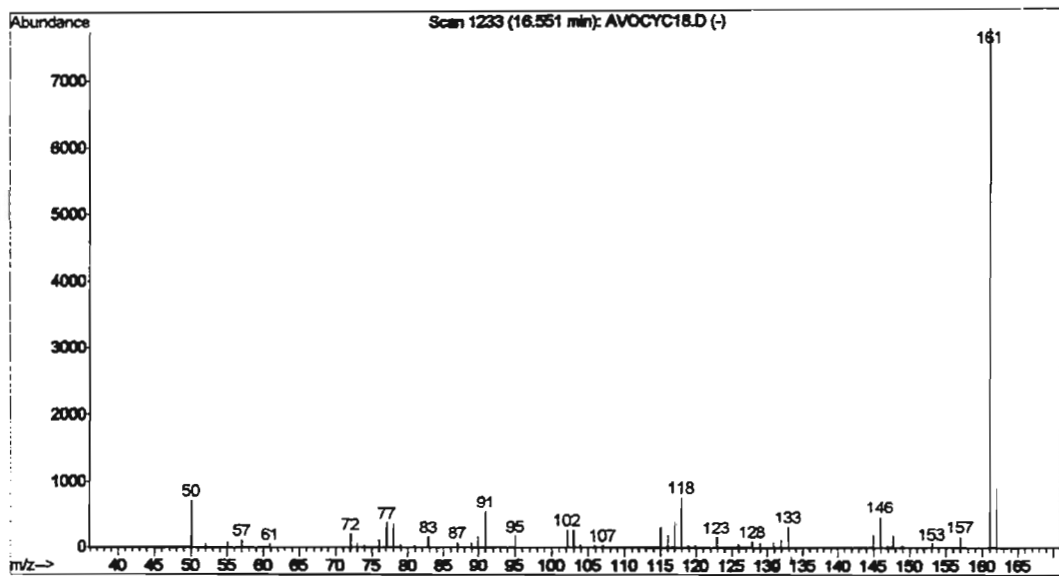
Figure B2.12:   Mass spectrum of 4,4'-di-*t*-butyl benzyl (Schwack and Rudolph [1995]) that eluted at 16.551 minutes in the chromatogram in Figure B2.1.
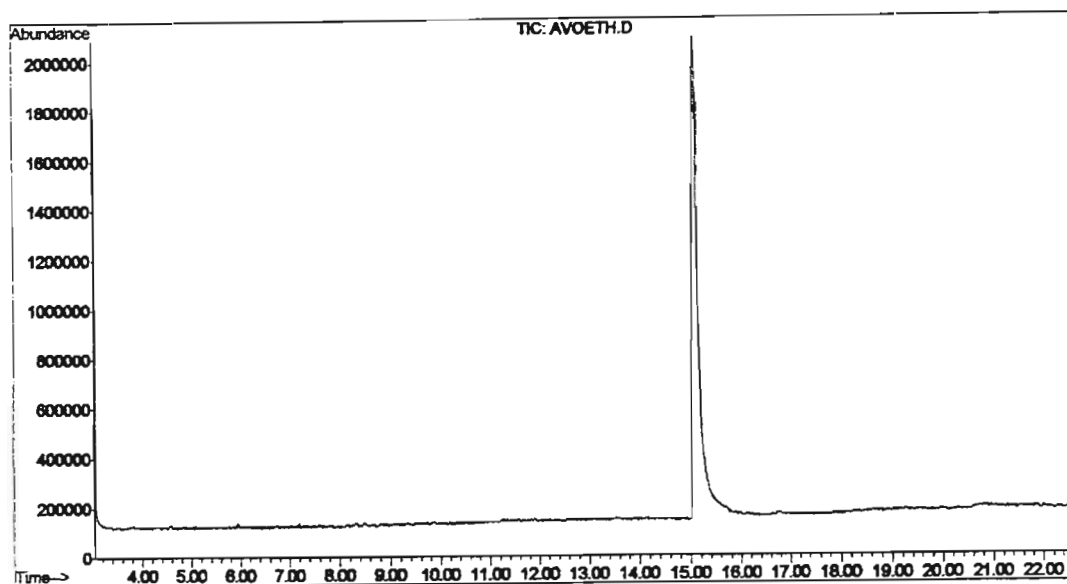
Figure B3.1: Total ion chromatogram of a 1×10^{-2} M avobenzone solution in ethyl acetate before irradiation, eluted through the HP-5MS column according to the conditions described in Section 2.7.
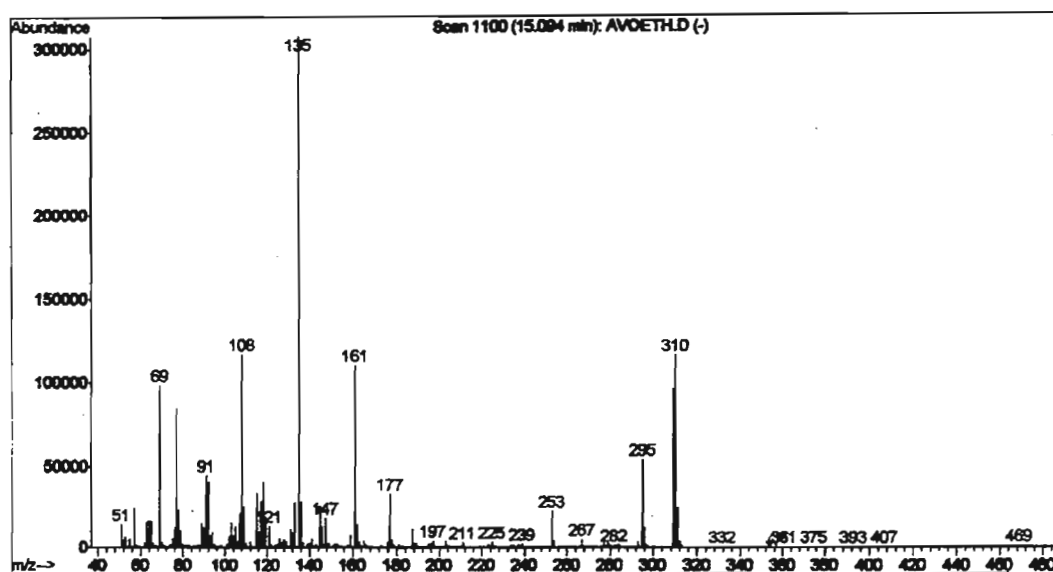
Figure B3.2: Mass spectrum of avobenzone that eluted at 15.094 minutes in the chromatogram in Figure B3.1.
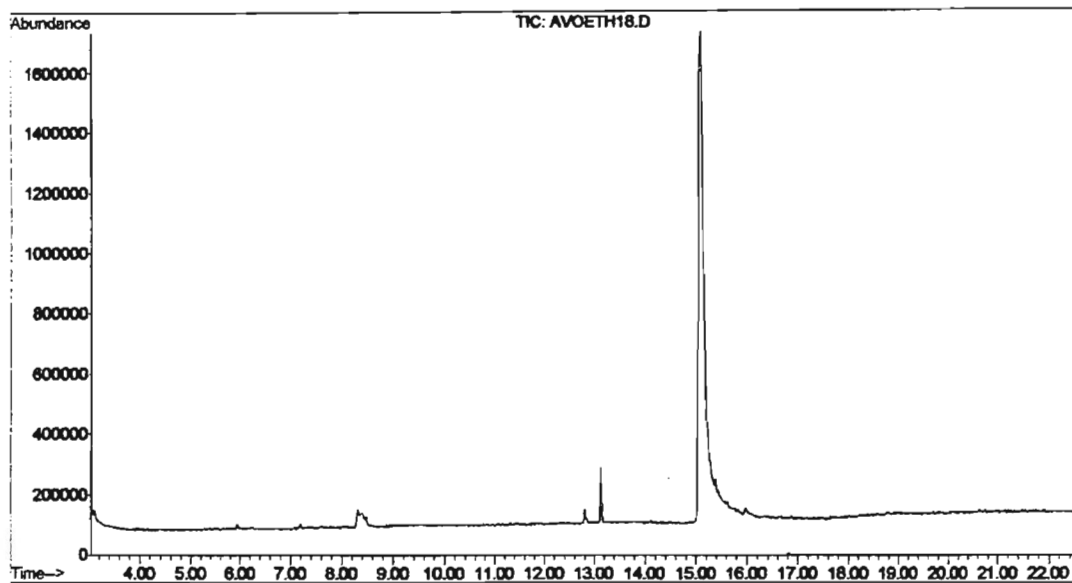
Figure B4.1:   Total ion chromatogram of a 1×10^{-2} M avobenzone solution in ethyl acetate after 18 hours of irradiation, eluted through the HP-5MS column according to the conditions described in Section 2.7.
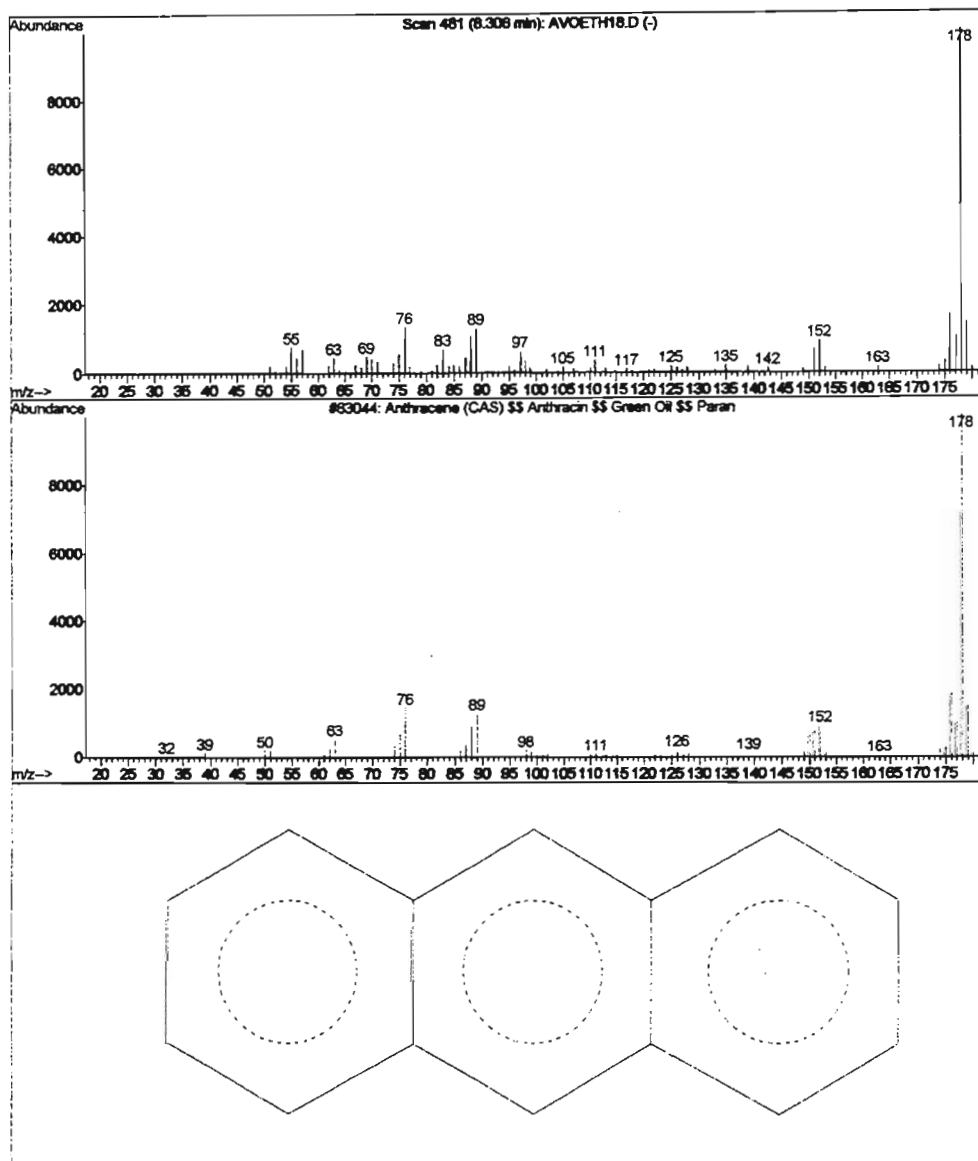
Figure B4.2:   Mass spectrum of anthracene, as matched by the Wiley275 library, which eluted at 8.306 minutes in the chromatogram in Figure B4.2.
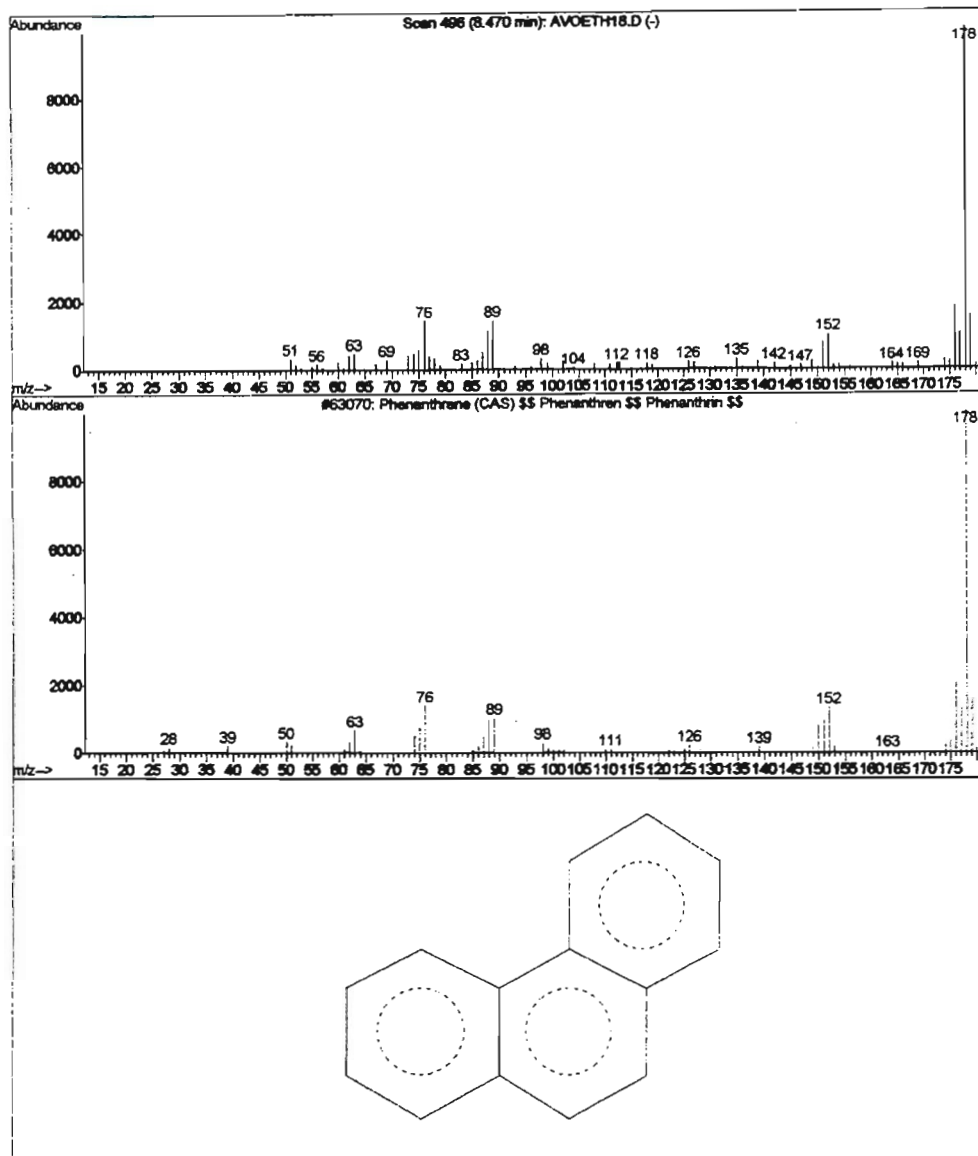
Figure B4.3:   Mass spectrum of phenanthrene, as matched by the Wiley275 library, which eluted at 8.481 minutes in the chromatogram in Figure B4.1.
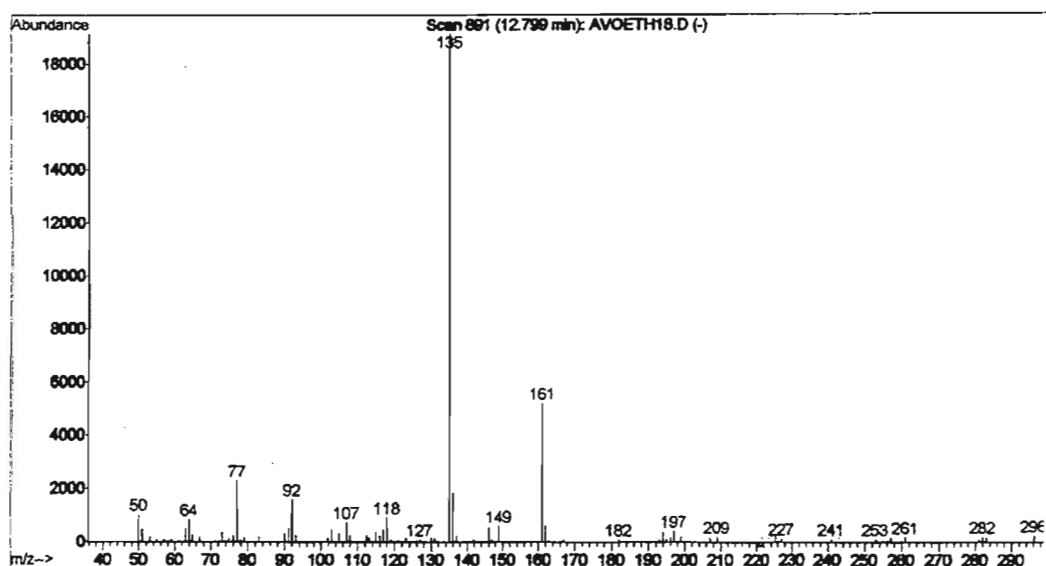
Figure B4.4: Mass spectrum of 4-*t*-butyl-4'-methoxy benzyl (Schwack and Rudolph [1995]) that eluted at 12.799 minutes in the chromatogram in Figure B4.1.
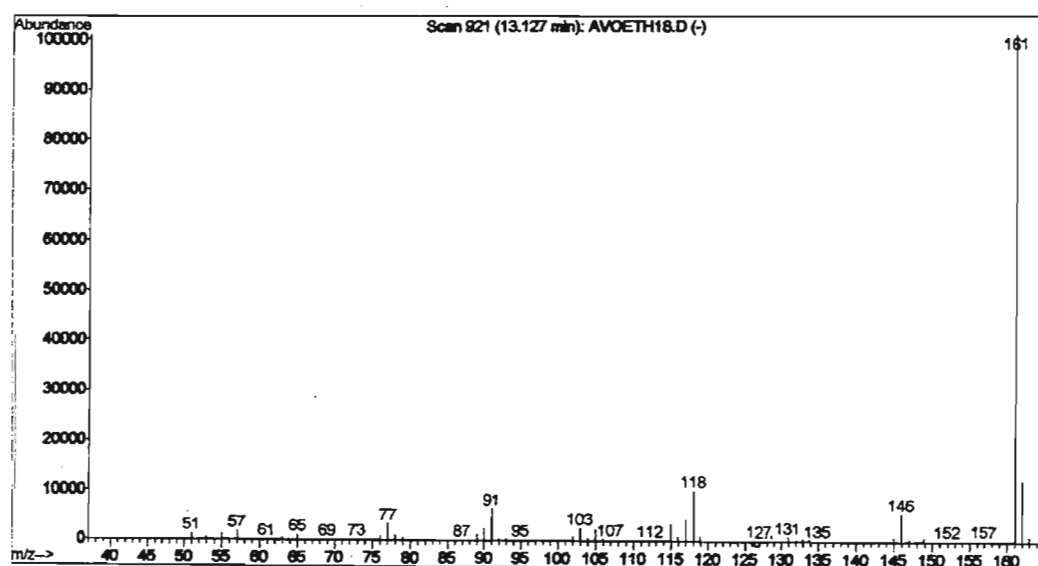
Figure B4.5: Mass spectrum of 4-t-butyl phenylglyoxal (Schwack and Rudolph [1995]) that eluted at 13.127 minutes in the chromatogram in Figure B4.1.
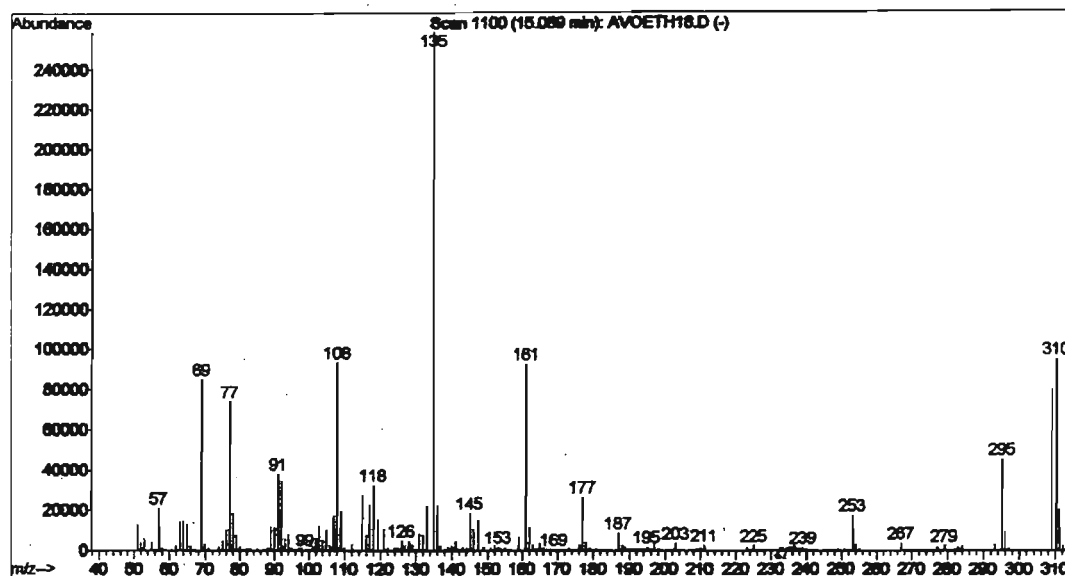
Figure B4.6:   Mass spectrum of avobenzone that eluted at 15.089 minutes in the chromatogram in Figure B4.1.
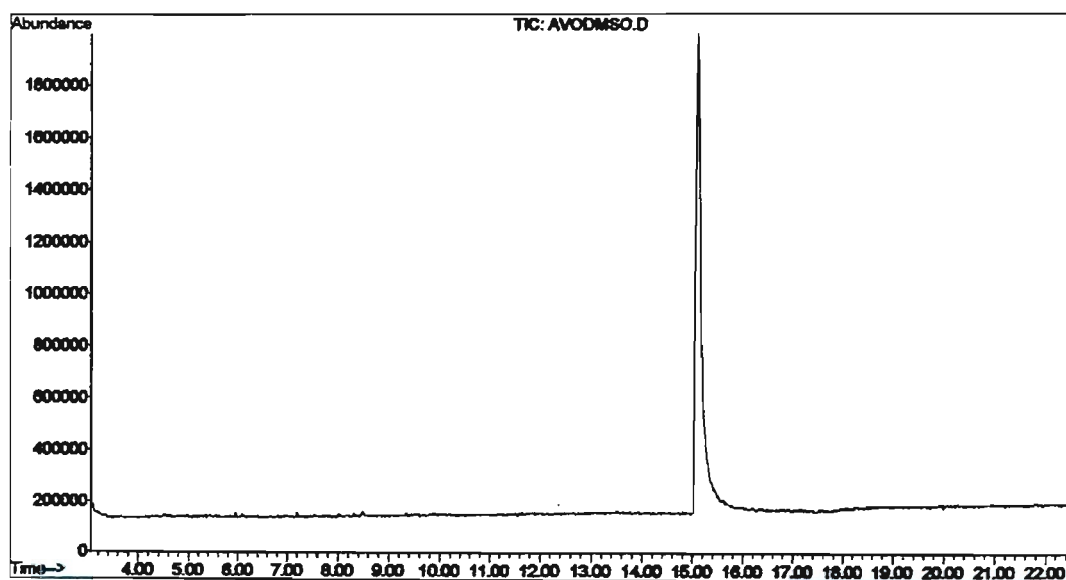
Figure B5.1:   Total ion chromatogram of a 1×10^{-2} M avobenzone solution in DMSO before irradiation, eluted through the HP-5MS column according to the conditions described in Section 2.7.
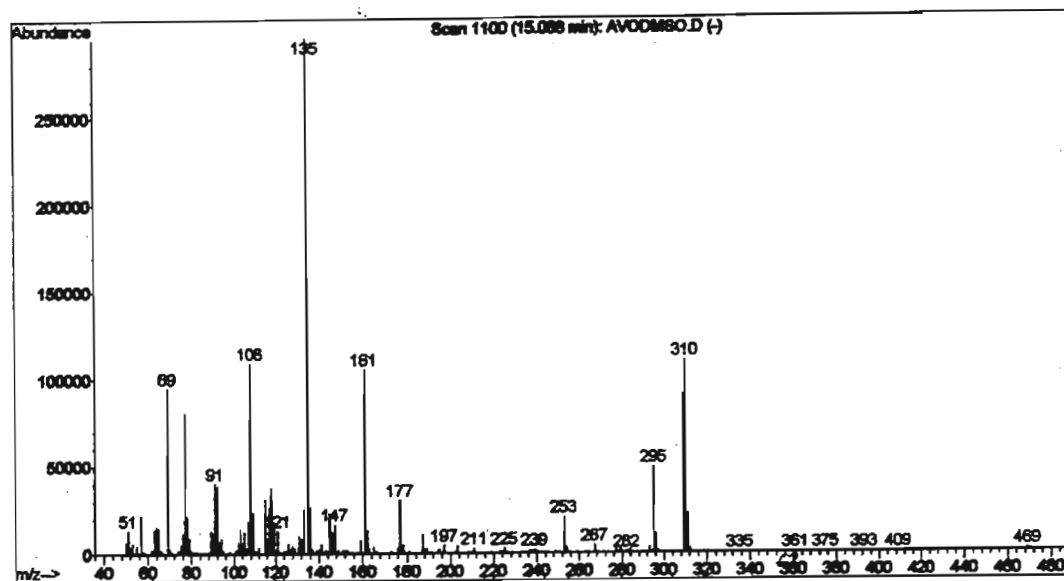
Figure B5.2:   Mass spectrum of avobenzone that eluted at 15.088 minutes in the chromatogram in Figure B5.1.
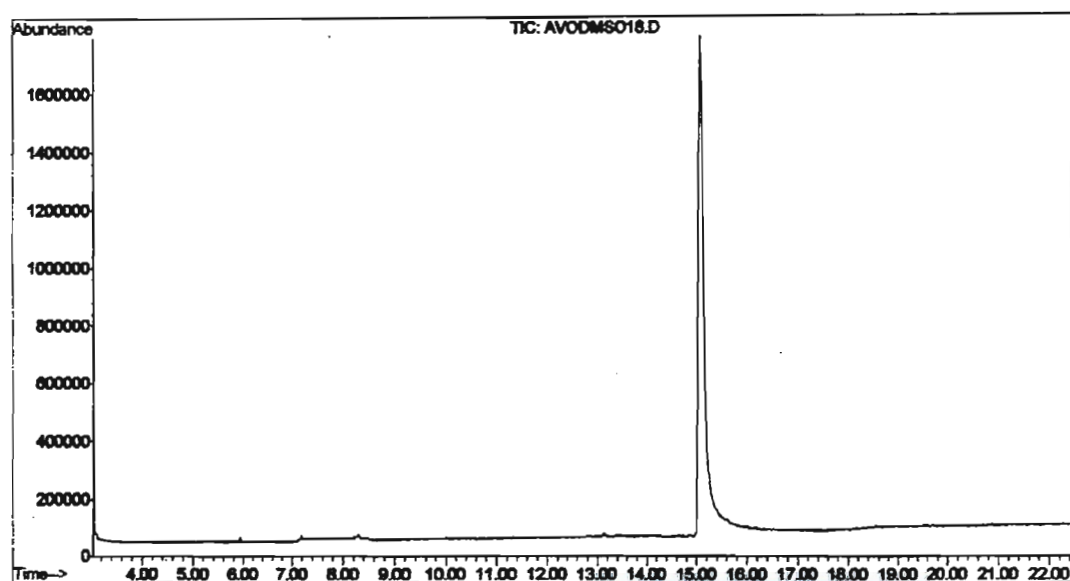
Figure B6.1:   Total ion chromatogram of a 1×10^{-2} M avobenzone solution in DMSO after 18 hours of irradiation, eluted through the HP-5MS column according to the conditions described in Section 2.7.
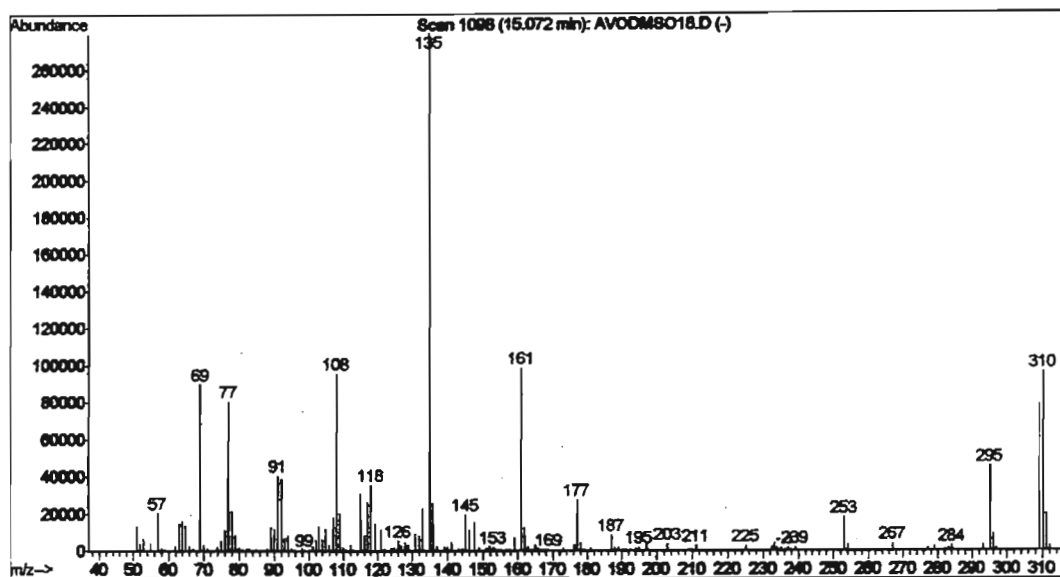
Figure B6.2:   Mass spectrum of avobenzone that eluted at 15.072 minutes in the chromatogram in Figure B6.1.

APPENDIX C

C.1: GC-MS results for the ethanol-water extracts
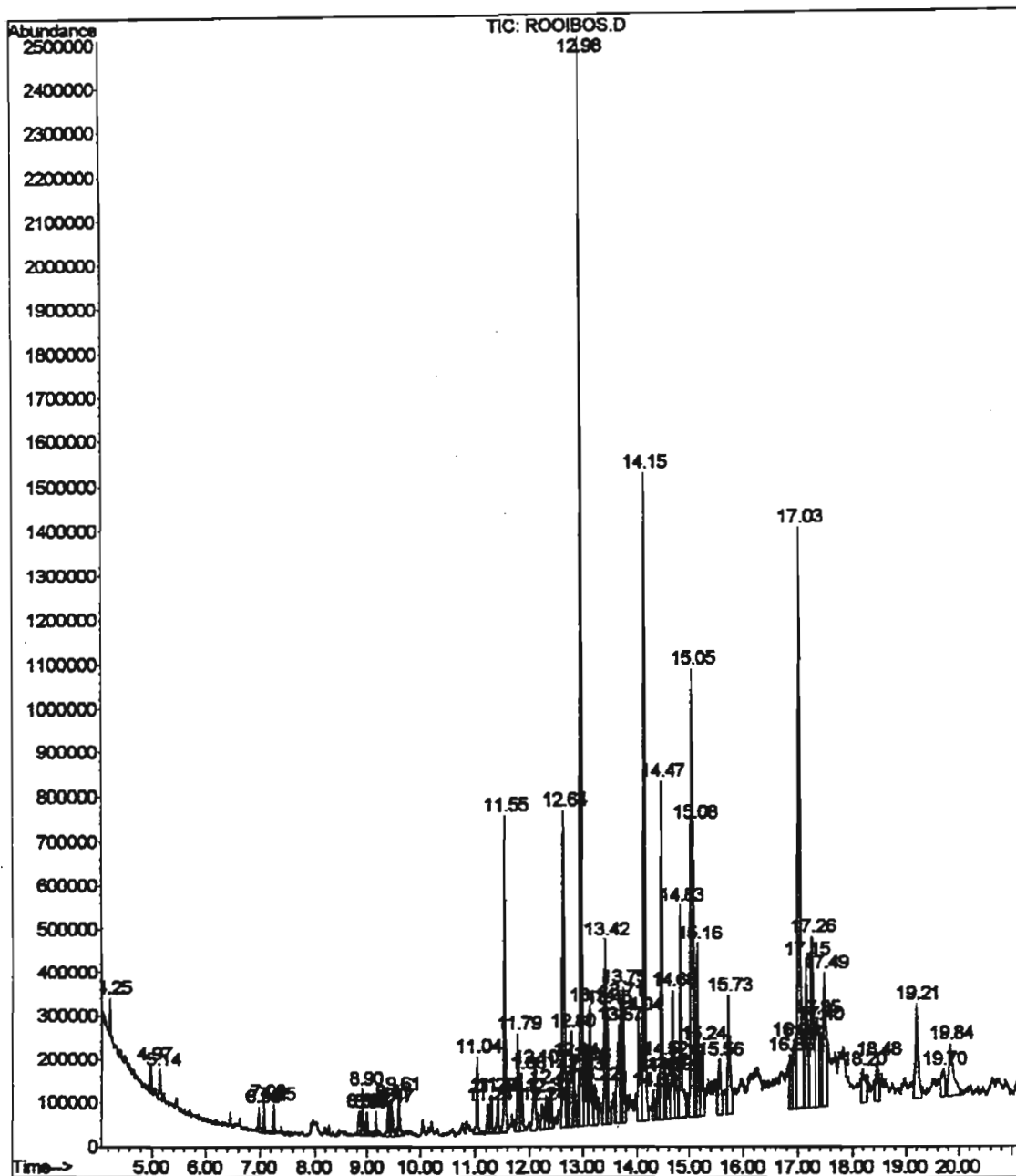
Figure C1.1: Total ion chromatogram of the ethanol-water Rooibos tea extract, derivatised by BSTFA/pyridine and eluted through the HP-5MS column of the Agilent 6890 GC-MS by conditions described in Section 2.7.2.1.
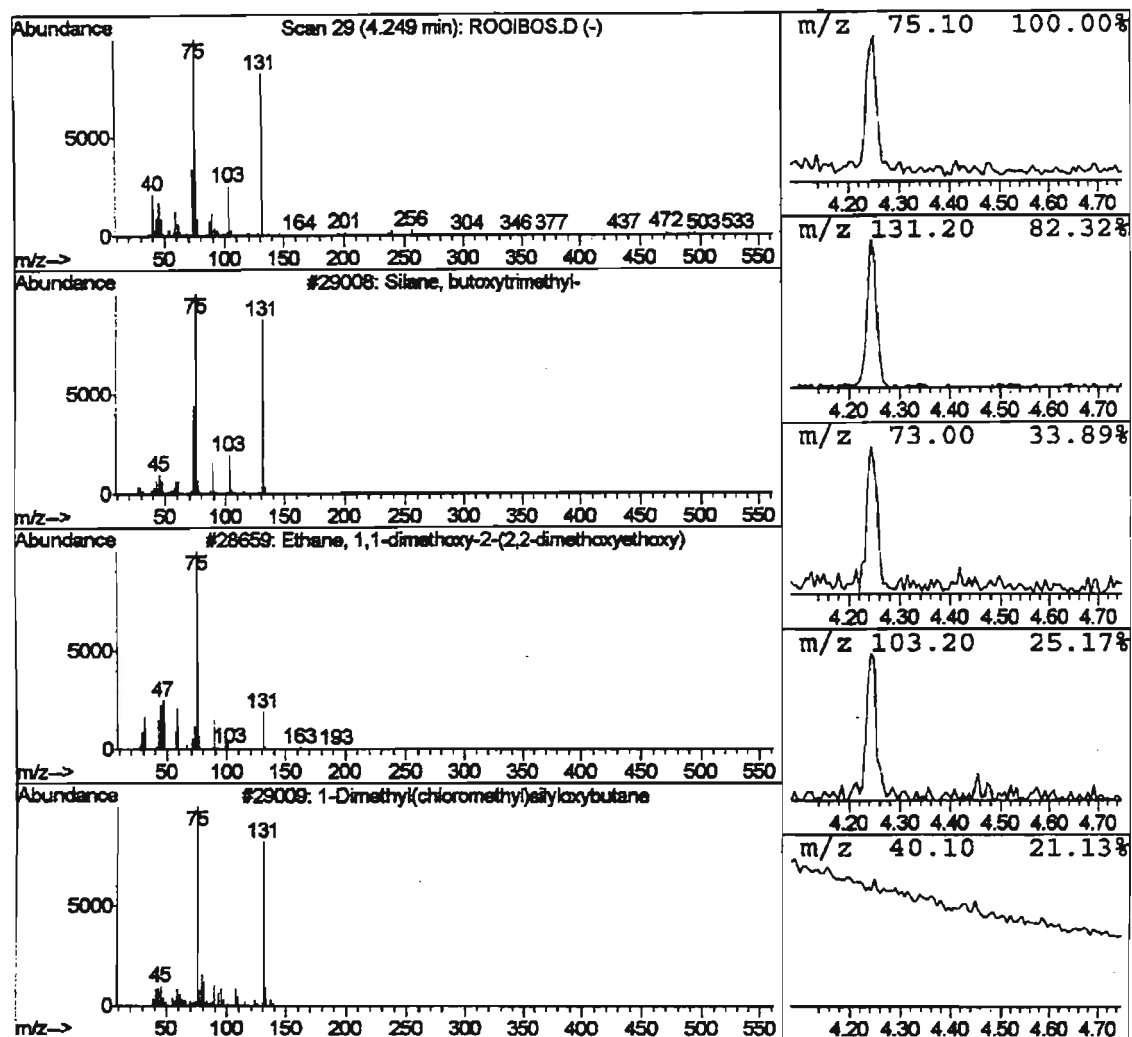
Figure C1.2:   Mass spectrum of an unknown compound eluting at 4.249 minutes. The mass spectrum of the unknown compound is at the top left corner, below it are the best matches from the NIST98 library, in descending order. On the left hand side are the abundances of each fragment peak in descending order.
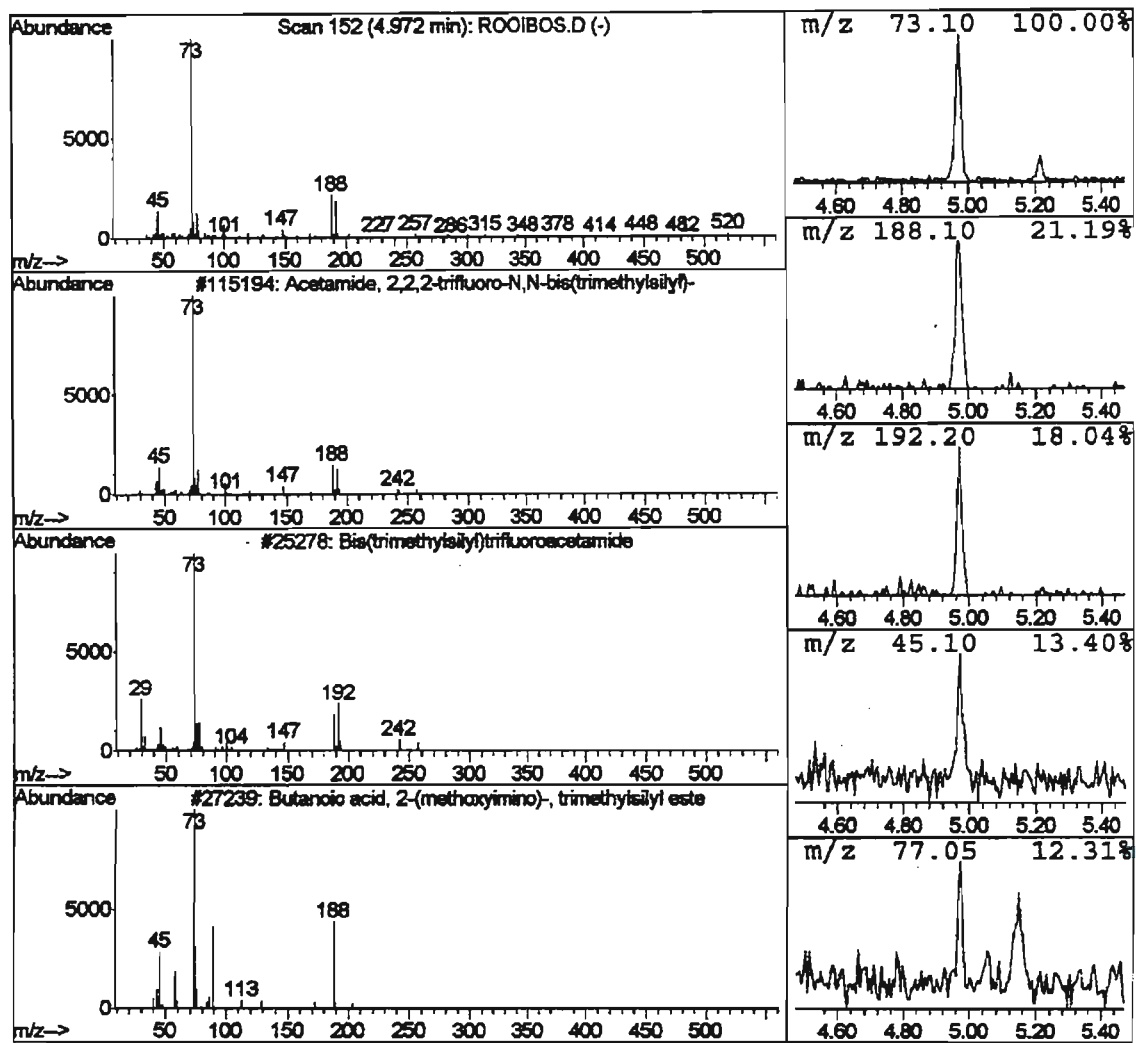
Figure C1.3: Mass spectrum of a derivatised BSTFA that elutes at 4.972 minutes. The fragmentation pattern matched that of a derivatised BSTFA present in the library.
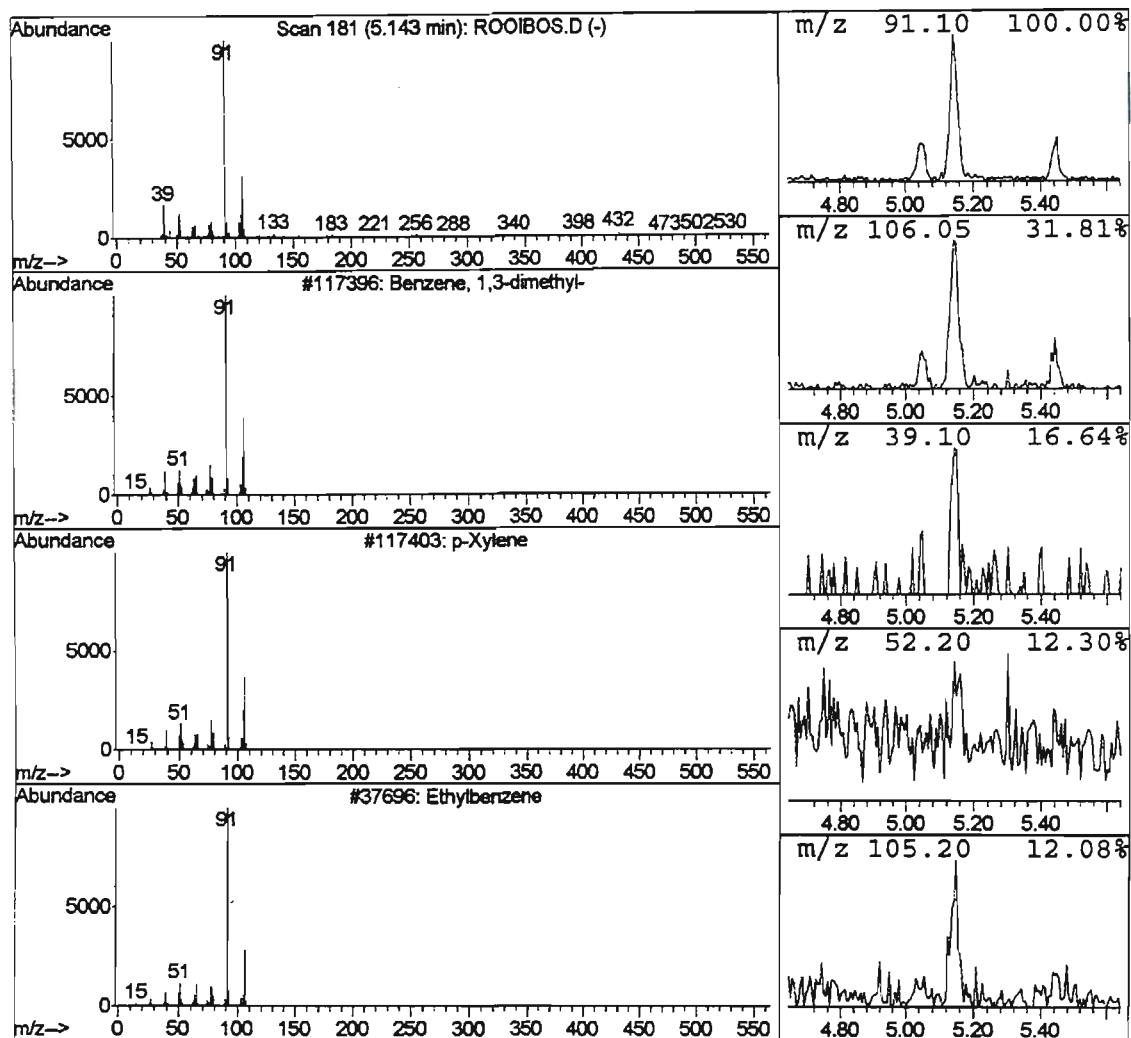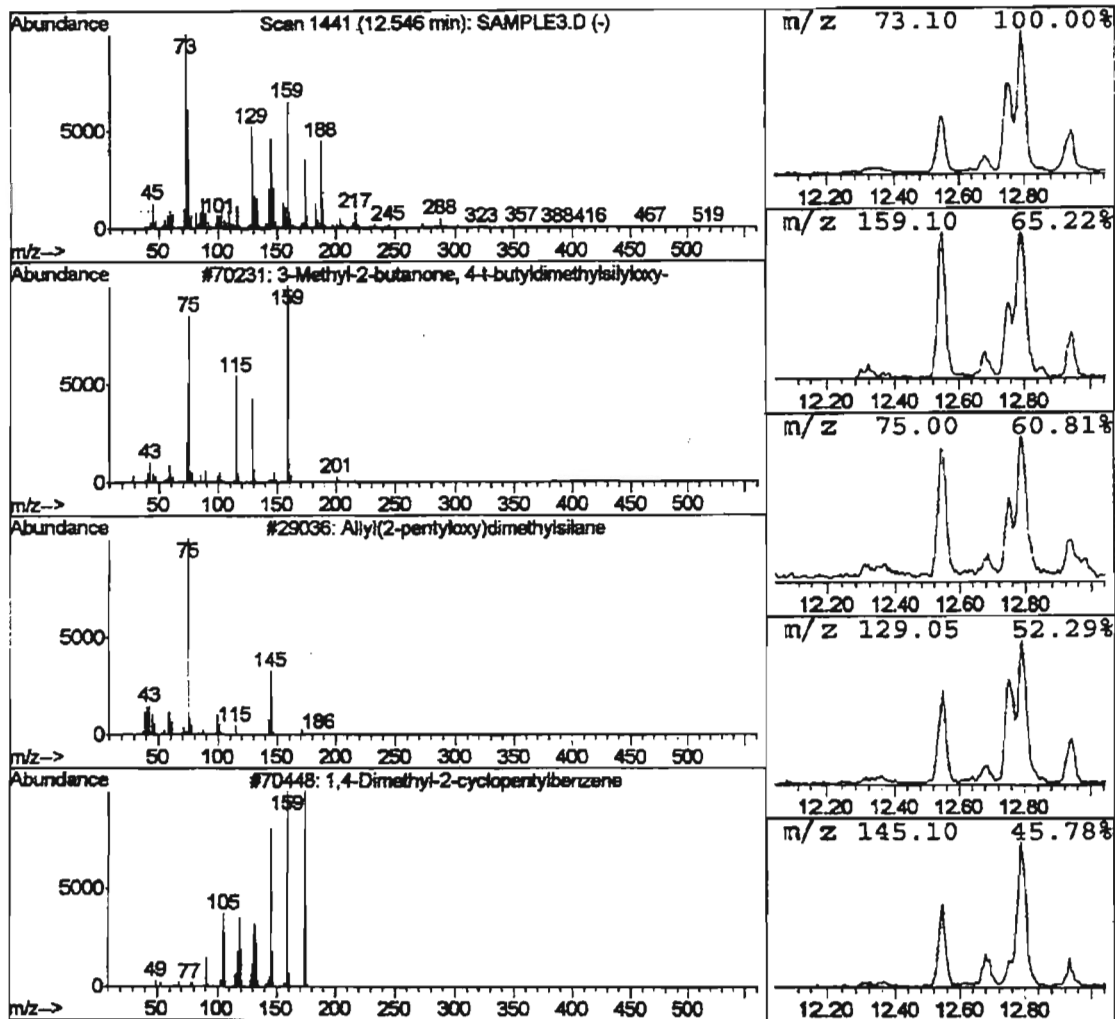
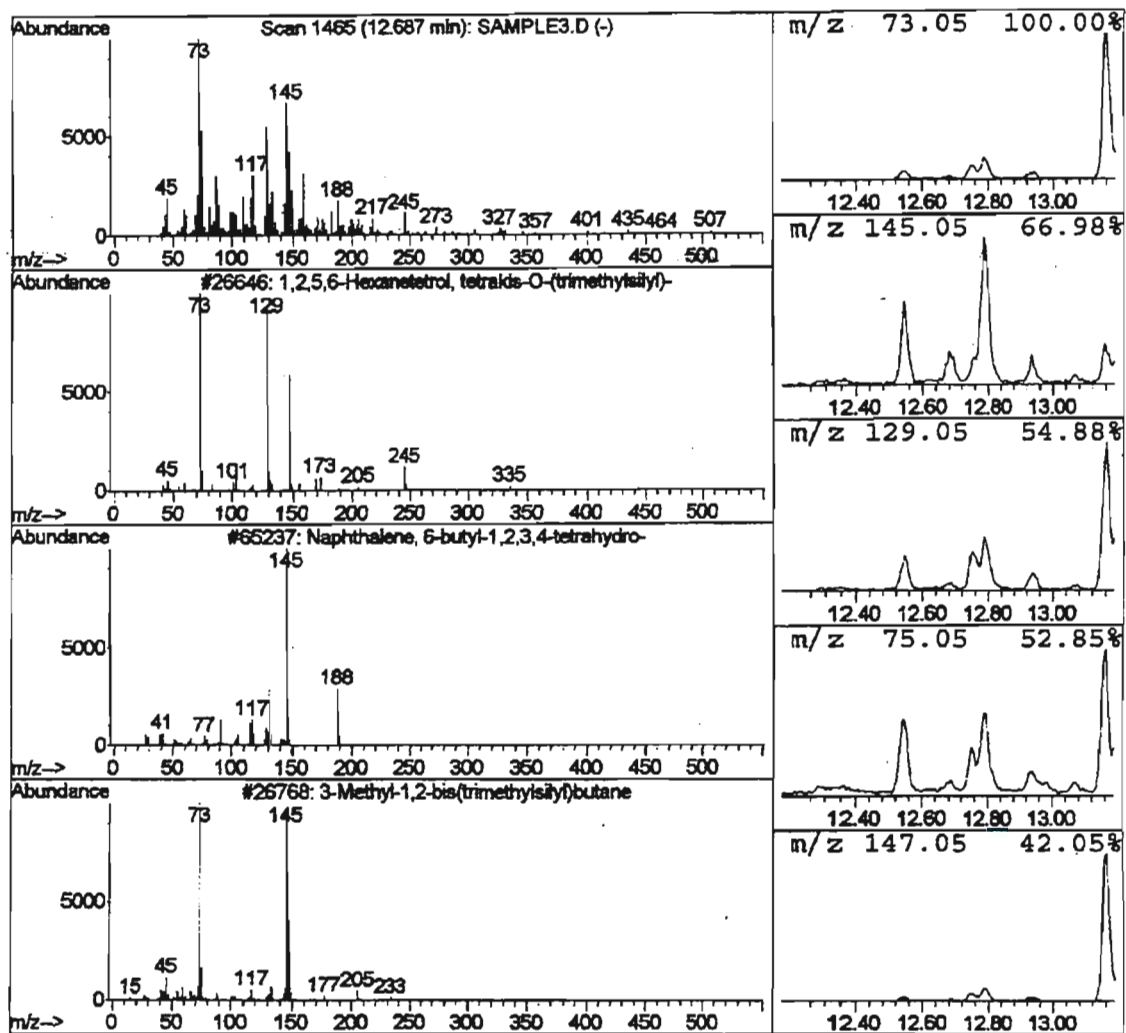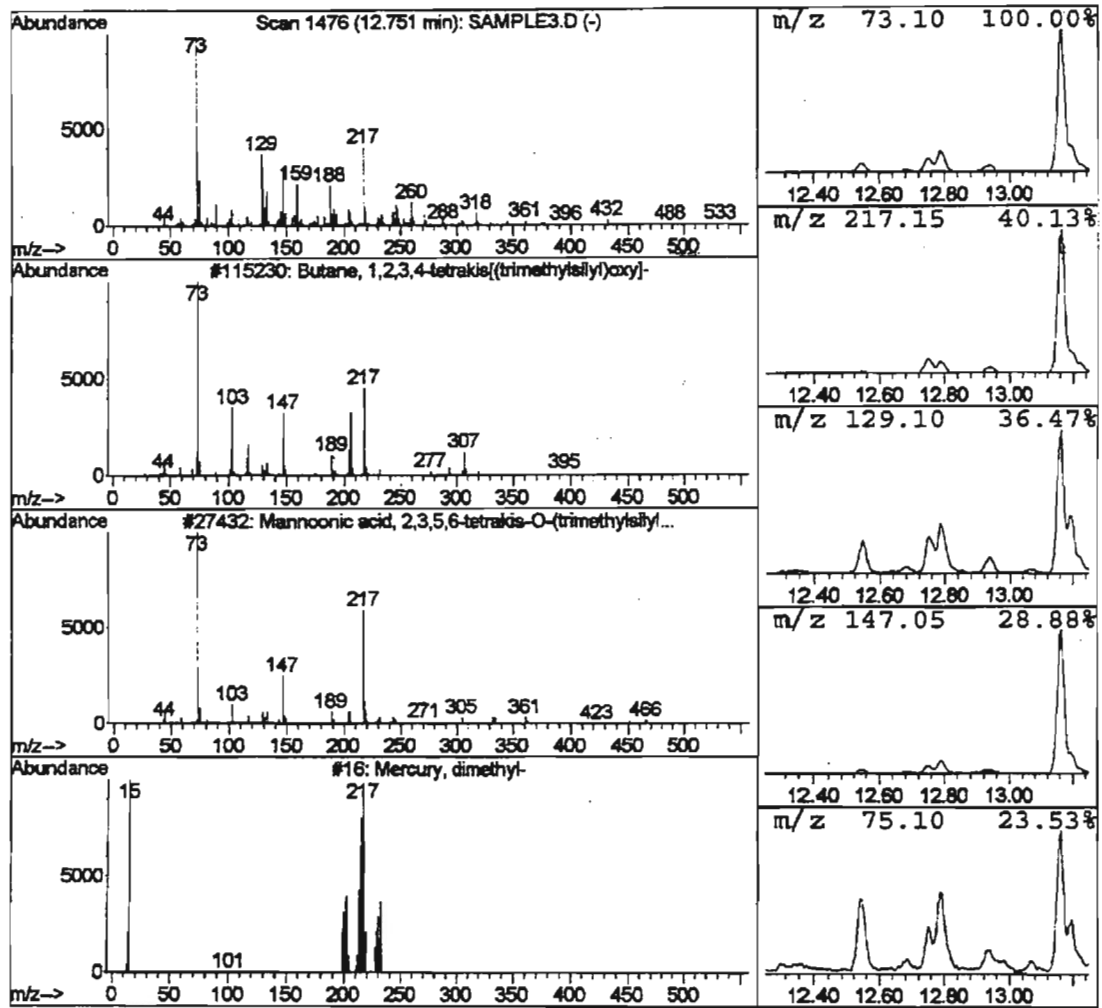Figure C1.4:   Mass spectrum of an unknown compound eluting at 5.143 minutes.
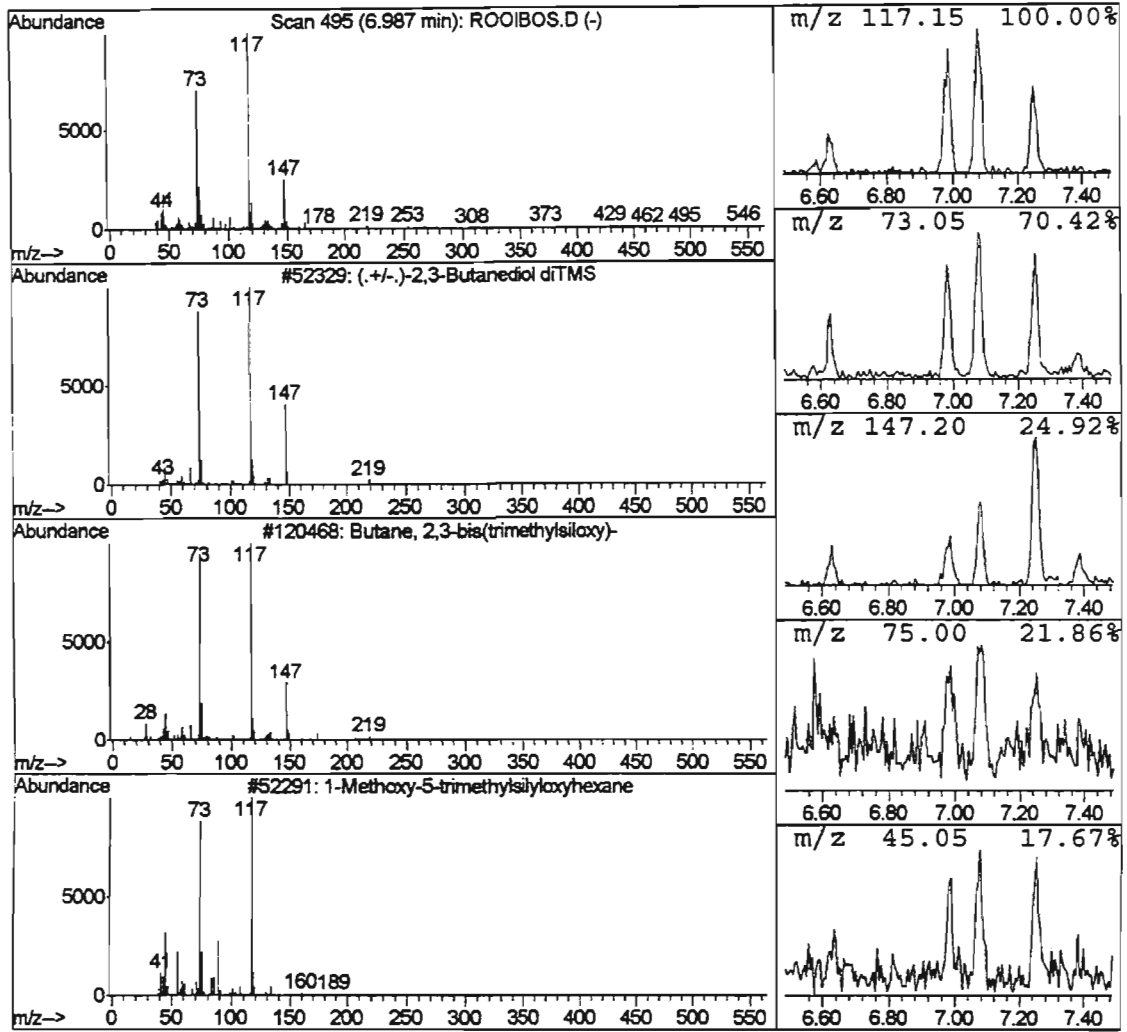
Figure C1.5:   Mass spectrum of an unknown compound eluting at 6.987 minutes.
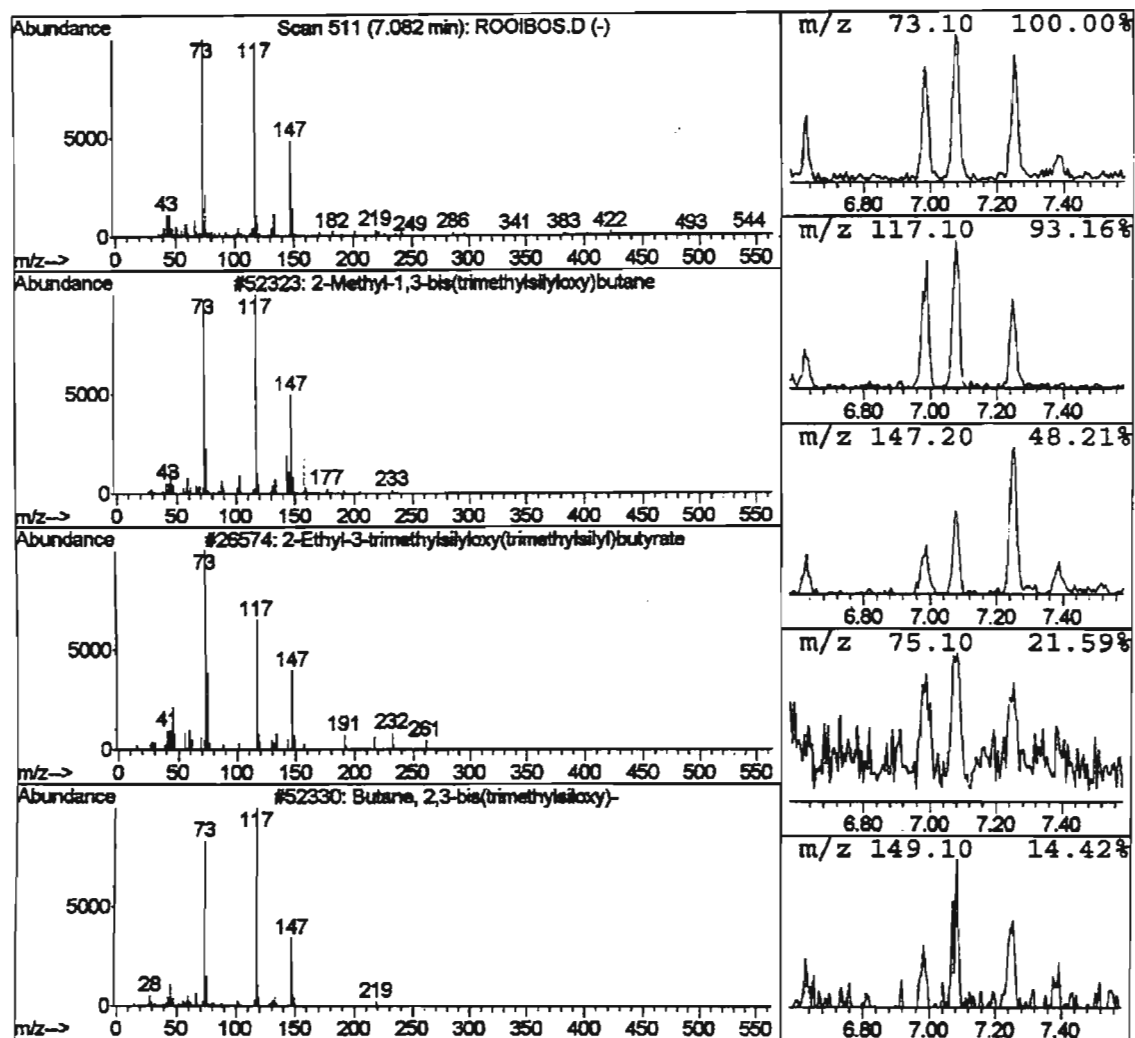
Figure C1.6:   Mass spectrum of an unknown compound eluting at 7.082 minutes.
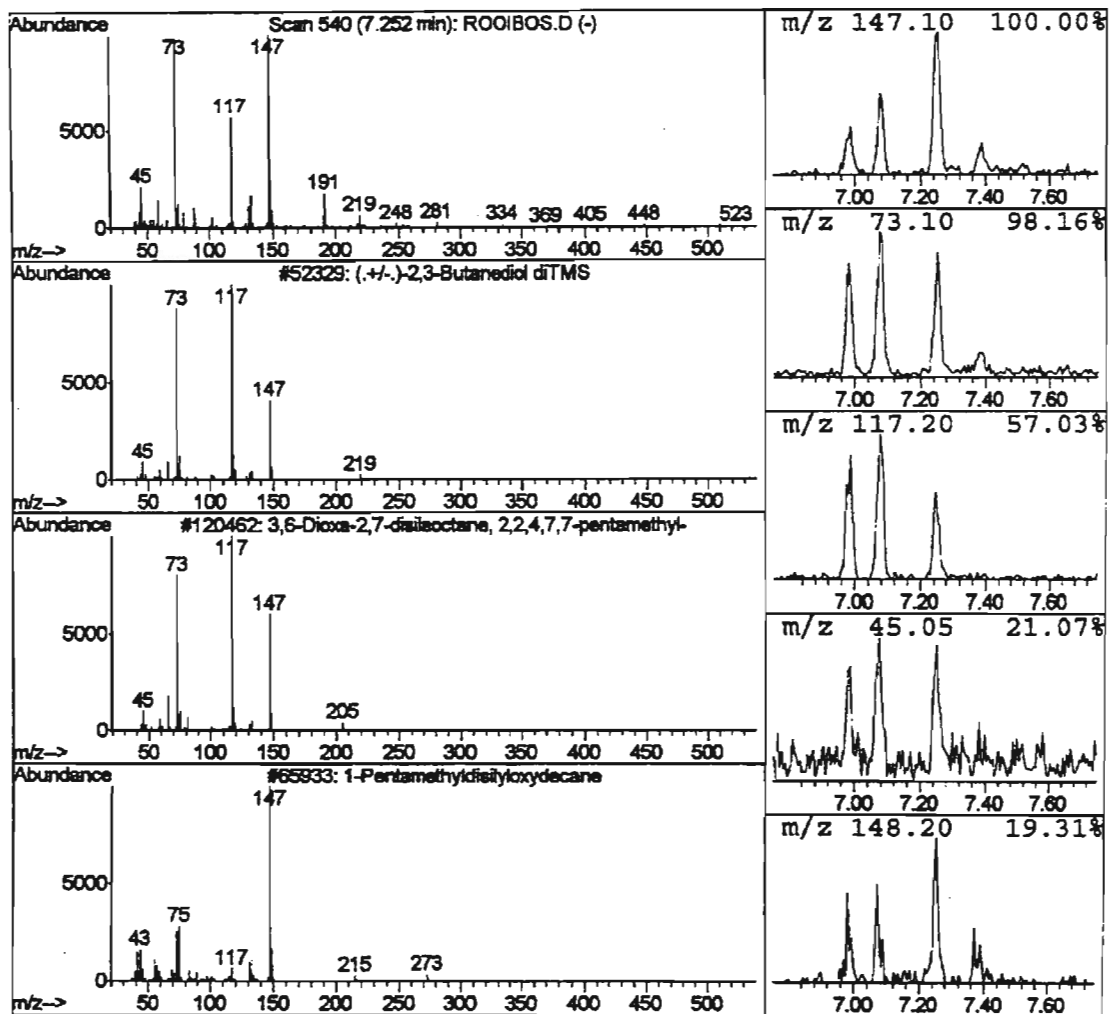
Figure C1.7:   Mass spectrum of an unknown compound eluting at 7.252 minutes.
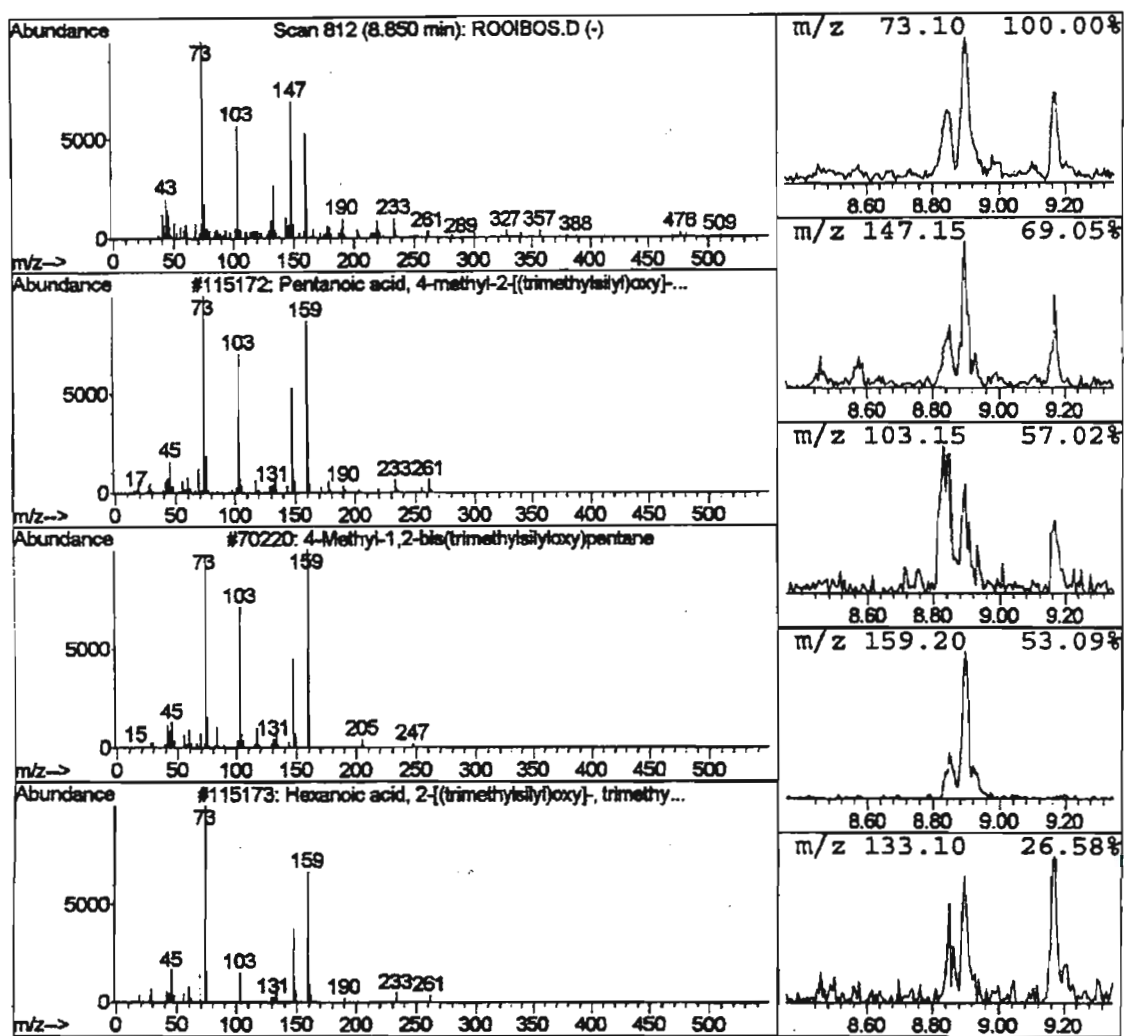
Figure C1.8:   Mass spectrum of an unknown compound eluting at 8.850 minutes.
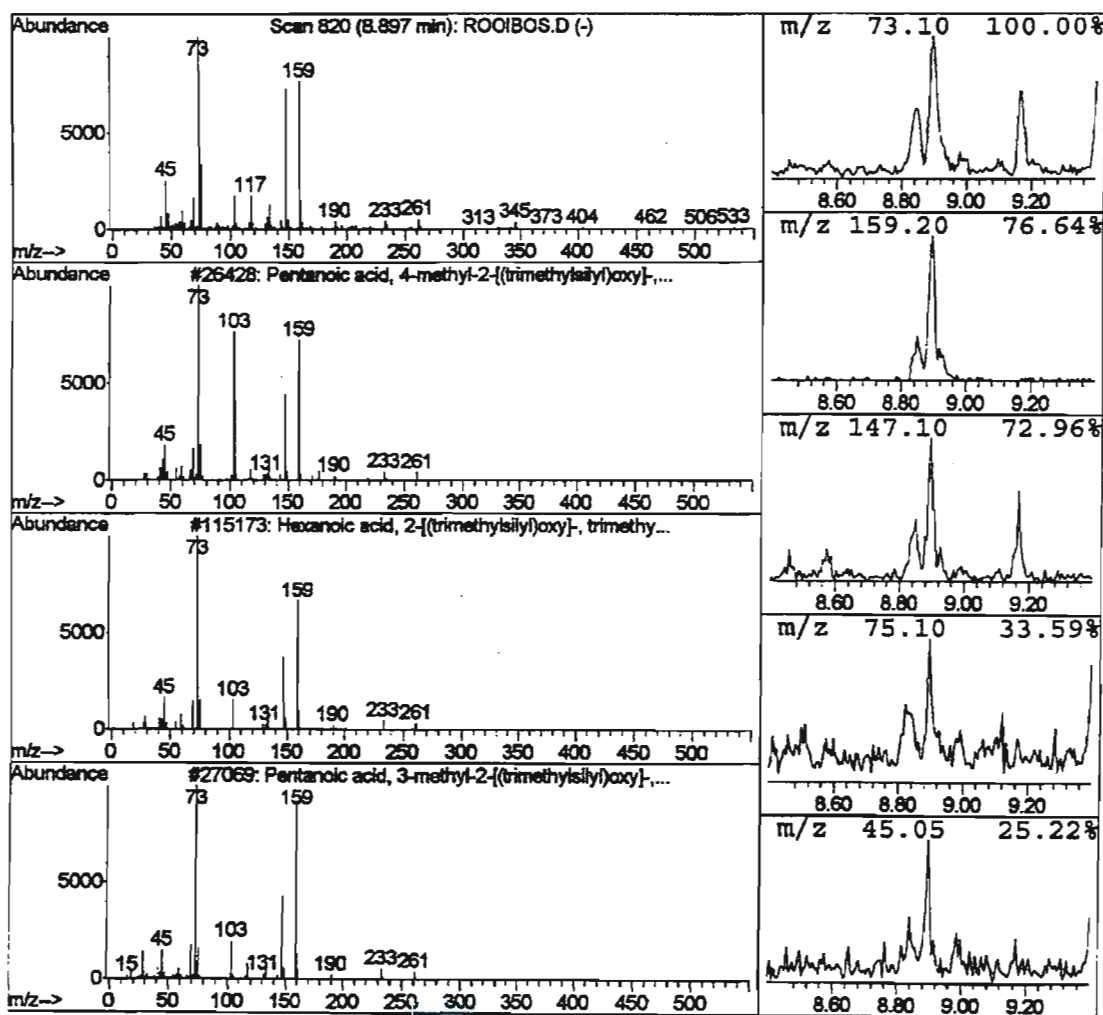
Figure C1.9:   Mass spectrum of an unknown compound eluting at 8.897 minutes.
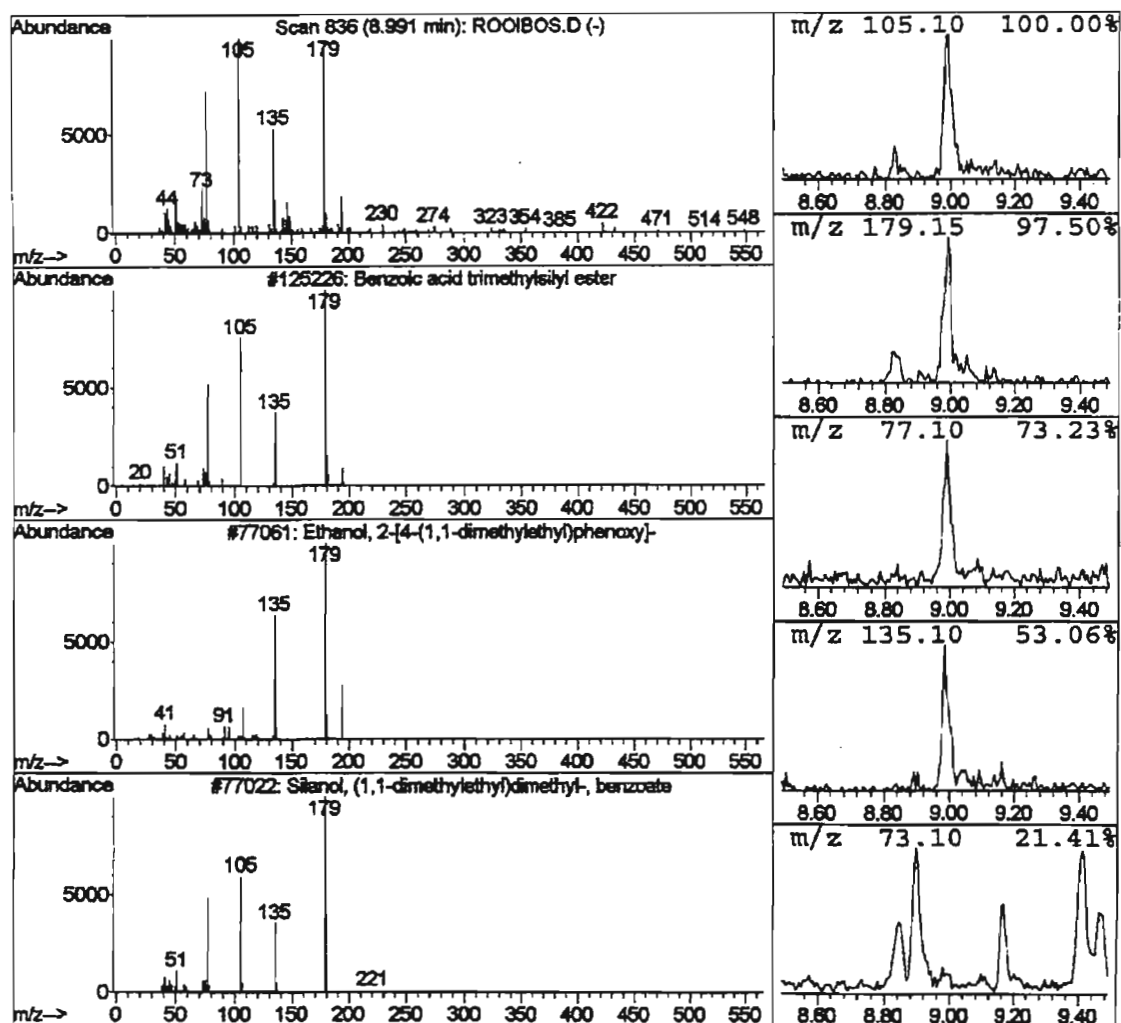
Figure C1.10:   Mass spectrum of a derivatised benzoic acid that elutes at 8.991 minutes. The
fragmentation pattern matched that of a derivatised benzoic acid present in the
library.
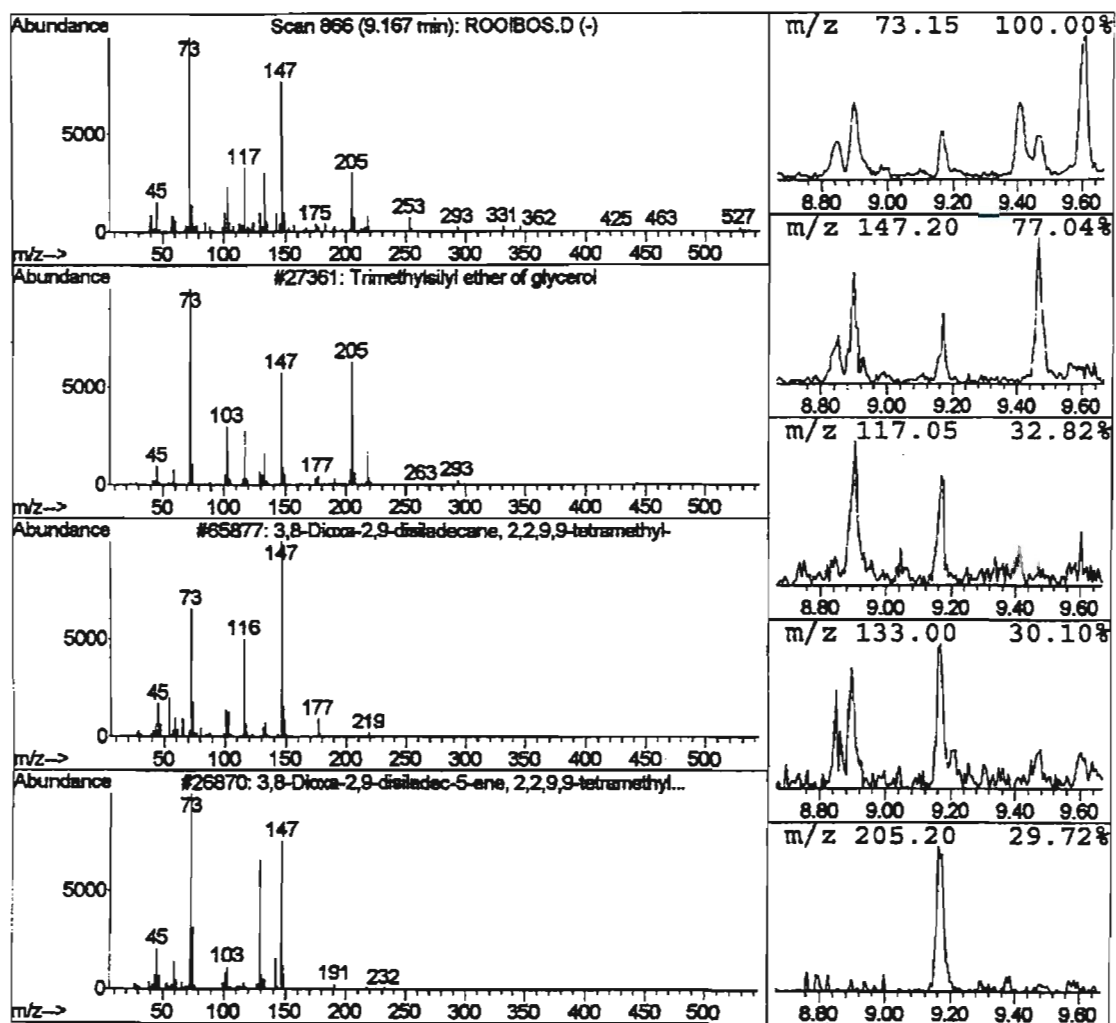
Figure C1.11:   Mass spectrum of an unknown compound eluting at 9.167 minutes.
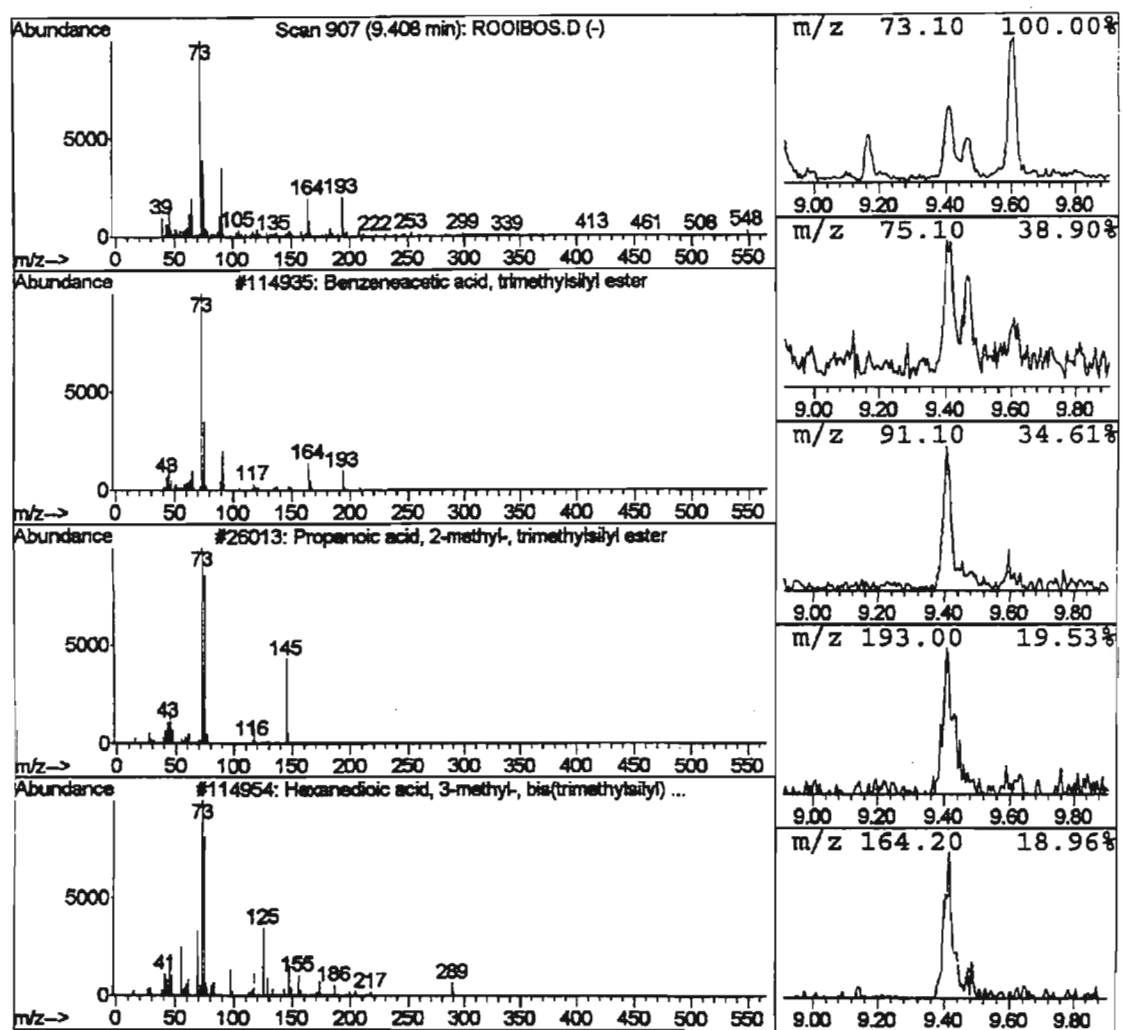
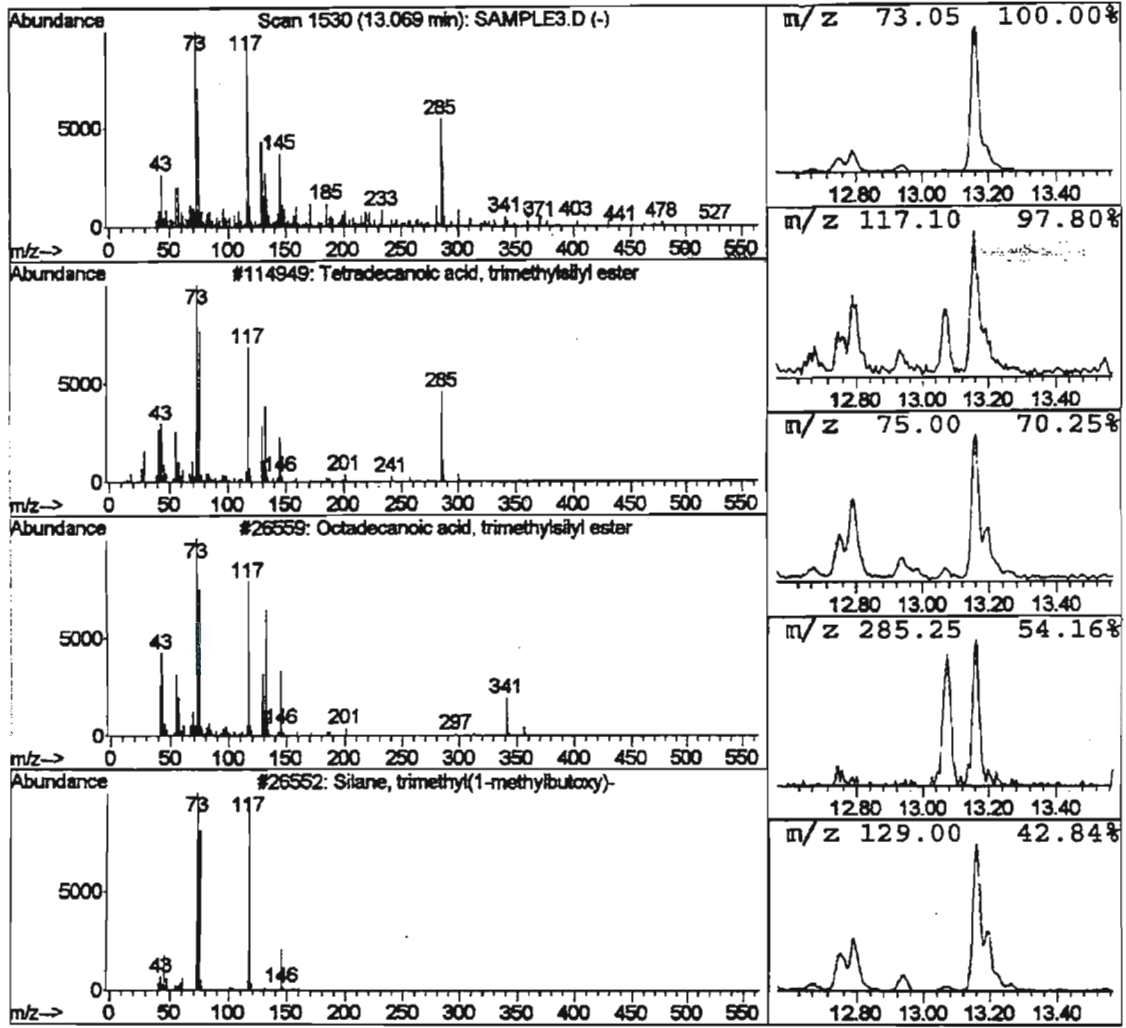Figure C1.12: Mass spectrum of an unknown compound eluting at 9.408 minutes.
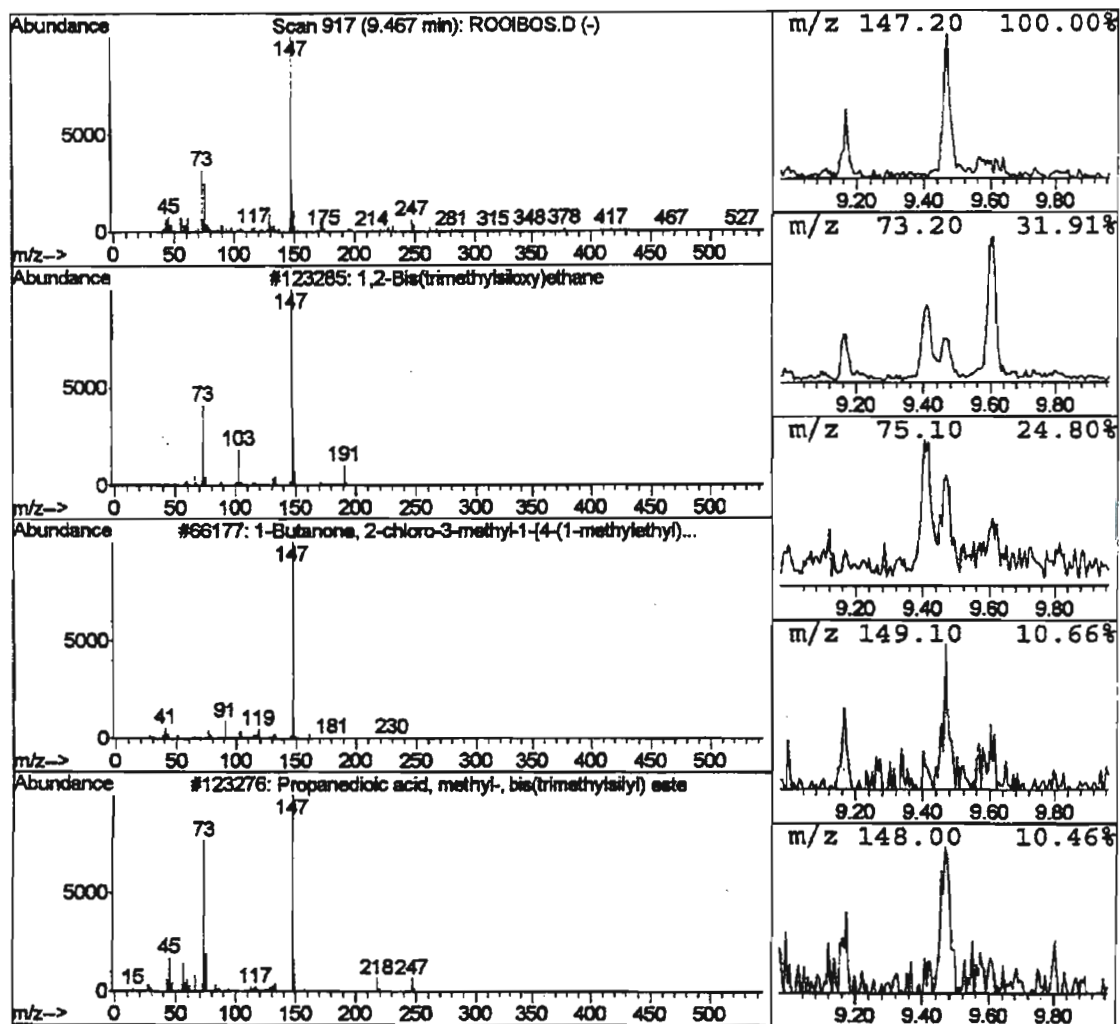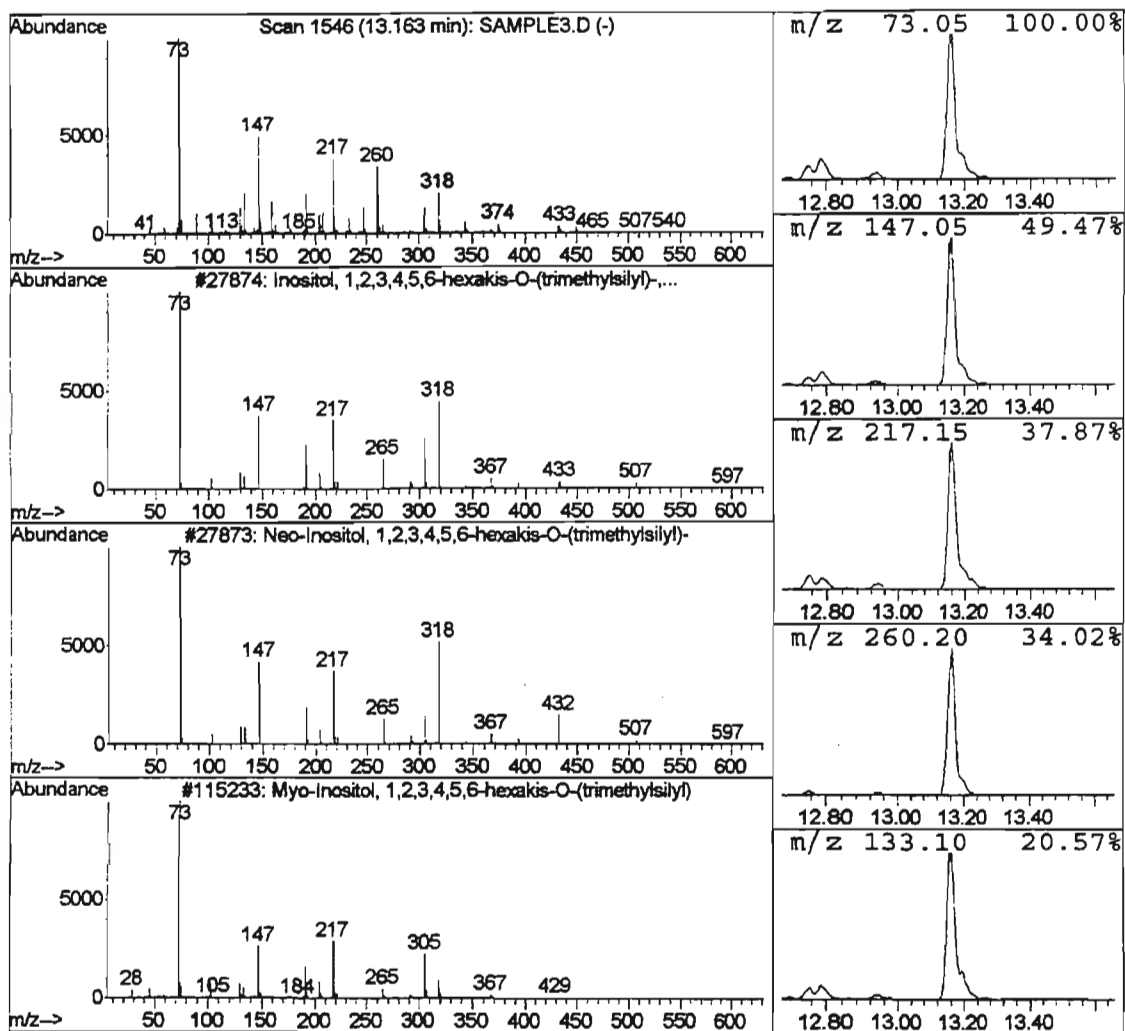
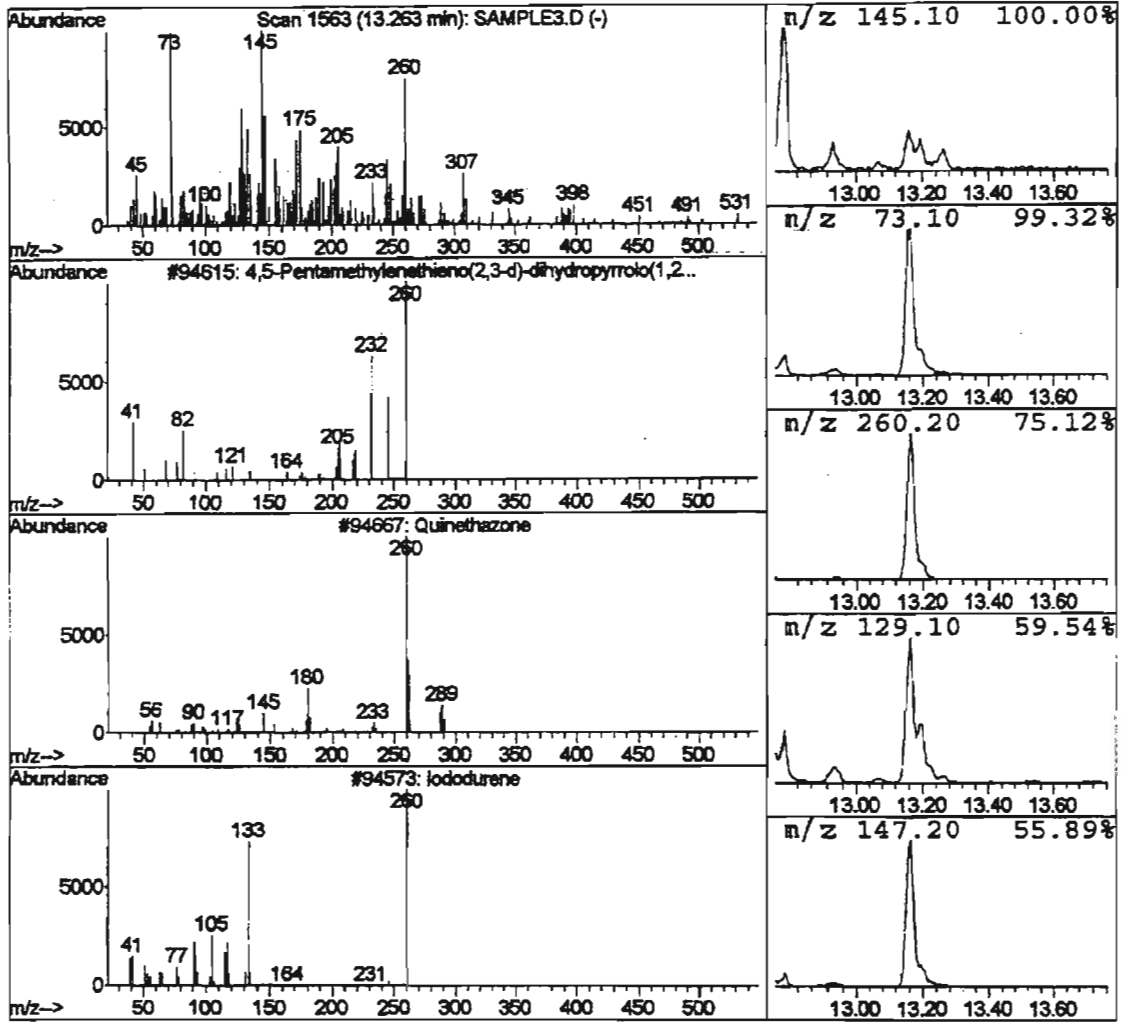Figure C1.13:   Mass spectrum of an unknown compound eluting at 9.467 minutes.
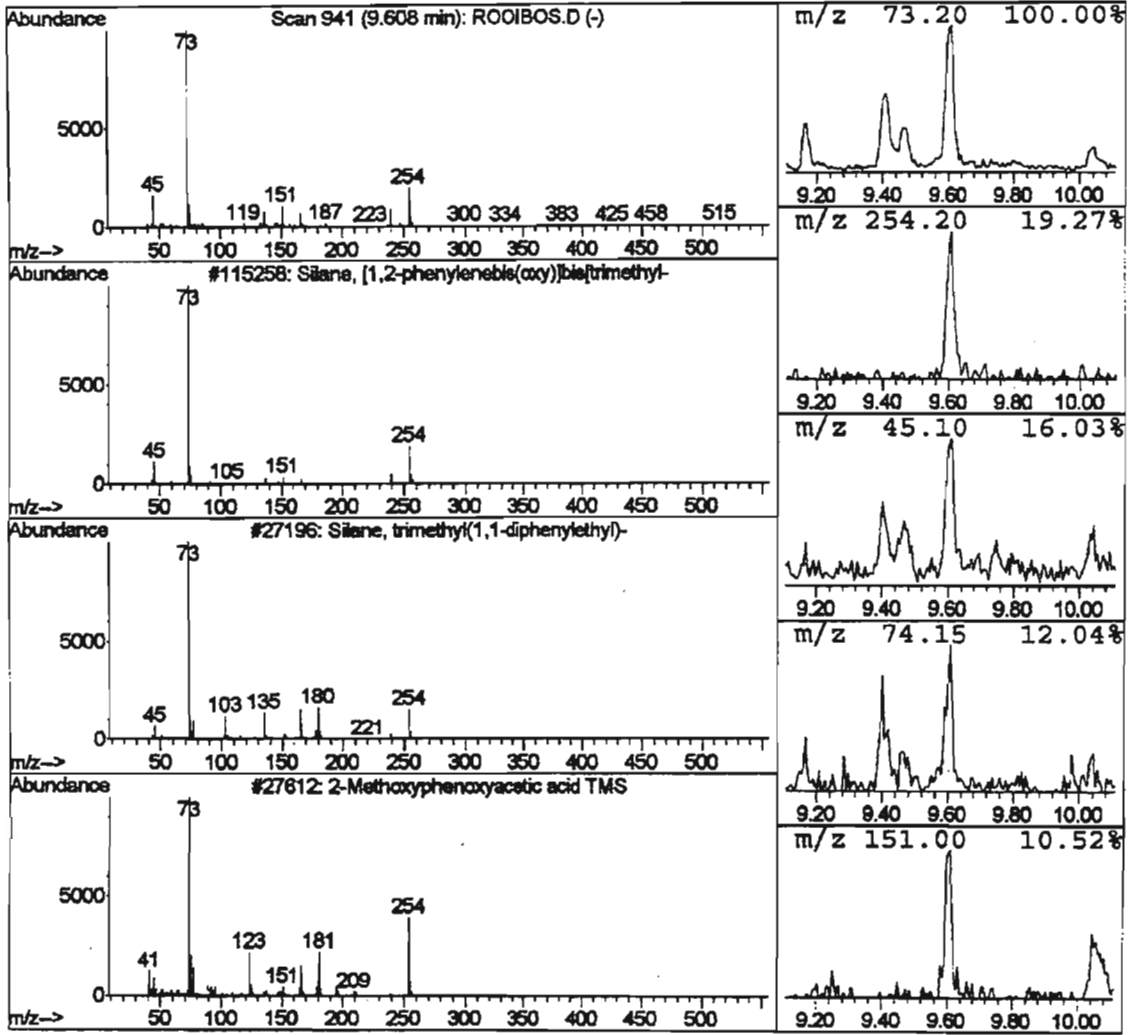
Figure C1.14:   Mass spectrum of an unknown compound eluting at 9.608 minutes.
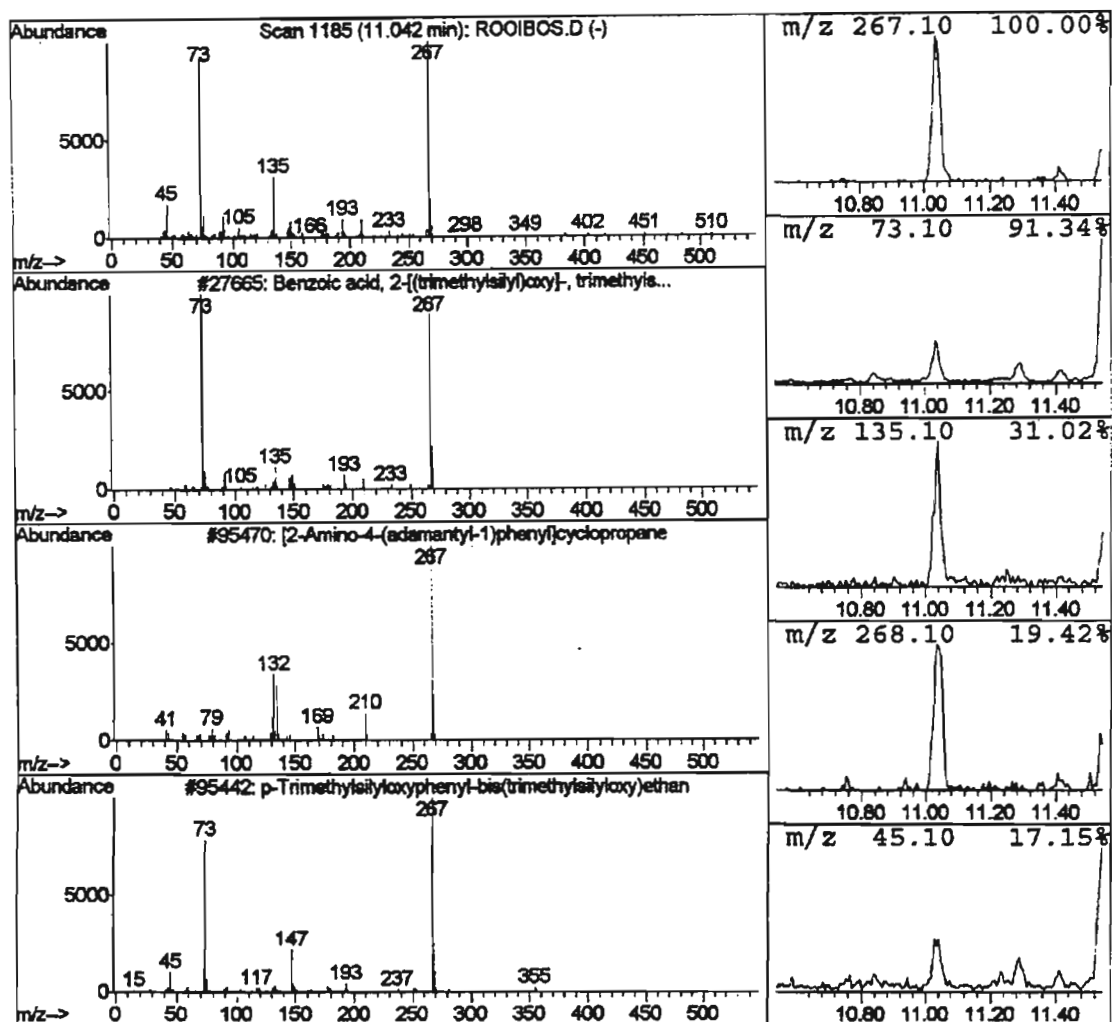
Figure C1.15:   Mass spectrum of a derivatised benzoic acid that elutes at 11.042 minutes. The fragmentation pattern matched that of a derivatised benzoic acid present in the library.
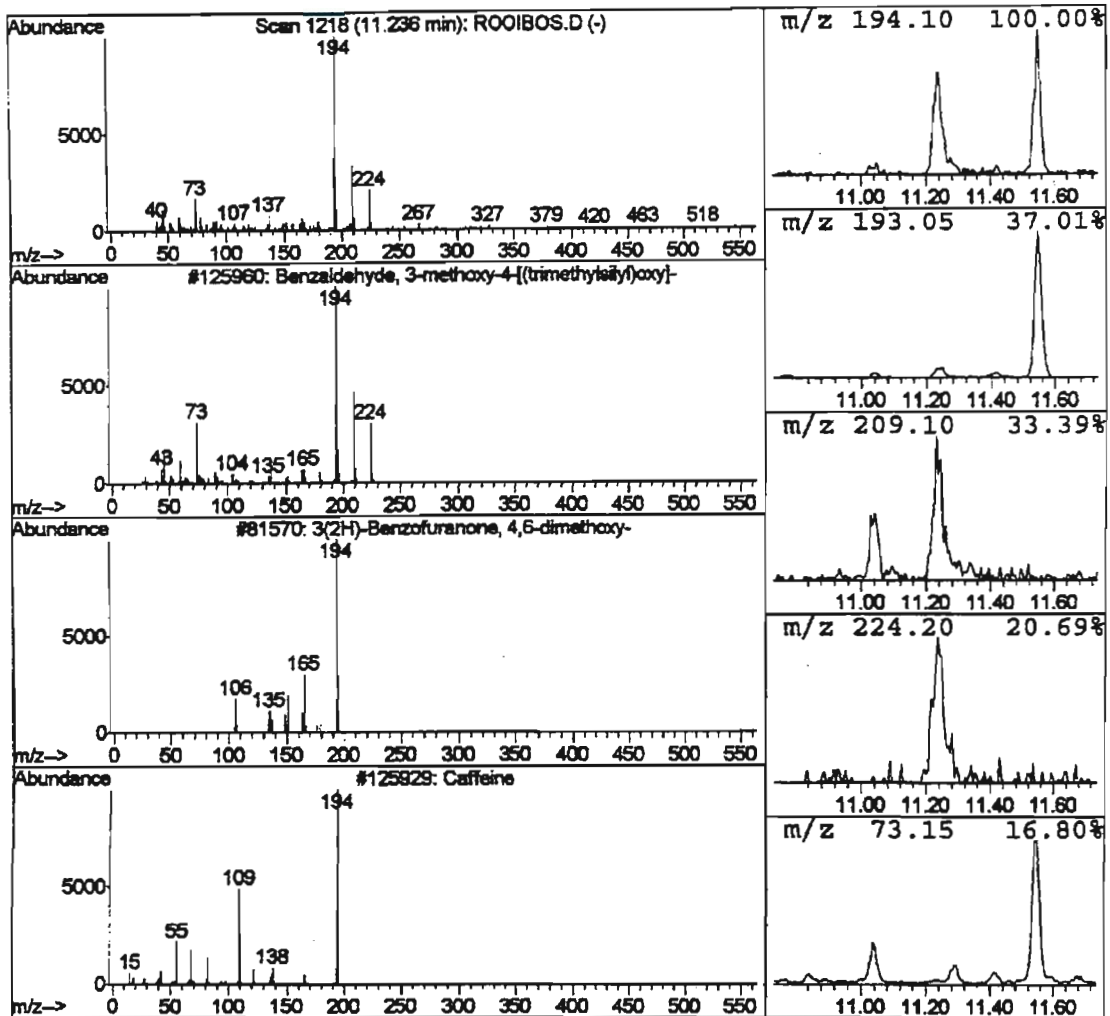
Figure C1.16:   Mass spectrum of a derivatised benzaldehyde that elutes at 11.236 minutes. The fragmentation pattern matched that of a derivatised benzaldehyde present in the library.
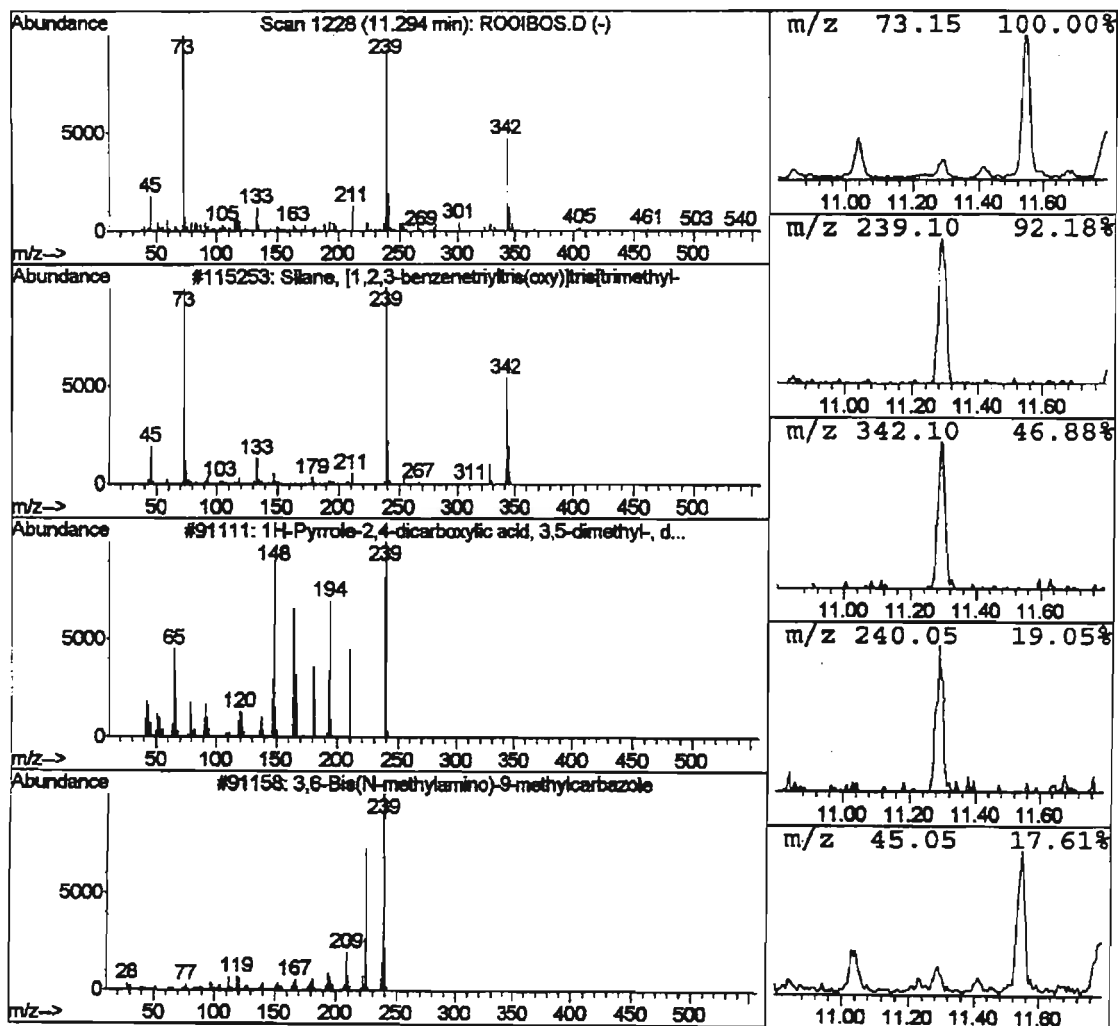
Figure C1.17:   Mass spectrum of an unknown compound eluting at 11.294 minutes.
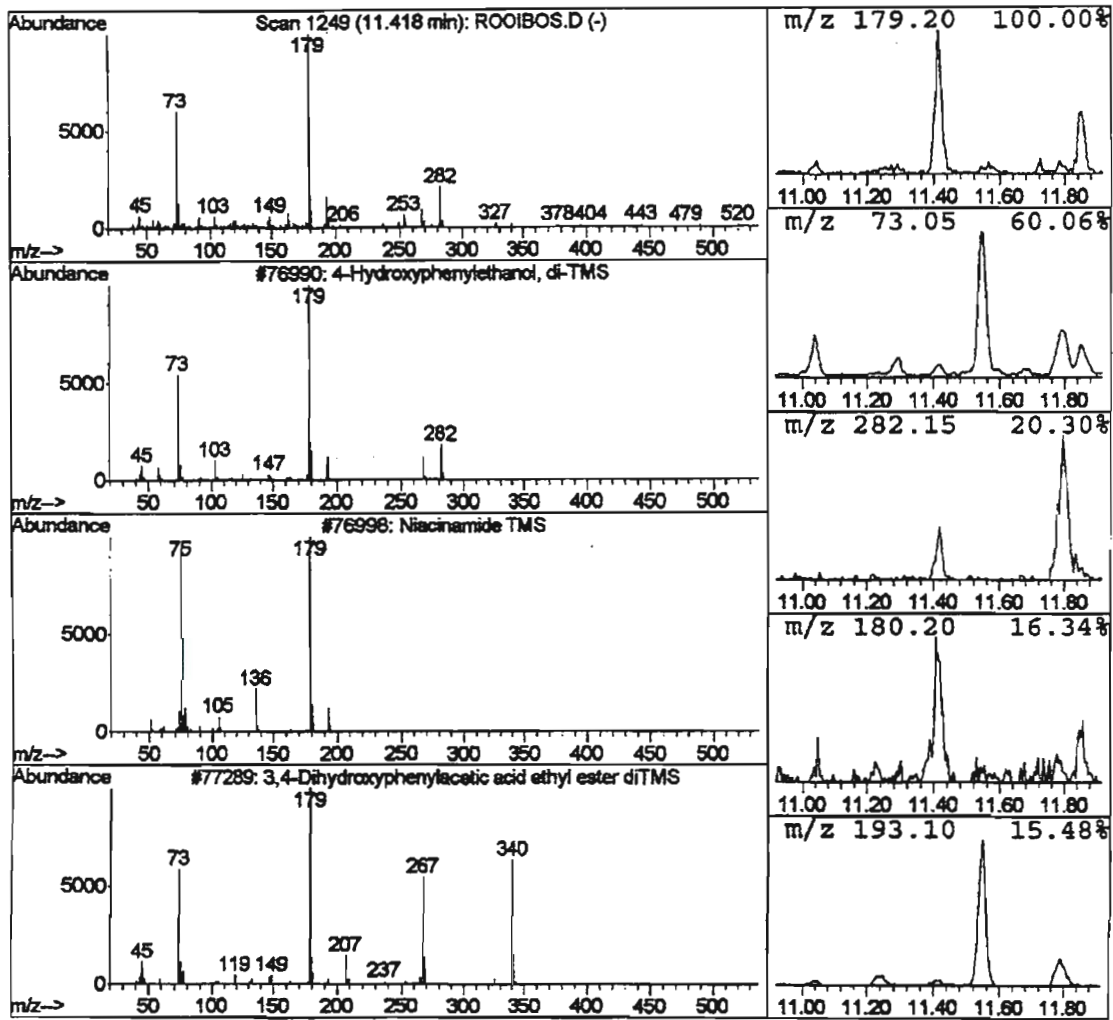
Figure C1.18: Mass spectrum of a derivatised 4-hydroxyphenyl ethanol that elutes at 11.418 minutes. The fragmentation pattern matched that of a derivatised 4-hydroxyphenyl ethanol present in the library.
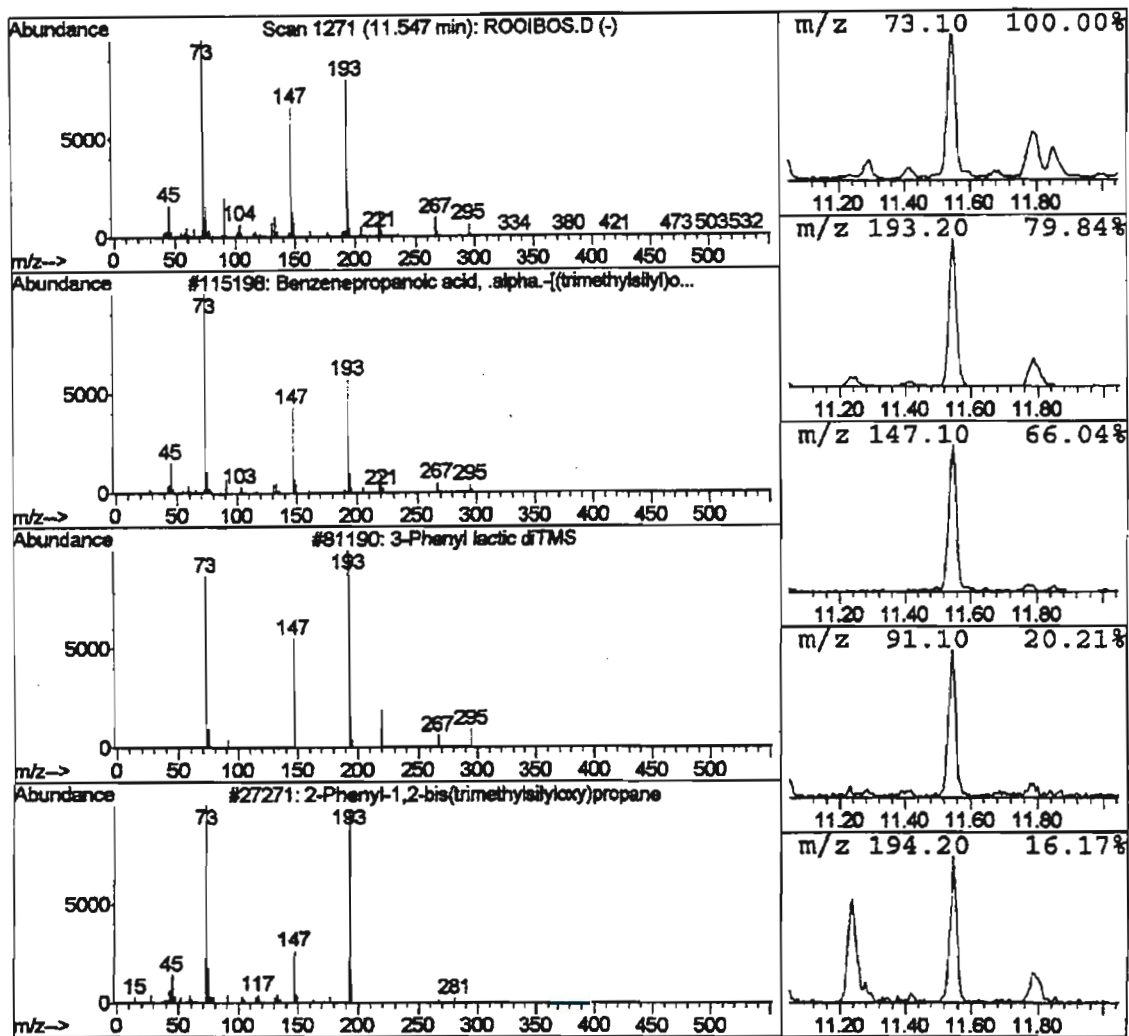
Figure C1.19: Mass spectrum of a derivatised benzenepropanoic acid that elutes at 11.547 minutes. The fragmentation pattern matched that of a derivatised benzenepropanoic acid present in the library.
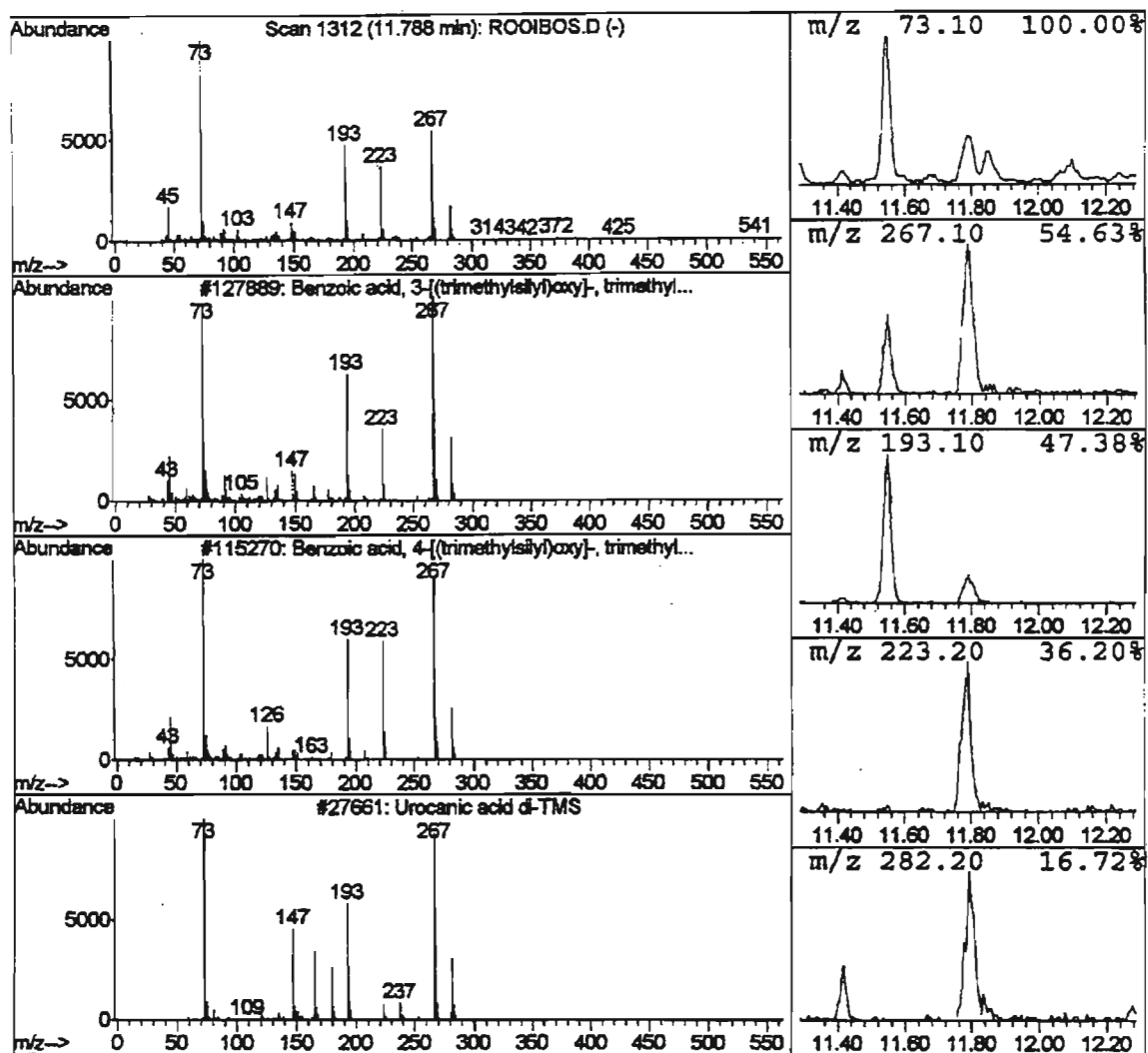
Figure C1.20: Mass spectrum of a derivatised benzoic acid that elutes at 11.788 minutes. The fragmentation pattern matched that of a derivatised benzoic acid present in the library.
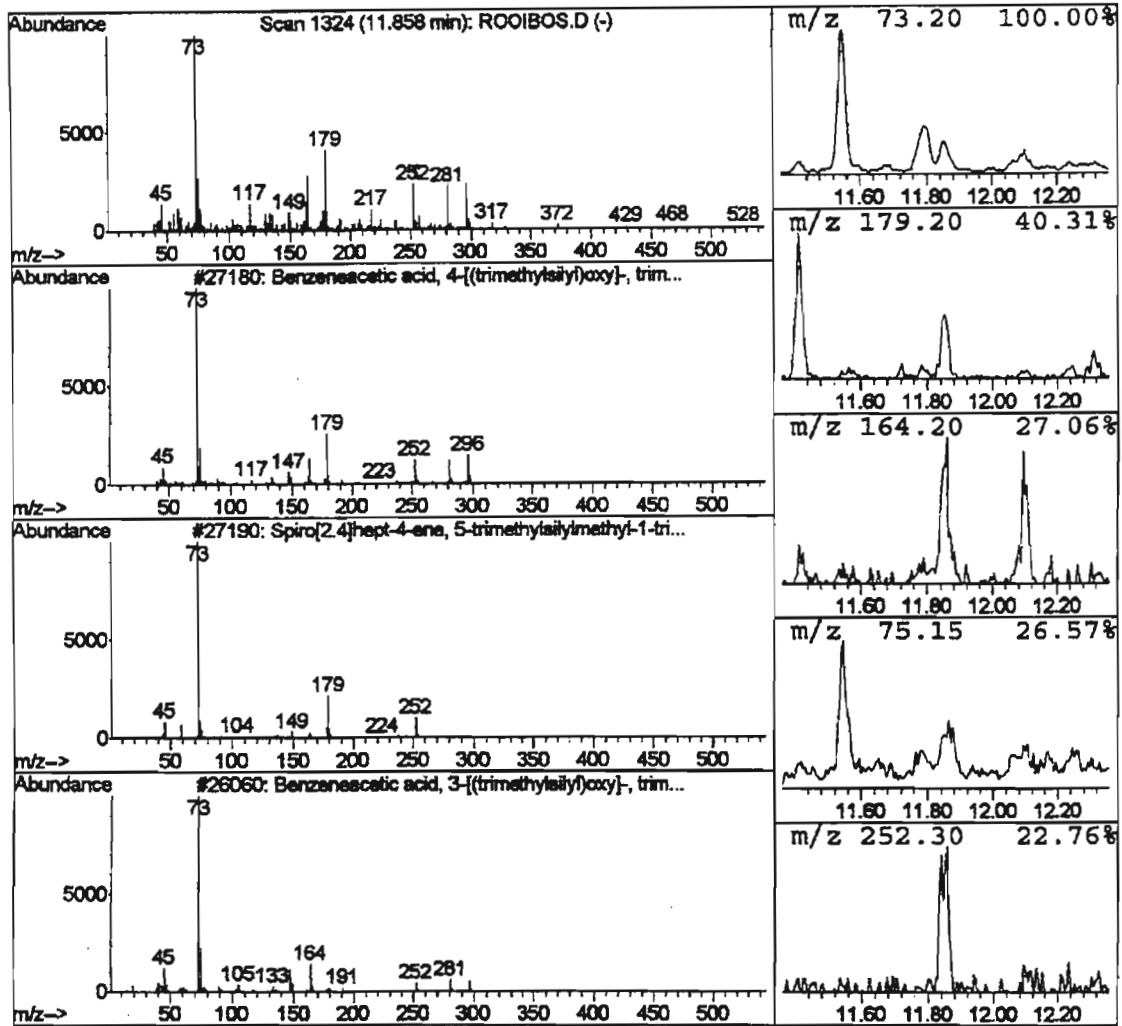
Figure C1.21: Mass spectrum of a derivatised benzeneacetic acid that elutes at 11.858 minutes. The fragmentation pattern matched that of a derivatised benzeneacetic acid present in the library.
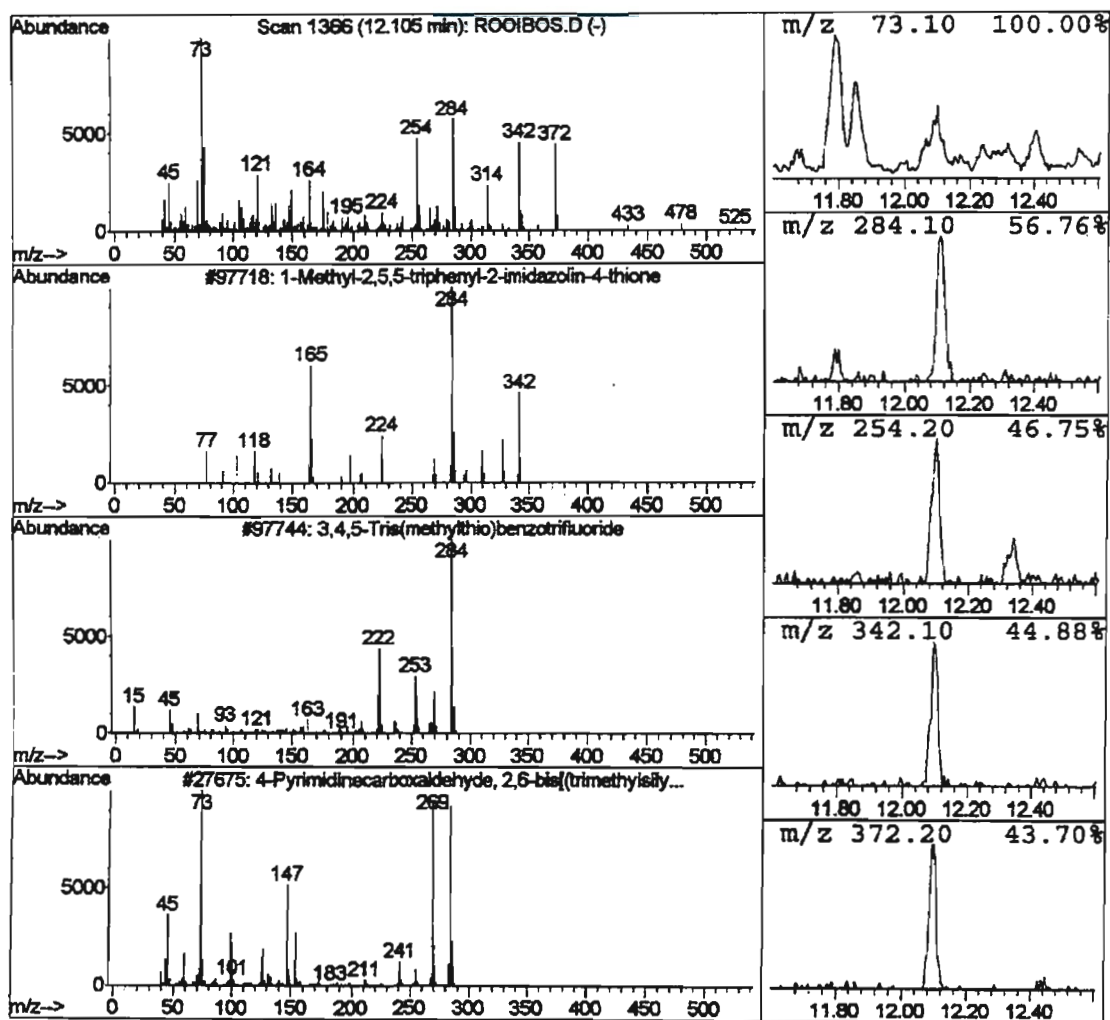
Figure C1.22:   Mass spectrum of an unknown compound eluting at 12.105 minutes.
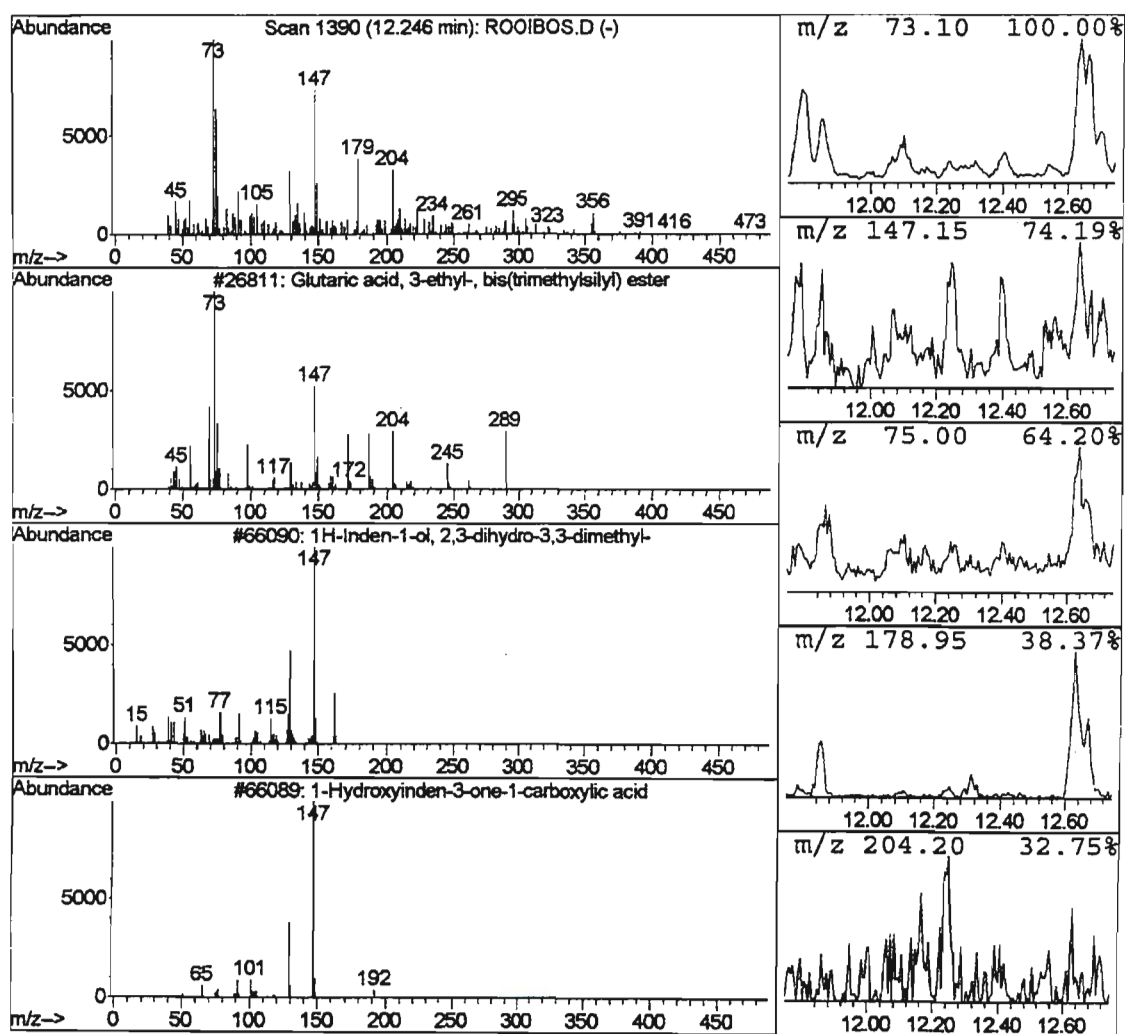
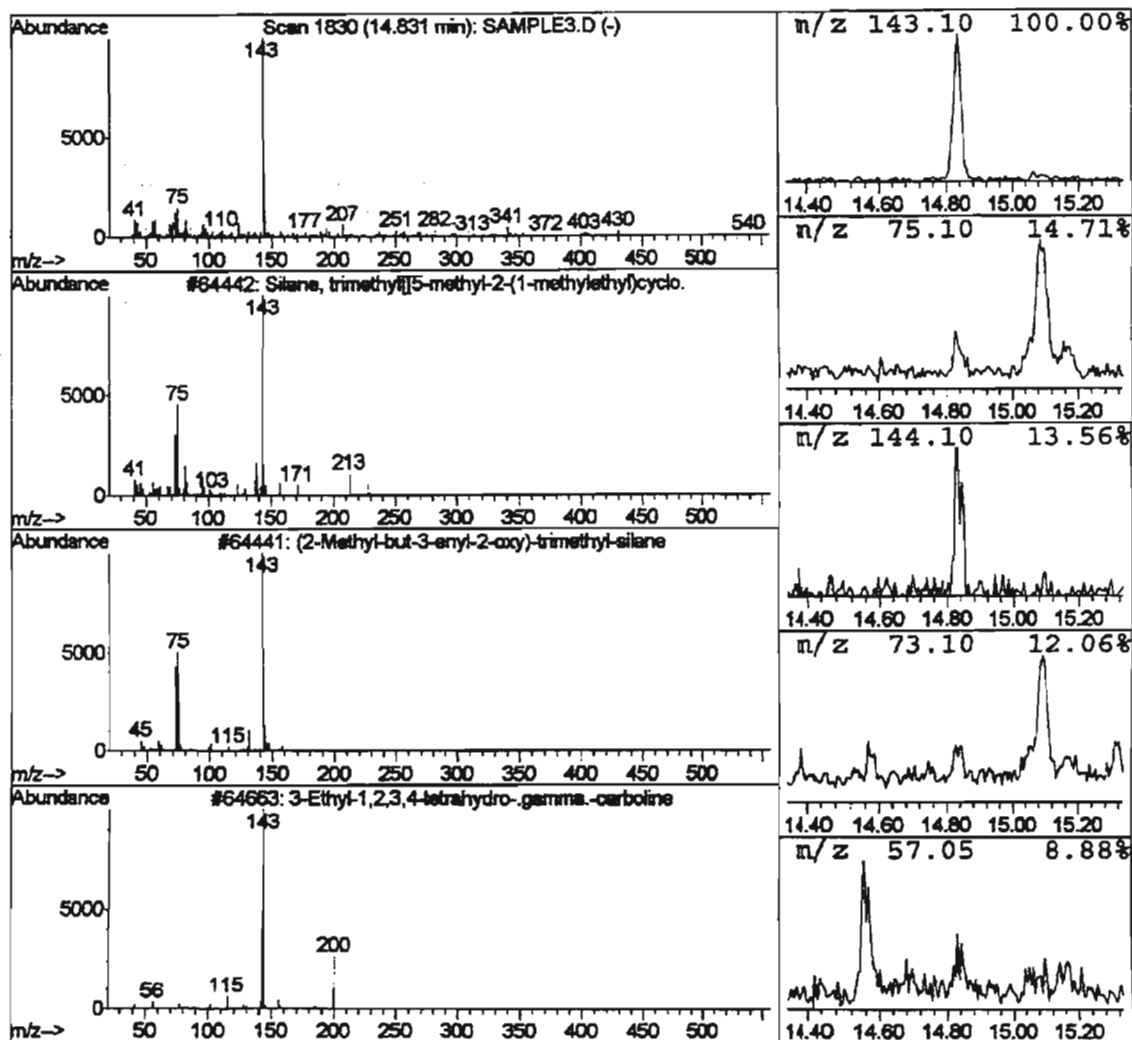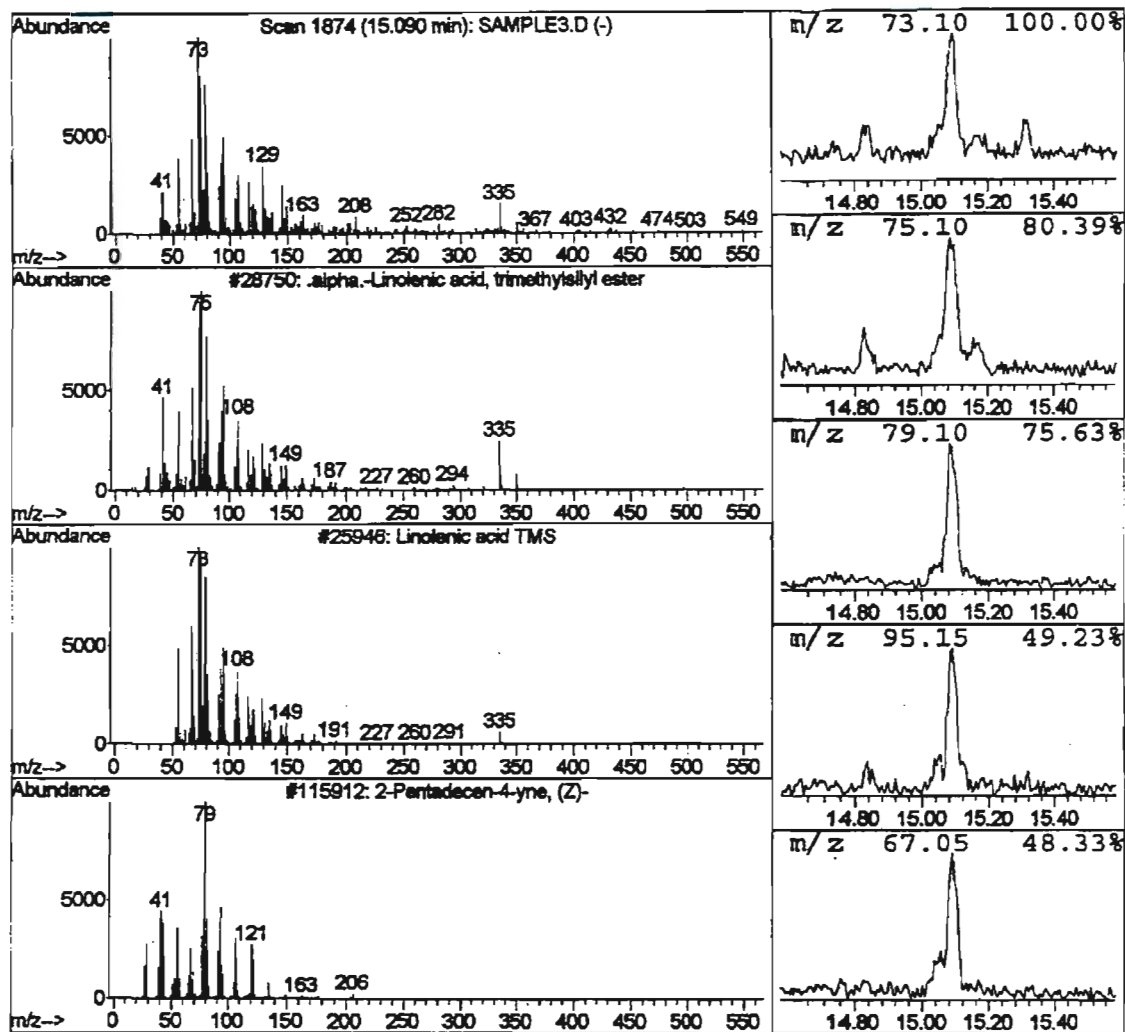Figure C1.23:   Mass spectrum of an unknown compound eluting at 12.246 minutes.
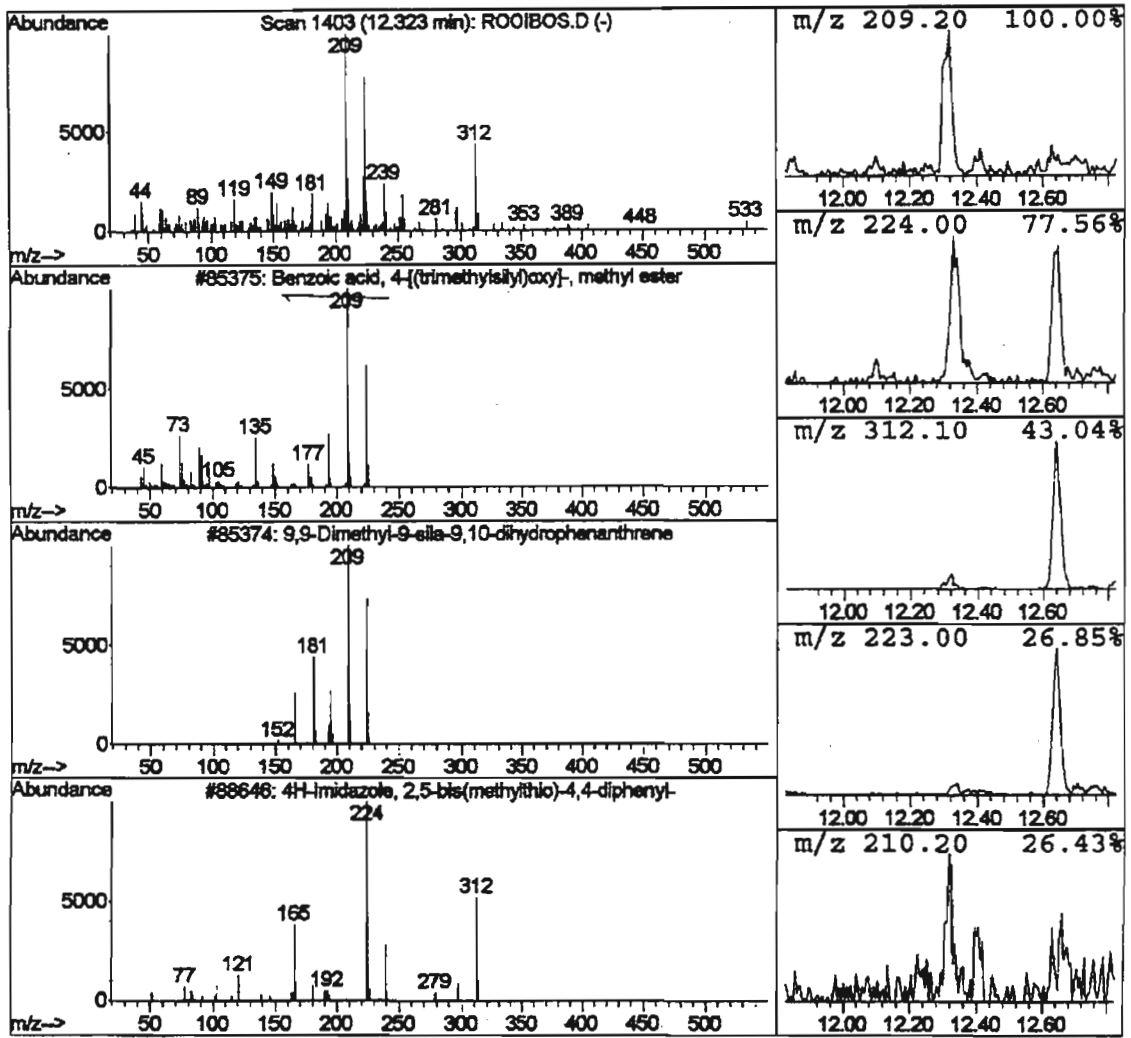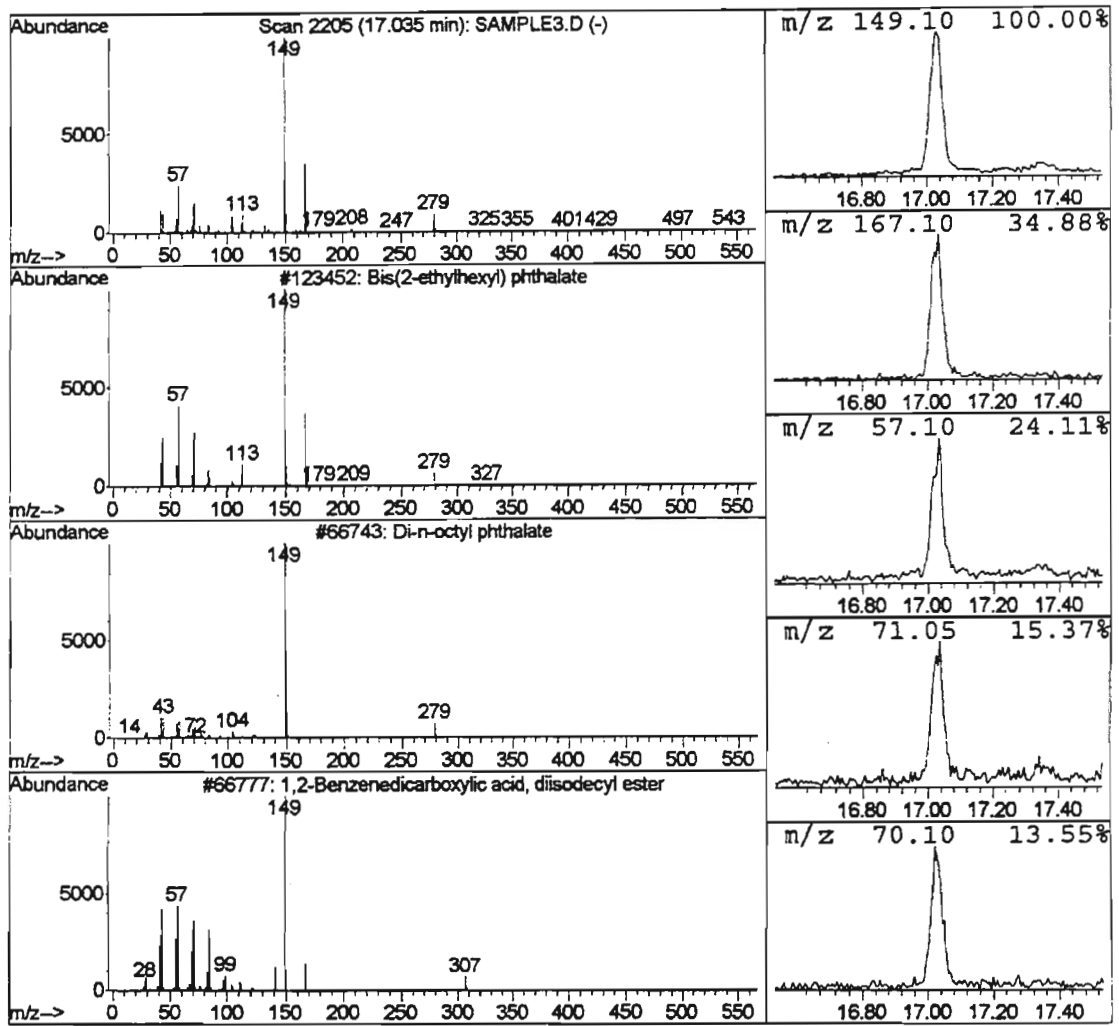
Figure C1.24: Mass spectrum of an unknown compound eluting at 12.323 minutes.
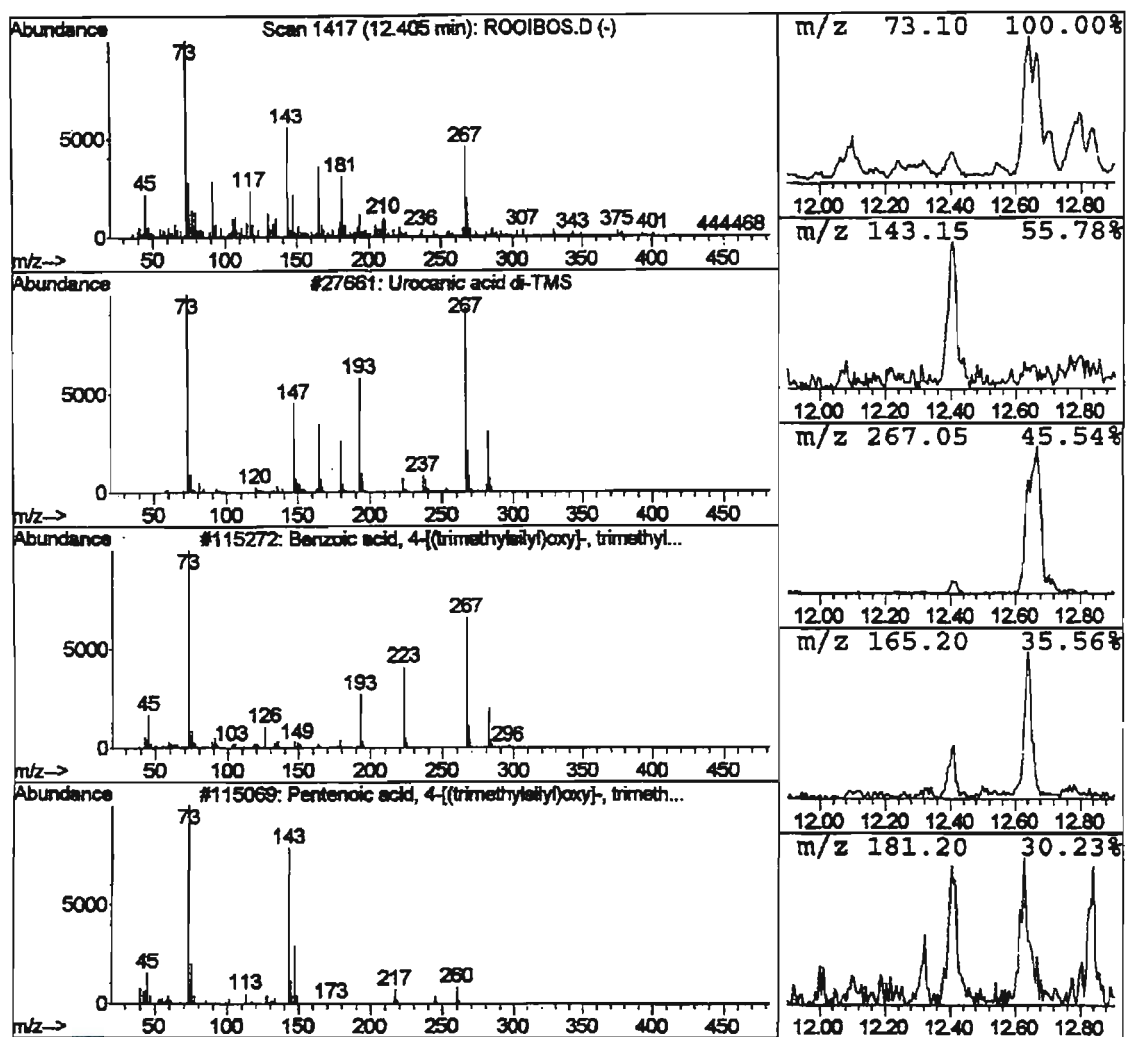
Figure C1.25:   Mass spectrum of an unknown compound eluting at 12.405 minutes.
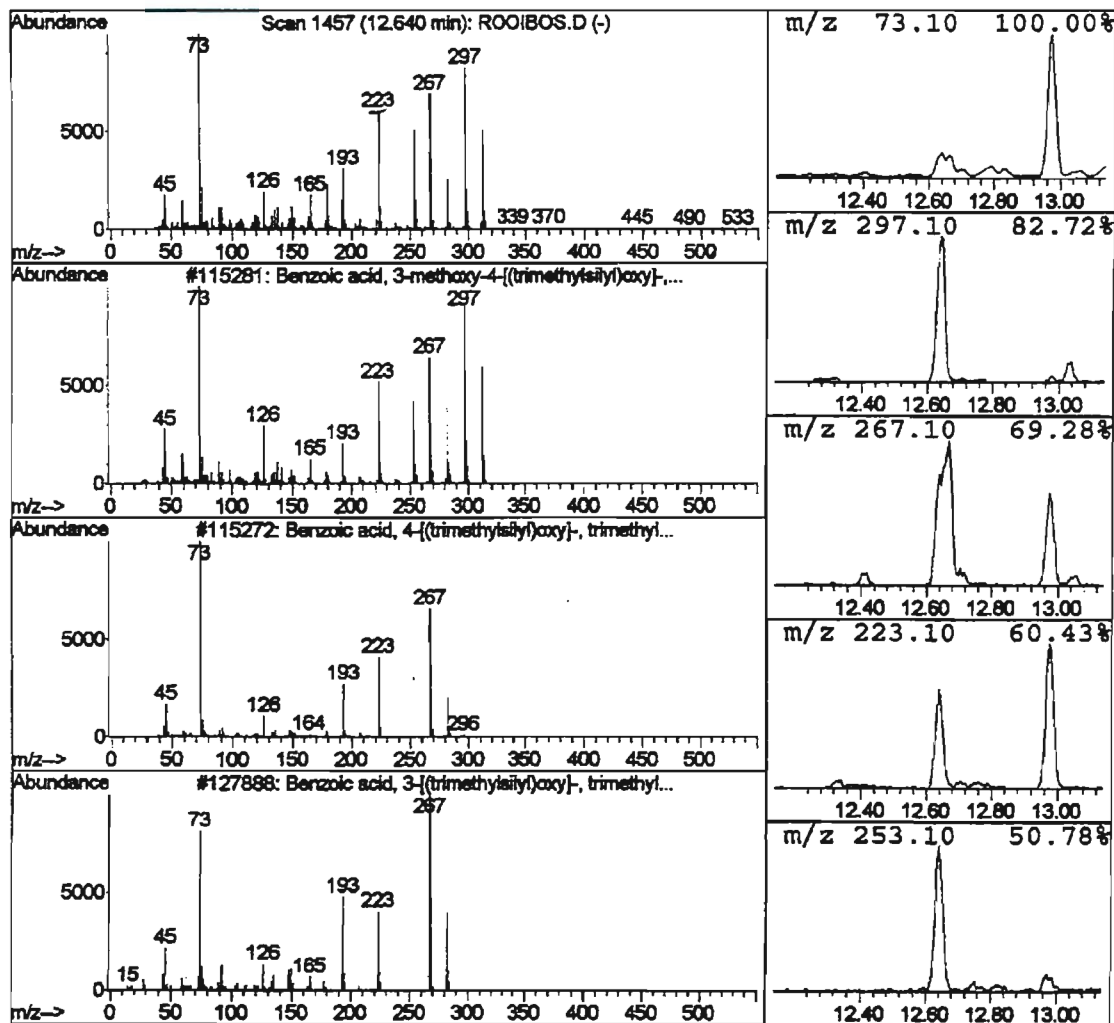
Figure C1.26:   Mass spectrum of a derivatised benzoic acid that elutes at 12.640 minutes. The fragmentation pattern matched that of a derivatised benzoic acid present in the library.
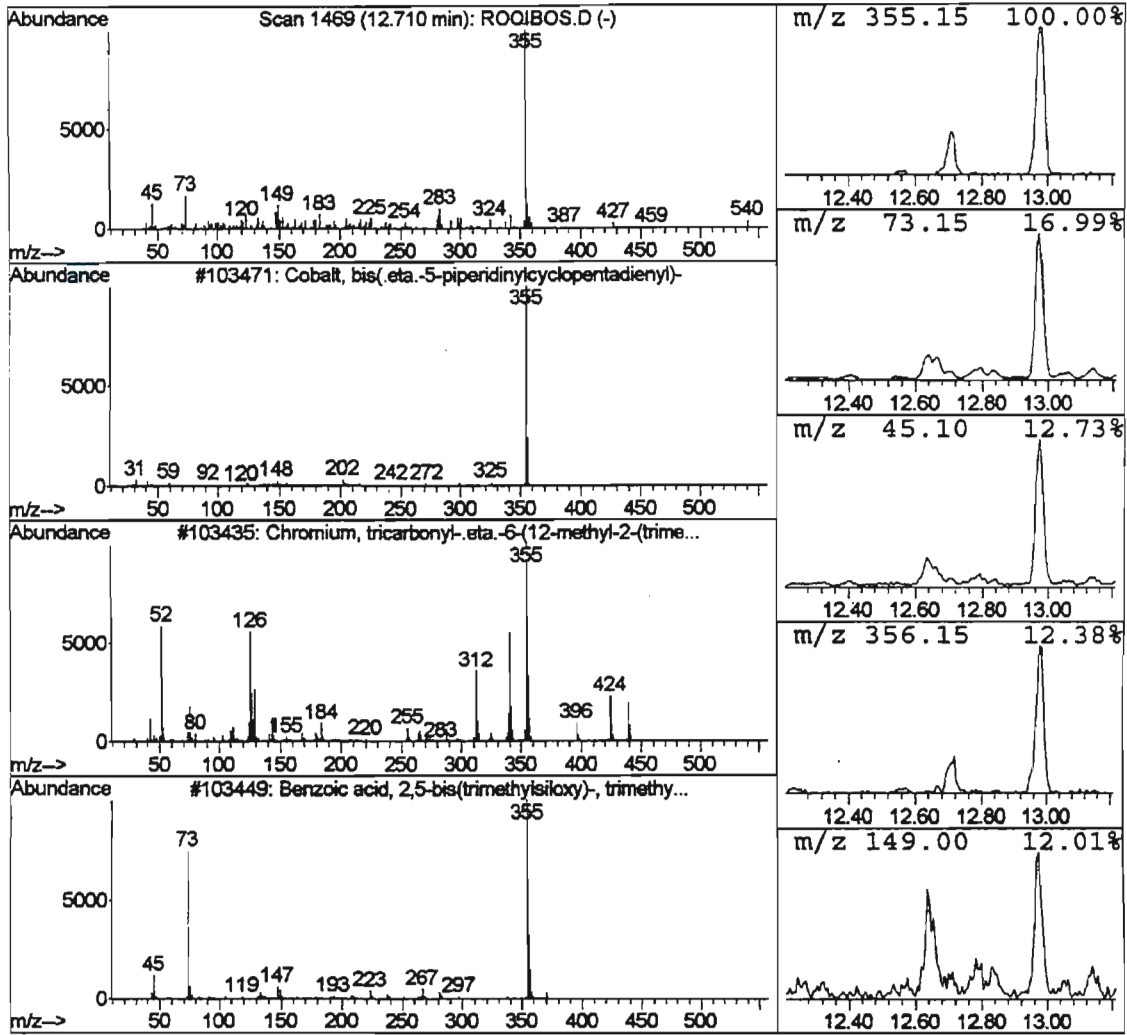
Figure C1.27: Mass spectrum of an unknown compound eluting at 12.710 minutes.
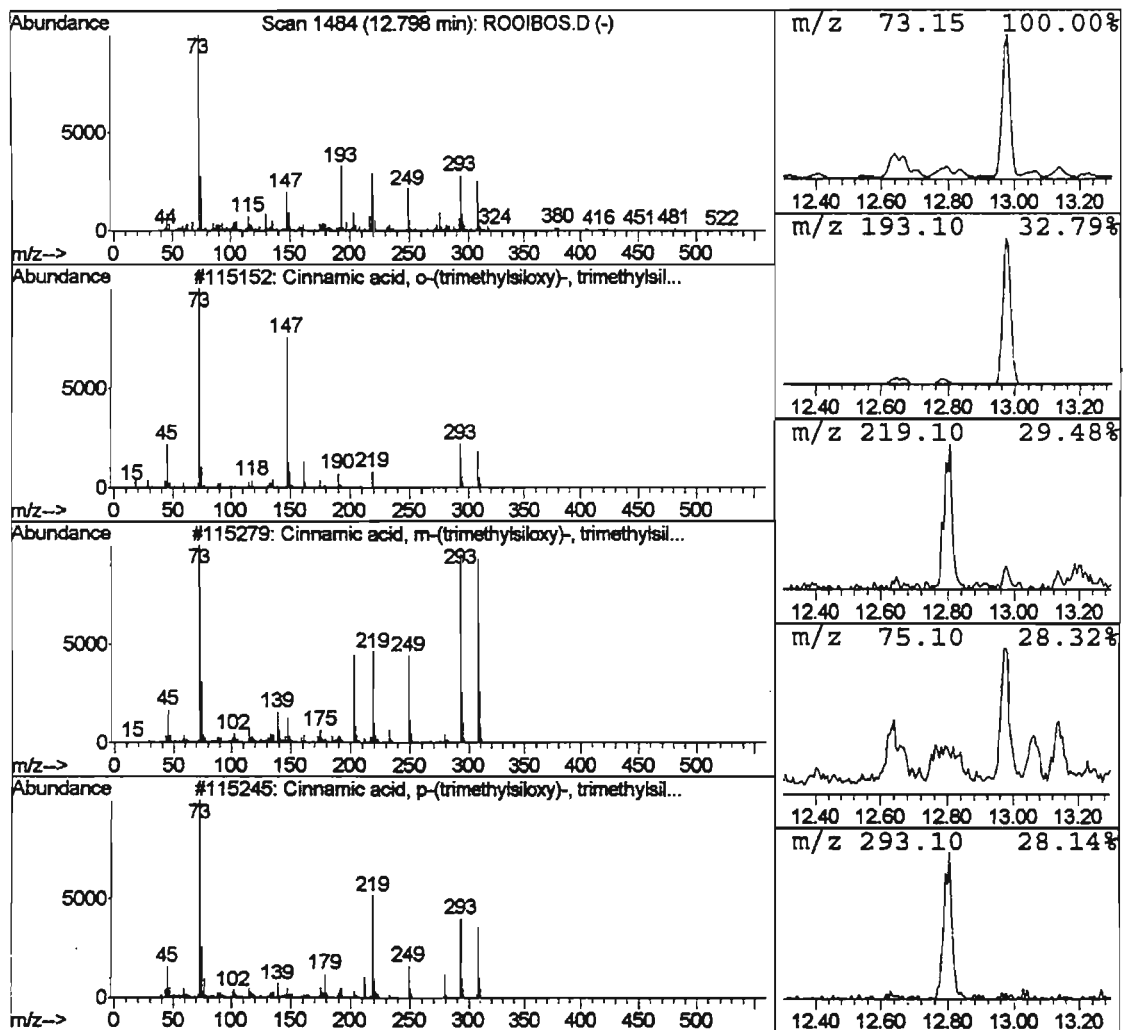
Figure C1.28: Mass spectrum of a derivatised *p*-coumaric acid that elutes at 12.798 minutes. The fragmentation pattern matched that of a derivatised *p*-coumaric reported by Owen *et al.* [2003].
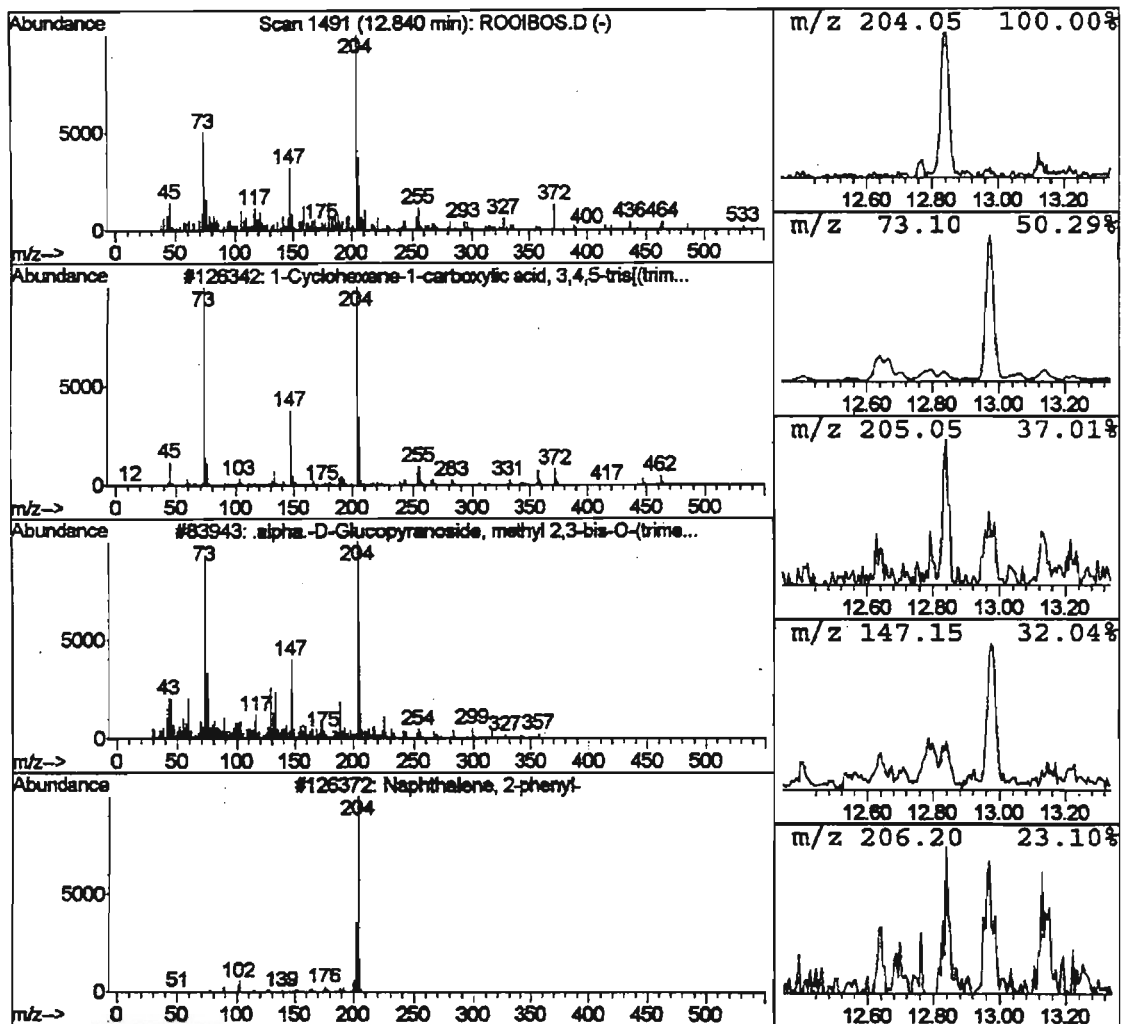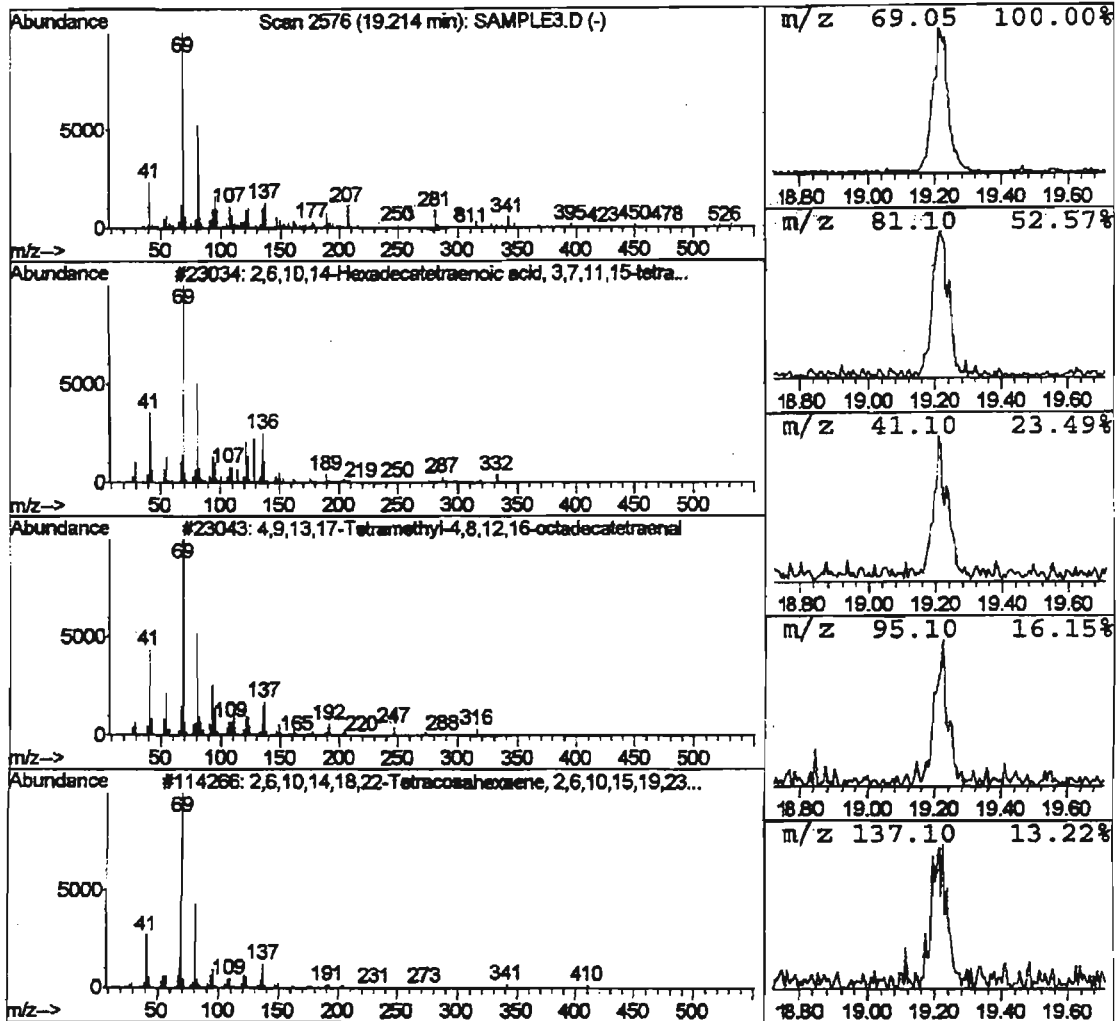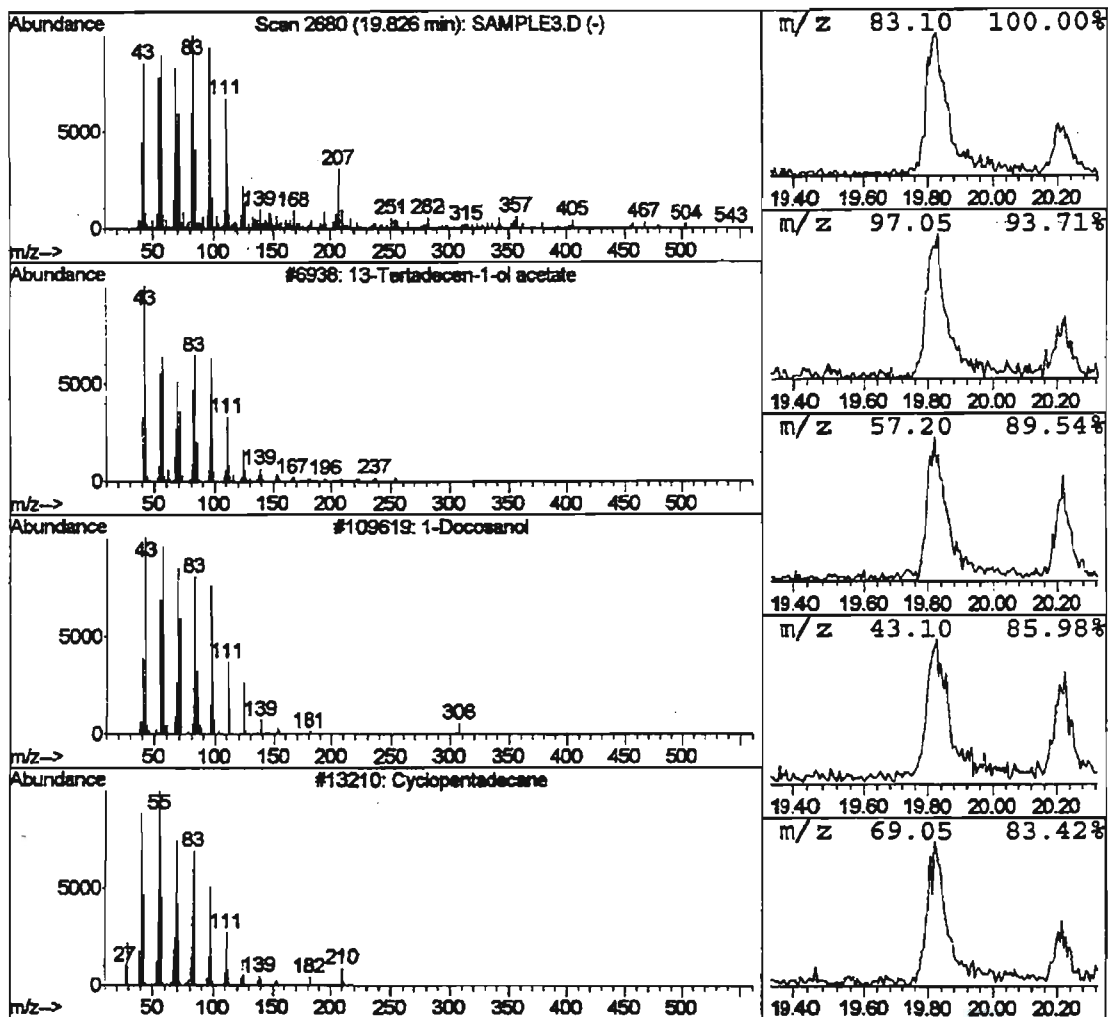
Figure C1.29:   Mass spectrum of an unknown compound eluting at 12.840 minutes.
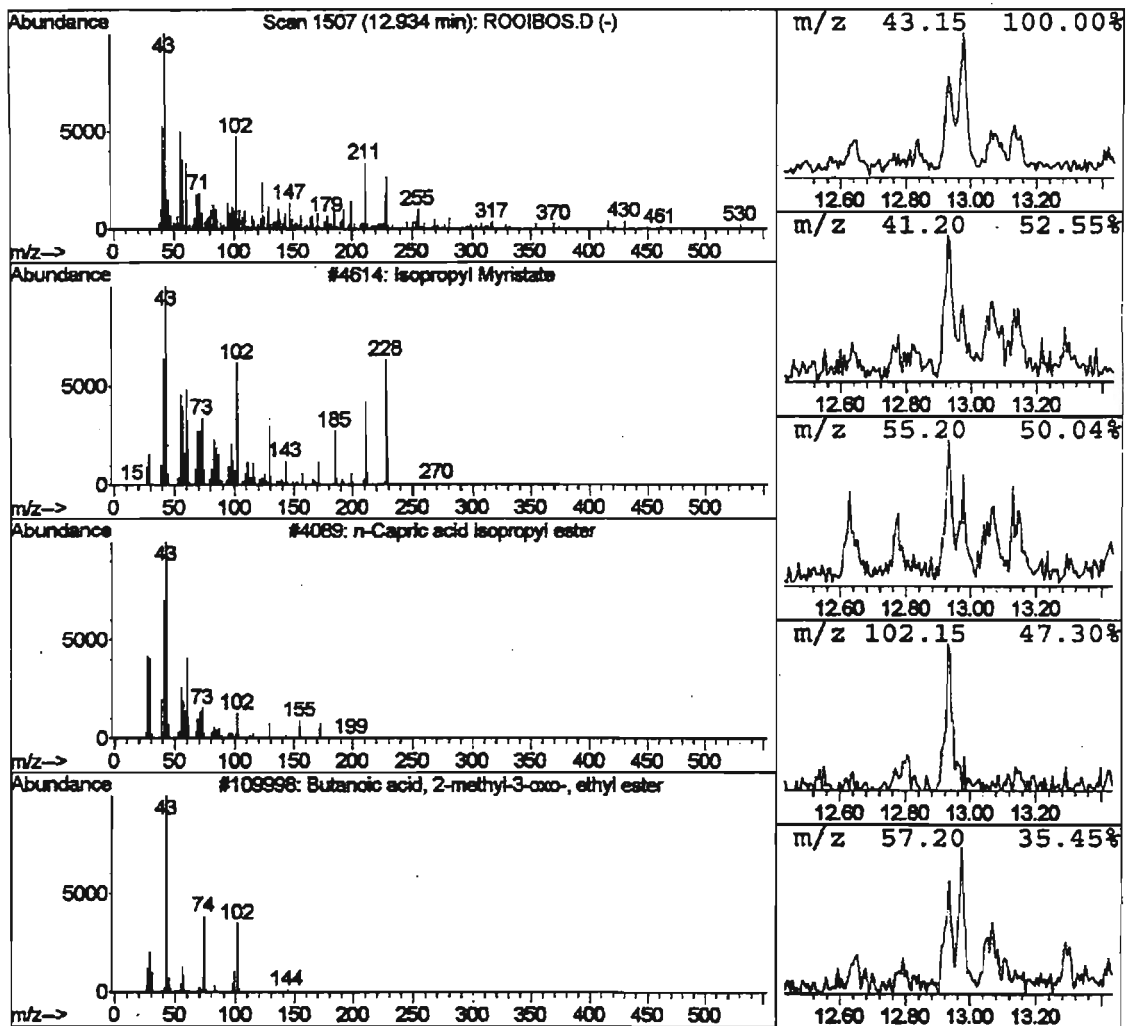
Figure C1.30:   Mass spectrum of an unknown compound eluting at 12.934 minutes.
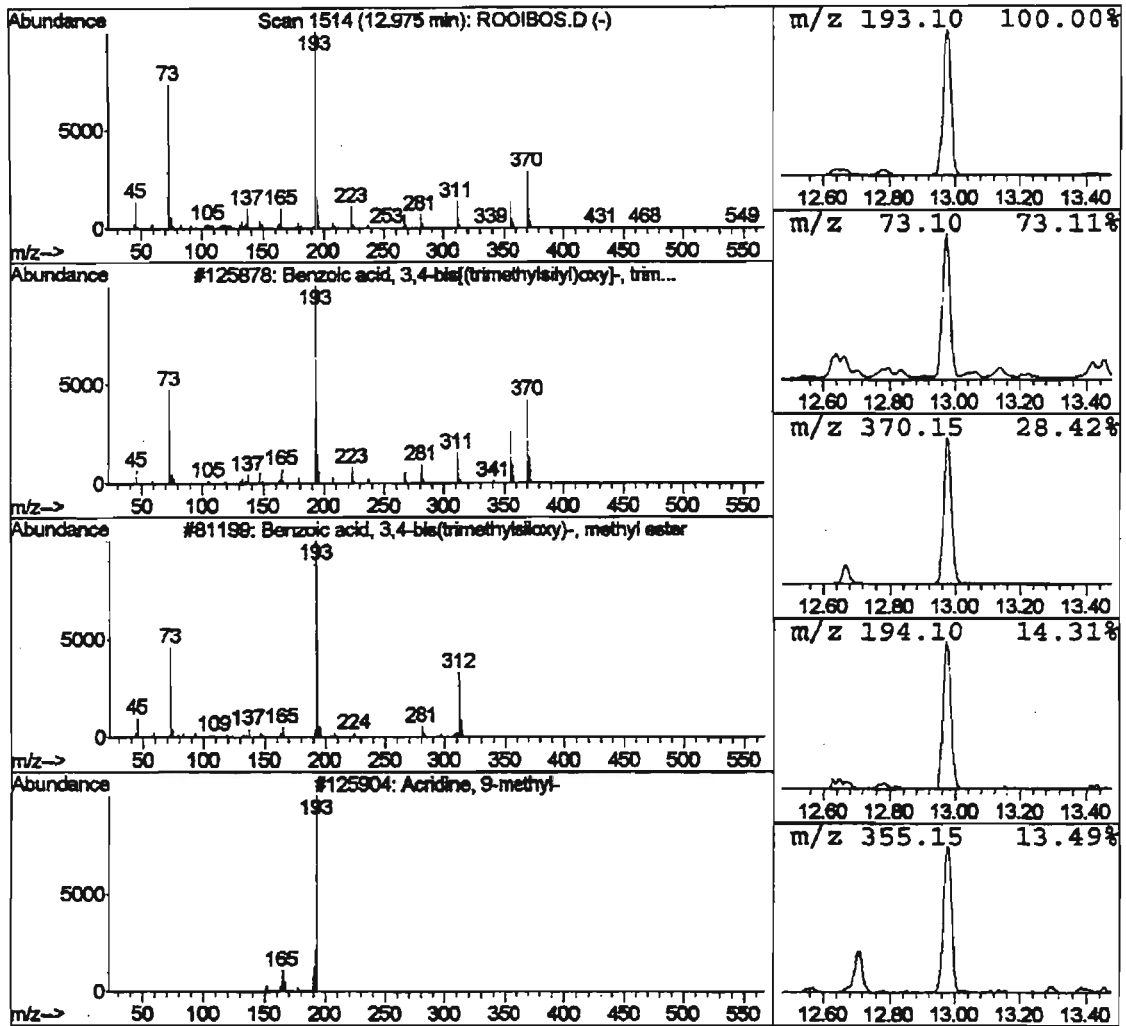
Figure C1.31: Mass spectrum of an unknown compound eluting at 12.975 minutes.
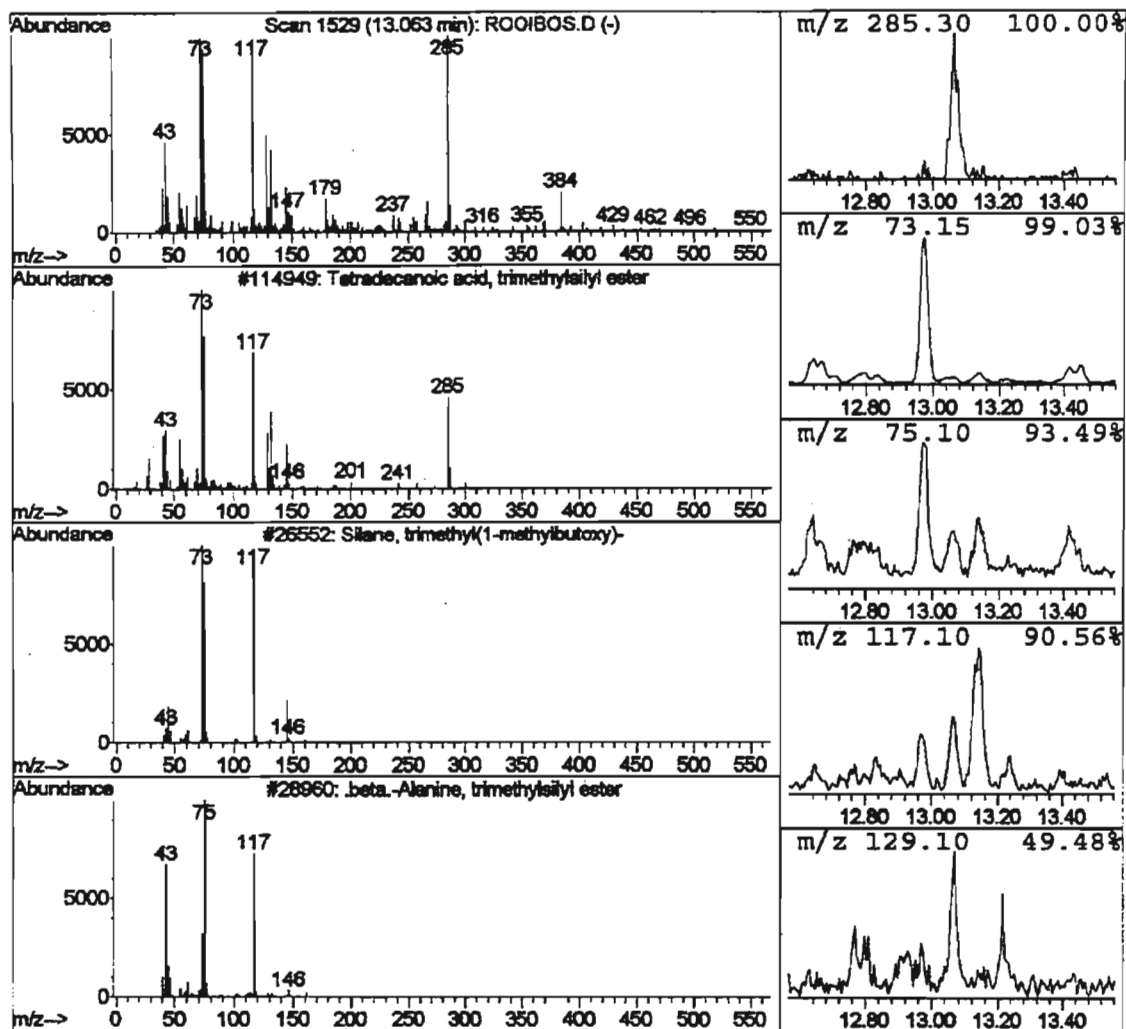
Figure C1.32: Mass spectrum of a derivatised tetradecanoic acid that elutes at 13.063 minutes. The fragmentation pattern matched that of a derivatised tetradecanoic acid present in the library.
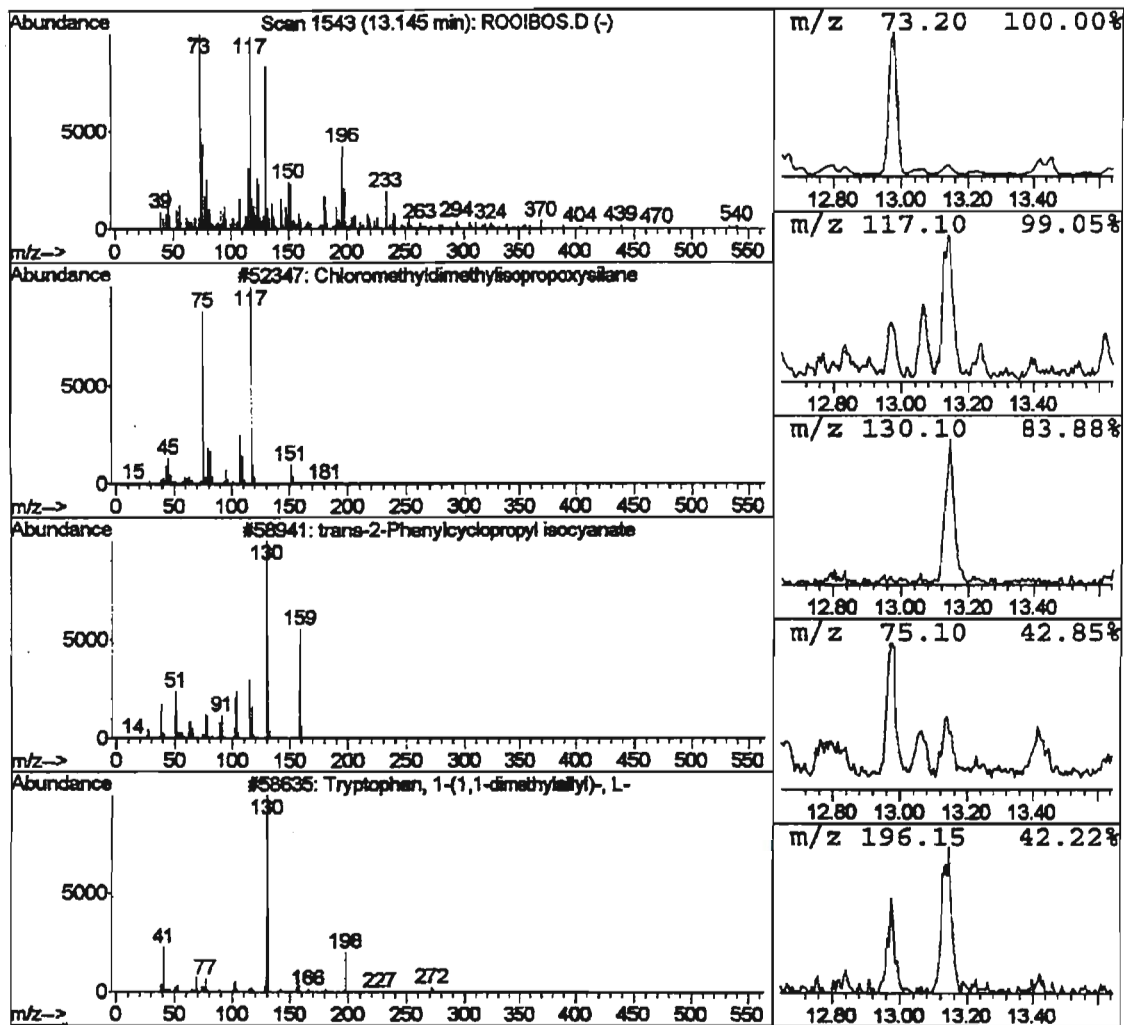
Figure C1.33:   Mass spectrum of an unknown compound eluting of 13.145 minutes.
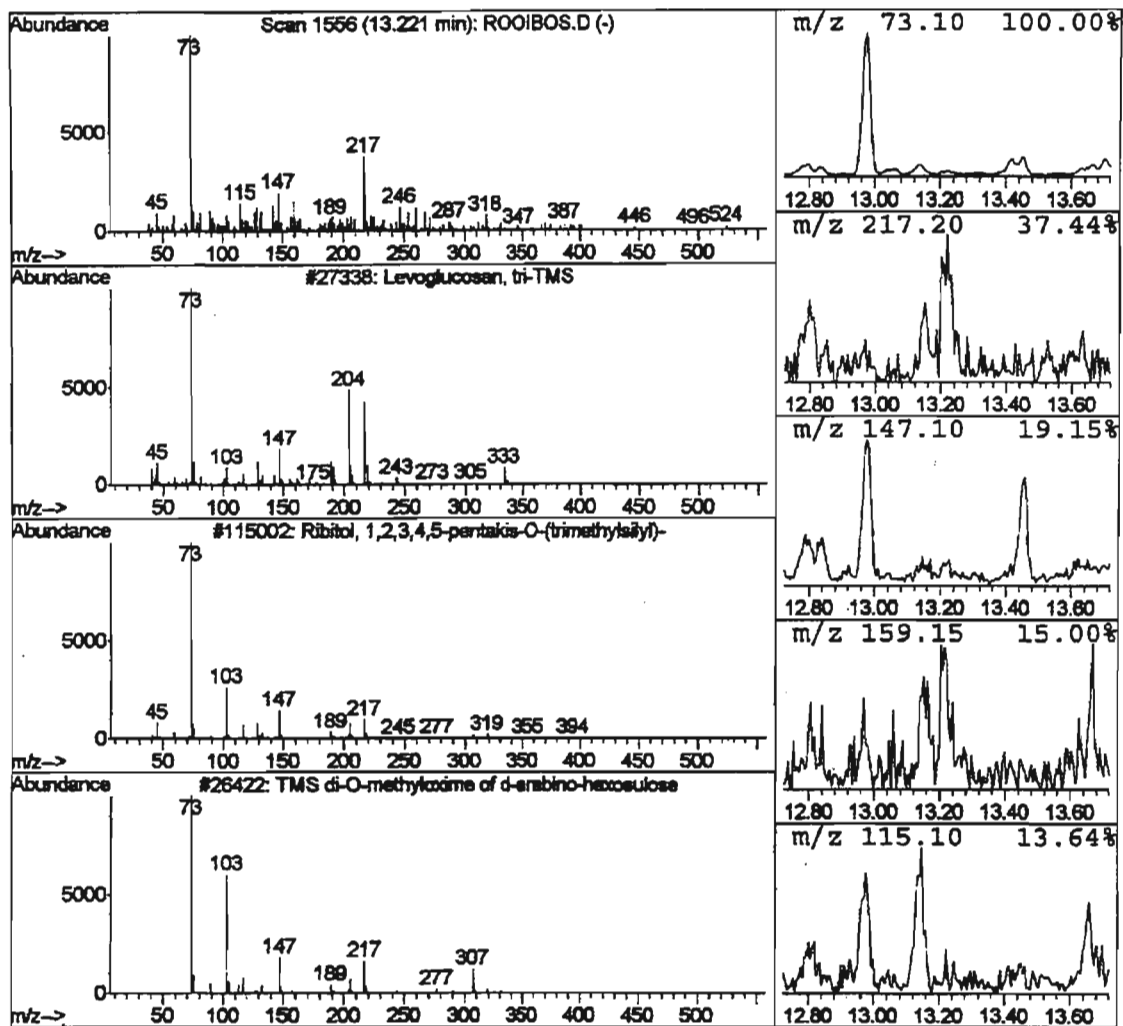
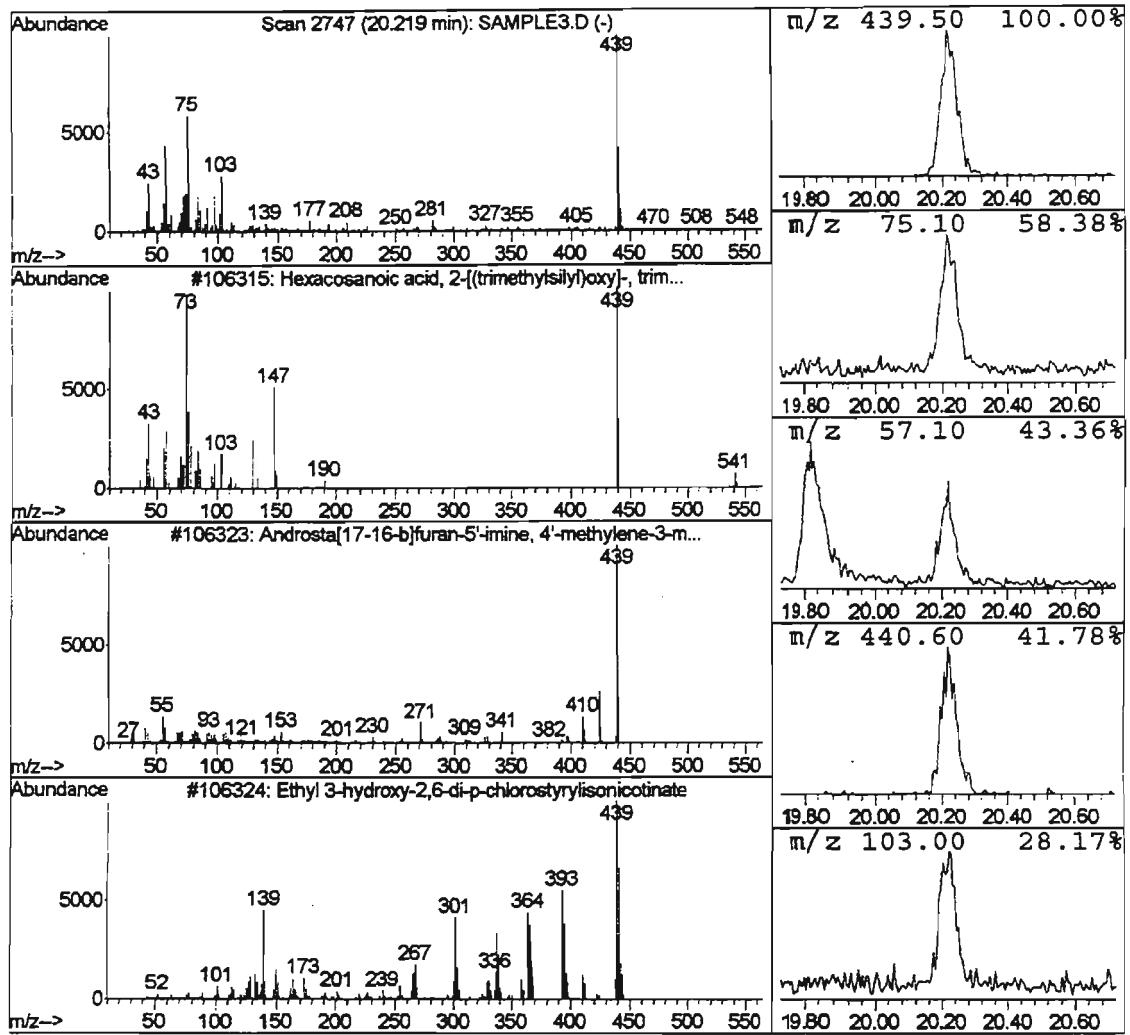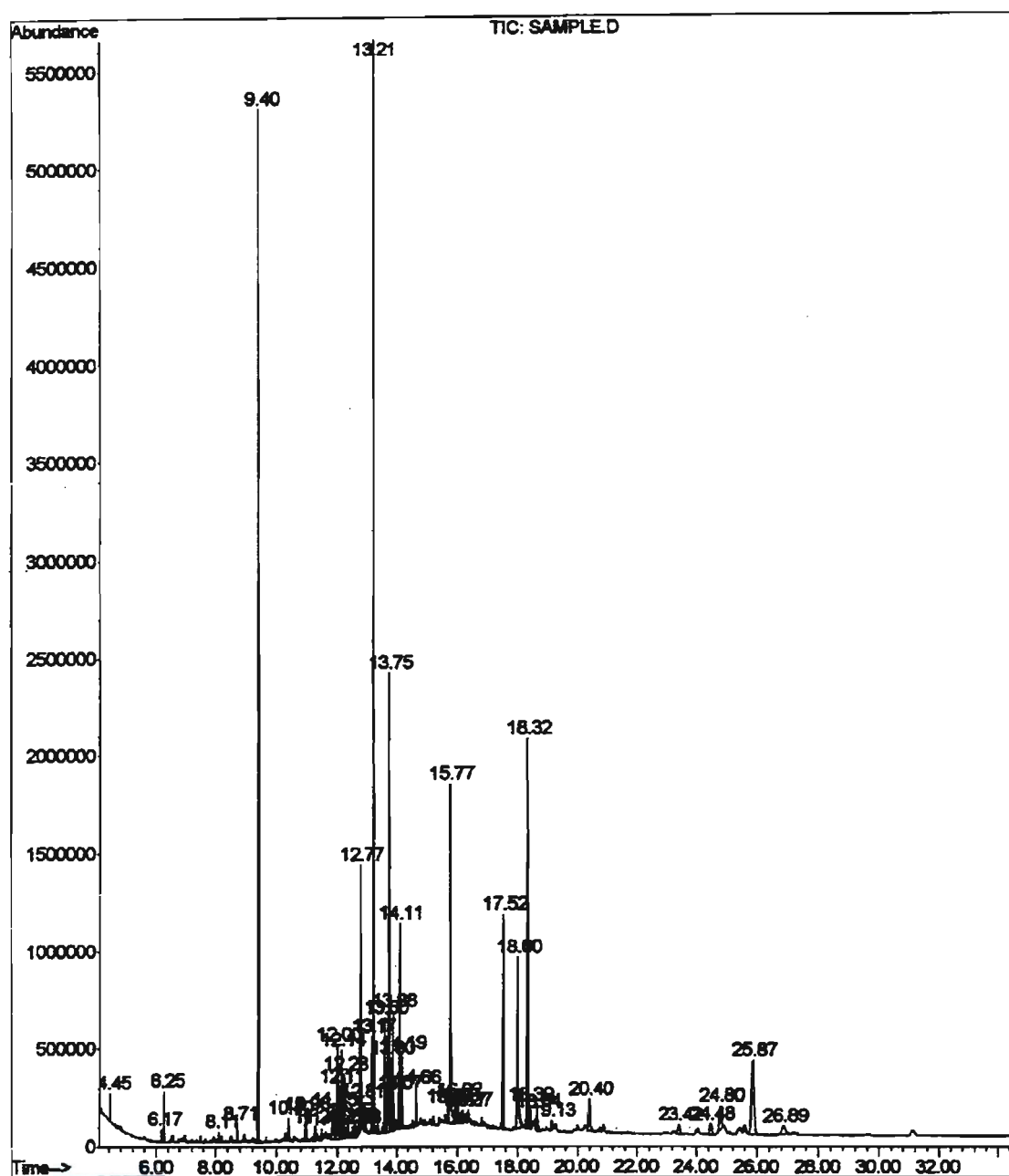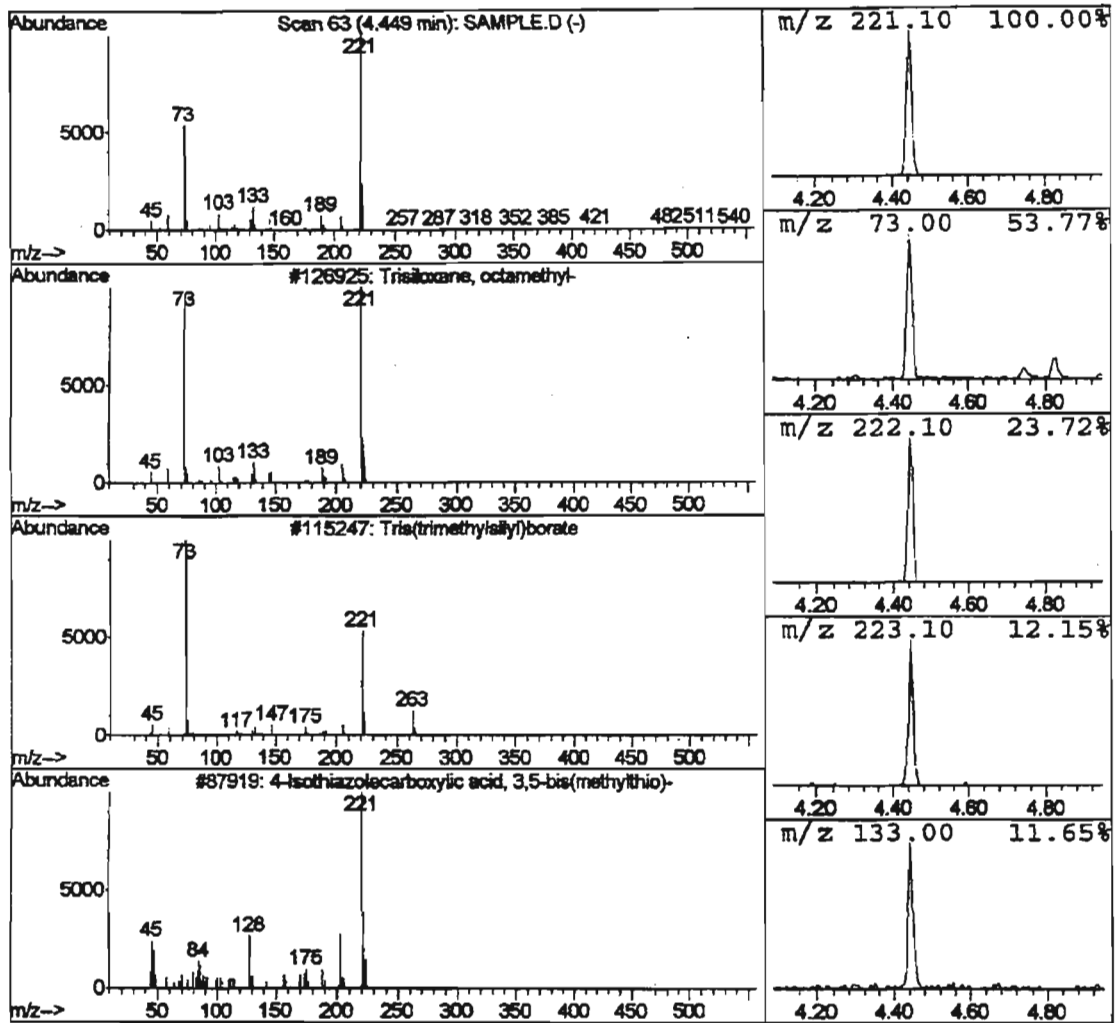Figure C1.34:   Mass spectrum of an unknown compound eluting at 13.221 minutes.
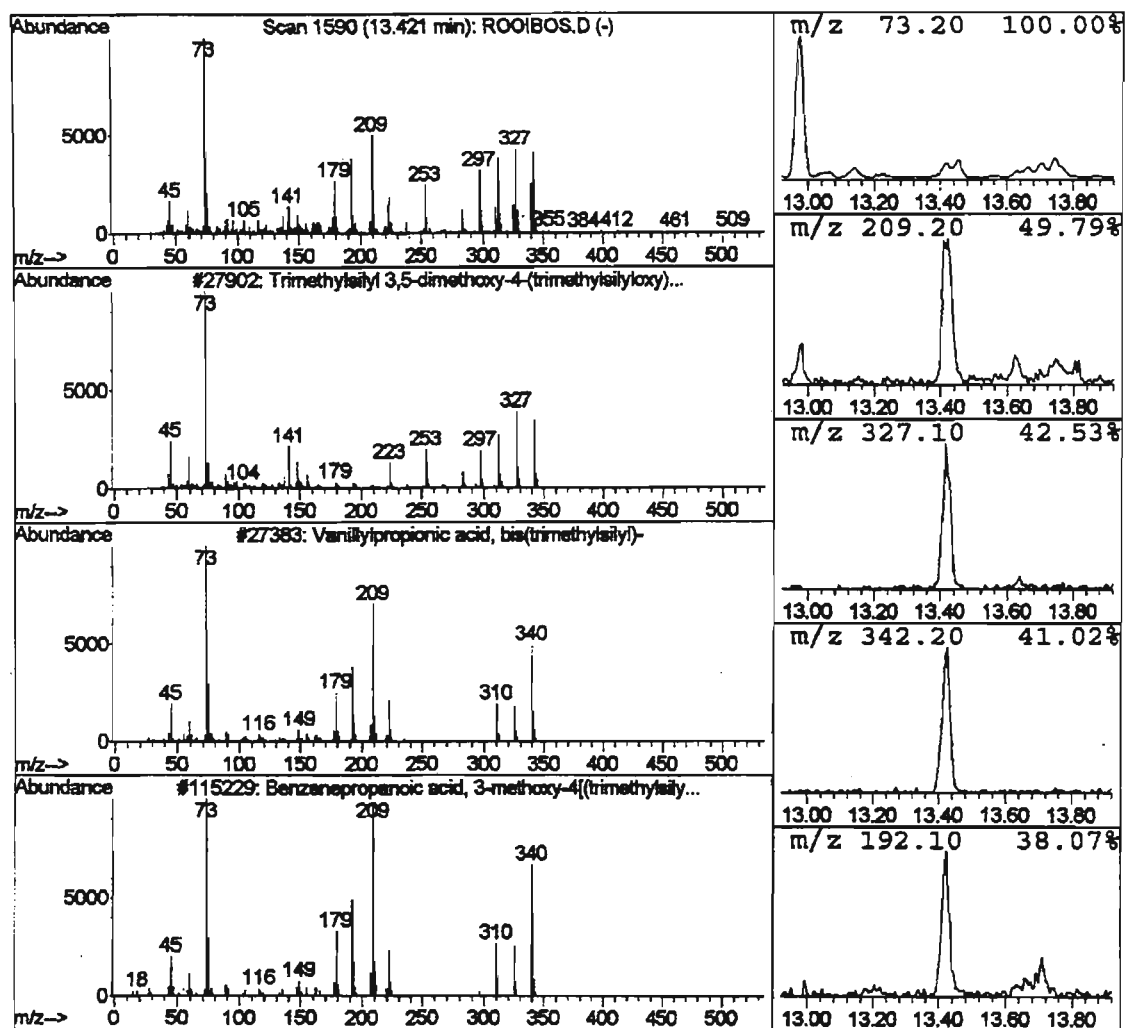
Figure C1.35:   Mass spectrum of a derivatised syringic acid that elutes at 13.421 minutes. The fragmentation pattern matched that of a derivatised syringic acid reported by Owen *et al.* [2003].
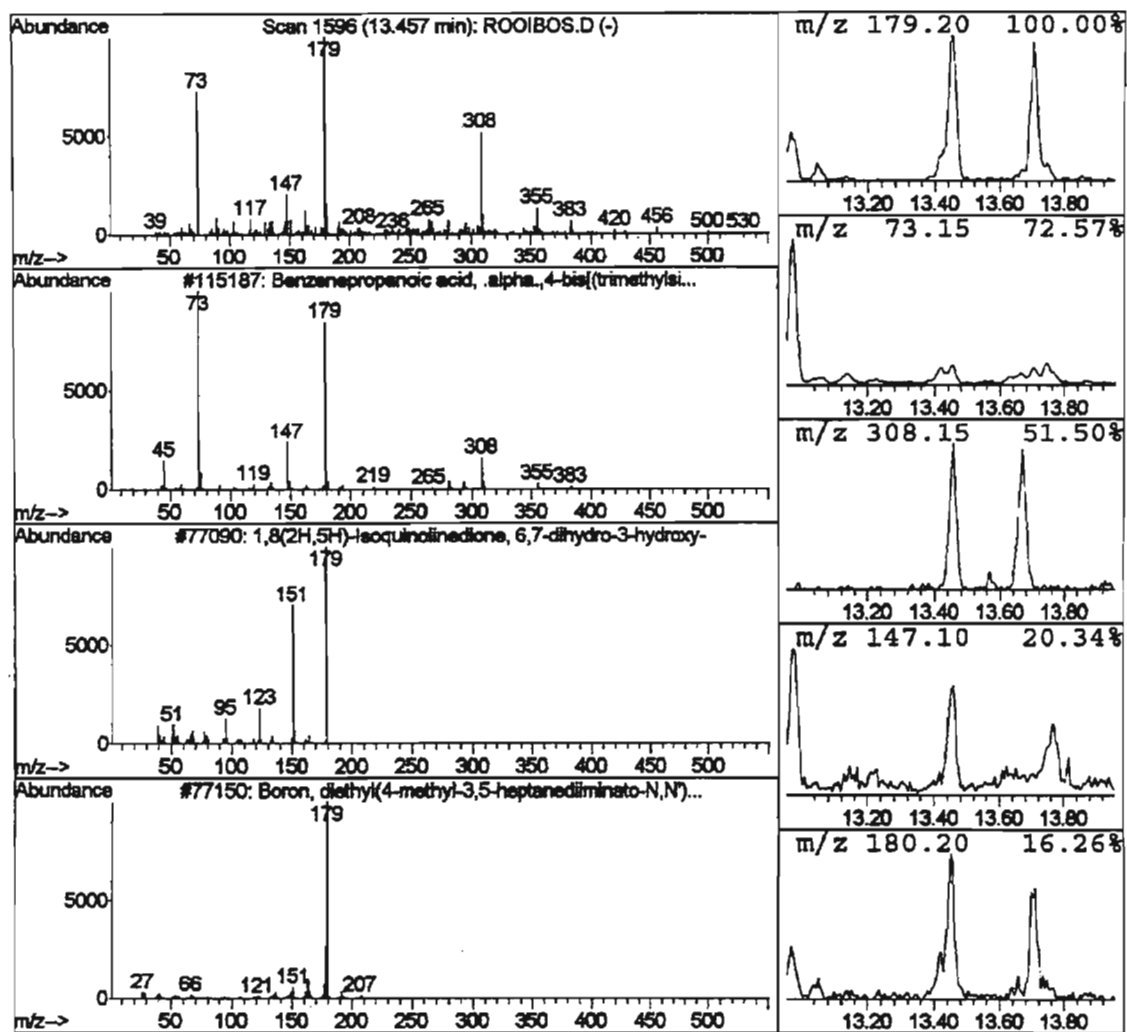
Figure C1.36: Mass spectrum of a derivatised benzenepropanoic acid that elutes at 13.457 minutes. The fragmentation pattern matched that of a derivatised benzenepropanoic acid present in the library.
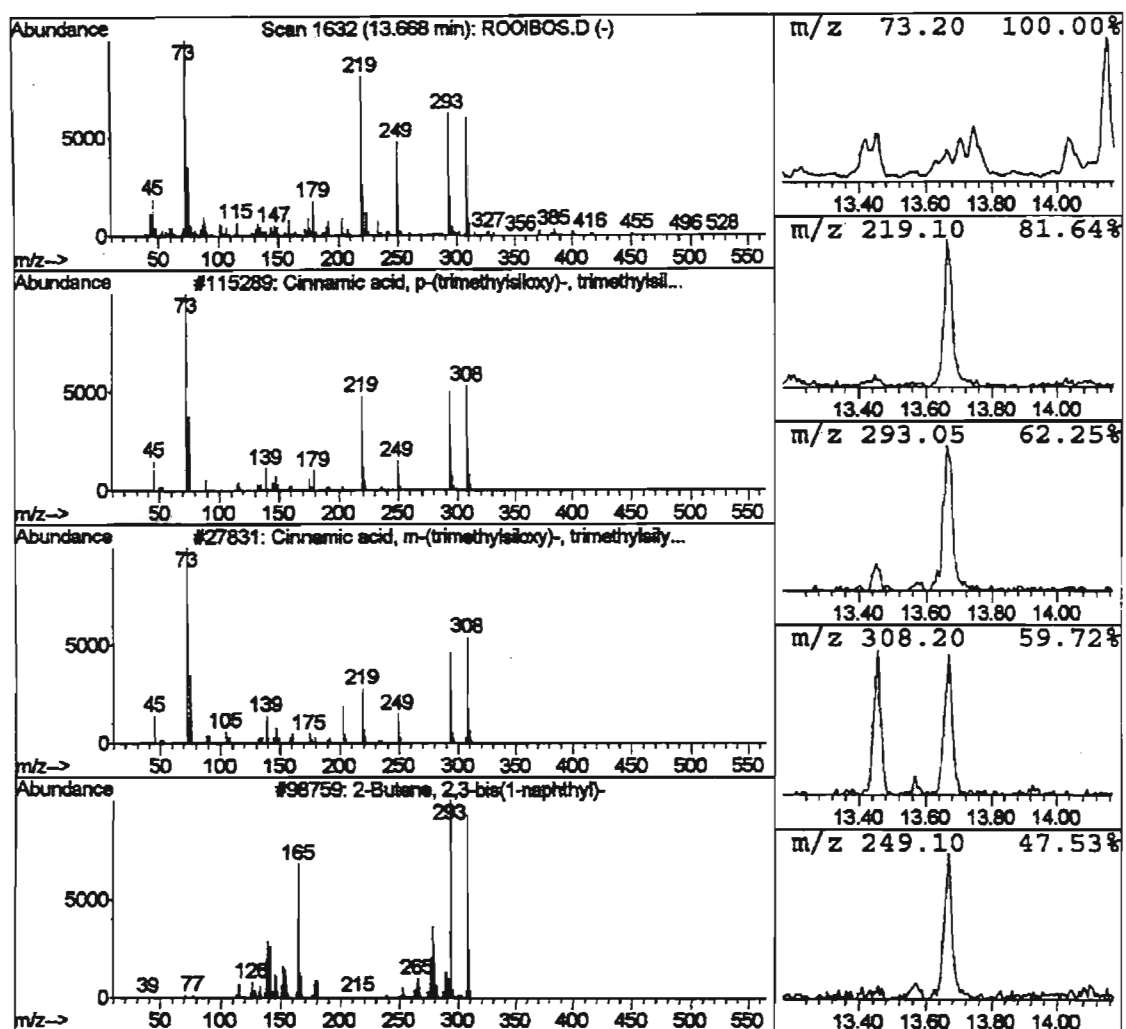
Figure Cl 37:   Mass spectrum of a derivatised cinnamic acid that elutes at 13.668 minutes.
The fragmentation pattern matched that of a derivatised cinnamic acid present in
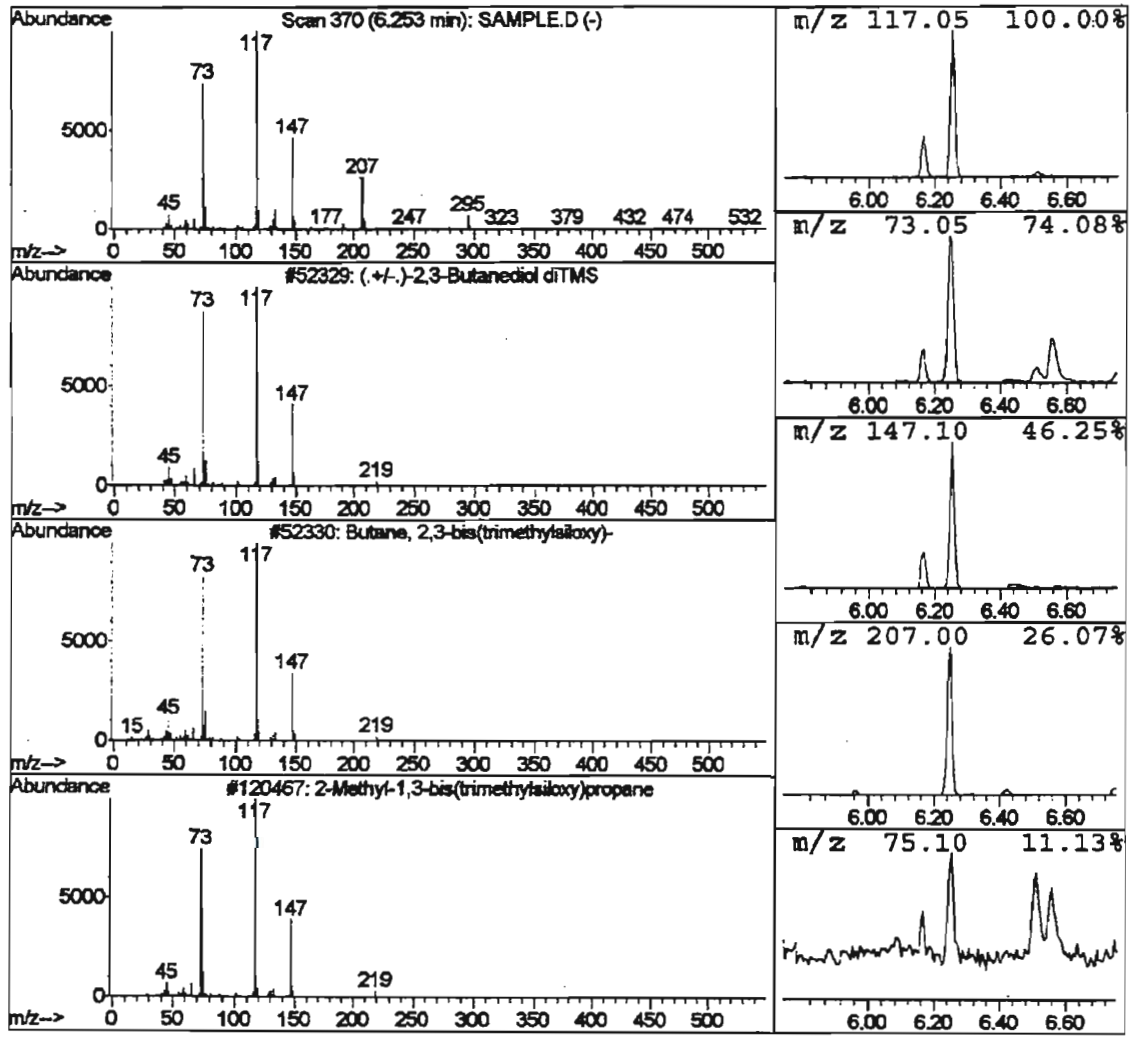the library.
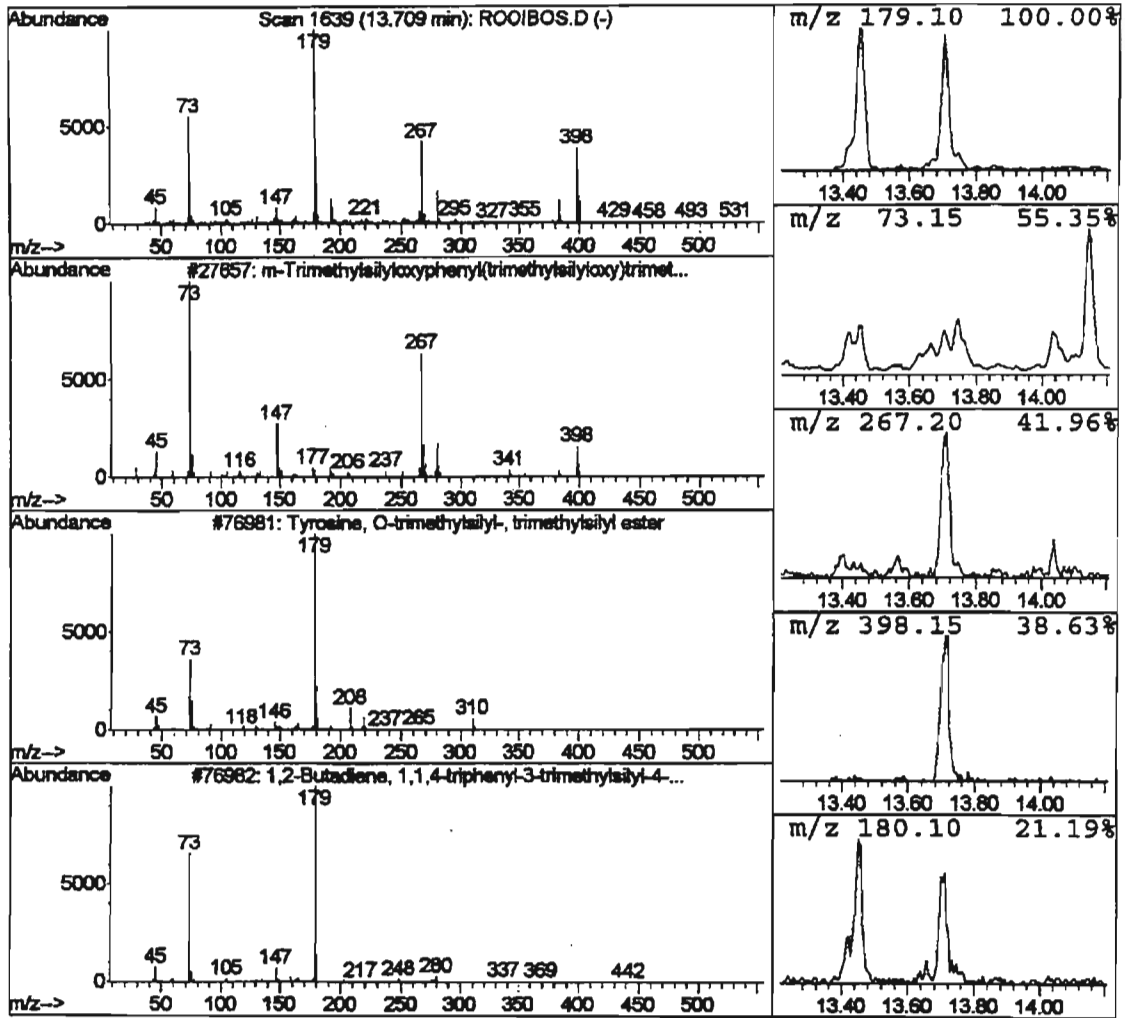
Figure C1.38:   Mass spectrum of an unknown compound eluting at 13.709 minutes.
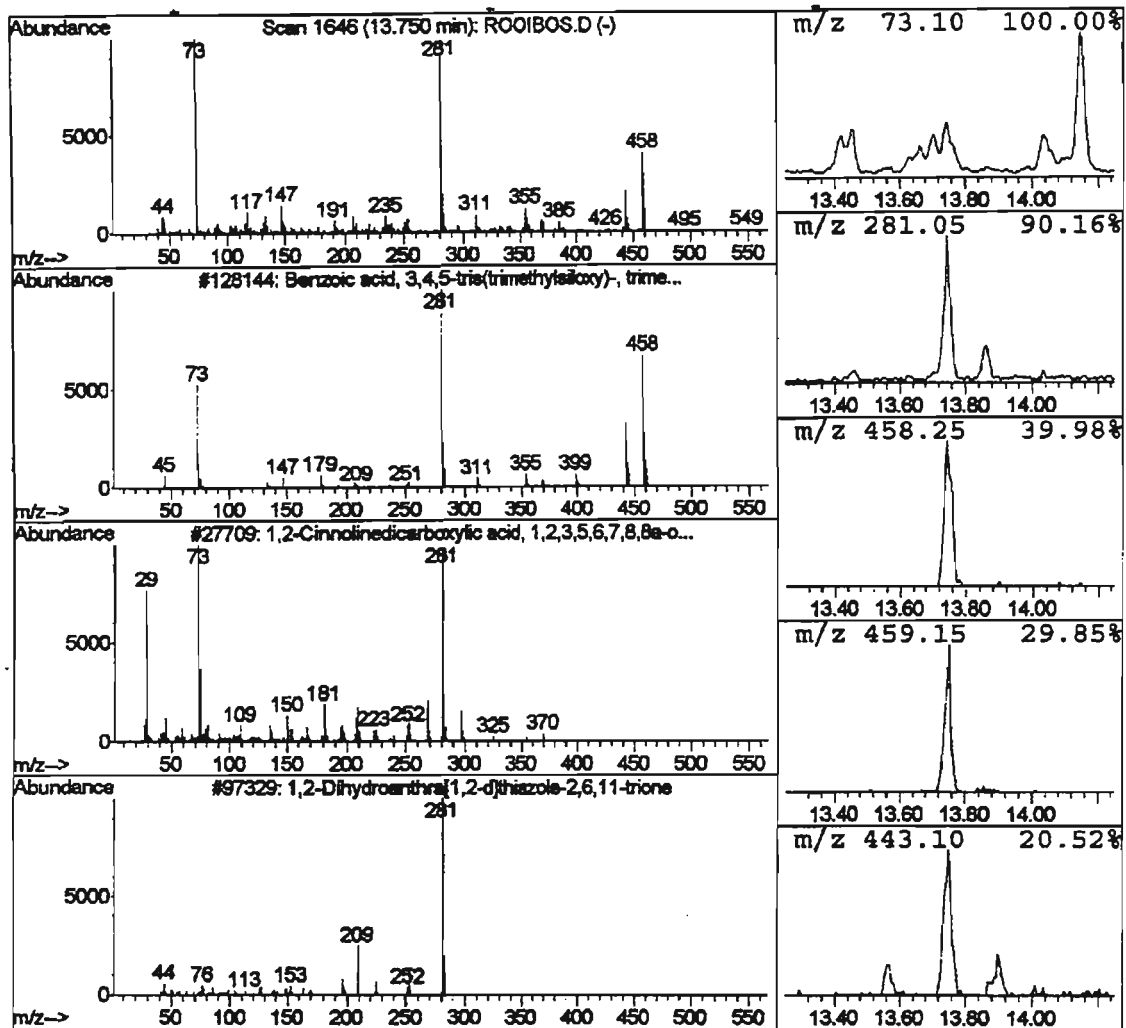
Figure C1.39: Mass spectrum of a derivatised gallic acid that elutes at 13.750 minutes. The
fragmentation pattern matched that of a derivatised gallic acid present in the
library and reported by Owen *et al.* [2003].
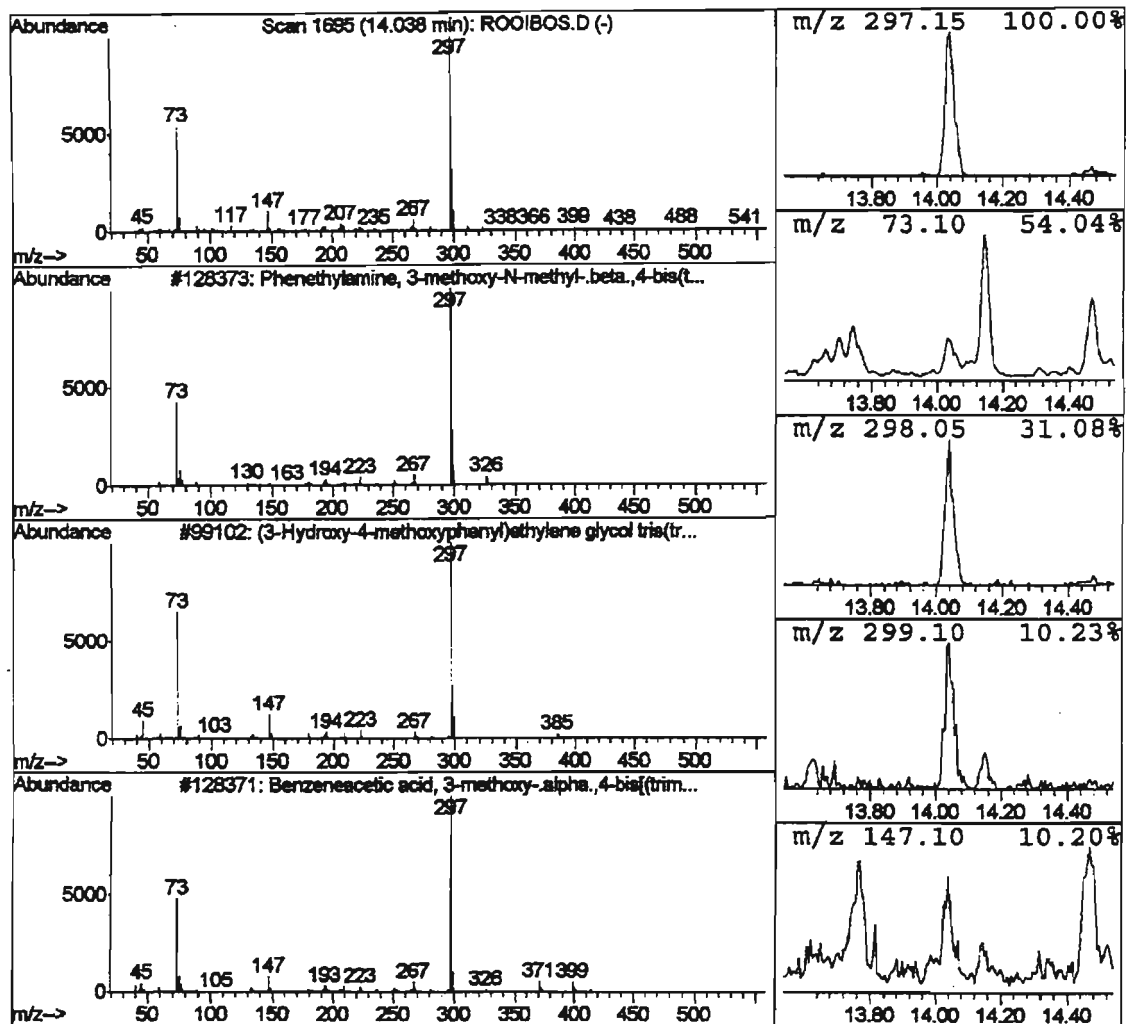
Figure C1.40:   Mass spectrum of an unknown compound eluting at 14.038 minutes.
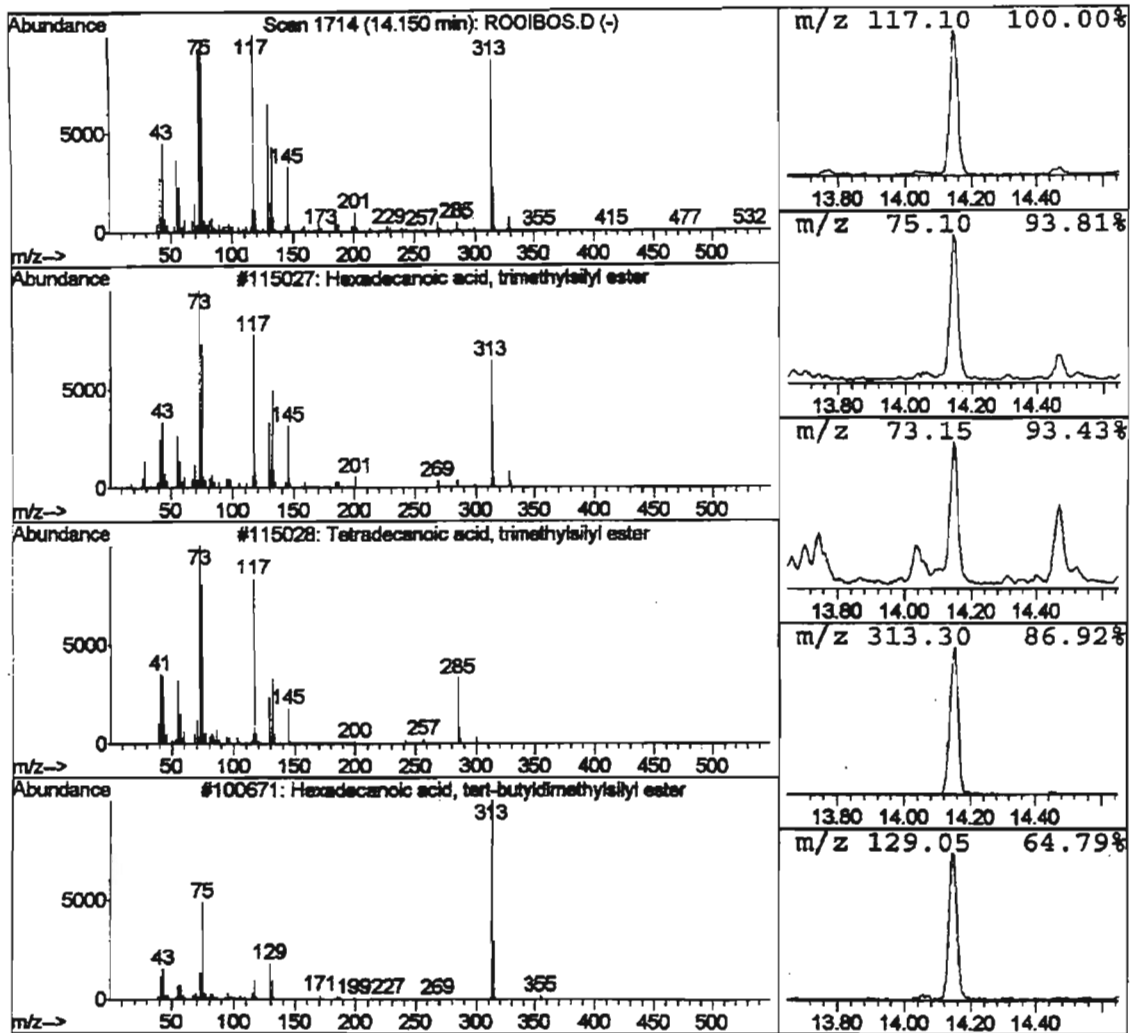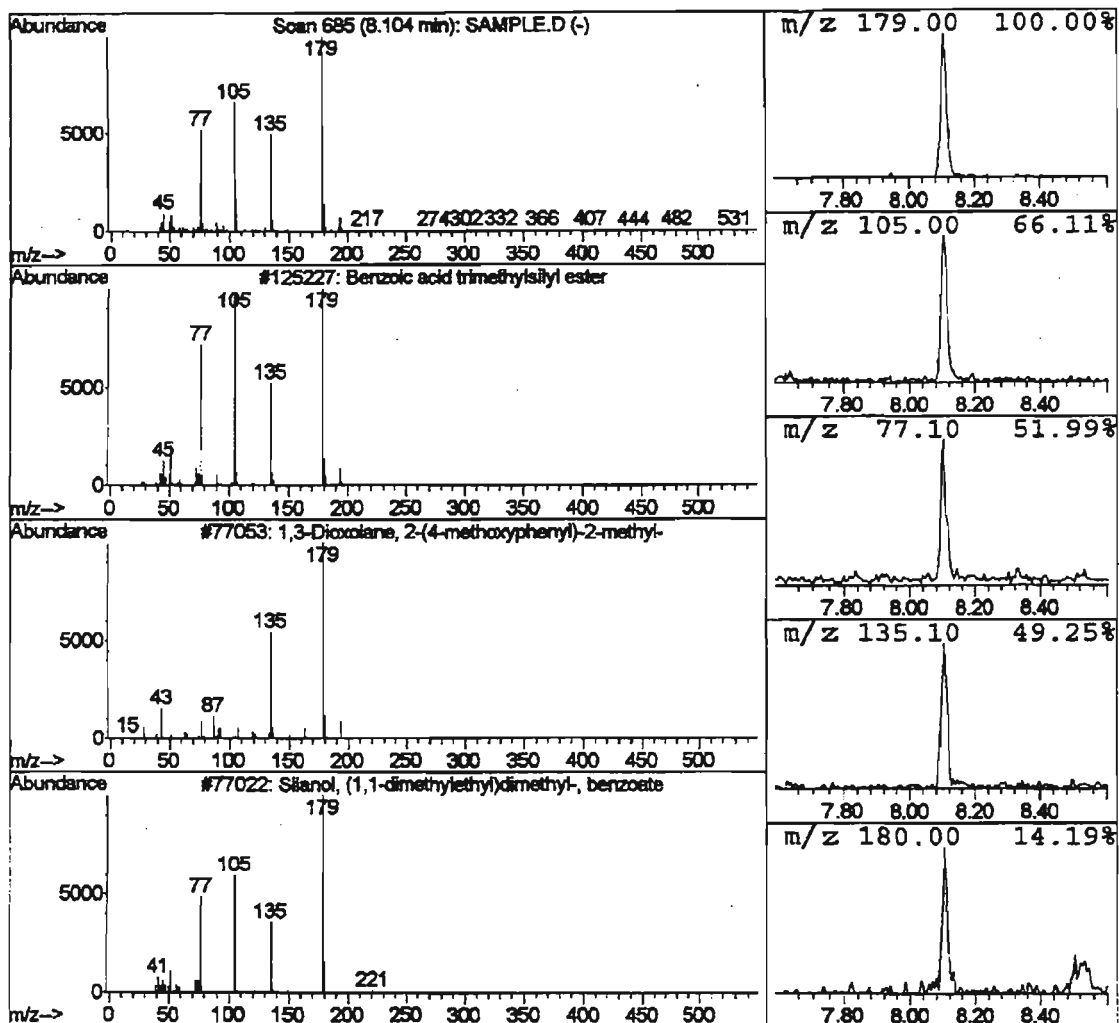
Figure C1.41:   Mass spectrum of a derivatised hexadecanoic acid that elutes at 14.150 minutes. The fragmentation pattern matched that of a derivatised hexadecanoic acid present in the library.
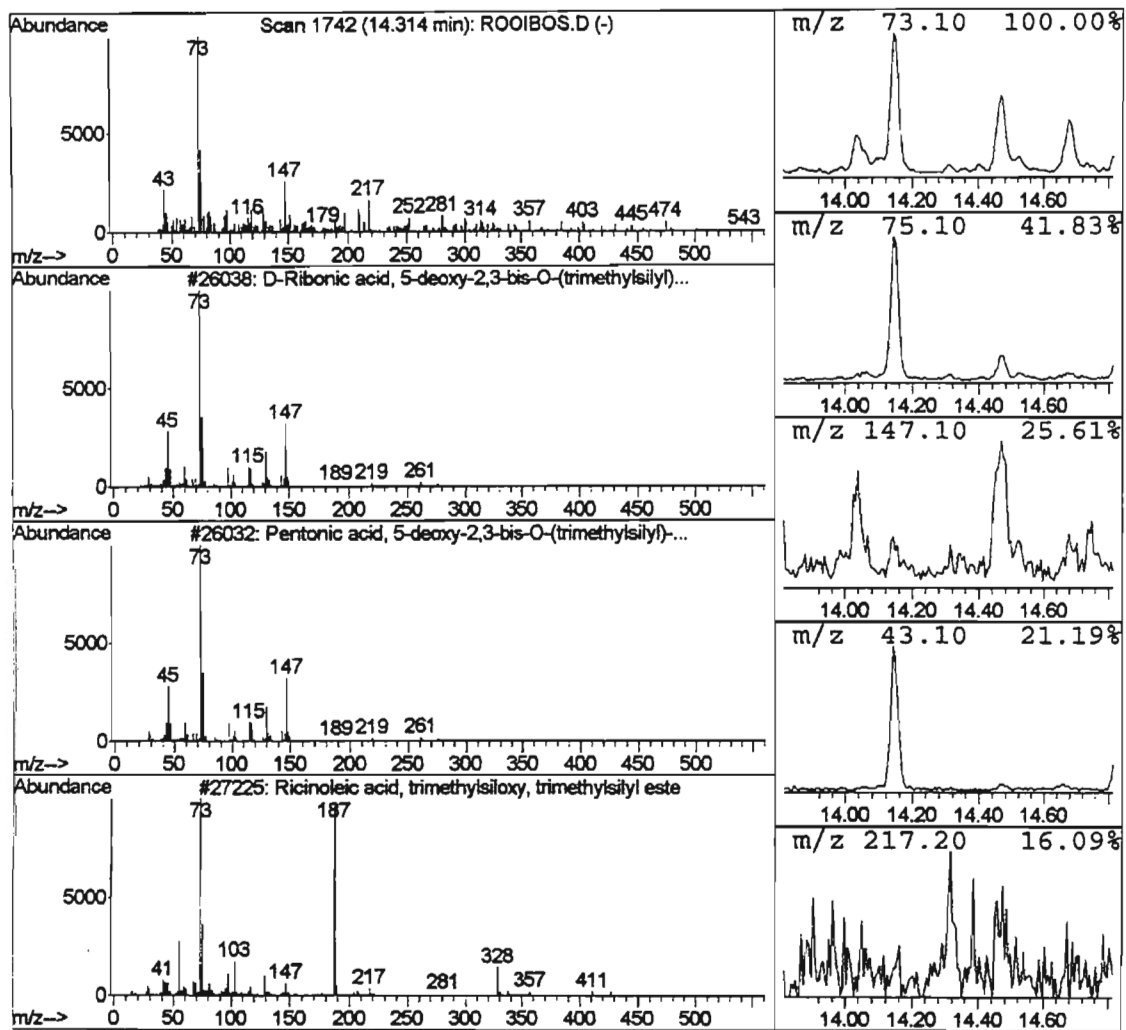
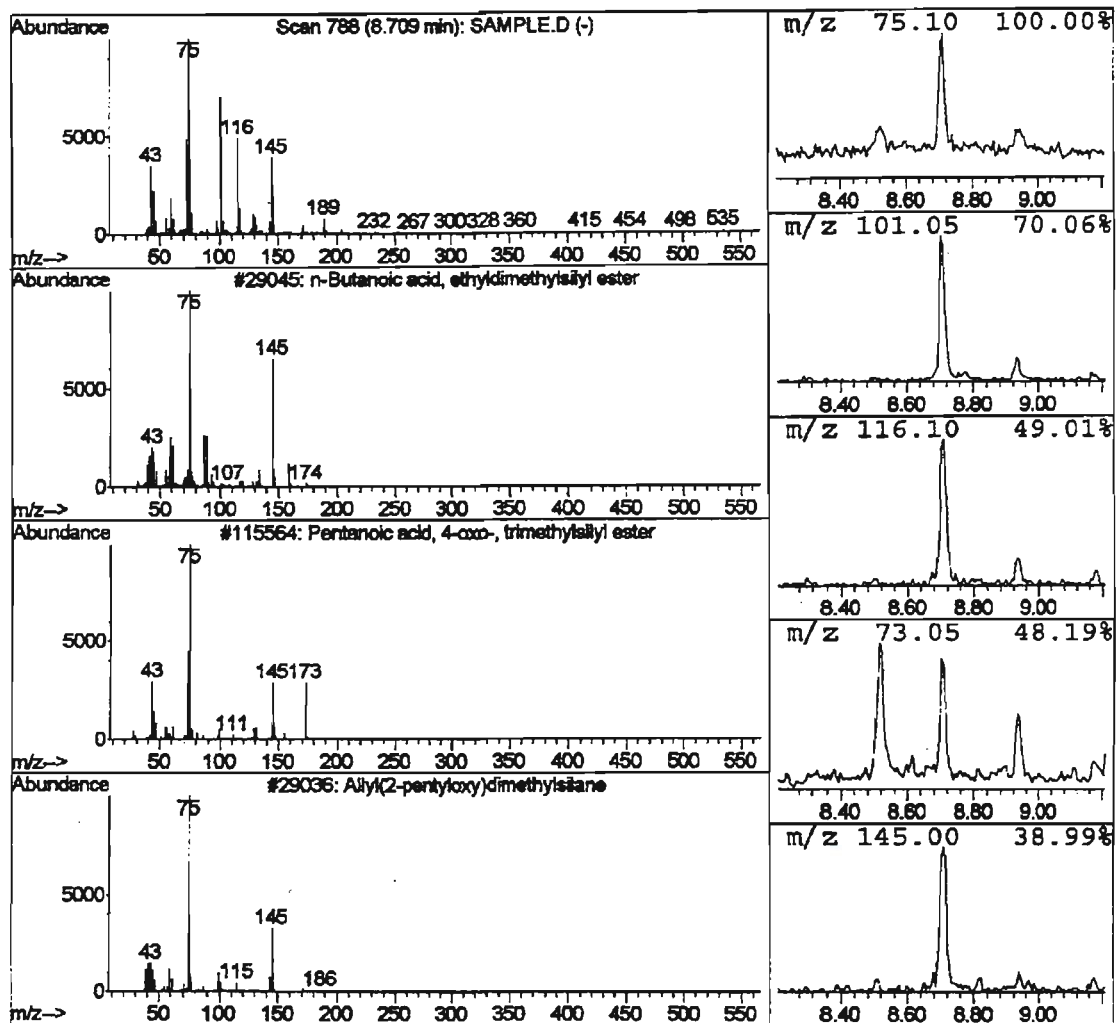Figure C1.42:   Mass spectrum of an unknown compound eluting at 14.314 minutes.
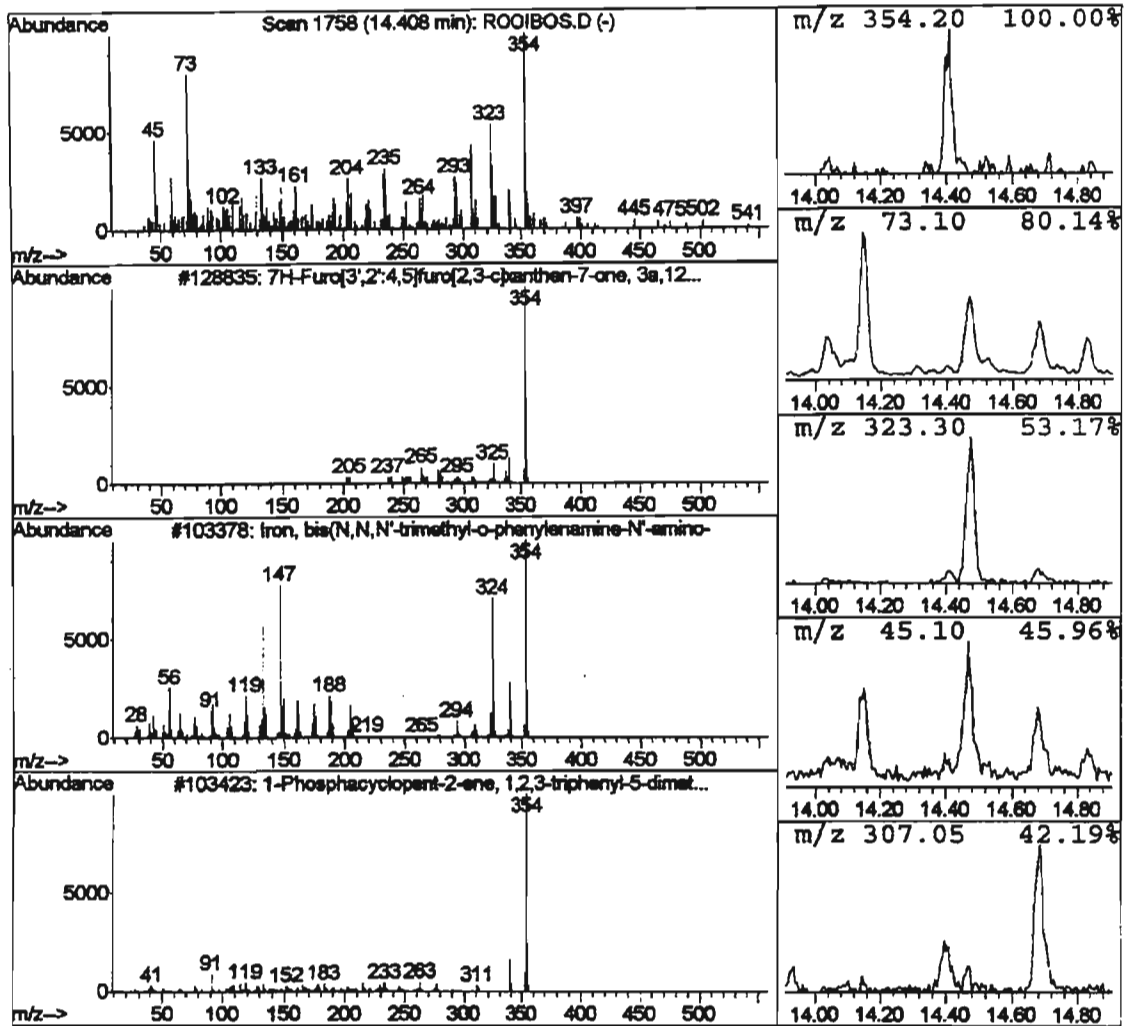
Figure C1.43:   Mass spectrum of an unknown compound eluting at 14.408 minutes.
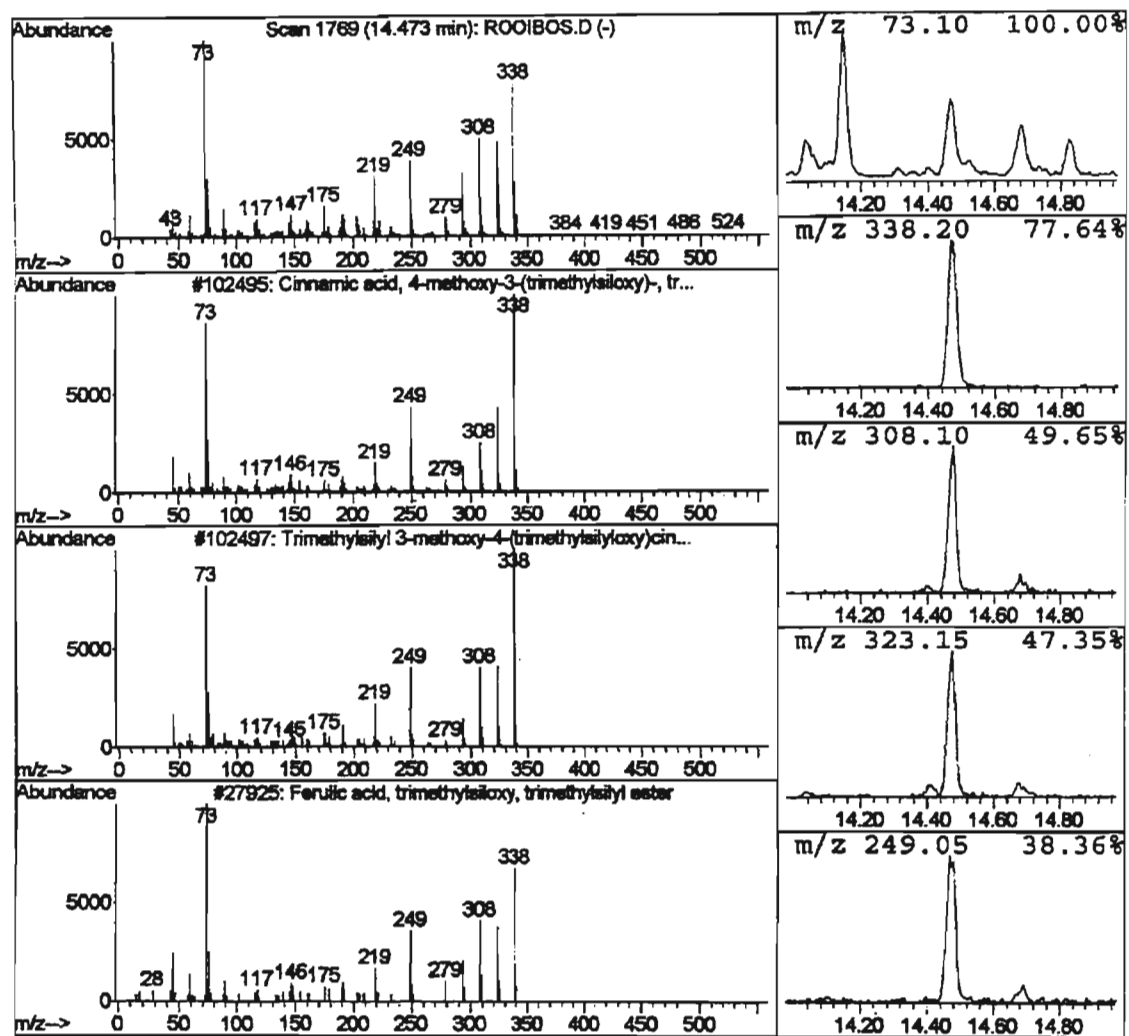
Figure C1.44: Mass spectrum of a derivatised ferulic acid that elutes at 14.473 minutes. The fragmentation pattern matched that of a derivatised ferulic acid present in the library.
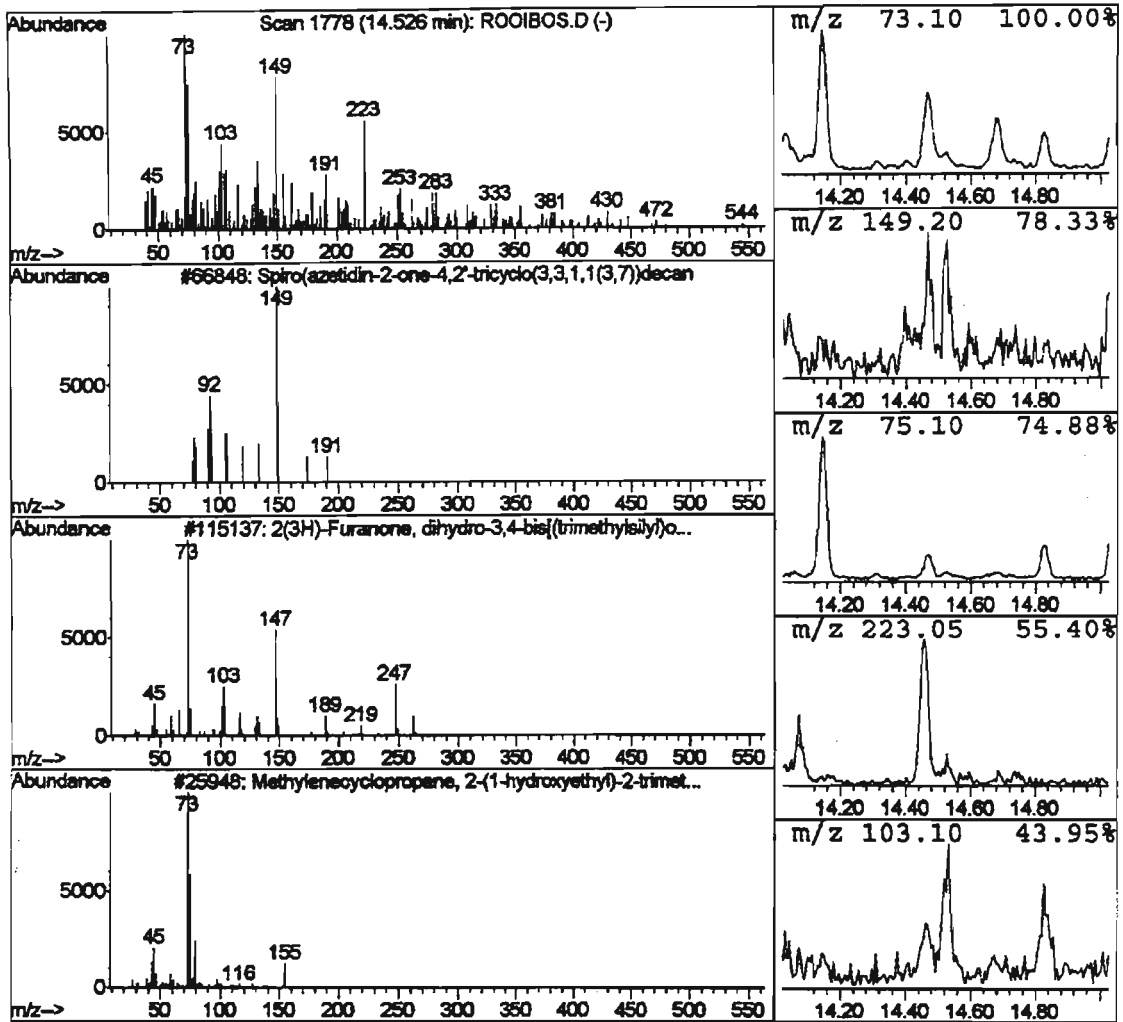
Figure C1.45:   Mass spectrum of an unknown compound eluting at 14.526 minutes.
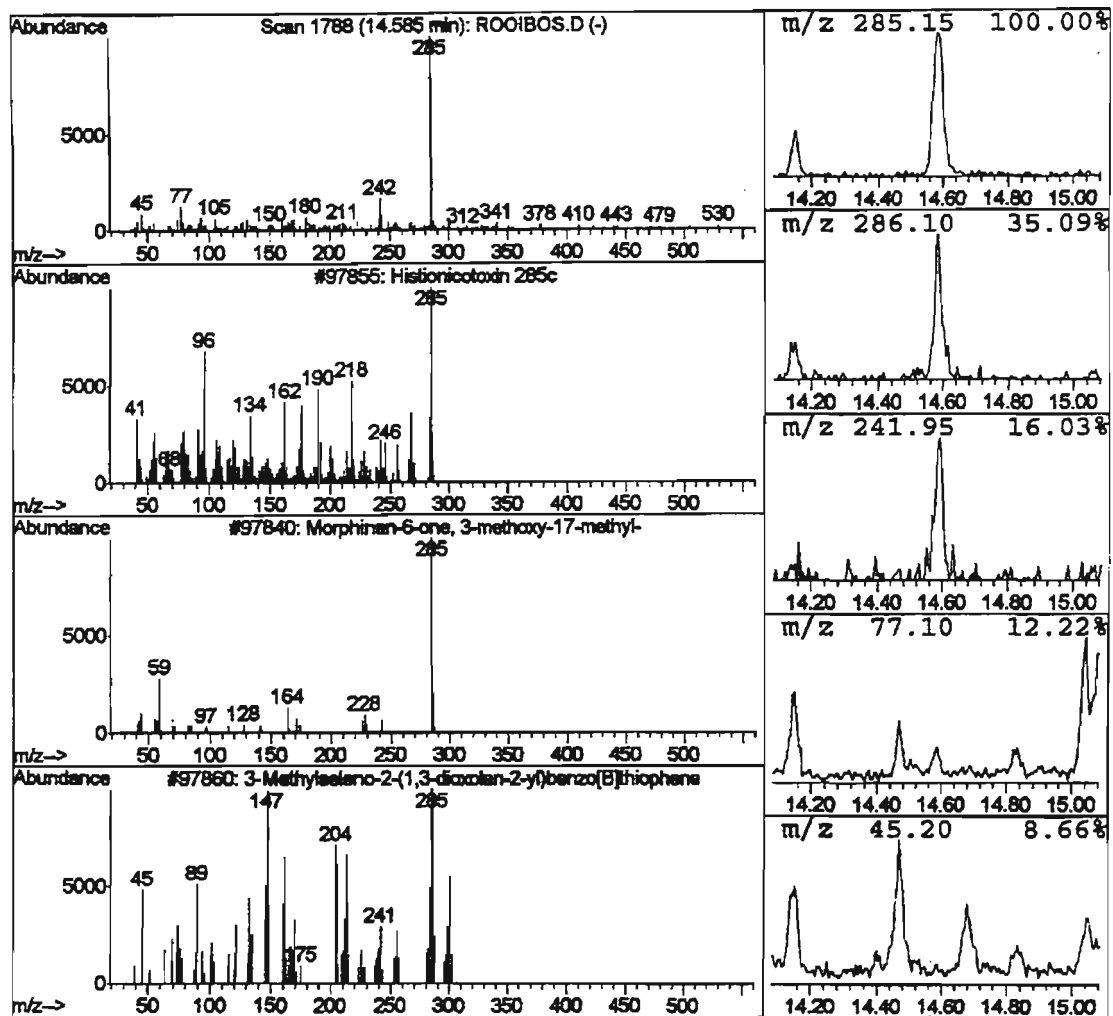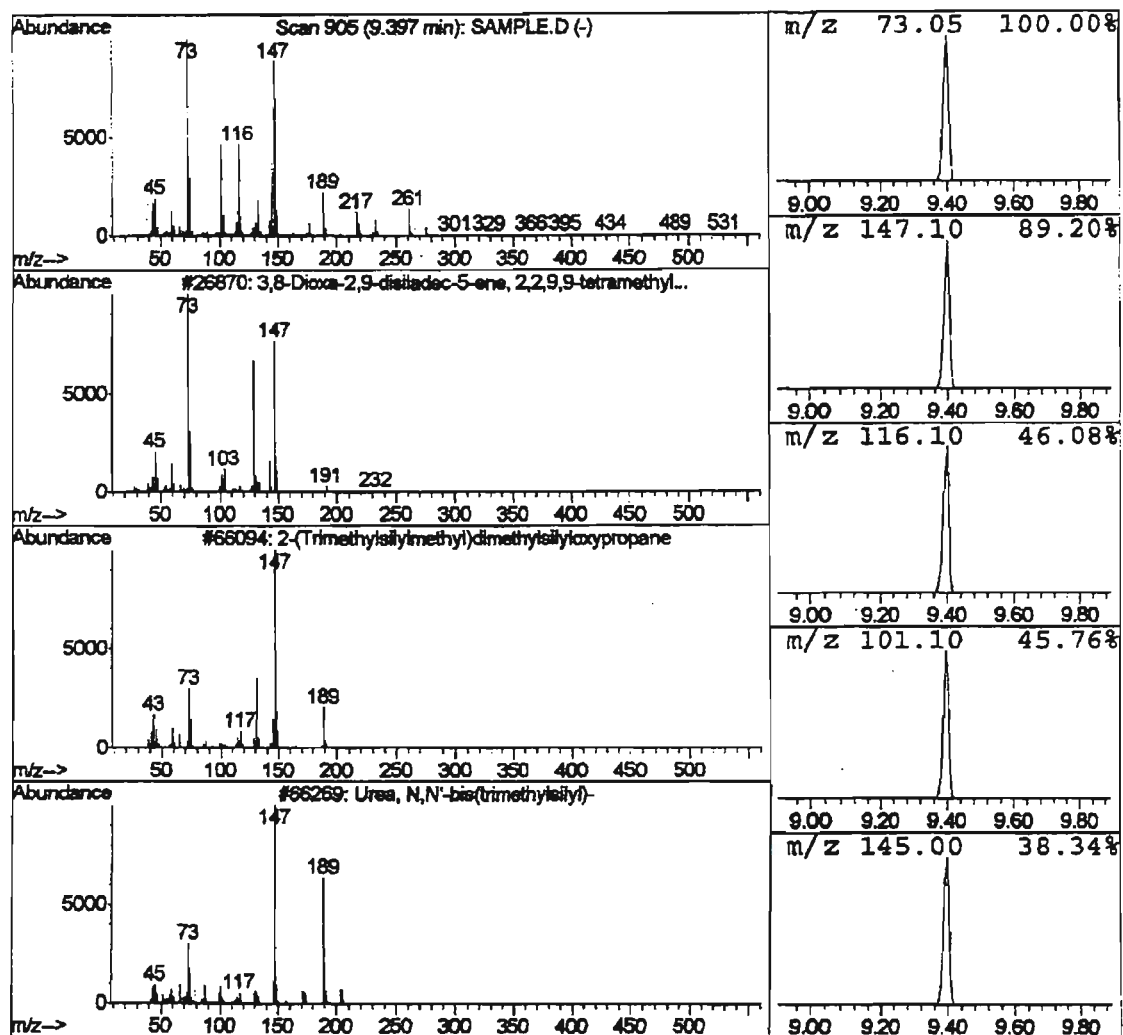
Figure C1.46:   Mass spectrum of an unknown compound eluting at 14.585 minutes.
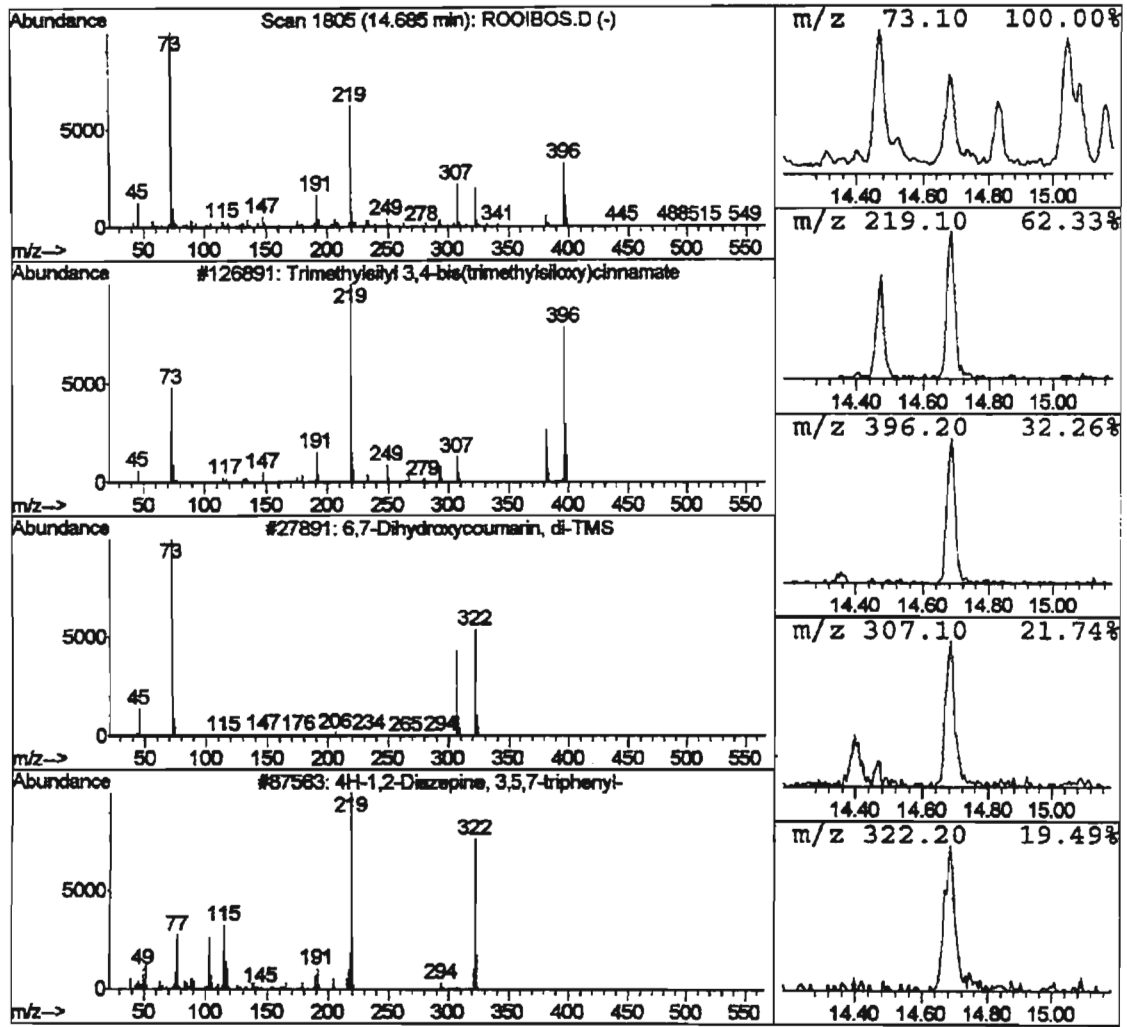
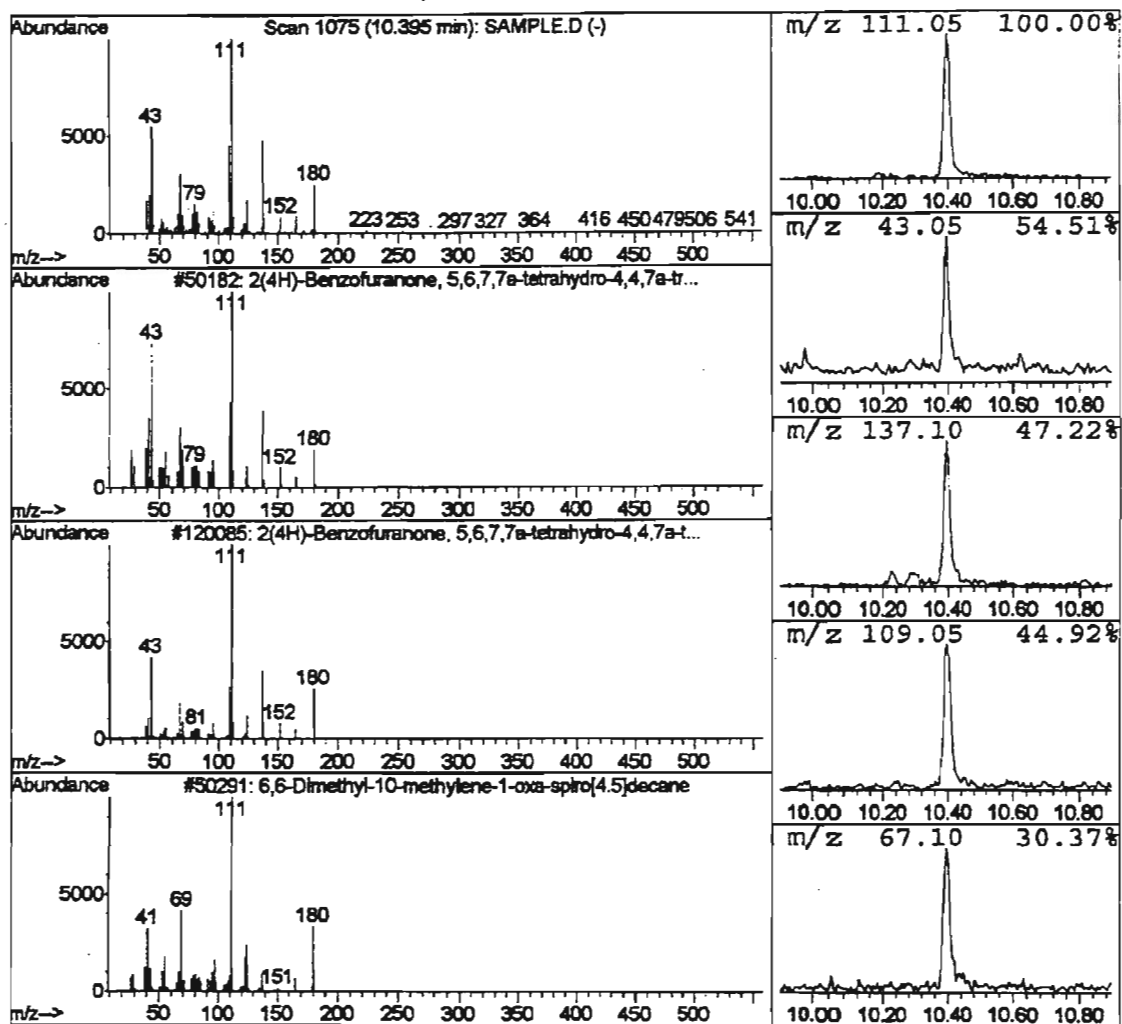Figure C1.47:   Mass spectrum of an unknown compound eluting at 14.685 minutes.
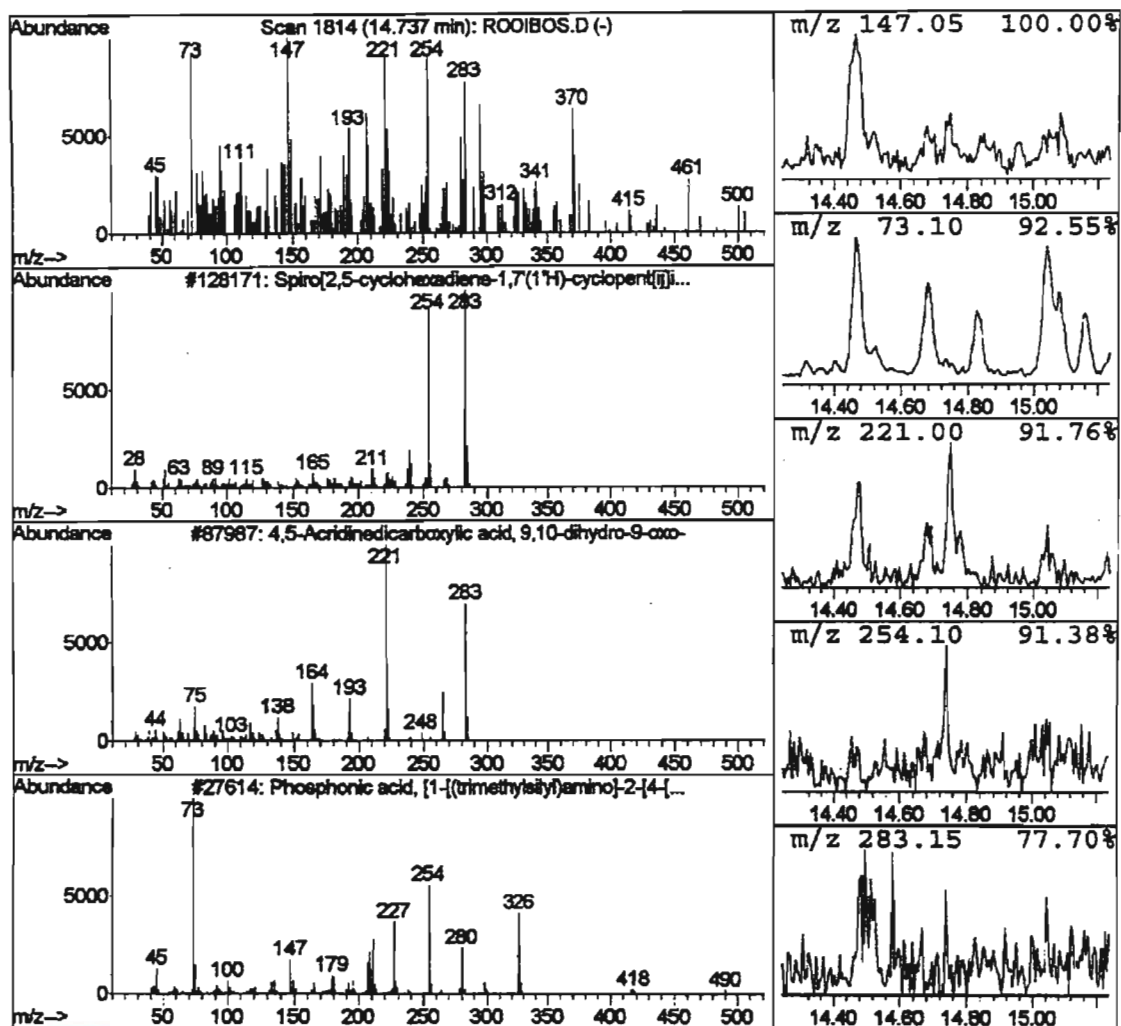
Figure C1.48:   Mass spectrum of an unknown compound eluting at 14.737 minutes.
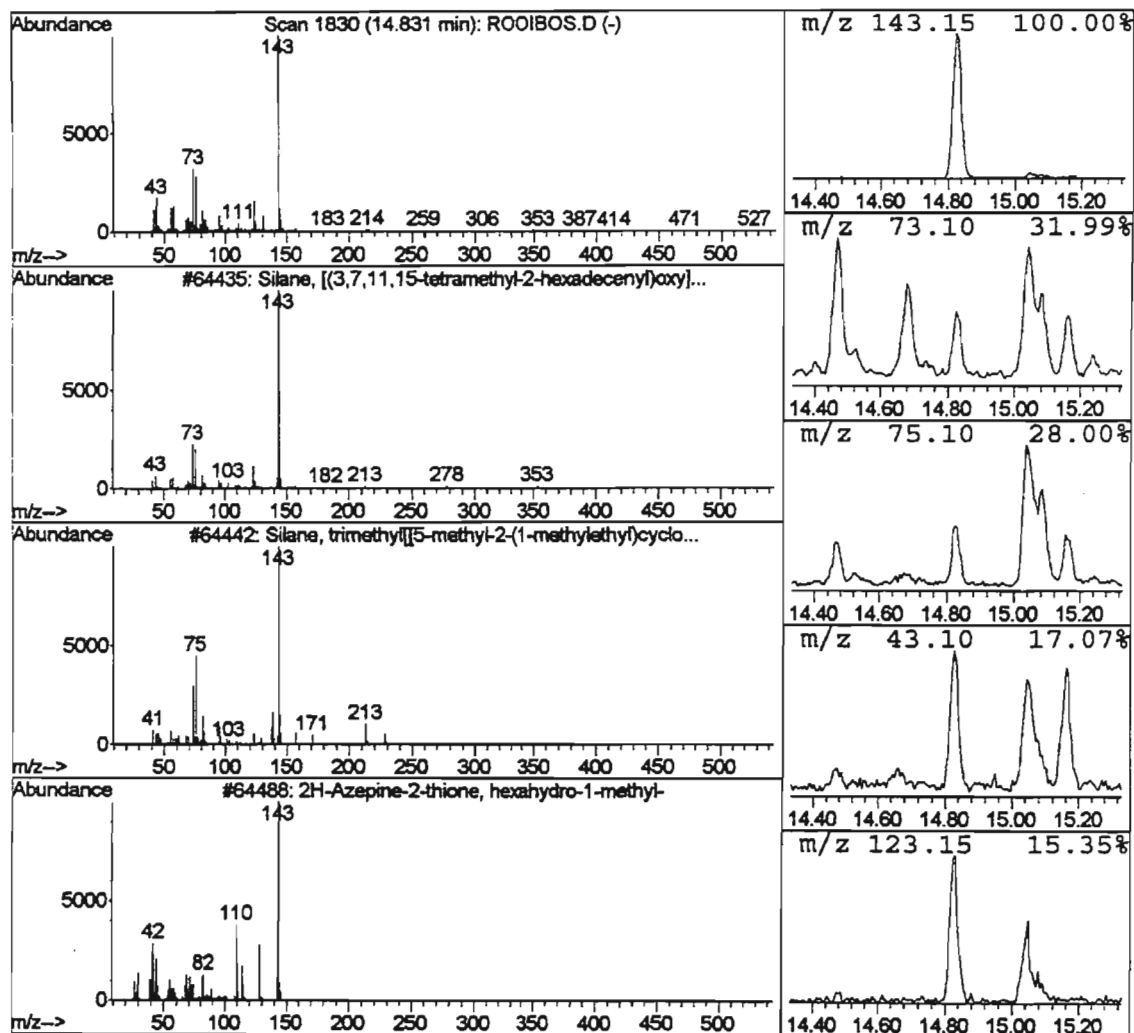
Figure C1.49: Mass spectrum of an unknown compound eluting at 14.831 minutes.
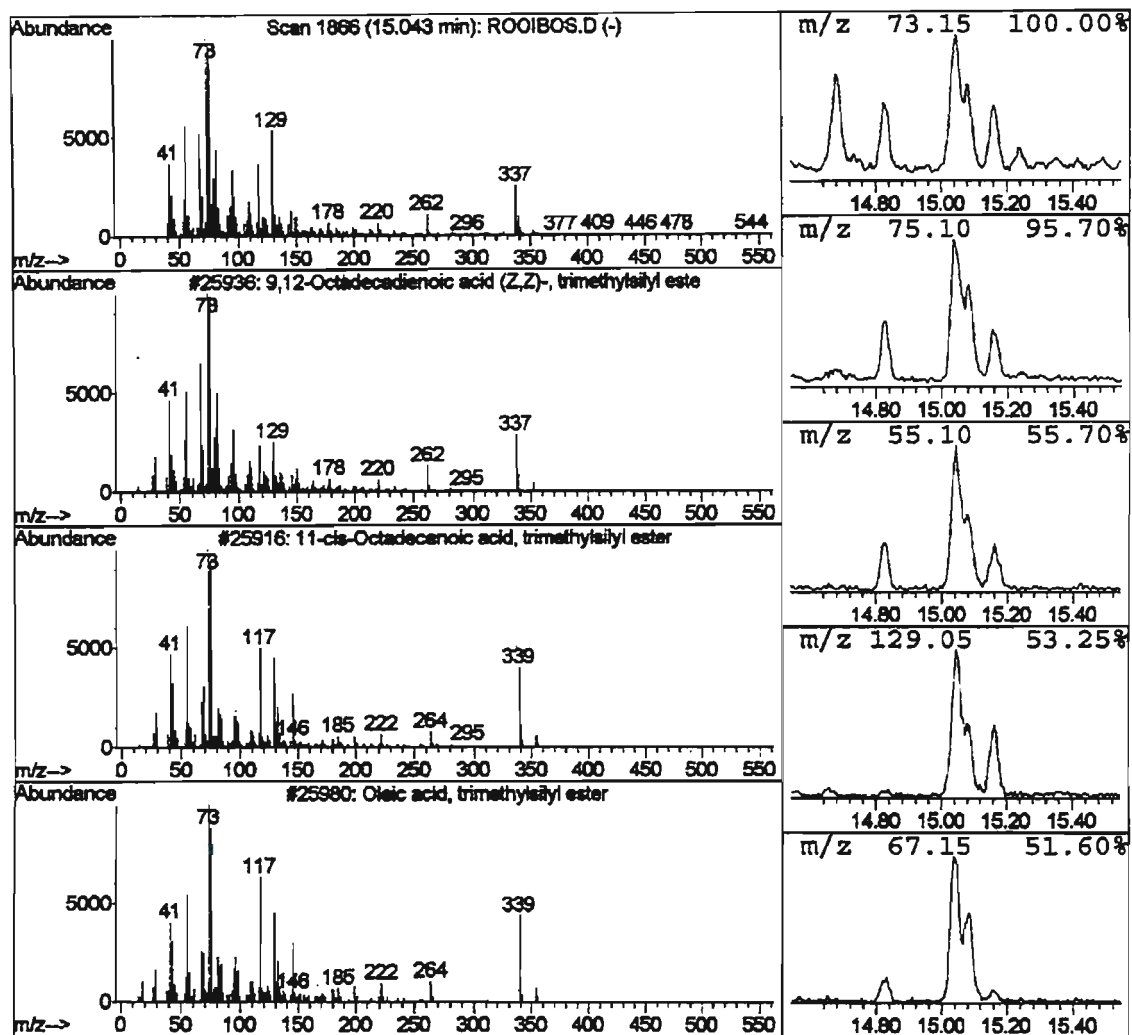
Figure C1.50:   Mass spectrum of an unknown compound eluting at 15.043 minutes.
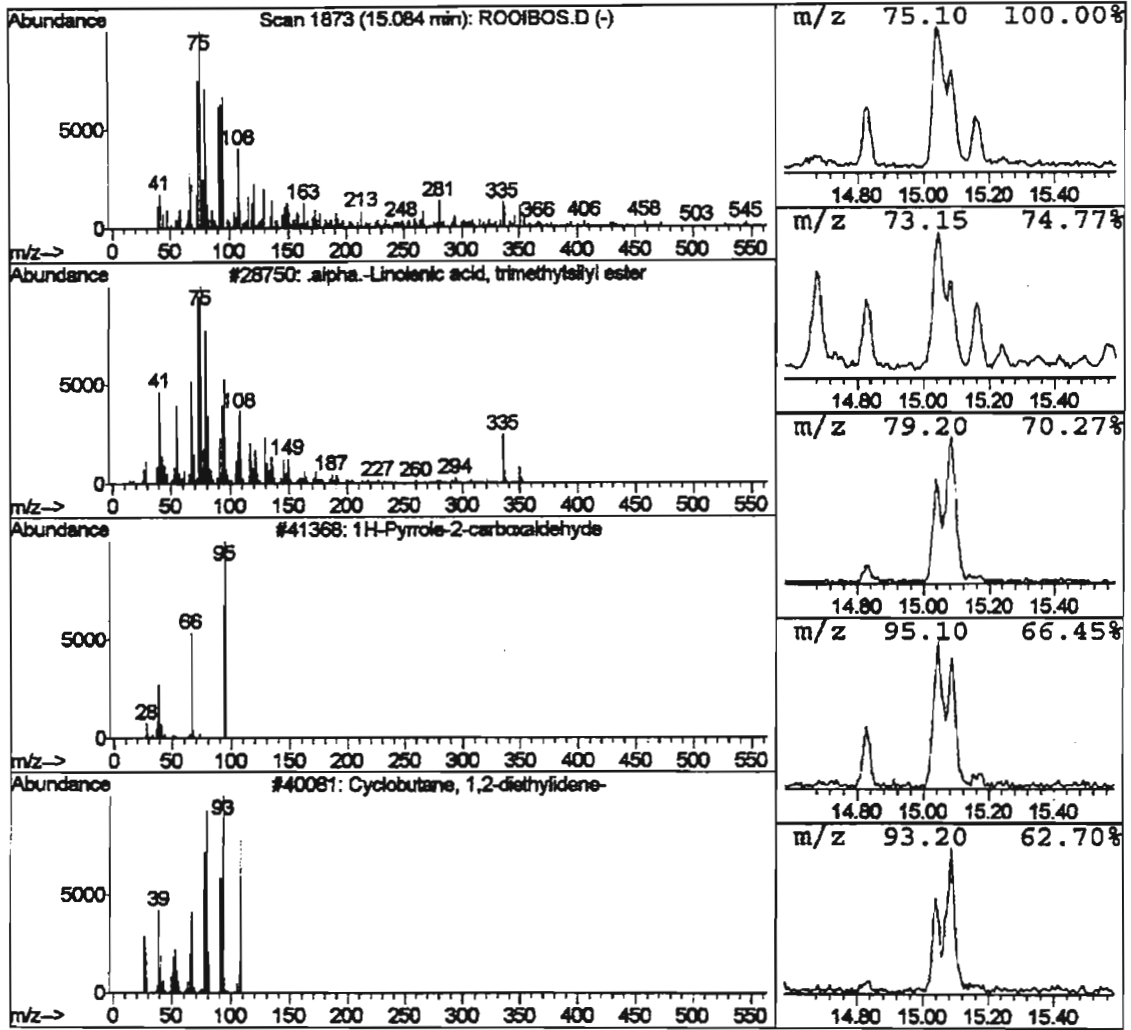
Figure C1.51:   Mass spectrum of an unknown compound eluting at 15.084 munutes.
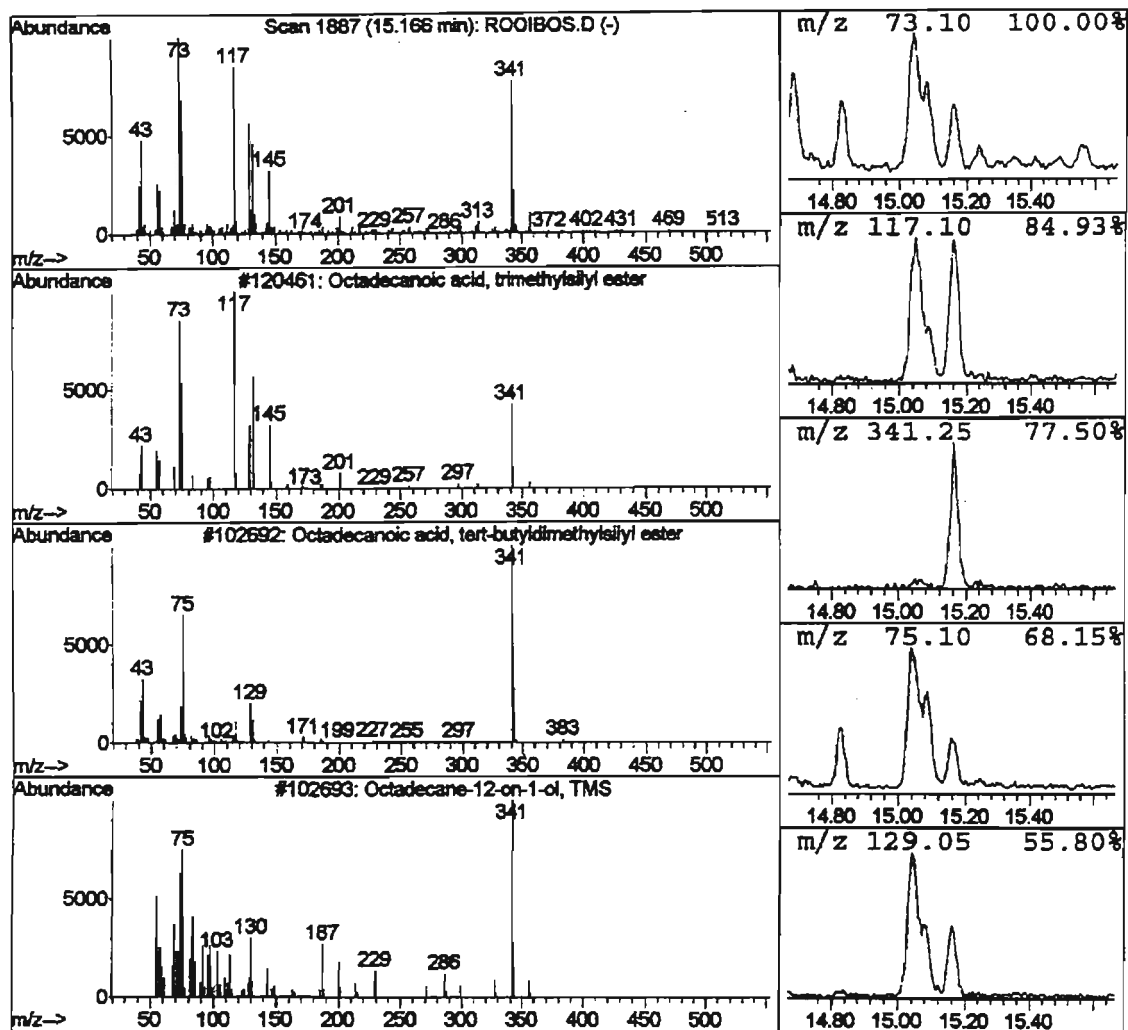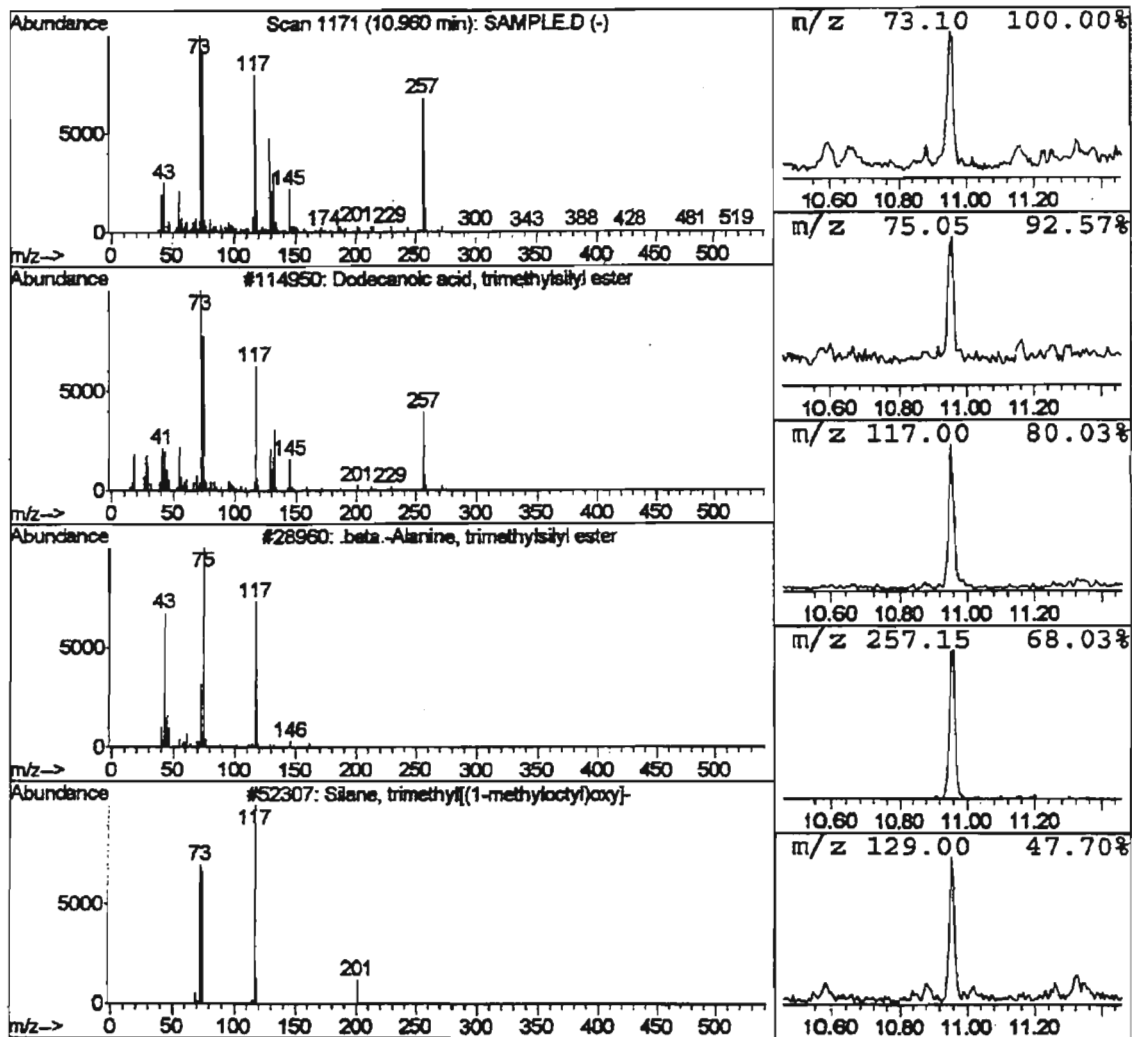
Figure C1.52:   Mass spectrum of a derivatised octadecanoic acid that elutes at 15.166 minutes. The fragmentation pattern matched that of a derivatised octadecanoic acid present in the library.
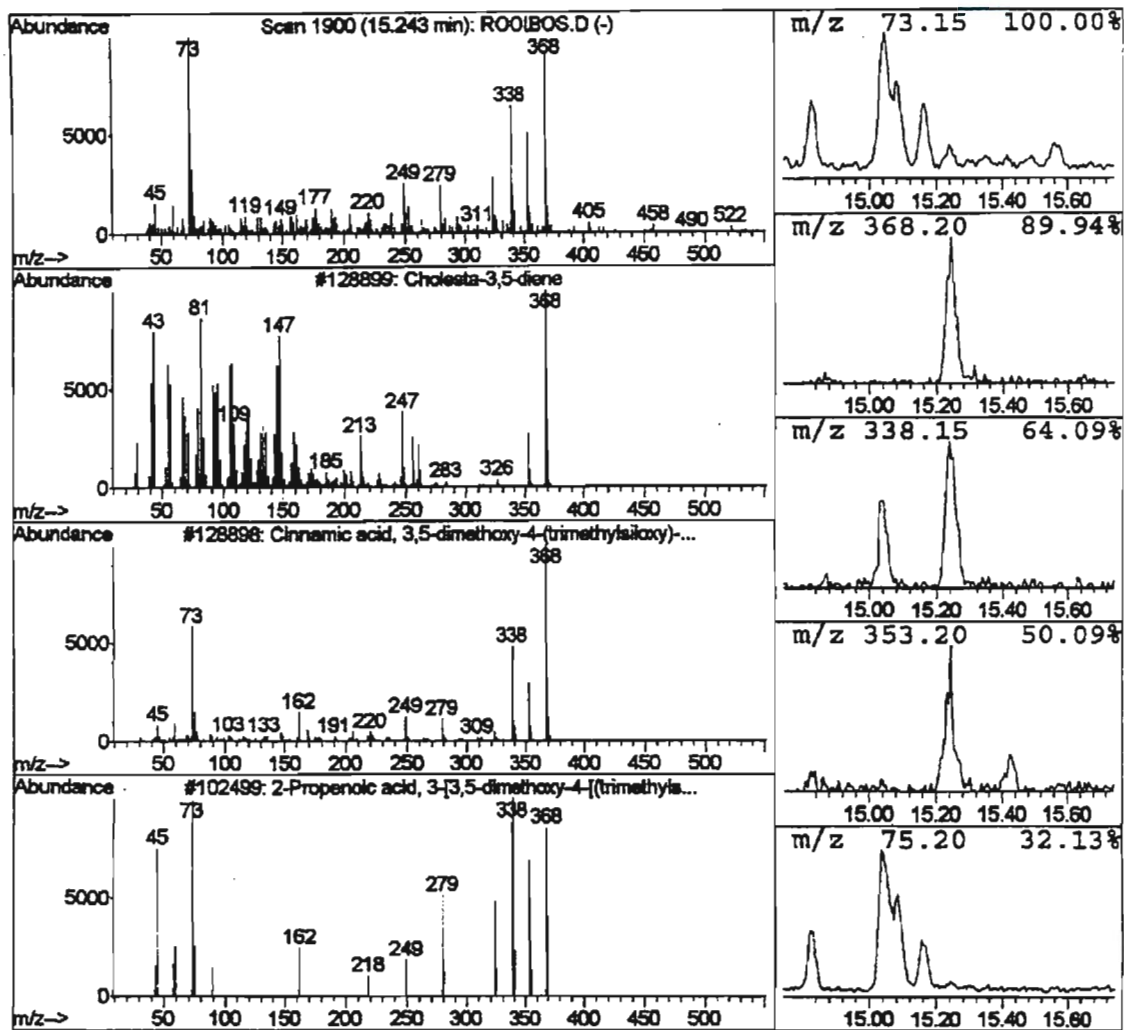
Figure C1.53: Mass spectrum of a derivatised cholesta-3,5-diene that elutes at 15.243 minutes. The fragmentation pattern matched that of a derivatised cholesta-3,5-diene present in the library.
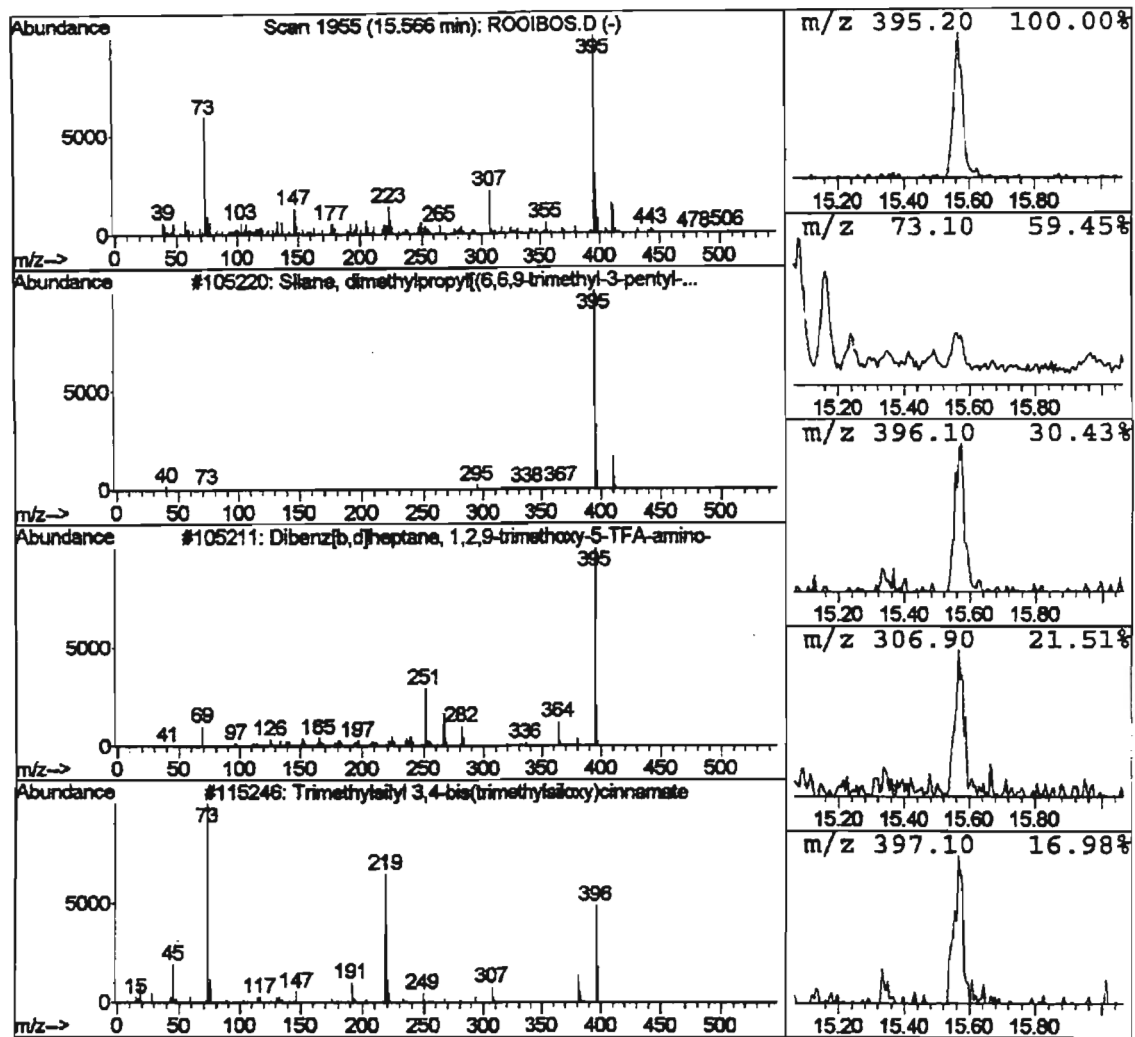
Figure C1.54:   Mass spectrum of an unknown compound eluting at 15.566 minutes.
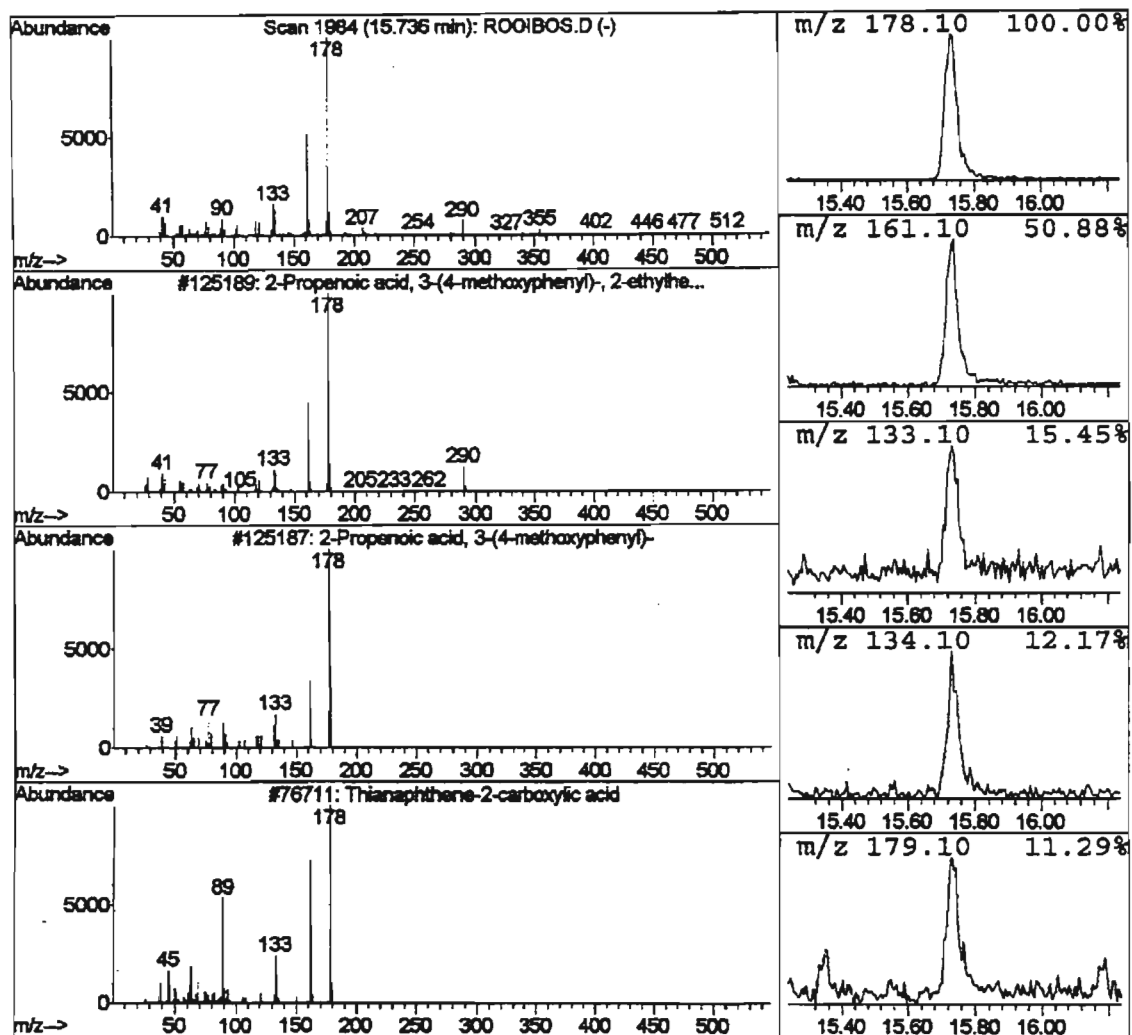
Figure C1.55: Mass spectrum of an EHMC impurity eluting at 15.736 minutes. The fragmentation pattern matched that of a derivatised EHMC present in the library.
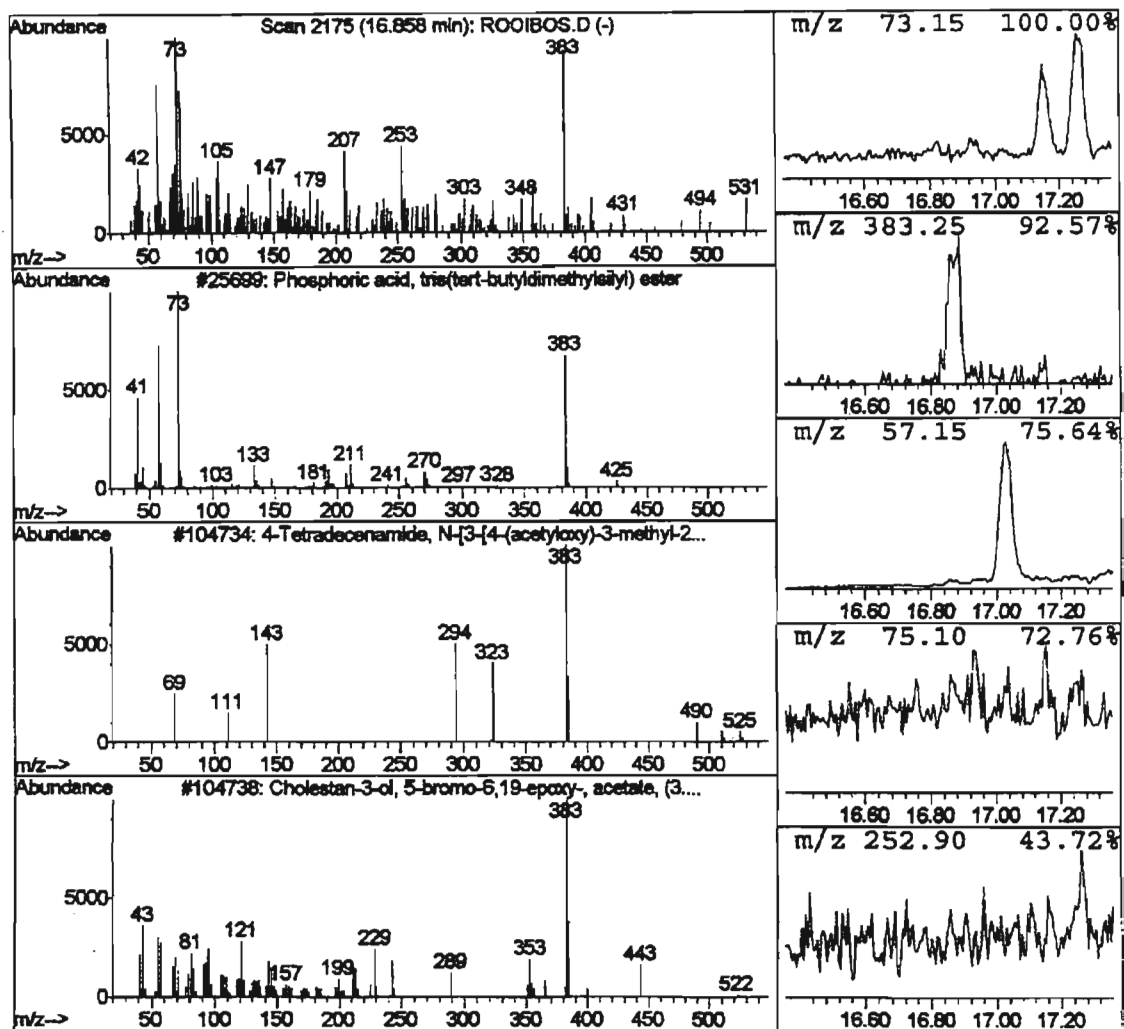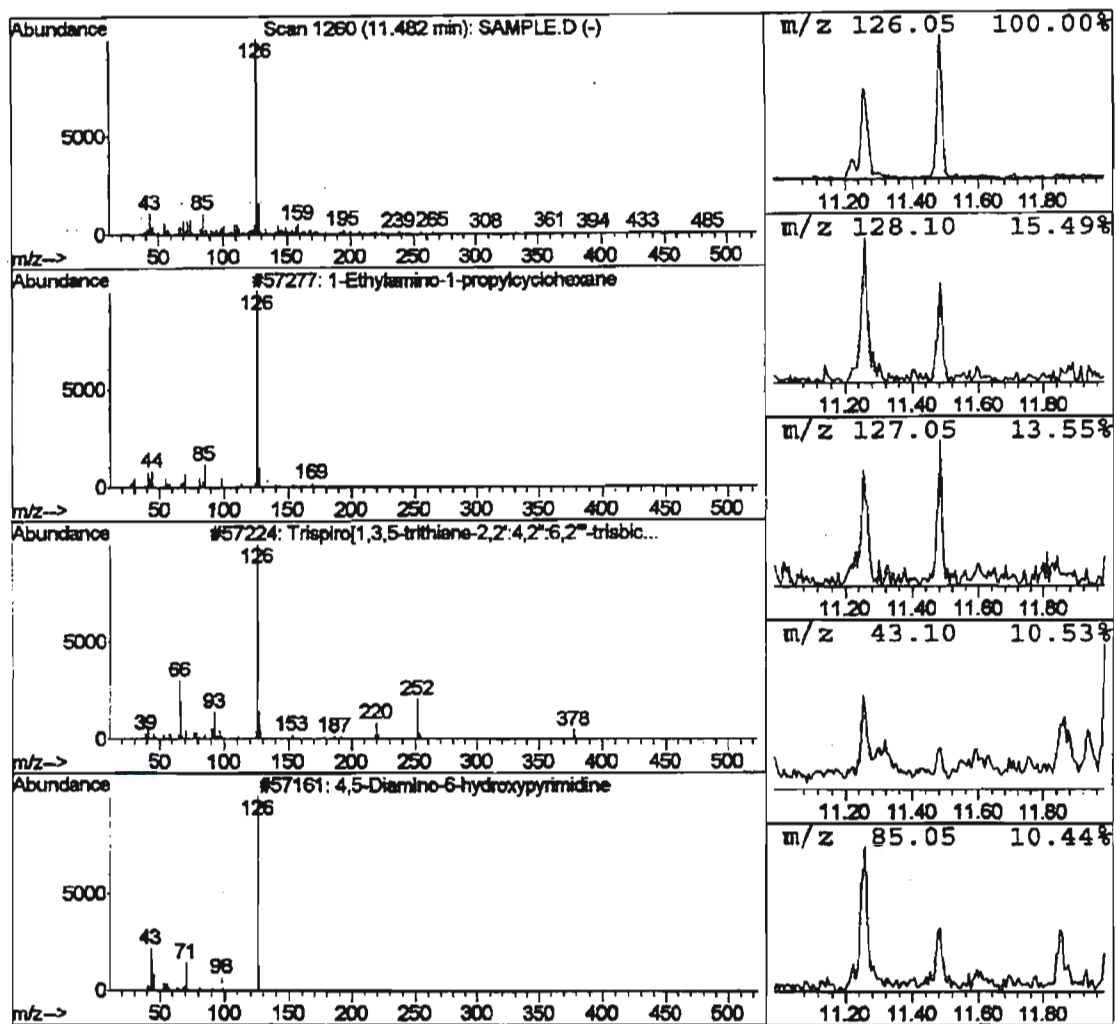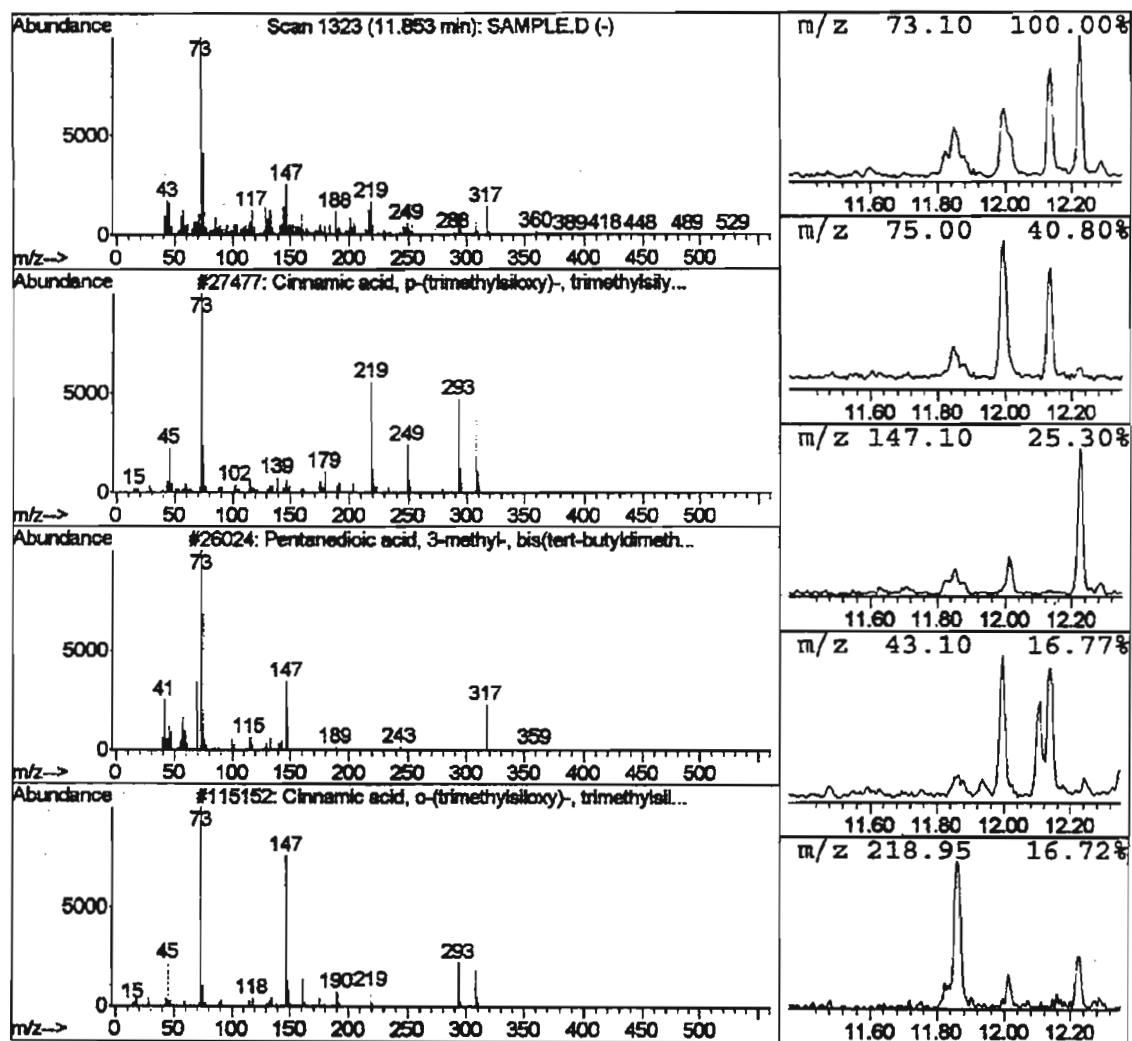
Figure C1.56:   Mass spectrum of an unknown compound eluting at 16.858 minutes.
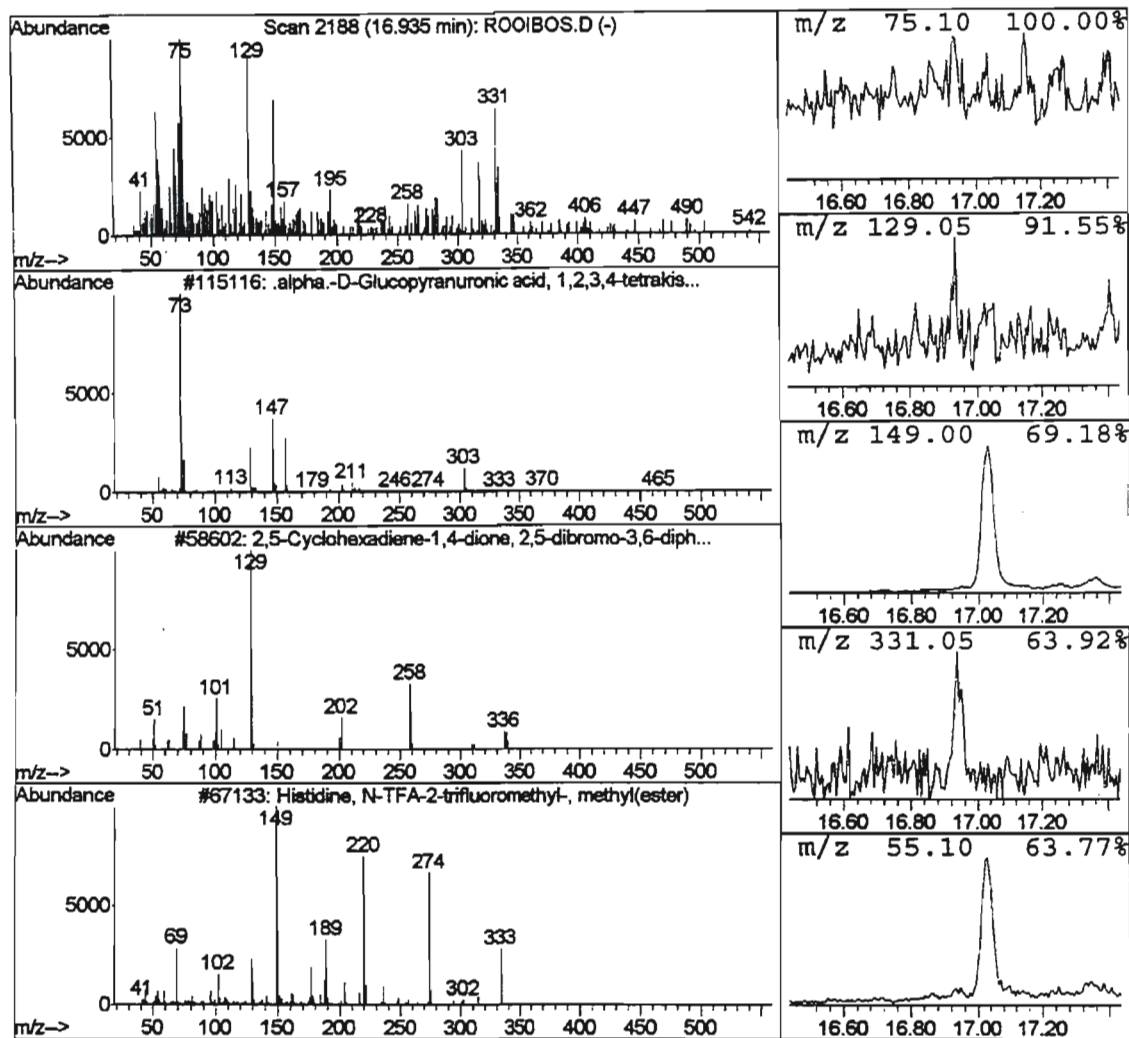
Figure C1.57: Mass spectrum of an unknown compound eluting at 16.935 minutes.
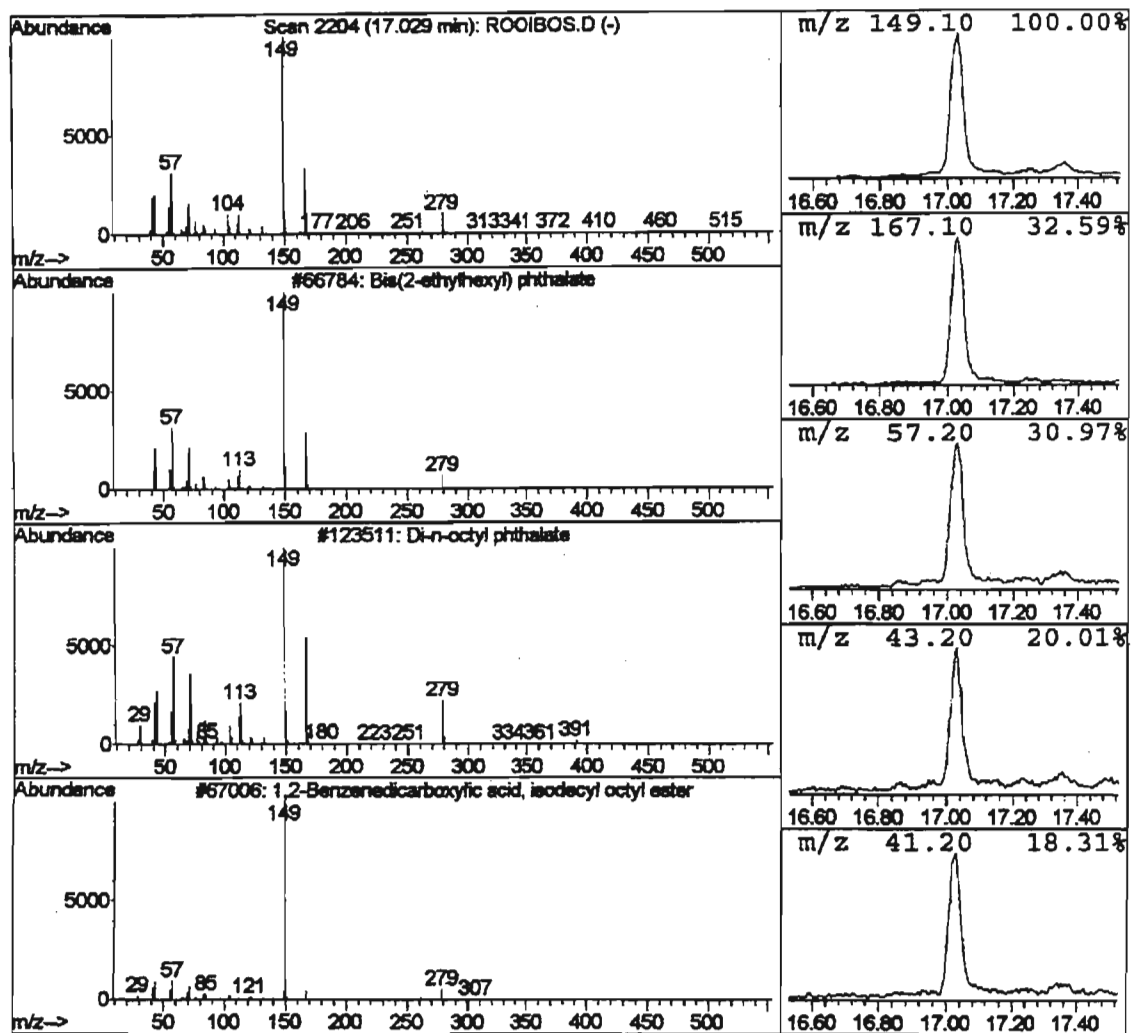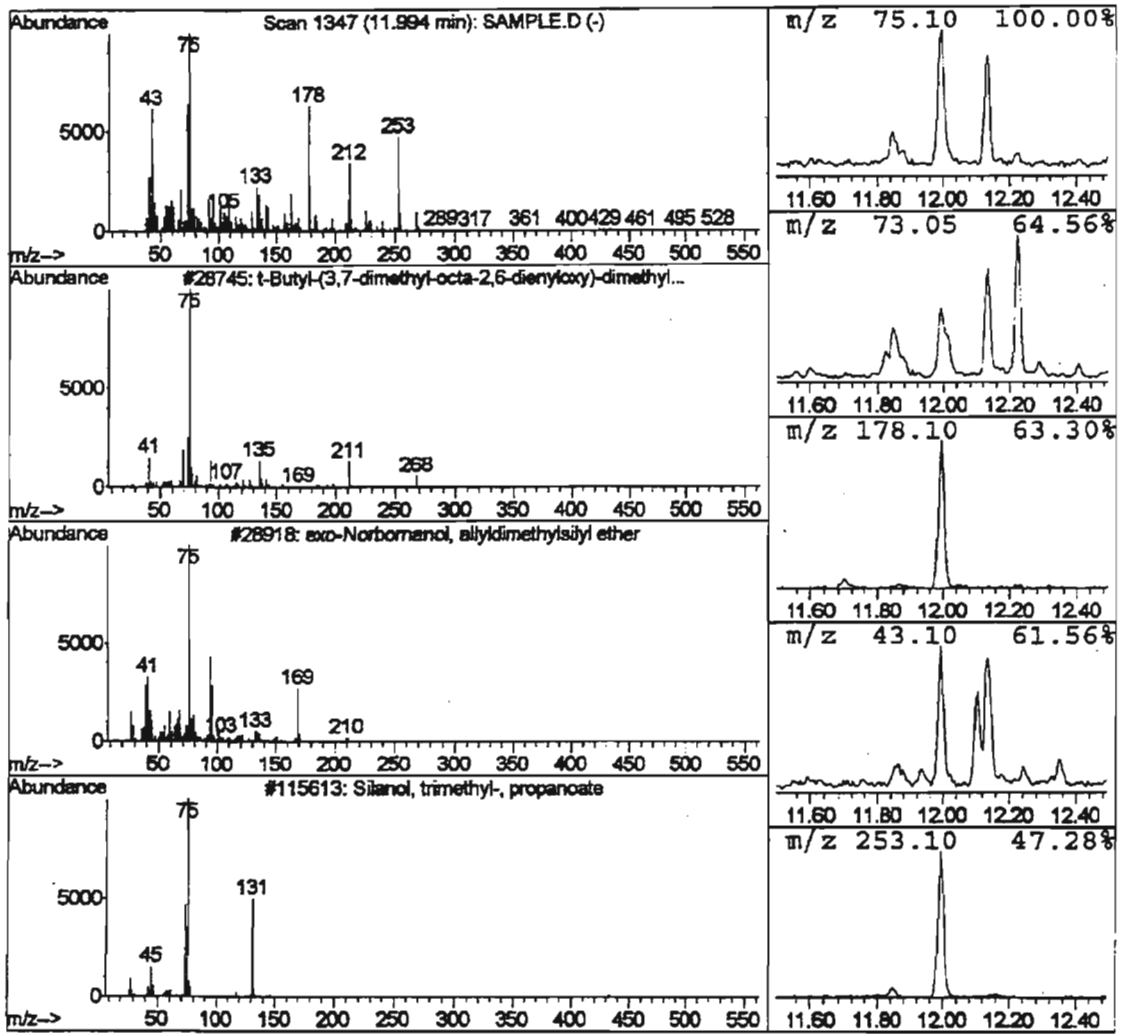
Figure C1.58: Mass spectrum of an unknown compound eluting at 17.029 minutes.
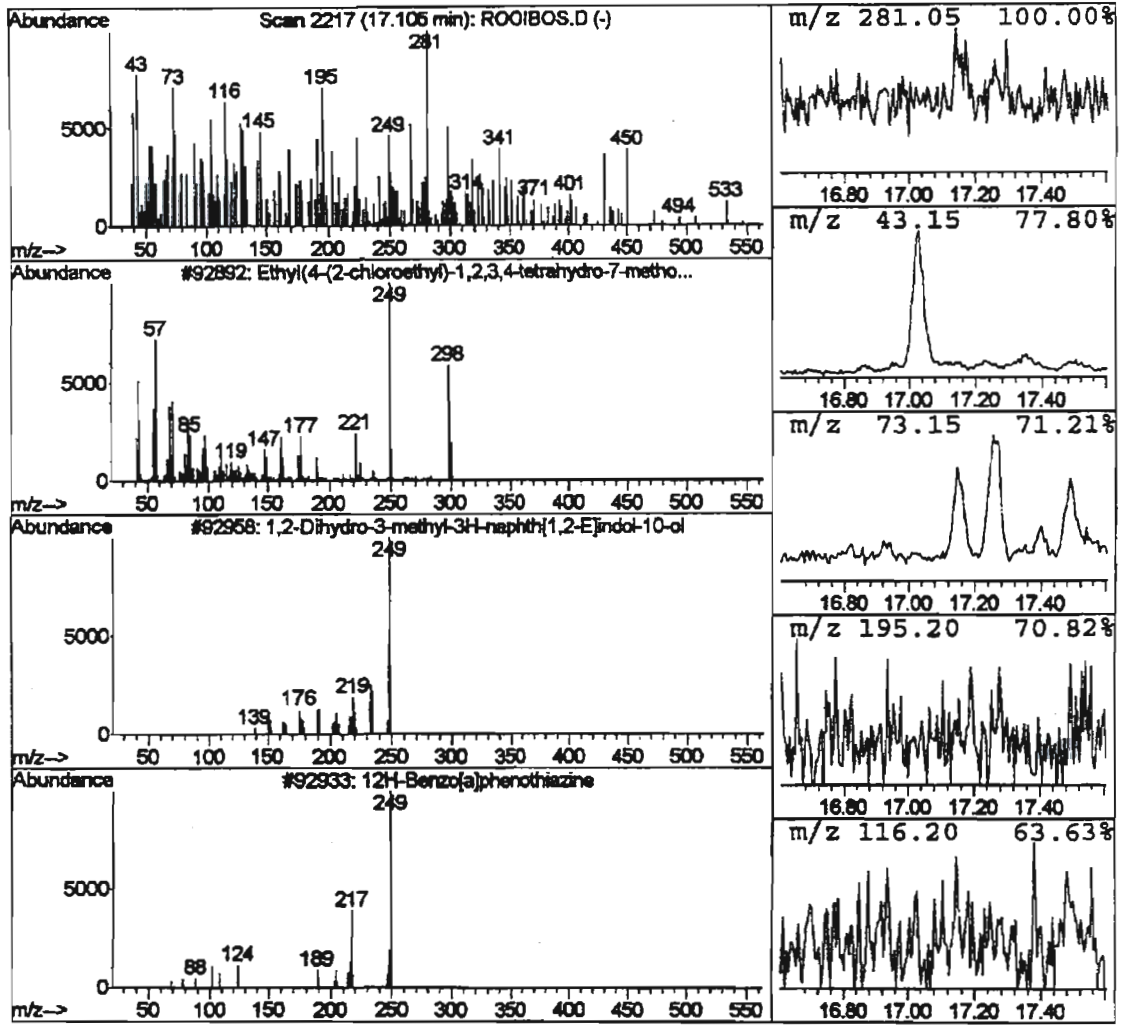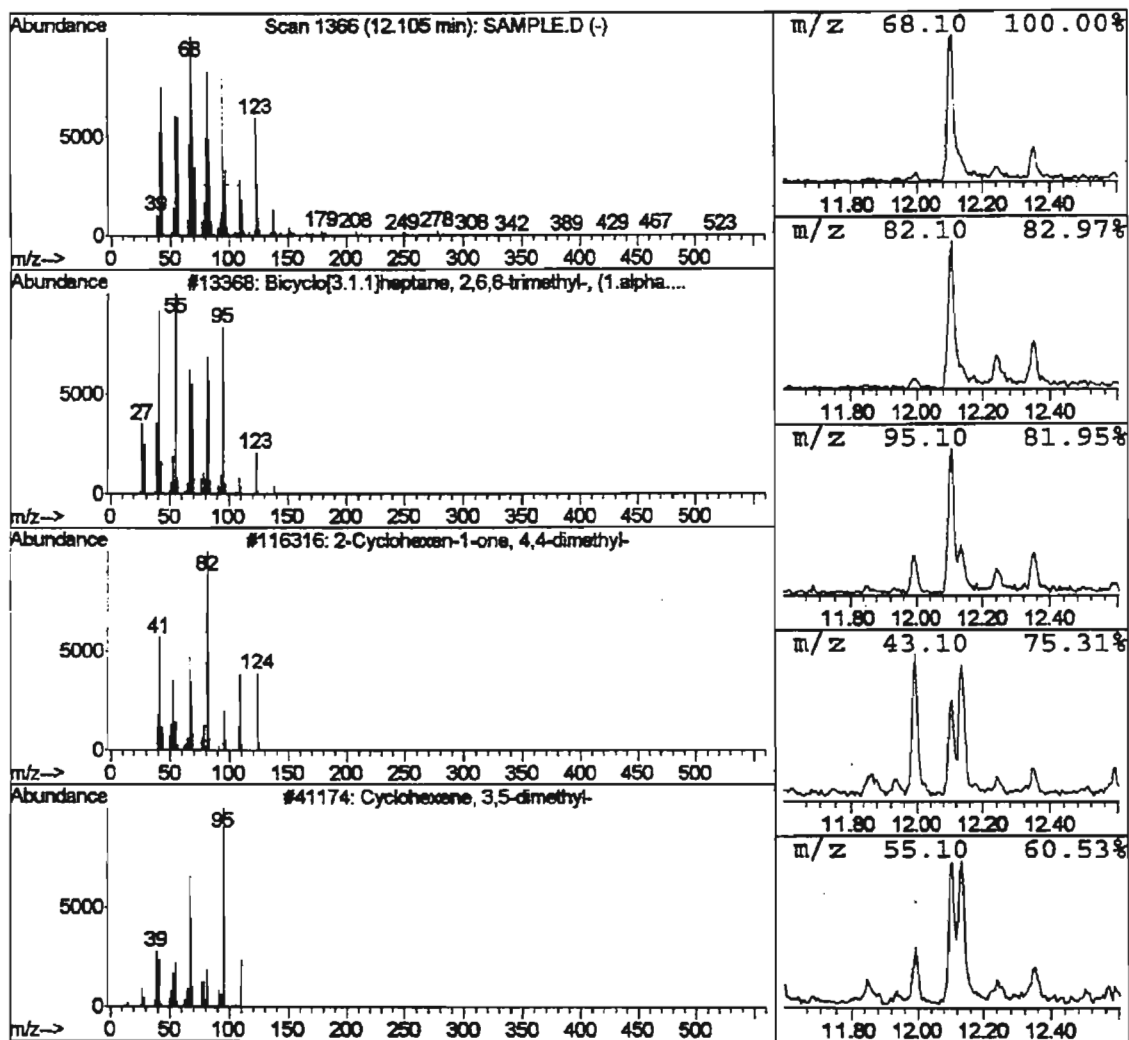
Figure C1.59:   Mass spectrum of an unknown compound eluting at 17.105 minutes.
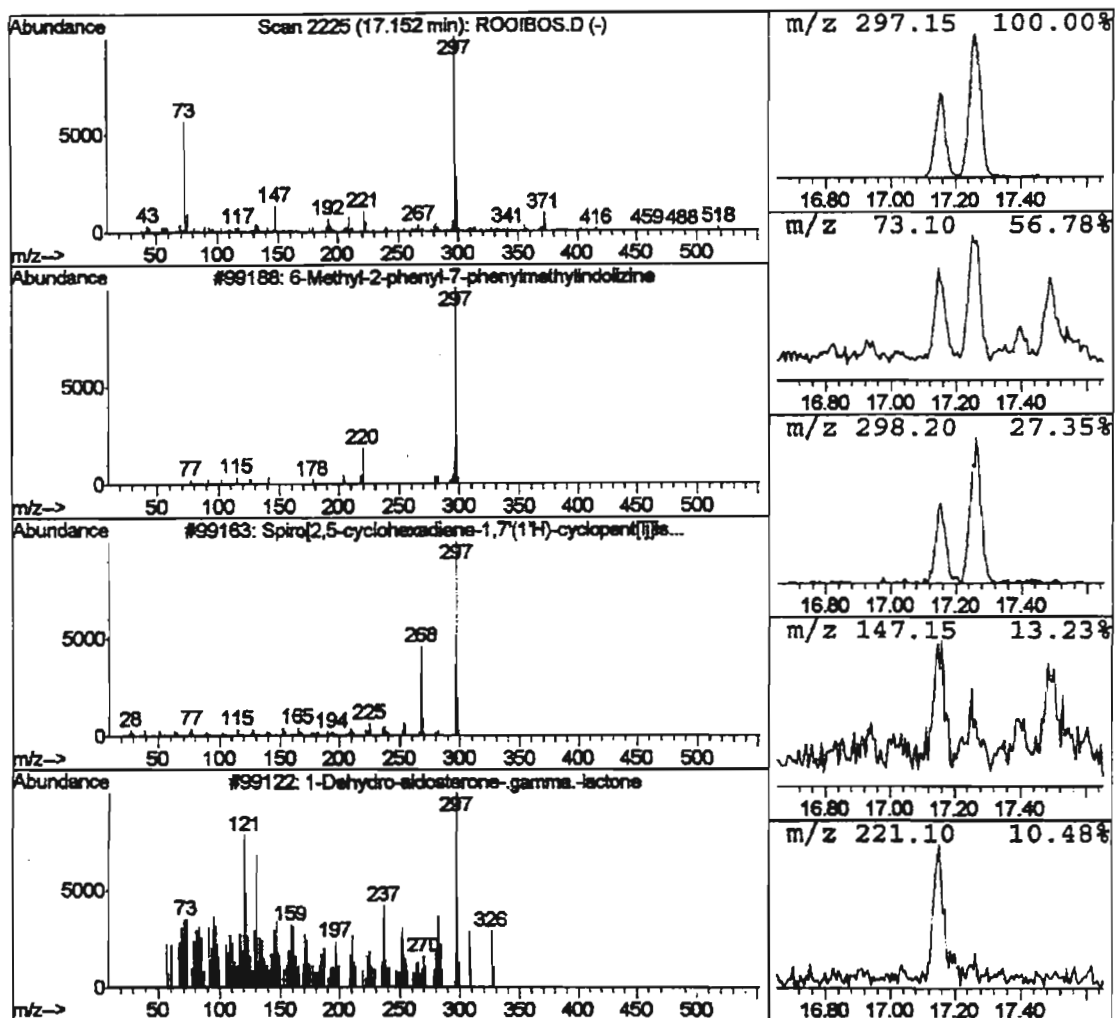
Figure C1.60: Mass spectrum of an unknown compound eluting at 17.152 minutes.
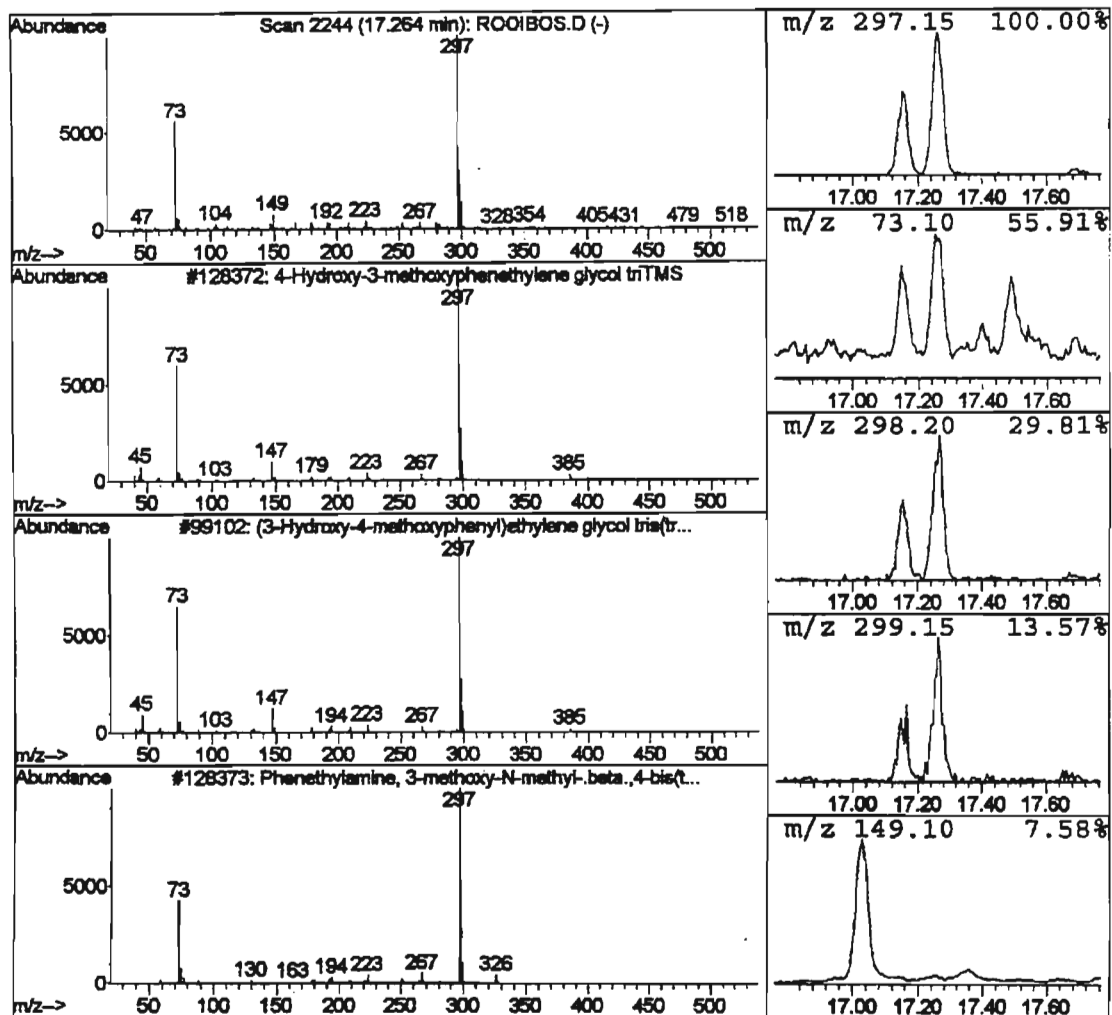
Figure C1.61:   Mass spectrum of a derivatised 4-hydroxy-3-menthoxyphenethylene glycol that elutes at 17.264 minutes.   The fragmentation pattern matched that of a derivatised 4-hydroxy-3-menthoxyphenethylene glycol present in the library.
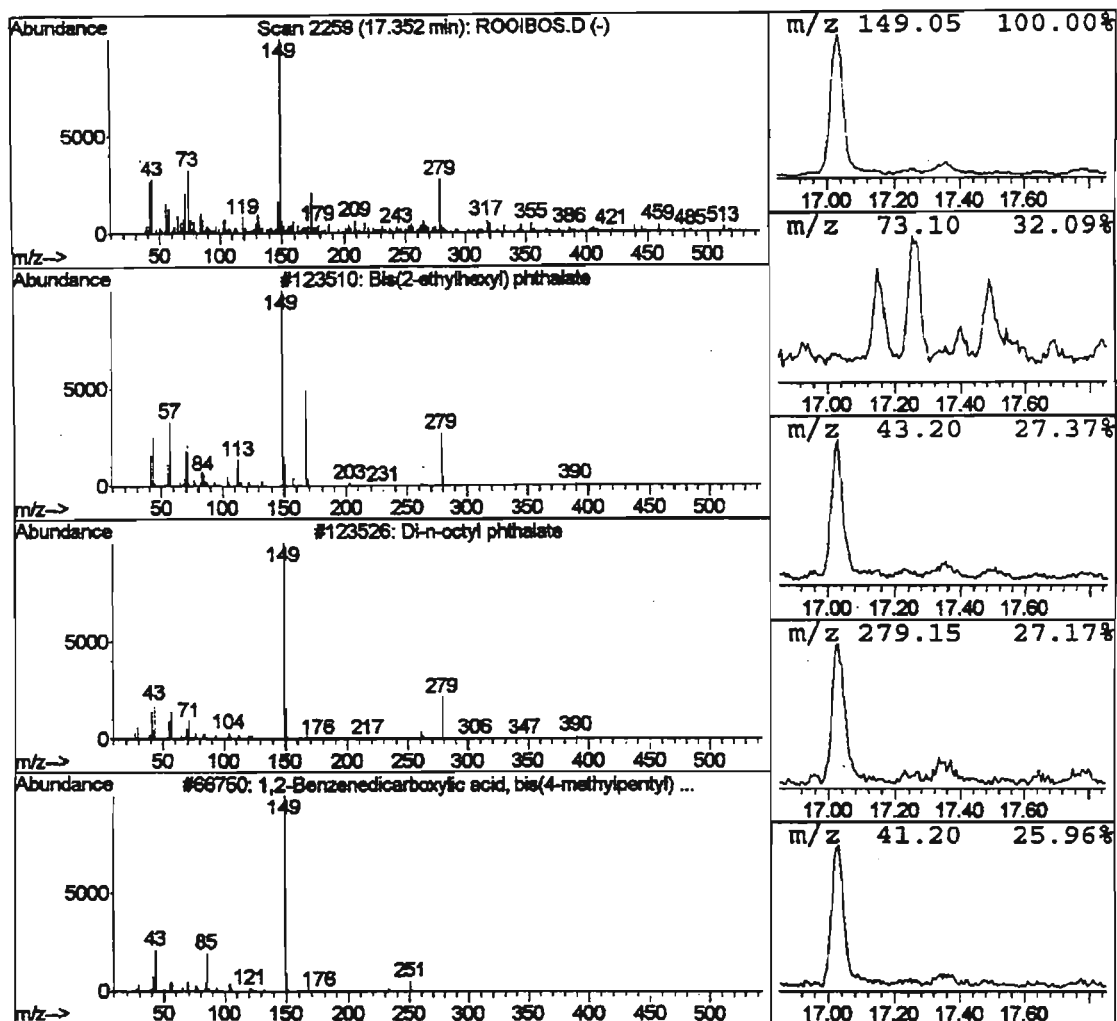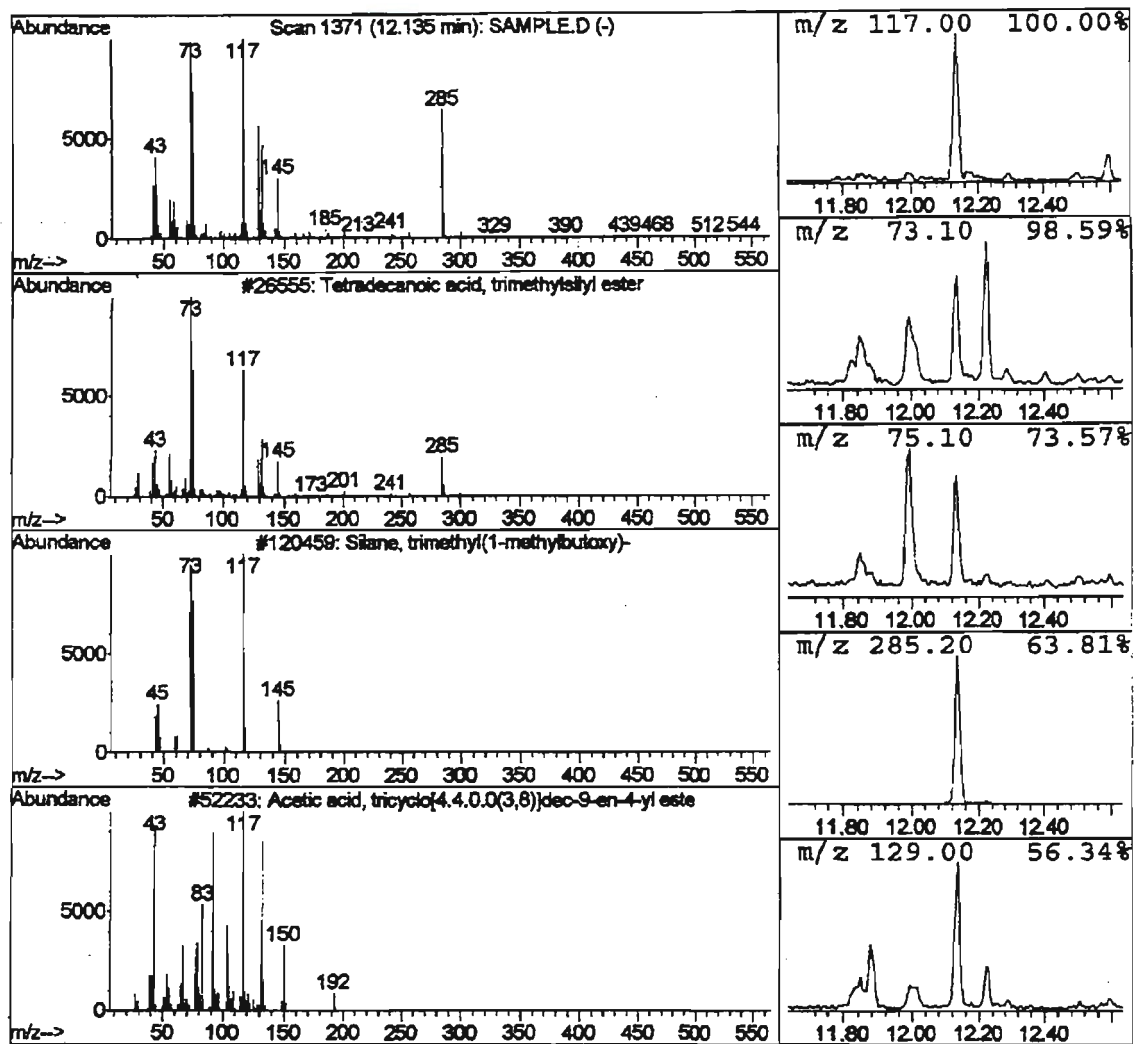
Figure C1.62: Mass spectrum of an unknown compound eluting at 17.352 minutes.
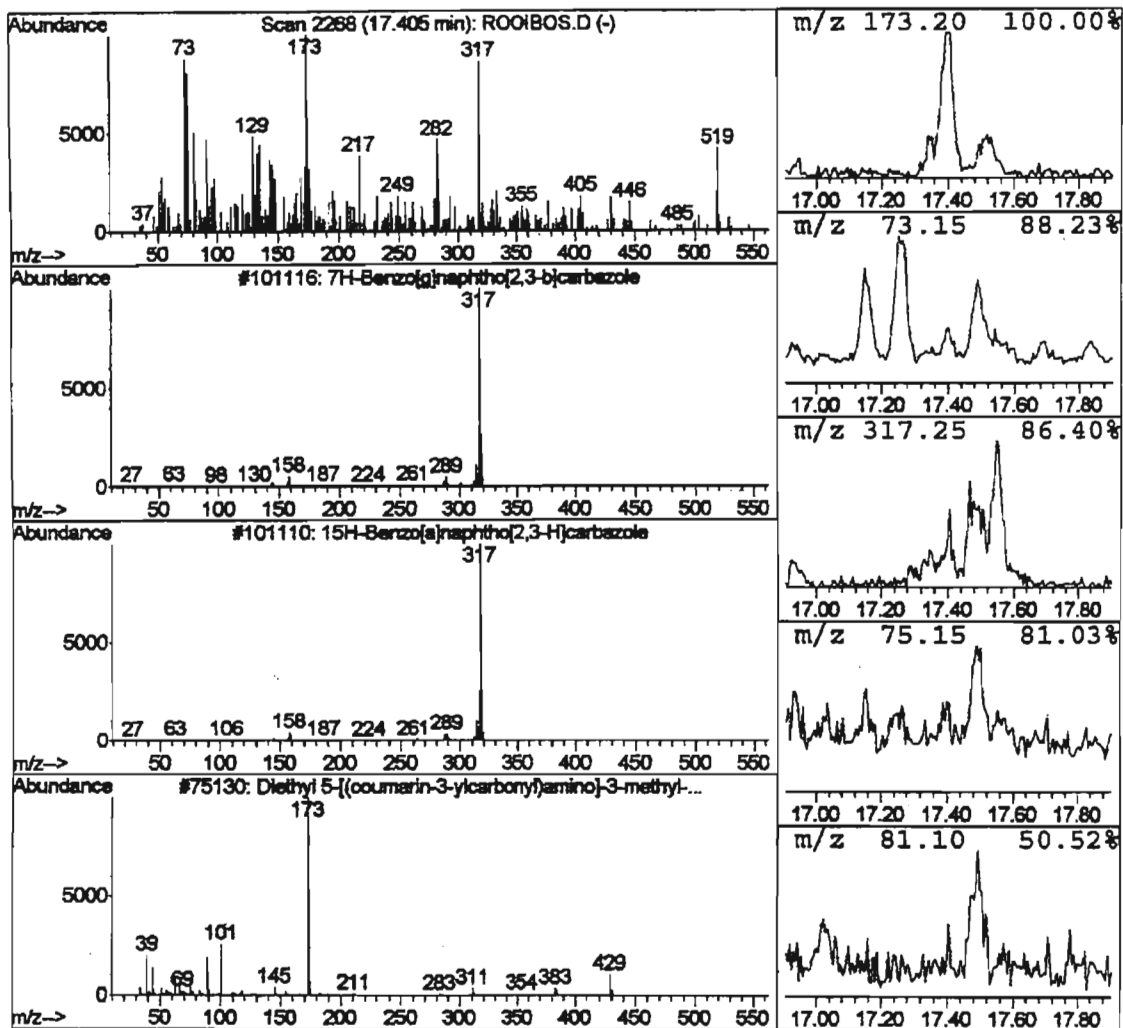
Figure C1.63: Mass spectrum of an unknown compound eluting at 17.405 minutes.
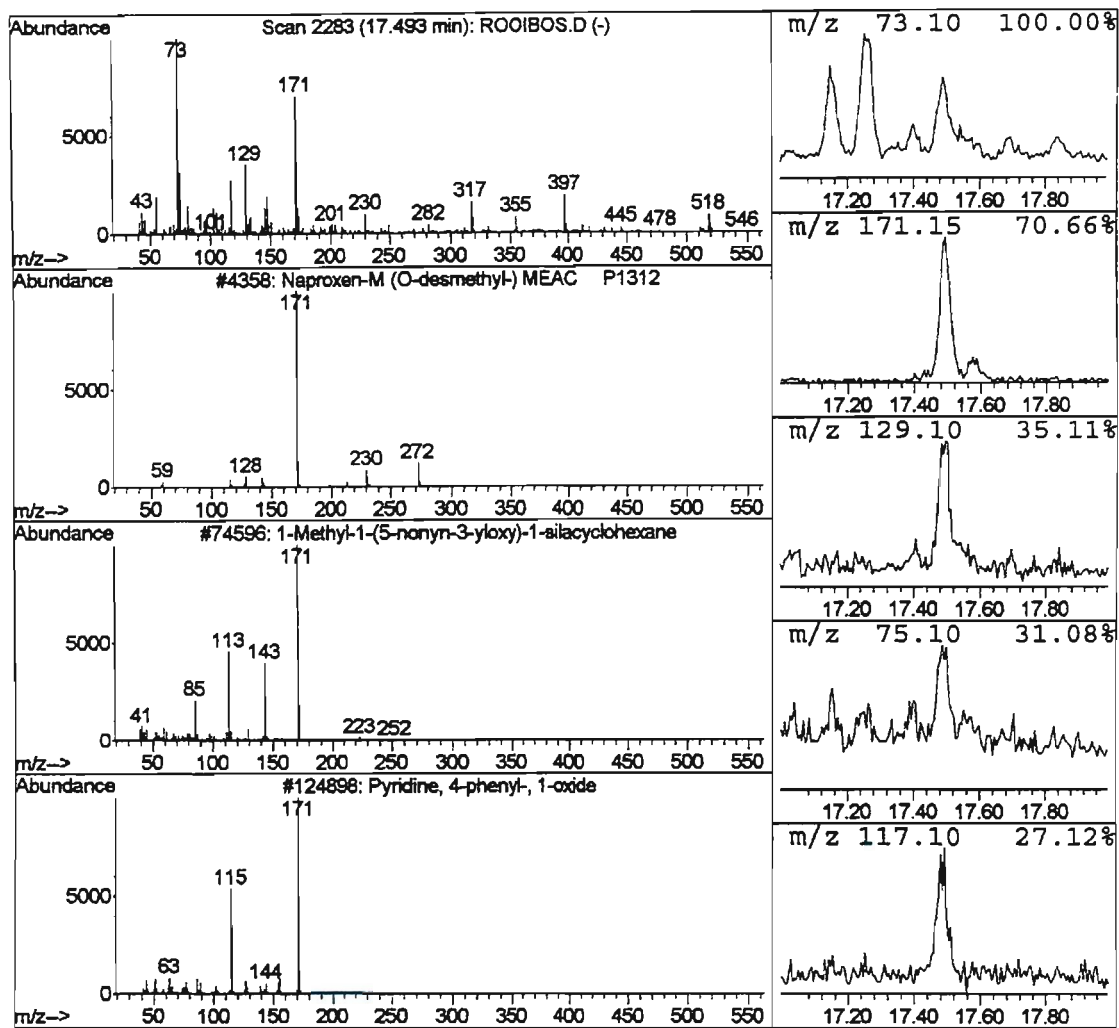
Figure C1.64:   Mass spectrum of an unknown compound eluting at 17.493 minutes.
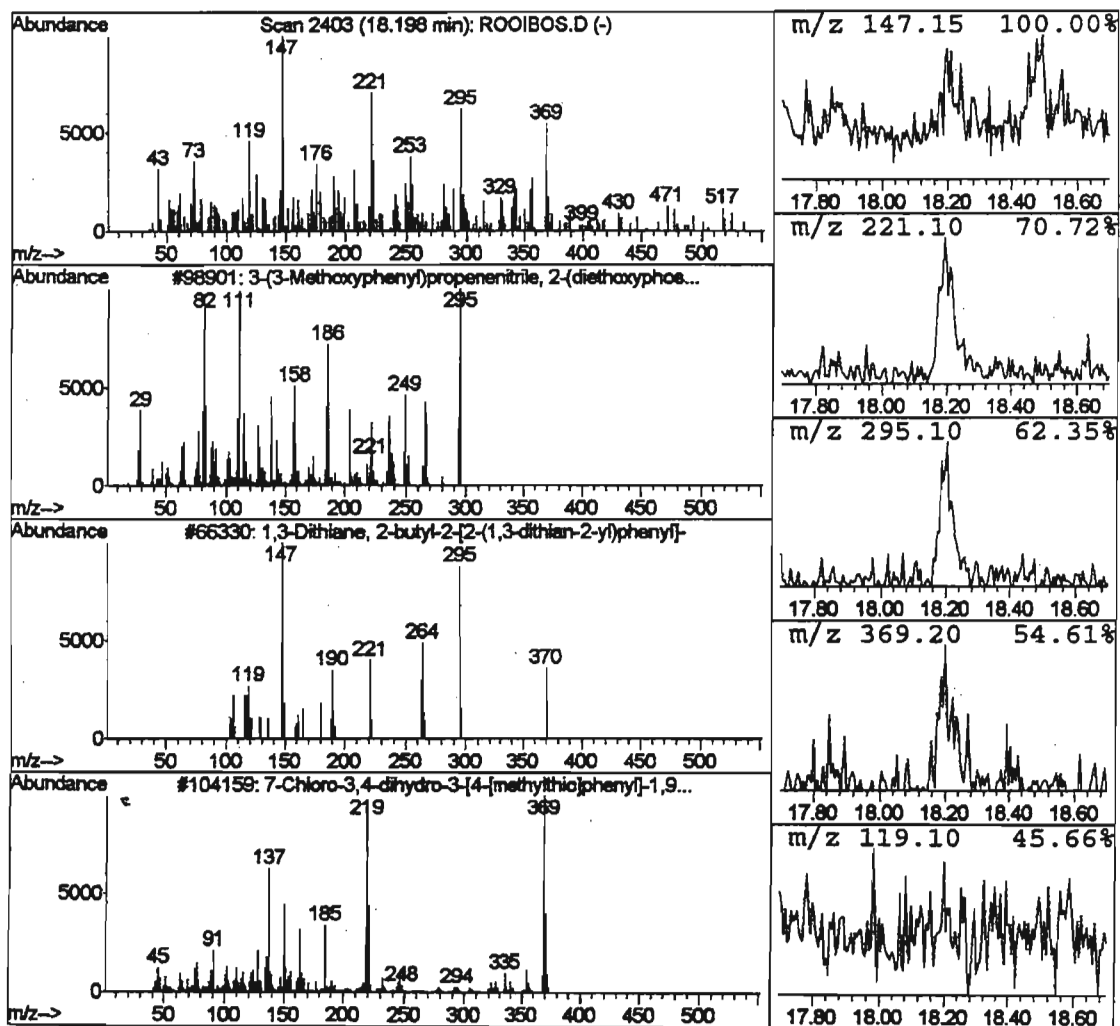
Figure C1.65:   Mass spectrum of an unknown compound eluting at 18.198 minutes.
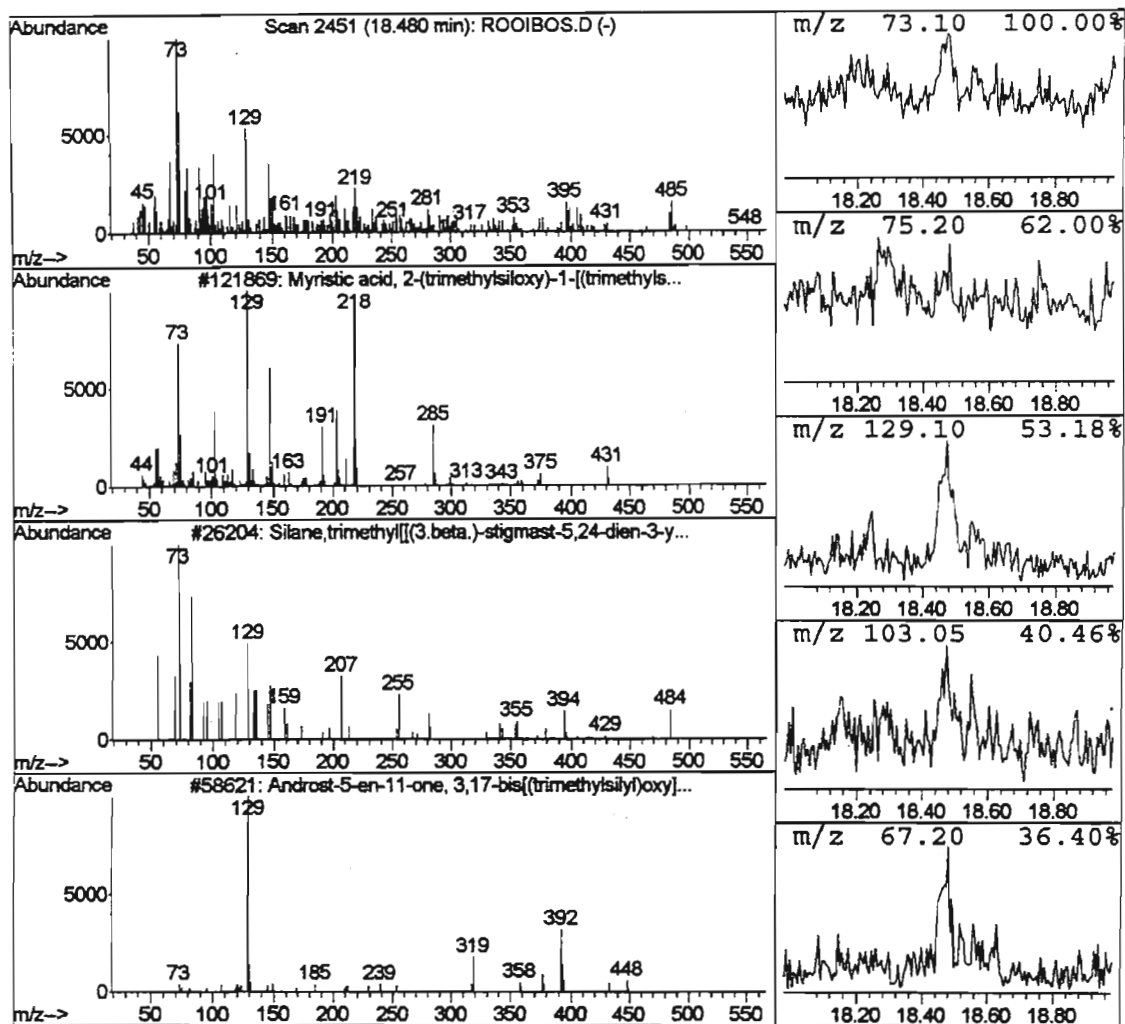
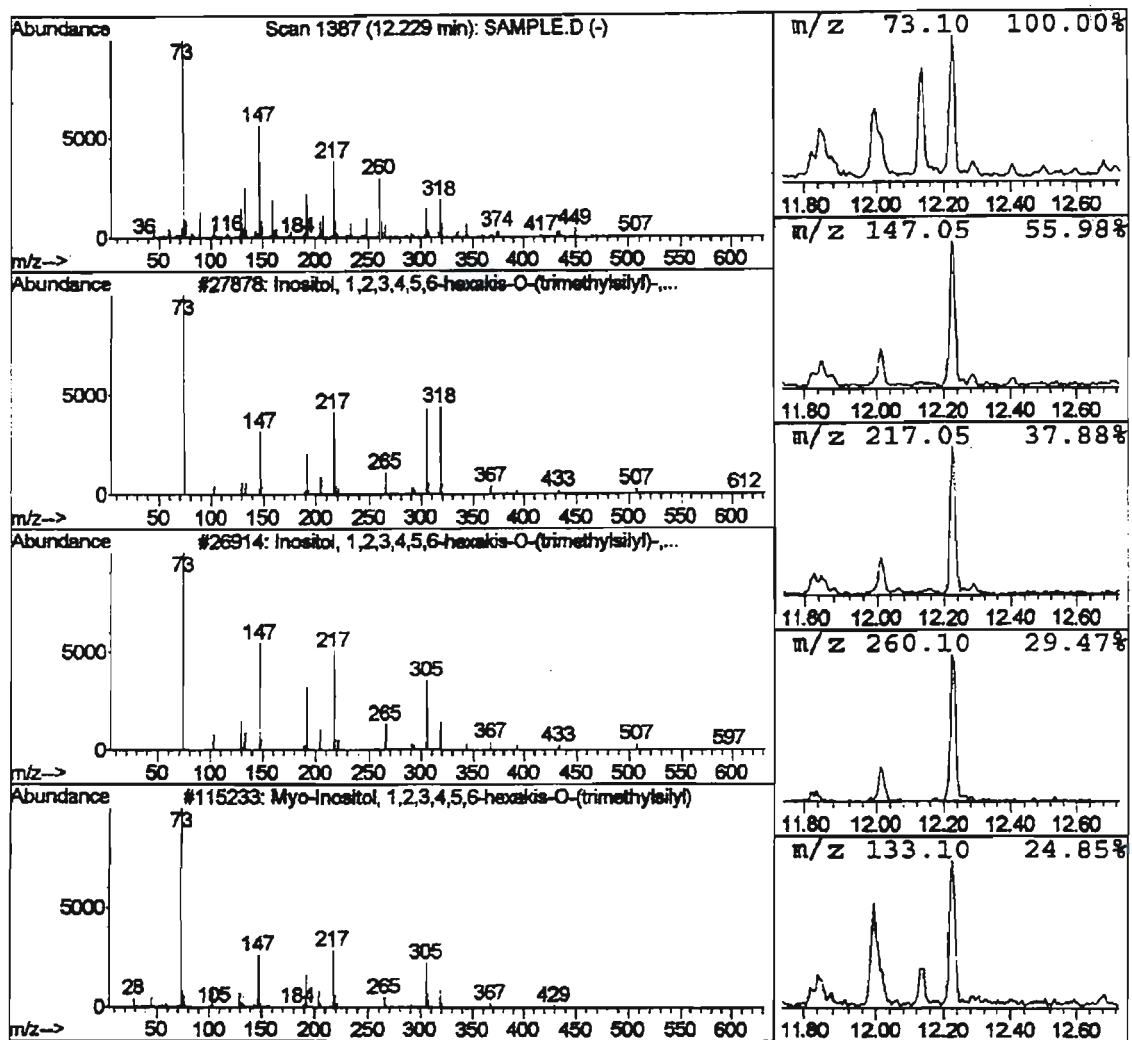Figure C1.66:   Mass spectrum of an unknown compound eluting at 18.480 minutes.
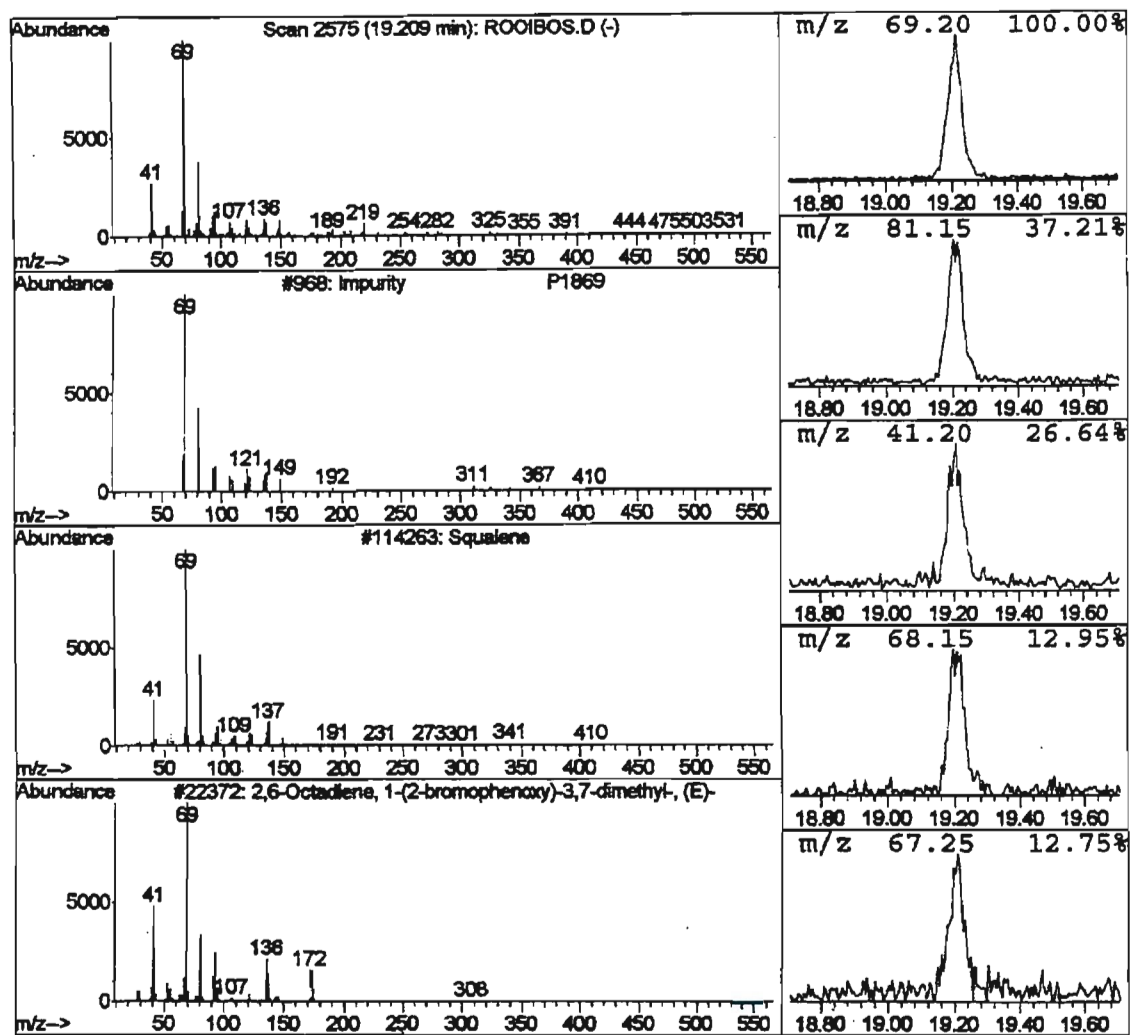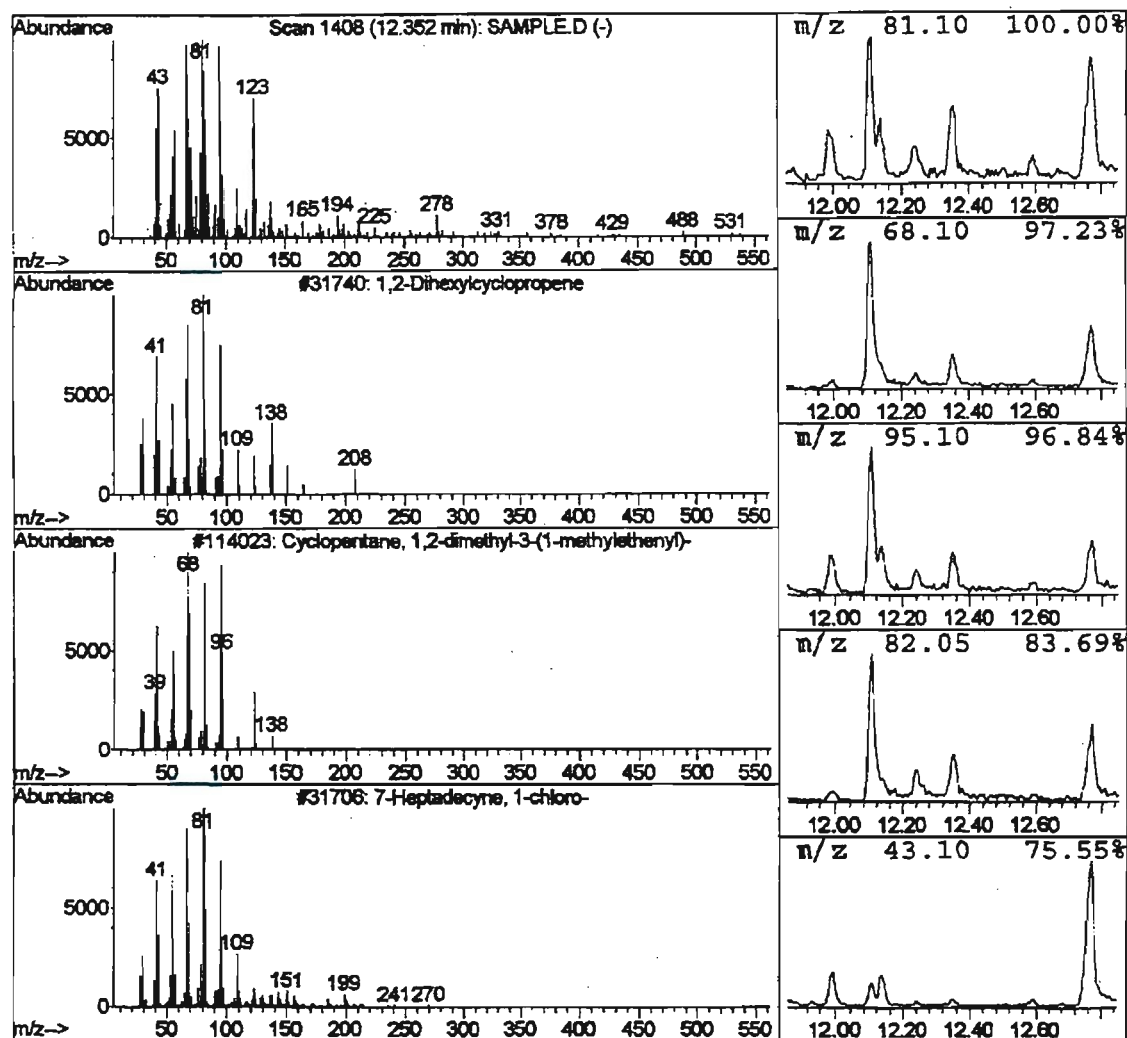
Figure C1.67:   Mass spectrum of an unknown compound eluting at 19.209 minutes.
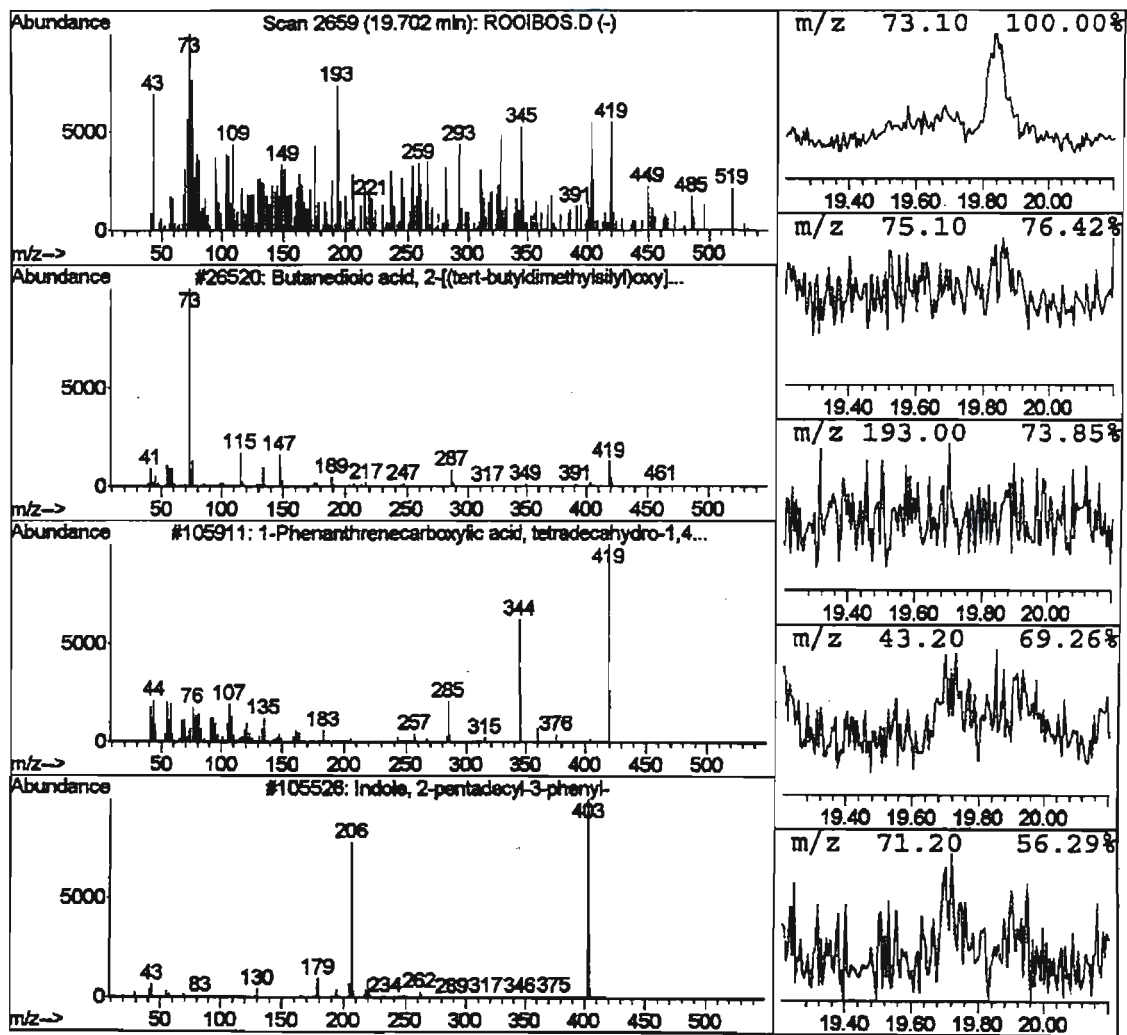
Figure C1.68:   Mass spectrum of an unknown compound eluting at 19.702 minutes.
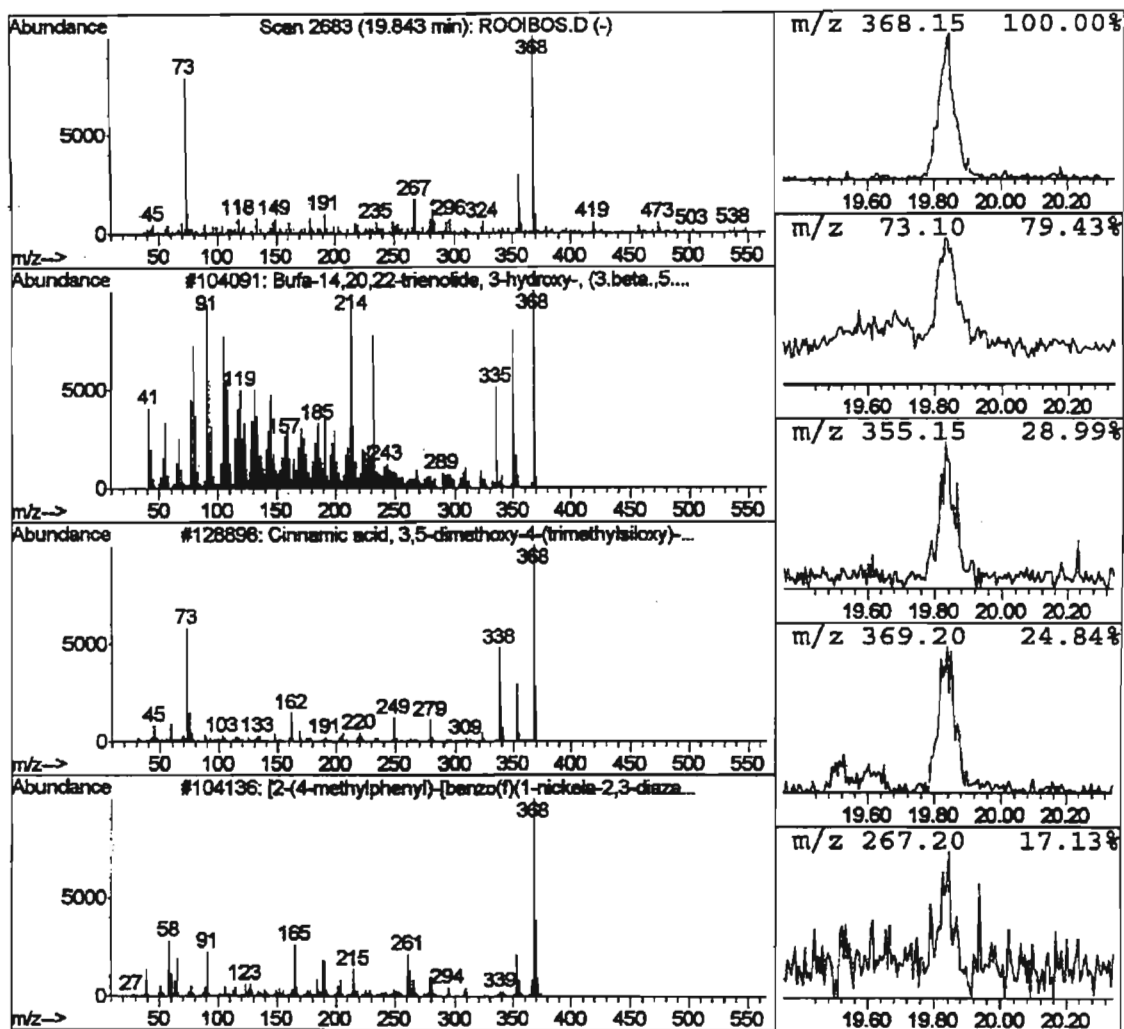
Figure C1.69: Mass spectrum of a possible catechin or epicatechin which eluted at 19.843 minutes. It was identified from the fragmentation reported by Donovan *et al.* [1998] and Luthia *et al.* [1997].
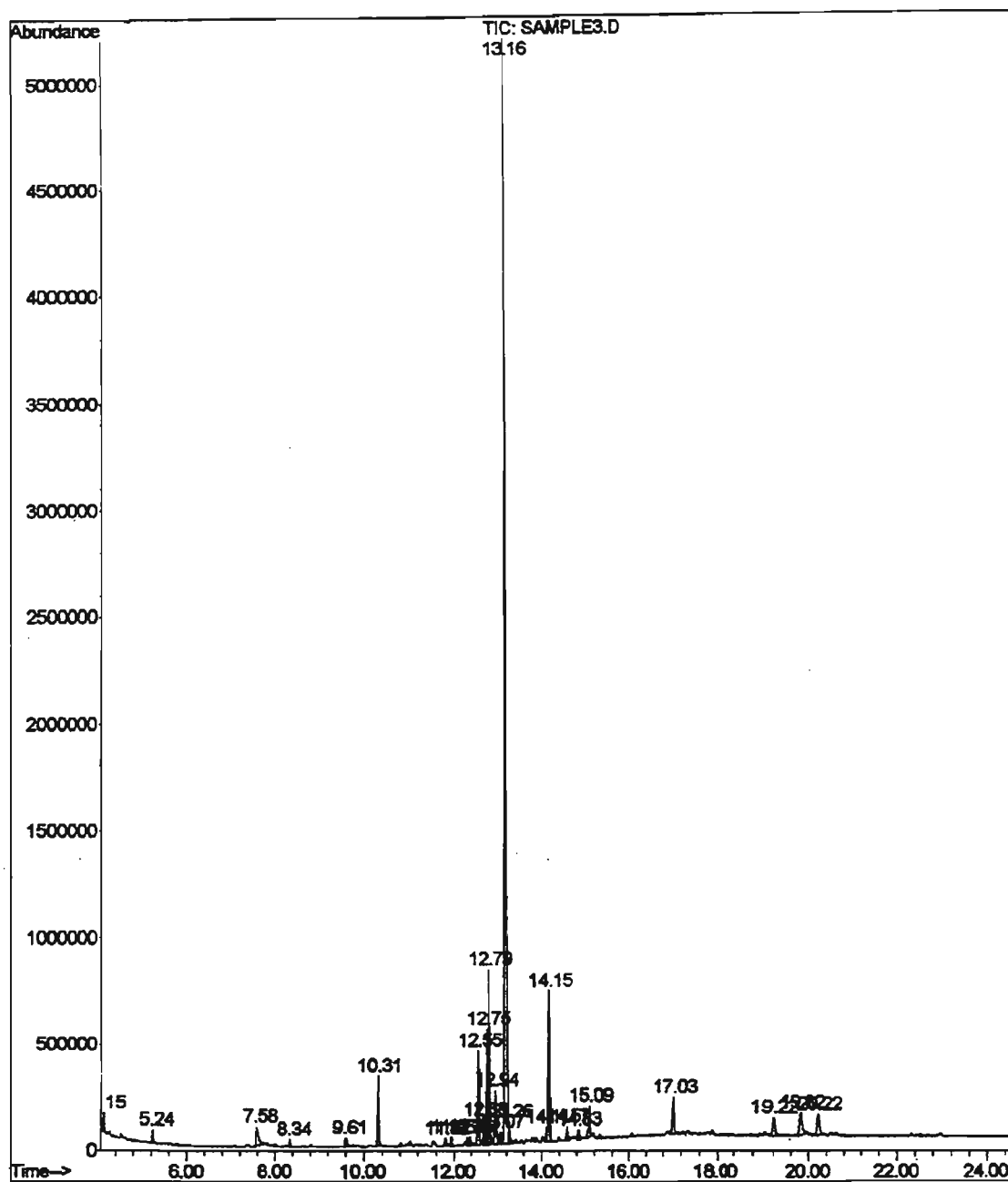
Figure C2.1: Total ion chromatogram of the ethanol-water Cancer Bush extract, derivatised by BSTFA/pyridine and eluted through the HP-5MS column of the Agilent 6890 GC-MS by conditions described in Section 2.7.2.1.
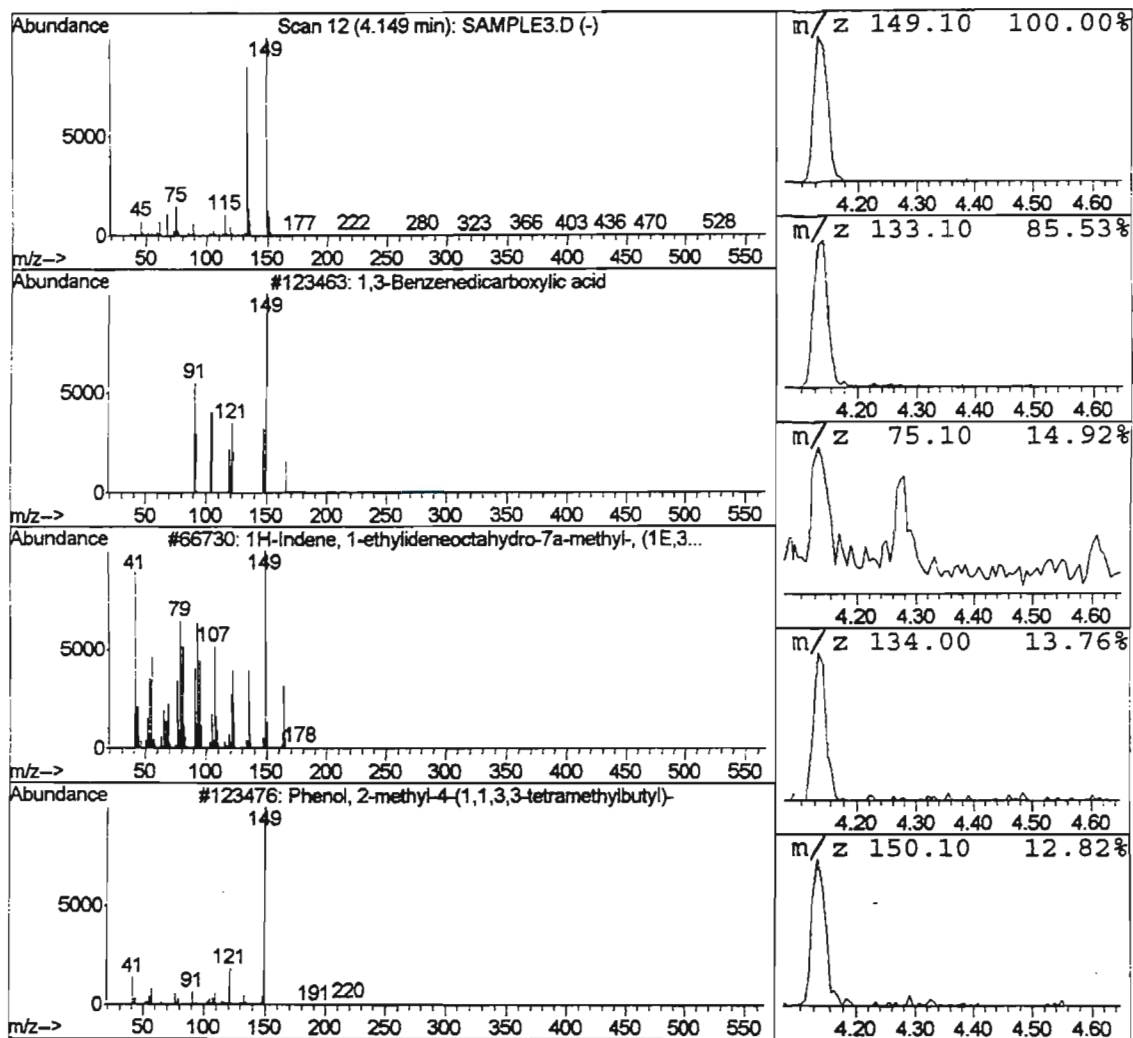
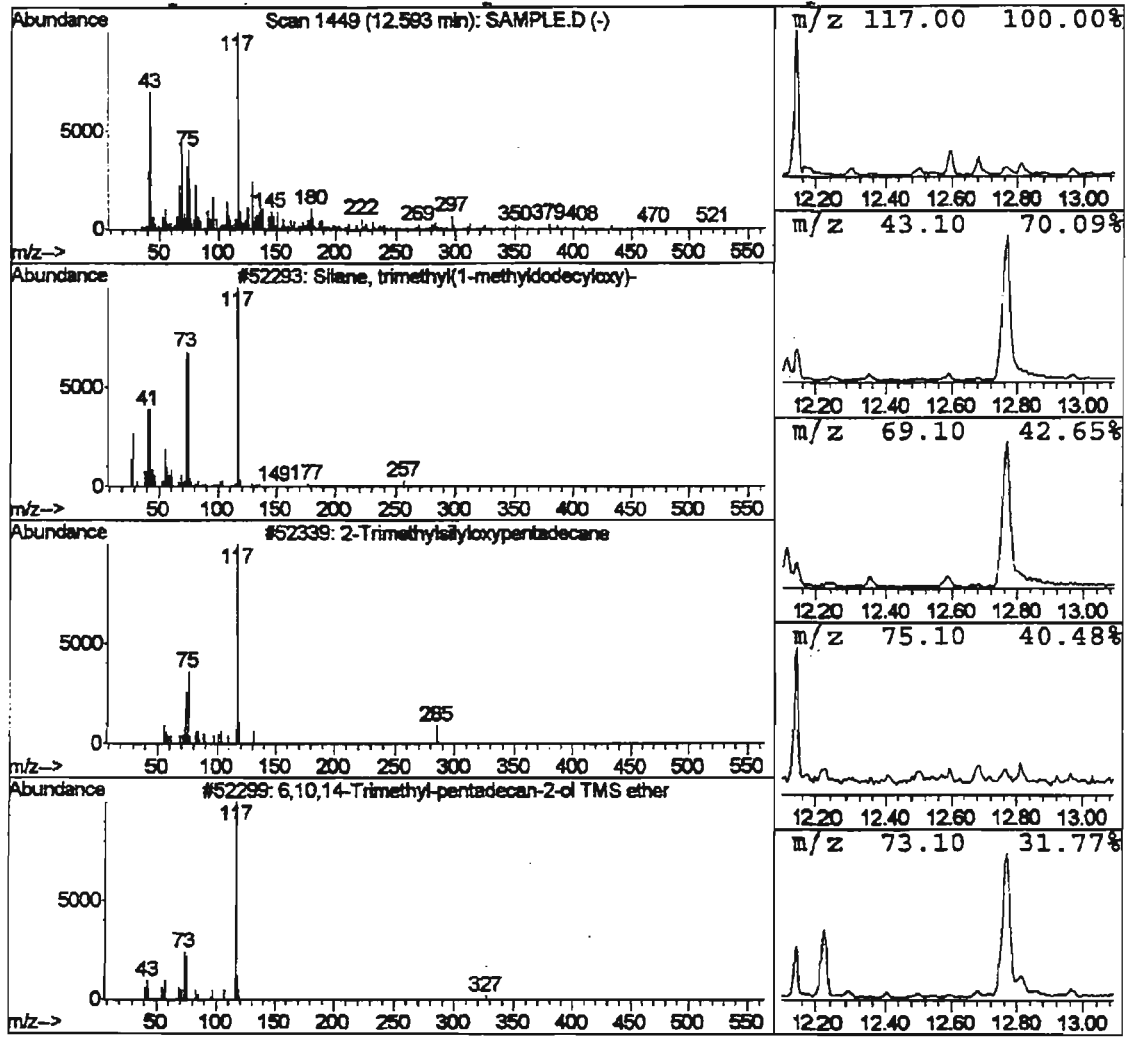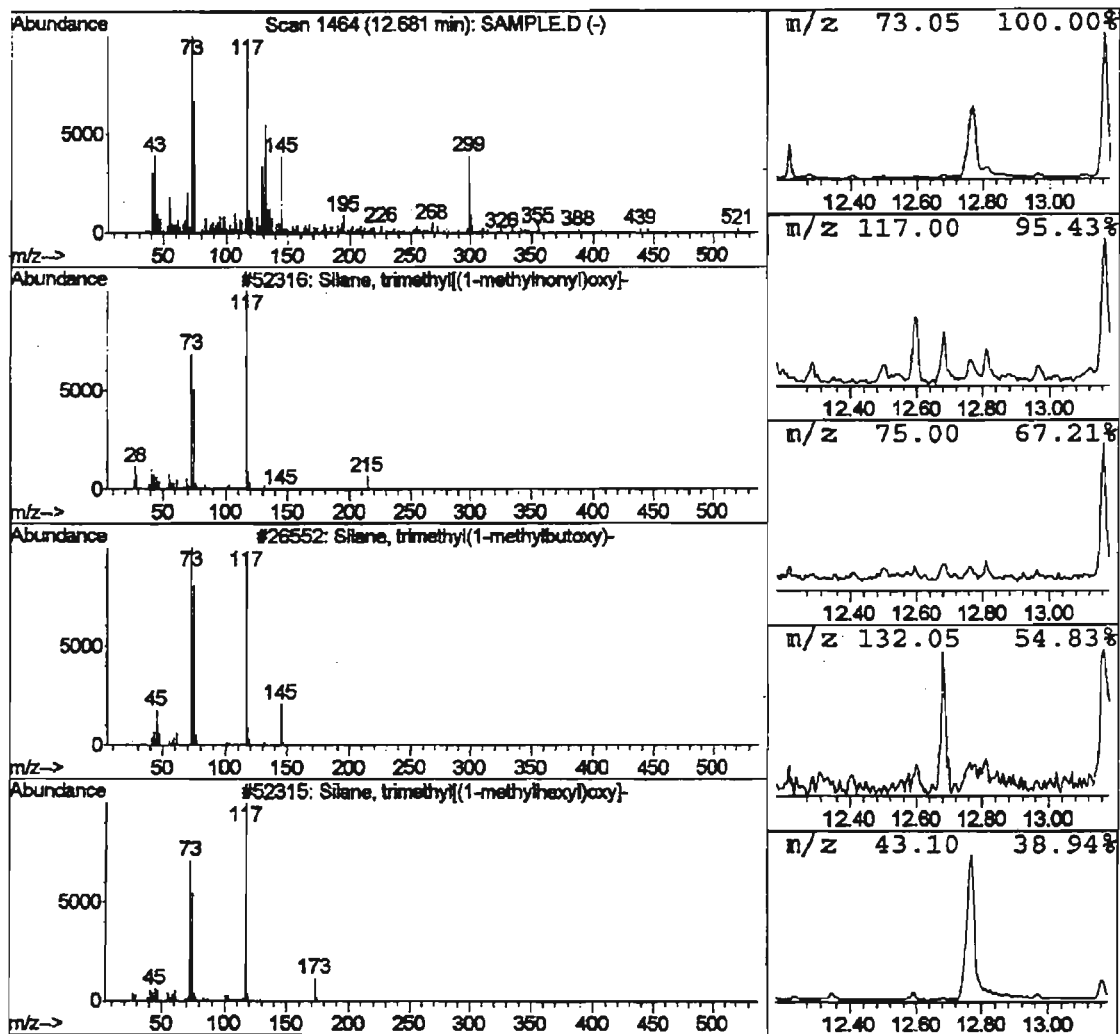Figure C2.2:   Mass spectrum of an unknown compound eluting at 4.149 minutes.
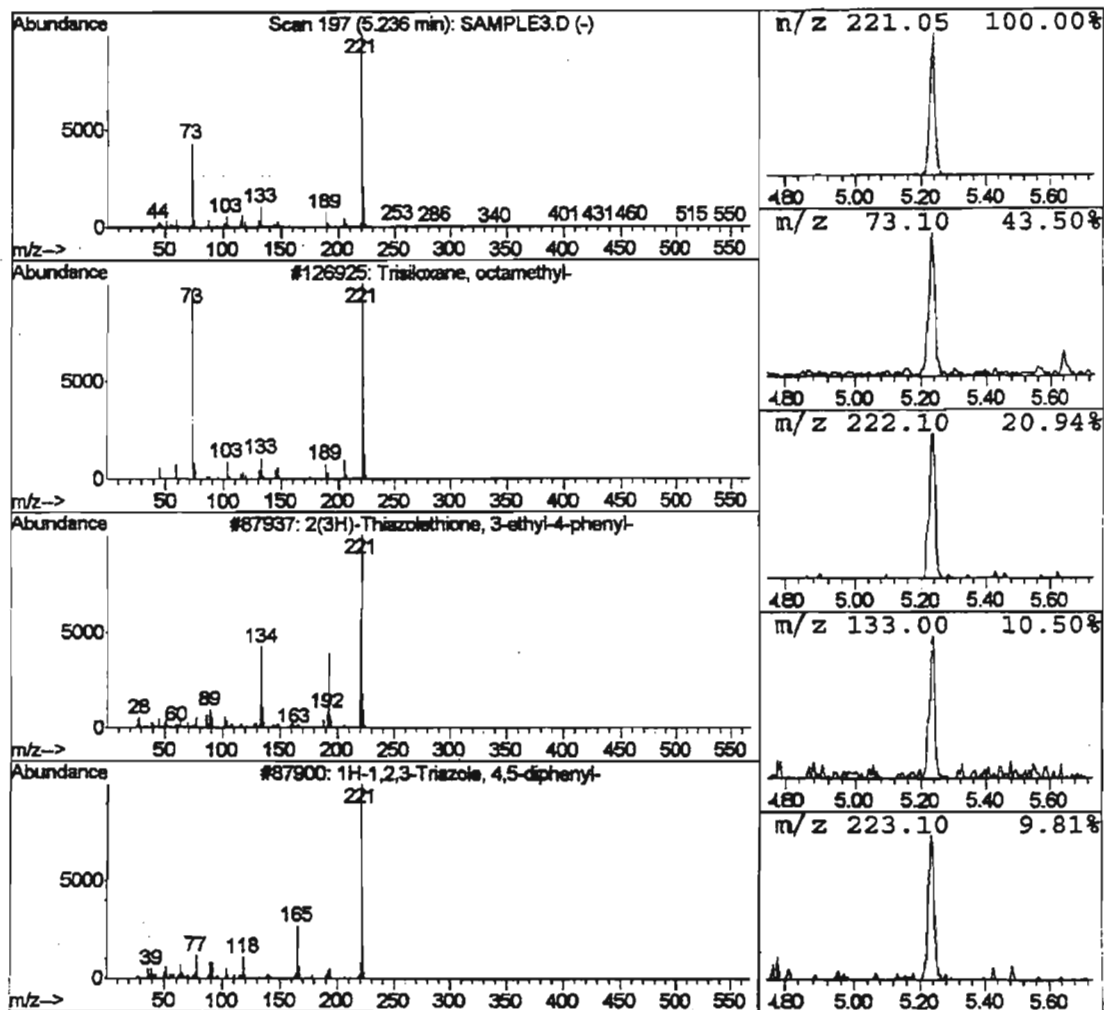
Figure C2.3:   Mass spectrum of an unknown compound eluting at 5.236 minutes.
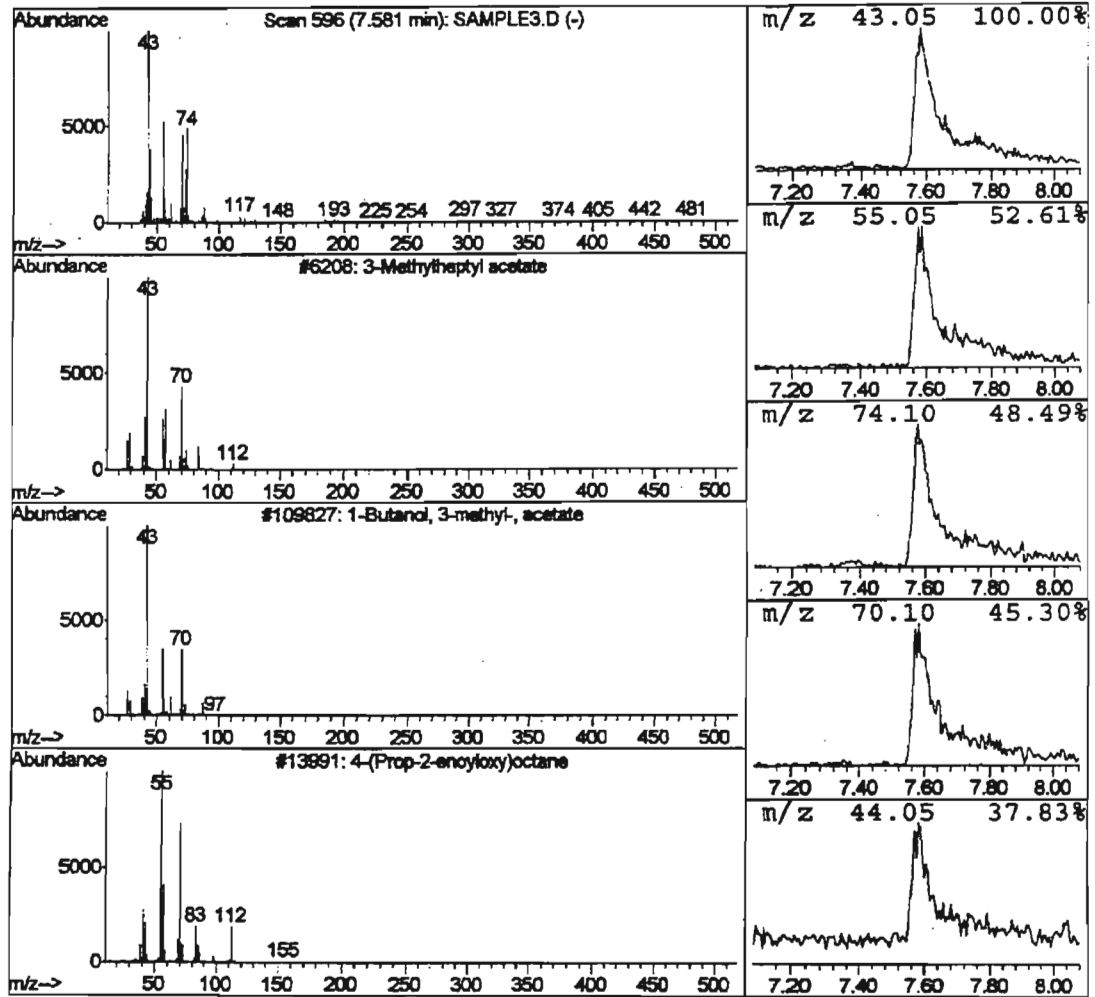
Figure C2.4:   Mass spectrum of an unknown compound eluting at 7.581 minutes.
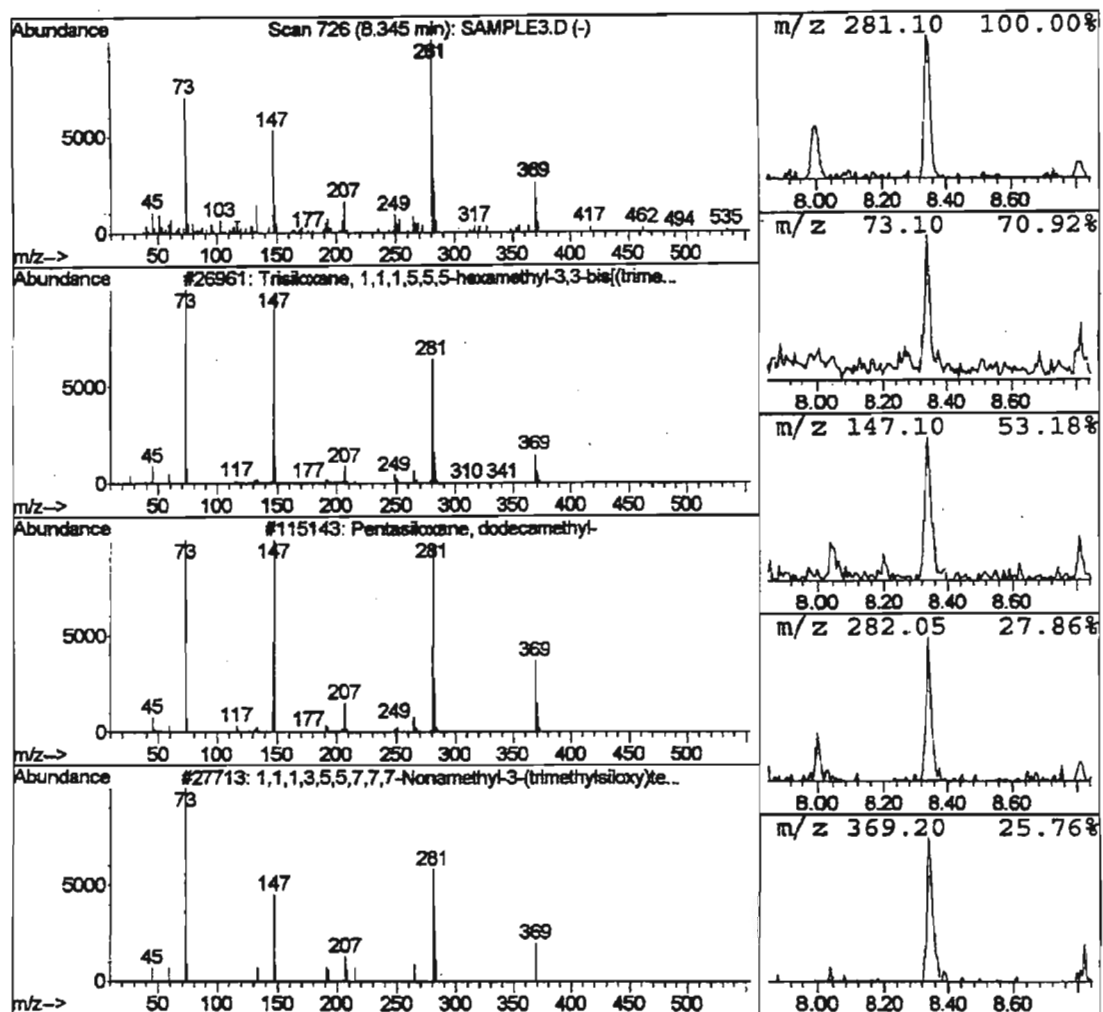
Figure C2.5: Mass spectrum of a possible derivatised quercetin compound which eluted at 8.345 minutes. It was identified from fragmentation reported by Tokusoglu *et al.* [2003].
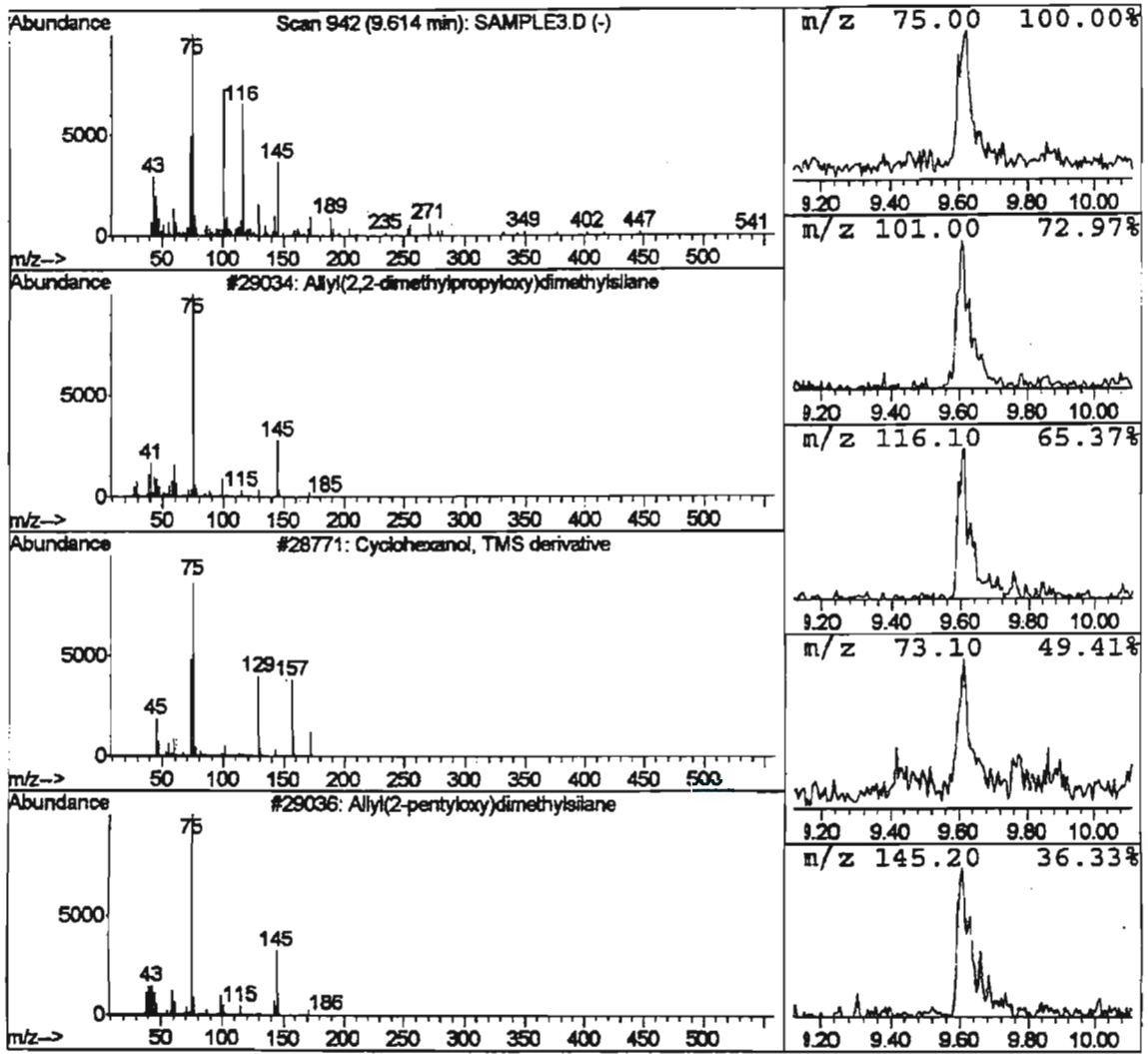
Figure C2.6:   Mass spectrum of an unknown compound eluting at 9.614 minutes.
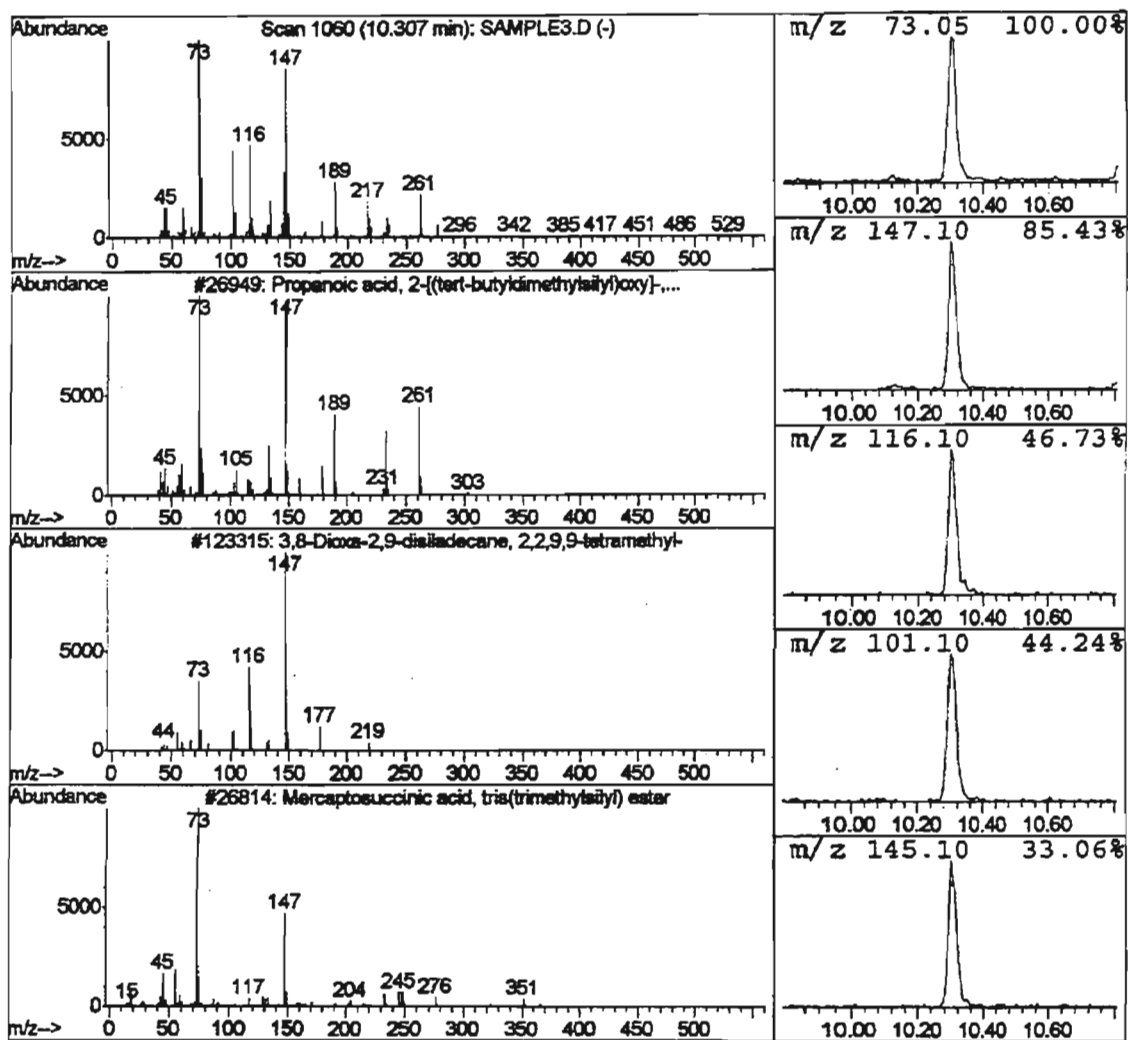
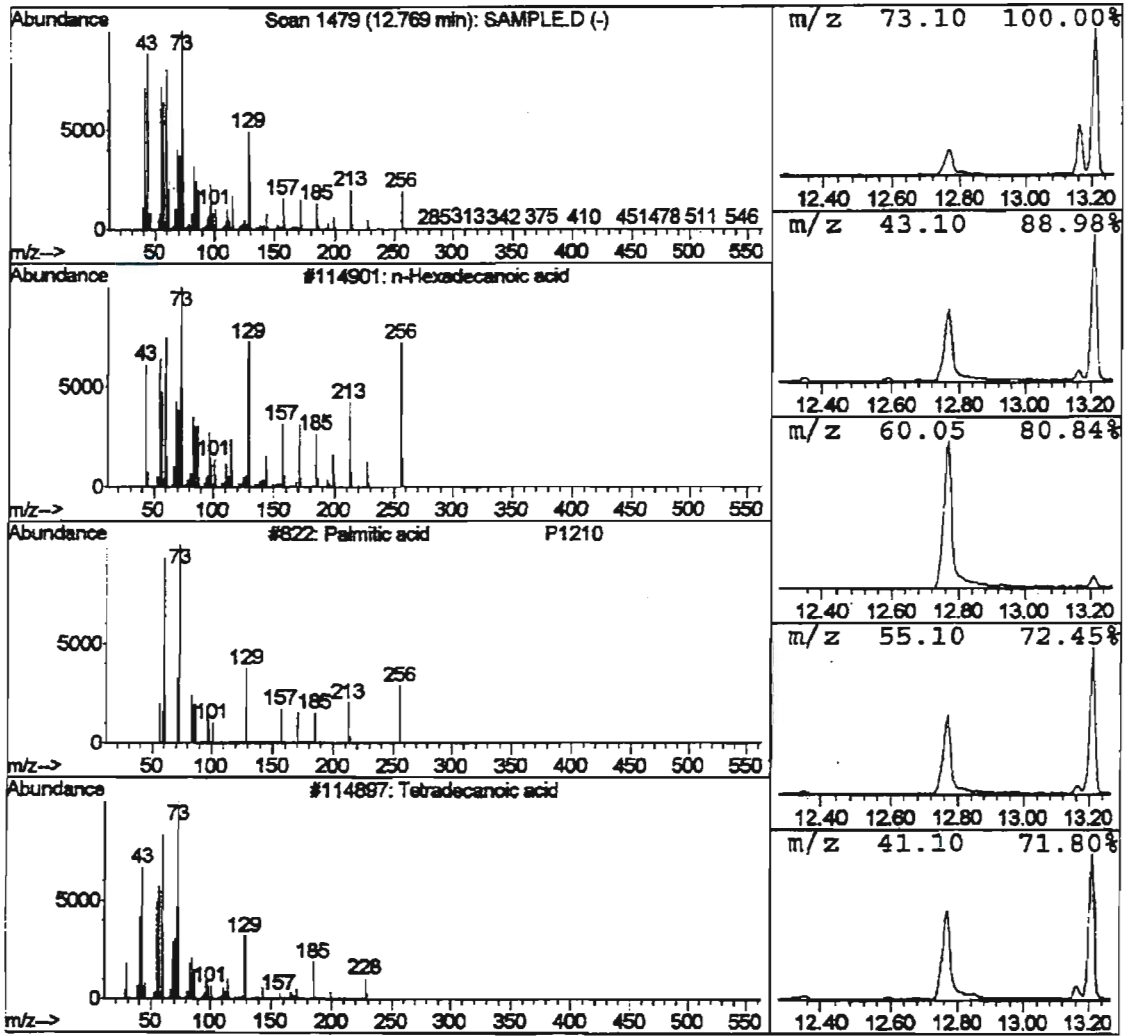Figure C2.7:   Mass spectrum of an unknown compound eluting at 10.307 minutes.
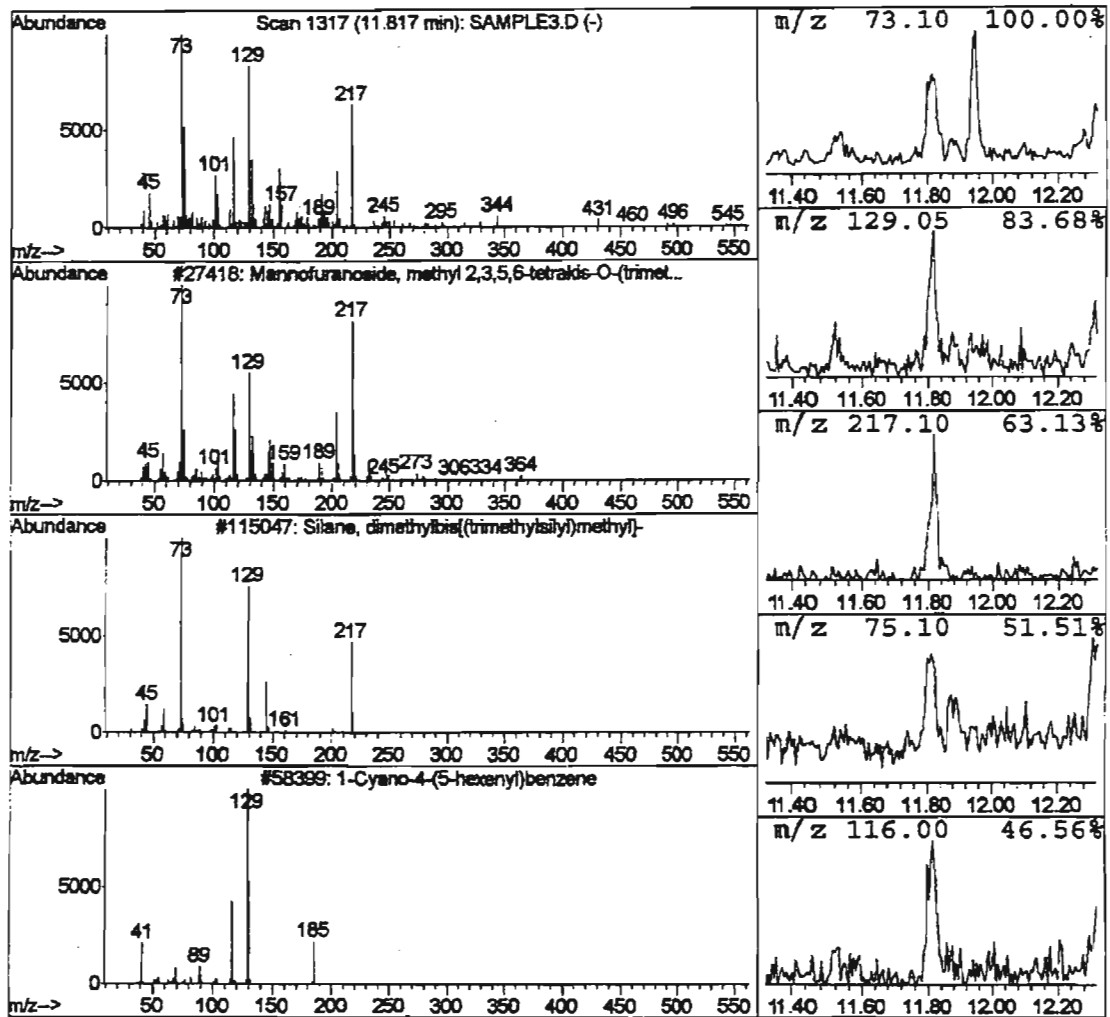
Figure C2.8: Mass spectrum of an unknown compound eluting at 11.817 minutes.
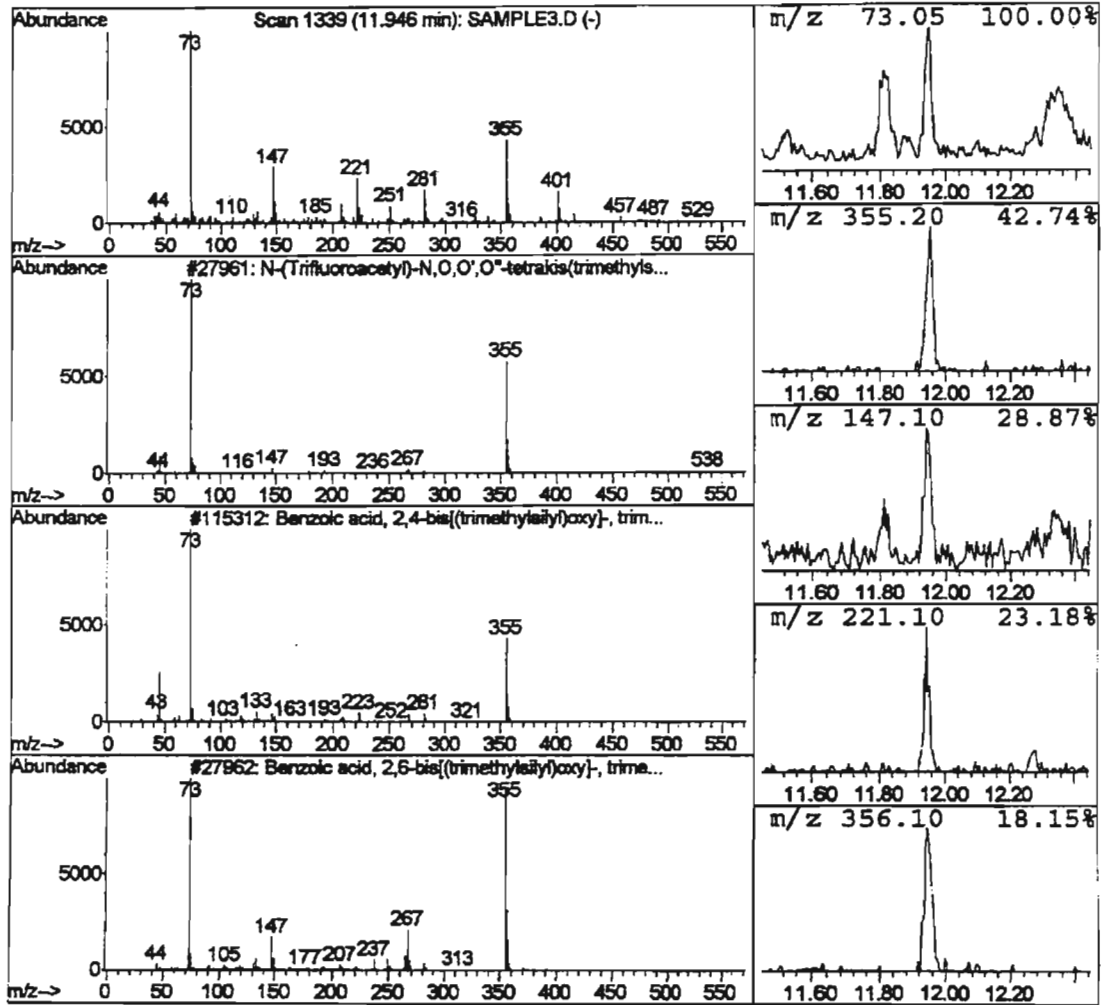
Figure C2.9:   Mass spectrum of an unknown compound eluting at 11.946 minutes.
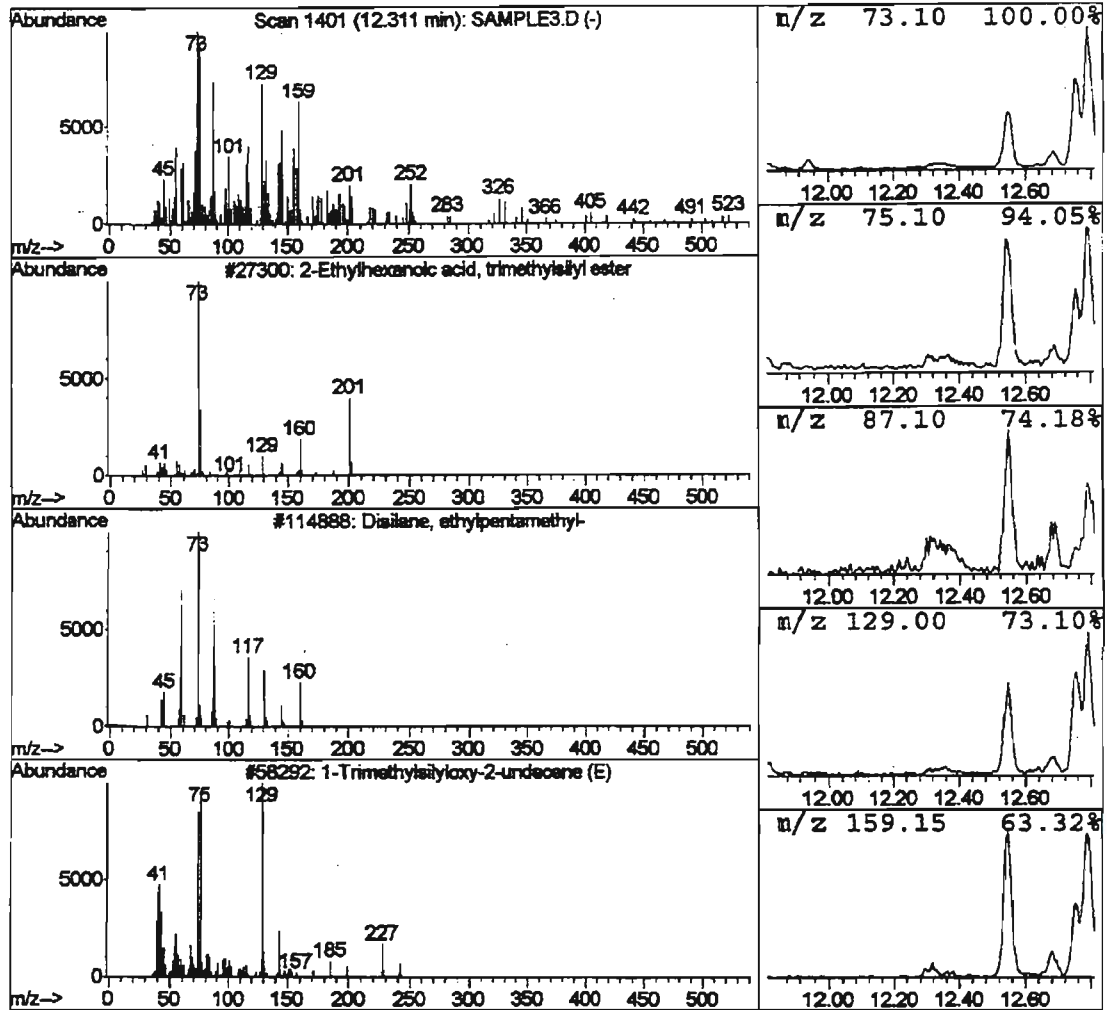
Figure C2.10:   Mass spectrum of an unknown compound eluting at 12.311 minutes.
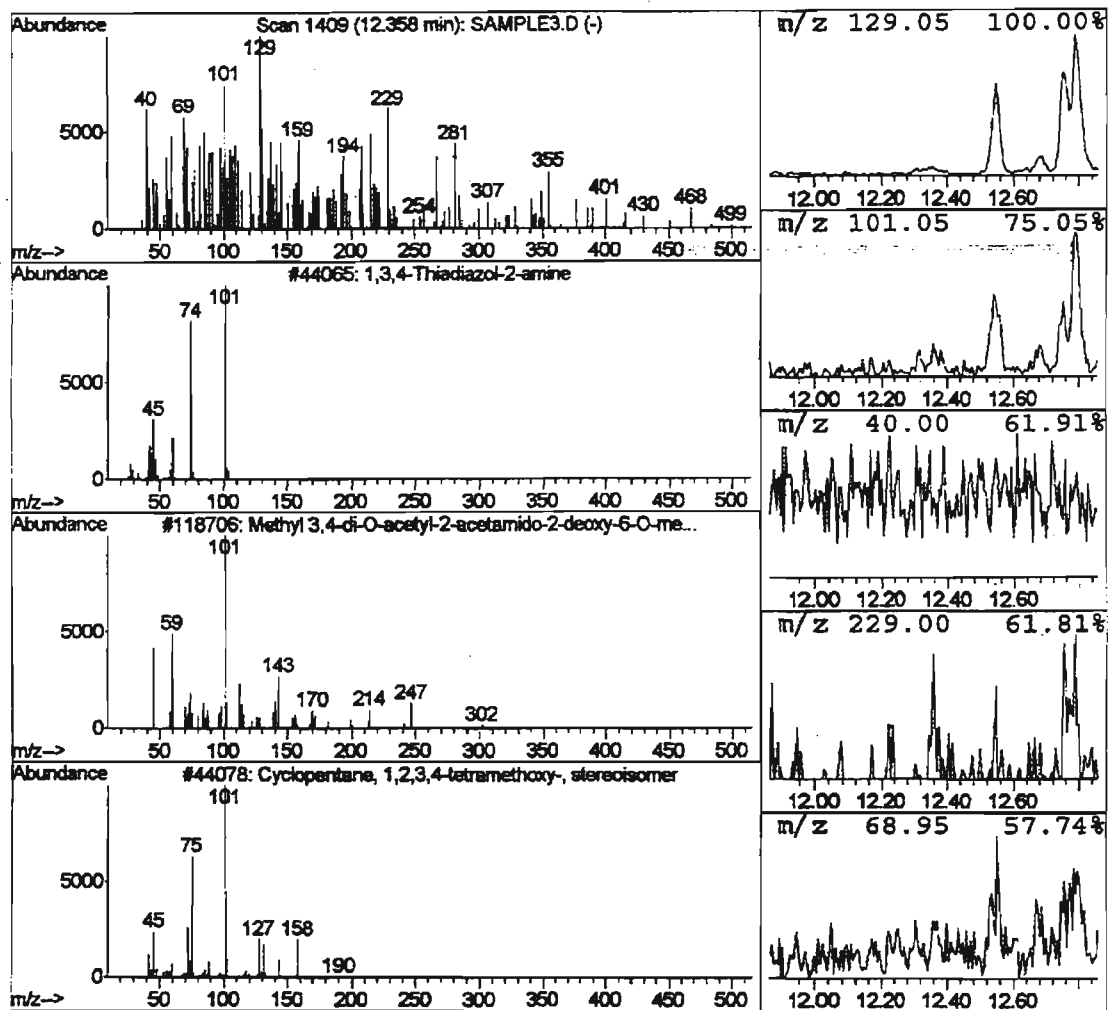
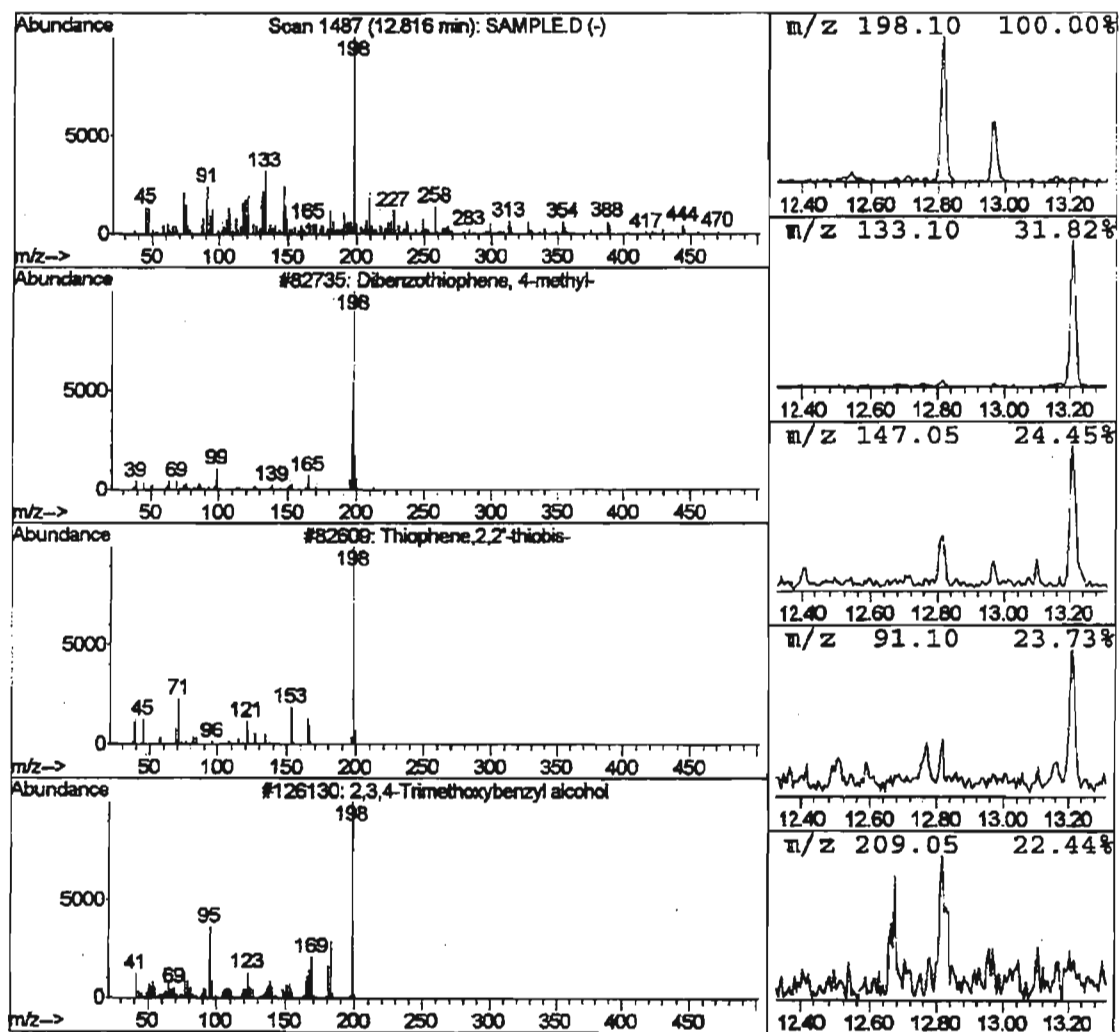Figure C2.11:   Mass spectrum of an unknown compound eluting at 12.358 minutes.

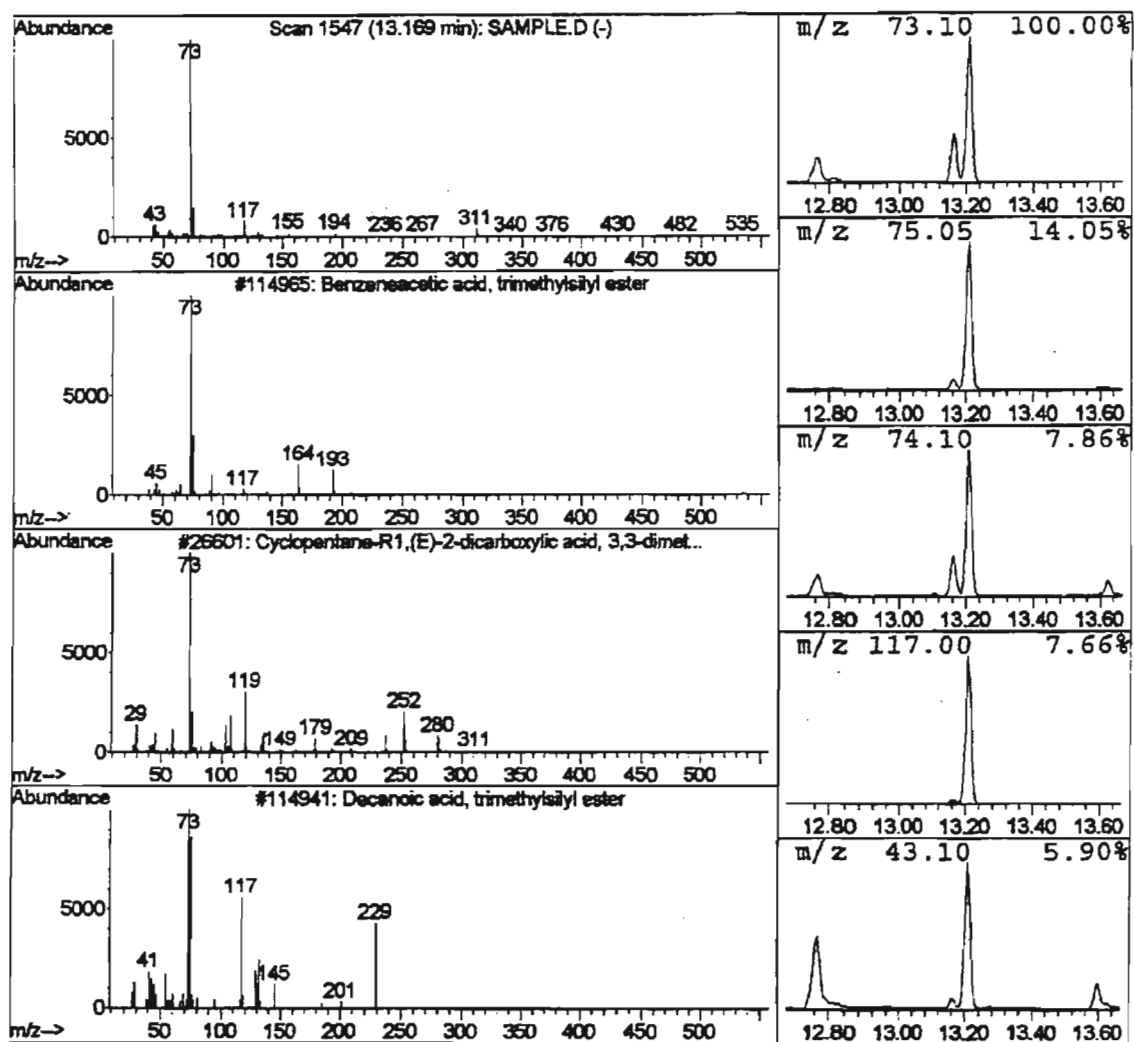Figure C2.12:   Mass spectrum of an unknown compound eluting at 12.546 minutes.

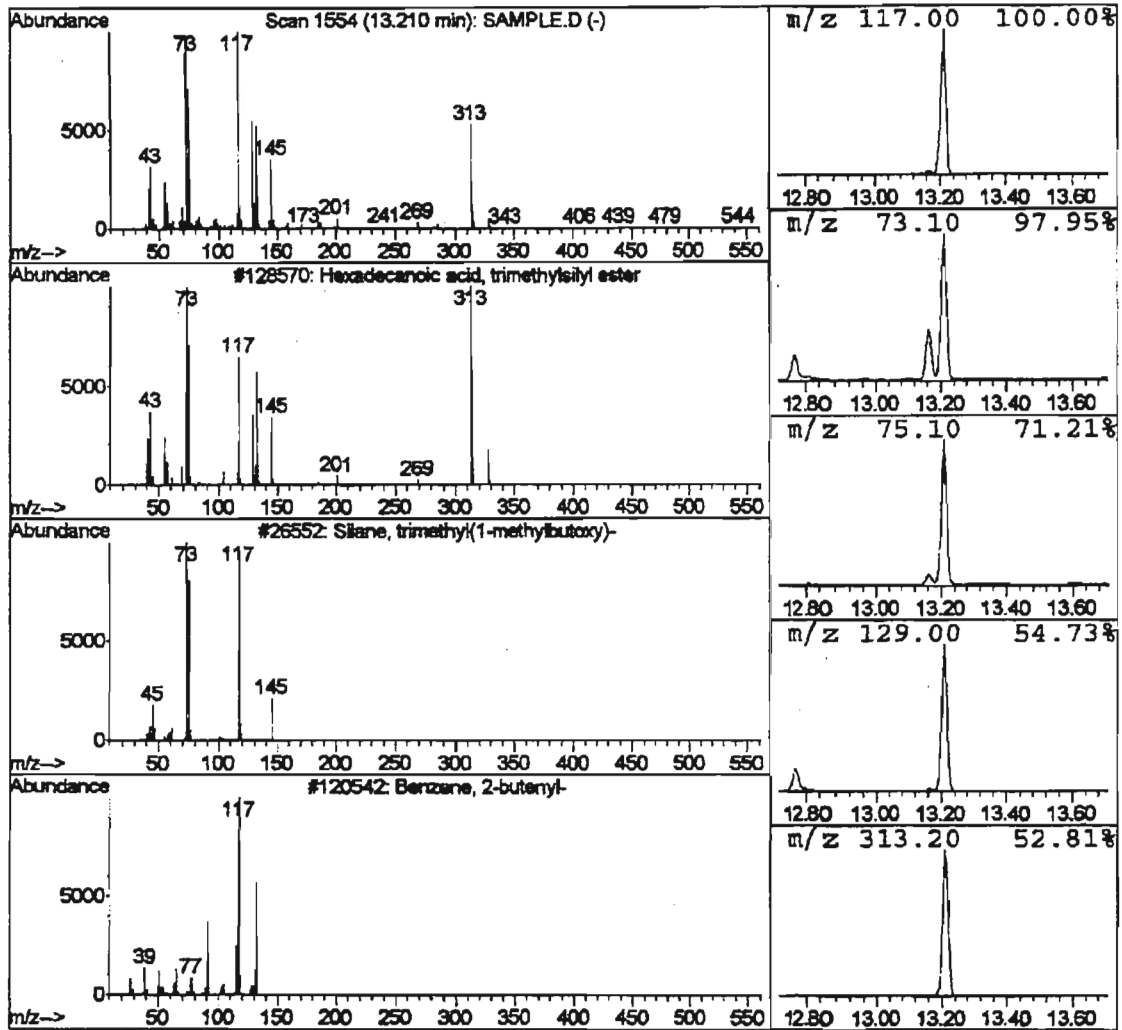Figure C2.13:   Mass spectrum of an unknown compound eluting at 12.687 minutes.

Figure C2.14:   Mass spectrum of an unknown compound eluting at 12.751 minutes.
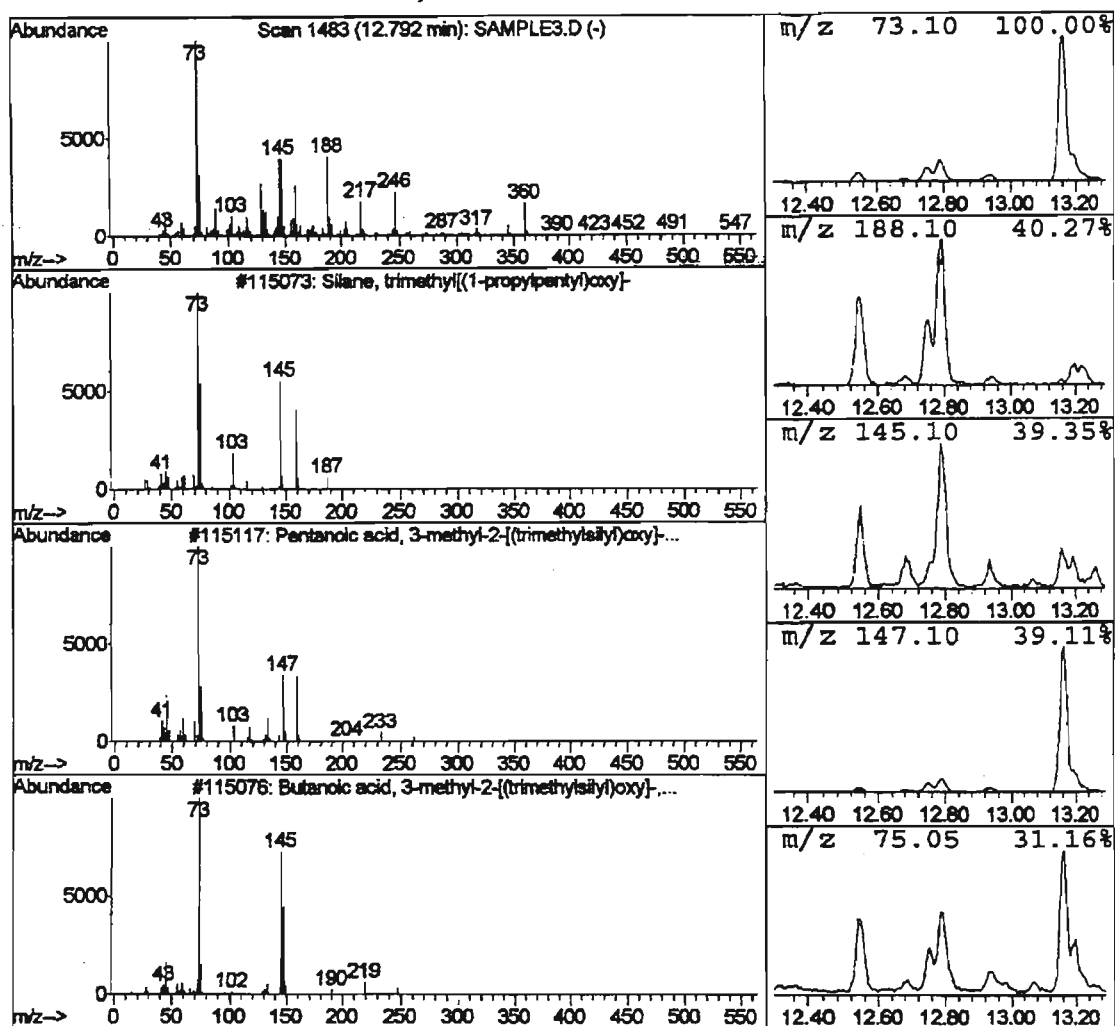
Figure C2.15: Mass spectrum of an unknown compound eluting at 12.792 minutes.
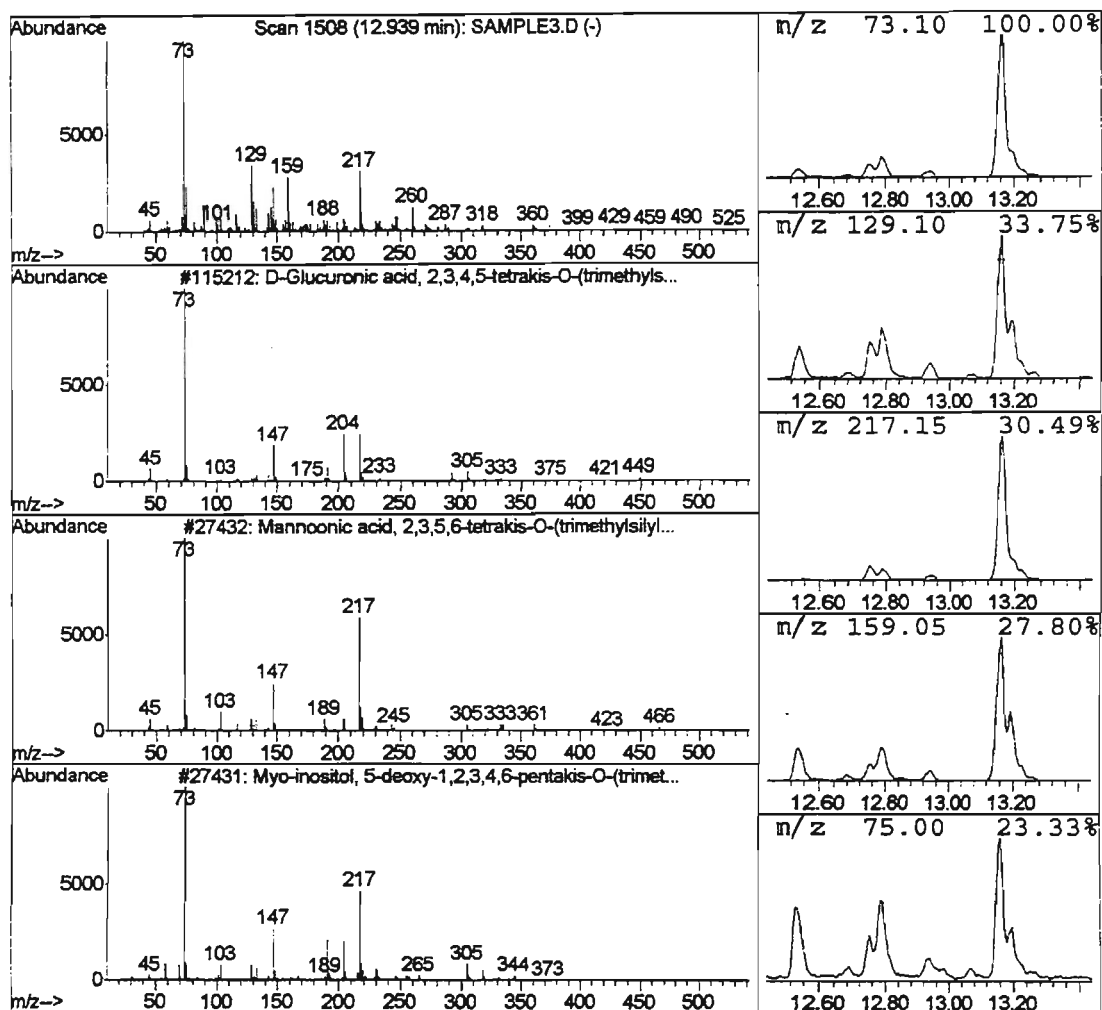
Figure C2.16: Mass spectrum of an unknown compound eluting at 12.939 minutes.

Figure C2.17:   Mass spectrum of an unknown compound eluting at 13.069 minutes.

Figure C2.18:   Mass spectrum of an unknown compound eluting at 13.163 minutes.

Figure C2.19:   Mass spectrum of an unknown compound eluting at 13.263 minutes.
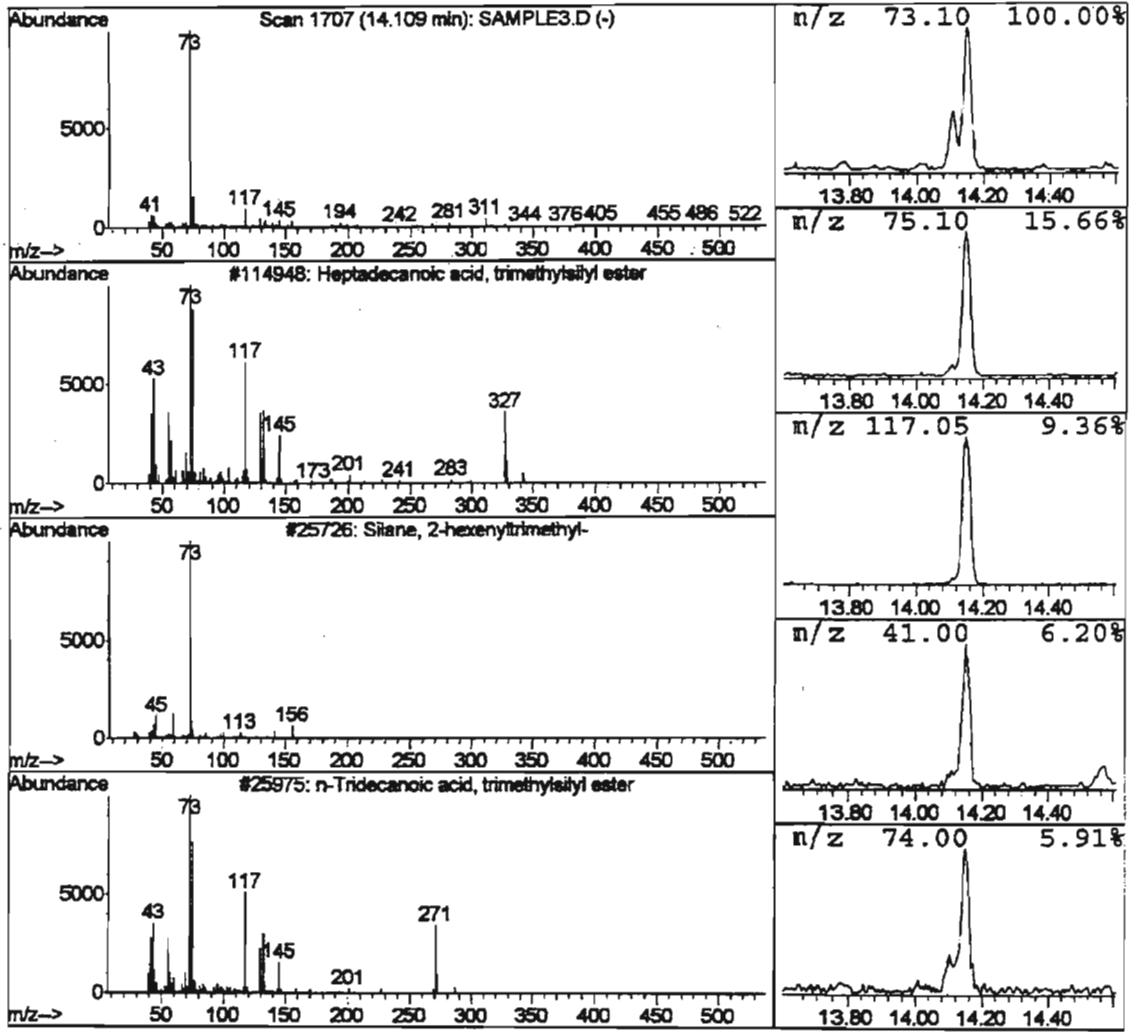
Figure C2.20:   Mass spectrum of an unknown compound eluting at 14.109 minutes.
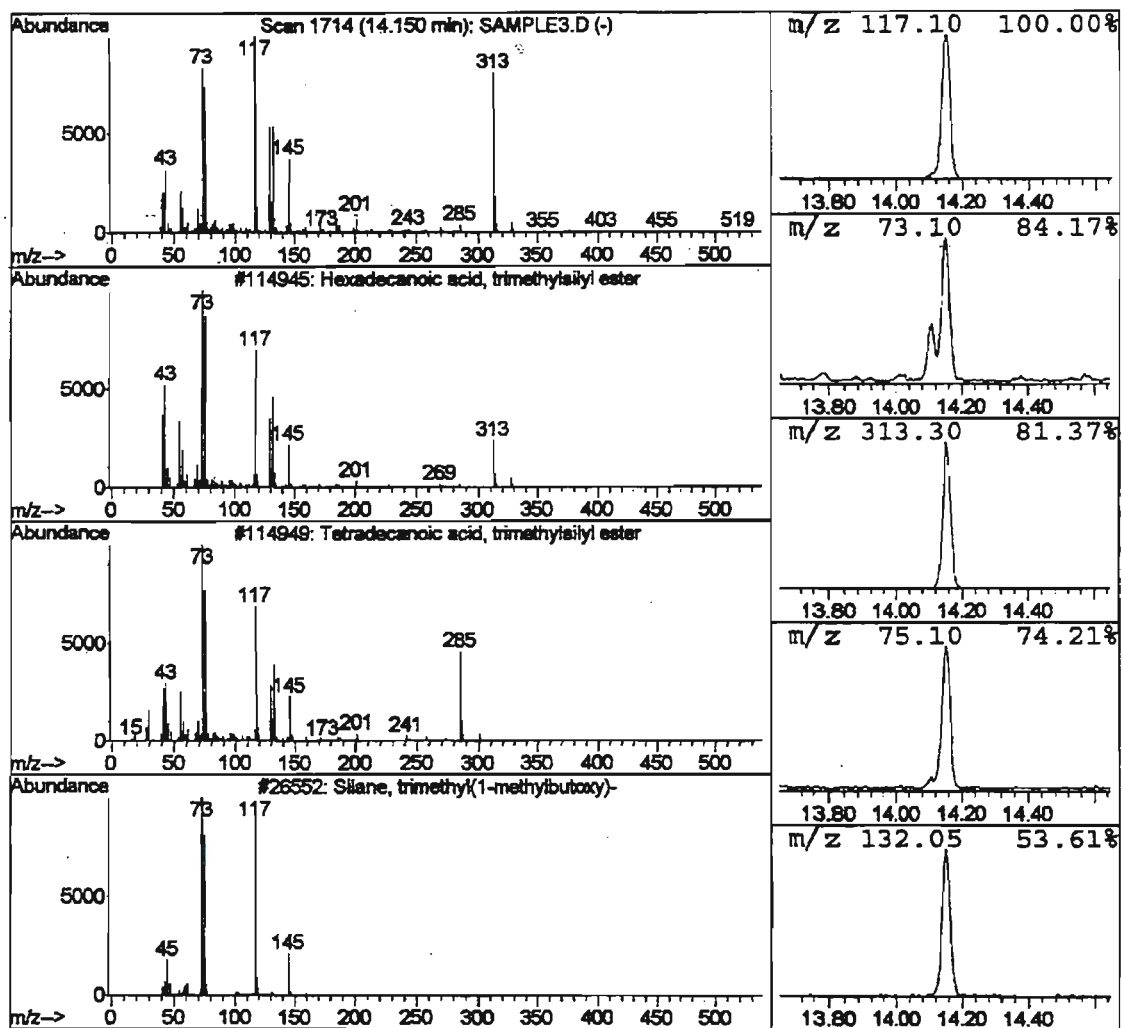
Figure C2.21: Mass spectrum of an unknown compound eluting at 14.150 minutes.
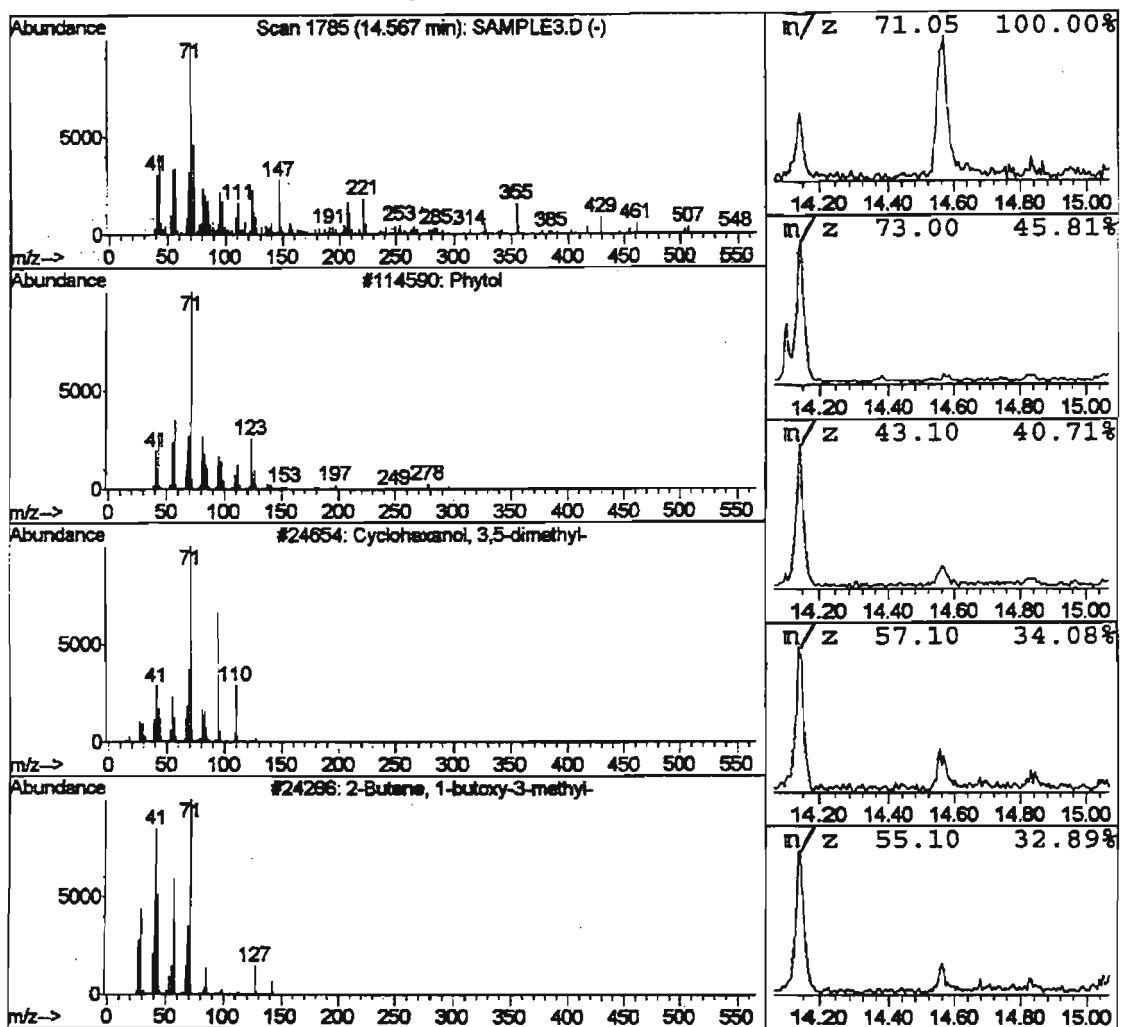
Figure C2.22:   Mass spectrum of an unknown compound eluting at 14.567 minutes.

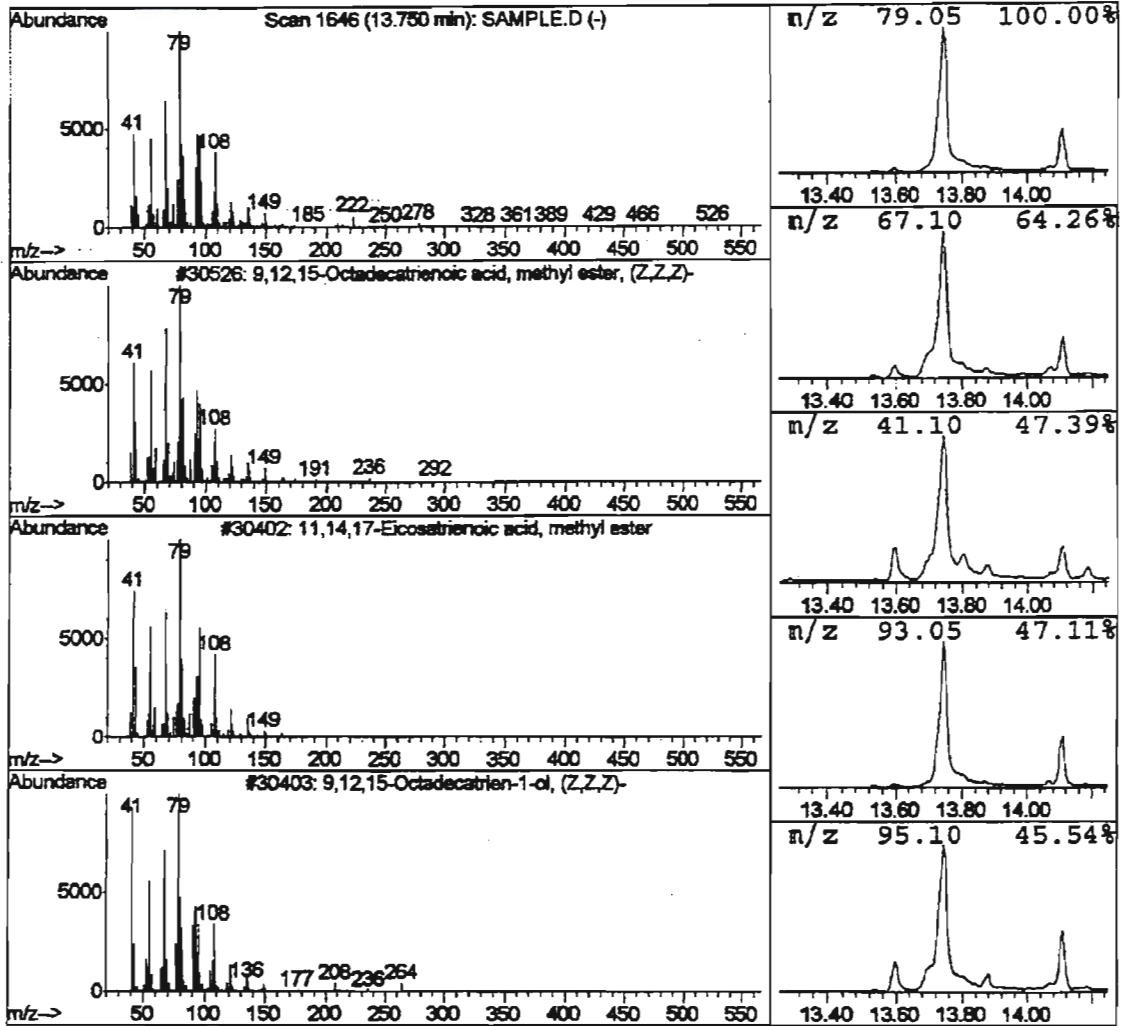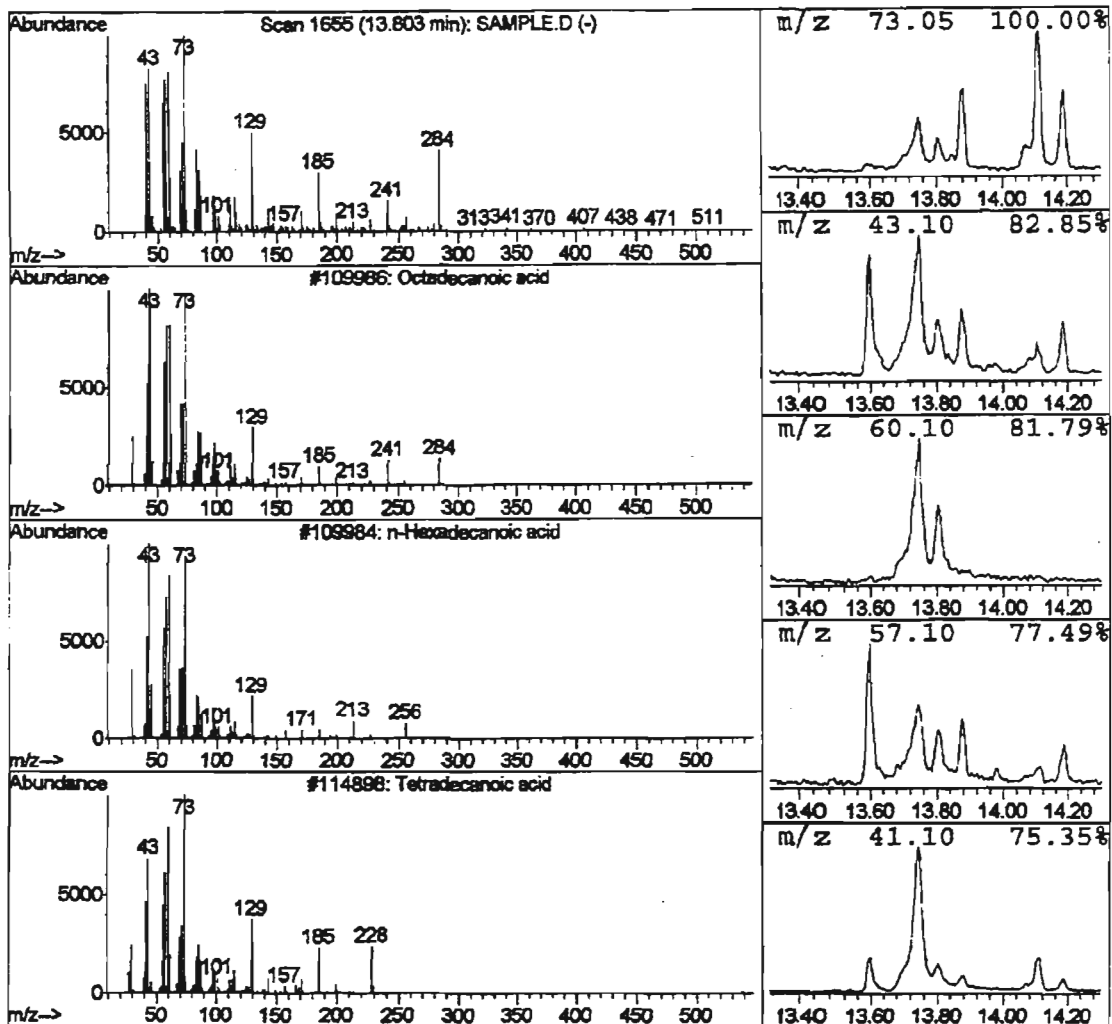Figure C2.23:   Mass spectrum of an unknown compound eluting at 14.831 minutes.

Figure C2.24: Mass spectrum of a derivatised alpha-linolenic acid that elutes at 15.090 minutes. The fragmentation pattern matched that of a derivatised alpha-linolenic acid present in the library.

Figure C2.25:   Mass spectrum of an unknown compound eluting at 17.035 minutes.

Figure C2.26: Mass spectrum of an unknown compound eluting at 19.214 minutes.

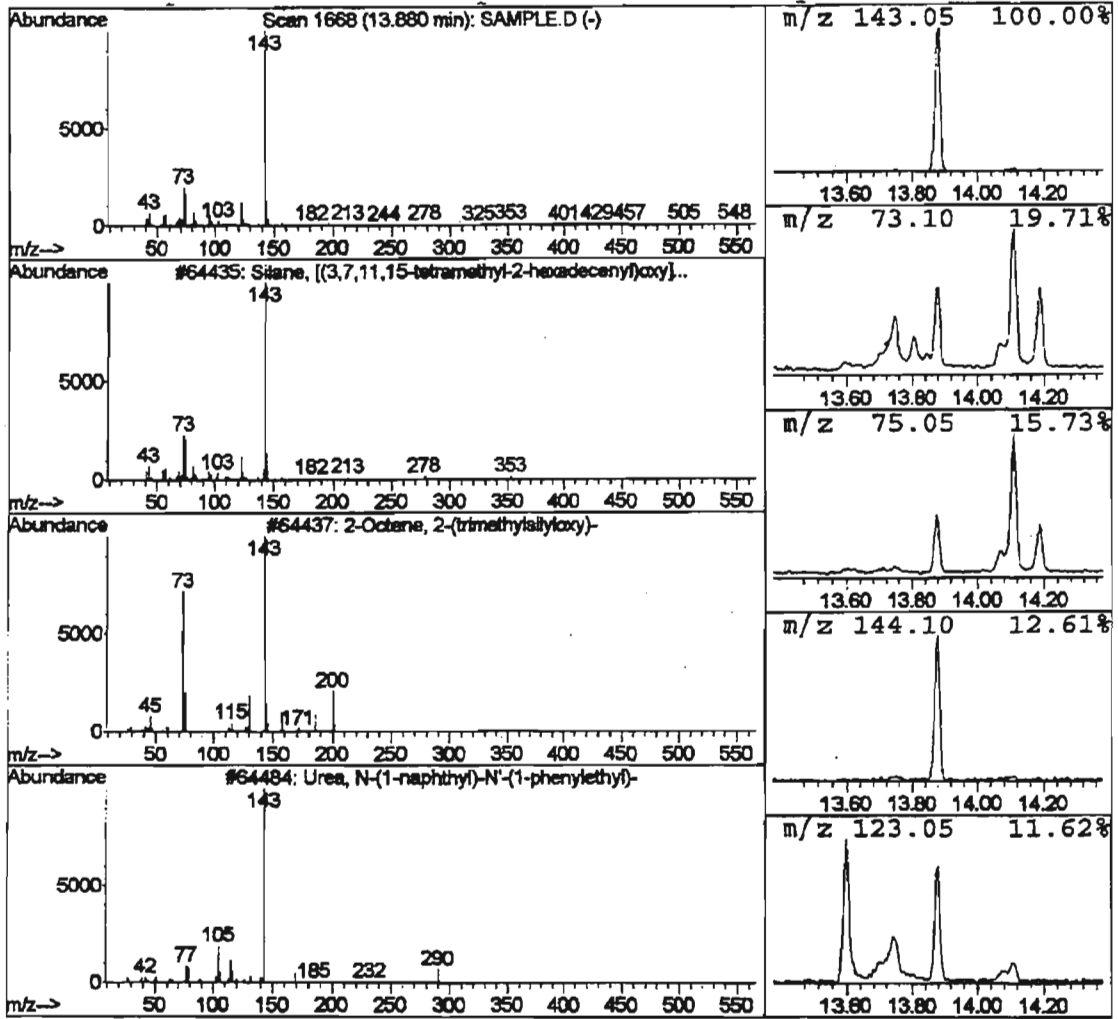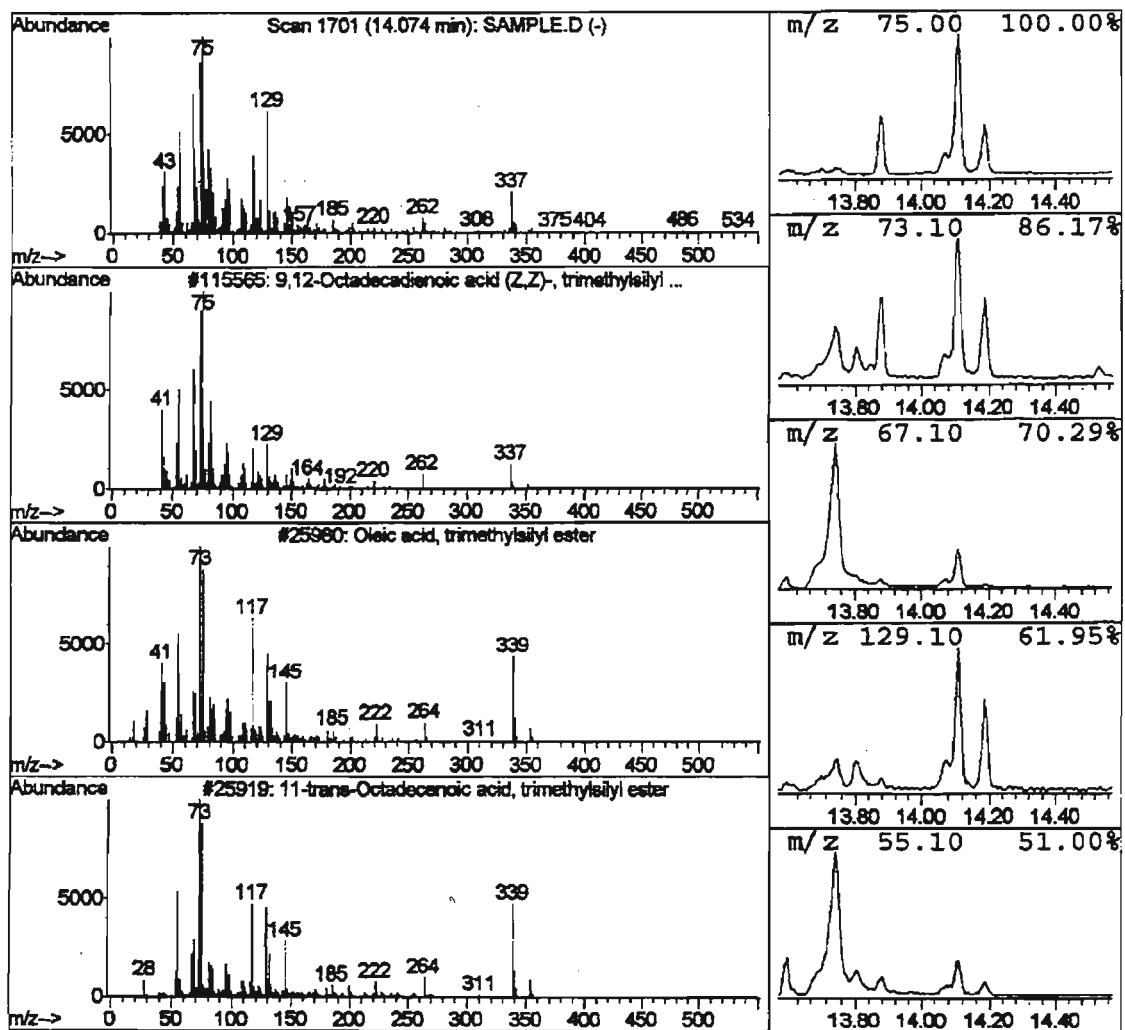Figure C2.27: Mass spectrum of an unknown compound eluting at 19.826 minutes.

Figure C2.28:   Mass spectrum of an unknown compound eluting at 20.219 minutes.

Figure C3.1:   Total ion chromatogram of the ethanol-water Cancer Bush extract, derivatised by BSA/pyridine and eluted through the HP-5MS column of the Agilent 6890 GC-MS by conditions described in Section 2.7.2.1.

Figure C3.2:   Mass spectrum of an unknown compound eluting at 4.449 minutes.
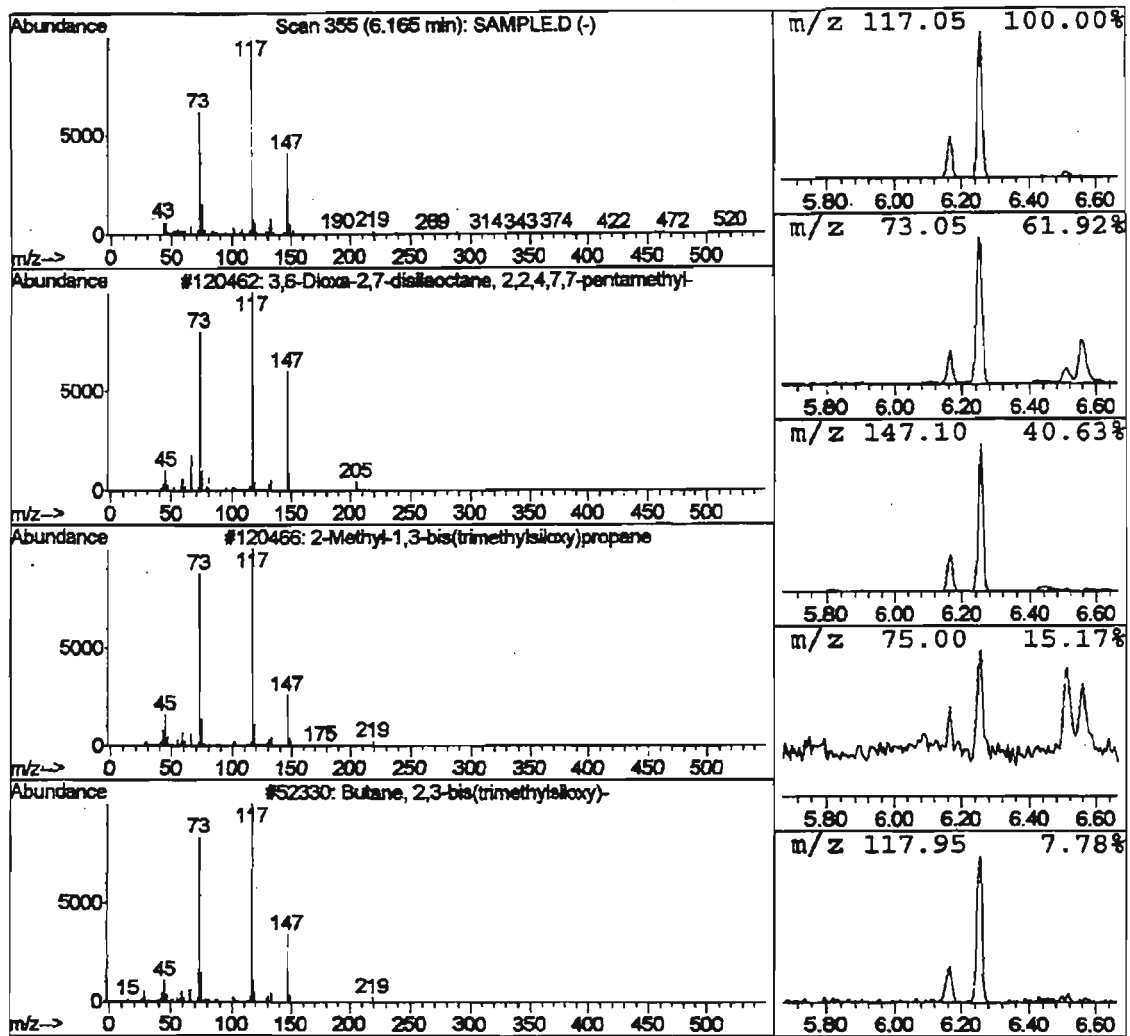
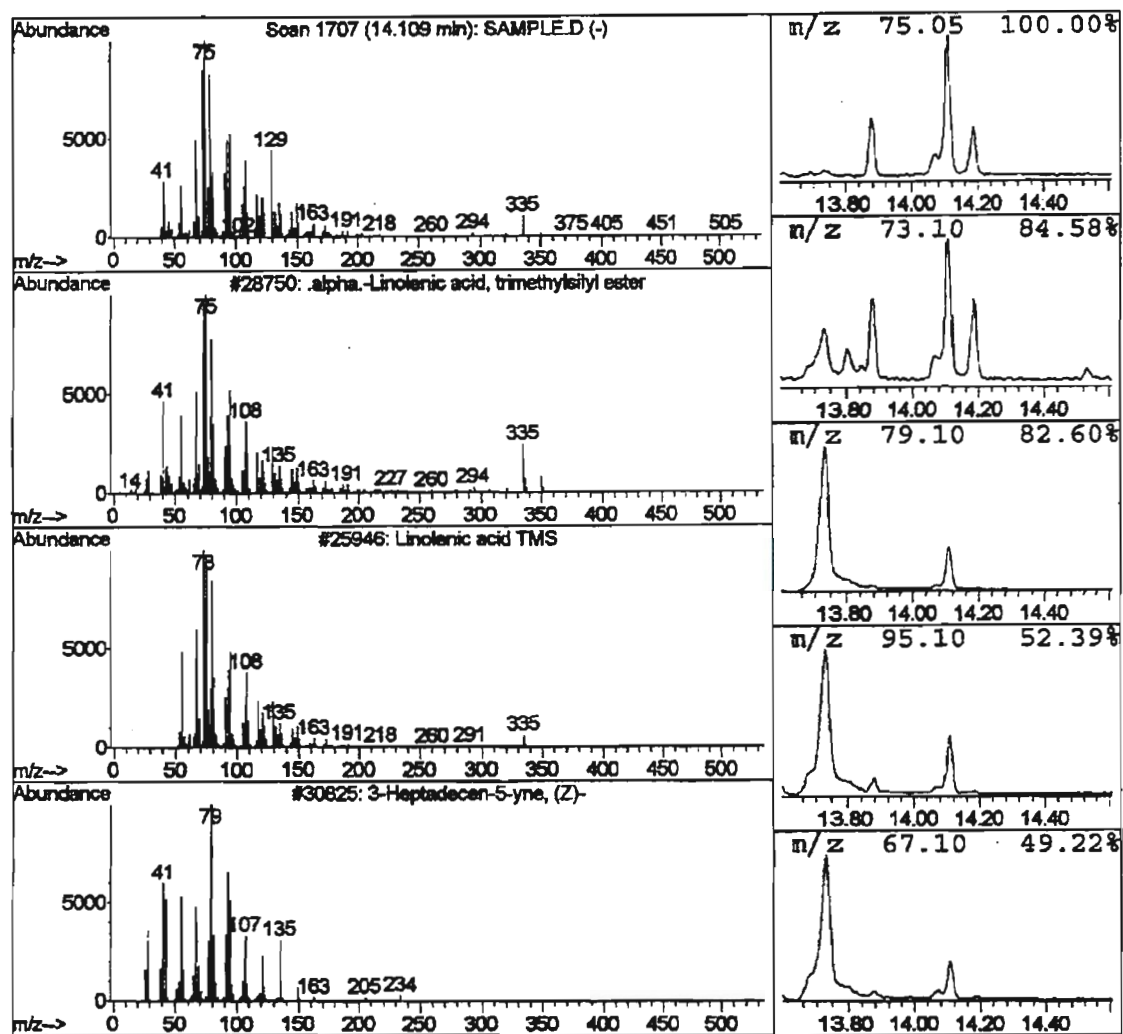Figure C3.3:   Mass spectrum of an unknown compound eluting at 6.165 minutes.

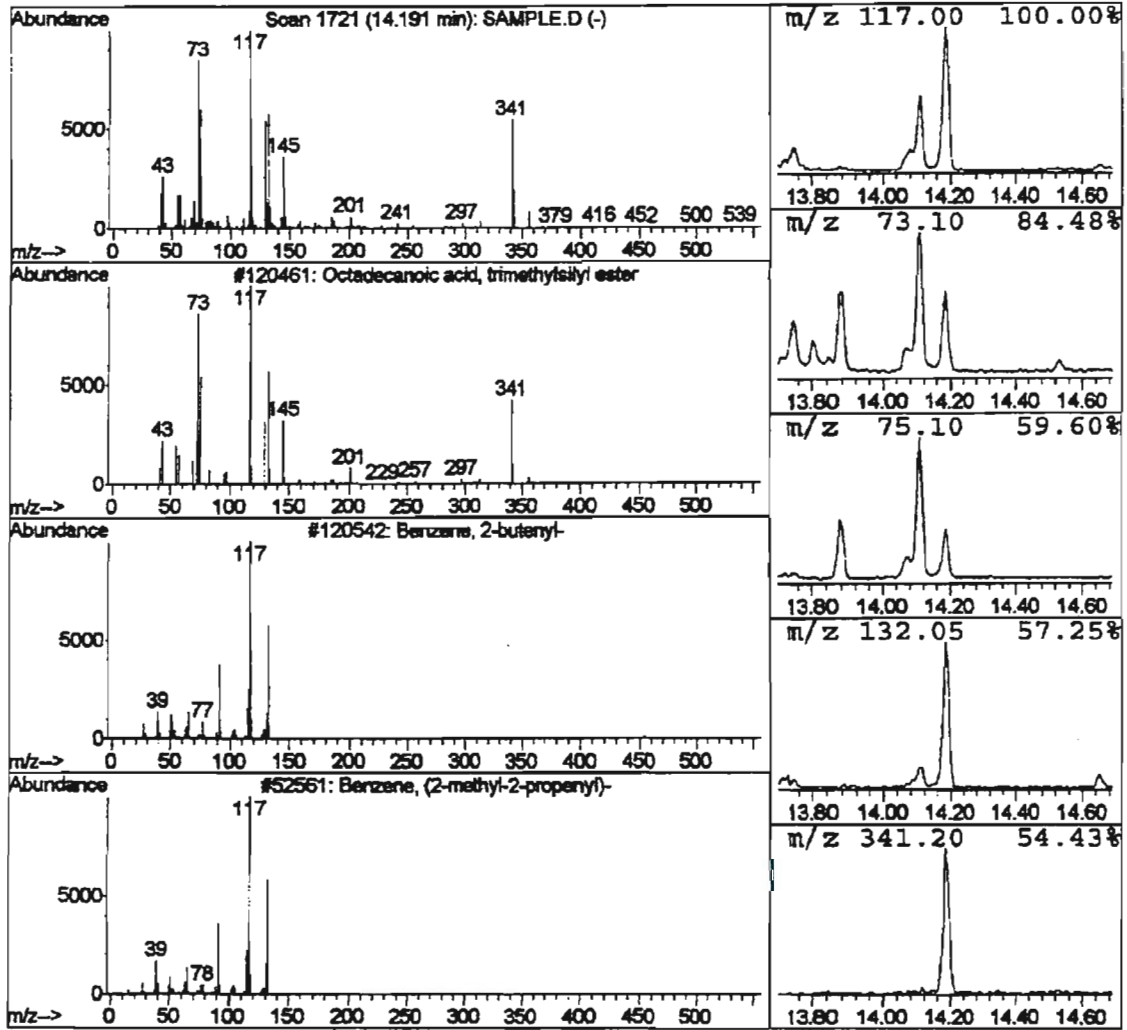Figure C3.4: Mass spectrum of an unknown compound eluting at 6.253 minutes.

Figure C3.5:   Mass spectrum of a derivatised benzoic acid that elutes at 8.104 minutes. The fragmentation pattern matched that of a derivatised benzoic acid present in the library.

Figure C3.6:   Mass spectrum of an unknown compound eluting at 8.709 minutes.

Figure C3.7:   Mass spectrum of an unknown compound eluting at 9.397 minutes.

Figure C3.8:   Mass spectrum of a derivatised benzofuranone that elutes at 10.395 minutes.
The fragmentation pattern matched that of a derivatised benzofuranone present
in the library.

Figure C3.9:   Mass spectrum of a derivatised dodecanoic acid that elutes at 10.960 minutes. The fragmentation pattern matched that of a derivatised dodecanoic acid present in the library.
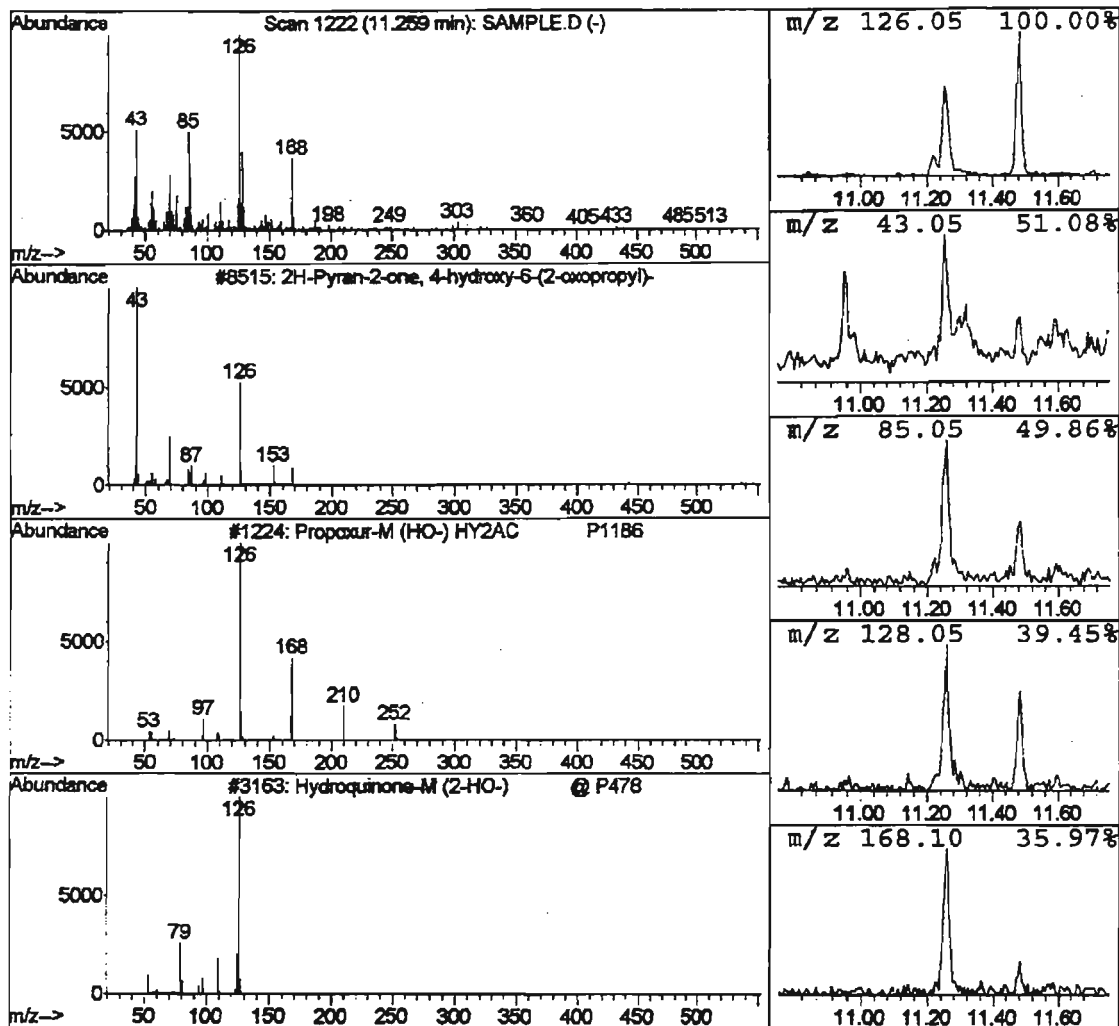
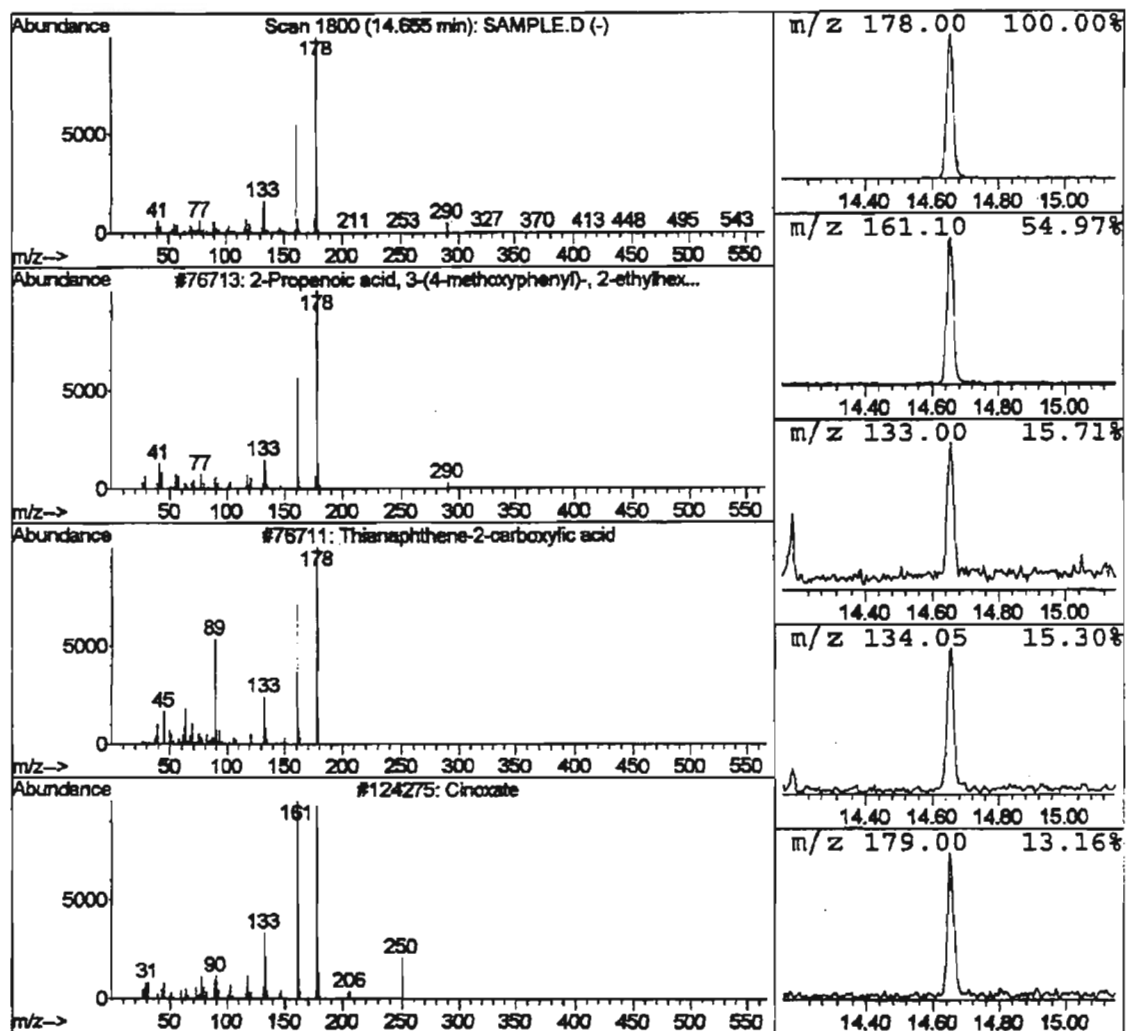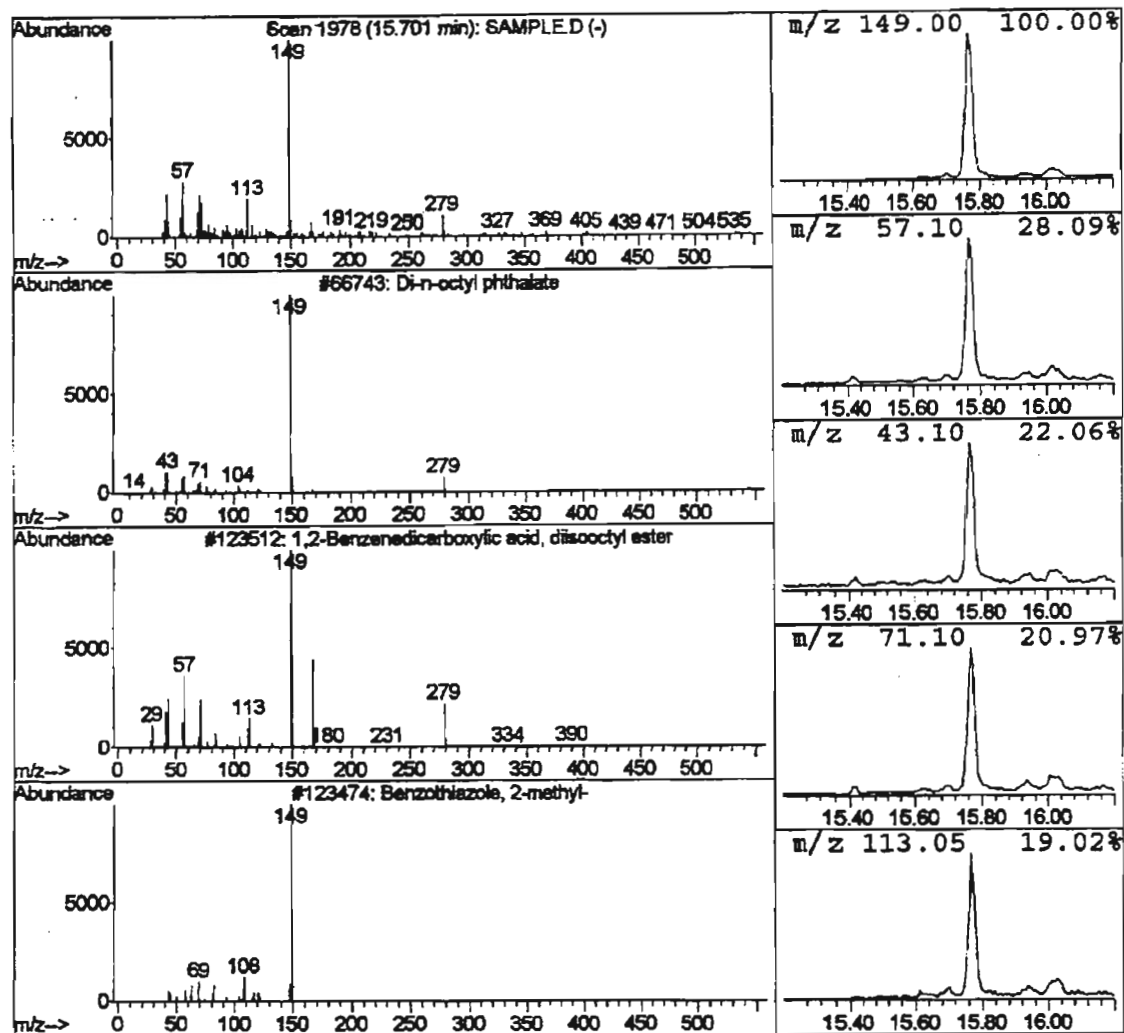Figure C3.10: Mass spectrum of an unknown compound eluting at 11.259 minutes.

Figure C3.11:   Mass spectrum of an unknown compound eluting at 11.482 minutes.

Figure C3.12:   Mass spectrum of an unknown compound eluting at 11.853 minutes.

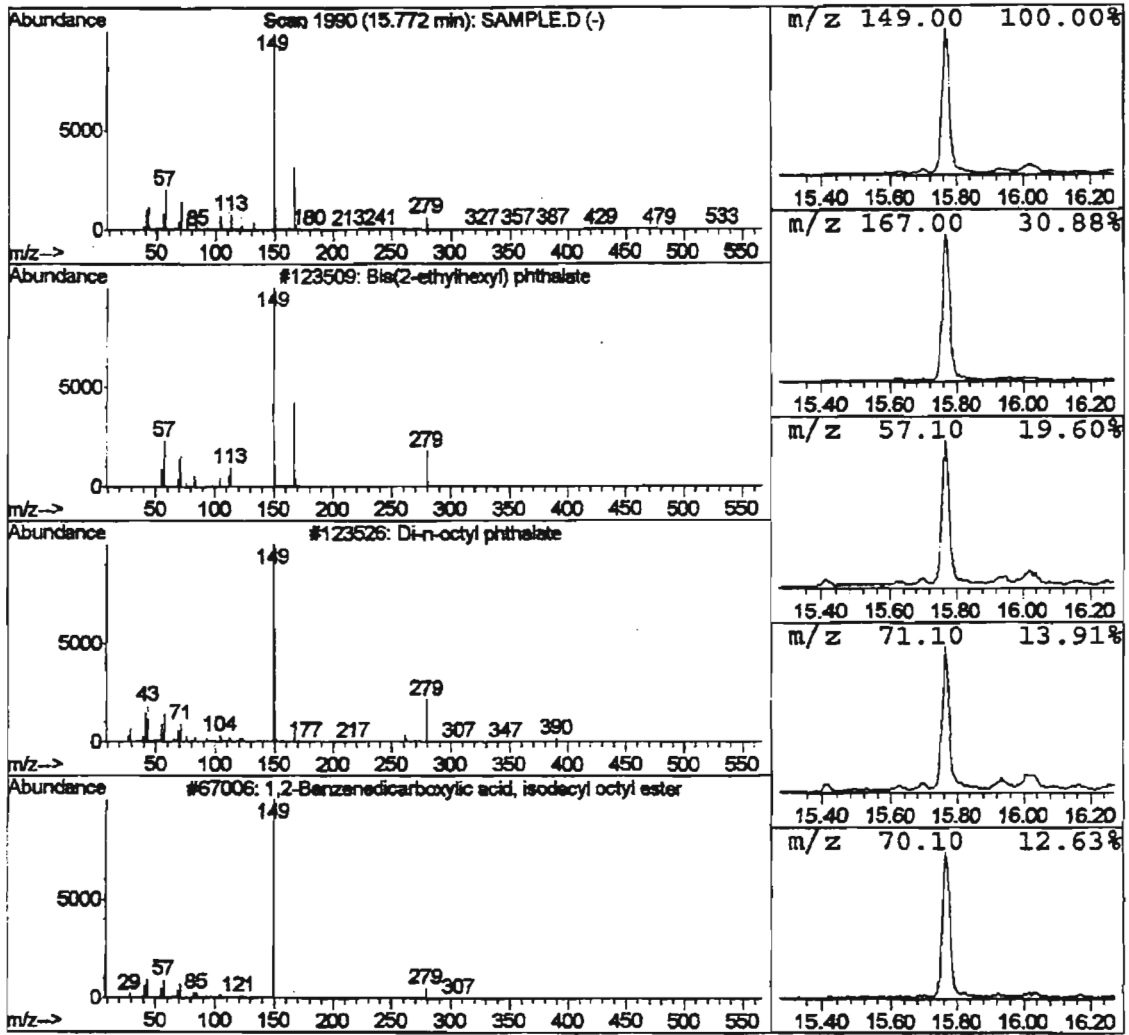Figure C3.13:   Mass spectrum of an unknown compound eluting at 11.994 minutes.

Figure C3.14:   Mass spectrum of an unknown compound eluting at 12.105 minutes.

Figure C3.15:   Mass spectrum of an unknown compound eluting at 12.135 minutes.
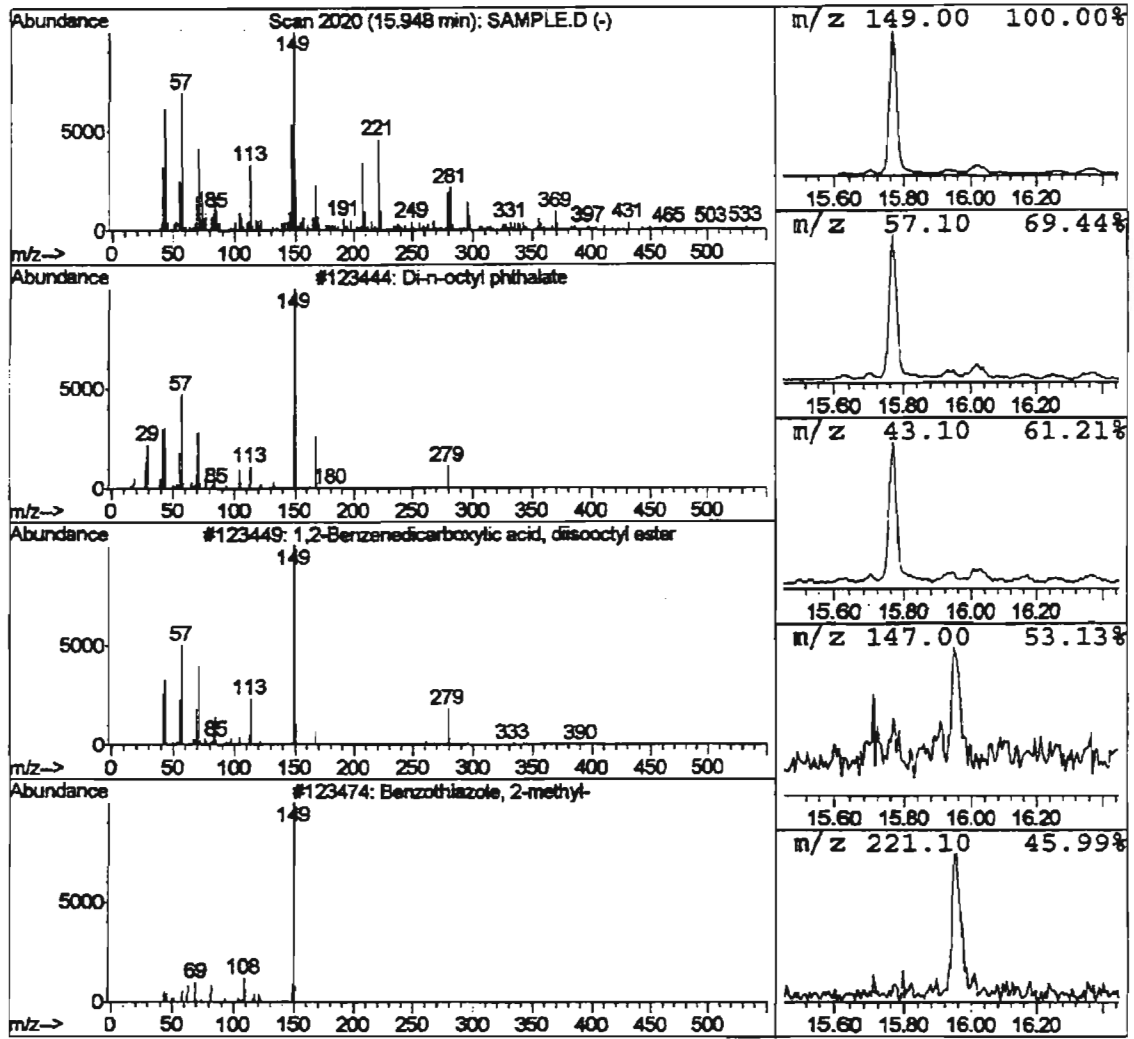
Figure C3.16:   Mass spectrum of an unknown compound eluting at 12.229 minutes.

Figure C3.17:   Mass spectrum of an unknown compound eluting at 12.352 minutes.
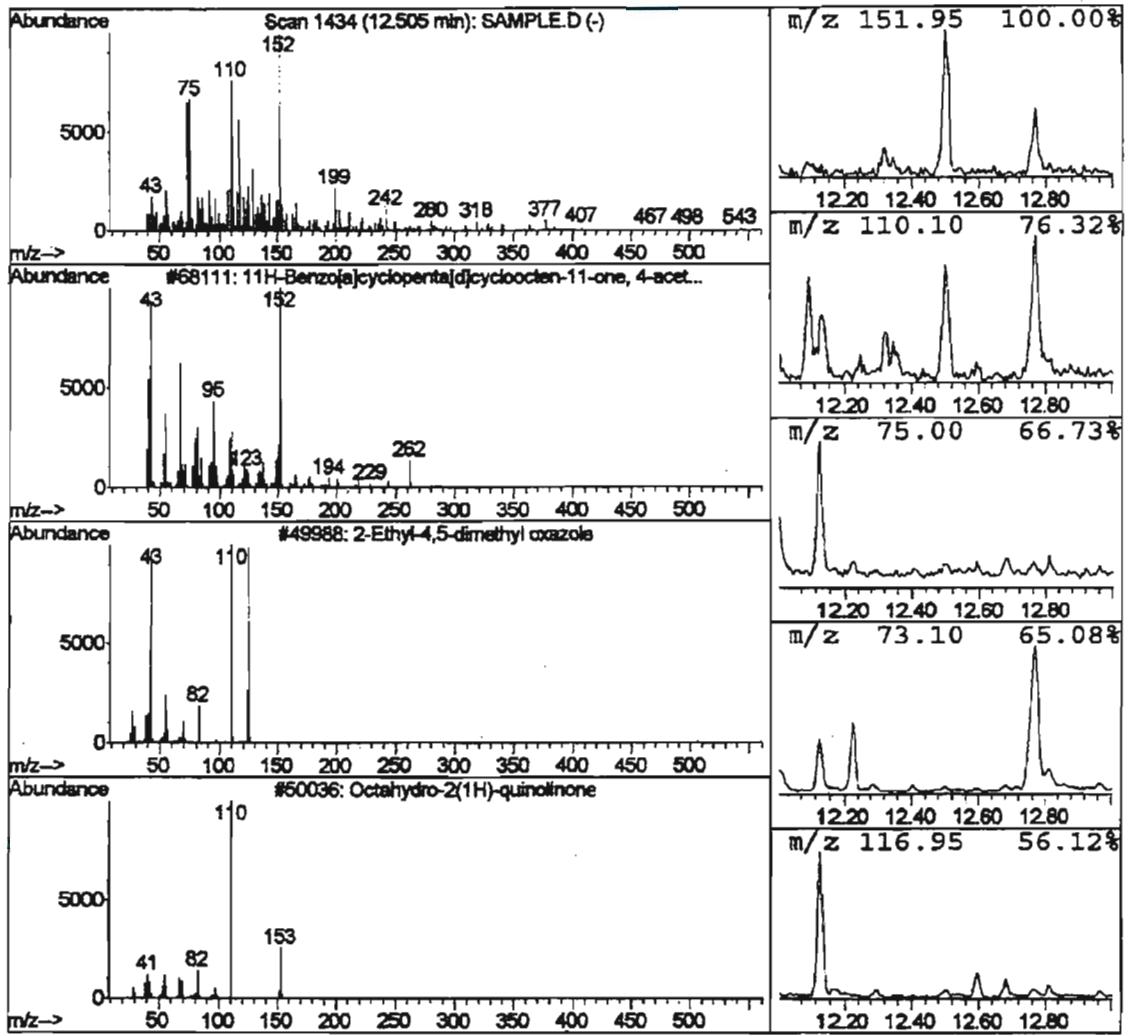
Figure C3.18:   Mass spectrum of an unknown compound eluting at 12.505 minutes.
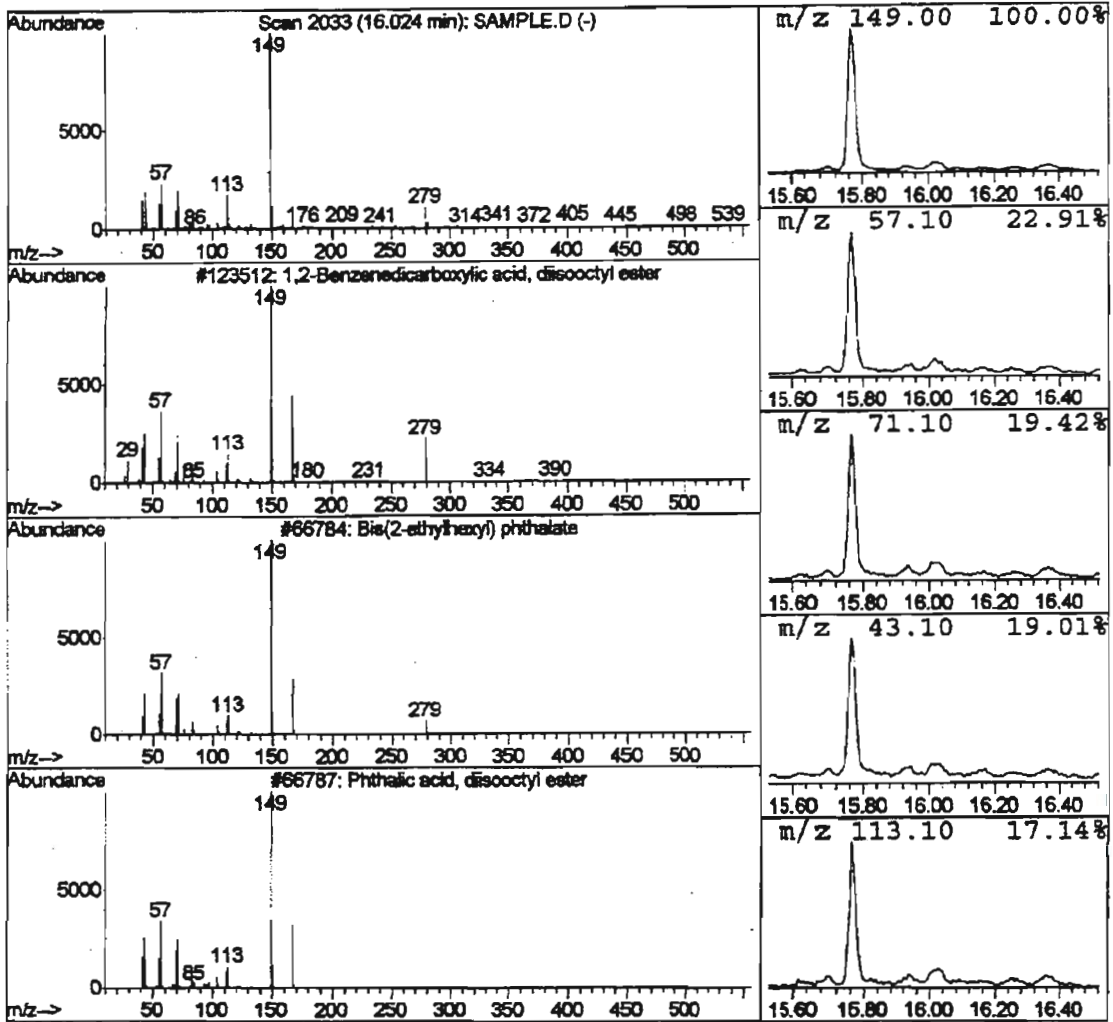
Figure C3.19:   Mass spectrum of an unknown compound eluting at 12.593 minutes.

Figure C3.20: Mass spectrum of an unknown compound eluting at 12.681 minutes.

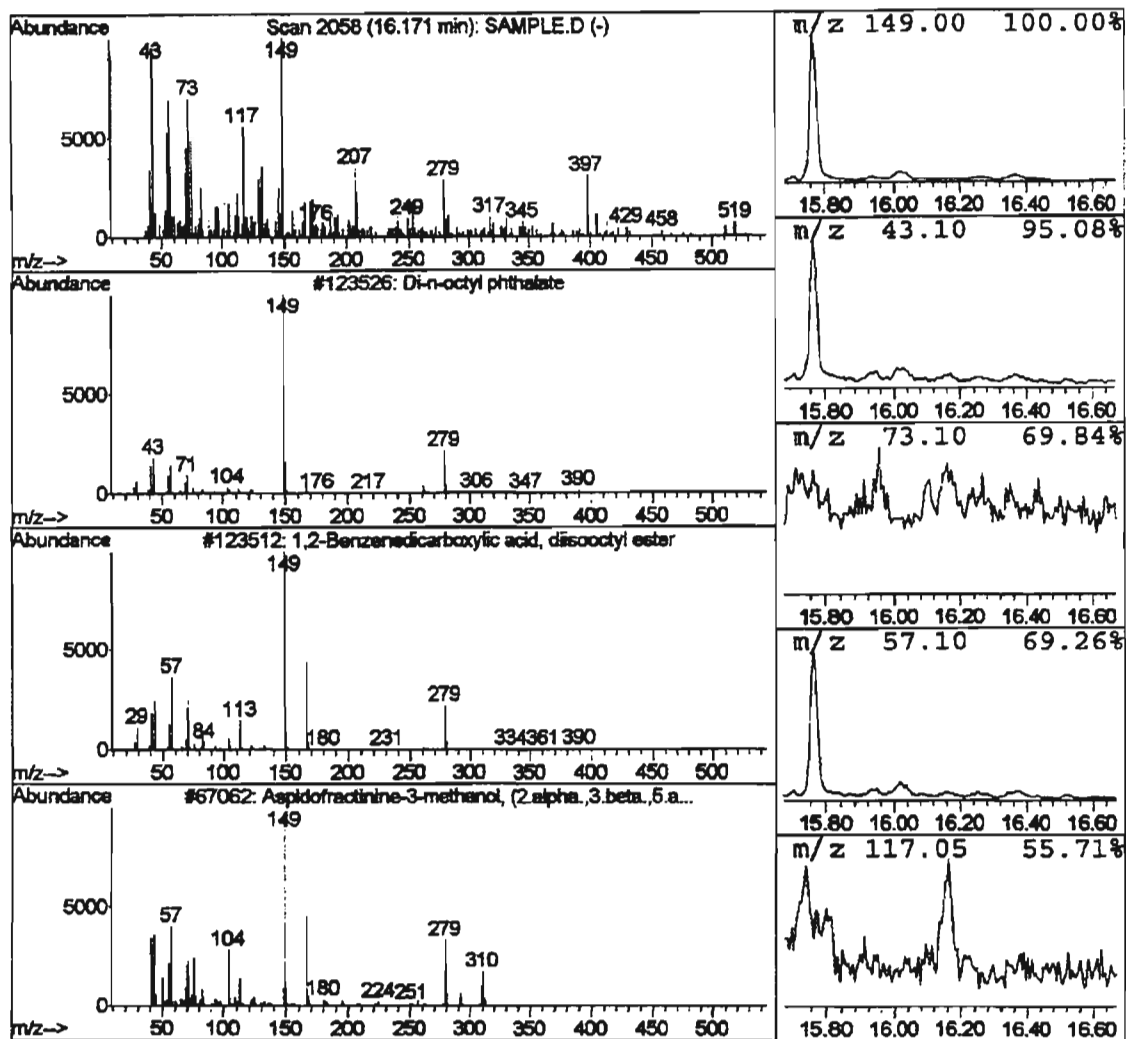Figure C3.21:   Mass spectrum of an unknown compound eluting at 12.769 minutes.

Figure C3.22:   Mass spectrum of an unknown compound eluting at 12.816 minutes.

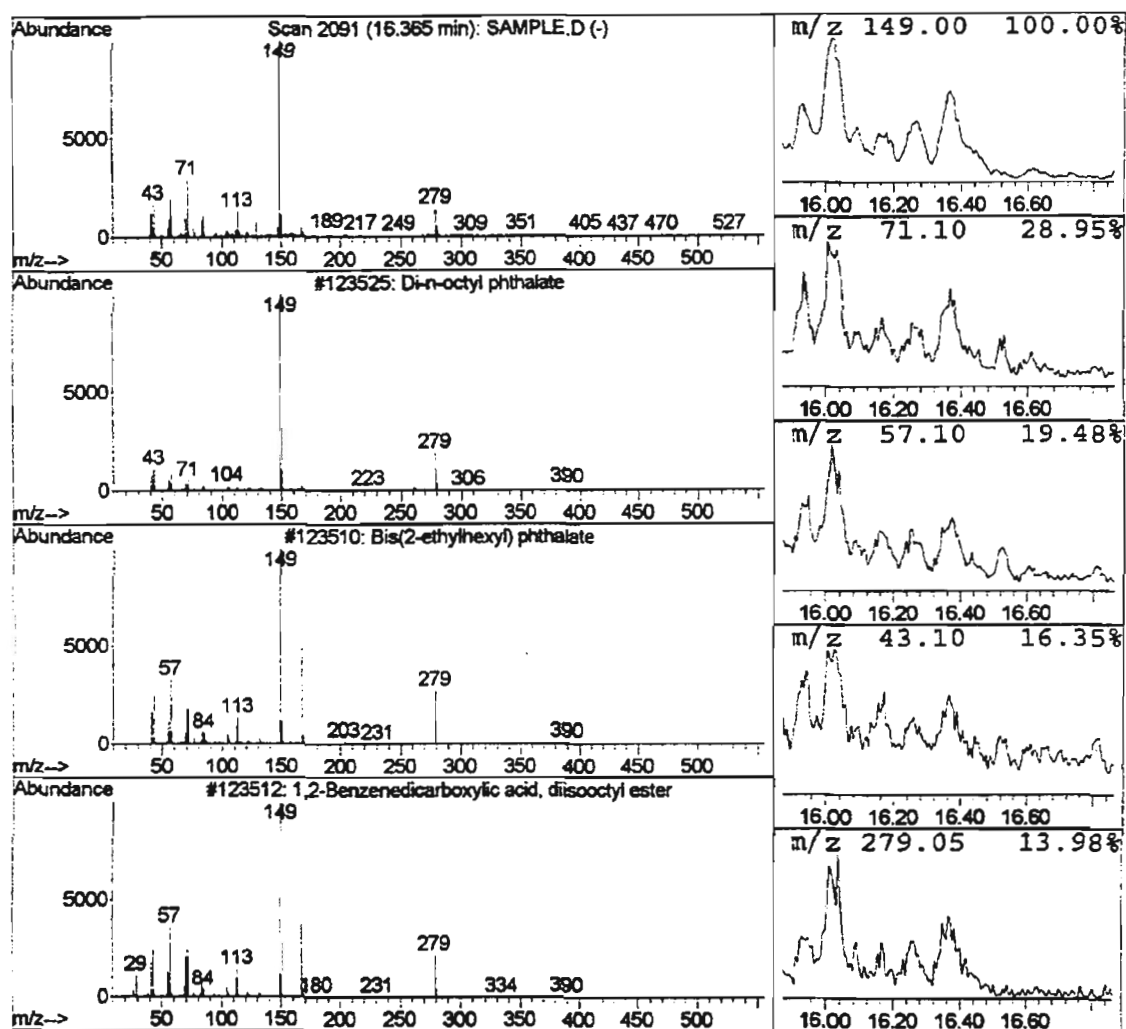Figure C3.23:   Mass spectrum of an unknown compound eluting at 13.169 minutes.

Figure C3.24: Mass spectrum of a derivatised hexadecanoic acid that elutes at 13.210 minutes. The fragmentation pattern matched that of a derivatised hexadecanoic acid present in the library.
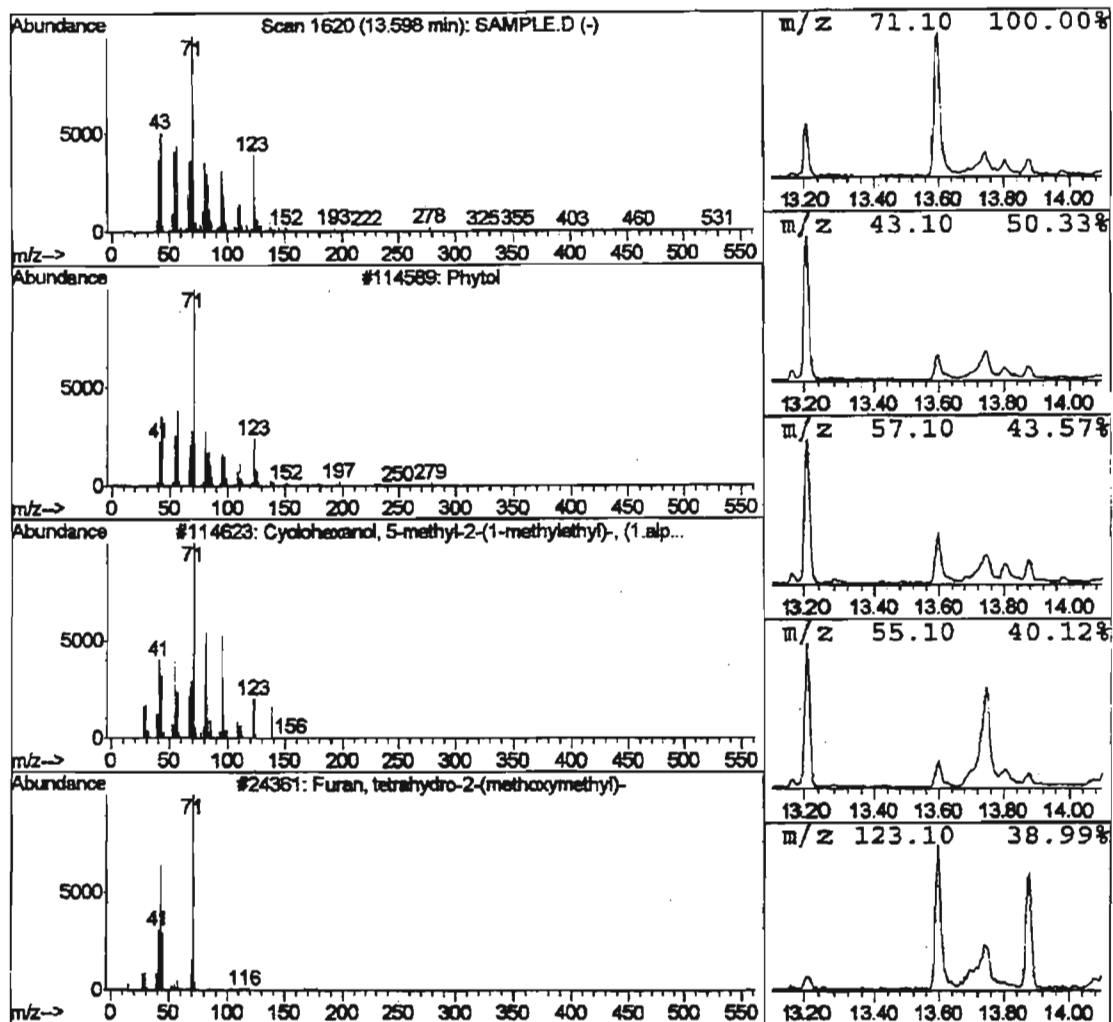
Figure C3.25:   Mass spectrum of an unknown compound eluting at 13.598 minutes.

Figure C3.26: Mass spectrum of a derivatised octadecatrienoic acid that elutes at 13.750 minutes. The fragmentation pattern matched that of a derivatised octadecatrienoic acid present in the library.

Figure C3.27: Mass spectrum of a derivatised octadecanoic acid that elutes at 13.803 minutes. The fragmentation pattern matched that of a derivatised octadecanoic acid present in the library.
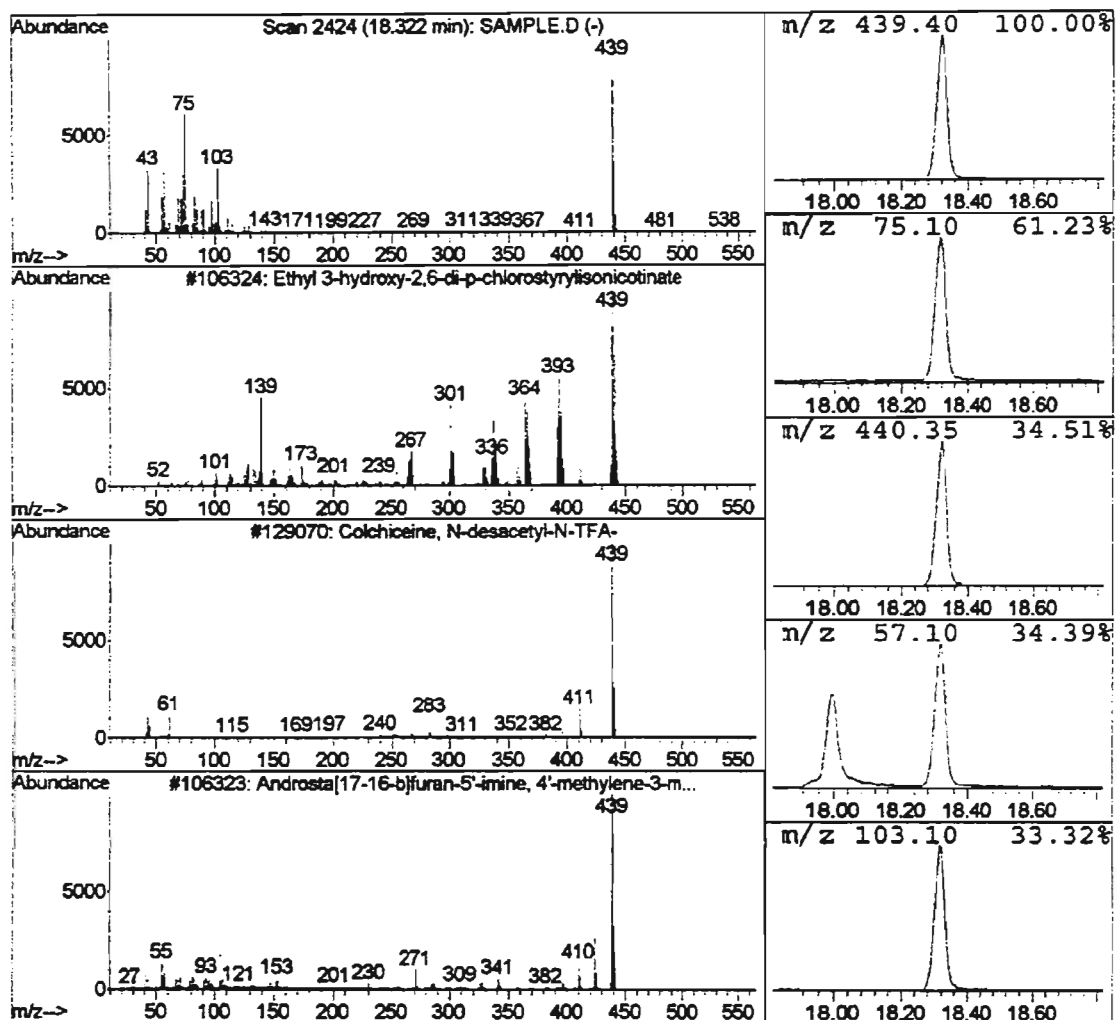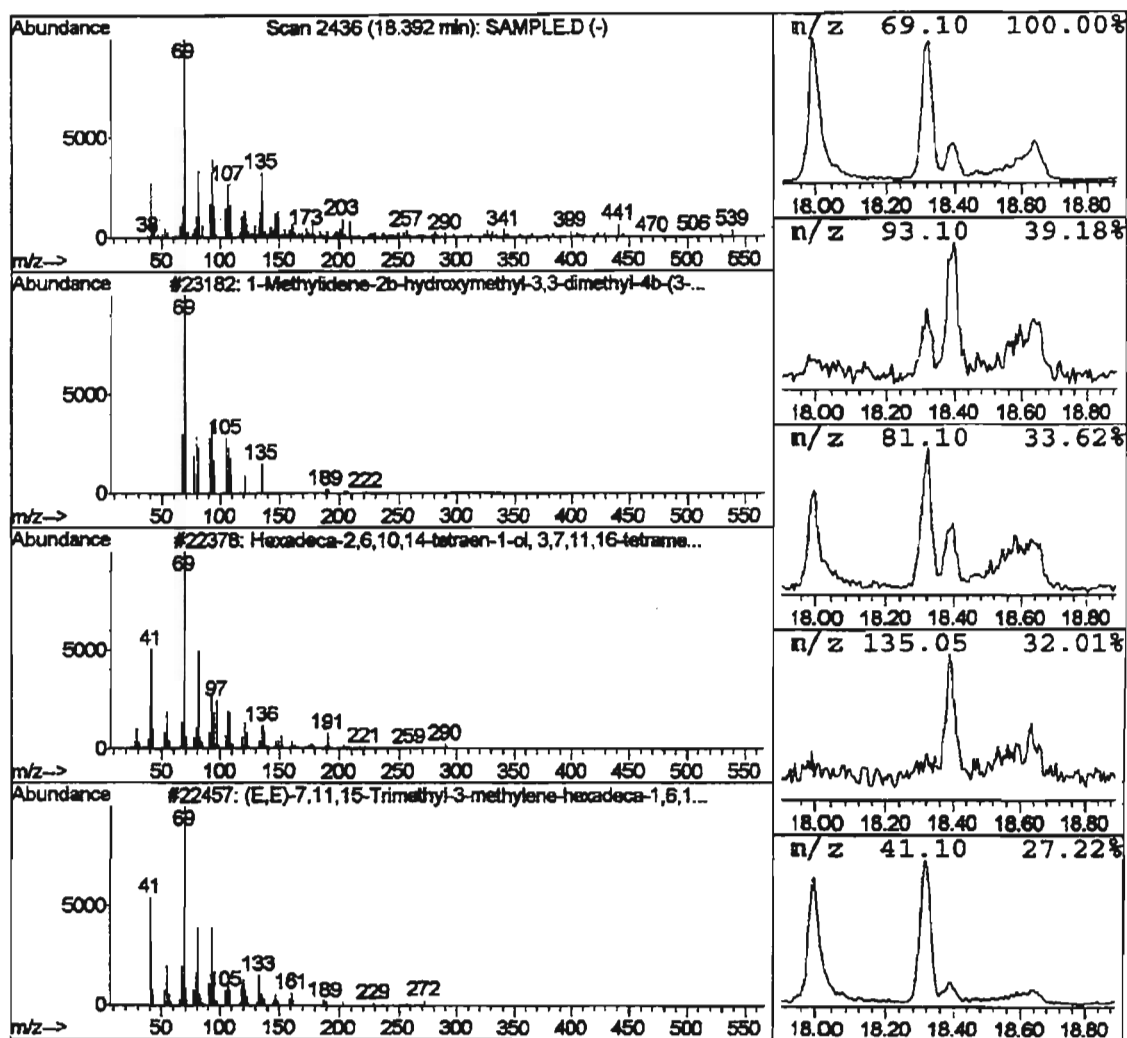
Figure C3.28:   Mass spectrum of an unknown compound eluting at 13.880 minutes.

Figure C3.29:   Mass spectrum of an unknown compound eluting at 14.074 minutes.

Figure C3.30: Mass spectrum of a derivatised alpha-linolenic acid that elutes at 14.109 minutes. The fragmentation pattern matched that of a derivatised alpha-linolenic acid present in the library.

Figure C3.31:   Mass spectrum of a derivatised octadecanoic acid that elutes at 14.191 minutes. The fragmentation pattern matched that of a derivatised octadecanoic acid present in the library.

Figure C3.32: Mass spectrum of an EHMC impurity eluting at 14.655 minutes. The fragmentation pattern matched that of a derivatised EHMC present in the library.
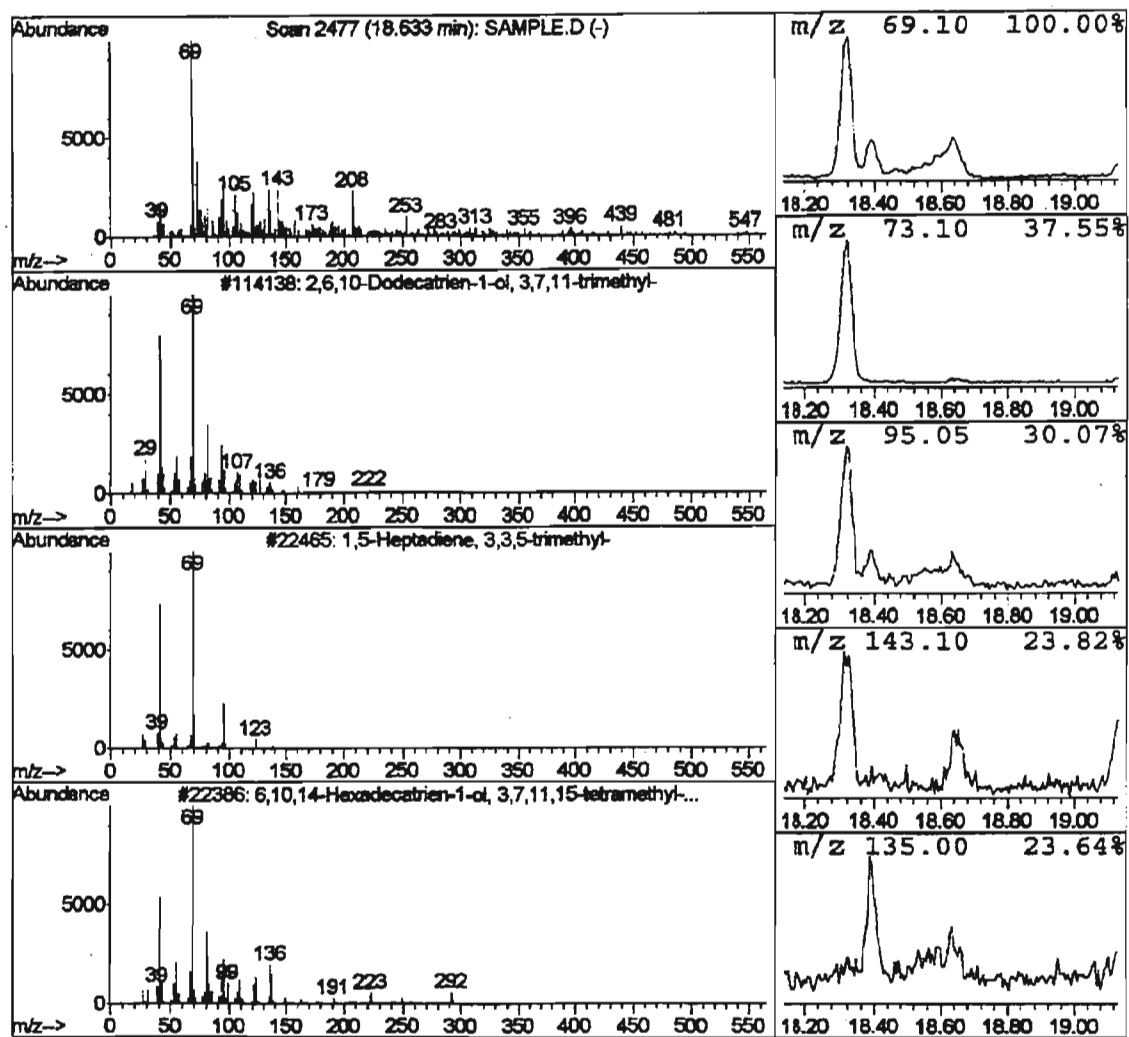
Figure C3.33:   Mass spectrum of an unknown compound eluting at 15.701 minutes.
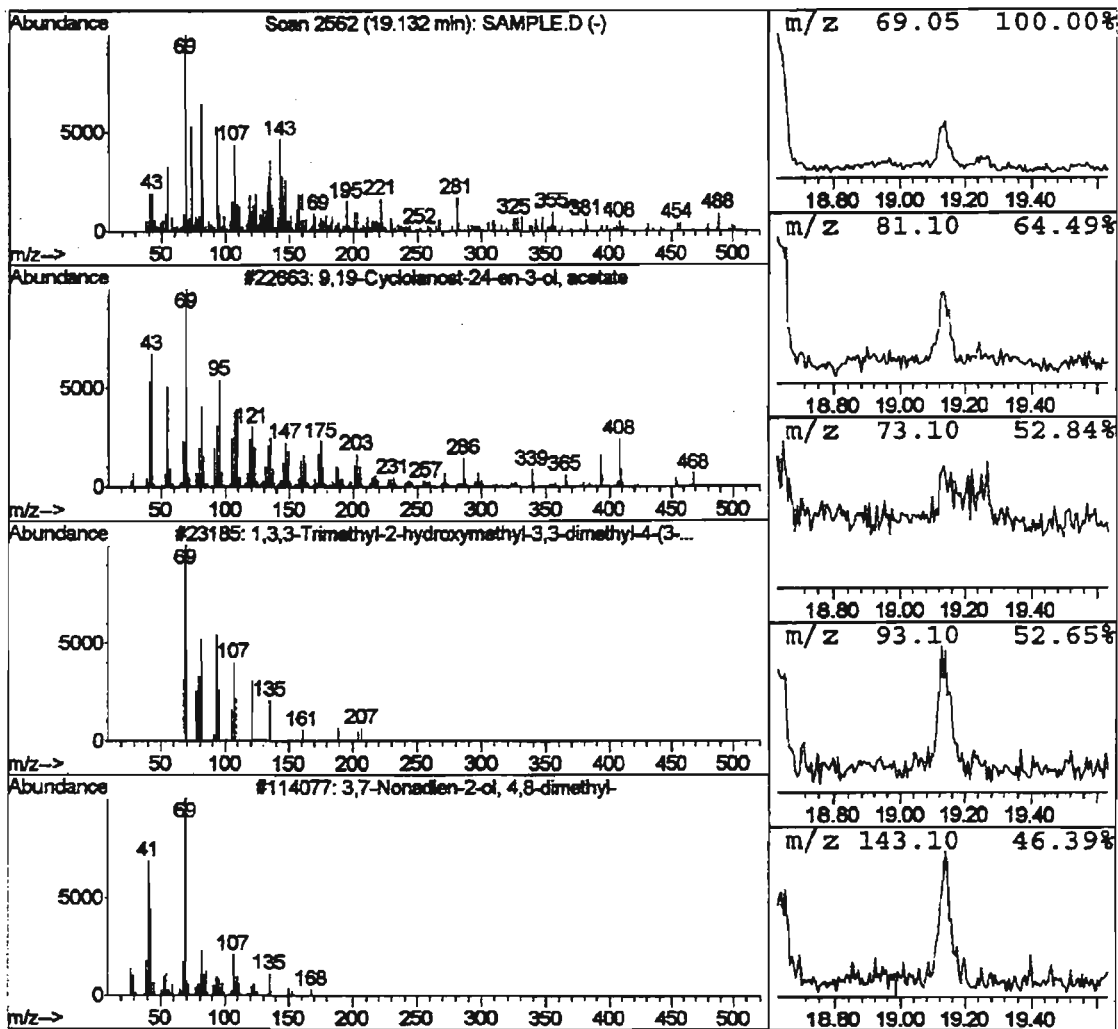
Figure C3.34: Mass spectrum of an unknown compound eluting at 15.772 minutes.

Figure C3.35:   Mass spectrum of an unknown compound eluting at 15.948 minutes.

Figure C3.36:   Mass spectrum of an unknown compound eluting at 16.024 minutes.

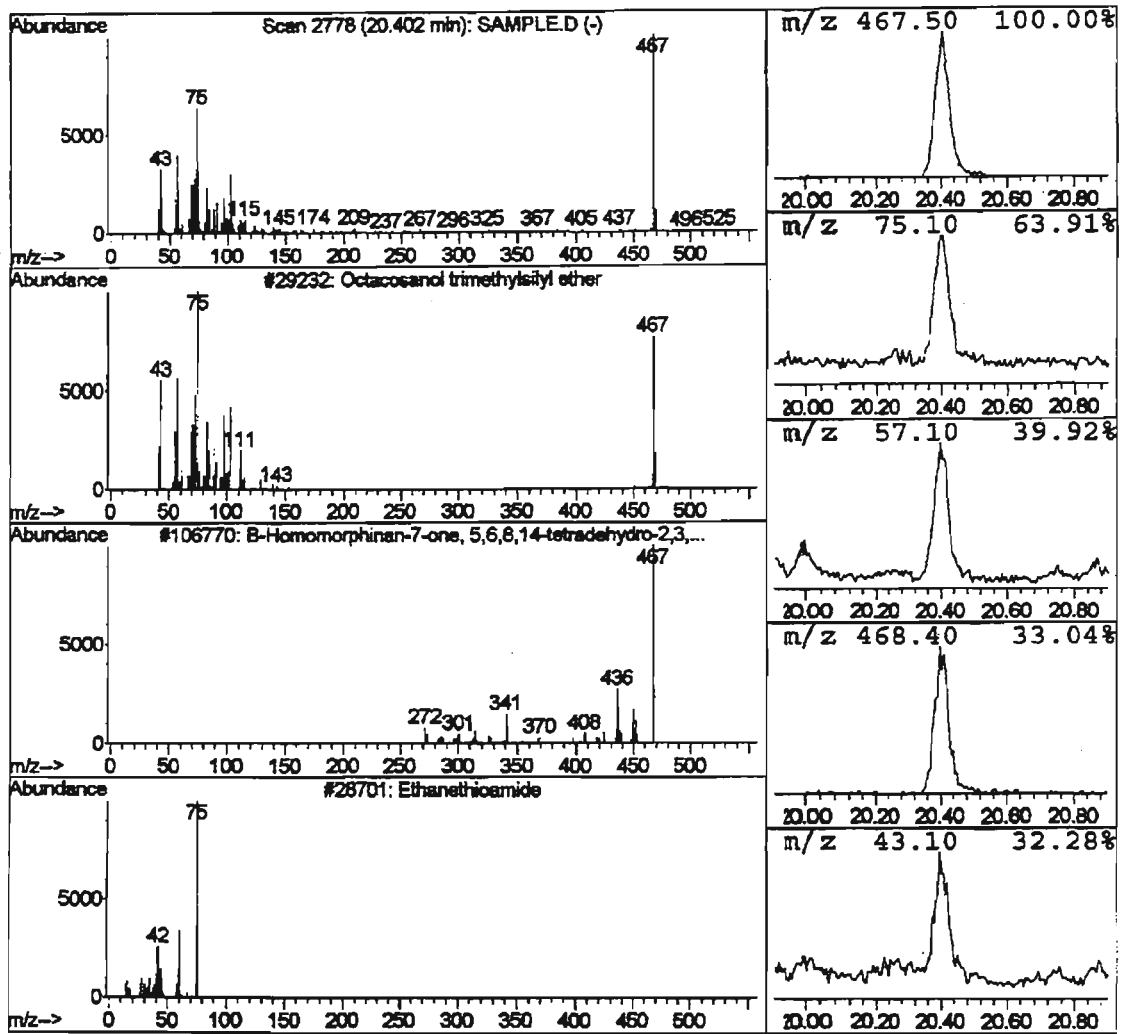Figure C3.37:   Mass spectrum of an unknown compound eluting at 16.171 minutes.

Figure C3.38:   Mass spectrum of an unknown compound eluting at 16.365 minutes.
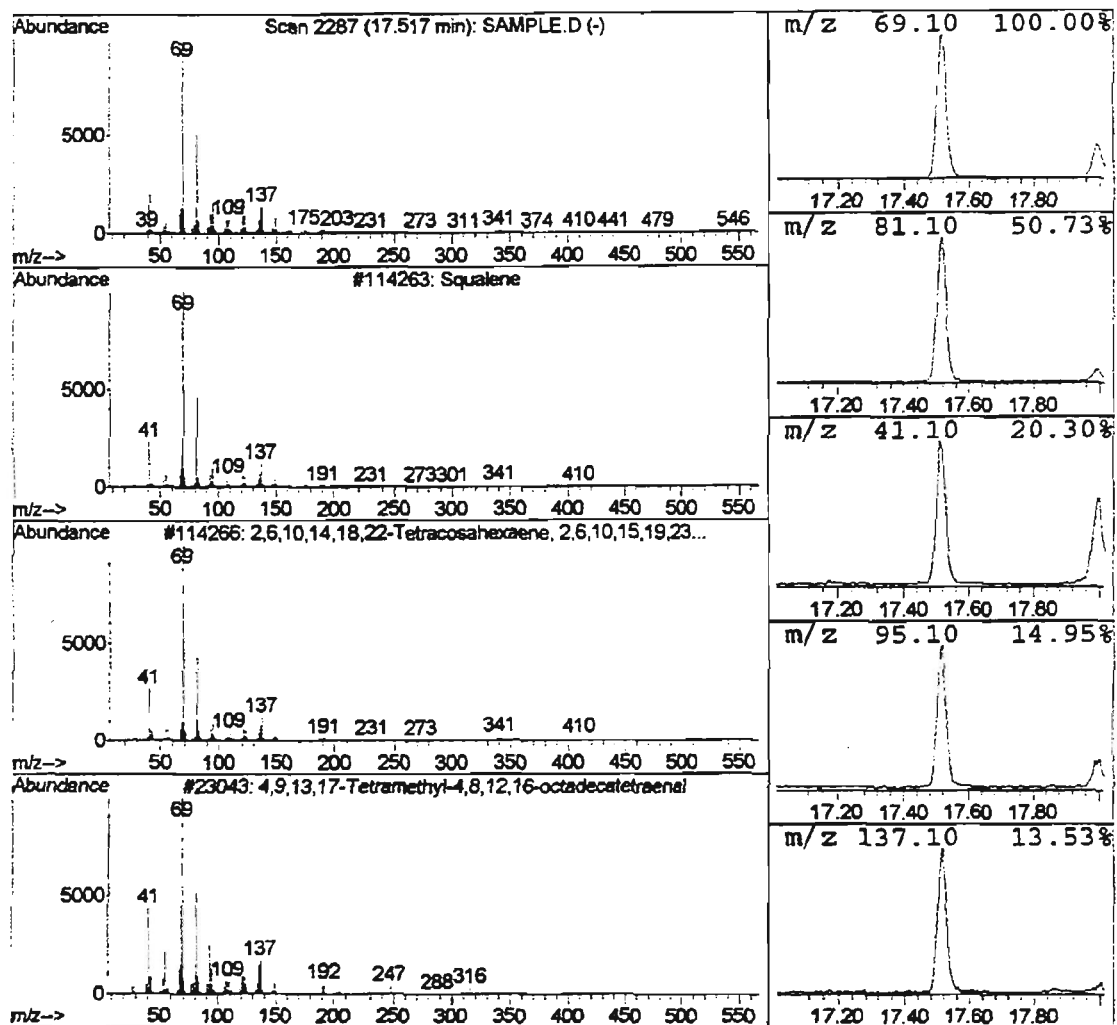
Figure C3.39: Mass spectrum of squalene that elutes at 17.517 minutes. The fragmentation
pattern matched that of squalene present in the library.
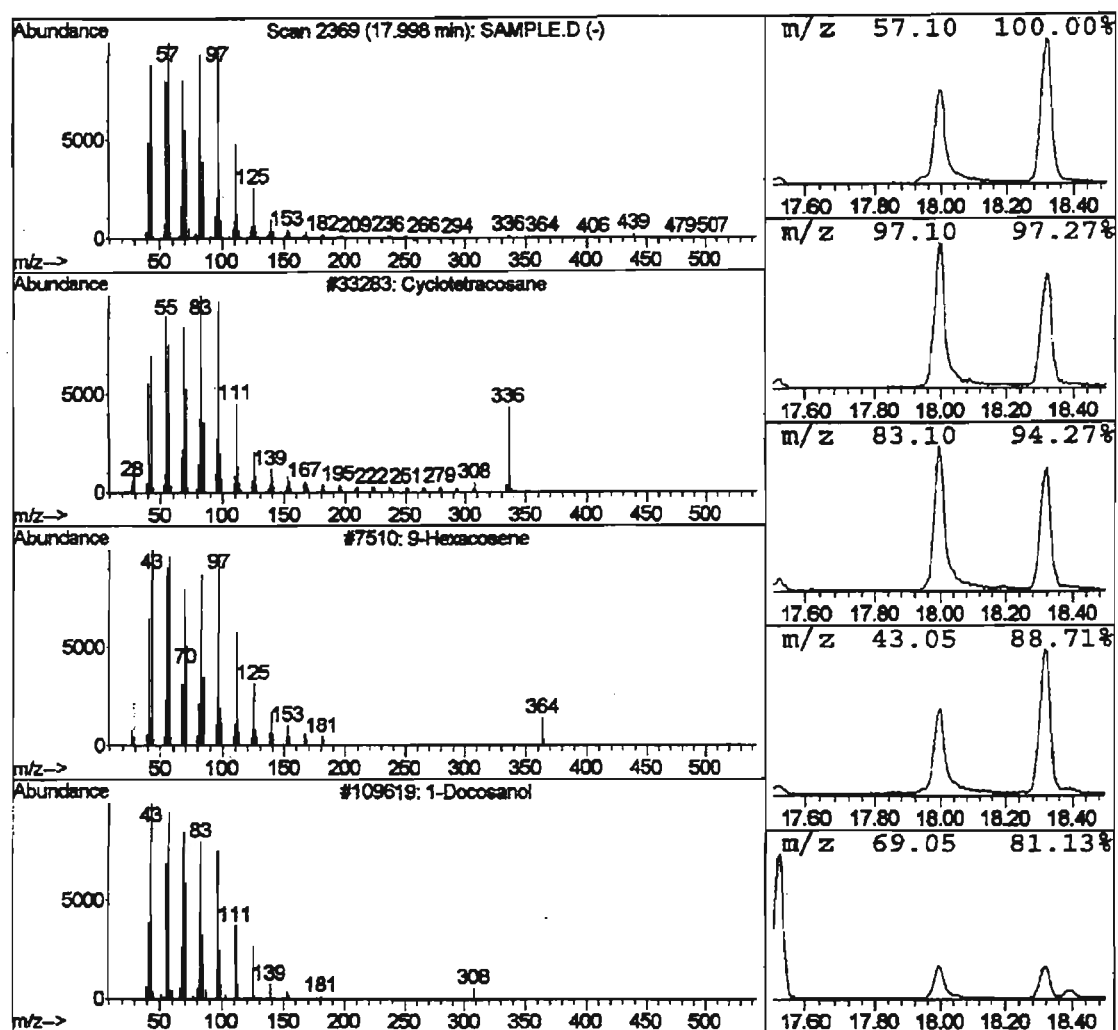
Figure C3.40: Mass spectrum of cyclotetracosane eluting at 17.998 minutes. The fragmentation pattern matched that of cyclotetracosane present in the library.
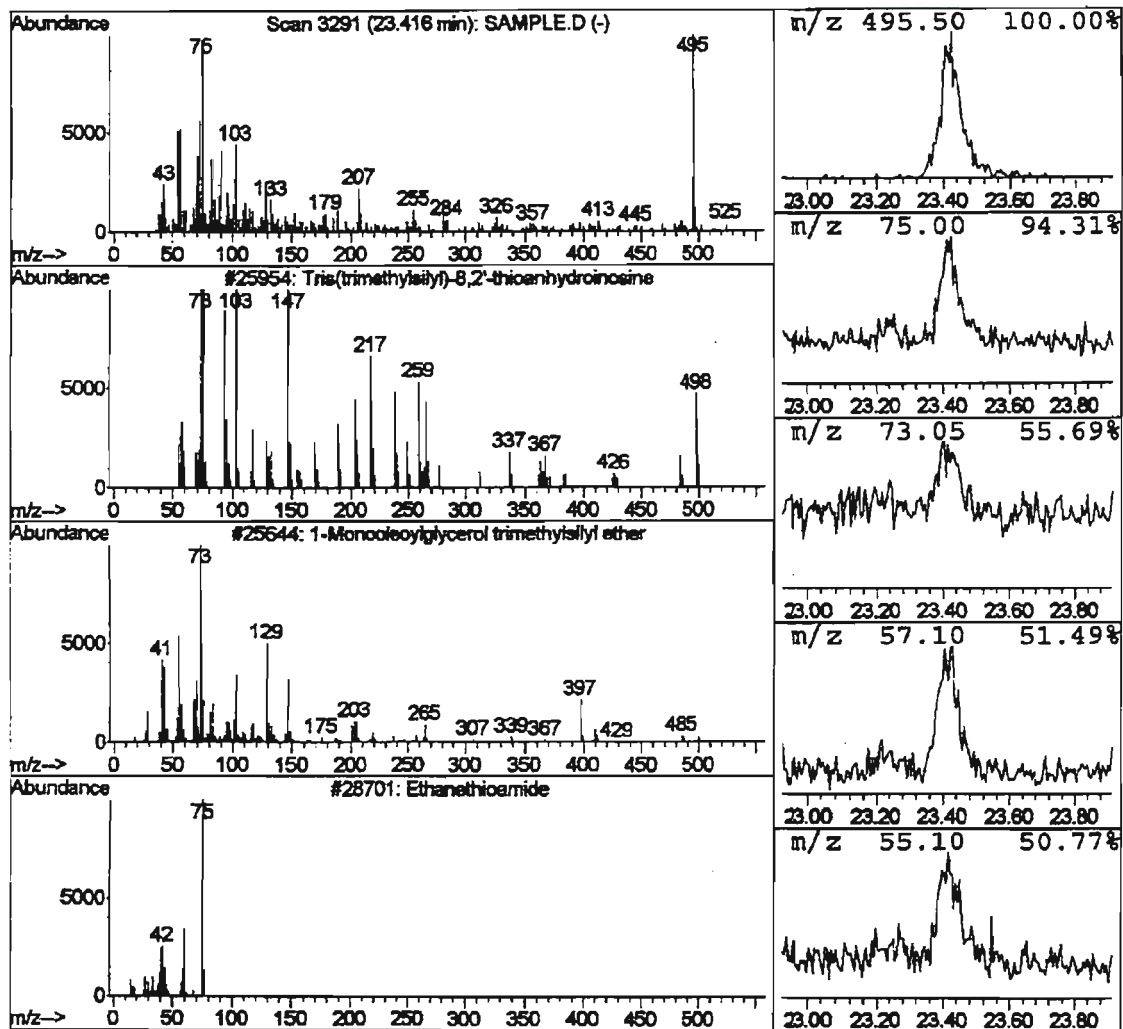
Figure C3.41:   Mass spectrum of an unknown compound eluting at 18.322 minutes.

Figure C3.42:   Mass spectrum of an unknown compound eluting at 18.392 minutes.

Figure C3.43:   Mass spectrum of an unknown compound eluting at 18.633 minutes.

Figure C3.44: Mass spectrum of an unknown compound eluting at 19.132 minutes.

Figure C3.45:   Mass spectrum of an unknown compound eluting at 20.402 minutes.
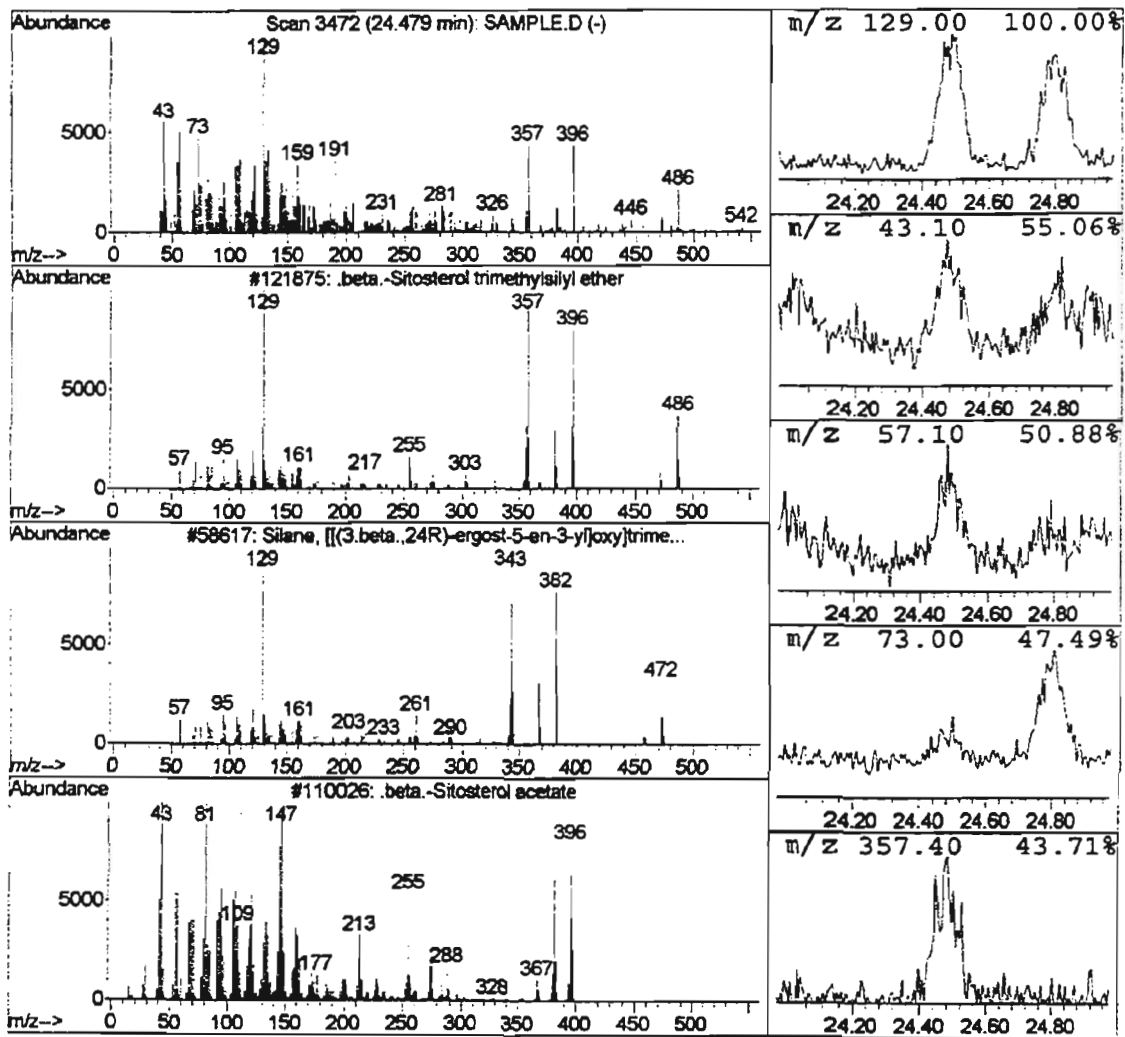
Figure C3.46:   Mass spectrum of an unknown compound eluting at 23.416 minutes.

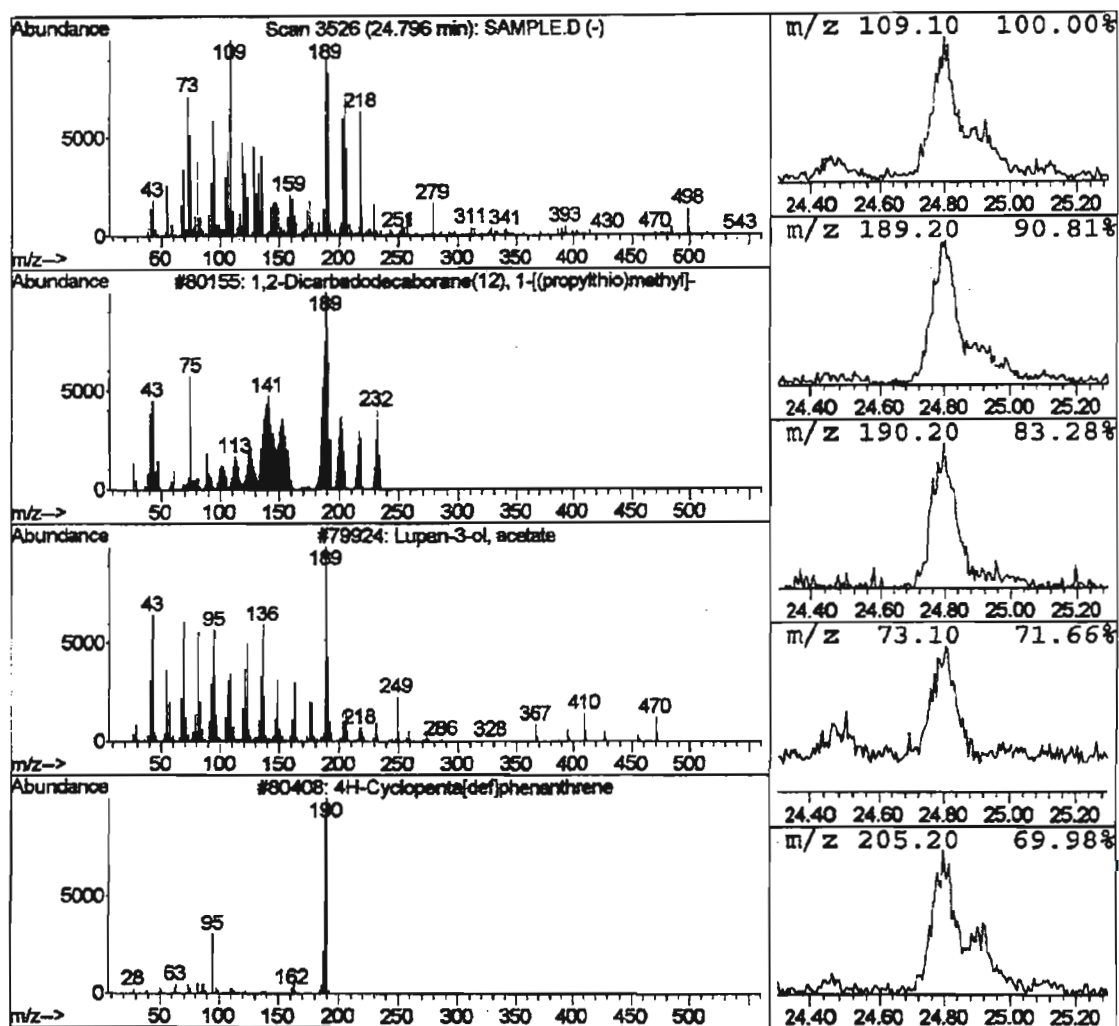Figure C3.47: Mass spectrum of an unknown compound eluting at 24.479 minutes.

Figure C3.48: Mass spectrum of an unknown compound eluting at 24.796 minutes.
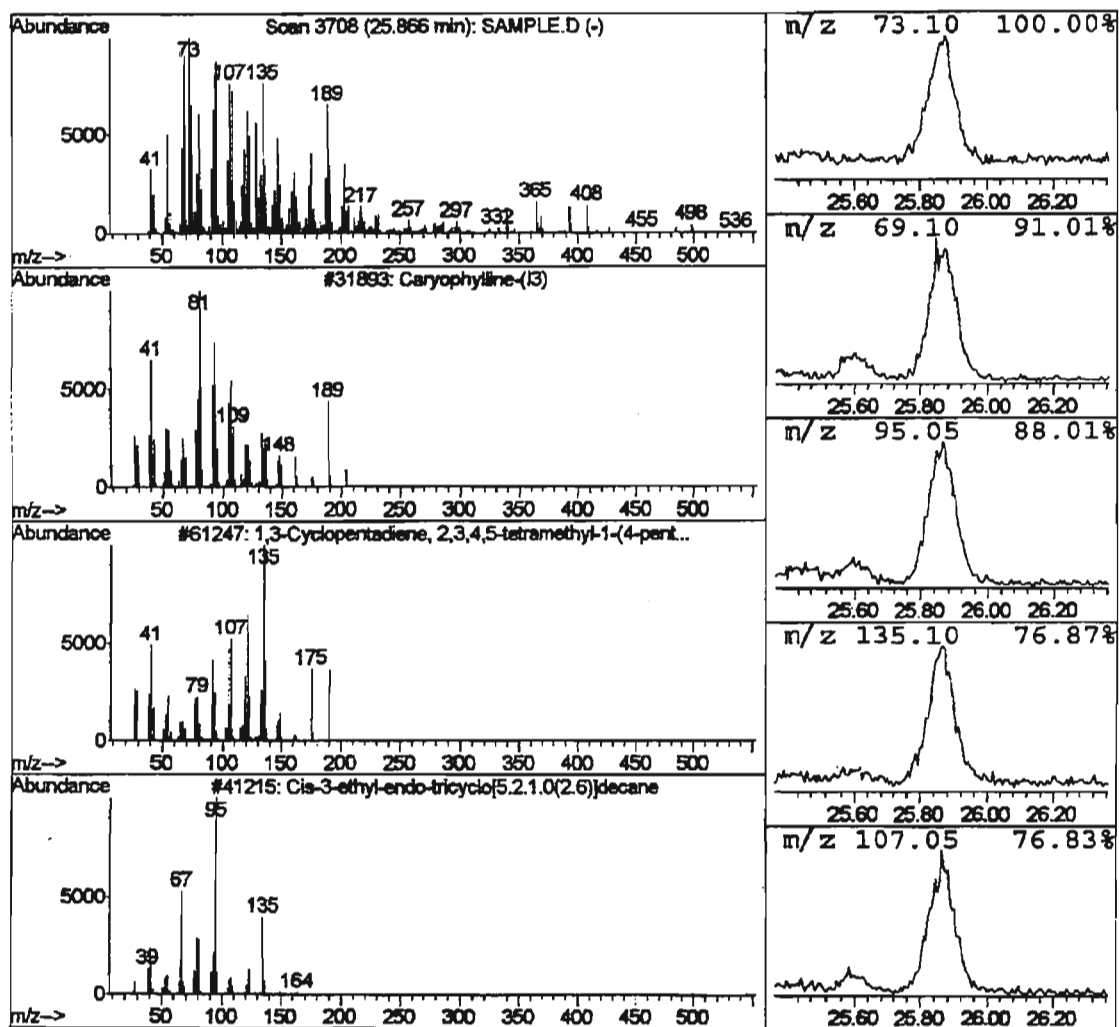
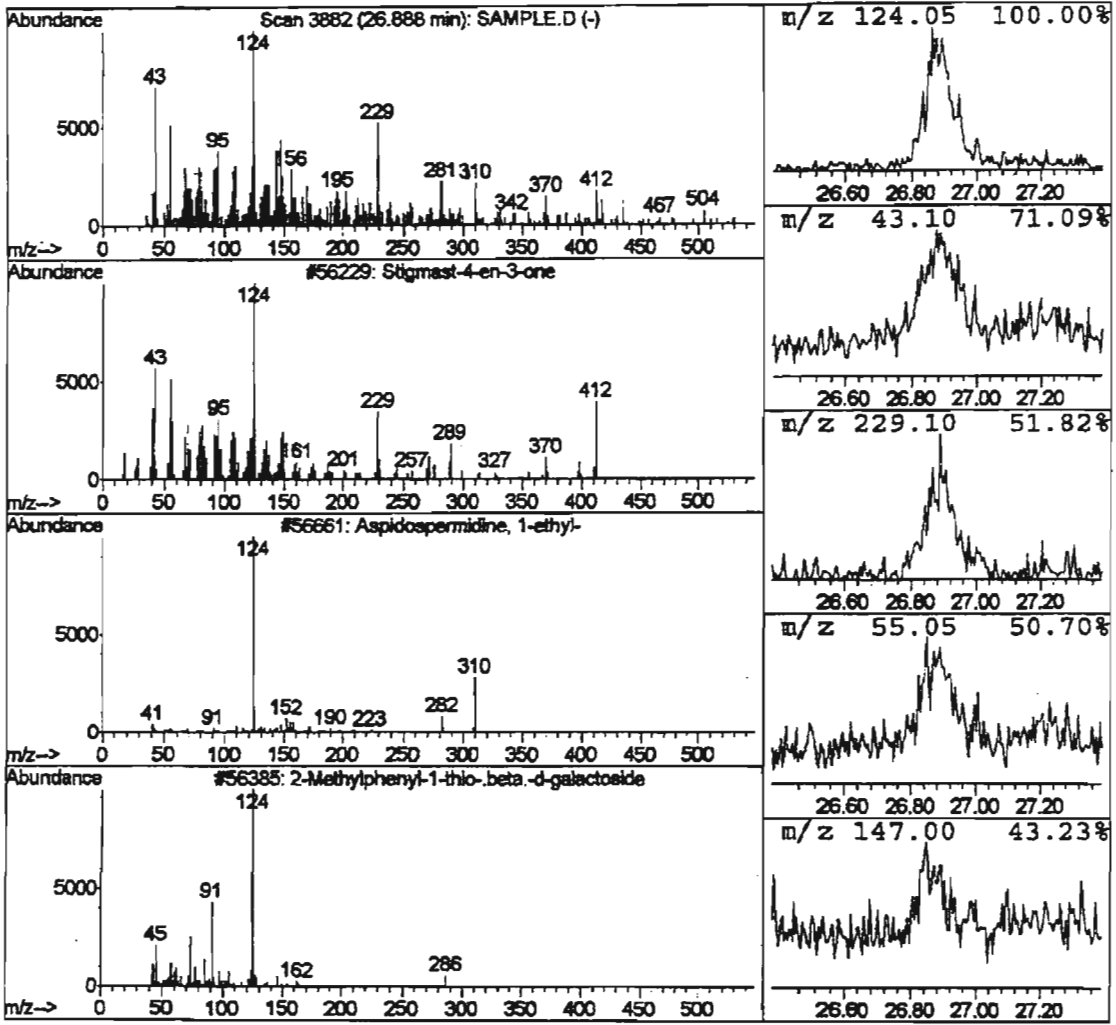Figure C3.49: Mass spectrum of an unknown compound eluting at 25.866 minutes.

Figure C3.50: Mass spectrum of an unknown compound eluting at 26.888 minutes.